frontiers | Research Topics

Systems biology and data-driven machine learning-based models in personalized cardiovascular medicine

Edited by
Miguel Hueso, Joan Carles Escolà-Gil, Noemi Rotllan Vila and Alfredo Vellido

Published in
Frontiers in Cardiovascular Medicine



FRONTIERS EBOOK COPYRIGHT STATEMENT

The copyright in the text of individual articles in this ebook is the property of their respective authors or their respective institutions or funders. The copyright in graphics and images within each article may be subject to copyright of other parties. In both cases this is subject to a license granted to Frontiers.

The compilation of articles constituting this ebook is the property of Frontiers.

Each article within this ebook, and the ebook itself, are published under the most recent version of the Creative Commons CC-BY licence. The version current at the date of publication of this ebook is CC-BY 4.0. If the CC-BY licence is updated, the licence granted by Frontiers is automatically updated to the new version.

When exercising any right under the CC-BY licence, Frontiers must be attributed as the original publisher of the article or ebook, as applicable.

Authors have the responsibility of ensuring that any graphics or other materials which are the property of others may be included in the CC-BY licence, but this should be checked before relying on the CC-BY licence to reproduce those materials. Any copyright notices relating to those materials must be complied with.

Copyright and source acknowledgement notices may not be removed and must be displayed in any copy, derivative work or partial copy which includes the elements in question.

All copyright, and all rights therein, are protected by national and international copyright laws. The above represents a summary only. For further information please read Frontiers' Conditions for Website Use and Copyright Statement, and the applicable CC-BY licence.

ISSN 1664-8714
ISBN 978-2-8325-3900-2
DOI 10.3389/978-2-8325-3900-2

About Frontiers

Frontiers is more than just an open access publisher of scholarly articles: it is a pioneering approach to the world of academia, radically improving the way scholarly research is managed. The grand vision of Frontiers is a world where all people have an equal opportunity to seek, share and generate knowledge. Frontiers provides immediate and permanent online open access to all its publications, but this alone is not enough to realize our grand goals.

Frontiers journal series

The Frontiers journal series is a multi-tier and interdisciplinary set of open-access, online journals, promising a paradigm shift from the current review, selection and dissemination processes in academic publishing. All Frontiers journals are driven by researchers for researchers; therefore, they constitute a service to the scholarly community. At the same time, the *Frontiers journal series* operates on a revolutionary invention, the tiered publishing system, initially addressing specific communities of scholars, and gradually climbing up to broader public understanding, thus serving the interests of the lay society, too.

Dedication to quality

Each Frontiers article is a landmark of the highest quality, thanks to genuinely collaborative interactions between authors and review editors, who include some of the world's best academicians. Research must be certified by peers before entering a stream of knowledge that may eventually reach the public - and shape society; therefore, Frontiers only applies the most rigorous and unbiased reviews. Frontiers revolutionizes research publishing by freely delivering the most outstanding research, evaluated with no bias from both the academic and social point of view. By applying the most advanced information technologies, Frontiers is catapulting scholarly publishing into a new generation.

What are Frontiers Research Topics?

Frontiers Research Topics are very popular trademarks of the *Frontiers journals series*: they are collections of at least ten articles, all centered on a particular subject. With their unique mix of varied contributions from Original Research to Review Articles, Frontiers Research Topics unify the most influential researchers, the latest key findings and historical advances in a hot research area.

Find out more on how to host your own Frontiers Research Topic or contribute to one as an author by contacting the Frontiers editorial office: frontiersin.org/about/contact

Systems biology and data-driven machine learning-based models in personalized cardiovascular medicine

Topic editors

Miguel Hueso — Bellvitge University Hospital, Spain
Joan Carles Escolà-Gil — Sant Pau Institute for Biomedical Research, Spain
Noemi Rotllan Vila — Sant Pau Institute for Biomedical Research, Spain
Alfredo Vellido — Universitat Politecnica de Catalunya, Spain

Citation

Hueso, M., Escolà-Gil, J. C., Vila, N. R., Vellido, A., eds. (2023). *Systems biology and data-driven machine learning-based models in personalized cardiovascular medicine*. Lausanne: Frontiers Media SA. doi: 10.3389/978-2-8325-3900-2

Table of contents

05 Editorial: Systems biology and data-driven machine learning-based models in personalized cardiovascular medicine
Miguel Hueso, Noemí Rotllan, Joan Carles Escolà-Gil and Alfredo Vellido

08 Machine Learning Patient-Specific Prediction of Heart Failure Hospitalization Using Cardiac MRI-Based Phenotype and Electronic Health Information
Aidan K. Cornhill, Steven Dykstra, Alessandro Satriano, Dina Labib, Yoko Mikami, Jacqueline Flewitt, Easter Prosio, Sandra Rivest, Rosa Sandonato, Andrew G. Howarth, Carmen Lydell, Cathy A. Eastwood, Hude Quan, Nowell Fine, Joon Lee and James A. White

19 Prediction and Risk Stratification of Cardiovascular Disease in Diabetic Kidney Disease Patients
Jingjing Ren, Dongwei Liu, Guangpu Li, Jiayu Duan, Jiancheng Dong and Zhangsuo Liu

30 Predicting acute kidney injury risk in acute myocardial infarction patients: An artificial intelligence model using medical information mart for intensive care databases
Dabei Cai, Tingting Xiao, Ailin Zou, Lipeng Mao, Boyu Chi, Yu Wang, Qingjie Wang, Yuan Ji and Ling Sun

44 Machine learning in predicting cardiac surgery-associated acute kidney injury: A systemic review and meta-analysis
Zhe Song, Zhenyu Yang, Ming Hou and Xuedong Shi

56 Machine learning prediction of atrial fibrillation in cardiovascular patients using cardiac magnetic resonance and electronic health information
Steven Dykstra, Alessandro Satriano, Aidan K. Cornhill, Lucy Y. Lei, Dina Labib, Yoko Mikami, Jacqueline Flewitt, Sandra Rivest, Rosa Sandonato, Patricia Feuchter, Andrew G. Howarth, Carmen P. Lydell, Nowell M. Fine, Derek V. Exner, Carlos A. Morillo, Stephen B. Wilton, Marina L. Gavrilova and James A. White

70 Machine learning derived ECG risk score improves cardiovascular risk assessment in conjunction with coronary artery calcium scoring
Shruti Siva Kumar, Sadeer Al-Kindi, Nour Tashtish, Varun Rajagopalan, Pingfu Fu, Sanjay Rajagopalan and Anant Madabhushi

82 Interpretable machine learning for 28-day all-cause in-hospital mortality prediction in critically ill patients with heart failure combined with hypertension: A retrospective cohort study based on medical information mart for intensive care database-IV and eICU databases
Shengxian Peng, Jian Huang, Jiewen Deng, Chenyu Sun, Juan Tang, Huaqiao Chen, Wenzhai Cao, Wei Wang, Xiangjie Duan, Xianglin Luo, Shuang Peng and Xiaozhu Liu

98 Using machine learning to find genes associated with sudden death
Kena Zhou, Congbo Cai, Yi He and Zhihua Chen

109 The predictive value of pressure recording analytical method for the duration of mechanical ventilation in children undergoing cardiac surgery with an XGBoost-based machine learning model
Mingwei Li, Shuangxing Wang, Hui Zhang, Hongtao Zhang, Yongjie Wu and Bing Meng

120 Prediction model of obstructive sleep apnea–related hypertension: Machine learning–based development and interpretation study
Yewen Shi, Lina Ma, Xi Chen, Wenle Li, Yani Feng, Yitong Zhang, Zine Cao, Yuqi Yuan, Yushan Xie, Haiqin Liu, Libo Yin, Changying Zhao, Shinan Wu and Xiaoyong Ren

132 5mC modification patterns provide novel direction for early acute myocardial infarction detection and personalized therapy
Yiqun Guo, Hua Jiang, Jinlong Wang, Ping Li, Xiaoquan Zeng, Tao Zhang, Jianyi Feng, Ruqiong Nie, Yulong Liu, Xiaobian Dong and Qingsong Hu

147 Machine learning-based integration develops biomarkers initial the crosstalk between inflammation and immune in acute myocardial infarction patients
Hongyu Li, Xinti Sun, Zesheng Li, Ruiping Zhao, Meng Li and Taohong Hu

167 Plasma protein profiling analysis in patients with atrial fibrillation before and after three different ablation techniques
Menglu Lin, Yangyang Bao, Zunhui Du, Yanting Zhou, Ning Zhang, Changjian Lin, Yinyin Xie, Ruihong Zhang, Qiheng Li, Jinwei Quan, Tingfang Zhu, Yuan Xie, Cathy Xu, Yun Xie, Yue Wei, Qingzhi Luo, Wenqi Pan, Lingjie Wang, Tianyou Ling, Qi Jin, Liqun Wu, Tong Yin and Yucai Xie

182 WGCNA combined with machine learning algorithms for analyzing key genes and immune cell infiltration in heart failure due to ischemic cardiomyopathy
XiangJin Kong, HouRong Sun, KaiMing Wei, LingWei Meng, Xin Lv, ChuanZhen Liu, FuShun Lin and XingHua Gu

198 Combining bioinformatics and machine learning to identify common mechanisms and biomarkers of chronic obstructive pulmonary disease and atrial fibrillation
Ziyi Sun, Jianguo Lin, Tianya Zhang, Xiaoning Sun, Tianlin Wang, Jinlong Duan and Kuiwu Yao

213 Segmenting computed tomograms for cardiac ablation using machine learning leveraged by domain knowledge encoding
Ruibin Feng, Brototo Deb, Prasanth Ganesan, Fleur V. Y. Tjong, Albert J. Rogers, Samuel Ruipérez-Campillo, Sulaiman Somani, Paul Clopton, Tina Baykaner, Miguel Rodrigo, James Zou, Francois Haddad, Matei Zahari and Sanjiv M. Narayan

frontiers | Frontiers in Cardiovascular Medicine

TYPE Editorial
PUBLISHED 27 October 2023
DOI 10.3389/fcvm.2023.1320110

Check for updates

OPEN ACCESS

EDITED AND REVIEWED BY
Neil Morgan,
University of Birmingham, United Kingdom

*CORRESPONDENCE
Miguel Hueso
✉ mhueso@idibell.cat

RECEIVED 11 October 2023
ACCEPTED 13 October 2023
PUBLISHED 27 October 2023

CITATION
Hueso M, Rotllan N, Escolà-Gil JC and Vellido A (2023) Editorial: Systems biology and data-driven machine learning-based models in personalized cardiovascular medicine. Front. Cardiovasc. Med. 10:1320110. doi: 10.3389/fcvm.2023.1320110

COPYRIGHT
© 2023 Hueso, Rotllan, Escolà-Gil and Vellido. This is an open-access article distributed under the terms of the Creative Commons Attribution License (CC BY). The use, distribution or reproduction in other forums is permitted, provided the original author(s) and the copyright owner(s) are credited and that the original publication in this journal is cited, in accordance with accepted academic practice. No use, distribution or reproduction is permitted which does not comply with these terms.

Editorial: Systems biology and data-driven machine learning-based models in personalized cardiovascular medicine

Miguel Hueso[1,2]*, Noemí Rotllan[3,4], Joan Carles Escolà-Gil[3,4] and Alfredo Vellido[5,6]

[1]Department of Nephrology, Hospital Universitari Bellvitge, and Institut d'Investigació Biomèdica de Bellvitge-IDIBELL, L'Hospitalet de Llobregat, Spain, [2]BigData and Artificial Intelligence Group (BigSEN Working Group) from the Spanish Society of Nephrology (SENEFRO), Spain, [3]Institut d'Investigacions Biomèdiques (IIB) Sant Pau, Barcelona, Spain, [4]CIBER de Diabetes y Enfermedades Metabólicas Asociadas (CIBERDEM), Madrid, Spain, [5]Department of Computer Science, Universitat Politècnica de Catalunya (UPC), Barcelona, Spain, [6]Intelligent Data Science and Artificial Intelligence (IDEAI-UPC) Research Center, Barcelona, Spain

KEYWORDS

personalized medicine, cardiovascular diseases, machine learning, artificial intelligence, systems biology

Editorial on the Research Topic
Systems biology and data-driven machine learning-based models in personalized cardiovascular medicine

1. Introduction

The fields of health and medicine have joined the rest of the other branches of life sciences in adopting computerized systems, digital communication, information processing, and an overall data-centrism. Artificial intelligence (AI) has emerged as one of the current drivers for this data-centric approach, particularly in the form of machine learning (ML) and, more specifically, deep learning (DL), which is one of its most successful sub-families.

This brief editorial paper provides an introduction to the 16 papers that contributed to the current special issue on systems biology and data-driven ML-based models in personalized cardiovascular medicine. The collection comprises original research, systematic reviews, and meta-analyses, and we are confident that it will be of great interest to the readers of this journal. Cardiovascular medicine is in fact one of the most active medical areas for the application of ML and AI techniques (1). The breadth and variety of topics broached by the works in this collection bear testimony to such a reality. In the next paragraphs, we shall characterize these studies according to the cardiovascular problem addressed, the ML approaches adopted, and any other relevant characteristics of the data analysis workflows.

The studies conducted by Cornhill et al. and Dykstra et al. have reported on the predictions of heart failure hospitalization and atrial fibrillation based on similar cardiac magnetic resonance (CMR) information. In both cases, the CMR data are combined with electronic health record (EHR) features, in addition to supplementary information such as patient health questionnaires. In the study conducted by Peng et al. the authors address

the problem of predicting all-cause in-hospital mortality for patients in the intensive care unit (ICU) with heart failure combined with hypertension. The data under analysis include gender, age, vital signs, laboratory tests, and comorbidities.

The study conducted by Ren et al. focuses on developing a predictive DL model for predicting the progression of cardiovascular disease (CVD), including coronary heart diseases, cerebrovascular diseases, congestive heart failure, and peripheral artery diseases in patients with diabetic kidney disease. The predictive model uses seven clinical variables, including age, smoking status, systolic blood pressure, total cholesterol, hemoglobin, high-density lipoprotein cholesterol levels, and urinary protein excretion. The best performing model, called DeepSurv, is used to develop an online tool for predicting CVD risk in patients with diabetic kidney disease.

Several papers (Cai et al., Guo et al., Li et al.) are devoted in predicting acute myocardial infarction (AMI). In the study conducted by Cai et al. the authors developed a predictive model for the risk stratification of acute kidney injury in patients with AMI using data from the Medical Information Mart for Intensive Care (MIMIC) IV database. Siva Kumar et al. in their study developed a quantitative electrocardiogram (ECG) risk score in conjunction with coronary artery calcification (CAC) to assess their ability in predicting major adverse cardiovascular events (MACE) in patients with at least one cardiovascular risk factor from the Community Benefit of No-charge Calcium Score Screening Program (CLARIFY) trial. A nomogram constructed by integrating the quantitative ECG risk score with CAC, age, and sex was found to be associated with MACE and demonstrated accurate discrimination between patients at high risk and those at low risk. The study conducted by Guo et al. identified the genes related with inflammation associated to the pathogenesis of AMI. This study performed, for the first time, a systematic analysis of biomarkers associated with the development from stable cardiovascular disease to AMI, specifically focusing on 5mC regulators. Interestingly, nine hub 5mC regulators were identified and validated by a robust model, leading to developing a diagnostic model that might be used to discriminate AMI from coronary artery disease. The study conducted by Li et al. focused on identifying the genes associated with heart failure induced by ischemic cardiomyopathy. Both papers utilized the data from the Gene expression Omnibus (GEO) and Genomic Spatial Event (GSE) databases. Weighted gene co-expression network analysis (WGCNA) is employed as a method in identifying potential functional modules. The CIBERSORT algorithm is used in characterizing immune cell infiltration.

In the study conducted by Kong et al. the authors employed a new proteomic assay platform called Olink multiplex cardiovascular disease III to assess the variations in protein expression in patients with acute phase atrial fibrillation who underwent cryoballoon ablation, radiofrequency balloon ablation, or radiofrequency ablation procedures. The pathway analysis revealed major changes in the cytokine–cytokine receptor interaction after the three different ablations, as well as in certain proteins associated with hemorrhage and coagulation. It should be noted that the scope of this exploratory study was rather constrained due to the small sample size and the focus on the proteins included in the Olink panel.

The problem of atrial fibrillation in patients with chronic obstructive pulmonary disease (COPD), using data from GEO and GSE databases, is addressed in the study conducted by Sun et al. These data were investigated using the WGCNA method and the STRING platform to construct a protein–protein interaction network. The CIBERSORT algorithm was used once again to characterize immune cell infiltration.

Shi et al. performed a retrospective observational study with 1,493 patients diagnosed with obstructive sleep apnea (OSA) admitted to the Department of Otorhinolaryngology—Head and Neck Surgery of the Second Affiliated Hospital of Xi'an Jiaotong University between October 2019 and December 2021. The authors used six different ML analyses and found that the gradient boosting machine (GBM) model was the best in assessing risk factors and predicting OSA-related hypertension. In addition to identifying several known risk factors, such as BMI, age/10, and minimum SaO_2/10, the multivariate logistic regression and SHAP analysis also found that CT90/10OSA, a novel variable related to sleep disorder, exhibits a strong association with CVD, metabolic disorders, and cognitive impairment.

The study conducted by Song et al. provided a systematic review and meta-analysis that examined the use of 60 ML models in predicting cardiac surgery-associated acute kidney injury (CSA-AKI). The study included a total of 255,943 patients from 38 eligible studies and found that NNET and Extreme Gradient Boosting (XGBoost) are more effective in the early prediction of CSA-AKI compared with logistic regression (LR).

In another study, Zhou et al. used ML on the Genotype-Tissue Expression project (GTEx) database to find genes associated with sudden death (SD). The SD group included 88 blood samples from 69 donors with fast death of natural causes (0–1 h) and 17 donors with intermediate death (1–24 h). In this case, the authors employed two different ML algorithms, namely Least Absolute Shrinkage and Selection Operator (LASSO) and the Support Vector Machine with Recursive Feature Elimination (SVM-RFE), in order to reduce errors. Consequently, the analysis revealed a correlation between two specific genes, MYL2 and TNNT3, and the occurrence of SD.

One of the main barriers to the application of ML methods in clinical medicine is the difficulty of obtaining sizeable samples of harmonized, properly curated, and representative (multi-center, international) data. Many of the studies in this collection reflect this limitation and would require further validation in data-richer contexts in order to guarantee reproducibility. In any case, the reported circumstances are varied, as some works use original data, whereas others resort to existing publicly available databases. Among the former, for instance, the CMR data used in the studies conducted by Cornhill et al. and Dykstra et al. are derived from a single center and encompass a substantial number of cases. In the study conducted by Shi et al. a single-center retrospective design was used. However, more patients from multiple sources are required to validate the robustness and repeatability of their model. Among the latter, Peng et al. utilized data from several thousands of patients from the MIMIC-IV and the eICU Collaborative Research Databases. The meta-analysis conducted by Song et al. utilized an uncharacteristically large multi-center data sample of 255,943 patients. An interesting alternative approach was used in the study conducted by Feng

et al. wherein the authors hypothesized that ML models can be effectively trained utilizing limited datasets by incorporating domain knowledge encoding.

The range of ML methods available to medical data scientists through open-access implementation is staggering. This issue reflects such variety: The most extreme example is the meta-analysis conducted by Song et al. where the performance of 60 ML models was compared. The studies conducted by Cornhill et al. and Dykstra et al. employed the Random Survival Forests as a statistical method. The research conducted by Peng et al. used a K-nearest neighbor method for missing data imputation. In addition, the study utilized the artificial neural networks (ANN), Naïve Bayes, and Random Forests (RF) as predictive models. In the study conducted by Cai et al. several analytical techniques such as RF, Bayesian analysis, SVM, XGBoost, Decision Trees, and LR to analyze the data. On the other hand, Li et al. utilized LASSO, RF, and SVM-REF for their analysis, while Guo et al. and Zhou et al. employed LASSO and SVM-RFE for their respective studies. The atrial fibrillation problem in Sun et al.'s study was analyzed using RF, SVM, XGBoost, and generalized linear models (GLM). Shi et al. employed LR, GBM, XGBoost, adaptive boosting (AdaBoost), bootstrapped aggregating (Bagging), and ANN for predicting OSA-related hypertension. XGBoost was also used in Li et al.'s study to assess the predictive value of a pressure recording analytical method for the duration of mechanical ventilation in children undergoing cardiac surgery, while LASSO and RF were also used in the study conducted by Lin et al. for the analysis of plasma protein profiling in patients with atrial fibrillation.

The lack of interpretability of ML models has recently emerged as a serious limitation in their implementation in medical settings (2). This topic has been investigated by Cai et al. and Shi et al. using the SHAP method to assess the relevance of input features. In addition, Lin et al. utilized an RF-related software package (in R) called *randomForestExplainer*.

This special issue offers an overview of the latest developments in AI and ML in the field of cardiovascular medicine. However, it is worth noting that future progress also points toward a more precise approach to treatment that takes into account individual differences in patient's genes, environmental factors, and lifestyle choices. This is a context in which AI and ML may help in improving diagnosis, drug discovery, and treatment personalization, perhaps with the help of new tools such as digital twins. The scalable storage of clinical data in data lakes that support fast multidimensional queries should enable data sharing and fuel clinical research. Finally, the emergence of large language models and generative AI, together with federated learning, may provide clinicians with powerful tools for bridging the gap between patients and devices, paving the way for interactive clinical decision support systems.

Author contributions

MH: Conceptualization, Writing – original draft, Writing – review & editing. NR: Conceptualization, Writing – original draft, Writing – review & editing. JE: Conceptualization, Writing – original draft, Writing – review & editing. AV: Conceptualization, Writing – original draft, Writing – review & editing.

Funding

The authors declare financial support was received for the research, authorship, and/or publication of this article.

AV acknowledges funding from the Spanish Ministry of Science and Innovation under project PID2022-143299OB-I00. This study was supported by the Instituto de Salud Carlos III project CIBERDEM (CB07/08/0016).

Acknowledgments

The authors would like to thank the CERCA program/ Generalitat de Catalunya (Barcelona, Spain) for institutional support.

Conflict of interest

The authors declare that the research was conducted in the absence of any commercial or financial relationships that could be construed as a potential conflict of interest.

The authors declared that they were an editorial board member of Frontiers, at the time of submission. This had no impact on the peer review process and the final decision.

Publisher's note

All claims expressed in this article are solely those of the authors and do not necessarily represent those of their affiliated organizations, or those of the publisher, the editors and the reviewers. Any product that may be evaluated in this article, or claim that may be made by its manufacturer, is not guaranteed or endorsed by the publisher.

References

1. Sánchez-Martínez S, Camara O, Piella G, Cikes M, González Ballester MA, Miron M, et al. Machine learning for clinical decision-making: challenges and opportunities in cardiovascular imaging. *Frontiers in Cardiovascular Medicine – Cardiovascular Imaging* (2022) 8:765693. doi: 10.3389/fcvm.2021.765693

2. Lisboa PJG, Saralajew S, Vellido A, Fernández-Domenech R, Villmann V. The coming of age of interpretable and explainable machine learning models. *Neurocomputing*. (2023) 535:25–39. doi: 10.1016/j.neucom.2023.02.040

frontiers | Frontiers in Cardiovascular Medicine

ORIGINAL RESEARCH
published: 16 June 2022
doi: 10.3389/fcvm.2022.890904

Machine Learning Patient-Specific Prediction of Heart Failure Hospitalization Using Cardiac MRI-Based Phenotype and Electronic Health Information

*Aidan K. Cornhill[1], Steven Dykstra[1], Alessandro Satriano[1,2,3], Dina Labib[1,2,3], Yoko Mikami[1,2,3], Jacqueline Flewitt[1], Easter Prosio[1], Sandra Rivest[1], Rosa Sandonato[1], Andrew G. Howarth[1,2,3], Carmen Lydell[1,2,3,4], Cathy A. Eastwood[3,5], Hude Quan[3,5], Nowell Fine[2,3], Joon Lee[5,6,7] and James A. White[1,2,3]**

[1] Stephenson Cardiac Imaging Centre, University of Calgary, Calgary, AB, Canada, [2] Division of Cardiology, Department of Cardiac Sciences, Libin Cardiovascular Institute of Alberta, Calgary, AB, Canada, [3] Libin Cardiovascular Institute of Alberta, Calgary, AB, Canada, [4] Department of Diagnostic Imaging, University of Calgary, Calgary, AB, Canada, [5] Department of Community Health Sciences, Cumming School of Medicine, University of Calgary, Calgary, AB, Canada, [6] Data Intelligence for Health Lab, Cumming School of Medicine, University of Calgary, Calgary, AB, Canada, [7] Department of Cardiac Science, Cumming School of Medicine, University of Calgary, Calgary, AB, Canada

Background: Heart failure (HF) hospitalization is a dominant contributor of morbidity and healthcare expenditures in patients with systolic HF. Cardiovascular magnetic resonance (CMR) imaging is increasingly employed for the evaluation of HF given capacity to provide highly reproducible phenotypic markers of disease. The combined value of CMR phenotypic markers and patient health information to deliver predictions of future HF events has not been explored. We sought to develop and validate a novel risk model for the patient-specific prediction of time to HF hospitalization using routinely reported CMR variables, patient-reported health status, and electronic health information.

Methods: Standardized data capture was performed for 1,775 consecutive patients with chronic systolic HF referred for CMR imaging. Patient demographics, symptoms, Health-related Quality of Life, pharmacy, and routinely reported CMR features were provided to both machine learning (ML) and competing risk Fine-Gray-based models (FGM) for the prediction of time to HF hospitalization.

Results: The mean age was 59 years with a mean LVEF of 36 ± 11%. The population was evenly distributed between ischemic (52%) and idiopathic non-ischemic cardiomyopathy (48%). Over a median follow-up of 2.79 years (IQR: 1.59–4.04) 333 patients (19%) experienced HF related hospitalization. Both ML and competing risk FGM based models achieved robust performance for the prediction of time to HF hospitalization. Respective 90-day, 1 and 2-year AUC values were 0.87, 0.83, and 0.80

OPEN ACCESS

Edited by:
Ali Yilmaz,
University Hospital Münster, Germany

Reviewed by:
Giulia Barbati,
University of Trieste, Italy
Minglong Chen,
The First Affiliated Hospital of Nanjing Medical University, China

***Correspondence:**
James A. White
jawhit@ucalgary.ca

Specialty section:
This article was submitted to Cardiovascular Imaging, a section of the journal Frontiers in Cardiovascular Medicine

Received: *07 March 2022*
Accepted: *10 May 2022*
Published: *16 June 2022*

Citation:
Cornhill AK, Dykstra S, Satriano A, Labib D, Mikami Y, Flewitt J, Prosio E, Rivest S, Sandonato R, Howarth AG, Lydell C, Eastwood CA, Quan H, Fine N, Lee J and White JA (2022) Machine Learning Patient-Specific Prediction of Heart Failure Hospitalization Using Cardiac MRI-Based Phenotype and Electronic Health Information. Front. Cardiovasc. Med. 9:890904. doi: 10.3389/fcvm.2022.890904

for the ML model, and 0.89, 0.84, and 0.80 for the competing risk FGM-based model in a holdout validation cohort. Patients classified as high-risk by the ML model experienced a 34-fold higher occurrence of HF hospitalization at 90 days vs. the low-risk group.

Conclusion: In this study we demonstrated capacity for routinely reported CMR phenotypic markers and patient health information to be combined for the delivery of patient-specific predictions of time to HF hospitalization. This work supports an evolving migration toward multi-domain data collection for the delivery of personalized risk prediction at time of diagnostic imaging.

Keywords: cardiovascular magnetic resonance imaging, machine learning, heart failure hospitalization, prediction, systolic heart failure (HF)

INTRODUCTION

Heart failure (HF) is estimated to affect approximately 64 million people worldwide (1) and is associated with a high incidence of disease-related hospitalization (2). HF hospitalization is increasingly prioritized as an important clinical outcome by patients and healthcare organizations given strong associations with morbidity, mortality and dominant contribution to healthcare expenditures (3). In 2017 it was estimated that each HF hospitalization incurred a mean cost of $14,631 USD with 40% of patients readmitted within 90 days (4). Of all patient populations, those with systolic HF provide greatest contributions to HF hospitalization costs (2), justifying an expanding focus on this population for risk modeling. While the prediction of HF re-admission early following index HF hospitalization has been explored from administrative health data (5–7), risk models for incident HF hospitalization applicable to broader HF populations are required. The deployment of such models at time of diagnostic imaging, delivering descriptors of disease with opportunity for the capture of contextual health information, provides an attractive solution for personalized prediction modeling.

Cardiovascular magnetic resonance (CMR) imaging has become a routinely engaged test for the diagnosis and management of systolic heart failure. This has been justified by its versatility for the delivery of a broad range of phenotypic markers that accurately differentiate ischemic from non-ischemic etiologies (8–10), describe patterns of tissue injury (8), identify valvular pathology (11), and deliver reference standard quantification of chamber volumes, function, and ventricular mass (12, 13). While demonstrated to provide independent value for the prediction of composite outcomes (14–17), the combined value of CMR-reported phenotypic features and contextual patient health information to deliver personalized predictions of HF-related outcomes remains unexplored.

We hypothesized that CMR-reported markers of disease contextualized to patient-reported and EHR-derived markers of health can permit patient-specific predictions of time to HF hospitalization. To achieve this, we explored both machine learning (ML)-based modeling and competing risk Fine-Gray (FGM)-based risk modeling techniques for individualized predictions of time to HF hospitalization at time of CMR.

MATERIALS AND METHODS

Dataset Available for Risk Modeling

CMR imaging data, patient-reported measures of health status and electronic health record (EHR) abstracted data was provided by the Cardiovascular Imaging Registry of Calgary (CIROC, NCT04367220). CIROC is a prospectively recruiting clinical outcomes Registry of the Libin Cardiovascular Institute engaging patients clinically referred for cardiac diagnostic imaging. Consenting patients undergoing CMR imaging between February 2015 and October 2019 for the evaluation of systolic HF and completing a minimum 1-year follow-up period were included. All data was collected at time of diagnostic test performance using a commercial workflow, data integration, and diagnostic test reporting software platform (cardioDI^{TM}, Cohesic Inc., Calgary).

Patients with chronic systolic HF resulting from ischemic cardiomyopathy or idiopathic non-ischemic cardiomyopathy were identified. All patients were required to have CMR-based confirmation of reduced global systolic function, defined as a left ventricular ejection fraction (LVEF) $\leq$ 50%. Recognizing the unique natural history of patients with specific non-ischemic cardiomyopathy states, all patients with confirmed cardiac amyloid, cardiac sarcoidosis, and hypertrophic cardiomyopathy were excluded. Patients with an acute cardiomyopathy state due to recent (within 90 days) acute coronary syndrome, takotsubo cardiomyopathy, per-partum cardiomyopathy, or viral infection (suspected or confirmed acute myocarditis) were also excluded. This established a final patient cohort with chronic systolic HF of either ischemic or idiopathic non-ischemic etiology. Ischemic cardiomyopathy (ICM) was defined by occurrence of prior myocardial infarction, percutaneous coronary intervention and/or coronary bypass surgery, or presence of ischemic (subendocardial) pattern injury on late

Abbreviations: CIROC, Cardiovascular Imaging Registry of Calgary; CMR, Cardiovascular Magnetic Resonance Imaging; CoxPH, Cox Proportional Hazard; EHR, Electronic Health Record; FGM, Fine-Gray (Model); HF, Heart Failure; HR-QOL, Health Related Quality of Life; LGE, Late Gadolinium Enhancement; LVEF, Left Ventricular Ejection Fraction; ML, Machine Learning; PPV, Positive Predictive Value; RSF, Random Survival Forest; tAUC, Time Dependent Area Under the Receiver Operating Characteristic Curve.

gadolinium enhancement (LGE) imaging corresponding to one or more vascular territories. Patients not meeting this criterion were classified as idiopathic non-ischemic dilated cardiomyopathy. For patients who underwent multiple CMR studies, the index study was used for prediction modeling.

A total of 8,773 unique patients enrolled in the CIROC Registry were considered. Of these, 2,455 had an LVEF $\leq$ 50% by CMR. Following application of the inclusion and exclusion criteria, 1,775 unique patients satisfied cohort eligibility.

The study was approved by the University of Calgary Conjoint Health Research Ethics Board. All subjects provided written informed consent. All research activities were performed in accordance with the Declaration of Helsinki.

Data Element Generation and Collection

Patient Reported Health Data

Patient health questionnaires were electronically deployed prior to each CMR examination to collect patient demographics, comorbid cardiac and non-cardiac illness, smoking, and alcohol history, patient-reported shortness of breath [based on New-York Heart Association (NYHA) classification], and HRQoL using the EQ-5D tool (18).

Cardiovascular Magnetic Resonance Imaging-Based Phenotype Data

CMR imaging was performed on 3 Tesla clinical scanners (Prisma or Skyra, Siemens Healthcare, Erlangen, Germany) using standardized imaging protocols inclusive of routine cine and LGE imaging techniques in sequential short-axis views and 2-, 3-, and 4-chamber long axis views. Quantitative image analysis was performed using standardized operating procedures developed according to guidelines of the Society for Cardiovascular Magnetic Resonance (19). Image analysis was performed using commercially available software (cvi**42**; Circle Cardiovascular Inc., Calgary) to obtain left ventricular (LV) and right ventricular (RV) volumes and function from semi-automated contour tracing of the endocardial and epicardial borders followed by manual adjustment. Papillary muscles were considered part of the LV mass. Maximal left atrial volume was assessed in the phase immediately prior to mitral valve opening using the bi-plane area-length method on matched 2- and 4-chamber cine images. All measurements were indexed to body surface area, where appropriate, using the Mosteller formula.

Standardized software was used to receive and code quantitative markers of chamber volumes and function, and to code disease-specific phenotypes (cardioDI^{TM}; Cohesic Inc., Calgary). LGE images were visually scored for the presence, extent, and pattern of fibrosis: the latter scored as subendocardial, mid-wall striae, right ventricular insertion site, mid-wall patchy, subepicardial, and diffuse patterns, as previously described (20, 21). Valvular pathology was coded based upon visually graded assessments of regurgitation and stenosis severity. The presence of pleural and pericardial effusions was routinely coded.

Electronic Health Record Abstracted Data

Electronic health information was abstracted from institutional EHR data warehouses and was inclusive of pharmacy, laboratory and ICD-10 coded diagnostic and procedural data. Historic data was abstracted at time of index CMR, and every 3-months perpetually thereafter. The primary clinical outcome of HF-related hospitalization was identified by ICD-10 coding registered in the Discharge Abstract Database System, using primary ICD-10 codes of I50.X. All documented events were manually adjudicated by medical chart review. Mortality data, used for competing risk analysis, was collected from Vital Statistics Alberta.

Statistical Analysis

Continuous variables are reported as means $\pm$ standard deviation whereas categorical variables are expressed as counts with percentages. Comparison between groups for continuous variables were performed using a Student's *t*-test or a Welch's *t*-test where appropriate. Chi-squared tests without a Yates Correction and Fishers Exact tests were used for comparison between groups for categorical variables. Univariable CoxPH analysis of baseline variables was performed to identify associations with the primary outcome, this used for identifying candidate variables for FGM-based modeling.

Risk Model Development

We aimed to develop and compare performance of machine learning (ML) and non-ML based modeling for the patient-specific prediction of time to HF hospitalization with reference comparison to a historic HF prediction model. As a ML-based approach we used Random Survival Forest (RSF) based modeling, this compared to a FGM-based model. For the development of our novel prediction models our study dataset was split into a 70% (n = 1,245) development and 30% (n = 530) holdout validation cohort, balanced for both event rate and follow-up duration. The development cohort was partitioned into five training and testing datasets for 5-fold cross-validation-based model development and selection. Within each cross-validation fold, missing data was independently imputed by multivariable feature imputation (Hmisc: aregImpute) (22). Manual variable reduction was executed to remove variables with a missingness rate $>$ 15% and those believed to have poor generalizability to other clinical settings (i.e., unique to the local institution). This led to 63 consistently available disease phenotype (imaging) and patient health variables for the development of our risk models (**Supplementary Table 1**).

Machine Learning Model Development and Performance Evaluation

For each development fold, 100 bootstrap samples with replacement were generated and 100 RSF models were trained for variable selection. These models were applied to out-of-bag data where variable importance was then assessed using permutation importance rank. The top 15 performing variables for each training fold were selected by their mean variable rank across all 100 out-of-bag datasets. A comprehensive grid search technique was used for hyperparameter tuning, as summarized in **Supplementary Table 2**. Optimized models in each training fold were applied to the test sets for final model evaluation and

selection using time-dependent area under the curve (tAUC) and C-index. Models containing a range of 13–17 features were assessed in the test set, comparing tAUC and C-index to identify the optimal number of model features. The final model was then applied to the holdout dataset where performance was assessed using C-index, tAUC, average positive predictive value (PPV), average recall and F1 score. A model threshold for discriminating "High" from "Low" risk cohorts was then defined by observing the inflection point of observed events across deciles of predicted risk in the development cohort. Cumulative incidence plots accounting for competing events and stratifying patients by predicted risk category were generated. Calibration plots were generated by plotting mean difference in predicted and observed event rates for each decile of risk across 100 bootstrap replicates at 2 years. The Aalen-Johansen method was used to account for competing events.

Competing Risk Fine-Gray-Based Models Risk Model Development and Performance Evaluation

For development of the FGM based model variable candidacy was defined by a threshold p-value of 0.1 in univariable analysis. Backward variable selection was performed to select features, based on order of variable exclusion. Highly correlated features were excluded using a threshold of a Pearson's coefficient greater than 0.7. The competing risk FGM model was applied to generate coefficients for each variable that could then be used to estimate 90 day, 1 and 2-year probability of HF hospitalization for individual patients, as previously described (23). The test dataset was used to assess model performance for each development and test fold, resulting in five candidate risk models. C-index and tAUC were then used to select an optimal model for validation in the holdout dataset. Model performance in the holdout dataset was assessed using C-index, tAUC, average PPV, average recall and F1 score. Calibration was assessed using the method described above.

MAGGIC Score-Based Risk Model Performance Evaluation

Originally developed for mortality prediction in systolic HF populations (24), the MAGGIC risk score served as the best available surrogate model for the estimation of HF outcomes in our referral population. MAGGIC risk scores were applied to the holdout cohort to provide matched assessments of performance vs. novel risk models.

All statistical analysis and modeling was performed in R version 4.0.3 and Python version 3.8.8 (25).

RESULTS

Population Characteristics

Our chronic systolic HF population consisted of 1,775 unique patients with a mean age of 59 ± 13 years and 24% being female. Baseline clinical and CMR characteristics are summarized in **Table 1**. The population was composed of 52% ischemic cardiomyopathy and 48% non-ischemic dilated cardiomyopathy patients.

During a median follow-up period of 2.79 years (IQR: 1.59–4.04) 333 patients (19%) experienced the primary outcome of HF hospitalization. Ninety-five patients (5%) died, 40 of these (2%) dying without prior HF hospitalization.

No significant differences were observed between development and validation cohorts **(Supplementary Table 3**). In the development cohort, 233 patients (19%) experienced the primary outcome over a median follow-up period of 2.8 (IQR: 1.59–4.04) years. In the validation cohort 100 patients (19%) experienced the primary outcome over a median follow-up period of 2.74 (1.58–4.04) years.

Machine Learning Risk Model Performance

The final RSF risk model contained15 predictive variables, 9 of which were sourced from the CMR-reported phenotype. The variable selection process produced a model containing LVESVi, LVEDVi, LVEF, RVESVi, RVEDVi, and RVEF. Given that end systolic volumes are implicit in a model containing end diastolic volumes and ejection fraction, two predictive late gadolinium enhancement patterns (subendocardial and mid-wall striae) were added to the model and performance in the test datasets compared. The model containing LGE features achieved higher C-index and tAUC values and this feature set was subsequently used to train the final RSF model. The mean permutation importance of each selected variables is shown in **Figure 1**. In the holdout cohort, the RSF model achieved a C-index of 0.77 and provided 90-day, 1 and 2-year AUC values of 0.87, 0.83, and 0.80, respectively (**Figure 2**). The RSF model delivered a mean PPV of 0.50 with an F1 score of 0.60 with good calibration across all deciles of risk (**Figure 3**). We defined patients with risk estimates above the seventh-risk decile to be "high-risk," these patients experiencing 66% of all observed outcomes in the holdout cohort. Cumulative incidence curves (**Figure 4**) for patients predicted to be "high-risk" vs. "low-risk" showed significantly higher occurrence of HF hospitalization. The respective event rates for high vs. low-risk cohorts were 19 vs. 0.6% ($p < 0.0001$) at 90 days; 28 vs. 4% ($p < 0.0001$) at 1-year; and at 35 vs. 7% ($p < 0.0001$) at 2-years.

Competing Risk Fine-Gray-Based Models Model Performance

Similar to machine learning-based modeling, variables from all data domains were shown to provide value toward an optimal FGM-based model with respective associations summarized in **Supplementary Table 4**. In holdout validation CIROC-HF-FGM delivered a mean C-index of 0.77 with 90-day, 1 and 2-year tAUC's of 0.89, 0.84, 0.80, respectively. The mean PPV and F1 score was 0.49 and 0.59, respectively (**Figure 2**). Similar to the ML-based model, patients with a predicted risk above the seventh-risk decile were defined as "high-risk." High-risk patients experienced 62% of all observed outcomes in the holdout cohort, with cumulative incidence curves shown in **Figure 4**. The respective event rates for high vs. low-risk groups were 18 vs. 1%

TABLE 1 | Baseline clinical and CMR characteristics of the study cohort.

Data domain	Full population	Event –	Event +	*p*-value
	***n* = 1,775**	***n* = 1,442**	***n* = 333**	
Patient reported health questionnaire				
Age (years)	59 ± 13	58 ± 13	63 ± 13	**<0.0001**
Female, *n* (%)	418 (24)	336 (23)	82 (25)	0.6079
Obesity, *n* (%)	638 (36)	510 (35)	128 (38)	0.2925
NYHA class III or IV, *n* (%)	439 (25)	313 (22)	126 (38)	**<0.0001**
Atrial fibrillation, *n* (%)	322 (18)	247 (17)	75 (23)	**0.0213**
CAD, *n* (%)	397 (22)	305 (21)	92 (28)	**0.0106**
Diabetes, *n* (%)	346 (19)	251 (17)	95 (29)	**<0.0001**
Hypertension, *n* (%)	688 (39)	524 (36)	164 (49)	**<0.0001**
Hyperlipidemia, *n* (%)	382 (22)	290 (20)	92 (28)	**0.0026**
Peripheral arterial disease, *n* (%)	22 (1)	16 (1)	6 (2)	0.3034
Pulmonary hypertension, *n* (%)	26 (1)	14 (1)	12 (4)	**0.0003**
COPD, *n* (%)	87 (5)	56 (4)	31 (9)	**<0.0001**
Smoking, *n* (%)	340 (19)	279 (19)	61 (18)	0.6669
Mobility issues (EQ5D), *n* (%)	518 (29)	366 (25)	152 (46)	**<0.0001**
Anxiety/depression (EQ5D), *n* (%)	539 (30)	435 (30)	104 (31)	0.7033
Pain issues (EQ5D), *n* (%)	598 (34)	457 (32)	141 (42)	**0.0002**
Self-care issues (EQ5D), *n* (%)	172 (10)	121 (8)	51 (15)	**0.0001**
Issues with usual activity (EQ5D), *n* (%)	649 (37)	474 (33)	175 (53)	**<0.0001**
Clinical patient history—administrative health data				
Prior hospitalization—1 year, *n* (%)	894 (50)	669 (46)	225 (68)	**<0.0001**
Prior hospitalization—3 years, *n* (%)	1,169 (66)	895 (62)	274 (82)	**<0.0001**
Two weeks hospitalized in prior year, *n* (%)	248 (14)	160 (11)	88 (26)	**<0.0001**
Ischemic cardiomyopathy, *n* (%)	919 (52)	710 (49)	209 (63)	**<0.0001**
History of atrial fibrillation, *n* (%)	396 (22)	292 (20)	104 (31)	**<0.0001**
CMR parameters				
LVEF (%)	36 ± 11	37 ± 10	31 ± 11	**<0.0001**
LVESV index (mL/m^2)	75 ± 36	71 ± 33	91 ± 42	**<0.0001**
LVEDV index (mL/m^2)	113 ± 37	110 ± 35	127 ± 44	**<0.0001**
LVMass index (g/m^2)	70 ± 21	68 ± 21	76 ± 23	**<0.0001**
RVEF (%)	47 ± 12	48 ± 11	44 ± 13	**<0.0001**
RVESV index (mL/m^2)	45 ± 21	44 ± 20	51 ± 27	**<0.0001**
RVEDV index (mL/m^2)	84 ± 24	83 ± 22	87 ± 30	**0.0260**
LA volume index (mL/m^2)	44 ± 18	42 ± 17	50 ± 20	**<0.0001**
Presence of any LGE pattern, *n* (%)	1,064 (60)	831 (58)	233 (70)	**<0.0001**
Subendocardial pattern, *n* (%)	695 (39)	533 (37)	162 (49)	**0.0001**
Non-ischemic pattern, *n* (%)	679 (38)	542 (38)	137 (41)	0.2290
Midwall striae, *n* (%)	304 (17)	232 (16)	72 (22)	**0.0157**
RV insertion site, *n* (%)	392 (22)	302 (21)	90 (27)	**0.0159**
Midwall patchy, *n* (%)	119 (7)	96 (7)	23 (7)	0.8697
Subepicardial, *n* (%)	111 (6)	97 (7)	14 (4)	**0.0866**
Diffuse, *n* (%)	26 (1)	20 (1)	6 (2)	0.5701
Medications				
ACE inhibitor or ARB, *n* (%)	1,498 (84)	1,182 (82)	316 (95)	**<0.0001**
Anti-arrhythmic, *n* (%)	98 (6)	68 (5)	30 (9)	**0.0020**
Anti-coagulant, *n* (%)	547 (31)	393 (27)	154 (46)	**<0.0001**
Anti-platelet (non-ASA), *n* (%)	275 (15)	221 (15)	54 (16)	0.6857
ASA, *n* (%)	803 (45)	624 (43)	179 (54)	**0.0005**
Beta-blocker, *n* (%)	1,492 (84)	1,181 (82)	311 (93)	**<0.0001**
Calcium channel blocker (dihydropyradine), *n* (%)	186 (10)	142 (10)	44 (13)	0.0707
Calcium channel blocker (non-dihydropyridines), *n* (%)	56 (3)	46 (3)	10 (3)	0.8603
Digoxin, *n* (%)	138 (8)	92 (6)	46 (14)	**<0.0001**

(Continued)

TABLE 1 | (Continued)

Data domain	Full population	Event –	Event +	*p*-value
	***n* = 1,775**	***n* = 1,442**	***n* = 333**	
Loop diuretic, *n* (%)	520 (29)	317 (22)	203 (61)	**<0.0001**
Thiazide diuretic, *n* (%)	136 (8)	108 (7)	28 (8)	0.5699
K-sparing diuretic, *n* (%)	718 (40)	529 (37)	189 (57)	**<0.0001**
Entresto, *n* (%)	178 (10)	142 (10)	36 (11)	0.5978
Glucose lowering, *n* (%)	310 (17)	212 (15)	98 (29)	**<0.0001**
Glucose lowering (DPP-4 inhibitors), *n* (%)	35 (2)	22 (2)	13 (4)	**0.0049**
Glucose lowering (SGLT 2 inhibitors), *n* (%)	38 (2)	32 (2)	6.0 (2)	0.6353
Insulin, *n* (%)	121 (7)	82 (6)	39 (12)	**0.0001**
Nitrates, *n* (%)	400 (23)	267 (19)	133 (40)	**<0.0001**
Statins, *n* (%)	1,005 (57)	778 (54)	227 (68)	**<0.0001**
Smoking cessation agents, *n* (%)	35 (2)	24 (2)	11 (3)	0.0525

Variables are described for the full population and those with and without occurrence of the primary clinical endpoint of heart failure related hospitalization.
Quantitative data is presented as means ± standard deviation, qualitative data is presented as counts and percentages. History of Atrial Fibrillation variable is derived from administrative EHR data, Atrial Fibrillation variable is patient reported.
ACE, angiotensin-converting enzyme; ARB, angiotensin II receptor blocker; BSA, body surface area; CAD, coronary artery disease; COPD, chronic obstructive pulmonary disease; EDV, end-diastolic volume; EF, ejection fraction; ESV, end-systolic volume; ICM, ischemic cardiomyopathy; LA, left atrial; LGE, late gadolinium enhancement; LV, left ventricular; NYHA, New York Heart Association; RV, right ventricular. Bold values indicates $p < 0.05$.

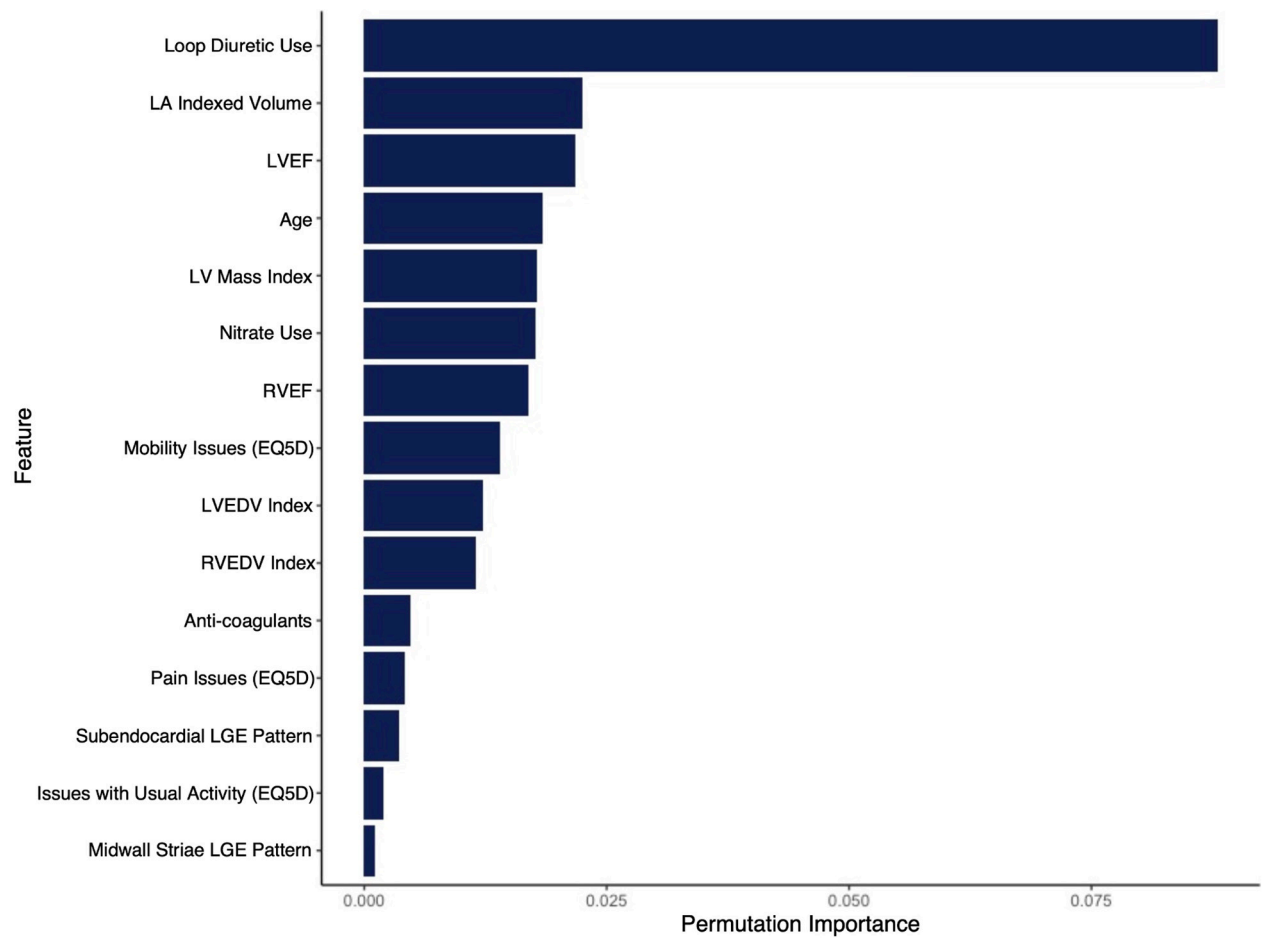
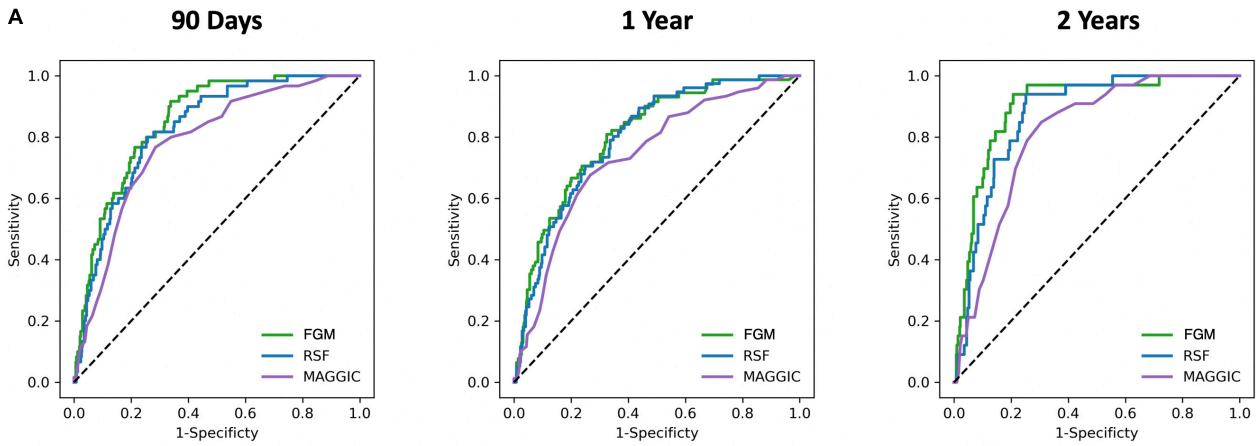


FIGURE 1 | Mean permutation importance values over 100 bootstrap samples for the features included in the final CIROC-HF-RSF model.



B

	C-index	90 days AUC	1 Year AUC	2 Years AUC
FGM Risk Score	0.77	0.89	0.84	0.80
RSF Model	0.77	0.87	0.83	0.80
MAGGIC Score	0.72	0.81	0.78	0.74

FIGURE 2 | (A) Receiver operating characteristic curves for the CIROC-HF-RSF Model, CIROC-HF-FGM Risk Model, and modified MAGGIC risk score at 90 days, 1 and 2 years follow-up in the holdout cohort. **(B)** Summary of CIROC-HF-RSF model, CIROC-HF-FGM Risk Model, and modified MAGGIC risk score performance in the holdout cohort.

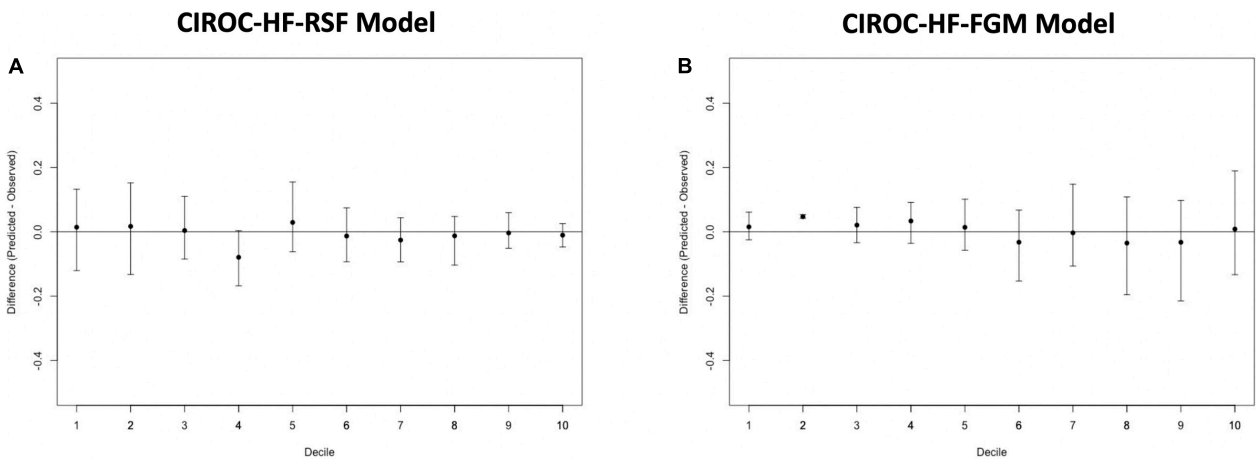


FIGURE 3 | Calibration plots for **(A)** CIROC-HF-RSF risk model, and **(B)** CIROC-HF-FGM risk model for the prediction of HF hospitalization in the holdout cohort. Plots display difference between observed and expected event rates at each decile of risk. Confidence intervals are derived from 100 bootstrapped datasets.

($p < 0.0001$) at 90-days; 28 vs. 3% ($p < 0.0001$) at 1-year; and 35 vs. 7% ($p < 0.0001$) at 2-years.

Comparison of CIROC-HF Risk Models to the MAGGIC Risk Score

Both CIROC-HF risk models were compared to the MAGGIC Risk Score (24) in the validation cohort. The MAGGIC Risk Score delivered a mean C-index of 0.72 with a respective 90-day, 1-year, 2-year tAUC's of 0.81, 0.78, 0.74. Comparisons of tAUC performance between the CIROC-HF risk models and MAGGIC Risk Score are shown in **Figure 2**, demonstrating superior performance for both novel CIROC-HF models.

DISCUSSION

In this study we demonstrated the capacity of routinely reported CMR disease markers to be contextualized by patient health information at the time of diagnostic testing for delivery of

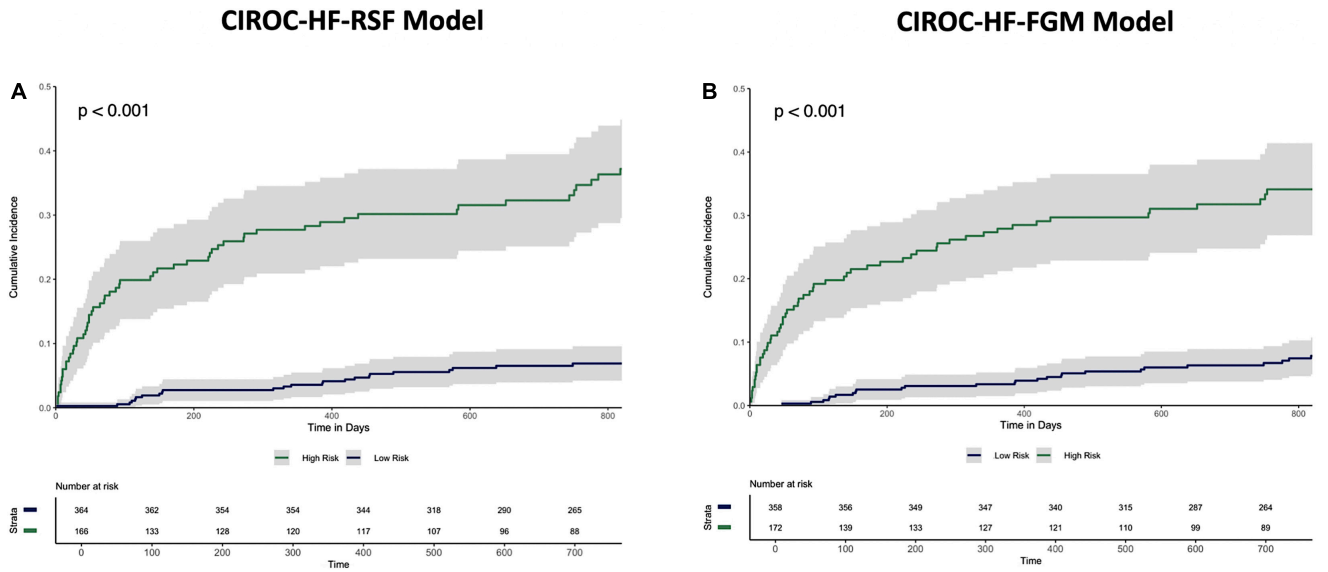


FIGURE 4 | Cumulative incidence curves describing time to HF hospitalization in the holdout dataset stratified by "High-risk" vs. "Low-risk" classification by the **(A)** CIROC-HF-RSF model, and **(B)** CIROC-HF-FGM Risk Model.

patient-specific estimations of time to HF hospitalization. Our modeling identified unique and independent value from each of the imaging phenotype, patient-reported health, and EHR data domains; their collective availability permitting improved prediction performance vs. the MAGGIC Risk Score. Using our ML-based model, patients classified to the high-risk category experienced a 34-fold higher occurrence of HF hospitalization at 90-days, 8-fold at 1-year, and 5-fold at 2-years. To our knowledge, this represents the first validated model for the prediction of HF hospitalization in HF patients undergoing CMR imaging.

HF hospitalization risk models have, to date, focussed on the prediction of re-admission following index hospitalizations for acute decompensation (5–7, 26–28). These models have consistently focussed on data sourced from in-patient electronic health records to identify those at higher likelihood of re-admission, typically at 90-days. All have struggled to achieve the performance of models trained to predict mortality (29, 30), suggesting elevated need to consider patient-specific disease phenotypes. The latter concept was explored in a study of 3,189 HF in-patients where multi-domain phenotypic data, gathered from routine echocardiography reporting, enabled prediction of all-cause early re-hospitalization with higher predictive accuracy than prior administrative data supported models, achieving an AUC of 0.76 at 90-days (31). While demonstrating value from multi-domain imaging phenotypes, this study was limited to high-risk inpatient populations, preventing generalizability to those patients routinely encountered by diagnostic imaging services.

Supported by a prior study showing incremental value from ML-based modeling for the prediction of HF re-admission using EHR sourced data (32), we postulated similar performance gains in our referral population. In contrast, we observed very similar performance for our modeled clinical outcome when compared to a FGM-based model provided matched multi-domain data resources. The exception was improved stability in time-dependent AUC seen using the ML-based approach at 2-years (**Figure 2**). However, a distinct advantage of ML-based modeling is its capacity to consider non-linear interactions between features without the limitations introduced by the proportional hazards assumption. Through this, we were afforded the opportunity to objectively evaluate the respective contributions of imaging phenotype, patient-reported health, and EHR-based markers have on the incident occurrence of HF hospitalization. As shown in **Figure 1**, we identified that current use of loop diuretics was the strongest contributor to model performance, followed by left atrial volume, LVEF, age and LV mass index. Other relevant features included volumetric markers of right ventricular health and patterns of myocardial fibrosis, these demonstrating the unique contributory value that CMR-based phenotyping can provide in this patient population. Collectively, these selected features appropriately represented phenotypic markers recognized to have strong predictive value in HF populations from prior studies (14, 15, 17, 20, 21, 33–46).

The capacity of contextual patient health information to contribute value for HF hospitalization prediction has been previously reported (47–49). To our knowledge, our current study is the first to describe the routine clinical deployment of patient-reported health questionnaires at time of diagnostic imaging for the delivery of this unique data domain. Of the top fifteen variables selected by our ML-based model, three were selected from the EQ-5D health related quality of life instrument (18). This demonstrates strong value from the synchronous capture of patient-reported measures of health at time of diagnostic testing, features recognized to be critical for the optimal prediction of HF-related events (29).

LIMITATIONS

This study was executed at a single tertiary care healthcare institution and therefore requires external site validation prior to deployment beyond the local environment. This is of particular importance for unique clinical environments that may be exposed to a local referral bias in diagnostic testing or have altered socio-demographic profiles. While systematically explored, we did not report results of other classification-based ML techniques for event prediction at specific time-points given lower performance metrics. Due to lack of routine performed surrounding the time of CMR imaging, we were unable to consider BNP or NT-proBNP values into our predictive models. In addition, given the high engagement of private out-patient echocardiography laboratories in clinical practice, direct comparison to models trained from echocardiographic variables in the same patient population was not feasible. Advanced CMR based markers of myocardial disease of recognized value, such as tissue mapping (50), were not undertaken in this large cohort study given desire for generalizability to routine practice and a high degree of vendor and hardware dependence for such measures.

CONCLUSION

In this study we developed and validated a machine learning based model for the prediction of time to HF hospitalization in systolic HF patients undergoing CMR. Our study was focussed on demonstrating the respective value provided by imaging phenotypes, patient-reported measures of health, and EHR-sourced data for the delivery of personalized HF predictions. Overall, our study supports strong value provided by the routine capture of multi-domain health data resources at time of diagnostic imaging, this approach facilitating the implementation of personalized outcome prediction.

DATA AVAILABILITY STATEMENT

The raw data supporting the conclusions of this article will be made available by the authors, upon appropriate request.

ETHICS STATEMENT

The studies involving human participants were reviewed and approved by the University of Calgary Conjoint Health Research Ethics Board. The patients/participants provided their written informed consent to participate in this study.

AUTHOR CONTRIBUTIONS

AC performed all data analysis, modeling, and manuscript authorship. JW conceived, designed, edited, and finalized manuscript content. SD developed data structures and data matching for the CIROC Registry. DL, YM, JF, SR, RS, EP, and AS assisted in data collection and adjudication. NF, CL, AH, HQ, and CE performed study design and manuscript review. JL assisted in data modeling. All authors contributed to the article and approved the submitted version.

FUNDING

This study was funded, in part, by the Calgary Health Foundation.

SUPPLEMENTARY MATERIAL

The Supplementary Material for this article can be found online at: https://www.frontiersin.org/articles/10.3389/fcvm.2022.890904/full#supplementary-material

REFERENCES

1. James SL, Abate D, Abate KH, Abay SM, Abbafati C, Abbasi N, et al. Global, regional, and national incidence, prevalence, and years lived with disability for 354 diseases and injuries for 195 countries and territories: a systematic analysis for the global burden of disease study 2017. *Lancet.* (2018) 392:1789–858. doi: 10.1016/S0140-6736(18)32279-7
2. Urbich M, Globe G, Pantiri K, Heisen M, Bennison C, Wirtz HS, et al. A systematic review of medical costs associated with heart failure in the USA (2014-2020). *Pharmacoeconomics.* (2020) 38:1219–36. doi: 10.1007/s40273-020-00952-0
3. Ruigomez A, Michel A, Martin-Perez M, Garcia Rodriguez LA. Heart failure hospitalization: an important prognostic factor for heart failure re-admission and mortality. *Int J Cardiol.* (2016) 220:855–61. doi: 10.1016/j.ijcard.2016.06.080
4. Kilgore M, Patel HK, Kielhorn A, Maya JF, Sharma P. Economic burden of hospitalizations of medicare beneficiaries with heart failure. *Risk Manag Healthc Policy.* (2017) 10:63–70. doi: 10.2147/RMHP.S130341
5. Formiga F, Masip J, Chivite D, Corbella X. Applicability of the heart failure readmission risk score: a first European study. *Int J Cardiol.* (2017) 236:304–9. doi: 10.1016/j.ijcard.2017.02.024
6. Lenzi J, Avaldi VM, Hernandez-Boussard T, Descovich C, Castaldini I, Urbinati S, et al. Risk-adjustment models for heart failure patients' 30-day mortality and readmission rates: the incremental value of clinical data abstracted from medical charts beyond hospital discharge record. *BMC Health Serv Res.* (2016) 16:473. doi: 10.1186/s12913-016-1731-9
7. Sudhakar S, Zhang W, Kuo YF, Alghrouz M, Barbajelata A, Sharma G. Validation of the readmission risk score in heart failure patients at a tertiary hospital. *J Card Fail.* (2015) 21:885–91. doi: 10.1016/j.cardfail.2015.07.010
8. Stirrat J, White JA. The prognostic role of late gadolinium enhancement magnetic resonance imaging in patients with cardiomyopathy. *Can J Cardiol.* (2013) 29:329–36. doi: 10.1016/j.cjca.2012.11.033
9. Mordi I, Bezerra H, Carrick D, Tzemos N. The combined incremental prognostic value of LVEF, late gadolinium enhancement, and global circumferential strain assessed by CMR. *JACC Cardiovasc Imaging.* (2015) 8:540–9. doi: 10.1016/j.jcmg.2015.02.005
10. McCrohon JA, Moon JC, Prasad SK, McKenna WJ, Lorenz CH, Coats AJ, et al. Differentiation of heart failure related to dilated cardiomyopathy and coronary artery disease using gadolinium-enhanced cardiovascular magnetic resonance. *Circulation.* (2003) 108:54–9. doi: 10.1161/01.CIR.0000078641.19365.4C
11. Gajjar K, Kashyap K, Badlani J, Williams RB, Biederman RWW. A review of the pivotal role of cardiac MRI in mitral valve regurgitation. *Echocardiography.* (2021) 38:128–41. doi: 10.1111/echo.14941
12. Grothues F, Smith GC, Moon JC, Bellenger NG, Collins P, Klein HU, et al. Comparison of interstudy reproducibility of cardiovascular magnetic resonance with two-dimensional echocardiography in normal subjects and in patients with heart failure or left ventricular hypertrophy. *Am J Cardiol.* (2002) 90:29–34. doi: 10.1016/s0002-9149(02)02381-0

13. Grothues F, Moon JC, Bellenger NG, Smith GS, Klein HU, Pennell DJ. Interstudy reproducibility of right ventricular volumes, function, and mass with cardiovascular magnetic resonance. *Am Heart J.* (2004) 147:218–23. doi: 10.1016/j.ahj.2003.10.005
14. Bluemke DA, Kronmal RA, Lima JA, Liu K, Olson J, Burke GL, et al. The relationship of left ventricular mass and geometry to incident cardiovascular events: the MESA (Multi-ethnic study of atherosclerosis) study. *J Am Coll Cardiol.* (2008) 52:2148–55. doi: 10.1016/j.jacc.2008.09.014
15. Modin D, Sengelov M, Jorgensen PG, Olsen FJ, Bruun NE, Fritz-Hansen T, et al. Prognostic value of left atrial functional measures in heart failure with reduced ejection fraction. *J Card Fail.* (2019) 25:87–96. doi: 10.1016/j.cardfail.2018.11.016
16. Wong TC, Piehler KM, Zareba KM, Lin K, Phrampus A, Patel A, et al. Myocardial damage detected by late gadolinium enhancement cardiovascular magnetic resonance is associated with subsequent hospitalization for heart failure. *J Am Heart Assoc.* (2013) 2:e000416. doi: 10.1161/JAHA.113.000416
17. Meyer P, Filippatos GS, Ahmed MI, Iskandrian AE, Bittner V, Perry GJ, et al. Effects of right ventricular ejection fraction on outcomes in chronic systolic heart failure. *Circulation.* (2010) 121:252–8. doi: 10.1161/CIRCULATIONAHA.109.887570
18. EuroQol Group. EuroQol–a new facility for the measurement of health-related quality of life. *Health Policy.* (1990) 16:199–208.
19. Hundley WG, Bluemke D, Bogaert JG, Friedrich MG, Higgins CB, Lawson MA, et al. Society for cardiovascular magnetic resonance guidelines for reporting cardiovascular magnetic resonance examinations. *J Cardiovasc Magn Reson.* (2009) 11:5.
20. Almehmadi F, Joncas SX, Nevis I, Zahrani M, Bokhari M, Stirrat J, et al. Prevalence of myocardial fibrosis patterns in patients with systolic dysfunction: prognostic significance for the prediction of sudden cardiac arrest or appropriate implantable cardiac defibrillator therapy. *Circ Cardiovasc Imaging.* (2014) 7:593–600. doi: 10.1161/CIRCIMAGING.113.001768
21. Halliday BP, Baksi AJ, Gulati A, Ali A, Newsome S, Izgi C, et al. Outcome in dilated cardiomyopathy related to the extent, location, and pattern of late gadolinium enhancement. *JACC Cardiovasc Imaging.* (2019) 12:1645–55. doi: 10.1016/j.jcmg.2018.07.015
22. White IR, Royston P, Wood AM. Multiple imputation using chained equations: issues and guidance for practice. *Stat Med.* (2011) 30:377–99. doi: 10.1002/sim.4067
23. Harrell F. *Regression Modeling Strategies*. 2nd ed. Berlin: Springer International Publishing (2015).
24. Pocock SJ, Ariti CA, McMurray JJ, Maggioni A, Kober L, Squire IB, et al. Predicting survival in heart failure: a risk score based on 39 372 patients from 30 studies. *Eur Heart J.* (2013) 34:1404–13. doi: 10.1093/eurheartj/ehs337
25. R Core Team. *R: A Language and Environment for Statistical Computing*. Vienna: R Foundation for Statistical Computing (2020).
26. Amarasingham R, Moore BJ, Tabak YP, Drazner MH, Clark CA, Zhang S, et al. An automated model to identify heart failure patients at risk for 30-day readmission or death using electronic medical record data. *Med Care.* (2010) 48:981–8. doi: 10.1097/MLR.0b013e3181ef60d9
27. Hammill BG, Curtis LH, Fonarow GC, Heidenreich PA, Yancy CW, Peterson ED, et al. Incremental value of clinical data beyond claims data in predicting 30-day outcomes after heart failure hospitalization. *Circ Cardiovasc Qual Outcomes.* (2011) 4:60–7. doi: 10.1161/CIRCOUTCOMES.110.954693
28. Tan BY, Gu JY, Wei HY, Chen L, Yan SL, Deng N. Electronic medical record-based model to predict the risk of 90-day readmission for patients with heart failure. *BMC Med Inform Decis Mak.* (2019) 19:193. doi: 10.1186/s12911-019-0915-8
29. Ouwerkerk W, Voors AA, Zwinderman AH. Factors influencing the predictive power of models for predicting mortality and/or heart failure hospitalization in patients with heart failure. *JACC Heart Fail.* (2014) 2:429–36. doi: 10.1016/j.jchf.2014.04.006
30. Rahimi K, Bennett D, Conrad N, Williams TM, Basu J, Dwight J, et al. Risk prediction in patients with heart failure: a systematic review and analysis. *JACC Heart Fail.* (2014) 2:440–6. doi: 10.1016/j.jchf.2014.04.008
31. Sarijaloo F, Park J, Zhong X, Wokhlu A. Predicting 90 day acute heart failure readmission and death using machine learning-supported decision analysis. *Clin Cardiol.* (2021) 44:230–7. doi: 10.1002/clc.23532
32. Shameer K, Johnson KW, Yahi A, Miotto R, Li LI, Ricks D, et al. Predictive modeling of hospital readmission rates using electronic medical record-wide machine learning: a case-study using mount sinai heart failure cohort. *Pac Symp Biocomput.* (2017) 22:276–87. doi: 10.1142/9789813207813_0027
33. Krittayaphong R, Boonyasirinant T, Saiviroonporn P, Thanapiboonpol P, Nakyen S, Ruksakul K, et al. Prognostic significance of left ventricular mass by magnetic resonance imaging study in patients with known or suspected coronary artery disease. *J Hypertens.* (2009) 27:2249–56. doi: 10.1097/HJH.0b013e3283309ac4
34. Dini FL, Cortigiani L, Baldini U, Boni A, Nuti R, Barsotti L, et al. Prognostic value of left atrial enlargement in patients with idiopathic dilated cardiomyopathy and ischemic cardiomyopathy. *Am J Cardiol.* (2002) 89:518–23. doi: 10.1016/s0002-9149(01)02290-1
35. Wong M, Staszewsky L, Latini R, Barlera S, Glazer R, Aknay N, et al. Severity of left ventricular remodeling defines outcomes and response to therapy in heart failure: valsartan heart failure trial (Val-HeFT) echocardiographic data. *J Am Coll Cardiol.* (2004) 43:2022–7. doi: 10.1016/j.jacc.2003.12.053
36. Gulati A, Jabbour A, Ismail TF, Guha K, Khwaja J, Raza S, et al. Association of fibrosis with mortality and sudden cardiac death in patients with nonischemic dilated cardiomyopathy. *JAMA.* (2013) 309:896–908. doi: 10.1001/jama.2013.1363
37. Gulati A, Ismail TF, Jabbour A, Alpendurada F, Guha K, Ismail NA, et al. The prevalence and prognostic significance of right ventricular systolic dysfunction in nonischemic dilated cardiomyopathy. *Circulation.* (2013) 128:1623–33. doi: 10.1161/CIRCULATIONAHA.113.002518
38. Doesch C, Dierks DM, Haghi D, Schimpf R, Kuschyk J, Suselbeck T, et al. Right ventricular dysfunction, late gadolinium enhancement, and female gender predict poor outcome in patients with dilated cardiomyopathy. *Int J Cardiol.* (2014) 177:429–35. doi: 10.1016/j.ijcard.2014.09.004
39. Purmah Y, Lei LY, Dykstra S, Mikami Y, Cornhill A, Satriano A, et al. Right ventricular ejection fraction for the prediction of major adverse cardiovascular and heart failure-related events: a cardiac MRI based study of 7131 patients with known or suspected cardiovascular disease. *Circ Cardiovasc Imaging.* (2021) 14:e011337. doi: 10.1161/CIRCIMAGING.120.011337
40. Mikami Y, Jolly U, Heydari B, Peng M, Almehmadi F, Zahrani M, et al. Right ventricular ejection fraction is incremental to left ventricular ejection fraction for the prediction of future arrhythmic events in patients with systolic dysfunction. *Circ Arrhythm Electrophysiol.* (2017) 10:e004067. doi: 10.1161/CIRCEP.116.004067
41. Abdi-Ali A, Miller RJH, Southern D, Zhang M, Mikami Y, Knudtson M, et al. LV mass independently predicts mortality and need for future revascularization in patients undergoing diagnostic coronary angiography. *JACC Cardiovasc Imaging.* (2018) 11:423–33. doi: 10.1016/j.jcmg.2017.04.012
42. Halliday BP, Gulati A, Ali A, Guha K, Newsome S, Arzanauskaite M, et al. Association between midwall late gadolinium enhancement and sudden cardiac death in patients with dilated cardiomyopathy and mild and moderate left ventricular systolic dysfunction. *Circulation.* (2017) 135:2106–15.
43. Di Marco A, Anguera I, Schmitt M, Klem I, Neilan TG, White JA, et al. Late gadolinium enhancement and the risk for ventricular arrhythmias or sudden death in dilated cardiomyopathy: systematic review and meta-analysis. *JACC Heart Fail.* (2017) 5:28–38. doi: 10.1016/j.jchf.2016.09.017
44. Alba AC, Gaztanaga J, Foroutan F, Thavendiranathan P, Merlo M, Alonso-Rodriguez D, et al. Prognostic value of late gadolinium enhancement for the prediction of cardiovascular outcomes in dilated cardiomyopathy: an international, multi-institutional study of the MINICOR group. *Circ Cardiovasc Imaging.* (2020) 13:e010105. doi: 10.1161/CIRCIMAGING.119.010105
45. Mikami Y, Cornhill A, Heydari B, Joncas SX, Almehmadi F, Zahrani M, et al. Objective criteria for septal fibrosis in non-ischemic dilated cardiomyopathy: validation for the prediction of future cardiovascular events. *J Cardiovasc Magn Reson.* (2016) 18:82. doi: 10.1186/s12968-016-0300-z
46. Mikami Y, Cornhill A, Dykstra S, Satriano A, Hansen R, Flewitt J, et al. Right ventricular insertion site fibrosis in a dilated cardiomyopathy referral population: phenotypic associations and value for the prediction of heart failure admission or death. *J Cardiovasc Magn Reson.* (2021) 23:79. doi: 10.1186/s12968-021-00761-0
47. Voors AA, Ouwerkerk W, Zannad F, van Veldhuisen DJ, Samani NJ, Ponikowski P, et al. Development and validation of multivariable models to

predict mortality and hospitalization in patients with heart failure. *Eur J Heart Fail.* (2017) 19:627–34. doi: 10.1002/ejhf.785
48. Bello NA, Claggett B, Desai AS, McMurray JJ, Granger CB, Yusuf S, et al. Influence of previous heart failure hospitalization on cardiovascular events in patients with reduced and preserved ejection fraction. *Circ Heart Fail.* (2014) 7:590–5. doi: 10.1161/CIRCHEARTFAILURE.113.001281
49. Rodríguez-Artalejo F, Guallar-Castillón P, Pascual CR, Otero CM, Montes AO, García AN, et al. Health-related quality of life as a predictor of hospital readmission and death among patients with heart failure. *Arch Intern Med.* (2005) 165:1274–9. doi: 10.1001/archinte.165.11.1274
50. Puntmann VO, Carr-White G, Jabbour A, Yu CY, Gebker R, Kelle S, et al. T1-mapping and outcome in nonischemic cardiomyopathy: all-cause mortality and heart failure. *JACC Cardiovasc Imaging.* (2016) 9:40–50.

Conflict of Interest: JW, AH, and JF were shareholders in Cohesic Inc. JW has received research funding from Siemens Healthineers, Circle Cardiovascular Inc., Pfizer Inc. AH received funding from Amgen. JW was Chief Medical Officer of Cohesic Inc.

The remaining authors declare that the research was conducted in the absence of any commercial or financial relationships that could be construed as a potential conflict of interest.

Publisher's Note: All claims expressed in this article are solely those of the authors and do not necessarily represent those of their affiliated organizations, or those of the publisher, the editors and the reviewers. Any product that may be evaluated in this article, or claim that may be made by its manufacturer, is not guaranteed or endorsed by the publisher.

Copyright © 2022 Cornhill, Dykstra, Satriano, Labib, Mikami, Flewitt, Prosio, Rivest, Sandonato, Howarth, Lydell, Eastwood, Quan, Fine, Lee and White. This is an open-access article distributed under the terms of the Creative Commons Attribution License (CC BY). The use, distribution or reproduction in other forums is permitted, provided the original author(s) and the copyright owner(s) are credited and that the original publication in this journal is cited, in accordance with accepted academic practice. No use, distribution or reproduction is permitted which does not comply with these terms.

frontiers | Frontiers in Cardiovascular Medicine

ORIGINAL RESEARCH
published: 24 June 2022
doi: 10.3389/fcvm.2022.923549

Prediction and Risk Stratification of Cardiovascular Disease in Diabetic Kidney Disease Patients

Jingjing Ren[1,2,3,4,5], *Dongwei Liu*[1,2,3,4], *Guangpu Li*[1,2,3,4,5], *Jiayu Duan*[1,2,3,4,5*], *Jiancheng Dong*[5*] and *Zhangsuo Liu*[1,2,3,4*]

[1] Department of Integrated Traditional and Western Nephrology, The First Affiliated Hospital of Zhengzhou University, Zhengzhou, China, [2] Research Institute of Nephrology, Zhengzhou University, Zhengzhou, China, [3] Henan Province Research Center for Kidney Disease, Zhengzhou, China, [4] Key Laboratory of Precision Diagnosis and Treatment for Chronic Kidney Disease in Henan Province, Zhengzhou, China, [5] Clinical Research Center of Big-data, The First Affiliated Hospital of Zhengzhou University, Zhengzhou, China

OPEN ACCESS

Edited by:
Chayakrit Krittanawong,
New York University, United States

Reviewed by:
Luis Miguel Ruilope,
University Hospital October 12, Spain
John Adeoye,
The University of Hong Kong, Hong Kong SAR, China
Vijay Viswanathan,
Prof. M. Viswanathan Diabetes Research Center, India
Filippo Cademartiri,
Gabriele Monasterio Tuscany Foundation (CNR), Italy

***Correspondence:**
Zhangsuo Liu
zhangsuoliu@zzu.edu.cn
Jiancheng Dong
dongjc@ntu.edu.cn
Jiayu Duan
jyduan@hotmail.com

Specialty section:
This article was submitted to Cardiovascular Epidemiology and Prevention, a section of the journal Frontiers in Cardiovascular Medicine

Received: 20 April 2022
Accepted: 30 May 2022
Published: 24 June 2022

Citation:
Ren J, Liu D, Li G, Duan J, Dong J and Liu Z (2022) Prediction and Risk Stratification of Cardiovascular Disease in Diabetic Kidney Disease Patients. Front. Cardiovasc. Med. 9:923549. doi: 10.3389/fcvm.2022.923549

Background: Diabetic kidney disease (DKD) patients are facing an extremely high risk of cardiovascular disease (CVD), which is a major cause of death for DKD patients. We aimed to build a deep learning model to predict CVD risk among DKD patients and perform risk stratifying, which could help them perform early intervention and improve personal health management.

Methods: A retrospective cohort study was conducted to assess the risk of the occurrence of composite cardiovascular disease, which includes coronary heart disease, cerebrovascular diseases, congestive heart failure, and peripheral artery disease, in DKD patients. A least absolute shrinkage and selection operator (LASSO) regression was used to perform the variable selection. A deep learning-based survival model called DeepSurv, based on a feed-forward neural network was developed to predict CVD risk among DKD patients. We compared the model performance with the conventional Cox proportional hazards (CPH) model and the Random survival forest (RSF) model using the concordance index (C-index), the area under the curve (AUC), and integrated Brier scores (IBS).

Results: We recruited 890 patients diagnosed with DKD in this retrospective study. During a median follow-up of 10.4 months, there are 289 patients who sustained a subsequent CVD. Seven variables, including age, high density lipoprotein (HDL), hemoglobin (Hb), systolic blood pressure (SBP), smoking status, 24 h urinary protein excretion, and total cholesterol (TC), chosen by LASSO regression were used to develop the predictive model. The DeepSurv model showed the best performance, achieved a C-index of 0.767(95% confidence intervals [CI]: 0.717–0.817), AUC of 0.780(95%CI: 0.721–0.839), and IBS of 0.067 in the validation set. Then we used the cut-off value determined by ROC (receiver operating characteristic) curve to divide the patients into different risk groups. Moreover, the DeepSurv model was also applied to develop an online calculation tool for patients to conduct risk monitoring.

Conclusion: A deep-learning-based predictive model using seven clinical variables can effectively predict CVD risk among DKD patients and perform risk stratification. An online calculator allows its easy implementation.

Keywords: machine learning, diabetic kidney disease, cardiovascular disease, prediction model, risk stratification

INTRODUCTION

Diabetic kidney disease (DKD) has been one of the most serious diabetic microvascular complications, implicating up to 50% of patients with diabetes and becoming the major cause of the end-stage renal disease (ESRD) worldwide (1–3). DKD patients are at high risk of developing cardiovascular disease (CVD), bringing a heavy burden on the public health system (4, 5). Reduction in renal function is considered as an independent risk factor and predictor of CVD (6, 7). Therefore, DKD patients are more susceptible to CVD than the general population, resulting in much worse functional outcomes, morbidity, and mortality (8, 9). Meanwhile, they also have under-treated problems because of the lack of awareness of the CVD risks. However, the mechanisms by which CVD occurs in patients with DKD have also not been fully clarified. The individual performance and prognosis are often heterogeneous. Accordingly, improving awareness of cardiovascular risk factors and conducting early intervention in high-risk patients may improve prognosis and slow the progress.

There are many risk factors associated with the high prevalence of CVD in DKD patients. Studies of risk factors and predictive tools for CVD are common among the general population, such as the Framingham, QRISK, and China-PAR models (10–12). But these models often excluded the populations with a decline in kidney function, so they cannot be fully applied to the DKD patients with high risk of cardiovascular events (13, 14). Researches on cardiovascular risk factors in this population are still limited. Network Initiative Cardiovascular and Renal Clinical Trialists (INI-CRCT) also advise that we should attach more importance to these patients to enhance their cardiovascular outcomes (15). Therefore, identifying these cardiovascular risk factors and patients at high risk is still a challenging problem.

In recent years, artificial intelligence, particularly deep learning is developing rapidly and has been applied to a variety of medical fields, such as disease prediction (16), machine vision (17) and diagnostic study (18), etc. Deep learning is superior in handling different types of data for its strong computing power (19). So far, there have been many deep learning methods were developed for survival analysis (20, 21). Katzman et al. also developed a novel deep feed-forward neural network based on Cox assumption called DeepSurv, which combined survival analysis with deep learning and had the advantage to perform a prediction of time-to-event data. It has been successfully applied in the survival analysis of multiple diseases and showed promising performance in predicting patients' outcomes, such as oncological diseases, Covid-19, and atherosclerotic cardiovascular disease (22–26). Several online calculation tools were constructed based on the DeepSurv method (27–29).

In this study, we aimed to develop a predictive model based on the deep learning method to predict the progression of CVD in DKD patients. It also can help us to investigate the associated risk factors, to provide treatment recommendations for better cardiovascular outcomes and support personalized medicine. Patients were stratified into different risk subgroups using the output risk values from the model. We further evaluated the performance of the DeepSurv model with the classical Cox proportional hazards (CPH) model and the Random survival forest (RSF) model using the concordance index (C-index), to prove that machine learning can effectively improve the predictive performance. Additionally, an easy-used online tool for calculating the incidence rate of CVD in DKD patients based on the predictive model was developed.

MATERIALS AND METHODS

Study Population

We retrospectively reviewed the patients who were diagnosed with DKD from the electronic medical records of the First Affiliated Hospital of Zhengzhou University from January 2013 to January 2020. DKD is defined as diabetic patients who performed persistent urinary albumin excretion or a reduction in estimated glomerular filtration rate (eGFR) for more than 3 months (2). Patients were required to have at least two hospitalizations, which allowed us to record patients' baseline data before a CV event (if any). The exclusion criteria were: (1) patients with incomplete clinical information ($n = 17$); (2) age <18 years ($n = 1$); (3) patients had history of cardiovascular diseases or coronary revascularization ($n = 1{,}065$); (4) patients with surgery, infection or injured at baseline ($n = 18$); and (5) patients with autoimmune disease or malignant tumor ($n = 45$). The selection process of patients is shown in **Supplementary Figure 1**.

Cardiovascular Outcomes

The CVD outcomes in this study were the first occurrence of a subsequent CVD, including coronary heart disease (coronary heart disease, myocardial infarction, angina, and coronary revascularization); cerebrovascular disease (hemorrhagic stroke and ischaemic stroke); congestive heart failure and peripheral arterial disease (amputations, aortic aneurysm, revascularization of the aorta or other peripheral arteries) and the combination of cardiovascular events. Outcomes were defined by the International Classification of Diseases, Tenth Revision (ICD-10) codes. The ICD-10 codes are summarized in **Supplemental Table 1**.

Statistical Analysis

we extracted the baseline patients' characteristics from the electronic medical records, including demographic details, comorbidities, physical examination measures, and laboratory values. If the missing-value ratio of a variable is more than 30%, the variable will be excluded. To impute the missing data, we applied multivariate imputation by chained equations (MICE) (30). After data imputation, we used the Z-score normalization method to normalize all variables to reduce the bias. The least absolute shrinkage and selection operator (LASSO) regression was performed to determine the significant clinical variables using 10-fold cross-validation (31). Furthermore, we used both univariate and multivariate cox regression analysis to assess the independent prognostic significance of the selected variables.

Modeling Process

The database was divided into two mutually exclusive datasets with balanced data distribution, 70% as a training set and 30% as an internal validation set. Continuous variables are presented as mean ± standard deviation (SD) and compared between groups using the *t*-test, or as median (interquartile range [IQR]) and compared by Mann–Whitney *U*-tests, depending on whether the data is normally distributed or not. Categorical variables are shown as frequency (percentage) and compared by the chi-squared test. The cumulative incidence rate of the two sets was plotted by the Kaplan-Meier method and then compared using the log-rank test. Deep Learning-based Survival Model (DeepSurv) was used to perform the task of predicting patient-individual cardiovascular risk using the preselected variables by LASSO regression. We applied Bayesian hyperparameter optimization including learning rate decay, dropout, and other hyperparameters, to prevent overfitting (32). The list of hyperparameters of DeepSurv was provided in the **Supplementary Table 2**. More details about the DeepSurv method are available online (https://github.com/jaredleekatzman/DeepSurv). After splitting the datasets into the training and validation sets, we trained the model performing a 5-fold cross-validation on the training set to assess for overfitting and determine the model validity. Then we estimated the model performance in the validation set.

Model Validation

After obtaining the output predicted individual risks with the DeepSurv model, the DKD patients were then divided into high-risk and low-risk groups based on the cut-off value determined by ROC (receiver operating characteristic) curve. The cumulative incidence curves were plotted using the Kaplan-Meier method and compared using the log-rank test to visualize the difference in the predicted cumulative incidence of patients in two risk groups. The importance values of the selected variables were calculated by their component weights in the DeepSurv model, indicating the univariate contribution to the model. Finally, we compared the performance of the DeepSurv model with the CPH model and RSF model as conventional prediction methods to verify its performance. The discrimination performance of the proposed methods was assessed using the C-index, integrated Brier score (IBS) (33), and the area under the receiver-operator characteristic curve (AUC) in both the training and validation cohorts. C-index is a commonly used indicator of survival prediction, which can reflect the ability to predict time-to-event data. IBS compares the predicted survival rate with the actual status of patients. Higher C-index, higher AUC, and smaller IBS indicate a stronger fit of the model. Then we plotted the calibration curves of the predicted individual risk probabilities of CVD events at 1, 3, and 5 year. Furthermore, for these four different cardiovascular diseases included in our study, a subgroup analysis was conducted to determine which of their outcomes has the best-predicted performance using the DeepSurv models. A simple depiction of our study design is shown in **Figure 1**. The study was reported according to the Transparent Reporting of a multivariable prediction model for Individual Prognosis or Diagnosis (TRIPOD) guidelines (**Supplementary Table 3**). Statistical analysis was completed with R v.4.1.1 and SPSS v.26 (IBM Corporation) software. Python v.3.7 and TensorFlow v.1.14 were used to implement DeepSurv models. A p-value <0.05 was considered statistically significant.

RESULTS

Patient Characteristics

A total of 890 patients were included in the final analysis. During a medium follow-up of 10.4 (IQR: 3.8–23.4) months, 284(31.91%) patients required rehospitalization due to subsequent cardiovascular events (128 cases of coronary heart diseases, 98 cerebrovascular diseases, 62 congestive heart failures, and 33 peripheral artery diseases; patients may have had >1 event). The median age for all patients was 52 years (IQR = 43–57), and that was 56 years (IQR = 48–65) for patients who sustained a subsequent CVD. Baseline demographic and clinical characteristics of the included patients, stratified by CVD outcomes are summarized in **Supplementary Table 4**. Patients were randomly divided into the training set (70%) and the validation set (30%), 606 patients in the training set, and 286 patients in the validation set. There were no statistically significant differences in the variables between the two groups (**Table 1**). **Figure 2** also showed that the cumulative incidence curves of the two sets were no statistically significant difference using the log-rank test ($p = 0.21$).

Variables Selection

There are 91 baseline clinical variables with at least 70% data completeness as candidate predictors used for LASSO regression. Seven variables, including age, high density lipoprotein (HDL), hemoglobin (Hb), systolic blood pressure (SBP), smoking status, 24 h urinary protein excretion, and total cholesterol (TC), were selected using the lambda with 1 SE of the minimum partial likelihood deviance. These variables are all easily available demographic, clinical characteristics, and laboratory results. Baseline characteristics of the selected variables were presented in **Table 2**. The results of the univariate analysis and multiple CPH regression analysis showed that each clinical parameter has independent prognostic power (**Supplementary Table 5**). To explore whether the correlation between variables would have an impact on the model, we applied the correlation-based heat map to calculate the correlation between every two factors. **Supplementary Figure 2** revealed that there were few correlations between the chosen variables (all correlation absolute values are <0.5).

Model Performance

After the feature selection process, all seven variables as independent predictors were used for the model development. We use the DeepSurv method to construct survival models to analyze individual CVD outcomes. A three-layer neural network with one input layer, one hidden layer, and one output layer is used to construct the predictive model. We used dropout, batch normalization, and L1 and L2 regularization

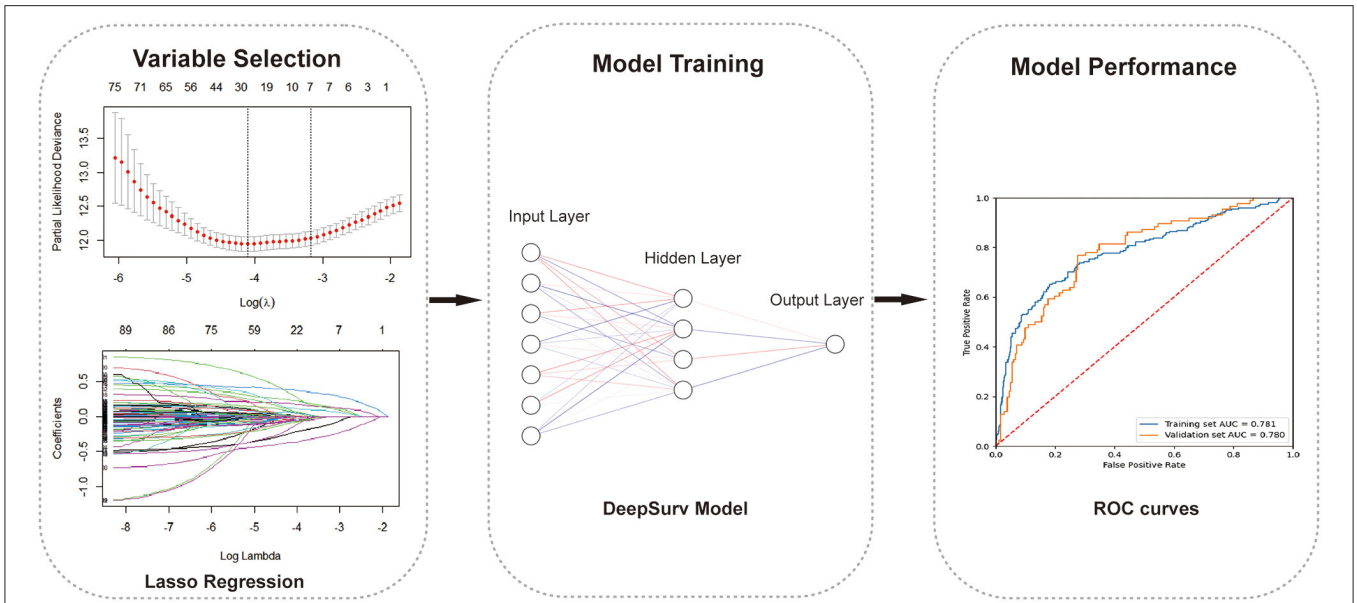


FIGURE 1 | The working process of this study. The study procedure consisted of variables selection, model building, and model evaluation.

TABLE 1 | Baseline characteristics in the training set and validation set.

	Total (n = 890)	Training set (n = 623)	Validation set (n = 267)	p-value
Smoking status				0.474
Never (%)	707 (79.4)	493 (79.1)	214 (80.2)	
Previous (%)	64 (7.2)	42 (6.7)	22 (8.2)	
Current (%)	119 (13.4)	88 (14.1)	31 (11.6)	
Age (years)	52 (45–60)	52 (45–60)	52 (45–60)	0.543
Systolic blood pressure (mmHg)	135 (126–148)	135 (126–148)	135 (125–149)	0.746
Total cholesterol (mmol/L)	4.5 (3.7–5.4)	4.6 (3.7–5.4)	4.5 (3.7–5.3)	0.615
Hemoglobin (g/L)	111 (94–131)	111 (95–130)	111 (92–132)	0.652
high density lipoprotein (mmol/L)	1.1(0.9–1.4)	1.1 (0.8–1.4)	1.1 (0.9–1.4)	0.390
24 h urinary protein (g)	2.7 (0.4–6.3)	2.7 (0.4–6.3)	2.8 (0.4–6.1)	0.296

Continuous variables are shown as mean (SD) or median (interquartile range) according to the distribution, and categorical variables are shown as frequency (percentage).

during training and selected adaptive moment (Adam) as the optimizer and Tanh as the activation function to reduce overfitting. The optimized hyperparameters for DeepSurv are shown in **Supplementary Table 6**. The 5-fold cross-validation in the training set was performed to prove the robustness of this model, with a mean AUC of 0.779(SD: 0.009), and a C-index of 0.793(SD: 0.012). To evaluate the DeepSurv model discriminative performance, we compared it with the CPH and RSF models using the C-index, AUC, and IBS. **Table 3** showed that the DeepSurv model performed best among the three survival models. The C-index of the DeepSurv model in the training and validation sets were 0.796 (95% CI: 0.761–0.831) and 0.796 (95% CI: 0.761–0.831). The AUC were 0.781 (95% CI:0.740–0.822) and 0.780 (95% CI: 0.721–0839) (**Figure 3**), and the IBS were 0.046 and 0.067 in the training and validation sets respectively. We assess the importance of the variables according to their weight in the DeepSurv model, indicating the univariate contribution to the model. It revealed that older age, lower HDL, lower Hb, higher 24 h urinary protein, smoking, higher SBP, and higher TC were significantly associated with the high risk of CVD (**Figure 4**). Age, HDL, and Hb were the three main relevant risk factors in the model. Subgroup analysis of four cardiovascular diseases showed that this model performed best in patients with congestive heart failure (**Table 4**), showed a C-index of 0.874 (95% CI: 0.822–0.826), and the AUC of 0.831 (95%CI: 0.770–0.892). The calibration curves of predicted event probabilities illustrated that this model has higher accuracy in predicting cardiovascular risk at 1 year (**Supplementary Figure 3**).

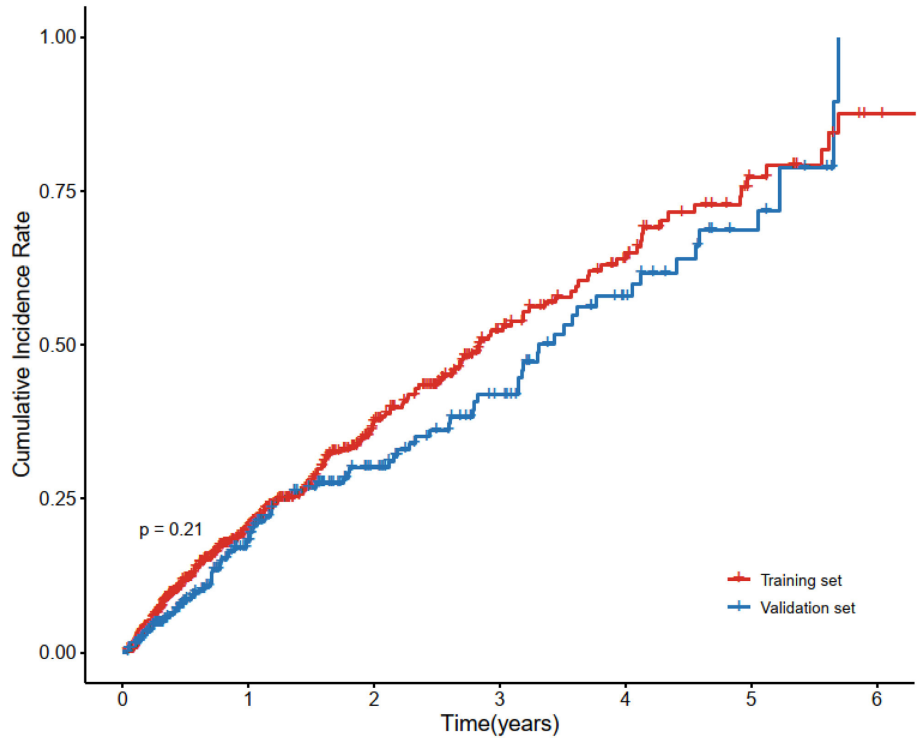


FIGURE 2 | Cumulative incidence curve of cardiovascular disease in the training set and validation set. Cardiovascular disease is the composite of coronary heart disease, cerebrovascular disease, congestive heart failure, and peripheral arterial disease. There was no statistically significant difference between the survival of the two sets using the log-rank test ($p = 0.21$).

TABLE 2 | Demographic and clinical characteristics of patients with or without CVD in the dataset.

	Total (*n* = 890)	**CVD** (*n* = 284)	**NO CVD** (*n* = 606)	***p*-value**
Smoking status				<0.001
Never (%)	707 (79.4)	191 (67.3)	516 (31.5)	
Previous (%)	64 (7.2)	25 (8.8)	39 (4.1)	
Current (%)	119 (13.4)	68 (23.9)	51 (11.2)	
Age (years)	52 (45–60)	56.4 ± 11.7	51 (43–57)	<0.001
Systolic blood pressure (mmHg)	135 (126–148)	142 (131.3–160)	133 (124.8–142)	<0.001
Total cholesterol (mmol/L)	4.5 (3.7–5.4)	4.9 (4.1–5.7)	4.3 (3.6–5.2)	<0.001
Hemoglobin (g/L)	111 (94–131)	107 (91–128)	113 (95.3–133)	0.007
High density lipoprotein (mmol/L)	1.1 (0.9–1.4)	1 (0.8–1.3)	1.1 (0.9–1.4)	0.002
24 h urinary protein (g)	2.7 (0.4–6.3)	3.2 (0.7–7.1)	2.5 (0.4–6)	0.042

Continuous variables are shown as mean (SD) or median (interquartile range) according to the distribution, and categorical variables are shown as frequency (percentage).

Risk Stratification

Furthermore, after calculating the predicted individual risk score, patients were divided into high-risk and low-risk groups based on the risk cut-off values (the sensitivity of 76.7% and specificity of 72.4%). 410 patients were classified as high risk and 480 patients were classified as low risk group. We plotted the cumulative incidence curves for the two risk subgroups. **Figure 5** illustrates that risk stratification based on the DeepSurv model can successfully stratify patients into different risk groups with significant differences ($p<0.01$).

Model Visualization

The best performing model, the DeepSurv model, was used to construct an easy-used online tool to predict CVD risk in DKD patients (http://model.51ehealth.com/). It can calculate the individual CVD risk and monitor the trend of the risk,

TABLE 3 | Performance of different models.

	C-index (95%CI)		AUC (95%CI)		IBS	
	Training set	Validation set	Training set	Validation set	Training set	Validation set
DeepSurv	0.796 (0.761–0.831)	0.767 (0.717–0.817)	0.781 (0.740–0.822)	0.780 (0.721–0839)	0.046	0.067
CPH	0.755 (0.719–0.790)	0.745 (0.691–0.800)	0.737 (0.698–0.776)	0.724 (0.659–0.789)	0.177	0.194
RSF	0.721 (0.681–0.761)	0.753 (0.700–0.806)	0.723 (0.680–0.766)	0.765 (0.704–0.826)	0.064	0.148

Model performance of DeepSurv, RSF, and CPH model in terms of C-index, AUC and IBS. CPH, cox proportional hazards regression; DeepSurv, deep learning-based survival model; RSF, random survival forest model; IBS, integrated brier scores; AUC, the area under the receiver-operator characteristic curve.

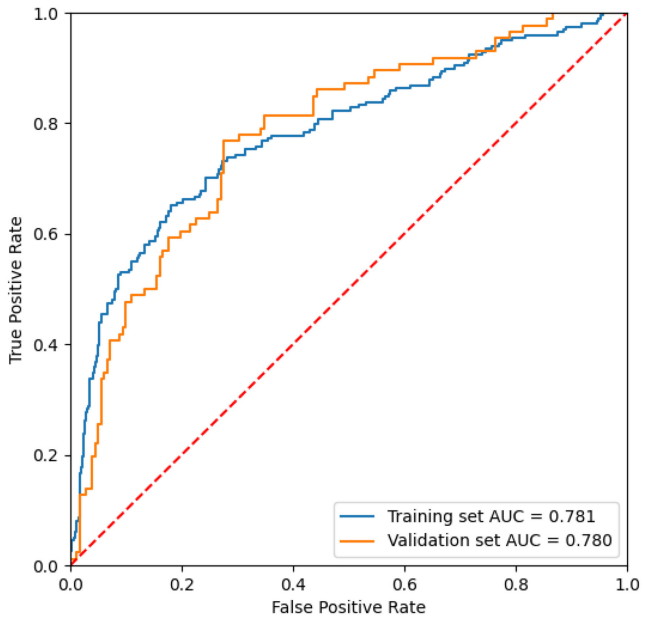


FIGURE 3 | Receiving operating characteristics (ROC) curves for the training set and validation set.

providing a more intuitive and understandable way to interpret the predictive model. The DeepSurv model was able to plot the predicted Kaplan-Meier survival curves for each patient. Meanwhile, for understanding convenience, we transformed the predicted time-to-event curves output from the model into curves of event incidence rates. DKD patients can input their personal information to get their risk stratification and the incidence of CVD for 1, 3, and 5 year. The interface of this risk calculator is shown in **Figure 6**. This online tool can also help physicians to choose the appropriate treatments and provide individual recommendations for the individuals to improve outcomes based on the output risk values.

DISCUSSION

The occurrence and progression of CVD is a crucial factor contributing to poor outcomes in patients with DKD (34). In this study, we developed a deep learning-based predictive model and an online tool to predict the CVD risk in DKD patients. Our model used seven clinical variables, including age, smoking status, SBP, TC, Hb, HDL, and 24 h urinary protein, as independent predictors, and had a promising performance in the validation set. Different from the previous CVD models, our model targets a specific population: DKD patients, which allows it to be applied with greater accuracy. The C-index, ROC curves, and IBS indicated that this deep-learning model had better model discrimination in analyzing patient-individual survival outcomes than the traditional models. Furthermore, the ability to classify patients into different risk groups based on their prognosis may benefit patients by identifying high CVD risk patients and attaching more importance to them. The application of an online tool translates the predictive model into clinical practice, which may be useful for risk calculation and risk monitoring in practical clinical applications. As a result, physicians can determine the most appropriate treatment strategy to implement personalized management based on the results of risk stratification and even improve the CVD outcomes.

This study applied deep learning methods to develop models for prediction and risk stratification of CVD among DKD patients without overfitting been observed, demonstrating that this deep learning-based survival predictive model showed better performance compared to the conventional statistical method. Despite the CPH model being the most widely used approach for survival analysis in analyzing time-to-event survival data (35–37), it has its inherent drawbacks (38). The Cox model assumes the effect of each covariate is proportional and it is unable to properly model non-linearities and interaction effects. Deep-learning methods can learn to solve non-linear and intricate relationships between covariates and individual outcomes efficiently and have advantages in processing large amounts and various types of data (39). But many deep learning methods also have problems with weak interpretation in clinical practice. In this study, DeepSurv methods can combine the deep learning method with the traditional Cox assumption for survival analysis of the non-linear effect using clinical variables to predict the CVD risk of DKD patients. We reveal that this model can significantly improve the prediction performance in terms of the C-index. It not only has good model discrimination but it also can be applied for clinical use for its good interpretability. It can generate predicted Cumulative incidence curves for individuals, thus identifying them into different risk groups. The superior performance of the DeepSurv model demonstrates its ability to handle the complex association of risk factors. In addition,

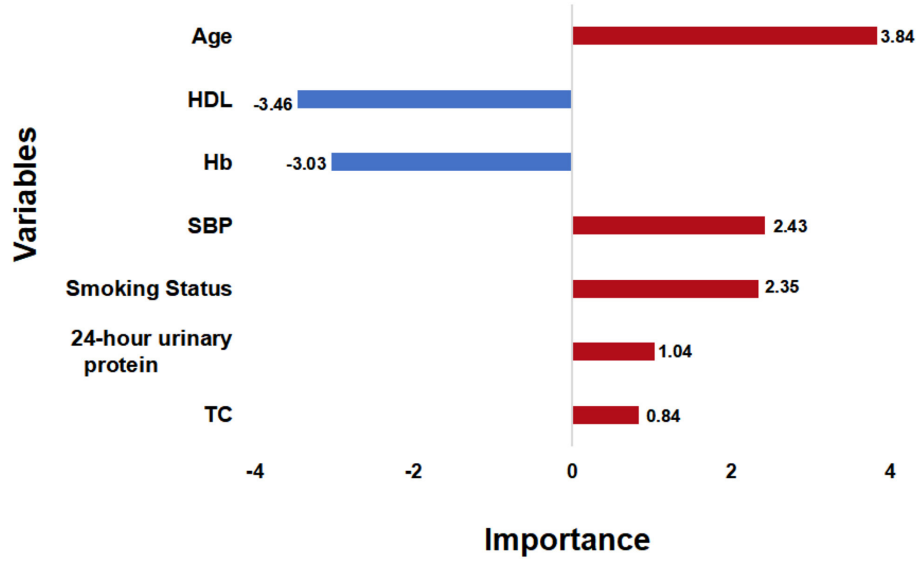


FIGURE 4 | Variable Importance. The importance score of the selected variables is calculated by their weights in the DeepSurv model. SBP, systolic blood pressure; TC, total cholesterol; Hb, hemoglobin; HDL, high density lipoprotein.

TABLE 4 | Subgroup analysis of the performance of different cardiovascular diseases.

Outcomes	C-index (95%CI)	AUC (95%CI)
Coronary heart disease	0.812 (0.768–0.856)	0.771 (0.722–0.820)
Cerebrovascular disease	0.844 (0.802–0.885)	0.806 (0.759–0.853)
Congestive heart failure	0.874 (0.822–0.826)	0.831 (0.770–0.892)
Peripheral artery disease	0.861 (0.789–0.934)	0.726 (0.646–0.806)

CI, confidence intervals.

the DeepSurv model has been widely applied to many survival analyses with a favorable prediction value (22, 23, 29). It also can provide a framework on which more datasets can be trained in the future in a broader population.

Numerous risk factors have been proved to be related to the high incidence of CVD in some DKD patients. In this study, we also demonstrated several recognized similar traditional risk predictors, consisting of age, SBP, smoking status, HDL, and TC, in consistent with the previous studies (40). A meta-analysis has shown that these traditional risk factors have been proved in previous classical predictive models based on the general population, including age, blood pressure, smoking status, and cholesterol levels (41). Age is a generally recognized risk factor for CVD (42). During aging, cardiac structural changes and functional dysfunction often occur caused by injury in fundamental cardiomyocytes (43). Hypertension is highly prevalent in chronic kidney disease (CKD) patients, which is widely recognized as a risk factor for the development of CVD (44–47). Reducing blood pressure is an important treatment strategy that not only slows the progression of renal failure but also decreases the risk of cardiovascular disease (48). Smoking is regarded as a crucial and modifiable predictor of the progression of CVD (49). The Study of Heart and Renal Protection (SHARP) found that smoking attributed to the high risk of vascular adverse complications among patients with chronic kidney disease, and may be changed by quitting smoking (50, 51). The potential benefits of cessation are even greater than those of pharmacological treatment for cardiovascular protection (52). There was a strong and inverse correlation between HDL and CVD risk in the DKD population (53). Through reverse cholesterol transport (RCT), HDL can protect against plaque formation and development in the prevention of CVD (54). TC concentration measurement is also proved to be important in the evaluation of CVD risk factors. Besides these traditional risk factors (55), we also found that anemia and high proteinuria play a significant role in the incidence of CVD among DKD patients. Anemia was found significantly associated with the occurrence of CVD events. Anemia can cause changes in ventricular structure (56). Long-term anemia will lead to decreased oxygen capacity and utilization disorders. The compensatory hyperdynamic circulation is needed to maintain normal oxygen supply, resulting in increased cardiac output and left ventricular hypertrophy (57). Anemia often contributes to recurrent and progressive cardiac and renal deterioration, which is also called cardiorenal anemia syndrome (CRAS) (58). Proteinuria, which can reflect kidney lesions, is also a predictive factor of cardiovascular events and mortality (59). A meta-analysis also showed that participants with proteinuria had a higher risk of stroke than non-participants (33). All these included variables were independently correlated with an increased risk of CVD progression. Identifying and increasing awareness of these risk factors for CVD is essential in the early intervention and appropriate treatment of DKD

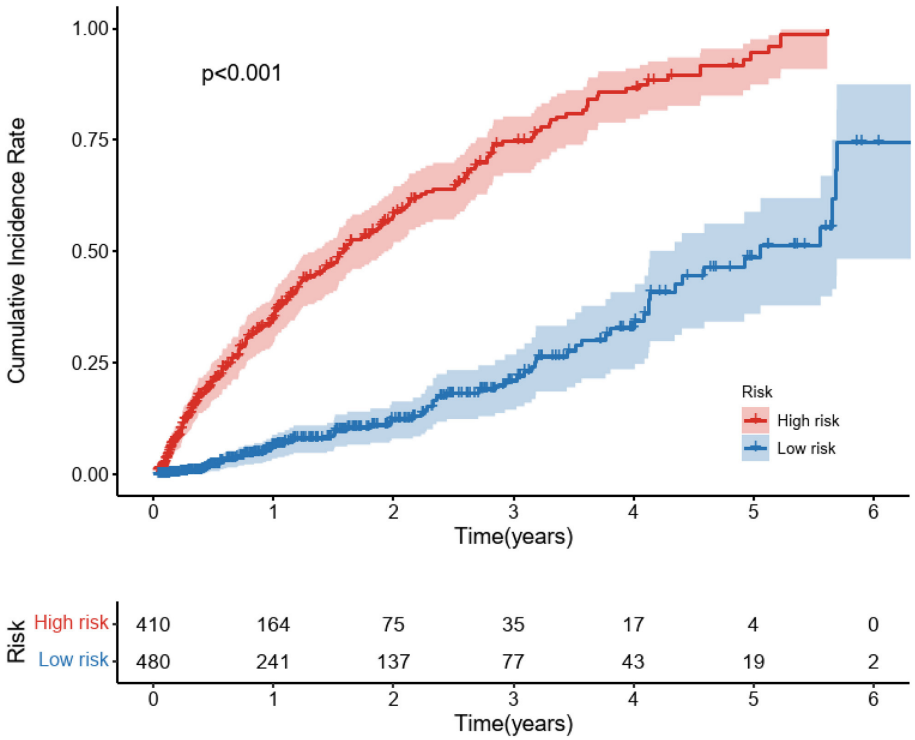


FIGURE 5 | Cumulative Incidence curves for predicted cardiovascular disease among diabetic kidney disease patients in different risk groups. Cardiovascular disease is the composite of coronary heart disease, cerebrovascular disease, congestive heart failure, and peripheral arterial disease. Patients were stratified into a high-risk group and a low-risk group based on the cut-off value of the ROC curve. The *P*-values between the high-risk and low-risk subgroups were calculated by the log-rank test.

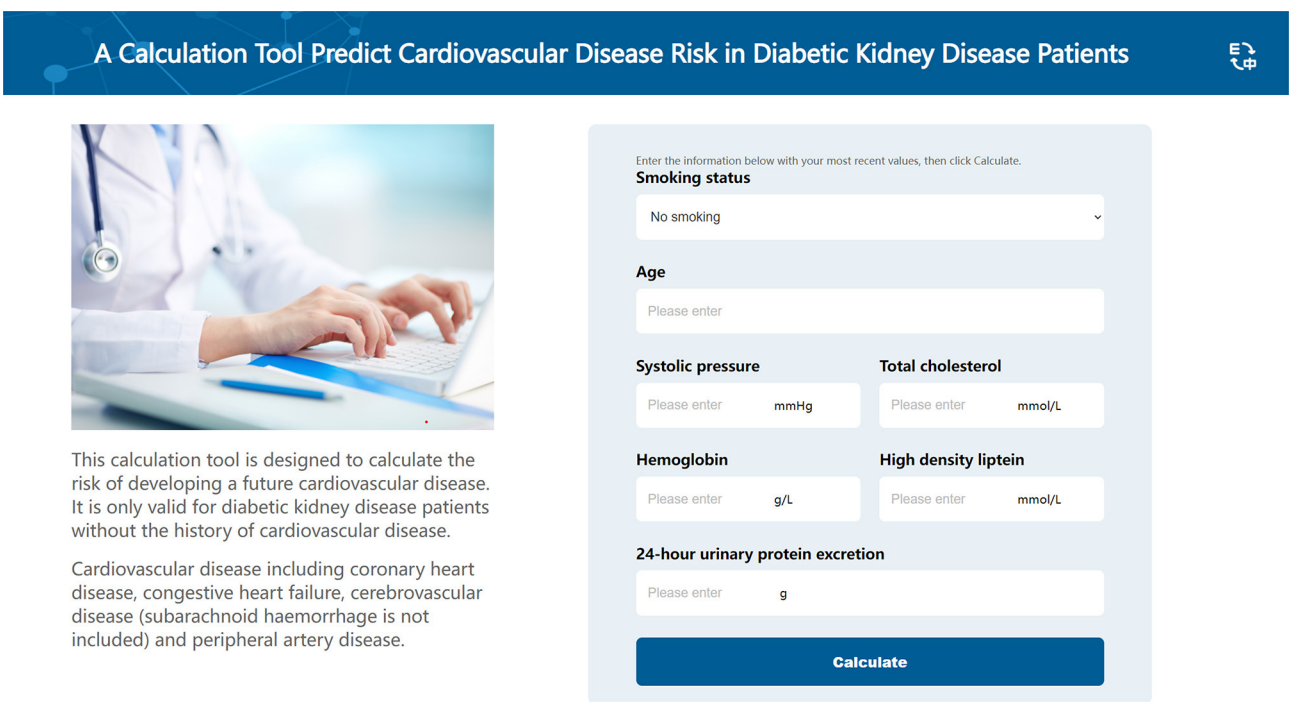


FIGURE 6 | The interface of the online calculation tool. This online calculation tool is used to predict the cardiovascular disease risk among diabetic kidney disease patients.

patients. New integrating approaches to prognostic factors could also increase the accuracy of prediction.

There are several limitations to this study. Firstly, this study was a retrospective single-center study. Further prospective research and multicenter datasets are needed to test the generalizability and validity of the model. Secondly, a relatively small number of patients included is also a limitation in our study. Although deep learning methods have advantages in processing data with small sample sizes, Replication in a broader population is needed to confirm the superior predictive potential. Thirdly, our model used only clinical variables. Although the use of these easily accessible variables facilitates the generalization and application of the models, multi-dimensional variables such as medical imaging, omics data, and histopathological information, may also have clinical significance in the occurrence of CVD. Finally, this predictive model is based on the Chinese population, and further validation is needed to verify whether it can be applied to other ethnicities.

In conclusion, we developed and validated a new predictive model with good discrimination to estimate CVD risk among patients with DKD using seven readily available clinical variables. A user-friendly online tool based on this model was developed for clinical implementation and patient surveillance.

DATA AVAILABILITY STATEMENT

The original contributions presented in the study are included in the article/**Supplementary Material**, further inquiries can be directed to the corresponding author/s.

ETHICS STATEMENT

The studies involving human participants were reviewed and approved by the Human Scientific Ethics Committee of the First Affiliated Hospital of Zhengzhou University. Written informed consent for participation was not required for this study in accordance with the National Legislation and the Institutional Requirements.

AUTHOR CONTRIBUTIONS

JR, JDo, DL, and JDu conceived and designed the study. GL collected the data. JR performed the statistical analysis, explained the results, and wrote the manuscript. JDu discussed the draft manuscript. JDo and ZL revised the manuscript. All the authors approved the submitted version of the manuscript.

FUNDING

This study was funded by the Young Scientists Fund of the National Natural Science Foundation of China (Grant No. 82103916), the General Program of the National Natural Science Foundation of China General Project (Grant No. 81970633), and the Major public welfare special projects in Henan Province (Grant No. 201300310600).

SUPPLEMENTARY MATERIAL

The Supplementary Material for this article can be found online at: https://www.frontiersin.org/articles/10.3389/fcvm.2022.923549/full#supplementary-material

REFERENCES

1. Microvascular complications and foot care: standards of medical care in diabetes-2019. *Diabetes care.* (2019) 42(Suppl. 1):S124–S38. doi: 10.2337/dc19-S011
2. Selby NM, Taal MW. An updated overview of diabetic nephropathy: diagnosis, prognosis, treatment goals and latest guidelines. *Diabetes Obes Metab.* (2020) 22(Suppl. 1):3–15. doi: 10.1111/dom.14007
3. Harding JL, Pavkov ME, Magliano DJ, Shaw JE, Gregg EW. Global trends in diabetes complications: a review of current evidence. *Diabetologia.* (2019) 62:3–16. doi: 10.1007/s00125-018-4711-2
4. Jankowski J, Floege J, Fliser D, Böhm M, Marx N. Cardiovascular disease in chronic kidney disease: pathophysiological insights and therapeutic options. *Circulation.* (2021) 143:1157–72. doi: 10.1161/CIRCULATIONAHA.120.050686
5. Maqbool M, Cooper ME, Jandeleit-Dahm KAM. Cardiovascular disease and diabetic kidney disease. *Semin Nephrol.* (2018) 38:217–32. doi: 10.1016/j.semnephrol.2018.02.003
6. Kühn A, van der Giet M, Kuhlmann MK, Martus P, Mielke N, Ebert N, et al. Kidney function as risk factor and predictor of cardiovascular outcomes and mortality among older adults. *Am J Kidney Dis.* (2021) 77:386–96.e1. doi: 10.1053/j.ajkd.2020.09.015
7. Chen J, Budoff MJ, Reilly MP, Yang W, Rosas SE, Rahman M, et al. Coronary artery calcification and risk of cardiovascular disease and death among patients with chronic kidney disease. *JAMA Cardiol.* (2017) 2:635–43. doi: 10.1001/jamacardio.2017.0363
8. Kelly D, Rothwell PM. Disentangling the multiple links between renal dysfunction and cerebrovascular disease. *J Neurol Neurosurg Psychiatry.* (2020) 91:88–97. doi: 10.1136/jnnp-2019-320526
9. Johansen KL, Garimella PS, Hicks CW, Kalra PA, Kelly DM, Martens S, et al. Central and peripheral arterial diseases in chronic kidney disease: conclusions from a kidney disease: improving global outcomes (Kdigo) controversies conference. *Kidney Int.* (2021) 100:35–48. doi: 10.1016/j.kint.2021.04.029
10. Corlin L, Short MI, Vasan RS, Xanthakis V. Association of the duration of ideal cardiovascular health through adulthood with cardiometabolic outcomes and mortality in the framingham offspring study. *JAMA cardiol.* (2020) 5:549–56. doi: 10.1001/jamacardio.2020.0109
11. Hippisley-Cox J, Coupland C, Brindle P. Development and validation of qrisk3 risk prediction algorithms to estimate future risk of cardiovascular disease: prospective cohort study. *BMJ.* (2017) 357:j2099. doi: 10.2337/dc19-S011
12. Yang X, Li J, Hu D, Chen J, Li Y, Huang J, et al. Predicting the 10-year risks of atherosclerotic cardiovascular disease in chinese population: the china-par project (Prediction for Ascvd Risk in China). *Circulation.* (2016) 134:1430–40. doi: 10.1161/CIRCULATIONAHA.116.022367
13. Zannad F, Rossignol P. Cardiovascular outcome trials in patients with advanced kidney disease: time for action. *Circulation.* (2017) 135:1769–71. doi: 10.1161/CIRCULATIONAHA.117.027338
14. Lai AC, Bienstock SW, Sharma R, Skorecki K, Beerkens F, Samtani R, et al. A Personalized approach to chronic kidney disease and cardiovascular disease: jacc review topic of the week. *J Am Coll Cardiol.* (2021) 77:1470–9. doi: 10.1016/j.jacc.2021.01.028

15. Rossignol P, Agarwal R, Canaud B, Charney A, Chatellier G, Craig JC, et al. Cardiovascular outcome trials in patients with chronic kidney disease: challenges associated with selection of patients and endpoints. *Eur Heart J.* (2019) 40:880–6. doi: 10.1093/eurheartj/ehx209
16. Schena FP, Anelli VW, Trotta J, Di Noia T, Manno C, Tripepi G, et al. Development and testing of an artificial intelligence tool for predicting end-stage kidney disease in patients with immunoglobulin a nephropathy. *Kidney Int.* (2021) 99:1179–88. doi: 10.1016/j.kint.2020.07.046
17. Bouteldja N, Klinkhammer BM, Bülow RD, Droste P, Otten SW. Freifrau von Stillfried S, et al. Deep learning-based segmentation and quantification in experimental kidney histopathology. *J Am Soc Nephrol.* (2021) 32:52–68. doi: 10.1681/ASN.2020050597
18. Yamashita R, Long J, Longacre T, Peng L, Berry G, Martin B, et al. Deep learning model for the prediction of microsatellite instability in colorectal cancer: a diagnostic study. *Lancet Oncol.* (2021) 22:132–41. doi: 10.1016/S1470-2045(20)30535-0
19. Wang F, Casalino LP, Khullar D. Deep learning in medicine-promise, progress, and challenges. *JAMA Intern Med.* (2019) 179:293–4. doi: 10.1001/jamainternmed.2018.7117
20. Lee C, Yoon J, Schaar MV. Dynamic-deephit: a deep learning approach for dynamic survival analysis with competing risks based on longitudinal data. *IEEE Trans Biomed Eng.* (2020) 67:122–33. doi: 10.1109/TBME.2019.2909027
21. Zhao L, Feng D. Deep neural networks for survival analysis using pseudo values. *IEEE J Biomed Health Inform.* (2020) 24:3308–14. doi: 10.1109/JBHI.2020.2980204
22. Shamout FE, Shen Y, Wu N, Kaku A, Park J, Makino T, et al. An artificial intelligence system for predicting the deterioration of covid-19 patients in the emergency department. *NPJ Digital Med.* (2021) 4:80. doi: 10.1038/s41746-021-00453-0
23. Byun SS, Heo TS, Choi JM, Jeong YS, Kim YS, Lee WK, et al. Deep learning based prediction of prognosis in non-metastatic clear cell renal cell carcinoma. *Sci Rep.* (2021) 11:1242. doi: 10.1038/s41598-020-80262-9
24. Adeoye J, Koohi-Moghadam M, Lo AWI, Tsang RK, Chow VLY, Zheng LW, et al. Deep learning predicts the malignant-transformation-free survival of oral potentially malignant disorders. *Cancers.* (2021) 13:6054. doi: 10.3390/cancers13236054
25. Moradmand H, Aghamiri SMR, Ghaderi R, Emami H. The role of deep learning-based survival model in improving survival prediction of patients with glioblastoma. *Cancer Med.* (2021) 10:7048–59. doi: 10.1002/cam4.4230
26. Hathaway QA, Yanamala N, Budoff MJ, Sengupta PP, Zeb I. Deep neural survival networks for cardiovascular risk prediction: the multi-ethnic study of atherosclerosis (mesa). *Comput Biol Med.* (2021) 139:104983. doi: 10.1016/j.compbiomed.2021.104983
27. Kim DW, Lee S, Kwon S, Nam W, Cha IH, Kim HJ. Deep learning-based survival prediction of oral cancer patients. *Sci Rep.* (2019) 9:6994. doi: 10.1038/s41598-019-43372-7
28. de Vries BCS, Hegeman JH, Nijmeijer W, Geerdink J, Seifert C, Groothuis-Oudshoorn CGM. Comparing three machine learning approaches to design a risk assessment tool for future fractures: predicting a subsequent major osteoporotic fracture in fracture patients with osteopenia and osteoporosis. *Osteoporosis Int.* (2021) 32:437–49. doi: 10.1007/s00198-020-05735-z
29. She Y, Jin Z, Wu J, Deng J, Zhang L, Su H, et al. Development and validation of a deep learning model for non-small cell lung cancer survival. *JAMA Network Open.* (2020) 3:e205842. doi: 10.1001/jamanetworkopen.2020.5842
30. Buuren S, Groothuis-Oudshoon K. Mice: multivariate imputation by chained equations in r. *J Stat Softw.* (2011):45:1–67. doi: 10.18637/jss.v045.i03
31. Ramsay IS, Ma S, Fisher M, Loewy RL, Ragland JD, Niendam T, et al. Model selection and prediction of outcomes in recent onset schizophrenia patients who undergo cognitive training. *Schizophr Res Cogn.* (2018) 11:1–5. doi: 10.1016/j.scog.2017.10.001
32. Feurer M, Jost T, Hutter F. Initializing bayesian hyperparameter optimization via meta-learning. In: *Proceedings of the Twenty-Ninth AAAI Conference on Artificial Intelligence*. Austin, Texas: AAAI Press (2015)
33. Ninomiya T, Perkovic V, Verdon C, Barzi F, Cass A, Gallagher M, et al. Proteinuria and stroke: a meta-analysis of cohort studies. *Am J Kidney Dis.* (2009) 53:417–25. doi: 10.1053/j.ajkd.2008.08.032
34. Santoro D, Gembillo G, Andò G. Glomerular filtration rate as a predictor of outcome in acute coronary syndrome complicated by atrial fibrillation. *J Clin Med.* (2020) 9:1466. doi: 10.3390/jcm9051466
35. Kaze AD, Santhanam P, Erqou S, Bertoni AG, Ahima RS, Echouffo-Tcheugui JB. Microvascular disease and cardiovascular outcomes among individuals with type 2 diabetes. *Diabetes Res Clin Pract.* (2021) 176:108859. doi: 10.1016/j.diabres.2021.108859
36. Lee HH, Lee H, Cho SMJ, Kim DW, Park S, Kim HC. On-treatment blood pressure and cardiovascular outcomes in adults with hypertension and left ventricular hypertrophy. *J Am Coll Cardiol.* (2021) 78:1485–95. doi: 10.1016/j.jacc.2021.08.015
37. Hou Y, Zhou Y, Hussain M, Budd GT, Tang WHW, Abraham J, et al. Cardiac risk stratification in cancer patients: a longitudinal patient-patient network analysis. *PLoS Med.* (2021) 18:e1003736. doi: 10.1371/journal.pmed.1003736
38. McGregor DE, Palarea-Albaladejo J, Dall PM, Hron K, Chastin S. Cox regression survival analysis with compositional covariates: application to modeling mortality risk from 24 h physical activity patterns. *Stat Methods Med Res.* (2020) 29:1447–65. doi: 10.1177/0962280219864125
39. Katzman JL, Shaham U, Cloninger A, Bates J, Jiang T, Kluger Y. Deepsurv: personalized treatment recommender system using a cox proportional hazards deep neural network. *BMC Med Res Methodol.* (2018) 18:e24. doi: 10.1186/s12874-018-0482-1
40. Rahman M, Hsu JY, Desai N, Hsu CY, Anderson AH, Appel LJ, et al. Central blood pressure and cardiovascular outcomes in chronic kidney disease. *Clin J Am Soc Nephrol.* (2018) 13:585–95. doi: 10.2215/CJN.08620817
41. Jiang W, Wang J, Shen X, Lu W, Wang Y, Li W, et al. Establishment and validation of a risk prediction model for early diabetic kidney disease based on a systematic review and meta-analysis of 20 cohorts. *Diabetes Care.* (2020) 43:925–33. doi: 10.2337/dc19-1897
42. Costantino S, Paneni F, Cosentino F. Aging, metabolism and cardiovascular disease. *J Physiol.* (2016) 594:2061–73. doi: 10.1113/JP270538
43. Picca A, Mankowski RT, Burman JL, Donisi L, Kim JS, Marzetti E, et al. Mitochondrial quality control mechanisms as molecular targets in cardiac aging. *Nat Rev Cardiol.* (2018) 15:543–54. doi: 10.1038/s41569-018-0059-z
44. Muntner P, Anderson A, Charleston J, Chen Z, Ford V, Makos G, et al. Hypertension awareness, treatment, and control in adults with ckd: results from the chronic renal insufficiency cohort (Cric) study. *Am J Kidney Dis.* (2010) 55:441–51. doi: 10.1053/j.ajkd.2009.09.014
45. Yan Z, Wang Y, Li S, Wang J, Zhang L, Tan H, et al. Hypertension control in adults with ckd in china: baseline results from the chinese cohort study of chronic kidney disease (C-Stride). *Am J Hypertens.* (2018) 31:486–94. doi: 10.1093/ajh/hpx222
46. Sarafidis PA Li S, Chen SC, Collins AJ, Brown WW, Klag MJ, et al. Hypertension awareness, treatment, and control in chronic kidney disease. *Am J Med.* (2008) 121:332–40. doi: 10.1016/j.amjmed.2007.11.025
47. McMullan CJ, Hickson DA, Taylor HA, Forman JP. Prospective analysis of the association of ambulatory blood pressure characteristics with incident chronic kidney disease. *J Hypertens.* (2015) 33:1939–46; discussion 46. doi: 10.1097/hjh.0000000000000638
48. Cheung AK, Rahman M, Reboussin DM, Craven TE, Greene T, Kimmel PL, et al. Effects of intensive BP control in CKD. *J Am Soc Nephrol.* (2017) 28:2812–23. doi: 10.1681/ASN.2017020148
49. Ding N, Sang Y, Chen J, Ballew SH, Kalbaugh CA, Salameh MJ, et al. Cigarette smoking, smoking cessation, and long-term risk of 3 major atherosclerotic diseases. *J Am Coll Cardiol.* (2019) 74:498–507. doi: 10.1016/j.jacc.2019.05.049
50. Staplin N, Haynes R, Herrington WG, Reith C, Cass A, Fellström B, et al. Smoking and adverse outcomes in patients with ckd: the study of heart and renal protection (Sharp). *Am J Kidney Dis.* (2016) 68:371–80. doi: 10.1053/j.ajkd.2016.02.052
51. Palmer SC, Mavridis D, Johnson DW, Tonelli M, Ruospo M, Strippoli GFM. Comparative effectiveness of calcimimetic agents for secondary hyperparathyroidism in adults: a systematic review and network meta-analysis. *Am J Kidney Dis.* (2020) 76:321–30. doi: 10.1053/j.ajkd.2020.02.439
52. Foley RN, Herzog CA, Collins AJ. Smoking and cardiovascular outcomes in dialysis patients: the united states renal data system wave 2 study. *Kidney Int.* (2003) 63:1462–7. doi: 10.1046/j.1523-1755.2003.00860.x
53. Jia C, Anderson JLC, Gruppen EG, Lei Y, Bakker SJL, Dullaart RPF, et al. High-density lipoprotein anti-inflammatory capacity

and incident cardiovascular events. *Circulation.* (2021) 143:1935–45. doi: 10.1161/CIRCULATIONAHA.120.050808
54. Barter P, Gotto AM, LaRosa JC, Maroni J, Szarek M, Grundy SM, et al. Hdl cholesterol, very low levels of Ldl cholesterol, and cardiovascular events. *N Engl J Med.* (2007) 357:1301–10. doi: 10.1056/NEJMoa064278
55. National Cholesterol Education Program (NCEP) Expert Panel on Detection, Evaluation, and Treatment of High Blood Cholesterol in Adults (Adult Treatment Panel III). Third report of the national cholesterol education program (Ncep) expert panel on detection, evaluation, and treatment of high blood cholesterol in adults (Adult Treatment Panel Iii) final report. *Circulation.* (2002) 106:3143–421. doi: 10.1161/circ.106.25.3143
56. Förhécz Z, Gombos T, Borgulya G, Pozsonyi Z, Prohászka Z, Jánoskuti L. Red cell distribution width in heart failure: prediction of clinical events and relationship with markers of ineffective erythropoiesis, inflammation, renal function, and nutritional state. *Am Heart J.* (2009) 158:659–66. doi: 10.1016/j.ahj.2009.07.024
57. Alonso N, Traveset A, Rubinat E, Ortega E, Alcubierre N, Sanahuja J, et al. Type 2 diabetes-associated carotid plaque burden is increased in patients with retinopathy compared to those without retinopathy. *Cardiovasc Diabetol.* (2015) 14:33. doi: 10.1186/s12933-015-0196-1
58. McCullough PA. Anemia of cardiorenal syndrome. *Kidney Int Suppl.* (2021) 11:35–45. doi: 10.1016/j.kisu.2020.12.001
59. Ohsawa M, Fujioka T, Ogasawara K, Tanno K, Okamura T, Turin TC, et al. High risks of all-cause and cardiovascular deaths in apparently healthy middle-aged people with preserved glomerular filtration rate and albuminuria: a prospective cohort study. *Int J Cardiol.* (2013) 170:167–72. doi: 10.1016/j.ijcard.2013.10.076

Conflict of Interest: The authors declare that the research was conducted in the absence of any commercial or financial relationships that could be construed as a potential conflict of interest.

Publisher's Note: All claims expressed in this article are solely those of the authors and do not necessarily represent those of their affiliated organizations, or those of the publisher, the editors and the reviewers. Any product that may be evaluated in this article, or claim that may be made by its manufacturer, is not guaranteed or endorsed by the publisher.

Copyright © 2022 Ren, Liu, Li, Duan, Dong and Liu. This is an open-access article distributed under the terms of the Creative Commons Attribution License (CC BY). The use, distribution or reproduction in other forums is permitted, provided the original author(s) and the copyright owner(s) are credited and that the original publication in this journal is cited, in accordance with accepted academic practice. No use, distribution or reproduction is permitted which does not comply with these terms.

frontiers | Frontiers in Cardiovascular Medicine

TYPE Original Research
PUBLISHED 07 September 2022
DOI 10.3389/fcvm.2022.964894

Check for updates

OPEN ACCESS

EDITED BY
Istvan Szokodi,
University of Pécs, Hungary

REVIEWED BY
Sorayya Malek,
University of Malaya, Malaysia
Ping Yan,
Central South University, China

*CORRESPONDENCE
Qingjie Wang
wang-qingjie@hotmail.com
Yuan Ji
jiyuan1213@aliyun.com
Ling Sun
sunling85125@hotmail.com

SPECIALTY SECTION
This article was submitted to Coronary Artery Disease, a section of the journal Frontiers in Cardiovascular Medicine

RECEIVED 09 June 2022
ACCEPTED 16 August 2022
PUBLISHED 07 September 2022

CITATION
Cai D, Xiao T, Zou A, Mao L, Chi B, Wang Y, Wang Q, Ji Y and Sun L (2022) Predicting acute kidney injury risk in acute myocardial infarction patients: An artificial intelligence model using medical information mart for intensive care databases.
Front. Cardiovasc. Med. 9:964894.
doi: 10.3389/fcvm.2022.964894

COPYRIGHT
© 2022 Cai, Xiao, Zou, Mao, Chi, Wang, Wang, Ji and Sun. This is an open-access article distributed under the terms of the Creative Commons Attribution License (CC BY). The use, distribution or reproduction in other forums is permitted, provided the original author(s) and the copyright owner(s) are credited and that the original publication in this journal is cited, in accordance with accepted academic practice. No use, distribution or reproduction is permitted which does not comply with these terms.

Predicting acute kidney injury risk in acute myocardial infarction patients: An artificial intelligence model using medical information mart for intensive care databases

Dabei Cai[1,2], Tingting Xiao[1], Ailin Zou[1], Lipeng Mao[1,2], Boyu Chi[1,2], Yu Wang[1], Qingjie Wang[1,2]*, Yuan Ji[1]* and Ling Sun[1,2]*

[1]Department of Cardiology, The Affiliated Changzhou No. 2 People's Hospital of Nanjing Medical University, Changzhou, China, [2]Graduate School of Dalian Medical University, Dalian Medical University, Dalian, China

Background: Predictive models based on machine learning have been widely used in clinical practice. Patients with acute myocardial infarction (AMI) are prone to the risk of acute kidney injury (AKI), which results in a poor prognosis for the patient. The aim of this study was to develop a machine learning predictive model for the identification of AKI in AMI patients.

Methods: Patients with AMI who had been registered in the Medical Information Mart for Intensive Care (MIMIC) III and IV database were enrolled. The primary outcome was the occurrence of AKI during hospitalization. We developed Random Forests (RF) model, Naive Bayes (NB) model, Support Vector Machine (SVM) model, eXtreme Gradient Boosting (xGBoost) model, Decision Trees (DT) model, and Logistic Regression (LR) models with AMI patients in MIMIC-IV database. The importance ranking of all variables was obtained by the SHapley Additive exPlanations (SHAP) method. AMI patients in MIMIC-III databases were used for model evaluation. The area under the receiver operating characteristic curve (AUC) was used to compare the performance of each model.

Results: A total of 3,882 subjects with AMI were enrolled through screening of the MIMIC database, of which 1,098 patients (28.2%) developed AKI. We randomly assigned 70% of the patients in the MIMIC-IV data to the training cohort, which is used to develop models in the training cohort. The remaining 30% is allocated to the testing cohort. Meanwhile, MIMIC-III patient data performs the external validation function of the model. 3,882 patients and 37 predictors were included in the analysis for model construction. The top 5 predictors were serum creatinine, activated partial prothrombin time, blood glucose concentration, platelets, and atrial fibrillation, (SHAP values are 0.670, 0.444, 0.398, 0.389, and 0.381, respectively). In the testing cohort, using top

20 important features, the models of RF, NB, SVM, xGBoost, DT model, and LR obtained AUC of 0.733, 0.739, 0.687, 0.689, 0.663, and 0.677, respectively. Placing RF models of number of different variables on the external validation cohort yielded their AUC of 0.711, 0.754, 0.778, 0.781, and 0.777, respectively.

Conclusion: Machine learning algorithms, particularly the random forest algorithm, have improved the accuracy of risk stratification for AKI in AMI patients and are applied to accurately identify the risk of AKI in AMI patients.

KEYWORDS

acute myocardia infarction, acute kidney injury, machine learning, random forest, area under the receiver operating characteristic curve

Introduction

Ischemic heart disease is a significant contributor to mortality in the global population, which is one of the leading causes of disability-adjusted life years (DALYs) in middle-aged and elderly patients (1). Acute myocardial infarction (AMI) is the most serious type of ischemic heart disease, which is one of the causes of Acute kidney injury (AKI) in patients. AKI occurs in a certain proportion of hospitalized patients with AMI. Studies have shown that the incidence of AKI during hospitalization in AMI patients ranges from 7.1 to 29.3% (2–4). The occurrence of AKI during hospitalization was independently associated with increased in-hospital mortality and long-term mortality post AMI (5–13). Several studies have also shown that AKI is associated with a significant increase in in-hospital mortality. Because there is unexpected and life-threatening characteristic of AMI, early identification of risk factors for AKI in patients with AMI is critical to improving overall prognosis, which can benefit patient management and overall treatment planning (14).

Machine learning is an important supporting technology for artificial intelligence. Machine learning is an algorithm that allows computers to "learn" automatically, analyze and construct models from data, and then use the models to make predictions for new samples. Machine learning predictive models are useful tools for identifying potential risk factors and predicting the occurrence of adverse events (15). In recent years, machine learning algorithms have been used increasingly in cardiovascular diseases. Combination with clinical big data, machine learning could help doctors predict risk accurately, therefore choose personalized medical treatment for patients. Than et al. developed a machine learning model and it could provide an individualized and objective assessment of the likelihood of myocardial infarction (16). Khera et al. reported three machine learning models which was developed with patients from the American College of Cardiology Chest Pain-MI Registry. They found that XGBoost and meta-classifier models offered improved prediction performance for high-risk individuals (17). Advanced machine learning methods were also used to predict the risk of tachyarrhythmia after AMI. The artificial neural network (ANN) model reached the highest accuracy rate, which is better than traditional risk scores (18). These studies indicated that machine learning is a reliable novel method for the clinic. Therefore, they broaden the new horizons for clinical researches.

MIMIC is a large, single-center, open-access database. MIMIC-III includes data on more than 58,000 admissions to Beth Israel Deaconess Medical Center in Boston from 2001 to 2012, including 38,645 adults and 7,875 newborns (19, 20). MIMIC-IV includes data from 524,740 admissions of 382,278 patients at the center from 2008 to 2019 (21, 22). The clinical records include demographic data, vital signs, laboratory test results, microbiological culture results, imaging data, treatment protocols, medication records, and survival information were recorded in MIMIC databases.

Due to the advantages of machine learning, we aim to develop machine learning models with AMI patients from Medical Information Mart for Intensive Care III and IV (MIMIC-III v1.4 and MIMIC-IV v1.0) databases to predict the risk of AKI.

Materials and methods

Data source

AMI patient data were extracted from the MIMIC-III v1.4 and MIMIC-IV v1.0 databases. The use of the MIMIC database was approved by the Institutional Review Board of the Beth Israel Deaconess Medical Center and Massachusetts Institute of Technology. We have obtained permission after application and completion of the course and test (record IDs: 44703031 and 44703032). Because all patient information in the database is anonymous, so informed consent was not required (23).

Patients enrollment and data collection

SQL (Structured Query Language) programming in Navicat Premium (version 15.0.12) was used for data extraction. ICD-9 (International Classification of Diseases, Ninth Revision) codes were used to identify patients with AMI, and Codes 41000–41092 were used to identify the patients with AMI. Exclusion criteria: (1) Patients who are younger than 18 years or older than 90 years; (2) Patients with deficient test results of serum creatinine and troponin; (3) Patients with missing data of more than 5% were excluded from the analysis. (4) Patients admitted to the hospital for a recurrent episode of AMI. We randomly assigned 70% of the patients in the MIMIC-IV data to the training cohort, which is used to develop models in the training cohort. The remaining 30% is allocated to the testing cohort. Meanwhile, MIMIC-III patient data performs the external validation function of the model.

After identifying eligible subjects, we collected clinical data including demographics, comorbidities, vital signs, and laboratory parameters. Comorbidities include Atrial Fibrillation (AF), Heart Failure (HF), Diabetes Mellitus (DM), Hypercholesterolemia, Hypertriglyceridemia, Hypertension, Respiratory Failure, Ventricular Tachycardia (VT), and Cardiogenic Shock. Vital signs collect the first recorded results at the time of hospitalization, including heart rate, respiratory rate, body temperature, arterial systolic blood pressure, arterial diastolic blood pressure, and mean blood pressure. Laboratory parameters were also obtained for the first time after admission. The research indicators are red blood cells (RBC), white blood cells (WBC), platelets, hemoglobin, glucose, hematocrit, blood urea nitrogen (BUN), creatinine, potassium, sodium, chloride, calcium, phosphorus, magnesium, bicarbonate, activated partial prothrombin time (APTT), prothrombin time (PT), International Normalized Ratio (INR), Creatine Kinase Isozyme-MB (CK-MB), Troponin-T (TNT).

Model construction and evaluation

Five machine learning models were constructed based on the features selected by the training cohort. The models used are: Decision Tree (DT) model, Support Vector Machine (SVM) model, Random Forest (RF) model, Naive Bayes (NB) model, and eXtreme Gradient Boosting (xGBoost) model. The 10-Fold cross-validation was used for model training. Among the five models, DT, SVM, RF, NB, and xGBoost are considered as the most common machine learning algorithms. DT (24) is very versatile machine learning model that can be used for both regression and classification. A decision tree is a tree-shaped structure in which each internal node represents a judgment on an attribute, each branch represents the output of a judgment result, and finally each leaf node represents a classification result. SVM (25) is a fast and dependable classification algorithm that performs very well with a limited amount of data. For classification, SVM works by creating a decision boundary in between our data points, that tries to separate it as best as possible. NB (26) is a model in a Bayesian classifier that trains a model with a dataset of known categories to achieve categorical judgment on data of unknown categories. The theoretical basis of NB is Bayesian decision theory. RF (27) is a kind of model that can be used both for regression and classification. It is one of the most popular ensemble methods, belonging to the specific category of bagging methods. This method can be described as techniques that use a group of weak learners together, in order to create a stronger, aggregated one. In our case, RF is an ensemble of many individual DT models. XGBoost (28) is an optimized distributed gradient boosting library designed to be highly efficient, flexible, and portable. It implements machine learning algorithms under the Gradient Boosting framework. The traditional logistic regression (LR) (29) model is also used for model construction. The nomogram (30) is used visualize regression models. and the calibration curve can be used as one of the evaluation indicators of the model. The calibration curve is used to evaluate the fit of the model (31). After the model is developed, data from the test cohort and validation cohort was used to further evaluate the performance of the model. The area under the receiver operating characteristic curve (AUC) and precision-recall curves was used to compare the performance of each model.

Study endpoint

The study endpoint was AKI during hospitalization, which is based on a comprehensive assessment by the glomerular filtration rate to reflect renal function at admission and the changes of serum creatinine levels after admission. Estimating Glomerular filtration rate (eGFR) by Modification of Diet in Renal Disease (MDRD) study equation at admission was calculated from first serum creatinine level and age (32). The calculation formula was showed as following: $(\text{eGFR}[\text{mL}/(\text{min}\cdot 1.73\ \text{m}^2) = 186\cdot(\text{Scr})^{-1.154}\cdot(\text{age})^{-0.203})$. The diagnosis of AKI was based on the latest international AKI clinical practice guidelines (33). The diagnostic criteria are met in any of the following three criteria: (a) increase in creatinine by $\geq$ 0.3 mg/dl ($\geq$26.5 μmol/l) within 48 h; (b) increase in creatinine to $\geq$ 1.5 times baseline, which is known or presumed to have occurred within the prior 7 days; (c) urine volume $<$ 0.5 ml/kg/h for 6 h.

Statistical analysis

In order to avoid excessive bias, the missing ratio of variables in this study was less than 5% and was imputed. Multiple imputation to account for missing data. The principle

of multiple imputation was roughly divided into several points. First, several data sets containing all the missing variables were generated. Second, these datasets were used to build several complementary models, usually using generalized linear models. Third, these models were integrated together and then the performance of the multiple complementary models was evaluated. Finally, the complete dataset was output (34, 35).

Frequency and percentage were used to describe the categorical variables, and the chi-square test or Fisher's exact test was used to identify differences between groups. The Shapiro-Wilk test was applied to continuous variables to confirm that they conformed to a normal distribution. All continuous variables in this study did not conform to a normal distribution and were described using the median and interquartile range (IQR), and the Mann–Whitney *U*-test was used to determine differences between different groups.

The training cohort consisted of 2,624 patients, including a heterogeneous sample of AKI and non-AKI patients, AKI patients accounted for only 29.4% of the entire cohort, whereas non-AKI patients accounted for 70.6% of the entire cohort. The proportions of these two categories are quite different, which may lead to lower prediction accuracy of the prediction model. Therefore, to solve the problem of classification imbalance, we used the synthetic minority oversampling technique (SMOTE) (36). The SMOTE method is an effective tool to solve the problem of data distribution imbalance. It is used in the training cohort to preprocess the data before the construction of the models.

The importance ranking of all variables was obtained by the SHapley Additive exPlanations (SHAP) method. SHAP could explain the output of any machine learning model. Its name came from the SHapley Additive exPlanation, inspired by cooperative game theory, SHAP constructed an additive explanatory model in which all features were considered as contributors. SHAP had a solid theoretical basis for achieving both local and global interpretability. The advantage of SHAP value was that it provided us not only SHAP values to evaluate feature importance, and it also showed us the positive or negative effects of the impact (37, 38).

R software (version 4.1.2) and Python software (version 3.10) were used for statistical analysis; GraphPad Prism (version 8.3.0) and Origin (version 9.1.0) was used to draw graphs; and $P < 0.05$ was considered statistically significant.

Results

Baseline characteristics

After applying the inclusion and exclusion criteria, 1,258 and 2,624 AMI patients were extracted from the MIMIC-III and MIMIC-IV database, respectively, and entered into the final analysis (**Figure 1**). In patients with AMI, the incidence of AKI was 25.8 and 29.4% in the MIMIC-III database and MIMIC-IV database, respectively. In the MIMIC-III group, there was no difference in the proportion of males in the AKI group and the non-acute kidney injury (non-AKI) group ($p = 0.79$), while the median age of the AKI group was significantly higher than that of the non-AKI group ($p < 0.001$). The proportion of males and median age in the AKI group were higher than those in the non-AKI group ($p < 0.05$, $p < 0.001$, respectively). Other baseline characteristics of the patients are shown in **Table 1**.

Feature selection for models

The SHAP graph group are shown in **Figure 2**, including single-sample feature influence map, feature distribution heat map under sample clustering, feature importance histogram, and feature density scatter plot. SHAP gives variables importance ranking, which relies on the xGBoost classification algorithm, and provides an intrinsic measure of the importance of each feature, called the Shap value (39). The top 5 predictors were serum creatinine, activated partial prothrombin time, blood glucose concentration, platelets, and atrial fibrillation (SHAP values are 0.670, 0.444, 0.398, 0.389, and 0.381, respectively). We then developed machine learning models which included top 5 variables, top 10 variables, top 15 variables, top 20 variables, top 25 variables, and all variables, respectively, according to the variable importance ranking.

Logistic regression model

A LR model was first developed that included the top 5 most important variables, creatinine, activated partial prothrombin time, glucose, platelets, and atrial fibrillation. The LR model was plotted the receiver operating characteristic (ROC) curve (**Figure 3**) in the training cohort, and the AUC was calculated to be 0.615 (**Figure 4**). Meanwhile, the Nomogram and the Calibration curves are shown in the training cohort, test cohort, and validation cohort (**Figure 3**). The LR model with all variables (LR-all) in training cohort achieved an AUC of 0.713, (95% CI: 0.693∼0.732) (**Figure 4**). Meanwhile, the LR-all model in test cohort, achieved an AUC of 0.694 (95% CI: 0.656∼0.733) (**Supplementary Figure 1**). In the validation cohort, the AUC of the LR model with top 20 variables (LR-20) performed best in validation cohort (with an AUC of 0.686, 95%CI: 0.653∼0.720) (**Figure 5**).

Machine learning models in the training cohort

Five machine learning models including RF, NB, SVM, xGBoost, DT were then developed. According to the order

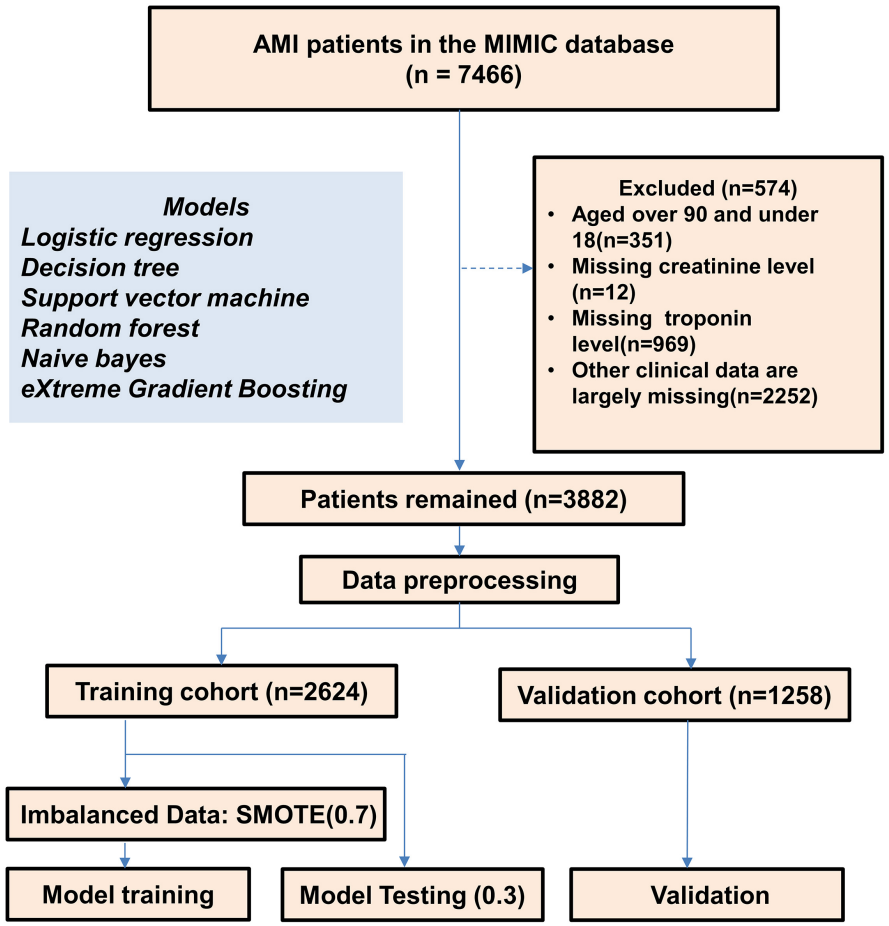


FIGURE 1
Flow diagram of the selection process of patients.

of variable importance, top 5 variables, top 10 variables, top 15 variables, top 20 variables, top 25 variables and models including all variables were successively developed. The machine learning models of using top 5 important features in training cohort were as follows: the RF model (RF-5), with an AUC of 1 (95% CI: 1); the NB model (NB-5), with an AUC of 0.744, (95% CI: 0.725∼0.763); the SVM model (SVM-5), with an AUC of 0.750 (95% CI: 0.730∼0.769); the xGBoost model (xGBoost-5), with an AUC of 1 (95% CI: 1); the DT model (DT-5), with an AUC of 0.682 (95% CI: 0.662∼0.703). All machine learning models outperformed the LR model in the training cohort. The RF-5 model and xGBoost-5 performed the best of all machine learning models. The DT-5 model has the worst performance. NB-5 and SVM-5 perform well in the training cohort. The SVM-5 model outperforms the NB-5 model. We gradually increased the number of included variables to develop different machine learning models. The ROC curves are shown for each model in the training cohort (Figure 4). The performances of all of the models are shown in the training cohort (Figure 4), and statistics for all models in the training cohort are shown in Supplementary Tables 1–6. There are, as the number of variables increased, dynamic plot of the area under the ROC curve for all machine learning models in training cohort (Figure 6).

Machine learning models in the test cohort

The other 30% of the data in MIMIC-IV is used as a test cohort to test the performance of each machine learning model. The machine learning models of the variable importance top 5 in test cohort were as follows: the RF-5 model, with an AUC of 0.696 (95% CI: 0.658∼0.734); the NB-5 model, with an AUC of 0.724 (95% CI: 0.687∼0.762); the SVM-5 model, with an AUC of 0.718 (95% CI: 0.680∼0.756); the xGBoost-5 model, with an AUC of 0.666 (95% CI: 0.626∼0.706); the DT-5 model, with an AUC of 0.663 (95% CI: 0.622∼0.704). The performance of the five machine learning models in the test cohort is better than that of the NB model, and the AUC of LR model with

TABLE 1 Baseline characteristics.

	MIMIC III (*n* = 1,258)			MIMIC IV (*n* = 2,624)		
	Non-AKI (*n* = 933)	AKI (*n* = 325)	*P*-value	Non-AKI (*n* = 1,851)	AKI (*n* = 773)	*P*-value
Demographic						
Male (*n*%)	639 (68.5%)	220 (67.7%)	0.79	1,164 (62.9%)	518 (67.0%)	0.045
Age (year)	65.1 [55.3,75.4]	69.2 [58.7,78.4]	<0.001	67.0 [57.0,75.0]	71.0 [61.0,78.0]	<0.001
Vital signs						
Heart rate (min^{-1})	83.0 [72.0,95.0]	87.0 [73.0,100.0]	<0.05	83.0 [73.0,95.0]	86.0 [74.0,100]	<0.001
Temperature (°C)	36.5 [36.0,36.8]	36.5 [35.9,37.1]	0.548	36.6 [36.4,36.8]	36.6 [36.3,36.9]	0.789
Respiratory rate (min^{-1})	17.0 [15.0,21.0]	19.0 [15.0,22.0]	<0.05	18.0 [15.0,22.0]	19.0 [16.0,24.0]	<0.001
ASP (mmHg)	119.8 [106.0,134.0]	116.0 [101.0,133.0]	0.055	118.0 [105.0,134.0]	113 [101.0,131.0]	<0.001
ADP (mmHg)	61.0 [52.0,70.0]	59.0 [50.0,68.0]	<0.05	66.0 [56.0,76.0]	61.0 [53.0,72.0]	<0.001
MAP (mmHg)	78.0 [68.0,88.0]	75.0 [66.0,84.0]	<0.05	80.0 [71.0,91.0]	77.0 [69.0,87.0]	<0.001
Laboratory results						
RBC (m/uL)	4.2 [3.8,4.7]	3.9 [3.4,4.5]	<0.001	4.0 [3.4,4.5]	3.8 [3.2,4.3]	<0.001
WBC (k/uL)	11.0 [8.7,14.7]	12.2 [8.4,15.2]	0.088	10.5 [8.0,13.7]	11.1 [8.0,15.8]	<0.05
Platelet (k/uL)	239.0 [194.0,297.5]	222.0 [175.0,292.5]	<0.05	211.0 [165.0,265.0]	197.0 [153.5,250.0]	<0.001
Hemoglobin (g/dL)	13.0 [11.4,14.4]	12.1 [10.4,13.6]	<0.001	12.0 [10.1,13.7]	11.2 [9.7,13.0]	<0.001
Hematocrit (%)	37.8 [34.0,41.6]	36.0 [31.3,40.0]	<0.001	36.5 [31.1,40.6]	34.9 [30.2,39.5]	<0.001
Glucose (mg/dL)	140.0 [114.0,187.0]	155.0[118.0,230.5]	<0.001	133.0 [109.0,178.0]	148.0 [113.0,203.0]	<0.001
BUN (mg/dL)	18.0 [14.0,26.0]	25.0 [17.0,37.0]	<0.001	19.0 [14.0,32.0]	25.0 [18.5,39.0]	<0.001
Potassium (mEq/L)	4.1 [3.8,4.5]	4.3 [3.9,4.7]	<0.001	4.2 [3.9,4.5]	4.3 [3.9,4.6]	<0.05
Sodium (mEq/L)	139.0 [136.0,140.0]	138.0 [135.0,140.0]	0.083	138.0 [136.0,140.0]	138.0 [135.0,141.0]	0.858
Chloride (mEq/L)	103.0 [100.0,106.0]	102.0 [101.0,107.0]	0.353	103.0 [99.0,105.0]	103.0 [99.0,105.0]	0.613
Calcium (mg/dL)	8.6 [8.2,9.1]	8.4 [7.9,8.9]	<0.001	8.7 [8.2,9.1]	8.5 [8.0,9.0]	<0.001
Magnesium (mg/dL)	1.9 [1.7,2.1]	1.9 [1.7,2.1]	0.468	2.0 [1.8,2.1]	2.0 [1.8,2.2]	0.900
Phosphate (mg/dL)	3.4 [2.9,4.0]	3.6[3.0,4.5]	<0.001	3.6 [3.0,4.2]	3.8 [3.2,4.6]	<0.001
Bicarbonate (mEq/L)	23.0 [21.0,26.0]	23.0 [20.0,25.0]	<0.05	23.0 [21.0,25.0]	22.0 [19.0,25.0]	<0.001
APTT (s)	31.6 [26.1,55.4]	35.2 [27.6,59.2]	<0.05	35.6 [28.8,55.5]	39.4 [29.4,65.2]	<0.05
INR	1.2 [1.1,1.3]	1.2 [1.1,1.4]	<0.05	1.2 [1.1,1.3]	1.2 [1.1,1.4]	<0.001
PT (s)	13.4 [12.5,14.6]	13.5 [12.8,15.0]	<0.05	12.7 [11.7,14.6]	13.3 [12.1,15.8]	<0.001
CK-MB (ng/mL)	32.0 [8.0,94.5]	26.0 [8.0,97.0]	0.633	20.0 [6.0,71.0]	18.0 [5.0,69.1]	0.431
TNT (ng/mL)	1.0 [0.8,4.0]	1.5[0.2,5.5]	<0.05	0.5 [0.1,2.3]	0.5 [0.1,2.3]	0.978
Creatinine (mg/dL)	1.0[0.8,1.3]	1.3 [0.9,1.6]	<0.001	1.0 [0.8,1.5]	1.4 [1.0,1.9]	<0.001
GFR [mL/(min·1.73 m^2)]	74.8 [55.8,95.8]	56.3 [38.1,82.7]	<0.001	72.0 [44.7,99.3]	52.1 [33.5,75.9]	<0.001
Comorbidities (*n*%)						
HF (*n*%)	327 (35.0%)	154 (47.4%)	<0.001	218 (11.8%)	100 (12.9%)	0.407
Cardiogenic shock (*n*%)	132 (14.1%)	85 (26.2%)	<0.001	85 (4.6%)	82 (10.4%)	<0.001
Atrial fibrillation (*n*%)	189 (19.9%)	110 (33.8%)	<0.001	501 (27.1%)	325 (42.0%)	<0.001
Hypertension (*n*%)	467 (50.1%)	144 (44.3%)	0.074	339 (18.3%)	96 (12.4%)	<0.001
Hyperlipidemia (*n*%)	273 (29.3%)	77(23.7%)	0.054	1,003 (54.2%)	339 (51.6%)	0.229
Hypercholesterolemia (*n*%)	154 (16.5%)	34 (10.5%)	<0.05	90 (4.9%)	39 (5.0%)	0.843
Respiratory failure (*n*%)	107 (11.5%)	72 (22.2%)	<0.001	70 (3.8%)	39 (5.0%)	0.162
DM (*n*%)	188 (20.2%)	86 (26.5%)	0.018	171 (9.2%)	77 (10.0%)	0.559
Ventricular tachycardia (*n*%)	119 (12.8%)	47 (14.5%)	0.434	90 (4.9%)	73 (9.4)	<0.001

Continuous variables are presented as the median and interquartile range (IQR). Counting data are presented as numbers and percentages. ASP, arterial systolic pressure; ADP, diastolic arterial pressure; MAP, mean arterial pressure; RBC, red blood cell; WBC, white blood cell; BUN, blood urea nitrogen; APTT, activated partial prothrombin time; INR, International Normalized Ratio; PT, prothrombin time; CK-MB, Creatine Kinase Isozyme-MB; TNT, Troponin-T; GFR, Glomerular Filtration Rate; HF, Heart Failure; DM, Diabetes Mellitus.

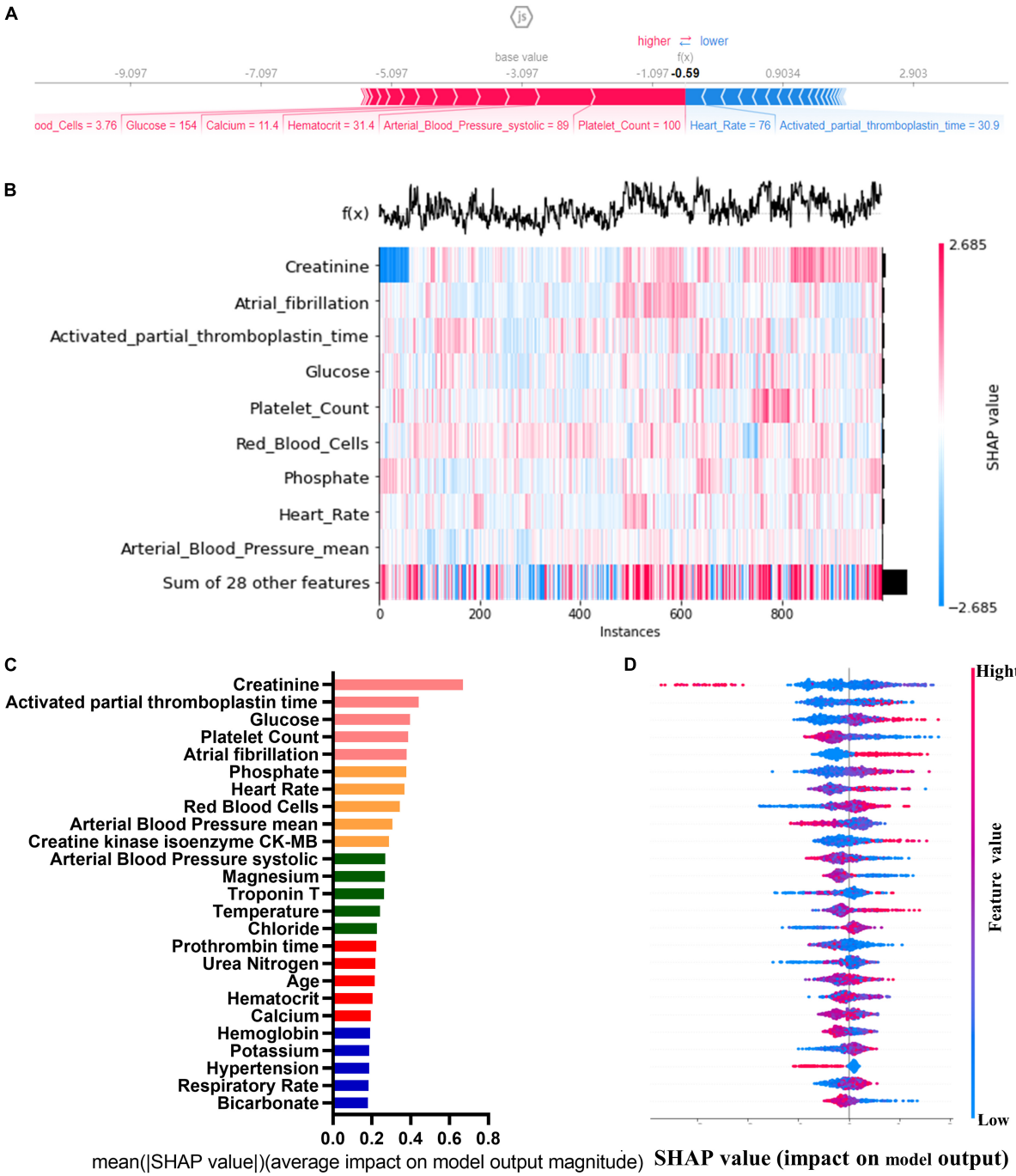


FIGURE 2
Single-sample feature impact map **(A)**; heat map of feature distribution under sample clustering **(B)**; histogram of feature importance **(C)**; scatter plot of feature density **(D)**.

top 5 variables (LR-5) has only 0.652 in the test cohort. The NB model is the best performer of all machine learning models in the test cohort. The NB model performed best when the variable importance top 20 variables were added to the model (AUC for NB-20 model: 0.739, 95% CI: 0.702∼0.776). The worst performing model is DT model with top 20 variables (AUC for DT-20 model: 0.663, 95% CI: 0.622∼0.704). xGBoost model performed general in the test cohort and their AUC increased when more variables were added (AUC for xGBoost-20 model: 0.689, 95% CI: 0.650∼0.728). But, the AUC of SVM model not increased when more variables were added (SVM-20 model: 0.687, 95% CI: 0.647∼0.727). And outperformed

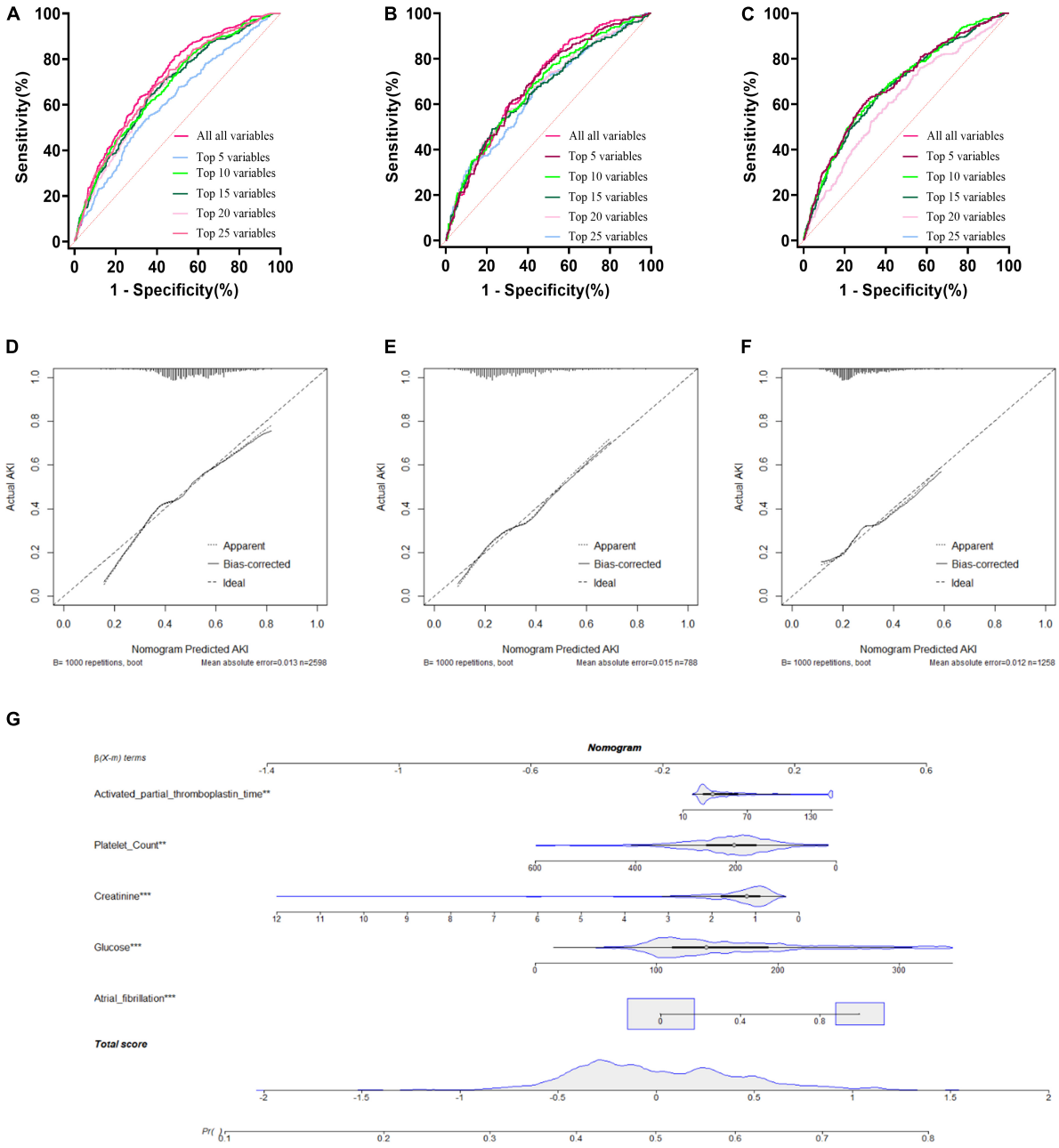


FIGURE 3
Logistic Regression model with different variables ROC curves; training cohort **(A)**; test cohort **(B)**; validation cohort **(C)**. Logistic Regression model calibration curve; training cohort **(D)**; test cohort **(E)**; validation cohort **(F)**. Logistic Regression model Nomogram **(G)**.

the RF-20 model (AUC for RF-20 model: 0.733, 95% CI: 0.695∼0.770). The ROC curves are shown for each model (**Supplementary Figure 1**). The performances of all models are shown in the test cohort (**Supplementary Figure 1**). Statistical measures of the performance of all models in the test cohort are shown in **Supplementary Tables 7–12**. There are, as the number of variables increased, dynamic plot of the area under the ROC curve for all machine learning models in test cohort (**Figure 6**).

Machine learning models in the validation cohort

Externally validated in a validation cohort of 1,258 cases, among all developed machine learning models, the RF model performed the best, followed by xGBoost, and the worst performing model was DT. The RF models were as follows in the external validation cohort: the RF-5 model, with an AUC of

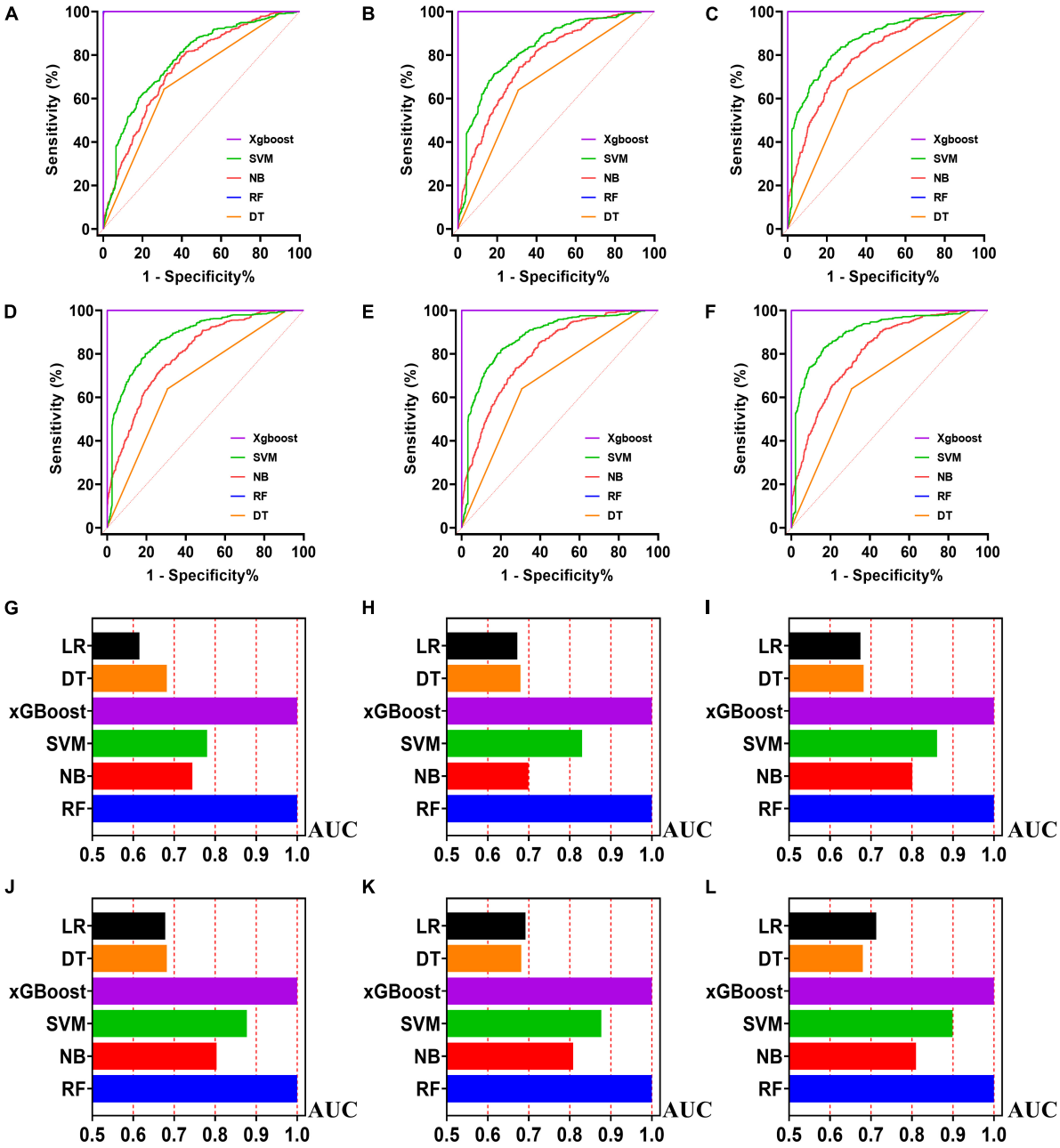


FIGURE 4
The ROC curves for machine learning models and the performances of all models in test cohort. The X-axis in 4G-4L represents the AUC values of each model. Top 5 variables **(A,G)**; top 10 variables **(B,H)**; top 15 variables **(C,I)**; top 20 variables **(D,J)**; top 25 variables **(E,K)**; models for all variables **(F,L)**.

0.711 (95% CI: 0.678∼0.744); the RF model with top 10 variables (RF-10), with an AUC of 0.754 (95% CI: 0.722∼0.786); the RF model with top 15 variables (RF-15), with an AUC of 0.778, (95% CI: 0.747∼0.808); the RF-20 model, with an AUC of 0.781, (95% CI: 0.750∼0.811); the RF model with top 25 variables (RF-25), with an AUC, 0.777 (95% CI: 0.746∼0.807); the RF model with all variables (RF-all), with an AUC of 0.770 (95% CI: 0.740∼0.801). The AUC of DT model with all variables (DT-all) in the validation cohort was 0.637 (95% CI: 0.602∼0.672). The AUC of LR-all was 0.686 (95% CI: 0.653∼0.720) in the validation cohort. The ROC curves are shown for each model (Figure 5). The performances of all models are shown in the validation cohort (Figure 5), and statistical measures of the performance for the variable importance top20 models in the validation

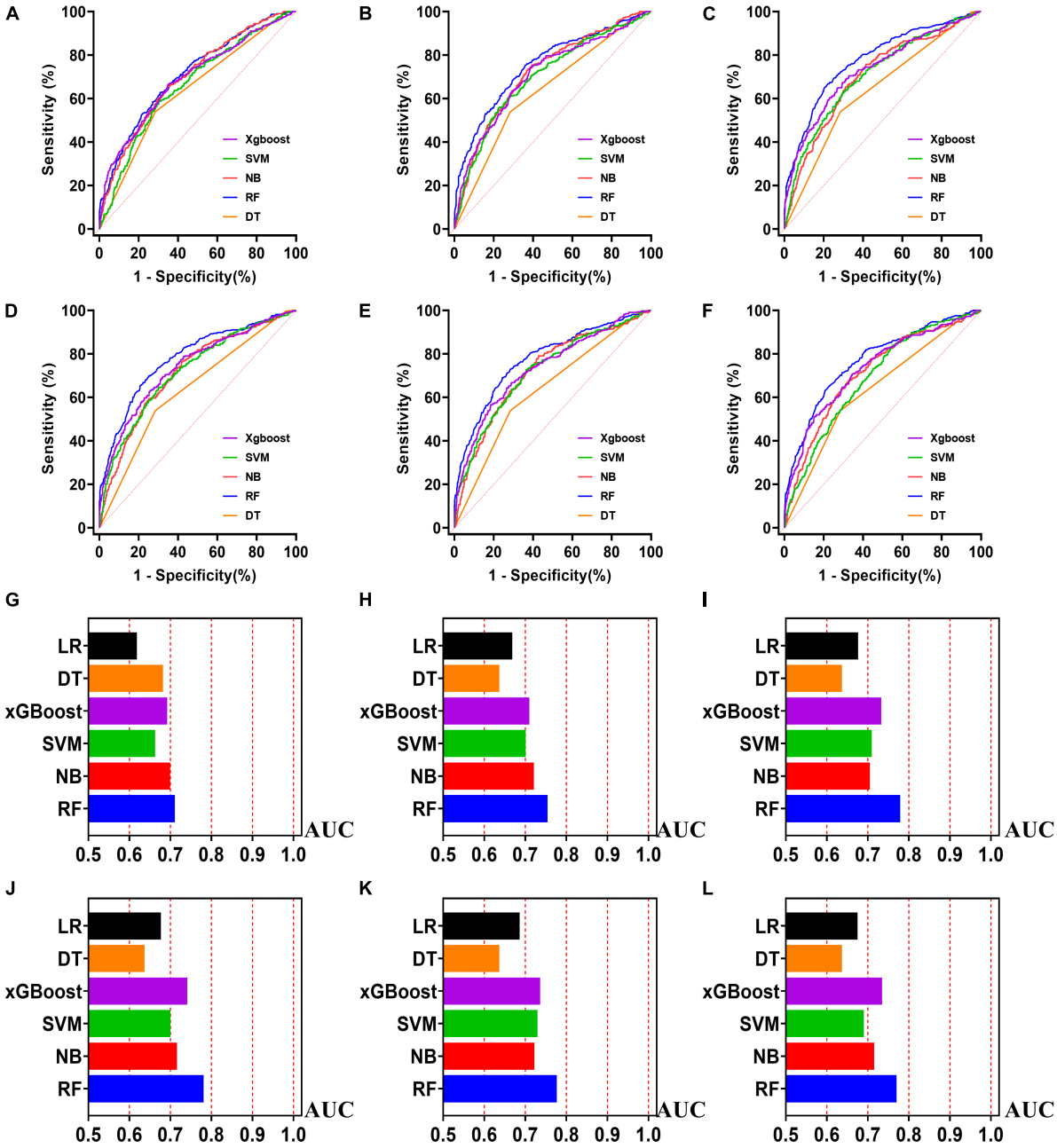


FIGURE 5
The ROC curves for machine learning models and the performances of all models in validation cohort. The X-axis in 5G-5L represents the AUC values of each model. Top 5 variables **(A,G)**; top 10 variables **(B,H)**; top 15 variables **(C,I)**; top 20 variables **(D,J)**; top 25 variables **(E,K)**; models for all variables **(F,L)**.

cohort (Table 2). Statistical measures of performance of other models are shown in the validation (Supplementary Tables 13–17). Meanwhile, there are, as the number of variables increased, dynamic plot of the area under the ROC curve for all machine learning models in validation cohort (Figure 6). Precision-recall curves of the six models with different variables in the validation cohort were showed in Supplementary Figures 2–7. The area under the precision-recall curves of each model was calculated. Consistent with the AUC values, it indicated that random forest outperformed the other five models in the validation cohort. Moreover, an application software program based on the top 20 predictors were developed for evaluating the risk of AKI. The AKI probability of each patient could be calculated after the patient was admitted to hospital (Figure 7).

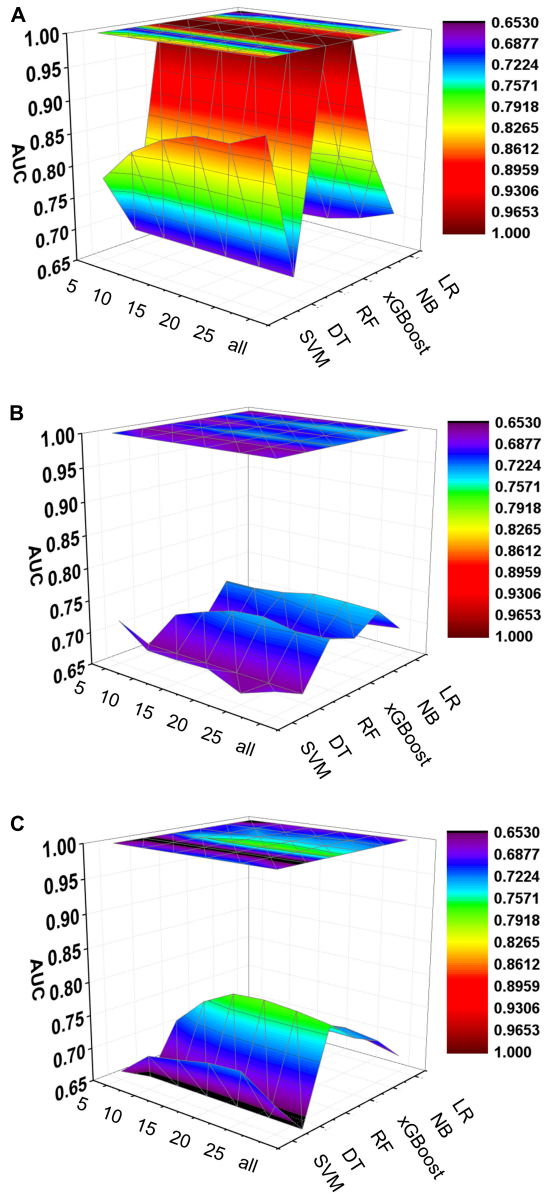


FIGURE 6
Dynamic plot of the area under the ROC curve for all machine learning models; training cohort **(A)**; test cohort **(B)**; validation cohort **(C)**. The x-axis represents the number of variables included in the model, the y-axis represents different kinds of models, and the z-axis represents the AUC values of each model.

Discussion

This study identified various clinical features associated with the risk of AKI in patients with AMI. Using a sophisticated machine learning approach, we found that creatinine, blood urea nitrogen, atrial fibrillation, glucose and hemoglobin were considered as the most important five features with AKI in patients with AMI. Among the six models, the RF model has the best performance with an AUC of 0.781 for the RF-20 model in the external validation cohort. The results of this study showed that the occurrence of AKI in patients with AMI was 28.2%. Compared with previously reported studies, the incidence of in-hospital AKI in patients with AMI reported in this study is close to the upper limit of normal (2–4). The possible reasons are follows; (a) firstly, we excluded patients with more than 5% missing data, which resulted in fewer hospitalizations for AMI overall and ultimately led to a higher incidence of AKI; (b) secondly, the median age of patients in each group was high (>65 years) for both MIMIC-III and MIMIC-IV, which suggest that general condition of our study population is not very optimistic, and they have poor resistance to injury.

Early identification of AKI in patients admitted for AMI improves overall outcomes (19). Therefore, identifying risk factors for AKI in patients with AMI can help to identify high-risk patients and to make appropriate clinical decisions. With the development of machine learning algorithms, the number of predictors that can be processed has largely been enriched. Therefore, advanced machine learning techniques allow researchers to develop more optimized models compared to traditional models (40). With such a model, cardiologists can be alerted in advance when a patient is admitted to the hospital with an AMI.

Zhou et al. reported a risk model for AKI prediction in AMI patients with LR analysis. The model calibrated well and performed better than traditional risk scores (41). With the development of concepts such as real-world research and precision treatment, the demand for medical big data processing by scientific researchers is increasing. Machine learning technology had a unique advantage in processing massive and high-dimensional data and conducting predictive evaluation, so in recent years, the application of machine learning method in the medical field had been deepening. Sun et al. developed several machine learning models and found that random forest model out performed outperformed LR in every comparison (36). Random forest methods improved the accuracy of AKI risk stratifying in AMI patients. The sample size of this study was relatively small and this was a single-center study, so we tried to explore a more robust AKI risk prediction model with a larger sample size from another canter. This study is an example of how machine learning methods works for evaluating AKI risk in AMI patients. Similarly, machine learning algorithms can be applied to other risk assessments of AMI patients, such as the risk of all-cause mortality, the risk of cardiac mortality and the incidence of major adverse cardiac event (MACE). The association between the risk factors and the risk of AKI is established by using artificial intelligence, and indicators such as patients' vital signs and laboratory test results are matched with AKI risks, which helps to improve the risk perception and recognition ability of the model. This innovative approach to risk assessment helps clinicians benefit from better individualized treatment decisions.

TABLE 2 The performance of six models containing the top 20 importance variables.

Model	AUC (CI 95%)	Accuracy	Sensitivity	Specificity
Support Vector Machine	0.720 (0.687~0.753)	0.684	0.697	0.646
Decision Trees	0.637 (0.602~0.672)	0.670	0.716	0.538
Random Forests	0.781 (0.750~0.811)	0.735	0.748	0.698
eXtreme Gradient Boosting	0.741 (0.708~0.773)	0.682	0.678	0.695
Naive Bayes	0.716 (0.684~0.749	0.628	0.582	0.763
Logistic regression	0.686 (0.653~0.720)	0.694	0.743	0.550

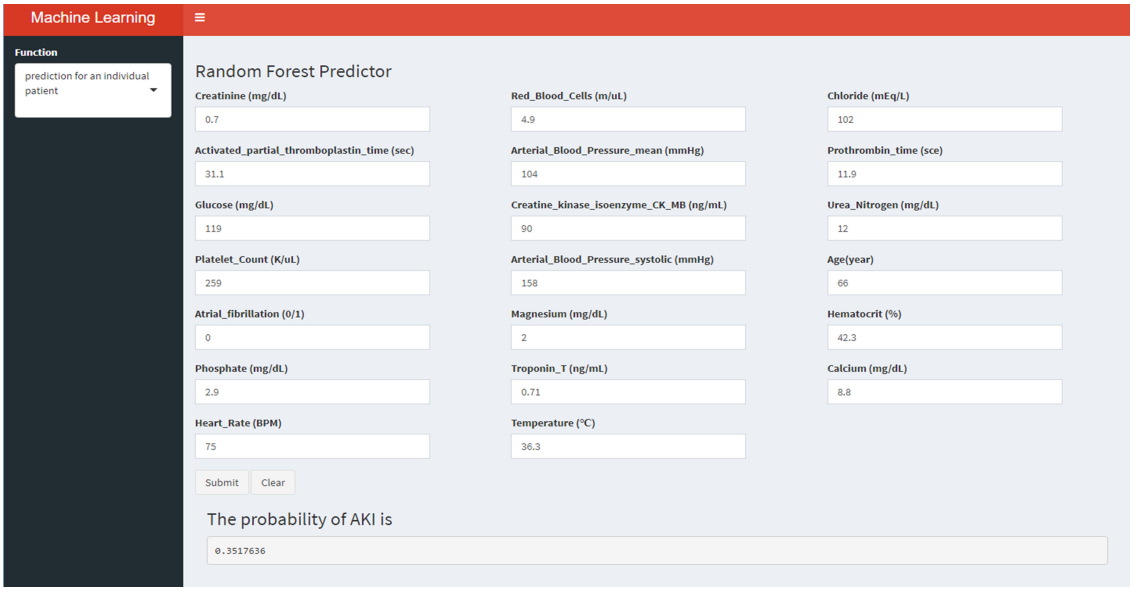


FIGURE 7
An example of the application software for predicting AKI risk in AMI patients.

In the present study, we used advanced statistical methods and specially processed data. The former includes five machine learning algorithm development models and traditional LR development models, with the 70% subset used for training cohort, and the 30% subset used for internal testing. Meanwhile, the data in MIMIC-III were used external validation and the ROCs to evaluate the models (28). Although there are many ways to filter the importance of variables, such as Boruta Algorithm and LASSO Regression (36, 42), SHAP method was used in the present study for feature selection. SHAP method not only shows the contribution of all features to the model output at the macro level with the feature density scatter plot, feature importance SHAP value and feature distribution heat map under sample clustering, but also shows the model output at the micro level through a single sample feature influence map (43, 44). Machine learning techniques help doctors analyze large amounts of information and are critical in optimizing medical practice. The latter is that we used the data in MIMIC-IV, the training and test cohort, to create a new dataset with a 1:1 ratio of AKI to non-AKI, addressing the imbalance of samples.

MIMIC, a high-quality database with a large sample size, was used in this study. There are several advantages for using the database. (a) Firstly, it is one of the few critical care databases that is freely accessible. (b) Secondly, the dataset spans more than a decade and contains a wealth of detailed information on patient care. (c) Thirdly, once the data usage agreement is accepted, the investigator's analysis is not subject to limitations, thereby enabling clinical research and education around the world. (d) Finally, data can be downloaded from multiple sources (45).

There are also some limitations in our study. Firstly, our model was developed retrospectively based on a single-center database. Missing data and input errors exist, such as C-reactive protein and N-terminal pro-brain natriuretic peptide, despite the very high quality of the MIMIC databases. Therefore, prospective validation of our model in another cohort is still required in the future (46, 47). Secondly, we trained the model and tested it using synthetic datasets due to the severe class imbalance of the extracted datasets, which could have led to, in the training cohort, over fitting of models cannot be

avoided and an overly optimistic assessment of its performance (48). Thirdly, this study only focused on the incidence of AKI during hospitalization, while other important prognostic indicators such as long-term mortality after discharge still require further investigation.

Conclusion

We have developed several machine learning prediction models based on the MIMIC database. Among them, the RF model has good performance and can be used to guide clinical practice.

Data availability statement

The datasets presented in this study can be found in online repositories. The names of the repository/repositories and accession number(s) can be found below: https://physionet.org/content/mimiciii-demo/1.4/ and https://physionet.org/content/mimiciv/1.0/.

Ethics statement

The studies involving human participants were reviewed and approved by the Beth Israel Women's Deaconess Medical Center and the MIT Institutional Review Board. The ethics committee waived the requirement of written informed consent for participation.

Author contributions

DC analyzed the data and wrote the manuscript. TX and YW collect the data. LM, AZ, and BC checked the integrity of the data and the accuracy of the data analysis. LS, QW, and YJ co-designed and revised the article. All authors read and approved the final manuscript.

Funding

This study was supported by grants from Young Talent Development Plan of Changzhou Health Commission (CZQM2020060), the National Natural Science Foundation of China (Grant No. 81901410), the Natural Science Foundation of Jiangsu Province (BK20221229), the Technology Development Fund of Nanjing Medical University (NMUB2020069), and the Changzhou Sci&Tech Program (Grant No. CJ20210059 and CE20225051).

Conflict of interest

The authors declare that the research was conducted in the absence of any commercial or financial relationships that could be construed as a potential conflict of interest.

Publisher's note

All claims expressed in this article are solely those of the authors and do not necessarily represent those of their affiliated organizations, or those of the publisher, the editors and the reviewers. Any product that may be evaluated in this article, or claim that may be made by its manufacturer, is not guaranteed or endorsed by the publisher.

Supplementary material

The Supplementary Material for this article can be found online at: https://www.frontiersin.org/articles/10.3389/fcvm.2022.964894/full#supplementary-material

References

1. GBD 2019 Diseases and Injuries Collaborators. Global burden of 369 diseases and injuries in 204 countries and territories, 1990-2019: a systematic analysis for the global burden of disease study 2019. *Lancet.* (2020) 396:1204–22. doi: 10.1016/S0140-6736(20)30925-9

2. Shacham Y, Leshem-Rubinow E, Steinvil A, Assa EB, Keren G, Roth A, et al. Renal impairment according to acute kidney injury network criteria among ST elevation myocardial infarction patients undergoing primary percutaneous intervention: a retrospective observational study. *Clin Res Cardiol.* (2014) 103:525–32. doi: 10.1007/s00392-014-0680-8

3. Tsai TT, Patel UD, Chang TI, Kennedy KF, Masoudi FA, Matheny ME, et al. Contemporary incidence, predictors, and outcomes of acute kidney injury in patients undergoing percutaneous coronary interventions: insights from the NCDR Cath-PCI registry. *JACC Cardiovasc Interv.* (2014) 7:1–9. doi: 10.1016/j.jcin.2013.06.016

4. Hwang SH, Jeong MH, Ahmed K, Kim MC, Cho KH, Lee MG, et al. Different clinical outcomes of acute kidney injury according to acute kidney injury network criteria in patients between ST elevation and non-ST elevation myocardial infarction. *Int J Cardiol.* (2011) 150:99–101. doi: 10.1016/j.ijcard.2011.03.039

5. Chertow GM, Normand SL, Silva LR, McNeil BJ. Survival after acute myocardial infarction in patients with end-stage renal disease: results from the cooperative cardiovascular project. *Am J Kidney Dis.* (2000) 35:1044–51.

6. Parikh CR, Coca SG, Wang Y, Masoudi FA, Krumholz HM. Long-term prognosis of acute kidney injury after acute myocardial infarction. *Arch Intern Med.* (2008) 168:987–95.

7. Goldberg A, Hammerman H, Petcherski S, Zdorovyak A, Yalonetsky S, Kapeliovich M, et al. Inhospital and 1-year mortality of patients who develop worsening renal function following acute ST-elevation myocardial infarction. *Am Heart J.* (2005) 150:330–7. doi: 10.1016/j.ahj.2004.09.055

8. Akhter MW, Aronson D, Bitar F, Khan S, Singh H, Singh RP, et al. Effect of elevated admission serum creatinine and its worsening on outcome in hospitalized patients with decompensated heart failure. *Am J Cardiol.* (2004) 94:957–60. doi: 10.1016/j.amjcard.2004.06.041

9. Hoste EA, Lameire NH, Vanholder RC, Benoit DD, Decruyenaere JM, Colardyn FA. Acute renal failure in patients with sepsis in a surgical ICU: predictive factors, incidence, comorbidity, and outcome. *J Am Soc Nephrol.* (2003) 14:1022–30. doi: 10.1097/01.asn.0000059863.48590.e9

10. de Mendonça A, Vincent JL, Suter PM, Moreno R, Dearden NM, Antonelli M, et al. Acute renal failure in the ICU: risk factors and outcome evaluated by the SOFA score. *Intensive Care Med.* (2000) 26:915–21.

11. Thakar CV, Worley S, Arrigain S, Yared JP, Paganini EP. Influence of renal dysfunction on mortality after cardiac surgery: modifying effect of preoperative renal function. *Kidney Int.* (2005) 67:1112–9.

12. Forman DE, Butler J, Wang Y, Abraham WT, O'Connor CM, Gottlieb SS, et al. Incidence, predictors at admission, and impact of worsening renal function among patients hospitalized with heart failure. *J Am Coll Cardiol.* (2004) 43:61–7.

13. Lassnigg A, Schmidlin D, Mouhieddine M, Bachmann LM, Druml W, Bauer P, et al. Minimal changes of serum creatinine predict prognosis in patients after cardiothoracic surgery: a prospective cohort study. *J Am Soc Nephrol.* (2004) 15:1597–605.

14. Wang C, Pei YY, Ma YH, Ma XL, Liu ZW, Zhu JH, et al. Risk factors for acute kidney injury in patients with acute myocardial infarction. *Chin Med J (Engl).* (2019) 132:1660–5.

15. Moll M, Qiao D, Regan EA, Hunninghake GM, Make BJ, Tal-Singer R, et al. Machine learning and prediction of all-cause mortality in COPD. *Chest.* (2020) 158:952–64.

16. Than M, Pickering J, Sandoval Y, Shah A, Tsanas A, Apple F, et al. Machine learning to predict the likelihood of acute myocardial infarction. *Circulation.* (2019) 140:899–909.

17. Khera R, Haimovich J, Hurley NC, McNamara R, Spertus JA, Desai N, et al. Use of machine learning models to predict death after acute myocardial infarction. *JAMA Cardiol.* (2021) 6:633–41.

18. Wang S, Li J, Sun L, Cai J, Wang S, Zeng L, et al. of machine learning to predict the occurrence of arrhythmia after acute myocardial infarction. *BMC Med Inform Decis Mak.* (2021) 21:301. doi: 10.1186/s12911-021-01667-8

19. Zhao Y, Zhou H, Tan W, Song Y, Qiu Z, Li S, et al. Prolonged dexmedetomidine infusion in critically ill adult patients: a retrospective analysis of a large clinical database multiparameter intelligent monitoring in intensive care III. *Ann Transl Med.* (2018) 6:304. doi: 10.21037/atm.2018.07.08

20. Wang B, Li D, Gong Y, Ying B, Cheng B. Association of serum total and ionized calcium with all-cause mortality incritically ill patients with acute kidney injury. *Clin Chim Acta.* (2019) 494:94–9. doi: 10.1016/j.cca.2019.03.1616

21. Zhang L, Wang Z, Xu F, Han D, Li S, Yin H, et al. Effects of stress hyperglycemia on short-term prognosis of patients without diabetes mellitus in coronary care unit. *Front Cardiovasc Med.* (2021) 8:683932. doi: 10.3389/fcvm.2021.683932

22. Wu WT, Li YJ, Feng AZ, Li L, Huang T, Xu AD, et al. Data mining in clinical big data: the frequently used databases, steps, and methodological models. *Mil Med Res.* (2021) 8:44. doi: 10.1186/s40779-021-00338-z

23. Han YQ, Yan L, Zhang L, Ouyang PH, Li P, Goyal H, et al. Red blood cell distribution width provides additional prognostic value beyond severity scores in adult critical illness. *Clin Chim Acta.* (2019) 498:62–7. doi: 10.1016/j.cca.2019.08.008

24. Chern CC, Chen YJ, Hsiao B. Decision tree-based classifier in providing telehealth service. *BMC Med Inform Decis Mak.* (2019) 19:104. doi: 10.1186/s12911-019-0825-9

25. Bhosale H, Ramakrishnan V, Jayaraman VK. Support vector machine-based prediction of pore-forming toxins (PFT) using distributed representation of reduced alphabets. *J Bioinform Comput Biol.* (2021) 19:2150028. doi: 10.1142/S0219720021500281

26. Maheswari S, Pitchai R. Heart disease prediction system using decision tree and naive bayes algorithm. *Curr Med Imaging Rev.* (2019) 15:712–7.

27. Kamińska JA. A random forest partition model for predicting NO(2) concentrations from traffic flow and meteorological conditions. *Sci Total Environ.* (2019) 651(Pt 1):475–83. doi: 10.1016/j.scitotenv.2018.09.196

28. Zhang Z, Ho KM, Hong Y. Machine learning for the prediction of volume responsiveness in patients with oliguric acute kidney injury in critical care. *Crit Care.* (2019) 23:112. doi: 10.1186/s13054-019-2411-z

29. Stoltzfus JC. Logistic regression: a brief primer. *Acad Emerg Med.* (2011) 18:1099–104.

30. Park SY. Nomogram: an analogue tool to deliver digital knowledge. *J Thorac Cardiovasc Surg.* (2018) 155:1793. doi: 10.1016/j.jtcvs.2017.12.107

31. Austin PC, Harrell FE Jr, van Klaveren D. Graphical calibration curves and the integrated calibration index (ICI) for survival models. *Stat Med.* (2020) 39:2714–42.

32. Delanaye P, Mariat C. The applicability of eGFR equations to different populations. *Nat Rev Nephrol.* (2013) 9:513–22.

33. Kellum JA, Lameire N. Diagnosis, evaluation, and management of acute kidney injury: a KDIGO summary (part 1). *Crit Care.* (2013) 17:204. doi: 10.1186/cc11454

34. Austin PC, White IR, Lee DS, van Buuren S. Missing data in clinical research: a tutorial on multiple imputation. *Can J Cardiol.* (2021) 37:1322–31.

35. Beesley LJ, Bondarenko I, Elliot MR, Kurian AW, Katz SJ, Taylor JM. Multiple imputation with missing data indicators. *Stat Methods Med Res.* (2021) 30:2685–700.

36. Sun L, Zhu W, Chen X, Jiang J, Ji Y, Liu N, et al. Machine learning to predict contrast-induced acute kidney injury in patients with acute myocardial infarction. *Front Med (Lausanne).* (2020) 7:592007. doi: 10.3389/fmed.2020.592007

37. Kim D, Antariksa G, Handayani MP, Lee S, Lee J. Explainable anomaly detection framework for maritime main engine sensor data. *Sensors (Basel).* (2021) 21:5200. doi: 10.3390/s21155200

38. Wojtuch A, Jankowski R, Podlewska S. How can SHAP values help to shape metabolic stability of chemical compounds? *J Cheminform.* (2021) 13:74. doi: 10.1186/s13321-021-00542-y

39. Yang M, Liu C, Wang X, Li Y, Gao H, Liu X, et al. An explainable artificial intelligence predictor for early detection of sepsis. *Crit Care Med.* (2020) 48:e1091–6. doi: 10.1097/CCM.0000000000004550

40. Churpek MM, Yuen TC, Winslow C, Meltzer DO, Kattan MW, Edelson DP. Multicenter comparison of machine learning methods and conventional regression for predicting clinical deterioration on the wards. *Crit Care Med.* (2016) 44:368–74. doi: 10.1097/CCM.0000000000001571

41. Zhou X, Sun Z, Zhuang Y, Jiang J, Liu N, Zang X, et al. Development and validation of nomogram to predict acute kidney injury in patients with acute myocardial infarction treated invasively. *Sci Rep.* (2018) 8:9769. doi: 10.1038/s41598-018-28088-4

42. McEligot AJ, Poynor V, Sharma R, Panangadan A. Logistic LASSO regression for dietary intakes and breast cancer. *Nutrients.* (2020) 12:2652. doi: 10.3390/nu12092652

43. Tseng PY, Chen YT, Wang CH, Chiu KM, Peng YS, Hsu SP, et al. Prediction of the development of acute kidney injury following cardiac surgery by machine learning. *Crit Care.* (2020) 24:478.

44. Zhao QY, Liu LP, Luo JC, Luo YW, Wang H, Zhang YJ, et al. A machine-learning approach for dynamic prediction of sepsis-induced coagulopathy in critically Ill patients with sepsis. *Front Med (Lausanne).* (2020) 7:637434. doi: 10.3389/fmed.2020.637434

45. Johnson AE, Pollard TJ, Shen L, Lehman LW, Feng M, Ghassemi M, et al. MIMIC-III, a freely accessible critical care database. *Sci Data.* (2016) 3:160035.

46. Ye XD, He Y, Wang S, Wong GT, Irwin MG, Xia Z. Heart-type fatty acid binding protein (H-FABP) as a biomarker for acute myocardial injury and long-term post-ischemic prognosis. *Acta Pharmacol Sin.* (2018) 39:1155–63. doi: 10.1038/aps.2018.37

47. Harada N, Okamura H, Nakane T, Koh S, Nanno S, Nishimoto M, et al. Pretransplant plasma brain natriuretic peptide and N-terminal probrain natriuretic peptide are more useful prognostic markers of overall survival after allogeneic hematopoietic cell transplantation than echocardiography. *Bone Marrow Transplant.* (2021) 56:1467–70. doi: 10.1038/s41409-021-01224-x

48. Hirano Y, Shinmoto K, Okada Y, Suga K, Bombard J, Murahata S, et al. Machine learning approach to predict positive screening of methicillin-resistant *Staphylococcus aureus* during mechanical ventilation using synthetic dataset from MIMIC-IV database. *Front Med (Lausanne).* (2021) 8:694520. doi: 10.3389/fmed.2021.694520

frontiers | Frontiers in Cardiovascular Medicine

TYPE Systematic Review
PUBLISHED 15 September 2022
DOI 10.3389/fcvm.2022.951881

Check for updates

OPEN ACCESS

EDITED BY
Robert Jeenchen Chen,
Stanford University, United States

REVIEWED BY
Giuseppe Filiberto Serraino,
Magna Græcia University of Catanzaro, Italy
Paul Philipp Heinisch,
German Heart, Germany

*CORRESPONDENCE
Zhenyu Yang
yangzhenyu2010@hotmail.com

SPECIALTY SECTION
This article was submitted to Heart Surgery, a section of the journal Frontiers in Cardiovascular Medicine

RECEIVED 24 May 2022
ACCEPTED 15 August 2022
PUBLISHED 15 September 2022

CITATION
Song Z, Yang Z, Hou M and Shi X (2022) Machine learning in predicting cardiac surgery-associated acute kidney injury: A systemic review and meta-analysis. *Front. Cardiovasc. Med.* 9:951881. doi: 10.3389/fcvm.2022.951881

COPYRIGHT
© 2022 Song, Yang, Hou and Shi. This is an open-access article distributed under the terms of the Creative Commons Attribution License (CC BY). The use, distribution or reproduction in other forums is permitted, provided the original author(s) and the copyright owner(s) are credited and that the original publication in this journal is cited, in accordance with accepted academic practice. No use, distribution or reproduction is permitted which does not comply with these terms.

Machine learning in predicting cardiac surgery-associated acute kidney injury: A systemic review and meta-analysis

Zhe Song[1], Zhenyu Yang[1]*, Ming Hou[1,2] and Xuedong Shi[2]

[1]Qinghai University Medical School, Xining, China, [2]Qinghai University Affiliated Hospital Intensive Care Unit, Xining, China

Background: Cardiac surgery-associated acute kidney injury (CSA-AKI) is a common complication following cardiac surgery. Early prediction of CSA-AKI is of great significance for improving patients' prognoses. The aim of this study is to systematically evaluate the predictive performance of machine learning models for CSA-AKI.

Methods: Cochrane Library, PubMed, EMBASE, and Web of Science were searched from inception to 18 March 2022. Risk of bias assessment was performed using PROBAST. Rsoftware (version 4.1.1) was used to calculate the accuracy and C-index of CSA-AKI prediction. The importance of CSA-AKI prediction was defined according to the frequency of related factors in the models.

Results: There were 38 eligible studies included, with a total of 255,943 patients and 60 machine learning models. The models mainly included Logistic Regression ($n = 34$), Neural Net ($n = 6$), Support Vector Machine ($n = 4$), Random Forest ($n = 6$), Extreme Gradient Boosting ($n = 3$), Decision Tree ($n = 3$), Gradient Boosted Machine ($n = 1$), COX regression ($n = 1$), κNeural Net ($n = 1$), and Naïve Bayes ($n = 1$), of which 51 models with intact recording in the training set and 17 in the validating set. Variables with the highest predicting frequency included Logistic Regression, Neural Net, Support Vector Machine, and Random Forest. The C-index and accuracy wer 0.76 (0.740, 0.780) and 0.72 (0.70, 0.73), respectively, in the training set, and 0.79 (0.75, 0.83) and 0.73 (0.71, 0.74), respectively, in the test set.

Conclusion: The machine learning-based model is effective for the early prediction of CSA-AKI. More machine learning methods based on noninvasive or minimally invasive predictive indicators are needed to improve the predictive performance and make accurate predictions of CSA-AKI. Logistic regression remains currently the most commonly applied model in CSA-AKI prediction, although it is not the one with the best performance. There are other models that would be more effective, such as NNET and XGBoost.

Systematic review registration: https://www.crd.york.ac.uk/; review registration ID: CRD42022345259.

KEYWORDS

thoracic surgery, machine learning, cardiac surgery-associated, acute kidney injury, meta-analysis

Introduction

Cardiac surgery-associated acute kidney injury (CSA-AKI) is a common complication following cardiac surgery, with its morbidity rising due to the increasing demand of cardiac surgery worldwide. The prevalence of cardiac surgery ranges from 0.5 to 500 per million in developing countries. Cardiac and vascular procedures are common risk factors in CSA-AKI, with 3% of the patients requiring renal replacement therapy. According to the Kidney Disease Improving Global Outcomes (KDIGO) criteria (1), AKI is defined as a sudden deterioration of renal function within a period of hours to days, and is characterized by the decrease of serum creatinine (SCr) levels, estimated glomerular filtration rate (eGFR), blood urea nitrogen (BUN), and urine output, with high morbidity and mortality. It can be divided into three stages based on either a decrease of urine output or an increase of SCr (2). AKI often requires high treatment costs, and inappropriate management for it can lead to chronic kidney disease (CKD) or end-stage renal disease (ESRD) (3). AKI induces not only short-term adverse events but long-term poor outcomes such as fluid and electrolyte disturbance. Even mild AKI is associated with poor patient survival according to the KDIGO (1) analysis. An analysis of recovery patterns after AKI shows that 41.2% of the patients could not have their renal function recovered before hospital discharge.

Cardiac and vascular surgery is one of the common risk factors for AKI. The incidence of CSA-AKI reaches up to 40% (4). Blood dynamics alteration following cardiac surgery causes a decrease in renal blood perfusion, and subsequently reduces eGFR, leading to necrosis of glomerular epithelial cells, which underlies the pathogenesis of CSA-AKI (5, 6).

Machine learning refers to computer simulation or implementation of human behavior to endow the computer with the ability of self-improvement so as to be capable of complex multitasking. It covers multiple disciplines such as mathematics, statistics, and computer science, and has been widely used in scientific research and industry. In recent years, machine learning has also been widely applied in disease prediction, and multiple studies on the use of machine learning in CSA-AKI prediction have been reported. However, its predictive value lacks evidence-based support. Therefore, we conducted this systematic review and meta-analysis to evaluate the predictive value of machine learning for CSA-AKI so as to provide evidence-based support for its clinical application (7).

Methods

This meta-analysis is carried out in strict accordance with The Preferred Reporting Items for Systematic Reviews and Meta-Analyses (PRISMA) 2020 statement, which has been preregistered on PROSPERO (Registration No. CRD420222345259).

Literature search

Cochrane Library, PubMed, EMBASE, and Web of Science were searched from inception to 18 March 2022. Search items were designed based on the combination of medical subject headings and free words, without language and region restriction. A literature search was conducted by Zhe Song (detailed search strategy is shown in Supplementary File 2).

Inclusion and exclusion criteria

Studies meeting the following criteria were included:

(1) Randomized controlled trial (RCT), prospective cohort study, nested case-control study, case-control study, and registration data on patients with cardiovascular diseases who had undergone heart surgery such as heart valve replacement and cardiac contrast.
(2) A complete predictive model was established;
(3) Published in English.

Exclusion criteria were:

(1) Study unrelated to CSA-AKI or only reported risk factors;
(2) Containing no outcome measures related to the effectiveness of a predictive model (e.g., RFC, sensitivity, specificity, accuracy, confusion matrix, etc.);
(3) Other study design: case reports, letters, conference summaries, reviews, etc.;
(4) Incomplete data or data unavailable.
(5) AKI staged using KDIGO (1) serum creatinine criteria; cardiac function graded *via* the American Heart Association guideline and ESC 2021 guideline (8, 9).

Literature search

All articles identified were imported into EndNote X9. Titles and abstracts of the articles were browsed following duplicate removal, and the full-texts of the remaining articles were retrieved and read to identify eligible studies. Literature search and screening were processed by two reviewers (SZ and YZY) independently, any disagreements were settled by a third reviewer (HM). The articles searching a flow chart are presented in Supplementary materials. Pieces of literature, which contain unclear information or missing critical data, were excluded from our study.

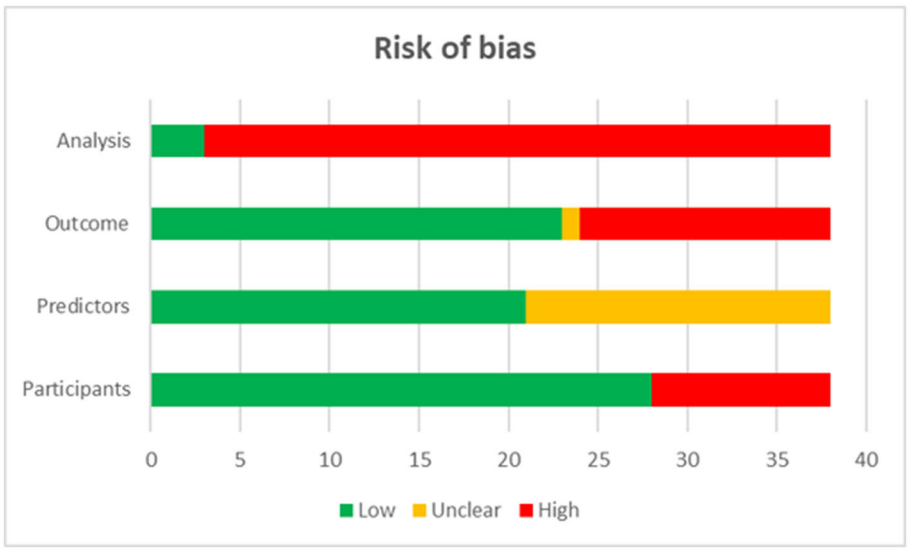


FIGURE 1
Quality assessment of included studies.

Data extraction

The data extraction form was designed according to the Modified CHARMS checklist (10), which mainly included: name of the first author, publication date, nation, duration of data hiring, study design (prospective and retrospective), types of validation (external, internal, random split, and time split), and sample size (total number, developments, and testing cluster). The development set was defined as all data sets other than the test set in this study due to the unclear description in each study.

Risk of bias assessment

We used the prediction model risk of bias assessment tool (PROBAST) (11) and the external prognostic validity model to assess the risk of bias in the included studies. PROBAST is a risk of the bias assessment tool designed for systematic reviews of diagnostic or prognostic prediction models. It contains four domains: participants, predictors, outcome, and statistical analysis. Items under each domain can be filled as "yes," "probably yes," "probably no," "no," and "no information," depending on the characteristics of the study. If a domain contains at least one item filled as "no" or "probably no," it would be graded as high risk. A domain with all the items filled as "yes" or "probably yes" would be graded as low risk. The overall risk of bias would be graded as low risk when all the domains are graded as low risk. The risk of bias assessment was performed by two reviewers independently.

Statistical analysis

We calculated and reported descriptive statistics to summarize the characteristics of the models. For prediction models that were examined in more than two independent datasets (excluding the model development dataset), a random-effect meta-analysis was performed to estimate the performance and accuracy. Prediction models, which were internally validated through bootstrapping or cross-validation and were externally validated in only two independent datasets, were also considered. We followed a recently published framework of meta-analysis for prediction models. If a measure of uncertainty (standard error or 95% confidence interval) was not available for the mean C-index, a formula was used to approximate the standard error of the mean C-index based on the number of events and number of participants. All data analyses were performed using the R software (Version 4.1.1).

Results

Study selection

There were 1,909 articles identified [Cochrane (n = 133), PubMed (n = 33), Embase (n = 231), Web of Science (n = 1,512)]. After removing 220 duplicates, titles and abstracts of the remaining 1,689 articles were browsed, and 38 studies (12–49) were finally included. A PRISMA flow diagram of the study selection process is shown in Supplementary File 4.

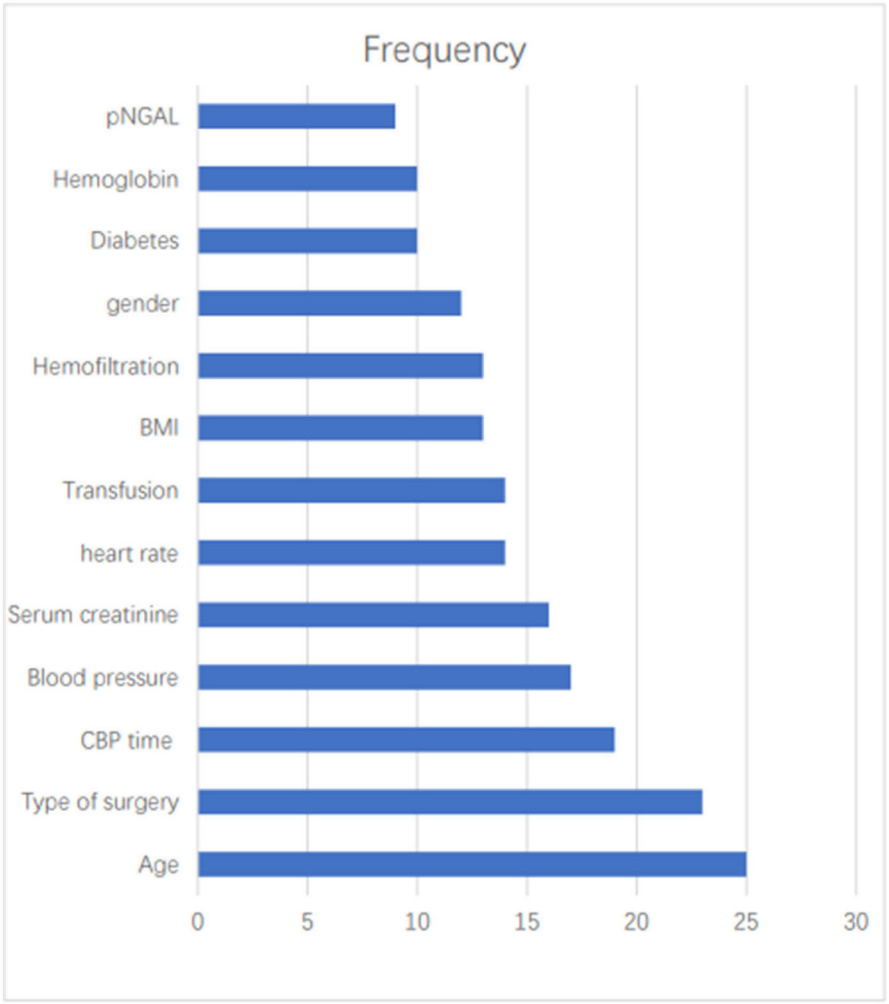


FIGURE 2
A frequency bar chart of predictors.

Characteristics of included studies

A total of 139,444 participants were involved, with 116,499 in the validation set. Data were collected from 12 countries. Among the included studies, 25 (about 66%) have been published in recent 5 years (2017–2022), indicating that research in the field of the machine learning-based prediction model has been a hotspot in recent years, and is of great value and significance.

These were 60 prognostic models for CSA-AKI included, 12 external validation models, and 7 random sampling validation models. The types of these 60 prognostic models include: Logistic Regression (12–16, 19–22, 24–35, 37–49) (n = 34), Neural Net (15, 17–19) (n = 6), Support Vector Machine (15, 16) (n = 4), Random Forest (15, 16, 30, 40) (n = 6), Extreme Gradient Boosting (15, 16, 49) (n = 3), Decision Tree (15, 16) (n = 3), Gradient Boosted Machine (19) (n = 1), COX regression (19) (n = 1), κ Neural Net (19) (n = 1), and Naïve Bayes (19) (n = 1). Characteristics of included studies are shown in Supplementary File 1.

Quality assessment

The quality assessment showed that 92.11% of included studies were graded as high risk in the domain of analysis, 36.84% were graded as high risk in the domain of outcomes, and 26.32% in that of participants (Figure 1).

Predictors

The most commonly used predictors were Age (n = 25, 41.67%), Types of surgery (n = 23, 38.33%), CBP time (n = 19,

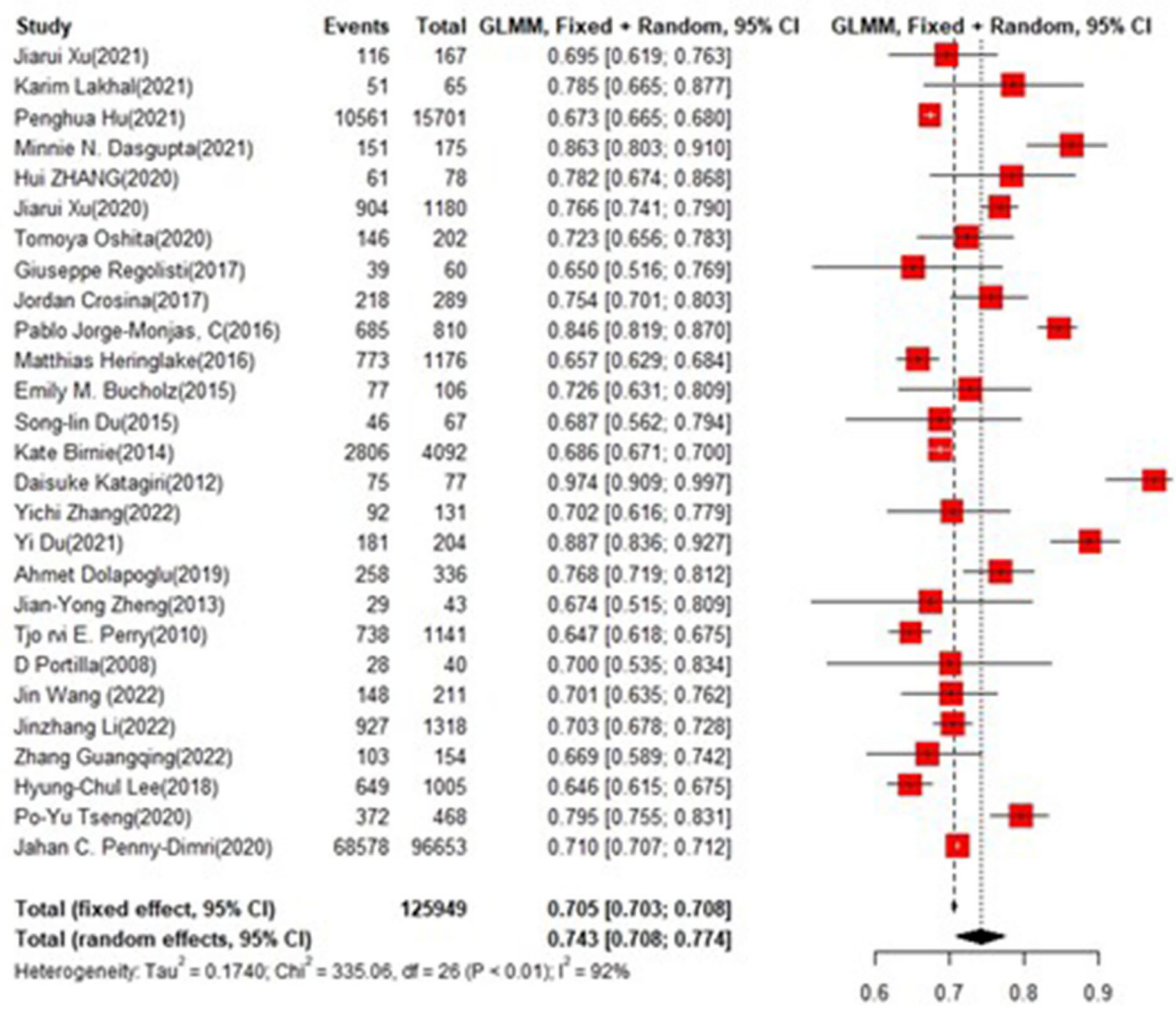


FIGURE 3
Accuracy of the machine learning-based model in the training set: logistic regression.

31.67%), Blood pressure ($n = 17$, 28.33%), SCr ($n = 16$, 26.67%), heart rate ($n = 14$, 23.33%), Transfusion ($n = 14$, 23.33%), BMI ($n = 13$, 21.67%), Hemofiltration ($n = 13$, 21.67%), gender ($n = 12$, 20.00%), diabetes ($n = 10$, 16.67%), Hemoglobin ($n = 10$, 16.67%), pNGAL ($n = 9$, 15.00%) (Figure 2).

Training set and test set accuracy

In the training set, the logistic regression model was the most commonly applied [$n = 27$, accuracy = 0.705 (0.703, 0.708)]. XGBoost showed to be of the best performance [$n = 3$, accuracy = 0.732 (0.715, 0.748)], with large modeling sample size (Figures 3, 4).

In the test set, logistic regression was also the most commonly applied model [$n = 10$, accuracy = 0.708 (0.705, 0.71)]. NNET was of the best effect [$n = 3$, accuracy = 0.711 (0.708, 0.713)], with large modeling sample size, so we think NNET has the best effect. XGBoost also showed an excellent effect in all models [accuracy = 0.755 (0.705, 0.802)], while its modeling sample size was limited (Figures 5, 6).

Training set and test set c-index

In the training set, logistic regression was the most commonly applied model [$n = 26$, c-index = 0.76 (0.75, 0.76)]. XGBoost showed to be of the best performance [$n = 3$, c-index =0.8 (0.78, 0.82)], with large modeling sample size. COX also showed a remarkable effect in all models [c-index = 0.9 (0.81, 1)], while its modeling sample size was limited (Figures 7, 8).

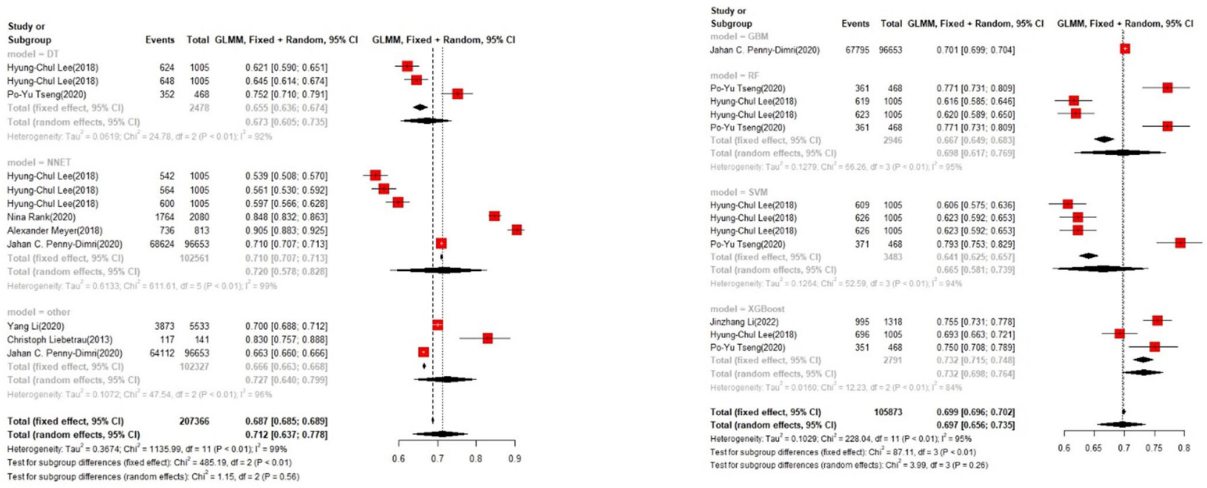


FIGURE 4
Accuracy of the machine learning-based model in the training set: other models.

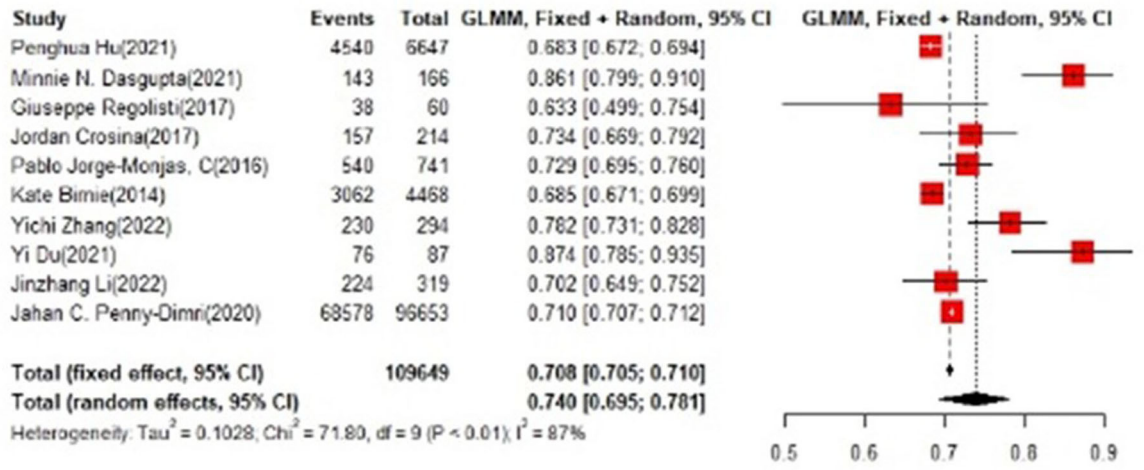


FIGURE 5
Accuracy of the machine learning-based model in the test set: logistic regression.

In the test set, logistic regression was also the most commonly applied model [$n = 8$, c-index = 0.75 (0.74, 0.76)]. NNET and XGBoost presented excellent performance, with the c-index of 0.89 (0.86, 0.92) and 0.81 (0.75, 0.88), respectively, while the modeling sample size of these two models was limited (Figures 9, 10).

Detailed results of data analyses are shown in Supplementary File 3.

Discussion

There were 38 studies, with 60 CSA-AKI models, 12 external validity models, and 7 random sampling models. Most of them were logistic regression models. Risk of bias assessment showed that there was a high risk of bias in the analyses of included studies, which might be related to the incomplete variables and limited sample size involved in the model, improper processing of missing data, internal verification of models, interpretation of complex data, and correlation between some predictors and CSA-AKI definition. Therefore, follow-up studies should take into account the selection and verification of models, expansion of samples, and application of multivariate analysis. Data screening should also be more scientific to obtain more clinically valuable results.

Cardiac surgery altered the hemodynamics leading to hypoperfusion in the kidneys. Cardiac Angio Pulmonary Bypass

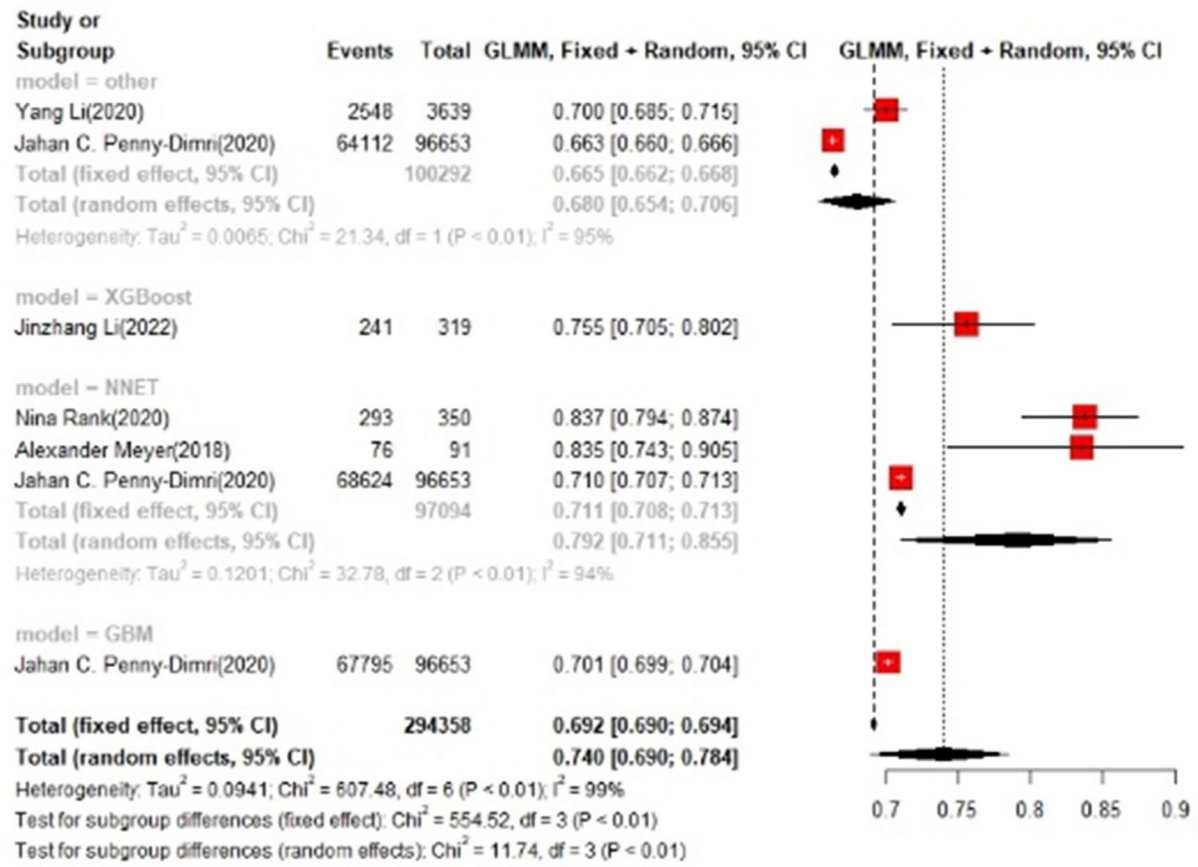


FIGURE 6
Accuracy of the machine learning-based model in the test set: other models.

can also induce hemodynamic disturbance directly and lead to acute kidney injury. Cardiac surgery-associated acute kidney injury (CSA-AKI) is a common and serious complication of cardiac surgery. There were more than 2 million people receiving cardiac surgery every year, and the incidence of CSA-AKI fluctuated between 5 and 42%. The occurrence of CSA-AKI is associated with high perioperative mortality, prolonged hospital stay, and heavy treatment costs. Pathogenesis of CSA-AKI should be further explored to elucidate the relationship between cardiac surgery undergoing and AKI occurring (2, 18).

Detailed mechanisms of CSA-AKI have not been fully elucidated. Ischemic reperfusion injury, activation of inflammatory cytokines cascades, oxidative stress, and nephrotoxic reaction might be involved in the pathogenesis of CSA-AKI (16, 19, 50). Hypotension may play a critical role in renal dysfunction, while the optimal mean arterial pressure (MAP) helpful to prevent CSA-AKI during CPB remains unknown. Almost all studies that assessed MAP during CPB were observational designs and were conducted to evaluate the correlation between hypotension and adverse neurologic outcomes. Griffin et al. (5) conducted a single-center RCT that included 300 patients who had known risk factors in AKI, and underwent elective cardiac surgery with normothermic CBP. They found that MAP during CPB was targeted to 50–60 mmHg in the control group, whereas that in the intervention group was targeted to 75–85 mmHg, and the overall mean MAP in the two groups was 60 ± 6 and 79 ± 6 mmHg, respectively. There was no intergroup difference in CSA-AKI, hospital LOS, and mortality.

AKI is a serious complication that can directly induce renal failure. The initiated injury process leads to irreversible renal function impairment that would continually deteriorate. Machine learning is capable of identifying the pathological factors of AKI so as to facilitate early intervention. Dong et al. (51) recruited 16,863 pediatric critical care patients aged from 1 month to 21 years, and used machine learning to predict pediatric AKI. Their findings were promising. Machine learning is a state-of-the-art approach to risk stratification. Interpretive modeling can use complex decision boundaries to help clinicians understand the risks specific to individual patients.

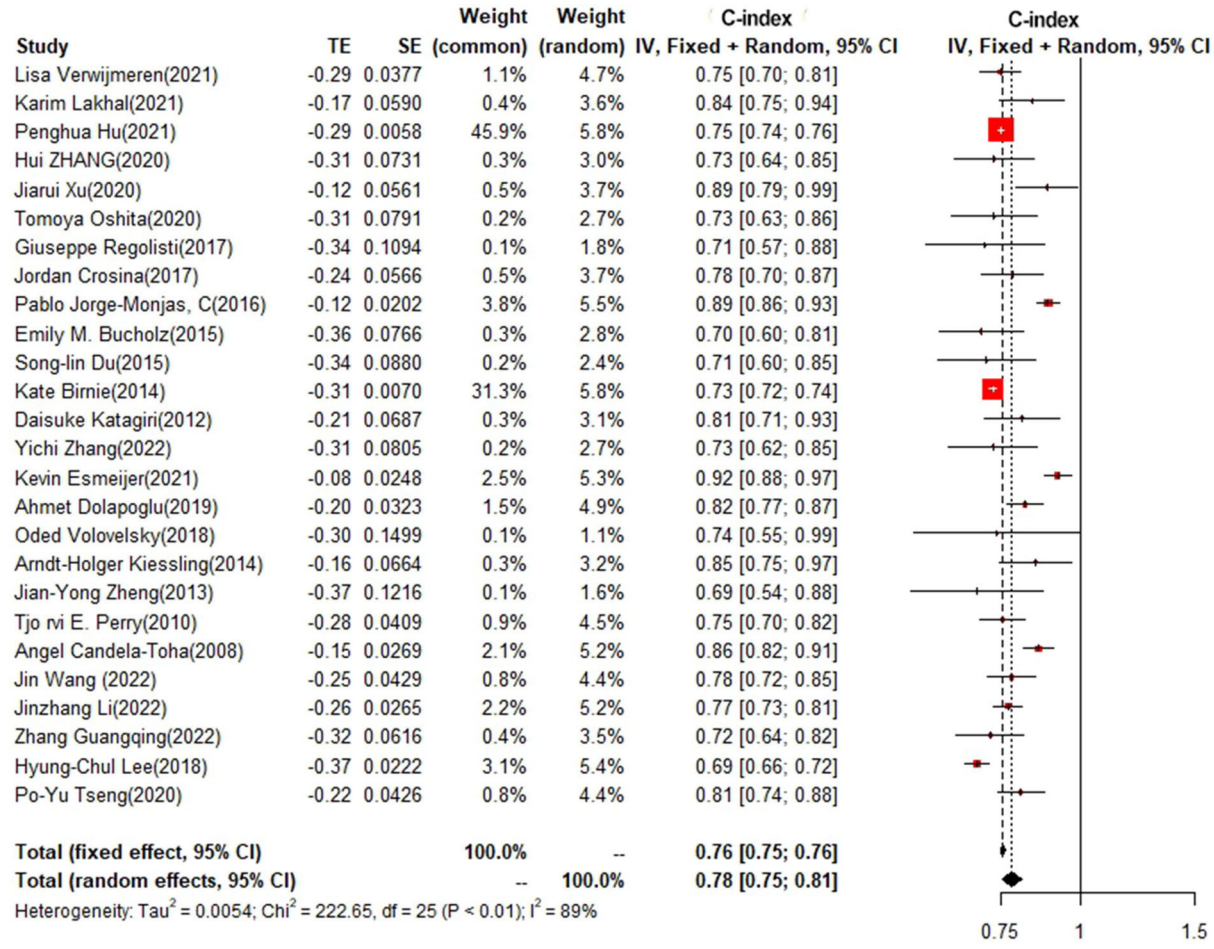


FIGURE 7
C-index in the training set: logistic regression.

The application of machine learning is driven by the development of big data analysis and the need for evidence-based care. The practicality of the combination of artificial intelligence and machine learning has aroused widespread interest in medical research. Machine learning has its own advantages in performance and scalability, and machine learning-based modeling from mass data presents to be helpful to the implementation of dynamic monitoring for multiple diseases (52–55). Some machine learning algorithms, such as Extreme Gradient Boost (XGBoost), can calculate and predict the relative size of variables in a specific result, which makes the level of insight into individual risk factors and their prognostic significance comparable to that of logistic regression models (56). Gradient Boosting (GBM) is a widely used method to predict the incidence of AKI (57). Huang et al. (58) proposed a GBM-based risk prediction model for AKI after percutaneous coronary intervention (PCI). They collected a large amount of data from 947,091 patients receiving PCI to construct a baseline model, and time verification was carried out through the data of more than 900,000 hospitalized patients. The AUC of the GBM model was 79% larger than that of the baseline linear regression model. Lee et al. (59) proposed an AKI-prediction model based on several machine learning algorithms, and compared their performance in patients undergoing liver transplantation and heart surgery. Both the studies found that GBM had the most reliable performance.

In conclusion, CSA-AKI is a complex and multifaceted syndrome with significant morbidity and mortality. The application of machine learning in nephrotic clinical practice, including CSA-AKI, has a promising prospect.

We found that age, SCr, type of surgery, BMI, CBP time, and blood pressure were significant predictors for CSA-AKI. A large multinational and multicenter RCT, which involved 4,752 participants from 19 different countries, reported that Patients who underwent cardiac surgery without CPB were significantly

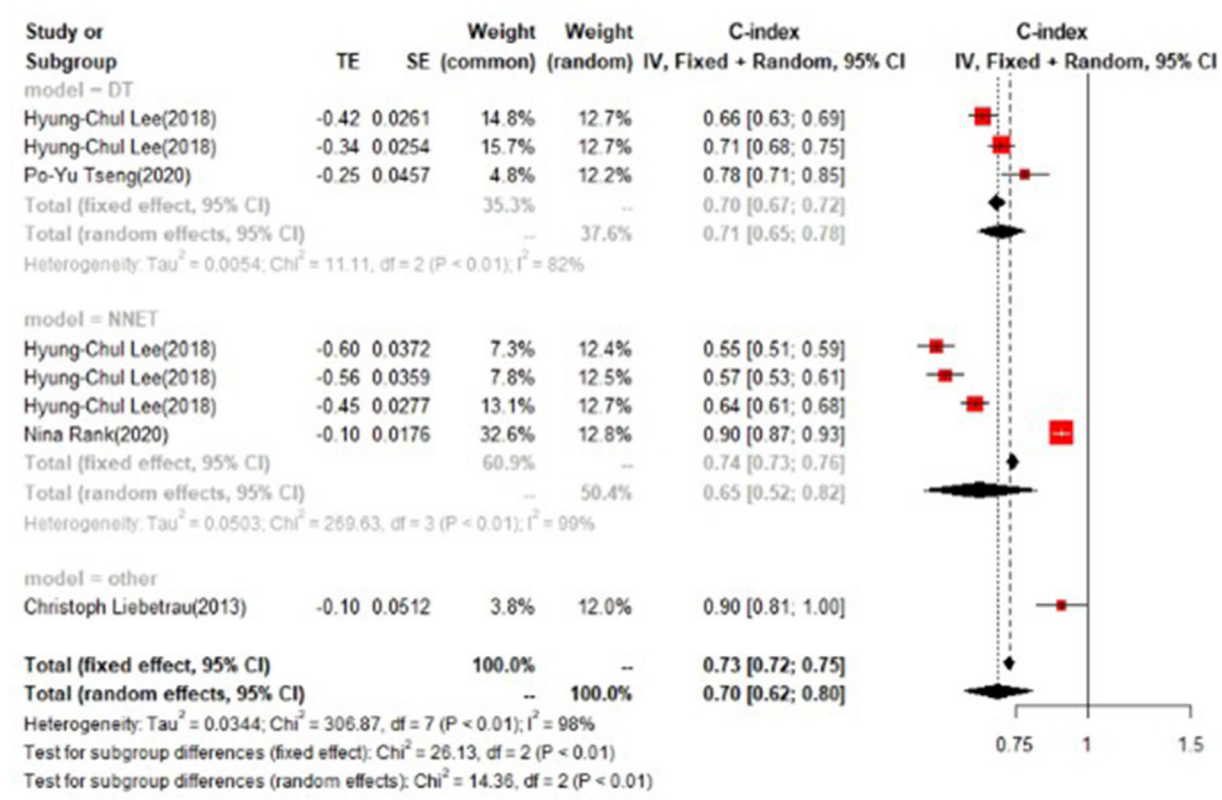


FIGURE 8
C-index in the training set: other models.

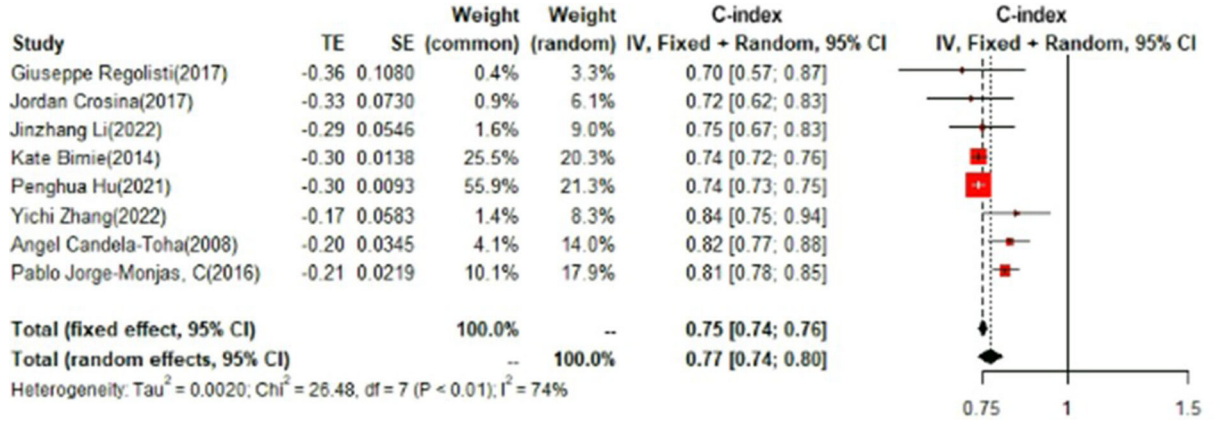


FIGURE 9
C-index in the test set: logistic regression.

less likely to have AKI 30 days after surgery [28 vs. 32.1%, RR = 0.87, 95% CI (80–0.96), $p = 5.01$] (17).

This systematic review and meta-analysis, based on a large sample size, showed that machine learning was effective in predicting the risk of CSA-AKI. Recently, the most common machine learning method is conventional logistic regression, followed by artificial neural networks, while SVM and RF are also commonly used. A study by Tseng et al. (16) demonstrated that machine learning could successfully predict CSA-AKI, which reflects the risks of cardiac surgery, enabling the

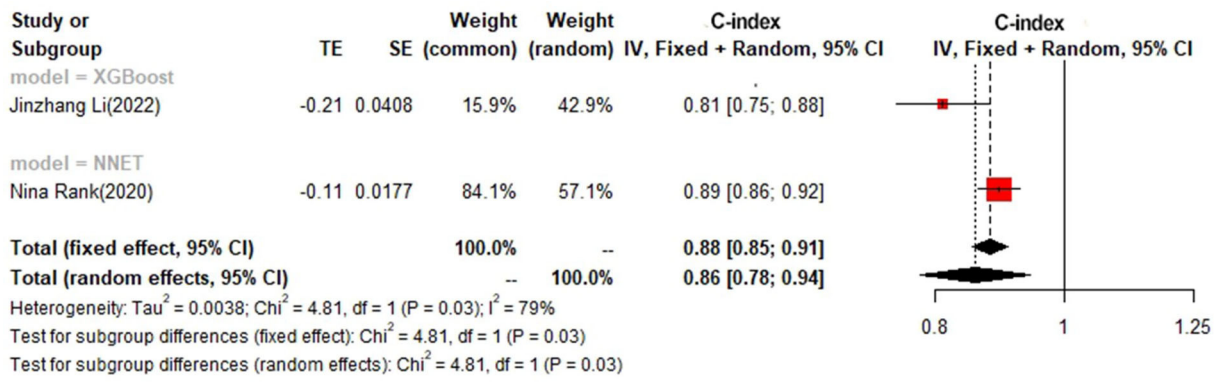


FIGURE 10
C-index in the test set: other models.

optimization of postoperative treatment processes to diminish the postoperative complications following cardiac operations.

This study also has some limitations: first, this study focused on the accuracy of the machine learning model and did not predict the risk factors of CSA-AKI. Second, some of the included models contained special variables (such as SCr and eGFR), which were related to the diagnosis of AKI, and these variables would be of value for further verification and research in subsequent studies.

Conclusion

Logistic regression remains the most commonly used model in CSA-AKI prediction, while it might not be the optimal option. Other models, such as NNET, XGBoost, and GBM, are of more remarkable performance. Using predictive models for early risk assessment has a relatively desirable effect on preventing CSA-AKI; however, it still needs to be further improved. Therefore, we look forward to more validated machine learning methods based on convenient, noninvasive, or minimally invasive predictive indicators that could be of remarkable performance and accuracy in the prediction of CSA-AKI.

Data availability statement

The original contributions presented in the study are included in the article/Supplementary material, further inquiries can be directed to the corresponding author.

Author contributions

ZS finished the entire research and bibliography retrieval. ZY was responsible for writing and review. MH and XS acted as the consultants. All authors contributed to the article and approved the submitted version.

Funding

This study is supported entirely by the ZS. The whole study was finished without any external financial support.

Conflict of interest

The authors declare that the research was conducted in the absence of any commercial or financial relationships that could be construed as a potential conflict of interest.

Publisher's note

All claims expressed in this article are solely those of the authors and do not necessarily represent those of their affiliated organizations, or those of the publisher, the editors and the reviewers. Any product that may be evaluated in this article, or claim that may be made by its manufacturer, is not guaranteed or endorsed by the publisher.

Supplementary material

The Supplementary Material for this article can be found online at: https://www.frontiersin.org/articles/10.3389/fcvm.2022.951881/full#supplementary-material

References

1. Stevens PE, Levin A, Kidney Disease: Improving Global Outcomes Chronic Kidney Disease Guideline Development Work Group Members. Evaluation and management of chronic kidney disease: synopsis of the kidney disease: improving global outcomes 2012 clinical practice guideline. *Ann Intern Med*. (2013) 158:825–30. doi: 10.7326/0003-4819-158-11-201306040-00007

2. Massoth C, Zarbock A, Meersch M. Acute kidney injury in cardiac surgery. *Crit Care Clin.* (2021) 37:267–78. doi: 10.1016/j.ccc.2020.11.009

3. Wang Y, Bellomo R. Cardiac surgery-associated acute kidney injury: risk factors, pathophysiology and treatment. *Nat Rev Nephrol.* (2017) 13:697–711. doi: 10.1038/nrneph.2017.119

4. Romagnoli S, Ricci Z, Ronco C. Perioperative acute kidney injury: prevention, early recognition, and supportive measures. *Nephron.* (2018) 140:105–10. doi: 10.1159/000490500

5. Griffin BR, Liu KD, Teixeira JP. Critical care nephrology: core curriculum 2020. *Am J Kidney Dis.* (2020) 75:435–52. doi: 10.1053/j.ajkd.2019.10.010

6. Azau A, Markowicz P, Corbeau JJ, Cottineau C, Moreau X, Baufreton C, et al. Increasing mean arterial pressure during cardiac surgery does not reduce the rate of postoperative acute kidney injury. *Perfusion.* (2014) 29:496–504. doi: 10.1177/0267659114527331

7. Deo RC. Machine learning in medicine. *Circulation.* (2015) 132:1920–30. doi: 10.1161/CIRCULATIONAHA.115.001593

8. Benjamin EJ, Virani SS, Callaway CW, Chamberlain AM, Chang AR, Cheng S, et al. Heart disease and stroke statistics-2018 update: a report from the American Heart Association. *Circulation.* (2018) 137:e67–e492. doi: 10.1161/CIR.0000000000000558

9. Vahanian A, Beyersdorf F, Praz F, Milojevic M, Baldus S, Bauersachs J, et al. 2021 ESC/EACTS Guidelines for the management of valvular heart disease: Developed by the Task Force for the management of valvular heart disease of the European Society of Cardiology (ESC) and the European Association for Cardio-Thoracic Surgery (EACTS). *Rev Esp Cardiol.* (2022) 75:524. doi: 10.1016/j.rec.2022.05.006

10. Moons KG, de Groot JA, Bouwmeester W, Vergouwe Y, Mallett S, Altman DG, et al. Critical appraisal and data extraction for systematic reviews of prediction modelling studies: the CHARMS checklist. *PLoS Med.* (2014) 11:e1001744. doi: 10.1371/journal.pmed.1001744

11. Wolff RF, Moons K, Riley RD, Whiting PF, Westwood M, Collins GS, et al. PROBAST: a tool to assess the risk of bias and applicability of prediction model studies. *Ann Intern Med.* (2019) 170:51–8. doi: 10.7326/M18-1376

12. Verwijmeren L, Bosma M, Vernooij LM, Linde EM, Dijkstra IM, Daeter EJ, et al. Associations between preoperative biomarkers and cardiac surgery-associated acute kidney injury in elderly patients: a cohort study. *Anesth Analg.* (2021) 133:570–7. doi: 10.1213/ANE.0000000000005650

13. Kiessling AH, Dietz J, Reyher C, Stock UA, Beiras-Fernandez A, Moritz A. Early postoperative serum cystatin C predicts severe acute kidney injury following cardiac surgery: a post-hoc analysis of a randomized controlled trial. *J Cardiothorac Surg.* (2014) 9:10. doi: 10.1186/1749-8090-9-10

14. Guangqing Z, Liwei C, Fei L, Jianshe Z, Guang Z, Yan Z, et al. Predictive value of neutrophil to lymphocyte ratio on acute kidney injury after on-pump coronary artery bypass: a retrospective, single-center study. *Gen Thorac Cardiovasc Surg.* (2022) 70:624–33. doi: 10.1007/s11748-022-01772-z

15. Lee HC, Yoon HK, Nam K, Cho YJ, Kim TK, Kim WH, et al. Derivation and validation of machine learning approaches to predict acute kidney injury after cardiac surgery. *J Clin Med.* (2018) 7:322. doi: 10.3390/jcm7100322

16. Tseng PY, Chen YT, Wang CH, Chiu KM, Peng YS, Hsu SP, et al. Prediction of the development of acute kidney injury following cardiac surgery by machine learning. *Crit Care.* (2020) 24:478. doi: 10.1186/s13054-020-03179-9

17. Rank N, Pfahringer B, Kempfert J, Stamm C, Kühne T, Schoenrath F, et al. Deep-learning-based real-time prediction of acute kidney injury outperforms human predictive performance. *NPJ Digit Med.* (2020) 3:139. doi: 10.1038/s41746-020-00346-8

18. Meyer A, Zverinski D, Pfahringer B, Kempfert J, Kuehne T, Sündermann SH, et al. Machine learning for real-time prediction of complications in critical care: a retrospective study. *Lancet Respir Med.* (2018) 6:905–14. doi: 10.1016/S2213-2600(18)30300-X

19. Penny-Dimri JC, Bergmeir C, Reid CM, Williams-Spence J, Cochrane AD, Smith JA. Machine learning algorithms for predicting and risk profiling of cardiac surgery-associated acute kidney injury. *Semin Thorac Cardiovasc Surg.* (2021) 33:735–45. doi: 10.1053/j.semtcvs.2020.09.028

20. Zhang H, Zhou K, Wang D, Zhang N, Liu J. The predictive value of the intraoperative Renal Pulsatility Index for acute kidney injury in patients undergoing cardiac surgery. *Minerva Anestesiol.* (2020) 86:1161–9. doi: 10.23736/S0375-9393.20.14460-2

21. Xu J, Jiang W, Li Y, Shen B, Shen Z, Wang Y, et al. Volume-associated hemodynamic variables for prediction of cardiac surgery-associated acute kidney injury. *Clin Exp Nephrol.* (2020) 24:798–805. doi: 10.1007/s10157-020-01908-6

22. Oshita T, Hiraoka A, Nakajima K, Muraki R, Arimichi M, Chikazawa G, et al. A better predictor of acute kidney injury after cardiac surgery: the largest area under the curve below the oxygen delivery threshold during cardiopulmonary bypass. *J Am Heart Assoc.* (2020) 9:e015566. doi: 10.1161/JAHA.119.015566

23. Li Y, Xu J, Wang Y, Zhang Y, Jiang W, Shen B, et al. A novel machine learning algorithm, Bayesian networks model, to predict the high-risk patients with cardiac surgery-associated acute kidney injury. *Clin Cardiol.* (2020) 43:752–61. doi: 10.1002/clc.23377

24. Zheng JY, Xiao YY, Yao Y, Han L. Is serum cystatin C an early predictor for acute kidney injury following cardiopulmonary bypass surgery in infants and young children? *Kaohsiung J Med Sci.* (2013) 29:494–9. doi: 10.1016/j.kjms.2013.01.004

25. Xu J, Jiang W, Li Y, Li H, Geng X, Chen X, et al. Association between syndecan-1, fluid overload, and progressive acute kidney injury after adult cardiac surgery. *Front Med.* (2021) 8:648397. doi: 10.3389/fmed.2021.648397

26. Zivkovic N, Elbaz-Greener G, Qiu F, Arbel Y, Cheema AN, Dvir D, et al. Bedside risk score for prediction of acute kidney injury after transcatheter aortic valve replacement. *Open heart.* (2018) 5:e000777. doi: 10.1136/openhrt-2018-000777

27. Regolisti G, Maggiore U, Cademartiri C, Belli L, Gherli T, Cabassi A, et al. Renal resistive index by transesophageal and transparietal echo-doppler imaging for the prediction of acute kidney injury in patients undergoing major heart surgery. *J Nephrol.* (2017) 30:243–53. doi: 10.1007/s40620-016-0289-2

28. Crosina J, Lerner J, Ho J, Tangri N, Komenda P, Hiebert B, et al. Improving the prediction of cardiac surgery-associated acute kidney injury. *Kidney Int Rep.* (2016) 2:172–9. doi: 10.1016/j.ekir.2016.10.003

29. Jorge-Monjas P, Bustamante-Munguira J, Lorenzo M, Heredia-Rodríguez M, Fierro I, Gómez-Sánchez E, et al. Predicting cardiac surgery-associated acute kidney injury: The CRATE score. *J Crit Care.* (2016) 31:130–8. doi: 10.1016/j.jcrc.2015.11.004

30. Heringlake M, Charitos EI, Erber K, Berggreen AE, Heinze H, Paarmann H. Preoperative plasma growth-differentiation factor-15 for prediction of acute kidney injury in patients undergoing cardiac surgery. *Crit Care.* (2016) 20:317. doi: 10.1186/s13054-016-1482-3

31. Shah KS, Taub P, Patel M, Rehfeldt M, Struck J, Clopton P, et al. Proenkephalin predicts acute kidney injury in cardiac surgery patients. *Clin Nephrol.* (2015) 83:29–35. doi: 10.5414/CN108387

32. Bucholz EM, Whitlock RP, Zappitelli M, Devarajan P, Eikelboom J, Garg AX, et al. Cardiac biomarkers and acute kidney injury after cardiac surgery. *Pediatrics.* (2015) 135:e945–56. doi: 10.1542/peds.2014-2949

33. Du SL, Zeng XZ, Tian JW, Ai J, Wan J, He JX. Advanced oxidation protein products in predicting acute kidney injury following cardiac surgery. *Biomarkers.* (2015) 20:206–11. doi: 10.3109/1354750X.2015.1062917

34. Birnie K, Verheyden V, Pagano D, Bhabra M, Tilling K, Sterne JA, et al. Predictive models for kidney disease: improving global outcomes (KDIGO) defined acute kidney injury in UK cardiac surgery. *Crit Care.* (2014) 18:606. doi: 10.1186/s13054-014-0606-x

35. Hu P, Mo Z, Chen Y, Wu Y, Song L, Zhang L, et al. Derivation and validation of a model to predict acute kidney injury following cardiac surgery in patients with normal renal function. *Ren Fail.* (2021) 43:1205–13. doi: 10.1080/0886022X.2021.1960563

36. Liebetrau C, Dörr O, Baumgarten H, Gaede L, Szardien S, Blumenstein J, et al. Neutrophil gelatinase-associated lipocalin (NGAL) for the early detection of cardiac surgery associated acute kidney injury. *Scand J Clin Lab Invest.* (2013) 73:392–9. doi: 10.3109/00365513.2013.787149

37. Katagiri D, Doi K, Honda K, Negishi K, Fujita T, Hisagi M, et al. Combination of two urinary biomarkers predicts acute kidney injury after adult cardiac surgery. *Ann Thorac Surg.* (2012) 93:577–83. doi: 10.1016/j.athoracsur.2011.10.048

38. Zhang Y, Zhao H, Su Q, Wang C, Chen H, Shen L, et al. Novel plasma biomarker-based model for predicting acute kidney injury after cardiac surgery: a case control study. *Front Med.* (2022) 8:799516. doi: 10.3389/fmed.2021.799516

39. Esmeijer K, Schoe A, Ruhaak LR, Hoogeveen EK, Soonawala D, Romijn F, et al. The predictive value of TIMP-2 and IGFBP7 for kidney failure and 30-day mortality after elective cardiac surgery. *Sci Rep.* (2021) 11:1071. doi: 10.1038/s41598-020-80196-2

40. Du Y, Wang XZ, Wu WD, Shi HP, Yang XJ, Wu WJ, et al. Predicting the risk of acute kidney injury in patients after percutaneous coronary intervention (PCI) or cardiopulmonary bypass (CPB) surgery: development and assessment of a nomogram prediction model. *Med Sci Monit.* (2021) 27:e929791. doi: 10.12659/MSM.929791

41. Dolapoglu A, Avci E, Kiris T, Bugra O. The predictive value of the prognostic nutritional index for postoperative acute kidney injury in patients undergoing on-pump coronary bypass surgery. *J Cardiothorac Surg.* (2019) 14:74. doi: 10.1186/s13019-019-0898-7

42. Lakhal K, Bigot-Corbel E, Sacchetto E, Chabrun F, Senage T, Figueres L, et al. Early recognition of cardiac surgery-associated acute kidney injury: (an observational pilot study). *BMC Anesthesiol.* (2021) 21:244. doi: 10.1186/s12871-021-01387-6

43. Volovelsky O, Gist KM, Terrell TC, Bennett MR, Cooper DS, Alten JA, et al. Early postoperative measurement of fibroblast growth factor 23 predicts severe acute kidney injury in infants after cardiac surgery. *Clin Nephrol.* (2018) 90:165–71. doi: 10.5414/CN109359

44. Perry TE, Muehlschlegel JD, Liu KY, Fox AA, Collard CD, Shernan SK, et al. Plasma neutrophil gelatinase-associated lipocalin and acute postoperative kidney injury in adult cardiac surgical patients. *Anesth Analg.* (2010) 110:1541–7. doi: 10.1213/ANE.0b013e3181da938e

45. Dasgupta MN, Montez-Rath ME, Hollander SA, Sutherland SM. Using kinetic eGFR to identify acute kidney injury risk in children undergoing cardiac transplantation. *Pediatr Res.* (2021) 90:632–6. doi: 10.1038/s41390-020-01307-3

46. Portilla D, Dent C, Sugaya T, Nagothu KK, Kundi I, Moore P, et al. Liver fatty acid-binding protein as a biomarker of acute kidney injury after cardiac surgery. *Kidney Int.* (2008) 73:465–72. doi: 10.1038/sj.ki.5002721

47. Candela-Toha A, Elías-Martín E, Abraira V, Tenorio MT, Parise D, de Pablo A, et al. Predicting acute renal failure after cardiac surgery: external validation of two new clinical scores. *Clin J Am Soc Nephrol.* (2008) 3:1260–5. doi: 10.2215/CJN.00560208

48. Wang J, Yu C, Zhang Y, Huang Y. A prediction model for acute kidney injury after pericardiectomy: an observational study. *Front Cardiovasc Med.* (2022) 9:790044. doi: 10.3389/fcvm.2022.790044

49. Li J, Gong M, Joshi Y, Sun L, Huang L, Fan R, et al. Machine learning prediction model for acute renal failure after acute aortic syndrome surgery. *Front Med.* (2022) 8:728521. doi: 10.3389/fmed.2021.728521

50. Sutherland L, Hittesdorf E, Yoh N, Lai T, Mechling A, Wagener G. Acute kidney injury after cardiac surgery: a comparison of different definitions. *Nephrology.* (2020) 25:212–8. doi: 10.1111/nep.13669

51. Dong J, Feng T, Thapa-Chhetry B, Cho BG, Shum T, Inwald DP, et al. Machine learning model for early prediction of acute kidney injury (AKI) in pediatric critical care. *Crit Care.* (2021) 25:288. doi: 10.1186/s13054-021-03724-0

52. Shorten G, Srinivasan KK, Reinertsen I. Machine learning and evidence-based training in technical skills. *Br J Anaesth.* (2018) 121:521–3. doi: 10.1016/j.bja.2018.04.012

53. Ghahramani Z. Probabilistic machine learning and artificial intelligence. *Nature.* (2015) 521:452–9. doi: 10.1038/nature14541

54. Quax S, van Gerven M. Emergent mechanisms of evidence integration in recurrent neural networks. *PLoS ONE.* (2018) 13:e0205676. doi: 10.1371/journal.pone.0205676

55. Abraham A, Pedregosa F, Eickenberg M, Gervais P, Mueller A, Kossaifi J, et al. Machine learning for neuroimaging with scikit-learn. *Front Neuroinf.* (2014) 8:14. doi: 10.3389/fninf.2014.00014

56. Kilic A. Artificial Intelligence and Machine Learning in Cardiovascular Health Care. *Ann Thorac Surg.* (2020) 109:1323–9. doi: 10.1016/j.athoracsur.2019.09.042

57. Koyner JL, Carey KA, Edelson DP, Churpek MM. The development of a machine learning inpatient acute kidney injury prediction model. *Crit Care Med.* (2018) 46:1070–7. doi: 10.1097/CCM.0000000000003123

58. Huang C, Murugiah K, Mahajan S, Li SX, Dhruva SS, Haimovich JS, et al. Enhancing the prediction of acute kidney injury risk after percutaneous coronary intervention using machine learning techniques: a retrospective cohort study. *PLoS Med.* (2018) 15:e1002703. doi: 10.1371/journal.pmed.1002703

59. Lee HC, Yoon SB, Yang SM, Kim WH, Ryu HG, Jung CW, et al. Prediction of acute kidney injury after liver transplantation: machine learning approaches vs. logistic regression model. *J Clin Med.* (2018) 7:428. doi: 10.3390/jcm7110428

frontiers | Frontiers in Cardiovascular Medicine

TYPE Original Research
PUBLISHED 28 September 2022
DOI 10.3389/fcvm.2022.998558

Check for updates

OPEN ACCESS

EDITED BY
Yael Yaniv,
Technion Israel Institute of Technology, Israel

REVIEWED BY
John Adeoye,
The University of Hong Kong, Hong Kong SAR, China
Jorge Rodríguez Capitán,
Centro de Investigación Biomédica en Red en Enfermedades Cardiovasculares (CIBERCV), Spain

*CORRESPONDENCE
James A. White
jawhit@ucalgary.ca

SPECIALTY SECTION
This article was submitted to Cardiovascular Imaging, a section of the journal Frontiers in Cardiovascular Medicine

RECEIVED 20 July 2022
ACCEPTED 05 September 2022
PUBLISHED 28 September 2022

CITATION
Dykstra S, Satriano A, Cornhill AK, Lei LY, Labib D, Mikami Y, Flewitt J, Rivest S, Sandonato R, Feuchter P, Howarth AG, Lydell CP, Fine NM, Exner DV, Morillo CA, Wilton SB, Gavrilova ML and White JA (2022) Machine learning prediction of atrial fibrillation in cardiovascular patients using cardiac magnetic resonance and electronic health information. *Front. Cardiovasc. Med.* 9:998558. doi: 10.3389/fcvm.2022.998558

COPYRIGHT
© 2022 Dykstra, Satriano, Cornhill, Lei, Labib, Mikami, Flewitt, Rivest, Sandonato, Feuchter, Howarth, Lydell, Fine, Exner, Morillo, Wilton, Gavrilova and White. This is an open-access article distributed under the terms of the Creative Commons Attribution License (CC BY). The use, distribution or reproduction in other forums is permitted, provided the original author(s) and the copyright owner(s) are credited and that the original publication in this journal is cited, in accordance with accepted academic practice. No use, distribution or reproduction is permitted which does not comply with these terms.

Machine learning prediction of atrial fibrillation in cardiovascular patients using cardiac magnetic resonance and electronic health information

Steven Dykstra[1,2], Alessandro Satriano[1,2,3], Aidan K. Cornhill[1,2], Lucy Y. Lei[1,2], Dina Labib[1,2], Yoko Mikami[1,2,3], Jacqueline Flewitt[1], Sandra Rivest[1,2], Rosa Sandonato[1,2], Patricia Feuchter[1,2,3], Andrew G. Howarth[1,2,3], Carmen P. Lydell[1,2,3], Nowell M. Fine[2], Derek V. Exner[2], Carlos A. Morillo[2], Stephen B. Wilton[2], Marina L. Gavrilova[4] and James A. White[1,2,3]*

[1]Stephenson Cardiac Imaging Centre, Libin Cardiovascular Institute of Alberta, University of Calgary, Calgary, AB, Canada, [2]Department of Cardiac Sciences, Cumming School of Medicine, University of Calgary, Calgary, AB, Canada, [3]Department of Diagnostic Imaging, Cumming School of Medicine, University of Calgary, Calgary, AB, Canada, [4]Department of Computer Science, University of Calgary, Calgary, AB, Canada

Background: Atrial fibrillation (AF) is a commonly encountered cardiac arrhythmia associated with morbidity and substantial healthcare costs. While patients with cardiovascular disease experience the greatest risk of new-onset AF, no risk model has been developed to predict AF occurrence in this population. We hypothesized that a patient-specific model could be delivered using cardiovascular magnetic resonance (CMR) disease phenotyping, contextual patient health information, and machine learning.

Methods: Nine thousand four hundred forty-eight patients referred for CMR imaging were enrolled and followed over a 5-year period. Seven thousand, six hundred thirty-nine had no prior history of AF and were eligible to train and validate machine learning algorithms. Random survival forests (RSFs) were used to predict new-onset AF and compared to Cox proportional-hazard (CPH) models. The best performing features were identified from 115 variables sourced from three data domains: (i) CMR-based disease phenotype, (ii) patient health questionnaire, and (iii) electronic health records. We evaluated discriminative performance of optimized models using C-index and time-dependent AUC (tAUC).

Results: A RSF-based model of 20 variables (CIROC-AF-20) delivered an overall C-index of 0.78 for the prediction of new-onset AF with respective tAUCs of 0.80, 0.79, and 0.78 at 1-, 2- and 3-years. This outperformed a novel CPH-based model and historic AF risk scores. At 1-year of follow-up, validation cohort patients classified as high-risk of future AF by CIROC-AF-20 went on to experience a 17.3% incidence of new-onset AF, being 24.7-fold higher risk than low risk patients.

Conclusions: Using phenotypic data available at time of CMR imaging we developed and validated the first described risk model for the prediction of new-onset AF in patients with cardiovascular disease. Complementary value was provided by variables from patient-reported measures of health and the electronic health record, illustrating the value of multi-domain phenotypic data for the prediction of AF.

KEYWORDS

machine learning, atrial fibrillation, risk prediction, random survival forest, Cox proportional-hazard models

Introduction

Atrial Fibrillation (AF) is the most common arrhythmia encountered in clinical practice, affecting over 30 million patients worldwide (1, 2). Beyond the age of 40, ∼26% of men and 23% of women will develop AF (3, 4), a diagnosis associated with elevated risk of cardioembolic stroke (5), reduced quality of life (4), and higher risk of heart failure (HF) related events (6–9). Targeted efforts to develop and validate AF risk scores have been described (6, 8, 10–12) leveraging data from healthy populations without cardiovascular disease. The Framingham Heart Study (6), Atherosclerosis Risk in Communities (ARIC) Study (12), and Cohorts for Heart and Aging Research in Genomic Epidemiology (CHARGE)-AF consortium (8) each constructed risk models with modest predictive accuracy. The C2HEST score demonstrated superior performance through broader inclusion of patient phenotypic features (11). However, while patients with established cardiovascular disease experiencing greatest incident risk of AF (4), no risk model has been developed in this population.

The prediction of cardiac outcomes in diseased referral populations is anticipated to require a central emphasis on patient-specific disease phenotypes followed by their contextualization to patient demographics, comorbid states, current pharmacologic care, and cardiovascular symptoms. In this study we tested the predictive utility of multi-domain data resources being routinely captured at time of diagnostic testing for the prediction of time to future AF in patients with cardiovascular disease. This was tested in 7,639 consecutive patients referred to cardiovascular magnetic resonance (CMR) at two tertiary care referral institution. Collective data resources were provided to machine learning based modeling for the patient-specific prediction of time to future AF. Prediction performance using machine learning was then compared to traditional statistical modeling using a Cox proportional-hazard models and published AF risk models.

Abbreviations: AF, Atrial Fibrillation; AUC, Area Under the Receiver Operator Characteristic Curve; CIROC, Cardiovascular Imaging Registry of Calgary; CPH, Cox Proportional-Hazards; CV, Cross Validation; EHR, Electronic Health Record; NND, Number Needed to Diagnose; NNP, Number Needed to Predict; RSF, Random Survival Forest; SCD, Sudden Cardiac Death; VHD, Valvular Heart Disease.

Materials and methods

Dataset available for risk modeling

Data from 9,448 unique patients was available from the Cardiovascular Imaging Registry of Calgary (CIROC, NCT04367220), a prospective clinical outcomes study of the Libin Cardiovascular Institute. Patients referred for CMR at two tertiary care centers were engaged at time of diagnostic testing to provide informed consent and complete a standardized patient health questionnaire. All imaging studies were triaged, protocolled, and interpreted using EHR-integrated software (cardioDI^{TM}, Cohesic Inc, Calgary) for the standardized collection of qualitative and quantitative phenotypic markers. Electronic health data was abstracted from the institutional data warehouse to provide patient-related laboratory, pharmacy, 12-lead ECG, Holter, and ICD-10 coded diagnostic and procedural data, as shown in Figure 1. Patients enrolled between February 2015 and November 2019 subsequently completing a minimum follow-up of 120 days were considered for model development and validation.

For the purposes of the described prediction model, all patients with a prior history of AF were excluded followed by the exclusion of patients with complex congenital heart disease (given their unique data model). Of 9,448 unique Registry patients, 7,802 met inclusion criteria with 7,639 having completed 120 days of clinical follow-up.

Data element generation and collection

Patient reported health data

A standardized patient reported health (PRH) questionnaire was used to collect baseline demographic information,

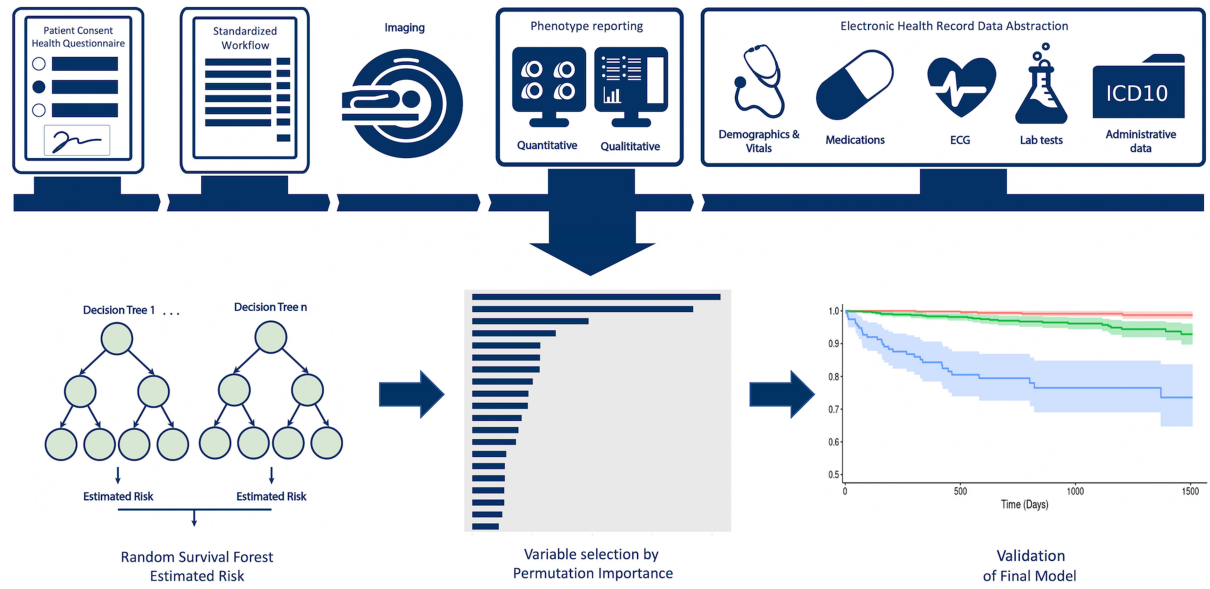


FIGURE 1
Central Illustration providing an overview of the multi-domain data collection and modeling process.

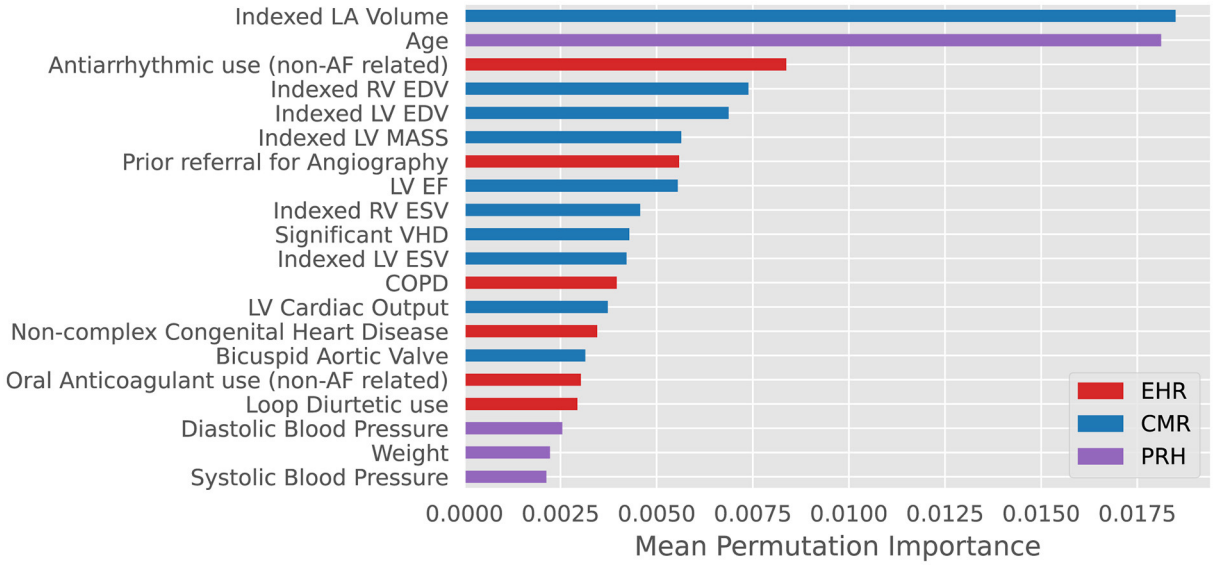


FIGURE 2
Top 20 variables for prediction of new-onset atrial fibrillation ranked by mean permutation importance calculated over 100 bootstrap samples of training data within each fold of cross-validation. VHD: valvular heart disease defined as ≥ moderate mitral or aortic valve insufficiency or stenosis. COPD: Chronic Obstructive Pulmonary Disease. EHR, Electronic Health Records; CMR, Cardiac Magnetic Resonance; PRH, Patient Reported Health (Questionnaires).

inclusive of ethnicity, education level, employment status, comorbid cardiac and non-cardiac diseases, alcohol consumption, smoking history, patient-reported shortness of breath based upon the New-York Heart Association (NYHA) classification, and QoL using the EQ-5D tool (13).

TABLE 1 Baseline Clinical Demographics in patient with and without the primary outcome of incident atrial fibrillation.

Baseline characteristics	Total cohort ($N = 7,639$)	Event – ($N = 7,325$)	Event + ($N = 314$)	p-value
Age (years)	52.2 ± 15.7	51.8 ± 15.7	62.1 ± 12.9	**<0.001**
Male, *n* (%)	4,520 (59.2)	4,301 (58.9)	219 (69.7)	**<0.001**
BSA (m^2)	1.9 ± 0.2	1.9 ± 0.2	2.0 ± 0.3	**0.002**
BMI (kg/m^2)	28.1 ± 6.2	28.0 ± 6.2	28.8 ± 6.7	**0.024**
SBP (mmHg)	116.4 ± 17.4	116.3 ± 17.4	117.0 ± 18.2	0.532
DBP (mmHg)	68.7 ± 12.3	68.7 ± 12.2	67.4 ± 13.1	0.076
NYHA class III or IV, *n* (%)	1,127 (14.8)	1,071 (14.6)	56 (17.8)	0.136
Previous angioplasty, *n* (%)	666 (8.7)	624 (8.5)	42 (13.4)	**0.004**
Previous bypass, *n* (%)	196 (2.6)	186 (2.5)	10 (3.2)	0.599
Smoker, *n* (%)	1,230 (16.1)	1,173 (16.0)	57 (18.2)	0.352
Alcohol consumption (>2 drinks per day), *n* (%)	203 (2.6)	197 (2.7)	6 (1.9)	0.509
Caffeine consumption (>2 drinks per day), *n* (%)	952 (12.5)	899 (12.3)	53 (16.9)	**0.020**
Comorbidities[a]				
Diabetes, *n* (%)	928 (12.1)	867 (11.8)	61 (19.4)	**<0.001**
Hypertension, *n* (%)	2,531 (33.1)	2,378 (32.5)	153 (48.7)	**<0.001**
Hyperlipidemia, *n* (%)	1,225 (16.0)	1,150 (15.7)	75 (23.9)	**<0.001**
COPD, *n* (%)	201 (2.6)	183 (2.5)	18 (5.7)	**<0.001**
Hypothyroidism, *n* (%)	582 (7.6)	565 (7.7)	17 (5.4)	0.163
Hyperthyroidism, *n* (%)	104 (1.4)	99 (1.4)	5 (1.6)	0.911
Medication use				
ACE-I or ARB, *n* (%)	3,498 (45.8)	3,309 (45.2)	189 (60.2)	**<0.001**
Antiarrhythmics[b], *n* (%)	116 (1.5)	94 (1.3)	22 (7.0)	**<0.001**
Anti-coagulant[b], *n* (%)	673 (8.8)	619 (8.5)	54 (17.2)	**<0.001**
Beta blocker, *n* (%)	3,397 (44.5)	3,202 (43.7)	195 (62.1)	**<0.001**
Calcium channel blocker,*n* (%)	995 (13.0)	933 (12.7)	62 (19.7)	**0.006**
Digoxin, n (%)	92 (1.2)	83 (1.1)	9 (2.9)	**0.013**
Oral hypoglycemic, *n* (%)	981 (12.8)	915 (12.5)	66 (21.0)	**<0.001**
Statin, *n* (%)	2,768 (36.2)	2,602 (35.5)	166 (52.9)	**<0.001**
Loop diuretic, *n* (%)	855 (11.2)	782 (10.7)	73 (23.2)	**<0.001**
Potassium sparing diuretic, *n* (%)	966 (12.6)	907 (12.4)	59 (18.8)	**0.001**
Thiazide diuretic, *n* (%)	631 (8.3)	580 (7.9)	51(16.2)	**<0.001**

BSA, body surface area; BMI, Body mass index; SBP, systolic blood pressure; DBP, diastolic blood pressure; NYHA, New York Heart Association; COPD, chronic obstructive pulmonary disease; ACE-I, angiotensin-converting enzyme inhibitor; ARB, angiotensin II receptor blocker. [a]Comorbidities were calculated from patient report health questionnaires. [b]not for the treatment of atrial fibrillation. Bold values indicate p-values ≤ 0.05.

CMR imaging-based disease phenotype

CMR imaging was performed on 3-T clinical scanners (Prisma or Skyra, Siemens Healthcare, Erlangen, Germany) using standardized protocols inclusive of breath-held cine and late gadolinium enhancement (LGE) imaging in sequential short-axis views and 2-,3-, and 4-chamber long axis views. Quantitative image analyses were performed using commercial software (cvi42; Circle Cardiovascular Inc., Calgary). Left ventricular (LV) and right ventricular (RV) volumes and function were assessed on short axis cine images using semi-automated contour tracing of the endocardial and epicardial borders followed by manual adjustment. Maximal left atrial volume was assessed in the phase immediately prior to mitral valve opening using the bi-plane area-length method. All measurements were indexed to body surface area (BSA), where appropriate, using the Mosteller formula (14). Chamber volumes, mass and function were coded by z-score comparison to age and sex-based reference values (15). LGE images were scored for the presence, distribution, and burden of fibrosis, as previously described (16, 17). All other disease features were coded in accordance with guidelines provided by the SCMR and European Association of Cardiovascular Imaging (EACVI) or the American Society of Echocardiography (ASE) (18, 19).

TABLE 2 Baseline imaging phenotypic features in patient with and without the primary outcome of incident atrial fibrillation.

CMR-imaging variables	Total cohort ($N = 7,639$)	Event – ($N = 7,325$)	Event + ($N = 314$)	p-value
Indexed LV EDV (ml/m^2)	87.5 ± 29.4	87.0 ± 29.0	98.0 ± 36.6	**<0.001**
Indexed LV ESV (ml/m^2)	41.7 ± 28.3	41.3 ± 28.0	49.8 ± 34.0	**<0.001**
LV EF (%)	55.4 ± 13.7	55.6 ± 13.6	52.8 ± 16.0	**<0.001**
Indexed LV Mass (g/m^2)	59.8 ± 19.9	59.4 ± 19.7	68.1 ± 23.0	**<0.001**
Indexed RV EDV (ml/m^2)	82.5 ± 23.3	82.3 ± 23.0	87.5 ± 30.1	**<0.001**
Indexed RV ESV (ml/m^2)	38.0 ± 17.1	37.8 ± 16.8	42.2 ± 22.1	**<0.001**
RV EF (%)	55.1 ± 9.7	55.2 ± 9.7	53.5 ± 11.0	**0.003**
Indexed LA Volume (ml/m^2)	35.9 ± 14.1	35.5 ± 13.8	44.3 ± 18.0	**<0.001**
Aortic stenosis[a], *n* (%)	124 (1.6)	101 (1.4)	23 (7.3)	**<0.001**
Aortic regurgitation[a], *n* (%)	68 (0.9)	57 (0.8)	11 (3.5)	**<0.001**
Mitral stenosis[a], *n* (%)	11 (0.1)	8 (0.1)	3 (1.0)	**0.002**
Mitral regurgitation[a], *n* (%)	140 (1.8)	121 (1.7)	19 (6.1)	**<0.001**

LV, left ventricular; RV, right ventricular; EDV, end diastolic volume; ESV, end systolic volume; EF: ejection fraction; LA, left atrial; All indexed values are indexed to body surface area (Mosteller formula); [a]≥ = moderate stenosis or insufficiency by imaging. Bold values indicate p-values ≤ 0.05.

Electronic health record-derived data

Electronic health information was abstracted from the institutional data warehouse, inclusive of laboratory, pharmacy, 12-lead ECG, Holter, and ICD-10 coded diagnostic and procedural data. ICD-10 coding was abstracted from the Discharge Abstract Database (DAD) and the National Ambulatory Care Reporting System (NACRS). 12-lead ECG and Holter data were obtained from archival systems (MUSE and MARS, GE Healthcare Milwaukee, USA) using custom scripts to extract vendor-coded detection of AF and identify text-based reporting of AF through internally validated natural language processing. Mortality data was obtained from Vital Statistics Alberta.

Primary clinical outcome

Patients were followed for the primary outcome of new-onset AF, defined as one or more of the following: (i) ICD-10 coded admission for AF (I48.0-I48.2, I48.9), atrial flutter (Aflut: I48.3-I48.4), (ii) any 12-lead ECG or Holter-based detection of AF, (iii) ICD-10 coded direct-current (DC) cardioversion (1HZ09) or ablative procedure (025S3ZZ, 025T3ZZ) for the treatment of AF. Atrial flutter was included in the primary outcome due to common co-existence, similar clinical management, and sequelae. A 2-month blackout period was applied to ensure outcomes were unrelated to any clinical events triggered by performance of diagnostic testing. The primary outcome was described in days from index CMR test performance.

Statistical analysis

Descriptive statistics are reported as mean ± standard deviation (SD) for continuous variables with categorical variables expressed in counts with percentages. Categorical data were compared using the chi-square test/Fisher's exact test, continuous data compared using Mann-Whitney U test for non-parametric variables and independent t-tests for dependent variables. Missing data points were excluded from comparison for respective variables. A total of 115 variables routinely captured at time of patient encounter by the CIROC Registry were considered for risk modeling (Supplementary Table 1), inclusive of imaging-based disease phenotype ($n = 33$), patient-reported health measures ($n = 48$), and EHR abstracted variables ($n = 34$). Variables with rare missing data (<15%) were imputed using Multivariate Imputation *via* Chained Equations (MICE) (20).

Variable selection and model development

Population data was split into training and validation datasets using 5-fold cross validation. In this process four training folds were combined (80%) and the remaining fold (20%) reserved as a hold-out for model validation. We performed a nested cross-validation for feature selection and hyperparameter tuning. Due to the relatively rare nature of new-onset AF, each outer fold was stratified to ensure balanced event rates across folds. The validation cohorts were used for

TABLE 3 Historic Cox Proportional Hazard model variables and corresponding variables chosen from the CIROC Registry.

C2HEST	**Training mean C-index:**	**0.70 ± 0.01**	
Original risk factors	**CIROC variables**	**HR (95% CI)**	***p*-values**
CAD	CAD	0.93 (0.66–1.32)	0.68
COPD	COPD	1.31 (0.76–2.26)	0.33
Hypertension	Hypertension	1.43 (1.11–1.86)	**0.01**
Elderly (age>75)	Age at scan	1.04 (1.03–1.05)	**<0.01**
Systolic HF	LVEF <50%	0.99 (0.98–1.00)	**0.05**
Thyroid disease (hyperthyroidism)	Thyroid disease (hyperthyroidism)	0.71 (0.23–2.21)	0.86
Aronson et al.	**Training mean C-index:**	**0.71 ± 0.01**	
Original risk factors	**CIROC variables**	**HR (95% CI)**	***p*-values**
Age	Age at Scan	1.05 (1.04–1.06)	**<0.01**
Female gender	Gender	0.67 (0.51–0.88)	**<0.01**
BMI	BMI	1.02 (1.00–1.04)	0.08
SBP > 160	SBP	0.99 (0.98–1.00)	**<0.01**
Previous MI	Previous MI	0.88 (0.63–1.22)	0.43
PAD	PAD	0.90 (0.22–3.65)	0.89
Hypertension	Hypertension	1.41 (1.08–1.84)	**0.01**
Previous HF	Previous HF	1.30 (0.88–1.92)	0.18
COPD	COPD	1.32 (0.76–2.27)	0.32
Inflammatory disease	Inflammatory disease	0.75 (0.31–1.83)	0.53
CHARGE-AF	**Training Mean C-index:**	**0.72 ± 0.01**	
Original risk factors	**CIROC variables**	**HR (95% CI)**	***p*-values**
Age	Age at Scan (years)	1.05 (1.04–1.06)	**<0.01**
Race (Caucasian)	Self-Reported Ethnicity (Caucasian)	1.43 (1.05–1.95)	**0.02**
Height	Height (m)	1.57 (0.38–6.40)	0.53
Weight	Weight (kg)	1.01 (1.00–1.01)	0.13
SBP	SBP (mmHg)	0.99 (0.98–1.00)	0.08
DBP	DBP (mmHg)	0.99 (0.98–1.01)	0.33
Current smoker	Active Smoker	1.37 (0.98–1.90)	0.06
Hypertensive medication	Hypertensive Medication	1.36 (1.03–1.79)	**0.03**
Diabetes	Diabetes	1.20 (0.86–1.68)	0.29
Previous HF	Previous HF	1.26 (0.85–1.86)	0.25
Previous MI	Previous MI	0.88 (0.63–1.23)	0.46

Overall model performance in the training dataset and adjusted hazards for the primary outcome of new-onset atrial fibrillation shown. CAD, coronary artery disease; COPD, chronic obstructive pulmonary disease; HF, heart failure; LVEF, left ventricular ejection fraction; BMI, body mass index; SBP, systolic blood pressure; MI, myocardial infarction; PAD, peripheral artery disease; DBP, diastolic blood pressure. Bold values indicate p-values ≤ 0.05.

estimation of final model performance and generalizability. Missing data was imputed using Python Scikit-Learns single iterative imputer (20) separately in each fold of the cross-validation process to ensure no data leakage.

Six independent risk models were trained to predict new-onset AF over 4-years of clinical follow-up. These included two random survival forest (RSF)-based models, a novel penalized Cox proportional-hazard (CPH) model using the least absolute shrinkage and selection operator (LASSO) for variable selection, and three CPH models based on variables from published AF risk scores [C2HEST (11), Aronson et al. (10), and CHARGE-AF (8)]. For CPH models, non-linearities in continuous variables were modeled using restricted cubic splines (21) and tested to ensure proportional hazard assumptions were satisfied by way of regression analysis relating Schoenfeld residuals to time. Clinical records were reviewed for patients taking anti-arrhythmic

10.3389/fcvm.2022.998558

TABLE 4 Model discriminative performance at 1-, 2-, and 3-years, as well as overall performance by C-index and time dependent AUC.

	Validation C-index (mean ± std)	Validation C-index stability (min–max)	Validation IBS (mean ± std)	Validation 1-year AUC (mean ± std)	Validation 2-year AUC (mean ± std)	Validation 3-year AUC (mean ± std)	Validation Mean AUC (mean ± std)
Cox PH models							
Aronson et al.	0.70 ± 0.03	0.67–0.75	0.034 ± 0.002	0.72 ± 0.03	0.71 ± 0.02	0.70 ± 0.02	0.71 ± 0.02
C2HEST	0.69 ± 0.02	0.65–0.73	0.034 ± 0.001	0.70 ± 0.04	0.70 ± 0.02	0.68 ± 0.02	0.70 ± 0.02
CHARGE-AF	0.71 ± 0.02	0.67–0.72	0.034 ± 0.002	0.72 ±0.03	0.71 ± 0.02	0.70 ± 0.03	0.72 ± 0.02
CIROC-AF-Cox	0.74 ± 0.02	0.71–0.79	0.033 ± 0.001	0.75 ± 0.02	0.75 ± 0.03	0.73 ± 0.03	0.75 ± 0.01
Random survival forests							
CIROC-AF-115	0.77 ± 0.02	0.74–0.79	0.031 ± 0.001	0.80 ± 0.04	0.80 ± 0.02	0.77 ± 0.02	0.79 ± 0.01
CIROC-AF-20	0.78 ± 0.01	0.75–0.81	0.031 ± 0.001	0.80 ± 0.02	0.79 ± 0.01	0.78 ± 0.02	0.77 ± 0.02

Validation: 5-fold cross-validation; C-index: Harrell's concordance index; IBS: Integrated Brier Score. AUC: time dependent (cumulative-dynamic) area under the receiver operating characteristic curve; CIROC-AF-Cox: LASSO-based variable selection. C-index Stability indicates the minimum and maximum validation c-indexes for each model across the 5-folds.

and anti-coagulant drugs to confirm prescription for non-AF related conditions.

RSF-based modeling was performed to consider non-linear interactions between variables and risk contribution to future events (22), an extension of Random Forest algorithms for right censored survival data (23). RSF also are fully data driven and independent of model assumption and can handle high dimensional data without the need for apriori feature selection (24). A RSF model was selected for its capacity to deliver an explainable prioritization of contributory model features in the form of permutation importance rank, this aimed at allowing for direct comparison to variables selected by traditional statistical modeling. First, we trained a RSF using all eligible ($n = 115$) CIROC variables (CIROC-AF-115). Second, with desire for a clinically translatable model, and recognizing that removal of variables with low predictive value can improve performance (25), we constructed a parsimonious RSF model using the 20 top performing variables (CIROC-AF-20), as shown in Figure 2. Variable performance was established by calculating each variable's permutation importance over 100 bootstrap samples from within the nested training cohort and training an RSF on each bootstrapped sample for the prediction of new-onset AF. Each variable's permutation importance was determined by the out-of-bag sample for each forest and its average importance calculated across the bootstraps (Figure 2). To determine optimal hyperparameters for each RSF-based model we performed an exhaustive grid search using a nested 5-fold CV in the training cohort (Supplementary Table 2). In the same fashion, the alpha parameter for LASSO was determined by hyperparameter tuning within the nested folds. Within each training fold data for LASSO CPH modeling was normalized to zero mean and unit variance, while categorical variables were one-hot encoded.

Performance evaluation

Each model's performance was assessed by discrimination and calibration measures. For discrimination we calculated the C-index, describing each model's ability to correctly rank event-free survival from patient scores, and the integrated brier score, which reports a measure of model performance over all time points. We reported mean C-index and integrated brier score over the five validation folds. Since C-index is shift invariant, time-dependent AUC is superior for assessing temporally sensitive risk predictions (26, 27) and was calculated at 1-, 2-, and 3-years, as well as mean value over the study duration. To assess calibration, we plotted the mean difference between predicted and observed rates of new-onset AF at each decile of risk for the best performing model's validation set, using 500 bootstrap estimates to generate 95% confidence intervals. Finally, for each risk model we compared the number needed to diagnose (NND) and the number needed to predict (NNP)

at 1-, 2-, and 3-years to permit a comparison of clinical utility across models. NND estimates the number of patients who must be evaluated to correctly detect the disease of interest, NNP the number to correctly predict this disease will occur in the future (28); the former being insensitive to variation in disease prevalence. All statistical analysis and modeling were performed in Python 3.6 and R 3.6.3. Model development and validation were done in accordance with the TRIPOD reporting guidelines (Supplementary Table 3).

Results

Study population characteristics

The baseline characteristics of 7,639 patients contributing to each prediction model are presented in Table 1. The mean age was 52.2 ± 15.7 years with 40.8% female. The prevalence of hypertension, diabetes and coronary artery disease was 33, 12, and 11%, respectively. Referral indications are provided in Supplementary Table 4. Imaging features showed a mean left ventricular ejection fraction (LVEF) of 55.5 ± 13.7%, right ventricular ejection fraction (RVEF) of 55.1 ± 9.7%, indexed left ventricular mass (LVMi) of 59.8 ± 19.9 g/m^2, and indexed left atrial volume (LAVi) of 35.9 ± 14.1 ml/m^2.

Following 17,697 patient-years of follow-up with median duration of 931 days (IQR 849), 314 patients (4.1%) experienced new-onset AF (crude incidence rate: 17.7 per 1,000 patient-years, with 283 diagnosed as atrial fibrillation and 31 diagnosed as atrial flutter). Patients experiencing AF showed significant differences in characteristics across all data domains (Table 1). Patients developing new-onset AF were older, more likely male, had higher rates of diabetes, hypertension, chronic obstructive pulmonary disease (COPD), hyperlipidemia, and taking more cardiovascular medications. Imaging-based phenotype revealed significantly higher LA and LV volumes, higher LV mass, lower LVEF and RVEF, and a higher prevalence of moderate-severe valvular disease (Table 2).

For model development and validation that 7,639 patients were spilt into 5 folds for cross validation. Each fold contains 1,527–1,528 patients, with 62–63 of them developing future atrial fibrillation in the following 4 years.

Historical cox proportional hazard AF risk model performance

Performance measures for CPH-based models trained using validated risk score variables (8, 10, 11) are listed in Table 3. Each showed similar discriminative performance with C-index scores of 0.70 to 0.72 averaged over the training folds. All models showed age and hypertension to be significant ($p < 0.01$) independent predictors. Model performance (mean C-index) for the C2HEST, Aronson, and CHARGE-AF models in validation datasets ranged between 0.69 and 0.71, with CHARGE-AF performing best at 0.71 ± 0.02. Each model showed a similar IBS of 0.034, indicating good performance and calibration across all time points. All models showed relatively stable validation c-indexes across each fold, with the largest difference between folds being 0.08 c-index. All historic models performed similarly over 1, 2, and 3 years by time dependent AUC (Table 4). AUC stability was modest, declining over time (Figure 3A).

LASSO-based cox proportional hazard model performance

The novel penalized-CPH model (CIROC-AF-Cox) reduced the variable set to 11 non-co-linear variables. CIROC-AF-Cox provided a mean C-index of 0.75 ± 0.01 over the training folds and mean validation C-index of 0.74 ± 0.02 and mean validation IBS of 0.034 ± 0.001. It showed similarly stable validation across each of the 5-folds (Table 4). CIROC-AF-Cox showed time-dependent AUC values at 1-, 2- and 3-years of 0.75 ± 0.02, 0.75 ± 0.03, 0.73 ± 0.03, and 0.75 ± 0.01, respectively. CIROC-AF-Cox showed improved stability in AUC values over time vs. historic models (Figure 3A).

Machine learning based AF risk prediction model performance

Our novel RSF-based models showed improved discrimination performance vs. historic CPH-based models, and vs. our novel CIROC-AF-Cox model. The CIROC-AF-115 model achieved a mean C-index of 0.77 ± 0.02, with the parsimonious CIROC-AF-20 model providing similar performance with mean C-index of 0.78 ± 0.01. Both RSF models had mean IBS of 0.033 ± 0.001 and showed model stability on par with the best CPH model (CHARGE-AF) with a maximum variation of 0.05 c-index between the folds. RSF models also outperformed CPH based approaches when assessed by time-dependent AUC. CIROC-AF-115 provided respective AUCs at 1-, 2- and 3-years of 0.80, 0.80, and 0.77 while CIROC-AF-20 provided respective AUCs of 0.80, 0.79, and 0.78 (Table 4).RSF Model stability was similar to the CPH models, declining slightly over the 4 year study time (50 days−1,450 days) (Figure 3A).

CIROC-AF-20 and CIROC-AF-Cox models were compared to determine how they correctly predicted low, intermediate, and high risk of incident AF. High risk was considered a predicted risk >4% per year, chosen as a 10-fold higher rate than the general population (29). Low risk was considered <1.5%. As shown in Figure 4, predicted risk estimates appropriately discriminated the future occurrence of AF. High risk patients

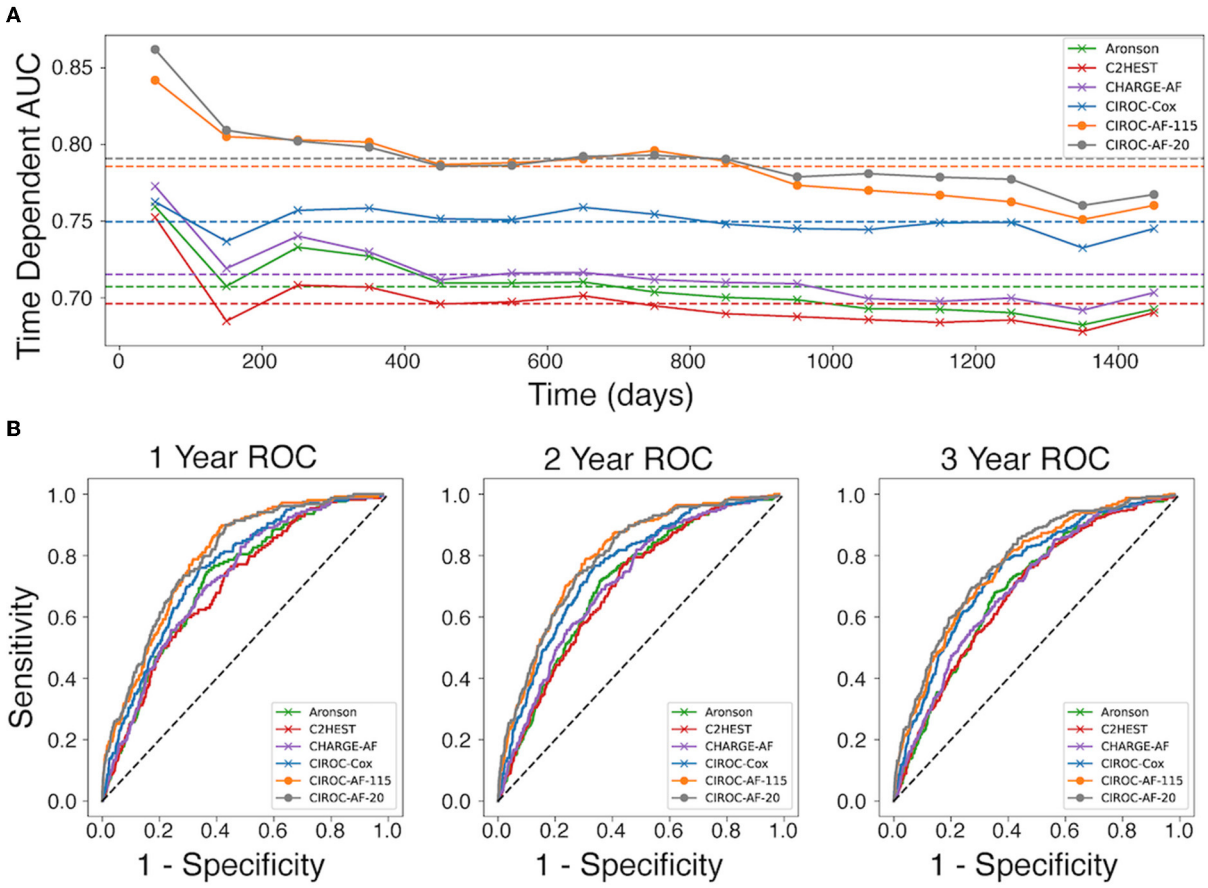


FIGURE 3
Comparison of discrimination performance for the prediction of new-onset atrial fibrillation. **(A)** Time-dependent AUC for CPH and RSF models averaged over the 5-fold validation cohorts, calculated at 15 time points for each model throughout the first 1,450 days. Dotted lines represent the mean time dependent AUC for each model. **(B)** Receiver operating characteristic (ROC) curves for each model generated at 1-year, 2-years, and 3-years.

predicted by CIROC-AF-20 experienced a 24.7-fold higher rate of AF at 1-year, 14.3-fold at 2-years, and 13.0-fold at 3-years vs. low-risk patients ($p < 0.001$ for all).

Time interval-based AUC performance and calibration

AUC curves for each model generated at 1-, 2-, and 3-years are shown in Figure 3B. RSF-based models showed improved discrimination across all time intervals vs. CIROC-AF-Cox and historic risk models. Calibration plots describing observed vs. predicted probabilities of new-onset AF at a 1-, 2-, and 3-years are shown in Figure 5. Both novel models showed good calibration across all deciles of predicted risk.

Clinical diagnostic performance

To compare diagnostically relevant performance markers, NND and NNP were calculated at 1-, 2- and 3-years. RSF models consistently outperformed CIROC-AF-Cox and all historic CPH models. RSF based models showed lowest NND between 1.97 and 2.32, with NNP ranging from 4.73 to 15.73 (Table 5).

Discussion

This study demonstrated the capacity for machine learning to deliver accurate patient-specific predictions of future AF occurrence in patients with cardiovascular disease using routinely reported CMR phenotypic markers contextualized to patient-reported and EHR-abstracted health information. Versus historic AF risk models (8, 10, 11) we observed

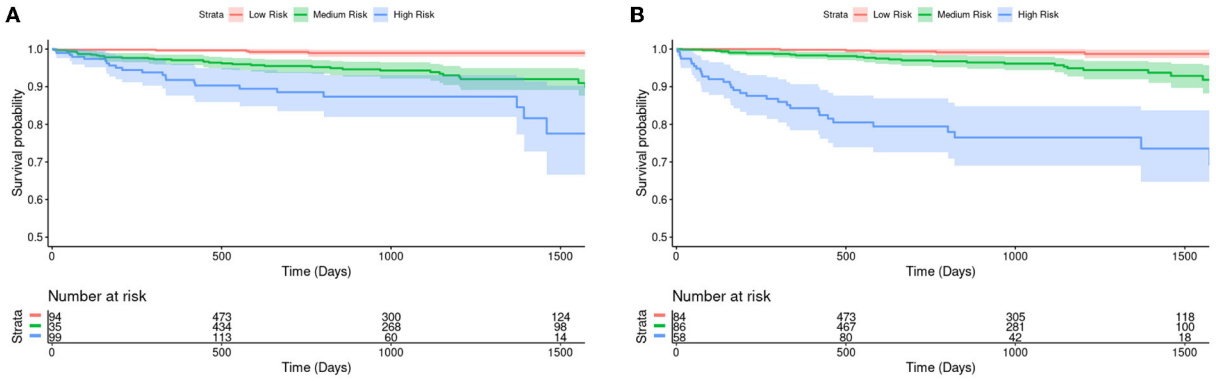


FIGURE 4
Kaplan-Meier survival curves and hazard ratios for risk of new-onset atrial fibrillation based on tertiles of predicted risk by **(A)** CIROC-AF-Cox and **(B)** CIROC-AF-20 models. The shaded area indicates a 95% confidence interval. Number at risk indicates the number of patients each model has predicted to be within each group at a given time. Intermediate risk is an estimated risk of > 1.5% and < 4%, where high risk is patients estimated at a risk of > 4%. These curves show a single fold's model performance on the fold's validation set. The log rank test *p*-values between each survival curve are shown in the table and have been adjusted *via* the Benjamini-Hochberg Procedure.

significant performance gains through expanded access to multiple data domains and through the use of machine learning-based methods.

With the exception of two studies focused in critically ill patients (30, 31), machine learning-based predictions of incident AF have been restricted to community practice settings using administrative health record data (32, 33). Despite the limited translation of these models to cardiovascular disease referral populations, these studies provided foundational evidence for machine learning to provide incremental value for the prediction of incident AF. Hill et al., used administrative health data from the UK Clinical Practice Research Datalink (CPRD) to predict future AF occurrence from 18 variables, delivering an AUC of 0.827 at 10-years vs. 0.725 using the CHARGE-AF risk score (32). A subsequent study confirmed similar findings but highlighted that much of the observed value in this referral population was being provided by conventional AF risk factors (33). Due to a low annual incidence of AF in community population settings, both studies required long term surveillance (e.g., 10-years) to identify patients at a meaningful risk of incident AF, this significantly limiting future implementation of cost-effective surveillance strategies. The alternate consideration of diagnostic testing data to assist in machine learning-based AF prediction has, to date, focused on 12-lead ECG data (34). In a single study, a model trained from ECG vector data in a community referral population showed potential for the identification of patients at elevated risk. However, whether such approaches can discriminate risk in patients with cardiovascular disease (where ECG abnormalities are more consistently observed) remains unknown. Our study uniquely focused on the prediction of AF risk in patients undergoing diagnostic imaging for cardiovascular disease, demonstrating the complementary value of disease phenotypic markers, patient-reported health measures, and EHR-abstracted health information to inform risk modeling. Importantly, all these data assets were routinely captured by, or automatically migrated to a central reporting solution. By eliminating any need for manual data collection or abstraction at time of diagnostic testing this study offers pragmatic evidence for the real-world delivery of multi-domain data collection in routine clinical practice.

As shown in Table 3, many predictors adopted by historical AF risk models (in primary care populations) failed to reach significance in patients with cardiovascular disease. Our machine learning based model objectively chose seven of the top 10 predictive variables from the imaging-based phenotype data domain. LA volume ranked first, a marker recognized as a dominant predictor of AF in both healthy (35–38) and disease-specific cohorts (29, 39). Left atrioventricular coupling index (LACI) and its change have also been shown to have an independent association with new-onset AF in the Multi-Ethnic Study of Atherosclerosis (MESA) (40). Incrementally, LVEF, LVEDVi and LV mass were important contributors; the latter acknowledged by CHARGE-AF (8). Of interest, RV EDVi was highly ranked, justifying value for multi-chamber phenotyping using CMR.

The cumulative risk of new-onset AF in our cardiovascular disease population was 4.1% at a median follow-up of 2.6 years; representing 17.7 AF events per 1,000 patient-years. This event confirms a higher incident risk of AF in this referral population vs. primary care where incident rates are between 4.0 and 6.7 events per 1,000 person-years (6, 8, 12, 29). This unique risk distribution emphasizes the need for population-specific risk models.

Finally, new-onset AF represents an ideal disease target for personalized prediction modeling at time of diagnostic

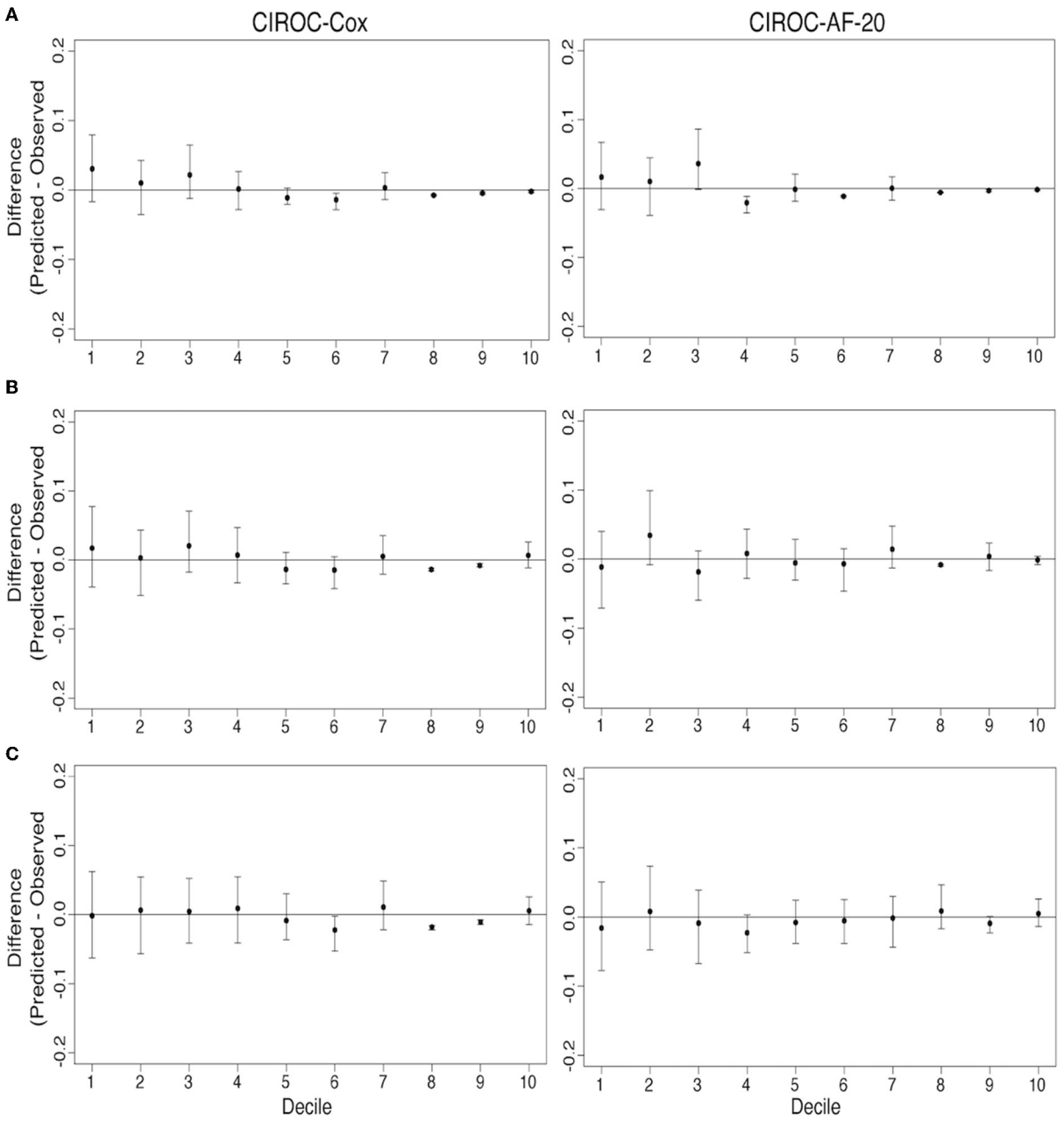


FIGURE 5
Comparison of model calibration for CIROC-AF-Cox and CIROC-AF-20 for new-onset atrial fibrillation prediction at **(A)** 1-year, **(B)** 2-years, and **(C)** 3-years. Differences between predicted and observed event rates is plotted across each decile of predicted risk. Black points indicate estimates from validation data sets and error bars indicate the 95% confidence interval from 500 bootstrapped validation data sets.

testing given the availability of validated therapies for reduction of cardio-embolic risk (41). With our model's observed 17.8% 1-year incident rate of new-onset AF in patients classified to be high-risk, actionable justification exists for the implementation of surveillance programs using Holter or wearable device-based tools for the prevention of AF-related cardiovascular events.

Limitations

Several important limitations are recognized for the current study. Our study was performed at two tertiary care hospitals within the same healthcare system. The initial study only validated the model through cross-validation and needs further hold-out validation and accordingly, external validation

TABLE 5 Number needed to diagnose (NND) and number needed to predict (NNP) performance indicators for all constructed prediction models of new-onset atrial fibrillation.

	1-Year NND (mean ± std)	2-Year NND (mean ± std)	3-Year NND (mean ± std)	1 Year NNP (mean ± std)	2 Year NNP (mean ± std)	3 Year NNP (mean ± std)
Cox PH models						
Aronson et al.	2.57 ± 0.66	2.74 ± 0.65	3.01 ± 0.64	17.91 ± 2.33	11.00 ± 2.67	6.58 ± 1.12
C2HEST	2.82 ± 0.47	2.92 ± 0.43	3.22 ± 0.46	21.29 ± 2.42	12.25 ± 2.30	7.02 ± 0.61
CHARGE-AF	2.51 ± 0.32	2.61 ± 0.26	2.96 ± 0.41	21.57 ± 4.56	10.53 ± 1.45	6.57 ± 1.27
CIROC-AF-Cox	2.17 ± 0.19	2.24 ± 0.32	2.36 ± 0.29	16.56 ± 4.32	8.71 ± 1.86	5.08 ± 0.70
Random survival forests						
CIROC-AF-115	1.97 ± 0.16	1.99 ± 0.08	2.32 ± 0.19	15.52 ± 1.04	8.00 ± 0.36	5.19 ± 0.53
CIROC-AF-20	2.03 ± 0.13	2.04 ± 0.09	2.18 ± 0.14	15.73 ± 1.77	7.62 ± 0.75	4.73 ± 0.57

NND: number needed to diagnose; the number of patients who need to be examined in order to correctly detect one person with the disease of interest in a study population of persons with and without the known disease. NNP: Number needed to predict; the number of patients who need to be examined in the patient population in order to correctly predict the diagnosis of one person.

prior to model implementation beyond our local institution. Incremental model calibrations through expanded population exposures are also advisable for all risk models, particularly to address varying ethnic distributions (42). Of the 7,639 studied patients, 5,195 (68%) were Caucasian. At time of risk modeling, the CIROC Registry had prospectively tracked clinical outcomes for a period of 4 years, and therefore uncertainty remains in the capacity of the presented model to deliver risk estimation beyond this period. Our models were trained using CMR-specific phenotypic variables. Matched echocardiographic data was not routinely available given high rates of private outpatient laboratory use, as is commonly encountered in cardiology practice. Accordingly, direct comparison to similar models trained from echocardiographic variables was not feasible. Implementation for other imaging modalities requires unique variable training and validation, recognizing unique differences in variable characteristics and referral bias. Similarly, our study did not include patients with congenital heart disease given unique anatomic phenotypes and disease profiles to routine adult cardiovascular disease. Accordingly, the current risk model is not applicable to this patient population. Finally, alternate machine learning-based techniques can be exploited for the prediction of outcomes from complex health data (32) and are planned for future investigation. In this inaugural study we did not comprehensively examine the comparative performance of alternate machine learning methodologies for survival-based prediction. Future research aimed at optimizing the presented AF prediction tool using alternate models is planned.

Conclusions

In this study we demonstrated capacity for multi-domain patient data collected at time of CMR-based phenotyping to support machine learning-based prediction of future AF in patients with cardiovascular disease. As the first described prediction model of AF risk in a cardiovascular disease population, our optimized model identified de-novo patients who experienced a 25-fold higher risk of incident AF over a 12-month period. This work provides foundational support for phenotype-based prediction modeling at time of diagnostic imaging for the delivery of personalized care. Future studies assessing the impact of AF prediction modeling at time of diagnostic imaging are warranted.

Data availability statement

The raw data supporting the conclusions of this article will be made available by the authors, without undue reservation.

Ethics statement

The studies involving human participants were reviewed and approved by Conjoint Health Research Ethics Board at the University of Calgary. The patients/participants provided their written informed consent to participate in this study.

Author contributions

SD performed all data analysis, statistical, machine learning based modeling, and manuscript authorship. JW was senior author and conceived, designed, edited, and finalized manuscript content. All other authors either assisted in data collection and adjudication (DL, YM, LL, AC, JF, SR, RS, AS, and PF), study design and manuscript review (NF, CL, AH, CM, SW, and DE) or data modeling (MG). All authors contributed to the article and approved the submitted version.

Funding

This study was partially funded by the Calgary Health Foundation.

Conflict of interest

Authors JW, AH, and JF each contributed to development of the novel software platform that is now supported by Cohesic Inc., and hold equity (shares) in this company. Author JW is the Chief Medical Officer of Cohesic Inc. Author JW has received research funding from Siemens Healthineers, Circle Cardiovascular Inc., and Pfizer Inc. Author AH has received funding from Amgen. Author SD receives funding from Alberta Innovates.

The remaining authors declare that the research was conducted in the absence of any commercial or financial relationships that could be construed as a potential conflict of interest.

Publisher's note

All claims expressed in this article are solely those of the authors and do not necessarily represent those of their affiliated organizations, or those of the publisher, the editors and the reviewers. Any product that may be evaluated in this article, or claim that may be made by its manufacturer, is not guaranteed or endorsed by the publisher.

Supplementary material

The Supplementary Material for this article can be found online at: https://www.frontiersin.org/articles/10.3389/fcvm.2022.998558/full#supplementary-material

References

1. Chugh SS, Havmoeller R, Narayanan K, Singh D, Rienstra M, Benjamin EJ, et al. Worldwide epidemiology of atrial fibrillation: a global burden of disease 2010. *Study Circulation.* (2014) 129:837–47. doi: 10.1161/CIRCULATIONAHA.113.005119

2. Stewart S, Hart C, Hole D, McMurray J. Population prevalence, incidence, and predictors of atrial fibrillation in the Renfrew/Paisley study. *Heart.* (2001) 86:516–21. doi: 10.1136/heart.86.5.516

3. Staerk L, Wang B, Preis SR, Larson MG, Lubitz SA, Ellinor PT, et al. Lifetime risk of atrial fibrillation according to optimal, borderline, or elevated levels of risk factors: cohort study based on longitudinal data from the Framingham Heart Study. *BMJ.* (2018) 361:k1453. doi: 10.1136/bmj.k1453

4. Staerk L, Sherer JA, Ko D, Benjamin EJ, Helm RH. Atrial fibrillation: epidemiology, pathophysiology, and clinical outcomes. *Circ Res.* (2017) 120:1501–17. doi: 10.1161/CIRCRESAHA.117.309732

5. O'Donnell MJ, Chin SL, Rangarajan S, Xavier D, Liu L, Zhang H, et al. Global and regional effects of potentially modifiable risk factors associated with acute stroke in 32 countries (INTERSTROKE): a case-control study. *Lancet.* (2016) 388:761–75. doi: 10.1016/S0140-6736(16)30506-2

6. Schnabel RB, Sullivan LM, Levy D, Pencina MJ, Massaro JM, D'Agostino RB, et al. Development of a risk score for atrial fibrillation (Framingham Heart Study): a community-based cohort study. *Lancet.* (2009) 373:739–45. doi: 10.1016/S0140-6736(09)60443-8

7. Chamberlain AM, Alonso A, Gersh BJ, Manemann SM, Killian JM, Weston SA, et al. Multimorbidity and the risk of hospitalization and death in atrial fibrillation: a population-based study. *Am Heart J.* (2017) 185:74–84. doi: 10.1016/j.ahj.2016.11.008

8. Alonso A, Krijthe BP, Aspelund T, Stepas KA, Pencina MJ, Moser CB, et al. Simple risk model predicts incidence of atrial fibrillation in a racially and geographically diverse population: the CHARGE-AF Consortium. *J Am Heart Assoc Cardiovasc Cerebrovasc Dis.* (2013) 2:e000102. doi: 10.1161/JAHA.112.000102

9. Schnabel RB, Rienstra M, Sullivan LM, Sun JX, Moser CB, Levy D, et al. Risk assessment for incident heart failure in individuals with atrial fibrillation. *Eur J Heart Fail.* (2013) 15:843–9. doi: 10.1093/eurjhf/hft041

10. Aronson D, Shalev V, Katz R, Chodick G, Mutlak D. Risk score for prediction of 10-year atrial fibrillation: a community-based study. *Thromb Haemost.* (2018) 118:1556–63. doi: 10.1055/s-0038-1668522

11. Li YG, Pastori D, Farcomeni A, Yang PS, Jang E, Joung B, et al. A simple clinical risk score (C2HEST) for predicting incident atrial fibrillation in Asian subjects. *Chest.* (2019) 155:510–8. doi: 10.1016/j.chest.2018.09.011

12. Chamberlain AM, Agarwal SK, Folsom AR, Soliman EZ, Chambless LE, Crow R, et al. A clinical risk score for atrial fibrillation in a biracial prospective cohort (from the atherosclerosis risk in communities (ARIC) study). *Am J Cardiol.* (2011) 107:85–91. doi: 10.1016/j.amjcard.2010.08.049

13. EuroQol Group. EuroQol–a new facility for the measurement of health-related quality of life. *Health Policy Amst Neth.* (1990) 16:199–208.

14. Mosteller RD. Simplified calculation of body-surface area. *N Engl J Med.* (1987) 317:1098. doi: 10.1056/NEJM198710223171717

15. Petersen SE, Aung N, Sanghvi MM, Zemrak F, Fung K, Paiva JM, et al. Reference ranges for cardiac structure and function using cardiovascular magnetic resonance (CMR) in Caucasians from the UK Biobank population cohort. *J Cardiovasc Magn Reson.* (2017) 19:1–19. doi: 10.1186/s12968-017-0327-9

16. Fine NM, Tandon S, Kim HW, Shah DJ, Thompson T, Drangova M, et al. Validation of sub-segmental visual scoring for the quantification of ischemic and nonischemic myocardial fibrosis using late gadolinium enhancement MRI. *J Magn Reson Imaging JMRI.* (2013) 38:1369–76. doi: 10.1002/jmri.24116

17. Satoh H, Sano M, Suwa K, Saitoh T, Nobuhara M, Saotome M, et al. Distribution of late gadolinium enhancement in various types of cardiomyopathies: Significance in differential diagnosis, clinical features and prognosis. *World J Cardiol.* (2014) 6:585–601. doi: 10.4330/wjc.v6.i7.585

18. Messroghli DR, Moon JC, Ferreira VM, Grosse-Wortmann L, He T, Kellman P, et al. Clinical recommendations for cardiovascular magnetic resonance mapping of T1, T2, T2 and extracellular volume: a consensus statement by the Society for Cardiovascular Magnetic Resonance (SCMR) endorsed by the European Association for Cardiovascular Imaging. *J Cardiovasc Magn Reson.* (2017) 19:75. doi: 10.1186/s12968-017-0389-8

19. Zoghbi WA, Adams D, Bonow RO, Enriquez-Sarano M, Foster E, Grayburn PA, et al. Recommendations for noninvasive evaluation of native valvular regurgitation: a report from the American Society of Echocardiography Developed in Collaboration with the Society for Cardiovascular Magnetic Resonance. *J Am Soc Echocardiogr.* (2017) 30:303–71. doi: 10.1016/j.echo.2017.01.007

20. Buuren Sv, Groothuis-Oudshoorn K. MICE: Multivariate Imputation by Chained Equations in R. *J Stat Softw.* (2011) 45:1–67. doi: 10.18637/jss.v045.i03

21. Roshani D, Ghaderi E. Comparing smoothing techniques for fitting the nonlinear effect of covariate in cox models. *Acta Inform Medica.* (2016) 24:38–41. doi: 10.5455/aim.2016.24.38-41

22. Kelly CJ, Karthikesalingam A, Suleyman M, Corrado G, King D. Key challenges for delivering clinical impact with artificial intelligence. *BMC Med.* (2019) 17:195. doi: 10.1186/s12916-019-1426-2

23. Ishwaran H, Kogalur UB, Blackstone EH, Lauer MS. Random survival forests. *Ann Appl Stat.* (2008) 2:841–60. doi: 10.1214/08-AOAS169

24. Wang H, Li G. A selective review on random survival forests for high dimensional data. *Quant Bio-Sci.* (2017) 36:85–96. doi: 10.22283/qbs.2017.36.2.85

25. Genuer R, Poggi JM, Tuleau-Malot C. Variable selection using random forests. *Pattern Recognit Lett.* (2010) 31:2225–36. doi: 10.1016/j.patrec.2010.03.014

26. Blanche P, Kattan MW, Gerds TA. The c-index is not proper for the evaluation of t-year predicted risks. *Biostatistics.* (2019) 20:347–57. doi: 10.1093/biostatistics/kxy006

27. Antolini L, Boracchi P, Biganzoli E. A time-dependent discrimination index for survival data. *Stat Med.* (2005) 24:3927–44. doi: 10.1002/sim.2427

28. Linn S, Grunau PD. New patient-oriented summary measure of net total gain in certainty for dichotomous diagnostic tests. *Epidemiol Perspect Innov*. (2006) 3:11. doi: 10.1186/1742-5573-3-11

29. Johansson C, Dahlqvist E, Andersson J, Jansson JH, Johansson L. Incidence, type of atrial fibrillation and risk factors for stroke: a population-based cohort study. Clin Epidemiol. *Volume.* (2017) 9:53–62. doi: 10.2147/CLEP.S122916

30. Bashar SK, Ding EY, Walkey AJ, McManus DD, Chon KH. Atrial fibrillation prediction from critically ill sepsis patients. *Biosensors.* (2021) 11:269. doi: 10.3390/bios11080269

31. Lip GYH, Genaidy A, Tran G, Marroquin P, Estes C. Incident atrial fibrillation and its risk prediction in patients developing COVID-19: a machine learning based algorithm approach. *Eur J Intern Med.* (2021) 91:53–8. doi: 10.1016/j.ejim.2021.04.023

32. Hill NR, Ayoubkhani D, McEwan P, Sugrue DM, Farooqui U, Lister S, et al. Predicting atrial fibrillation in primary care using machine learning. Azuero A, editor. *PLOS ONE.* (2019) 14:e0224582. doi: 10.1371/journal.pone.0224582

33. Tiwari P, Colborn KL, Smith DE, Xing F, Ghosh D, Rosenberg MA. Assessment of a machine learning model applied to harmonized electronic health record data for the prediction of incident atrial fibrillation. *JAMA Netw Open.* (2020) 3:e1919396. doi: 10.1001/jamanetworkopen.2019.19396

34. Raghunath S, Pfeifer JM, Ulloa-Cerna AE, Nemani A, Carbonati T, Jing L, et al. Deep neural networks can predict new-onset atrial fibrillation from the 12-lead ECG and help identify those at risk of atrial fibrillation–related stroke. *Circulation.* (2021) 143:1287–98. doi: 10.1161/CIRCULATIONAHA.120.047829

35. Tsang TSM, Barnes ME, Bailey KR, Leibson CL, Montgomery SC, Takemoto Y, et al. Left atrial volume: important risk marker of incident atrial fibrillation in 1655 older men and women. *Mayo Clin Proc.* (2001) 76:467–75. doi: 10.4065/76.5.467

36. Tsang TSM, Gersh BJ, Appleton CP, Tajik AJ, Barnes ME, Bailey KR, et al. Left ventricular diastolic dysfunction as a predictor of the first diagnosed nonvalvular atrial fibrillation in 840 elderly men and women. *J Am Coll Cardiol.* (2002) 40:1636–44. doi: 10.1016/S0735-1097(02)02373-2

37. Abhayaratna WP, Fatema K, Barnes ME, Seward JB, Gersh BJ, Bailey KR, et al. Left atrial reservoir function as a potent marker for first atrial fibrillation or flutter in persons ≥ 65 years of age. *Am J Cardiol.* (2008) 101:1626–9. doi: 10.1016/j.amjcard.2008.01.051

38. Habibi M, Samiei S, Venkatesh BA, Opdahl A, Helle-Valle TM, Zareian M, et al. CMR-measured left atrial volume and function and incident atrial fibrillation: results from the multi-ethnic study of atherosclerosis (MESA). *Circ Cardiovasc Imaging.* (2016) 9:e004299. doi: 10.1161/CIRCIMAGING.115.004299

39. Christopher M, Kramer MD, John P, DiMarco MD, Paul Kolm P, Carolyn Y, et al. Predictors of major atrial fibrillation endpoints in the national heart, lung, and blood institute HCMR. *Clin Electrophysiol.* (2021) 7:1376–86. doi: 10.1016/j.jacep.2021.04.004

40. Pezel T, Ambale-Venkatesh B, Quinaglia T, Heckbert SR, Kato Y, de Vasconcellos HD, et al. Change in left atrioventricular coupling index to predict incident atrial fibrillation: the multi-ethnic study of atherosclerosis (MESA). *Radiology.* (2022) 303:317–26. doi: 10.1093/ehjci/jeab289.377

41. Hart RG, Pearce LA, Aguilar MI. Meta-analysis: antithrombotic therapy to prevent stroke in patients who have nonvalvular atrial fibrillation. *Ann Intern Med.* (2007) 146:857–67. doi: 10.7326/0003-4819-146-12-200706190-00007

42. Alonso A, Roetker NS, Soliman EZ, Chen LY, Greenland P, Heckbert SR. Prediction of atrial fibrillation in a racially diverse cohort: the multi-ethnic study of atherosclerosis (MESA). *J Am Heart Assoc Cardiovasc Cerebrovasc Dis.* (2016) 5:e003077. doi: 10.1161/JAHA.115.003077

frontiers | Frontiers in Cardiovascular Medicine

TYPE Original Research
PUBLISHED 05 October 2022
DOI 10.3389/fcvm.2022.976769

Check for updates

OPEN ACCESS

EDITED BY
Jinwei Tian,
The Second Affiliated Hospital of Harbin Medical University, China

REVIEWED BY
Neal Yuan,
University of California, San Francisco, United States
Shirin Jimenez,
Stanford University, United States

*CORRESPONDENCE
Shruti Siva Kumar
shruti.sivakumar1993@gmail.com

†These authors have contributed equally to this work

SPECIALTY SECTION
This article was submitted to General Cardiovascular Medicine, a section of the journal Frontiers in Cardiovascular Medicine

RECEIVED 23 June 2022
ACCEPTED 05 September 2022
PUBLISHED 05 October 2022

CITATION
Siva Kumar S, Al-Kindi S, Tashtish N, Rajagopalan V, Fu P, Rajagopalan S and Madabhushi A (2022) Machine learning derived ECG risk score improves cardiovascular risk assessment in conjunction with coronary artery calcium scoring.
Front. Cardiovasc. Med. 9:976769.
doi: 10.3389/fcvm.2022.976769

COPYRIGHT
© 2022 Siva Kumar, Al-Kindi, Tashtish, Rajagopalan, Fu, Rajagopalan and Madabhushi. This is an open-access article distributed under the terms of the Creative Commons Attribution License (CC BY). The use, distribution or reproduction in other forums is permitted, provided the original author(s) and the copyright owner(s) are credited and that the original publication in this journal is cited, in accordance with accepted academic practice. No use, distribution or reproduction is permitted which does not comply with these terms.

Machine learning derived ECG risk score improves cardiovascular risk assessment in conjunction with coronary artery calcium scoring

Shruti Siva Kumar[1*†], Sadeer Al-Kindi[2,3†], Nour Tashtish[2,3], Varun Rajagopalan[2,3], Pingfu Fu[4], Sanjay Rajagopalan[2,3] and Anant Madabhushi[5]

[1]Department of Biomedical Engineering, Case Western Reserve University, Cleveland, OH, United States, [2]Harrington Heart and Vascular Institute, University Hospitals, Cleveland, OH, United States, [3]School of Medicine, Case Western Reserve University, Cleveland, OH, United States, [4]Department of Population and Quantitative Health Sciences, Case Western Reserve University, Cleveland, OH, United States, [5]Wallace H. Coulter Department of Biomedical Engineering, Radiology and Imaging Sciences, Biomedical Informatics (BMI) and Pathology, Georgia Institute of Technology and Emory University, Research Health Scientist, Atlanta Veterans Administration Medical Center, Atlanta, GA, United States

Background: Precision estimation of cardiovascular risk remains the cornerstone of atherosclerotic cardiovascular disease (ASCVD) prevention. While coronary artery calcium (CAC) scoring is the best available non-invasive quantitative modality to evaluate risk of ASCVD, it excludes risk related to prior myocardial infarction, cardiomyopathy, and arrhythmia which are implicated in ASCVD. The high-dimensional and inter-correlated nature of ECG data makes it a good candidate for analysis using machine learning techniques and may provide additional prognostic information not captured by CAC. In this study, we aimed to develop a quantitative ECG risk score (eRiS) to predict major adverse cardiovascular events (MACE) alone, or when added to CAC. Further, we aimed to construct and validate a novel nomogram incorporating ECG, CAC and clinical factors for ASCVD.

Methods: We analyzed 5,864 patients with at least 1 cardiovascular risk factor who underwent CAC scoring and a standard ECG as part of the CLARIFY study (ClinicalTrials.gov Identifier: NCT04075162). Events were defined as myocardial infarction, coronary revascularization, stroke or death. A total of 649 ECG features, consisting of measurements such as amplitude and interval measurements from all deflections in the ECG waveform (53 per lead and 13 overall) were automatically extracted using a clinical software (GE Muse™ Cardiology Information System, GE Healthcare). The data was split into 4 training (S_{tr}) and internal validation (S_v) sets [S_{tr} (1): S_v (1): 50:50; S_{tr} (2): S_v (2): 60:40; S_{tr} (3): S_v (3): 70:30; S_{tr} (4): S_v (4): 80:20], and the results were compared across all the subsets. We used the ECG features derived from S_{tr} to develop eRiS. A least absolute shrinkage and selection operator-Cox (LASSO-Cox) regularization model was used for data dimension reduction, feature selection, and eRiS construction. A Cox-proportional hazards model was used to assess the benefit of using an eRiS alone (M_{ecg}), CAC alone (M_{cac}) and a combination of eRiS and CAC ($M_{ecg+cac}$) for MACE prediction. A nomogram (M_{nom}) was further constructed by integrating eRiS with CAC and demographics (age and sex). The primary endpoint of the study was the assessment of the performance

of M_{ecg}, M_{cac}, $M_{ecg+cac}$ and M_{nom} in predicting CV disease-free survival in ASCVD.

Findings: Over a median follow-up of 14 months, 494 patients had MACE. The feature selection strategy preserved only about 18% of the features that were consistent across the various strata (S_{tr}). The M_{ecg} model, comprising of eRiS alone was found to be significantly associated with MACE and had good discrimination of MACE (C-Index: 0.7, $p = <2e\text{-}16$). eRiS could predict time-to MACE (C-Index: 0.6, $p = <2e\text{-}16$ across all S_v). The $M_{ecg+cac}$ model was associated with MACE (C-index: 0.71). Model comparison showed that $M_{ecg+cac}$ was superior to M_{ecg} ($p = 1.8e\text{-}10$) or M_{cac} ($p < 2.2e\text{-}16$) alone. The M_{nom}, comprising of eRiS, CAC, age and sex was associated with MACE (C-index 0.71). eRiS had the most significant contribution, followed by CAC score and other clinical variables. Further, M_{nom} was able to identify unique patient risk-groups based on eRiS, CAC and clinical variables.

Conclusion: The use of ECG features in conjunction with CAC may allow for improved prognostication and identification of populations at risk. Future directions will involve prospective validation of the risk score and the nomogram across diverse populations with a heterogeneity of treatment effects.

KEYWORDS

machine learning, artificial intelligence, atherosclerotic cardiovascular diseases (ASCVD), electrocardiogram (ECG), risk assessment/classification, nomogram

Introduction

Cardiovascular disease is the leading cause of death in the United States, with significant morbidity and cost of care (1). While cardiovascular mortality has declined in recent decades, the rate of decline appears to be decelerating, thought to be related to the increasing prevalence and exposure to risk factors such as unhealthy diet, obesity, physical inactivity, hyperlipidemia, hypertension and high alcohol use (2). Therefore, primary prevention of atherosclerotic cardiovascular disease (ASCVD) remains an important public health goal but requires precise identification of at-risk individuals.

Current approaches for risk evaluation are dependent on probabilistic risk scores, which are poorly calibrated, do not perform well across populations and do not provide individual risk assessment. The Pooled Cohort Equations (PCE) (1), which is a sex- and race-specific tool for estimating 10-year absolute rates of ASCVD is based on nine clinical variables. While PCE is in routine clinical use in the U.S., its CV risk overestimation (3, 4) and suboptimal calibration in specific patient populations have been noted (5–9), leading to updated clinical practice guidelines in 2019 (10, 11). While cardiac death was originally defined in the PCE as only those related to coronary heart disease, other types of cardiac death, such as those related to fatal arrhythmias or heart failure, also occur and may not be captured by the PCE (12–17) Coronary artery calcium (CAC), a marker of atherosclerosis, is an essential predictor of coronary artery disease, incident cardiovascular events and all-cause mortality (18–21). CAC combined with traditional clinical risk factors in an ML model, have been associated with superior risk prediction when compared to PCE and CAC alone (22). Also, combining CAC with traditional risk scores are better predictors of 1-year MACE and early revascularization (23, 24). However CAC may still not capture risk in the context of other indications such as for arrhythmic events.

ECG features have been used to diagnose or predict cardiovascular events. For instance, heterogeneity of R-wave and T-wave morphology and ST-segment elevation have been used to diagnose ventricular arrhythmias (25, 26). ST-segment elevation myocardial infarction (STEMI) has also been used for chronic HF prediction (27). QRS duration and morphology including left bundle branch block have been used for assessing ventricular dyssynchrony and predicting heart failure (28). Similarly, QT-prolongation and T-wave abnormalities are associated with increased risk for arrhythmia (29) and SCD (30), respectively. However, these individual ECG markers require manual assessment and can thus, be prone to subjective interpretation and variable clinical decisions. Recently, machine learning (ML) have been employed to analyze the 12-lead, high-dimensional ECG signal automatically, providing a more quantitative and reproducible alternative to more subjective interpretation (31, 32). Neural networks on ECGs have been shown to outperform

manual QTc measurements for life-threatening ventricular arrhythmia prediction (33, 34) and also as predictive tools for ventricular dysfunction (35, 36), coronary artery disease (37), atrial fibrillation (38, 39), myocardial hypertrophy (40) and ischemic heart disease (41). Although ML frameworks on ECGs lack direct interpretability, they have been used to detect the most relevant waves (P-wave, QRS complex or T-wave), contributing to diagnosis of CVDs (42). Additionally, ML frameworks have shown to detect both, clinically significant and other subtle features that are not traditionally used by cardiologists (42).

Given the significant value and success of ML-aided techniques over manual assessment for cardiovascular disease diagnosis and prediction, traditional ASCVD risk calculators can potentially be augmented by features derived from ECG using ML. In addition to ECG and other clinical predictors, inclusion of CAC may improve cardiovascular risk stratification beyond using CAC or ECG alone. This study sought to address three objectives: (1) To evaluate the utility of ML on ECG data (hand-crafted features) to predict MACE, (2) To evaluate the additive benefit of ECG on CAC scores to predict MACE and (3) To construct a nomogram with ECG and clinical variables to assess its predictive capability of MACE. By including ECG and CAC in a single model using a large prospective cohort (5,864 patients), a novel ASCVD-specific risk calculator is presented, one that addresses some of the limitations associated with the PCE.

Methods

Study design and participants

We used data from the Community Benefit of No-charge Calcium Score Screening Program (CLARIFY, ClinicalTrials.gov Identifier: NCT04075162), a prospective cohort study of patients with at least one cardiovascular risk factor who underwent no-charge coronary artery calcium scoring at University Hospitals Health Systems (UHHS), comprising 11 hospitals and >31 health centers across Ohio. We included participants with at least 1 cardiovascular risk factor and with a clinically available 12 lead electrocardiogram in CLARIFY who underwent CAC between January 1st, 2014, to November 4th, 2020. Cardiovascular events were identified from the electronic medical records as part of the registry and included heart failure, myocardial infarction, coronary revascularization, stroke, and death. Available patient factors included CAC, age, female, race, smoking status, body mass index, blood pressure, serum lipids (total cholesterol, low-density lipoprotein, high-density lipoprotein, triglycerides). The 10-year predicted risk of atherosclerotic cardiovascular disease was calculated for individuals with available variables using the AHA/ACC pooled cohort equations.

ECG feature extraction

During an ECG test, each patient's data is automatically processed through GE Muse^{TM} Cardiology Information System (Milwaukee, WI, USA) using the validated GE Marquette^{TM} 12SL^{TM} ECG analysis program (43). For each 12-lead ECG test, a total of 649 ECG features (53 per lead and 13 overall) were extracted. These features consisted of measurements such as amplitude and interval measurements from all deflections in the ECG waveform in each of the 12 leads (Supplementary Table 1). These 649 features along with cardiovascular event outcomes were extracted for all CLARIFY patients and were made available for subsequent analysis.

Feature selection and model construction

For this analysis, patients in the CLARIFY trial were split randomly into training (S_{tr}) and validation sets (S_v) using a stratification technique to preserve the same proportion of those who had an adverse CV event vs. those without an event during their follow-up period. Four split sizes were implemented [S_{tr} (1): S_v (1): 50:50, S_{tr} (2): S_v (2): 60:40, S_{tr} (3): S_v (3): 70:30, S_{tr} (4): S_v (4): 80:20], and the results were compared across all the subsets.

The least absolute shrinkage and selection operator (LASSO) (44) method was used to select the most useful predictive features from the patients in S_{tr}. The value of the tuning parameter in the LASSO-Cox model (λ) was averaged out *via* 10 cross-validations to minimize error. An advantage of the LASSO based analysis is the sparse solution associated with it, resulting in unimportant features being assigned a weight of 0. As a result, only the most discriminative features are preserved using this strategy. After selecting the top features, the corresponding LASSO coefficients were used for the eRiS construction. eRiS was calculated for each patient *via* a linear combination of selected features that were weighted by their respective coefficients. Hence, for each patient, a new composite ECG-risk score is added as a single feature (Figure 1).

A Cox-proportional hazards model was used to assess the benefit of using an eRiS alone (M_{ecg}), CAC alone (M_{cac}) and a combination of eRiS and CAC ($M_{ecg+cac}$) for ASCVD that is prognostic of adverse CV disease-free survival. These models were then further validated on S_v. M_{nom} was constructed by integrating eRiS with CAC and clinical covariates (age and sex) (Figure 1). This was developed on S_{tr} and then validated on S_v. To validate M_{nom} against the standard PCE based risk calculator (1), we extracted the estimated 10-year ASCVD risk from PCE for patients in this study. This information was available for only 1,291 patients out of the 5,864 eligible patients analyzed in this study.

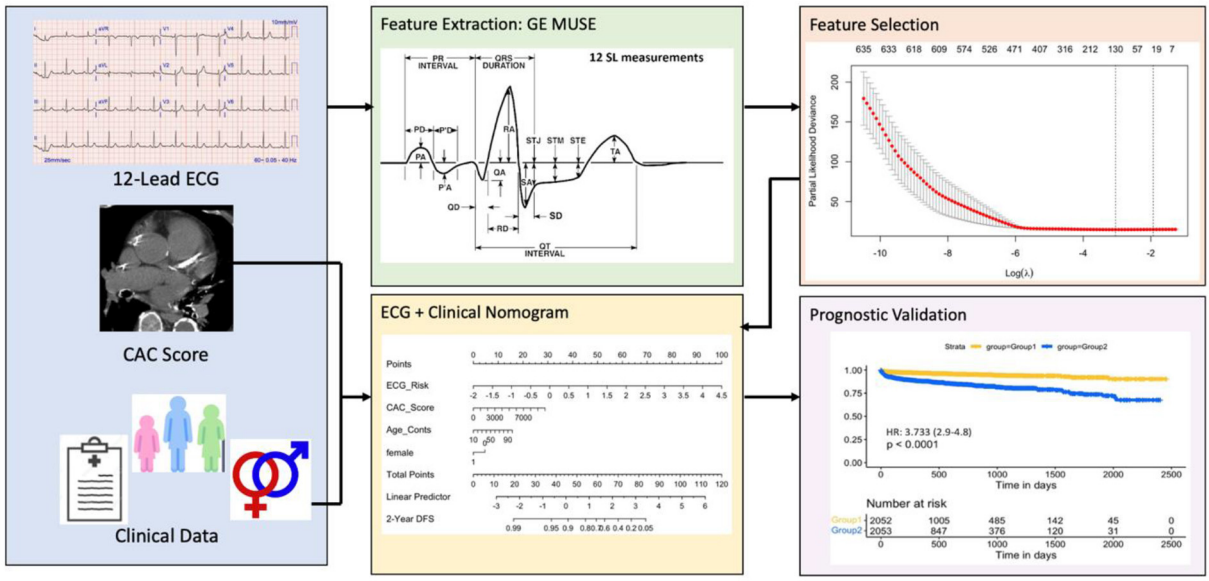


FIGURE 1
Overall workflow. The first step involves collecting ECG tests, manual CAC scores and clinical data from eligible patients. The ECG features are then automatically extracted using the commercially available GE MUSE software. Top ECG features were selected using the LASSO feature selection method and used for constructing eRiS. M_{nom} was constructed using clinical features and eRiS. M_{ecg} and M_{nom} were validated for prognostic performance and predicting downstream MACE events. LASSO: least absolute shrinkage and selection operator; eRiS: ECG risk score, Mecg: Cox PH model using eRiS alone; Mnom: Nomogram with eRiS, CAC and clinical factors.

Outcomes

The primary endpoint of the study was the prognostic performance of M_{ecg}, M_{cac}, $M_{ecg+cac}$ and M_{nom} with respect to CV risk prediction, which was measured from the date of CAC scoring to the time of composite cardiovascular event. Patients who were alive and did not have an event were censored at the date of last follow-up. We validated whether performance of M_{nom} was statistically better when compared to $M_{ecg+cac}$ and M_{ecg}. A second objective of our study was to assess whether eRiS in addition to CAC score ($M_{ecg+cac}$) could provide additional benefit to CAC when predicting CV risk. Other objectives of our study were to assess whether M_{ecg} and M_{nom} could be used to identify patient cohorts at higher probability for developing major adverse cardiovascular events (MACE: defined as composite of myocardial infarction, coronary revascularization, stroke, heart failure, or death).

Statistical analysis

The risk determination of M_{ecg} and M_{cac} was validated using hazard ratios (HR) (95% CI) and Harrell's concordance index. Further, the fit for the combination model $M_{ecg+cac}$ was evaluated against M_{ecg} and M_{cac} using ANOVA. The benefit of addition of eRiS to CAC in CV risk prediction was evaluated using C-indices and HRs of eRiS and CAC. For prognostic stratification, eRiS values were used to divide the training cohort into two groups for which MACE-free survival and HRs were calculated. The prognostic performance of M_{ecg} was validated using Kaplan-Meier survival analysis, log-rank test, HR (95% CI), and Harrell's concordance index [C index (95% CI)]. Univariate analysis of eRiS and the clinical variables was performed. Multivariable Cox-regression analysis was used to investigate the relationships between the various covariates and 2-year MACE-free survival. To assess nomogram risk discrimination, C indices were calculated from the nomogram for eRiS alone, CAC alone and clinical risk factors alone.

Results

Patient population

A total of 5,864 eligible patients were included in this study. Baseline characteristics are listed in Table 1. Over a median follow-up of 14.3 months, 73 died (1.2%), 220 had heart failure (HF) (3.8%), 71 had myocardial infarction (MI) (1.2%), 104 had stroke (1.8%), 235 had MACE (Death/MI/Stroke), 106 had Revascularization (coronary artery bypass graft surgery/percutaneous coronary intervention) (1.8%), and 494 had composite MACE (8.4%). CAC score distribution was skewed to the right with 37% patients with CAC score 0, and mean score 250 [0–9,479].

TABLE 1 Patient baseline characteristics.

Variables	
Calcium score	19.5 [0.0–217.0] ($n = 5,864$)*
Age	60.0 [53.0–67.0] ($n = 5,864$)*
Gender	Female: 53% ($n = 3,091$)
	Male: 47% ($n = 2,773$)
Race	White: 83% ($n = 4,854$)
	Black: 14% ($n = 834$)
	Other: 1.6% ($n = 92$)
	Unknown: 1.4% ($n = 84$)
Smoking status	Non-Smokers: 61% ($n = 3,592$)
	Smokers: 39% ($n = 2,272$)
Body mass index (kg/m^2)	29.57 [25.9–34.2] ($n = 5,533$)*
	Unknown: 6% ($n = 331$)
Systolic blood pressure (mmHg)	130 [120–142] ($n = 5,567$)*
	Unknown: 5% ($n = 297$)
Diastolic blood pressure (mmHg)	80 [72–84] ($n = 5,568$)*
	Unknown: 5% ($n = 296$)
High-density lipoprotein cholesterol	50 [41–61.5] ($n = 3,772$)*
(HDL-C), mg/dl	Unknown: 36% ($n = 2,092$)
Low-density lipoprotein cholesterol	113 [88–140] ($n = 3768$)*
(LDL-C), mg/dl	Unknown: 36% ($n = 2,096$)
Total cholesterol, mg/dl	193 [163–223] ($n = 3,846$)*
	Unknown: 34% ($n = 2,018$)
Triglycerides, mg/dl	114 [81–165] ($n = 3,744$)*
	Unknown: 36% ($n = 2,120$)

*Median [IQR].

ECG-based risk score construction

The LASSO-Cox regularization model resulted in preservation of 89, 119, 89, and 115 features, respectively, with 27 features being common to all across S_{tr} (1), S_{tr} (2), S_{tr} (3) and S_{tr} (4). The selected features are listed in Supplementary Table 2. This feature selection methodology preserved only about 18% of the initial extracted features, representing the highly correlated nature of the signal itself.

Cox proportional model analysis

ECG-risk score alone model (M_{ecg})

A Cox proportional model (M_{ecg}) comprising of eRiS alone predicted time-to-MACE across all data splits (C-Index: 0.6, p = <2e-16 across all S_v): S_v (1) [HR: 2.98 (2.3–3.87)], S_v (2) [HR: 2.26 (1.77–2.9)], S_v (3) [HR: 5.09 (4.14–6.25)], S_v (4) [HR: 2.74 (2.04–3.67)]. Association of downstream MACE events to eRiS was visualized in Figure 2. It was observed that patients with higher eRiS score tended to have a higher probability of a MACE event.

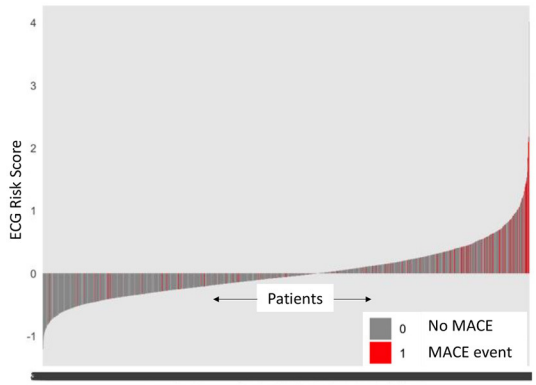


FIGURE 2
ECG risk score predicts MACE events. Patients with higher ECG risk score (eRiS) correlate with occurrence of MACE events, demonstrating the value of considering ECG as a factor in determining probability of a MACE event. X-axis denotes patients arranged in ascending value of eRiS scores.

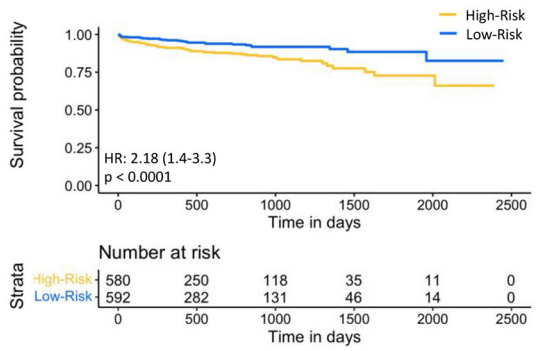


FIGURE 3
Kaplan-Meier plot for MACE-free survival according to eRiS-based risk groups in S_v. The eRiS threshold of −0.055 showed two distinct groups of high vs. low MACE-free survival in S_v (4).

For prognostic validation, two groups were identified in S_{tr} using eRiS median threshold. For instance, in S_{tr} (4), threshold was −0.055, below which patients were observed to have low risk of MACE (and hence increased MACE-free survival) and above which patients were observed to have high risk of MACE (hence decreased MACE-free survival). Kaplan-Meier for MACE-free survival were plotted to visualize patient MACE survival over follow-up time in our validation group (Figure 3).

CAC alone model (M_{cac})

M_{cac} was found to be significantly associated with CV events. (C-index 0.7, $p = <2e\text{-}16$).

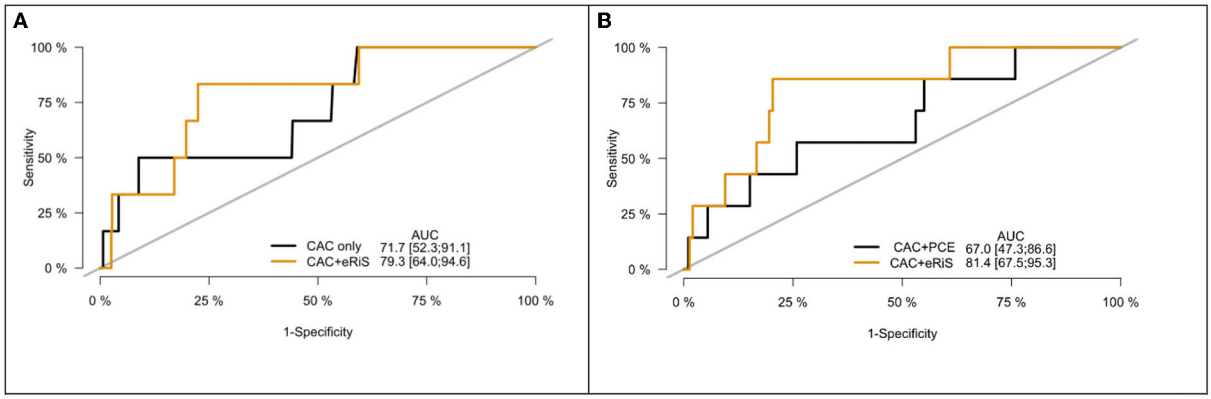


FIGURE 4
Receiver operating characteristic (ROC) curve for CAC only vs. eRiS+CAC shows the benefit of adding eRiS to CAC for better prediction of the probability of a MACE event in **(A)**. CAC+eRiS showed better performance than CAC+PCE (C-index: 0.72 vs. 0.67) for patients who had PCE available in **(B)**.

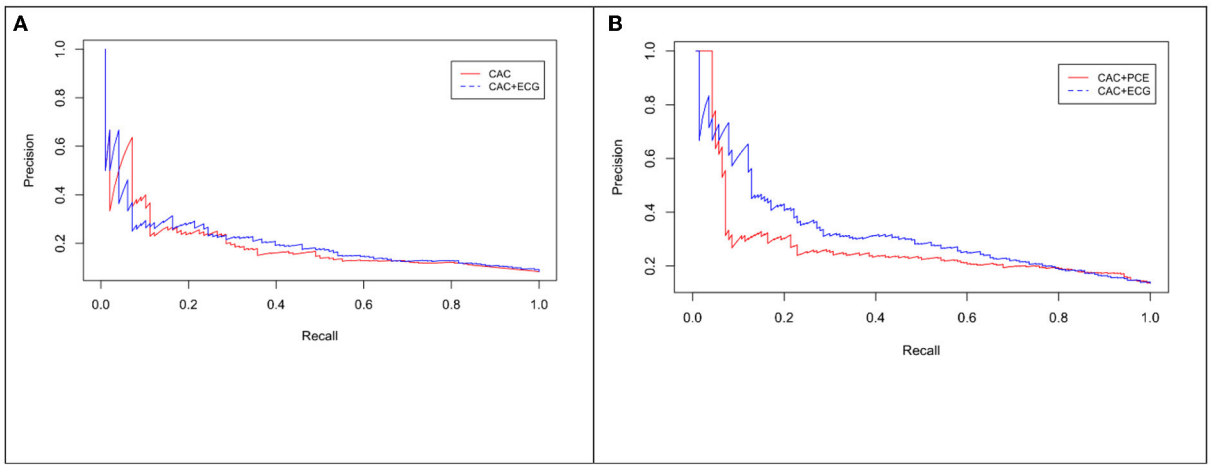


FIGURE 5
Precision-Recall (PR) curve for CAC only vs. eRiS+CAC shows the benefit of adding eRiS to CAC for better prediction of the probability of a MACE event in **(A)** (Average F1 statistic 0.20 vs. 0.21. PR AUC: 0.68 vs. 0.71). **(B)** CAC+eRiS showed better performance than CAC+PCE for patients who had PCE available (Average F1 statistic 0.28 vs. 0.30. PR AUC: 0.68 vs. 0.71).

ERiS ± CAC model ($M_{ecg±cac}$)

$M_{ecg+cac}$ was significantly associated with cardiovascular events (C-index: 0.65, p = <2e-16). Model comparison using ANOVA showed that $M_{ecg+cac}$ performed in a manner that was statistically superior when compared to M_{cac} (p < 2.2e-16) (Figures 4A, 5A). M $_{ecg+cac}$ also performed better in comparison to $M_{CAC+PCE}$ (p < 2.2e-16) (Figures 4B, 5B). Additionally, the adjustment of CAC to eRiS score did not attenuate HR for eRiS. Figure 6 shows this for S_v (4). Similar results were seen for other splits.

$M_{ecg+cac}$ was used to divide the population into 4 groups: (1) eRiS<median and CAC=0; (2) eRiS<median and CAC>0; (3) eRiS> median and CAC=0; (4) eRiS> median and CAC>0 (Figures 6, 7). As seen in the figure, worst prognosis was seen in the group with higher eRiS and CAC score, showing the additive benefit of ECG to CAC for MACE survival prediction. Similar groupings were seen when eRiS alone was used to divide S_{tr} into 4 groups, although higher HRs were observed between high and low risk patients with the eRiS+CAC model. These observations were validation on the held-out validation datasets (S_v).

We also evaluated reclassification index into high vs. low risk based of eRiS and CAC scores. We considered a threshold of −0.055 (eRiS median threshold in training data) for ECG and

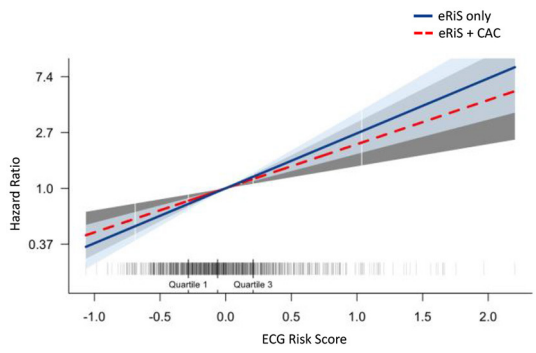


FIGURE 6
Additive benefit of eRiS to CAC: Hazard ratio is not attenuated when eRiS is adjusted by CAC score, indicating a strong relationship with MACE which is not weakened by the addition of CAC. Similar results were seen with other splits.

400 for CAC for this analysis. In S_v (4), 41% of patients with CAC score of 0 were reclassified as high risk by ECG. Further, 38% of patients with CAC>400 were reclassified as low risk by ECG.

ECG, CAC and clinical factors nomogram (M_{nom})

The calibration curve for the nomogram showed agreement between predicted survival and actual survival, and the C index for M_{nom} was 0.76. As shown in Figure 8, the ECG risk score had the most significant contribution, followed by CAC score and other clinical variables.

M_{nom} was also used to divide the population into high, medium and low risk groups using thresholds of 20 and 60% MACE free survival. As illustrated in Figure 9, M_{nom} predictions resulted in high and low risk groups. The two groups were significantly different in terms of their survival

ECG risk score-based nomogram vs. PCE for MACE survival prediction

M_{nom} was found to be statistically superior in terms of prognosis, to M_{PCE} across all Sv (C-index: 0.71 vs. 0.68; $p < 0.001$).

Discussion

Current ACC/AHA guidelines for atherosclerotic cardiovascular disease (ASCVD) risk assessment involves incorporation of traditional risk factors but does not include additional dimensions of risk that may be conveyed through other modalities such as coronary artery calcium (CAC) and electrocardiography (ECG). Improving prediction of major adverse cardiovascular events (MACE) risk can help identify at risk patients who may benefit from treatment interventions. Conversely, identification of patients who are at low risk of MACE, might help prevent the potentially harmful impact of unnecessary treatments. In this study, we developed and validated a novel ECG and CAC-based nomogram, that was not only associated with likelihood of MACE but, improved cardiovascular risk stratification when compared to the frequently used PCE for ASCV risk estimation calculator.

CT-based coronary artery calcium scoring has shown to be the single best predictor of CHD and CVD and is currently endorsed by clinical practice guidelines in select populations (21, 45, 46). CAC scoring, however, has modest discrimination for total CVD events (e.g., inclusive of heart failure event and arrhythmic events), which is becoming an important composite outcome. Additionally, CAC does not involve electrophysiologic parameters present in ECG (e.g., QRS width, q-waves, AV block) that can be markers of CV risk. Therefore, one of the main objectives of this study was to combine both electrophysiological and CT-based diagnostic information to improve CV risk prediction and prognosis when compared to either using ECG or CAC alone.

Previous studies have assessed associations of ECG with CAC in certain cardiac conditions. For instance, one study noted CAC scores being higher with ECG abnormalities as compared to those with normal ECGs and an elevated CAC burden with myocardial disease (47). In another study, QT interval duration significantly correlated with CAC in diabetic patients (48). Further, presence of both CAC and abnormal ECG has been associated with the highest rate of coronary events (49). Our study differs from these works in that we employed ML on a standard 12-lead ECG to automatically select relevant features and use these features to construct a risk score which was then tested for additive prognostic ability with CAC. Our ECG-CAC model was significantly associated with cardiovascular events in our dataset comprising of 5,864 patients. Additionally, our ECG-CAC model performed in a manner that was statistically superior compared to ECG or CAC alone or CAC-PCE, thus demonstrating the value of combining ECG and CAC for MACE prediction. We also demonstrated the risk reclassification by incorporating both ECG and CAC into MACE prediction. For patients with CAC score of 0, a higher risk predicted by ECG features may help guide clinical decision-making toward statin prescription recommendations.

A dedicated nomogram was developed demonstrating the relative contribution of ECG, CAC with traditional clinical factors for CV risk prediction. As seen in the nomogram, ECG risk score, which is currently not included in routine clinical practice for ASCVD risk prediction, was the most significant contributor to risk prediction. When tested against PCE for

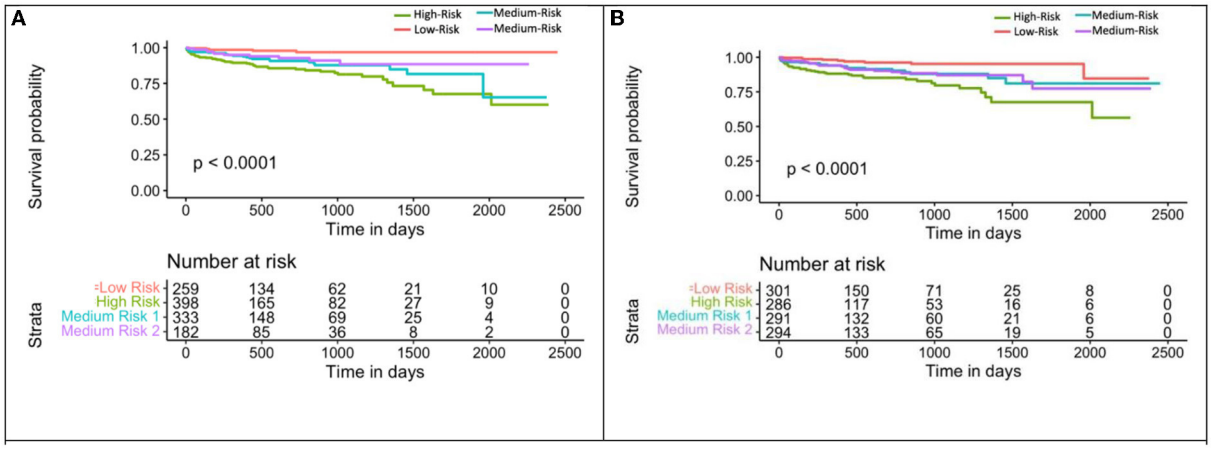


FIGURE 7
Kaplan-Meier plot for MACE-free survival according to eRiS+CAC and eRiS only risk groups in S_V (4). **(A)** The eRiS+CAC threshold showed worse prognosis for patients with high eRiS combined with high CAC score. HR between high and low risk: 6.72 [4.42–10.22]. **(B)** Similar observation seen in eRiS based segregation. HR between high and low risk: 5.22 [2.54–10.75].

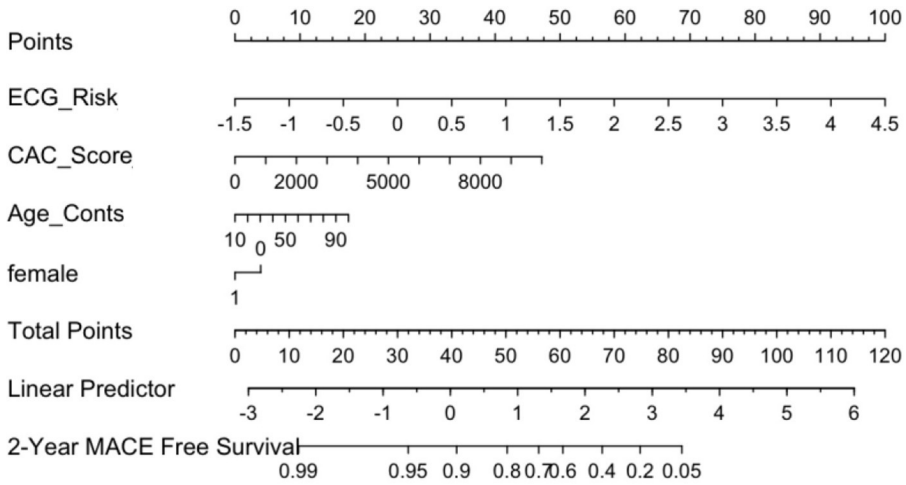


FIGURE 8
ECG Nomogram (M_{nom}) demonstrates relative contribution of each covariate in MACE prediction. ECG risk score has the most significant contribution, followed by CAC score and other clinical variables.

patients with this information, our nomogram performed at a level that was statistically superior to PCE. This suggests that incorporation of anatomic imaging (CAC), physiologic data (ECG) and clinical variables is superior to employing each stream of data independently. Our nomogram was also used to assess high vs. low risk patients based on their ECG risk scores and clinical variables. Patients in the low-risk group had higher survival rates compared to the high-risk patients. These findings appear to suggest that our novel tool, when deployed in the clinic, could be used for triaging patients far superior to PCE. ECG signals are routinely used as part of CAC imaging for image gating and thus are routinely available. A fully automated platform incorporating ECG, CAC and clinical variables can be envisioned for accurate risk prediction.

Much prior work around developing an ECG risk score has been based on using specific leads or ECG waveforms to predict CV risk/events (50). One study, for instance, used P-wave variables to stratify patients into 3 risk groups (51). Manually annotated features from ECG reports have been used to calculate an ECG risk score, associated with sudden cardiac death and risk stratification (52). ECG risk equation based on age, sex, QT interval, heart rate, and T axis was shown to be comparable to the Framingham risk score and yielded significant improvement in risk classification (53). Although ECG based risk scores have

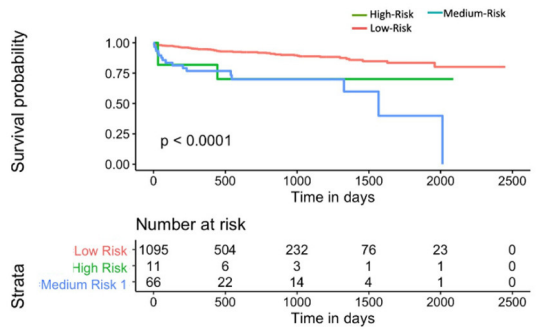


FIGURE 9
Kaplan-Meier plot for MACE-free survival according to M_{nom} risk groups for S_v (4) [C-index 0.6 (se = 0.023)]. HR between high and low risk: 3.24 [1.02–10.30].

been proposed in the past, most of these were not employed in a way to take advantage of the entire 12-lead signal. Additionally, to our knowledge, no study has tested the impact of ECG-based risk score in conjunction with CAC scoring to predict MACE.

Due to the high-dimensional electrophysiological information captured in a single 12-lead ECG test, previous studies have utilized sophisticated ML techniques, including deep learning (DL) to automatically diagnose and predict various cardiovascular outcomes (54). For instance, convolutional neural networks (CNN) on ECGs have identified patients with atrial fibrillation with high accuracy (39). DL models have also been developed to automatically interpret ECG abnormality types (55). Similarly, DL algorithms on routine 12-lead ECGs have been used to detect low ejection fraction (36), arrhythmia detection (56), aortic stenosis (57), atrial fibrillation (58), heart failure (59) and even all-cause mortality (60). Additionally, wavelets have also been used to extract features from ECGs for LV diastolic dysfunction detection using ML models (61). Also, unsupervised ML of ECG have been used to stratify which CRT candidates may have better response to resynchronization therapy beyond using QRS duration and left bundle branch block (62). However, all prior studies have relied upon DL methodologies employing neural networks or ML models. While these approaches are powerful and do not require domain level expertise to employ, the abstract nature of DL transformations often preclude any clear, clinically meaningful explanation of the features that drive the model predictions.

Recognizing that adoption of automated signal analysis platforms into clinical practice will require not only convincing statistical demonstrations but also clear, transparent, and biologically inspired methods, we chose to employ a "hand-crafted" feature-engineering approach in this work. This approach relied on using clinically validated ECG features automatically extracted from the GE Muse™ Cardiology Information System. Our risk score comprised of ECG features selected from a standard 12-lead ECG using ML to preserve the most important features. A major advantage of our score is the fact that no manual annotation is required to define the ECG features. As seen in this study, the ML derived ECG risk score was able to improve stratification of high-risk ASCVD patients, thus potentially helping physicians with identification of such patients. Another strength of this study was the relatively large sample size, and the inclusion of the CAC score, which is arguably considered the best marker of MACE risk.

This study did have its limitations. First, the ECG features used here were those that were automatically extracted from the GE MUSE system. Although this widely available clinical software has been validated with manual annotations, disadvantages might include inability to capture other subtle features in the ECG waveform beyond what is offered from the system. Second, the patient datasets used in this study consisted only of those who were part of the UH health system and are subject to referral bias. Although ECG, ECG-CAC and the subsequent nomogram showed consistent performance with respect to predicting patients with MACE, this tool needs to be validated prospectively in an external cohort with a diverse population in a multi-institution setting. In this current study, we were unable to compare to the MESA 10 -year CHD risk with CAC model, which may be current standard of care for many clinicians when making decisions from CAC scores. This will be considered in future analyses. Third, effects of treatment, if any, has not been considered in this study. Future studies could be directed toward adding more treatment-related variables into the nomogram, thus capturing the heterogeneity in the ASCVD prediction effects. As shown in this study, CAC score along with the ECG provided an additive benefit in ASCVD risk prediction. This suggests that assessing features from the CAC score itself such as CT radiomics features (63) with ECG omics, might provide even better risk stratification.

Conclusion

We developed and validated an ECG risk score-based model, ECG incorporated with CAC and a novel nomogram, with ECG, CAC and clinical factors. These models were implemented on various training-validation dataset sizes and the ECG features extracted were overall consistent. The nomogram identified high vs. low risk patients for downstream MACE with high separability. Following prospective multi-site validation, the ECG score could be incorporated in the electronic medical systems of patients which would enable personalization of treatment regimens with the addition of ECG based information. Specifically, it could be employed as a clinical decision tool to enable triaging patients based on ECG, CAC and the patient-specific clinical factors. Future testing is needed to evaluate how clinical CVD outcomes may be affected by incorporating this risk estimation tool into primary prevention efforts.

Data availability statement

The raw data supporting the conclusions of this article can be made available by the authors upon IRB approval and data sharing agreement.

Ethics statement

The studies involving human participants were reviewed and approved by UH Institutional Review Board with waiver of consent [Community Benefit of No-charge Calcium Score Screening Program-CLARIFY (NCT04075162)].

Author contributions

SS and SA-K: contributed equally toward data analysis, model building, and manuscript writing. SA-K, NT, and VR: access and acquisition of data. PF: statistical expertise. SR and AM: guidance on entire study, from data collection to data analysis, and manuscript writing. All authors contributed to the article and approved the submitted version.

Funding

Research reported in this publication was supported by the National Cancer Institute under (award numbers R01CA268287A1, U01CA269181, R01CA26820701A1, R01CA249992-01A1, R01CA202752-01A1, R01CA208236-01A1, R01CA216579-01A1, R01CA220581-01A1, R01CA257612-01A1, 1U01CA239055-01, 1U01CA248226-01, and 1U54CA254566-01), National Heart, Lung and Blood Institute (1R01HL15127701A1 and R01HL15807101A1), National Institute of Biomedical Imaging and Bioengineering 1R43EB028736-01, National Center for Research Resources under award number 1 C06 RR12463-01, VA Merit Review Award IBX004121A from the United States Department of Veterans Affairs Biomedical Laboratory Research and Development Service the Office of the Assistant Secretary of Defense for Health Affairs, through the Breast Cancer Research Program (W81XWH-19-1-0668), the Prostate Cancer Research Program (W81XWH-20-1-0851), the Lung Cancer Research Program (W81XWH-18-1-0440, W81XWH-20-1-0595), the Peer Reviewed Cancer Research Program (W81XWH-18-1-0404, W81XWH-21-1-0345, W81XWH-21-1-0160), the Kidney Precision Medicine Project (KPMP) Glue Grant, and sponsored research agreements from Bristol Myers-Squibb, Boehringer-Ingelheim, Eli-Lilly and Astrazeneca. The funder was not involved in the study design, collection, analysis, interpretation of data, the writing of this article, or the decision to submit it for publication.

Conflict of interest

AM is an equity holder in Picture Health, Elucid Bioimaging, and Inspirata Inc. Currently he serves on the advisory board of Picture Health, Aiforia Inc, and SimBioSys. He also currently consults for Biohme, SimBioSys and Castle Biosciences. He also has sponsored research agreements with AstraZeneca, Boehringer-Ingelheim, Eli-Lilly and Bristol Myers-Squibb. His technology has been licensed to Picture Health and Elucid Bioimaging. He is also involved in 3 different R01 grants with Inspirata Inc.

The remaining authors declare that the research was conducted in the absence of any commercial or financial relationships that could be construed as a potential conflict of interest.

Publisher's note

All claims expressed in this article are solely those of the authors and do not necessarily represent those of their affiliated organizations, or those of the publisher, the editors and the reviewers. Any product that may be evaluated in this article, or claim that may be made by its manufacturer, is not guaranteed or endorsed by the publisher.

Author disclaimer

The content is solely the responsibility of the authors and does not necessarily represent the official views of the National Institutes of Health, the U.S. Department of Veterans Affairs, the Department of Defense, or the United States Government.

Supplementary material

The Supplementary Material for this article can be found online at: https://www.frontiersin.org/articles/10.3389/fcvm.2022.976769/full#supplementary-material

References

1. Goff DC, Lloyd-Jones DM, Bennett G, Coady S, D'Agostino RB, Gibbons R, et al. 2013 ACC/AHA guideline on the assessment of cardiovascular risk: a report of the American College of Cardiology/American Heart Association Task Force on Practice Guidelines. *J Am Coll Cardiol.* (2014) 63:2935–59. doi: 10.1016/j.jacc.2013.11.005

2. Libby P, Buring JE, Badimon L, Hansson GK, Deanfield J, Bittencourt MS, et al. Atherosclerosis. *Nat Rev Dis Primer.* (2019) 5:1–18. doi: 10.1038/s41572-019-0106-z

3. Akintoye E, Briasoulis A, Afonso L. Biochemical risk markers and 10-year incidence of atherosclerotic cardiovascular disease: independent predictors, improvement in pooled cohort equation, and risk reclassification. *Am Heart J.* (2017) 193:95–103. doi: 10.1016/j.ahj.2017.08.002

4. Kuragaichi T, Kataoka Y, Miyakoshi C, Miyamoto T, Sato Y. External validation of pooled cohort equations using systolic blood pressure intervention trial data. *BMC Res Notes.* (2019) 12:271. doi: 10.1186/s13104-019-4293-1

5. Nanna MG, Peterson ED, Wojdyla D, Navar AM. The accuracy of cardiovascular pooled cohort risk estimates in U.S older adults. *J Gen Intern Med.* (2020) 35:1701–8. doi: 10.1007/s11606-019-05361-4

6. Khera R, Pandey A, Ayers CR, Carnethon MR, Greenland P, Ndumele CE, et al. Performance of the pooled cohort equations to estimate atherosclerotic cardiovascular disease risk by body mass index. *JAMA Netw Open.* (2020) 3:e2023242–e2023242. doi: 10.1001/jamanetworkopen.2020.23242

7. Damen JA, Pajouheshnia R, Heus P, Moons KGM, Reitsma JB, Scholten RJPM, et al. Performance of the Framingham risk models and pooled cohort equations for predicting 10-year risk of cardiovascular disease: a systematic review and meta-analysis. *BMC Med.* (2019) 17:109. doi: 10.1186/s12916-019-1340-7

8. Ridker PM, Cook NR. The pooled cohort equations 3 years on. *Circulation.* (2016) 134:1789–91. doi: 10.1161/CIRCULATIONAHA.116.024246

9. Rana JS, Tabada GH, Solomon MD, Lo JC, Jaffe MG, Sung SH, et al. Accuracy of the atherosclerotic cardiovascular risk equation in a large contemporary, multiethnic population. *J Am Coll Cardiol.* (2016) 67:2118–30. doi: 10.1016/j.jacc.2016.02.055

10. Arnett DK, Blumenthal RS, Albert MA, Buroker AB, Goldberger ZD, Hahn EJ, et al. 2019 ACC/AHA guideline on the primary prevention of cardiovascular disease: a report of the American College of Cardiology/American Heart Association Task Force on Clinical Practice Guidelines. *Circulation.* (2019) 140:e596–646. doi: 10.1161/CIR.0000000000000725

11. Lloyd-Jones DM, Braun LT, Ndumele CE, Smith SC, Sperling LS, Virani SS, et al. Use of risk assessment tools to guide decision-making in the primary prevention of atherosclerotic cardiovascular disease: a special report from the American Heart Association and American College of Cardiology. *Circulation.* (2019) 139:e1162–77. doi: 10.1161/CIR.0000000000000638

12. Ning H, Kershaw KN, Allen NB, Wilkins J, Lloyd-Jones DM. Association of health-related quality of life with atherosclerotic cardiovascular disease: lifetime risk pooling project. *Am J Prev Cardiol.* (2021) 7:100222. doi: 10.1016/j.ajpc.2021.100222

13. Agarwala A, Liu J, Ballantyne CM, Virani SS. The use of risk enhancing factors to personalize ASCVD risk assessment: evidence and recommendations from the 2018 AHA/ACC multi-society cholesterol guidelines. *Curr Cardiovasc Risk Rep.* (2019) 13:18. doi: 10.1007/s12170-019-0616-y

14. Orimoloye OA, Budoff MJ, Dardari ZA, Mirbolouk M, Uddin SMI, Berman DS, et al. Race/ethnicity and the prognostic implications of coronary artery calcium for all-cause and cardiovascular disease mortality: the coronary artery calcium consortium. *J Am Heart Assoc.* (2018) 7:e010471. doi: 10.1161/JAHA.118.010471

15. Al Rifai M, Cainzos-Achirica M, Kanaya AM, Kandula NR, Dardardi Z, Joshi PH, et al. Discordance between 10-year cardiovascular risk estimates using the ACC/AHA 2013 estimator and coronary artery calcium in individuals from 5 racial/ethnic groups: comparing MASALA and MESA. *Atherosclerosis.* (2018) 279:122–9. doi: 10.1016/j.atherosclerosis.2018.09.015

16. Shaw LJ, Min JK, Nasir K, Xie JX, Berman DS, Miedema MD, et al. Sex differences in calcified plaque and long-term cardiovascular mortality: observations from the CAC consortium. *Eur Heart J.* (2018) 39:3727–35. doi: 10.1093/eurheartj/ehy534

17. Leigh A, McEvoy JW, Garg P, Carr JJ, Sandfort V, Oelsner EC, et al. Coronary artery calcium scores and atherosclerotic cardiovascular disease risk stratification in smokers. *JACC Cardiovasc Imaging.* (2019) 12:852–61. doi: 10.1016/j.jcmg.2017.12.017

18. Budoff MJ, Shaw LJ, Liu ST, Weinstein SR, Tseng PH, Flores FR, et al. Long-term prognosis associated with coronary calcification: observations from a registry of 25,253 patients. *J Am Coll Cardiol.* (2007) 49:1860–70. doi: 10.1016/j.jacc.2006.10.079

19. Lin A, Kolossváry M, Motwani M, Išgum I, Maurovich-Horvat P, Slomka PJ, et al. Artificial intelligence in cardiovascular imaging for risk stratification in coronary artery disease. *Radiol Cardiothorac Imaging.* (2021) 3:e200512. doi: 10.1148/ryct.2021200512

20. Blaha MJ, Whelton SP, Al Rifai M, Dardari Z, Shaw LJ, Al-Mallah MH, et al. Comparing risk scores in the prediction of coronary and cardiovascular deaths: coronary artery calcium consortium. *JACC Cardiovasc Imaging.* (2021) 14:411–21. doi: 10.1016/j.jcmg.2019.12.010

21. Yeboah J, Young R, McClelland RL, Delaney JC, Polonsky TS, Dawood FZ, et al. Utility of nontraditional risk markers in atherosclerotic cardiovascular disease risk assessment. *J Am Coll Cardiol.* (2016) 67:139–47. doi: 10.1016/j.jacc.2015.10.058

22. Nakanishi R, Slomka PJ, Rios R, Betancur J, Blaha MJ, Nasir K, et al. Machine learning adds to clinical and CAC assessments in predicting 10-year CHD and CVD deaths. *JACC Cardiovasc Imaging.* (2021) 14:615–25. doi: 10.1016/j.jcmg.2020.08.024

23. Anderson JL, Le VT, Min DB, Biswas S, Minder CM, McCubrey RO, et al. Comparison of three atherosclerotic cardiovascular disease risk scores with and without coronary calcium for predicting revascularization and major adverse coronary events in symptomatic patients undergoing positron emission tomography-stress testing. *Am J Cardiol.* (2020) 125:341–8. doi: 10.1016/j.amjcard.2019.10.044

24. Al Rifai M, Cainzos-Achirica M, Kianoush S, Mirbolouk M, Peng A, Comin-Colet J, et al. Coronary artery calcium: recommendations for risk assessment in cardiovascular prevention guidelines. *Curr Treat Options Cardiovasc Med.* (2018) 20:89. doi: 10.1007/s11936-018-0685-0

25. Verrier RL, Nearing BD, D'Avila A. Spectrum of clinical applications of interlead ECG heterogeneity assessment: From myocardial ischemia detection to sudden cardiac death risk stratification. *Ann Noninvasive Electrocardiol.* (2021) 26:e12894. doi: 10.1111/anec.12894

26. Bergonti M, Saenen J, Heidbuchel H, Sarkozy A. ST-segment elevation: one sign, many shadows. *JACC Case Rep.* (2021) 3:1360–2. doi: 10.1016/j.jaccas.2021.05.023

27. Oleynikov VE, Averyanova EV, Oreshkina AA, Burko NV, Barmenkova YA, Golubeva AV, et al. A multivariate model to predict chronic heart failure after acute ST-segment elevation myocardial infarction: preliminary study. *Diagn Basel Switz.* (2021) 11:1925. doi: 10.3390/diagnostics11101925

28. Andersen DC, Kragholm K, Petersen LT, Graff C, Sørensen PL, Nielsen JB, et al. Association between vectorcardiographic QRS area and incident heart failure diagnosis and mortality among patients with left bundle branch block: a register-based cohort study. *J Electrocardiol.* (2021) 69:30–5. doi: 10.1016/j.jelectrocard.2021.09.002

29. Ether ND, Jantre SR, Sharma DB, Leishman DJ, Bailie MB, Lauver DA. Improving corrected QT; why individual correction is not enough. *J Pharmacol Toxicol Methods.* (2021) 113:107126. doi: 10.1016/j.vascn.2021.107126

30. Holkeri A, Eranti A, Haukilahti MAE, Kerola T, Kenttä TV, Noponen K, et al. Prognostic significance of flat T-waves in the lateral leads in general population. *J Electrocardiol.* (2021) 69:105–10. doi: 10.1016/j.jelectrocard.2021.10.001

31. Attia ZI, Harmon DM, Behr ER, Friedman PA. Application of artificial intelligence to the electrocardiogram. *Eur Heart J.* (2021) 42:ehab649. doi: 10.1093/eurheartj/ehab649

32. Mincholé A, Camps J, Lyon A, Rodríguez B. Machine learning in the electrocardiogram. *J Electrocardiol.* (2019) 57:S61–4. doi: 10.1016/j.jelectrocard.2019.08.008

33. Prifti E, Fall A, Davogustto G, Pulini A, Denjoy I, Funck-Brentano C, et al. Deep learning analysis of electrocardiogram for risk prediction of drug-induced arrhythmias and diagnosis of long QT syndrome. *Eur Heart J.* (2021) 42:3948–61. doi: 10.1093/eurheartj/ehab588

34. Hannun AY, Rajpurkar P, Haghpanahi M, Tison GH, Bourn C, Turakhia MP, et al. Cardiologist-level arrhythmia detection and classification in ambulatory electrocardiograms using a deep neural network. *Nat Med.* (2019) 25:65–9. doi: 10.1038/s41591-018-0268-3

35. Vaid A, Johnson KW, Badgeley MA, Somani SS, Bicak M, Landi I, et al. Using deep-learning algorithms to simultaneously identify right and left ventricular

dysfunction from the electrocardiogram. *JACC Cardiovasc Imaging.* (2022) 15:395–410. doi: 10.1016/j.jcmg.2021.08.004

36. Yao X, McCoy RG, Friedman PA, Shah ND, Barry BA, Behnken EM, et al. ECG AI-guided screening for low ejection fraction (EAGLE): rationale and design of a pragmatic cluster randomized trial. *Am Heart J.* (2020) 219:31–6. doi: 10.1016/j.ahj.2019.10.007

37. Li H, Wang X, Liu C, Li P, Jiao Y. Integrating multi-domain deep features of electrocardiogram and phonocardiogram for coronary artery disease detection. *Comput Biol Med.* (2021) 138:104914. doi: 10.1016/j.compbiomed.2021.104914

38. Zhang H, Dong Z, Sun M, Gu H, Wang Z, TP-CNN. A detection method for atrial fibrillation based on transposed projection signals with compressed sensed ECG. *Comput Methods Programs Biomed.* (2021) 210:106358. doi: 10.1016/j.cmpb.2021.106358

39. Attia ZI, Noseworthy PA, Lopez-Jimenez F, Asirvatham SJ, Deshmukh AJ, Gersh BJ, et al. An artificial intelligence-enabled ECG algorithm for the identification of patients with atrial fibrillation during sinus rhythm: a retrospective analysis of outcome prediction. *Lancet Lond Engl.* (2019) 394:861–7. doi: 10.1016/S0140-6736(19)31721-0

40. Siontis KC, Liu K, Bos JM, Attia ZI, Cohen-Shelly M, Arruda-Olson AM, et al. Detection of hypertrophic cardiomyopathy by an artificial intelligence electrocardiogram in children and adolescents. *Int J Cardiol.* (2021) 340:42–7. doi: 10.1016/j.ijcard.2021.08.026

41. Al Hinai G, Jammoul S, Vajihi Z, Afilalo J. Deep learning analysis of resting electrocardiograms for the detection of myocardial dysfunction, hypertrophy, and ischaemia: a systematic review. *Eur Heart J Digit Health.* (2021) 2:416–23. doi: 10.1093/ehjdh/ztab048

42. Bodini M, Rivolta MW, Sassi R. Opening the black box: interpretability of machine learning algorithms in electrocardiography. *Philos Trans R Soc Math Phys Eng Sci.* (2021) 379:20200253. doi: 10.1098/rsta.2020.0253

43. Tison GH, Zhang J, Delling FN, Deo RC. Automated and interpretable patient ECG profiles for disease detection, tracking, and discovery. *Circ Cardiovasc Qual Outcomes.* (2019) 12:e005289. doi: 10.1161/CIRCOUTCOMES.118.005289

44. Tibshirani R. Regression shrinkage and selection *via* the Lasso. *J R Stat Soc Ser B Methodol.* (1996) 58:267–88. doi: 10.1111/j.2517-6161.1996.tb02080.x

45. Kavousi M, Elias-Smale S, Rutten JHW, Leening MJG, Vliegenthart R, Verwoert GC, et al. Evaluation of newer risk markers for coronary heart disease risk classification: a cohort study. *Ann Intern Med.* (2012) 156:438–44. doi: 10.7326/0003-4819-156-6-201203200-00006

46. Möhlenkamp S, Lehmann N, Moebus S, Schmermund A, Dragano N, Stang A, et al. Quantification of coronary atherosclerosis and inflammation to predict coronary events and all-cause mortality. *J Am Coll Cardiol.* (2011) 57:1455–64. doi: 10.1016/j.jacc.2010.10.043

47. Möhlenkamp S, Schmermund A, Lehmann N, Roggenbuck U, Dragano N, Stang A, et al. Subclinical coronary atherosclerosis and resting ECG abnormalities in an unselected general population. *Atherosclerosis.* (2008) 196:786–94. doi: 10.1016/j.atherosclerosis.2007.01.012

48. Nelson MR, Daniel KR, Carr JJ, Freedman BI, Prineas RJ, Bowden DW, et al. Associations between electrocardiographic interval durations and coronary artery calcium scores: the diabetes heart study. *Pacing Clin Electrophysiol PACE.* (2008) 31:314–21. doi: 10.1111/j.1540-8159.2008.00991.x

49. Grossman C, Ehrlich S, Shemesh J, Koren-Morag N, Grossman E. Coronary artery calcium and exercise electrocardiogram as predictors of coronary events in asymptomatic adults. *Am J Cardiol.* (2015) 115:745–50. doi: 10.1016/j.amjcard.2014.12.039

50. Tan SY, Sungar GW, Myers J, Sandri M, Froelicher V. A simplified clinical electrocardiogram score for the prediction of cardiovascular mortality. *Clin Cardiol.* (2009) 32:82–6. doi: 10.1002/clc.20288

51. Alexander B, Milden J, Hazim B, Haseeb S, Bayes-Genis A, Elosua R, et al. New electrocardiographic score for the prediction of atrial fibrillation: The MVP ECG risk score (morphology-voltage-P-wave duration). *Ann Noninvasive Electrocardiol.* (2019) 24:e12669. doi: 10.1111/anec.12669

52. Aro AL, Reinier K, Rusinaru C, Uy-Evanado A, Darouian N, Phan D, et al. Electrical risk score beyond the left ventricular ejection fraction: prediction of sudden cardiac death in the Oregon Sudden Unexpected Death Study and the Atherosclerosis Risk in Communities Study. *Eur Heart J.* (2017) 38:3017–25. doi: 10.1093/eurheartj/ehx331

53. Shah AJ, Vaccarino V, Janssens ACJW, Flanders WD, Kundu S, Veledar E, et al. An electrocardiogram-based risk equation for incident cardiovascular disease from the national health and nutrition examination survey. *JAMA Cardiol.* (2016) 1:779–86. doi: 10.1001/jamacardio.2016.2173

54. Kashou AH, May AM, Noseworthy PA. Artificial intelligence-enabled ECG: a modern lens on an old technology. *Curr Cardiol Rep.* (2020) 22:57. doi: 10.1007/s11886-020-01317-x

55. Lai C, Zhou S, Trayanova NA. Optimal ECG-lead selection increases generalizability of deep learning on ECG abnormality classification. *Philos Transact A Math Phys Eng Sci.* (2021) 379:20200258. doi: 10.1098/rsta.2020.0258

56. Parvaneh S, Rubin J, Babaeizadeh S, Xu-Wilson M. Cardiac arrhythmia detection using deep learning: a review. *J Electrocardiol.* (2019) 57S:S70–S74. doi: 10.1016/j.jelectrocard.2019.08.004

57. Kwon J-M, Lee SY, Jeon K-H, Lee Y, Kim K-H, Park J, et al. Deep learning-based algorithm for detecting aortic stenosis using electrocardiography. *J Am Heart Assoc.* (2020) 9:e014717. doi: 10.1161/JAHA.119.014717

58. Hill NR, Arden C, Beresford-Hulme L, Camm AJ, Clifton D, Davies DW, et al. Identification of undiagnosed atrial fibrillation patients using a machine learning risk prediction algorithm and diagnostic testing (PULsE-AI): study protocol for a randomised controlled trial. *Contemp Clin Trials.* (2020) 99:106191. doi: 10.1016/j.cct.2020.106191

59. Kwon JM, Kim KH, Jeon KH, Kim HM, Kim MJ, Lim SM, et al. Development and validation of deep-learning algorithm for electrocardiography-based heart failure identification. *Korean Circ J.* (2019) 49:629–39. doi: 10.4070/kcj.2018.0446

60. Raghunath S, Ulloa Cerna AE, Jing L, vanMaanen DP, Stough J, Hartzel DN, et al. Prediction of mortality from 12-lead electrocardiogram voltage data using a deep neural network. *Nat Med.* (2020) 26:886–91. doi: 10.1038/s41591-020-0870-z

61. Kagiyama N, Piccirilli M, Yanamala N, Shrestha S, Farjo PD, Casaclang-Verzosa G, et al. Machine learning assessment of left ventricular diastolic function based on electrocardiographic features. *J Am Coll Cardiol.* (2020) 76:930–41. doi: 10.1016/j.jacc.2020.06.061

62. Feeny AK, Rickard J, Trulock KM, Patel D, Toro S, Moennich LA, et al. Machine learning of 12-lead QRS waveforms to identify cardiac resynchronization therapy patients with differential outcomes. *Circ Arrhythm Electrophysiol.* (2020) 13:e008210. doi: 10.1161/CIRCEP.119.008210

63. Song Y, Hoori A, Wu H, Al-Kindi S, Durieux JC, Terry JG, et al. Improved reproducibility of CT calcium score using blind deconvolution. *Med Imaging 2021 Biomed Appl Mol Struct Funct Imaging.* (2021) 11600:212–7. doi: 10.1117/12.2580484

frontiers | Frontiers in Cardiovascular Medicine

TYPE Original Research
PUBLISHED 12 October 2022
DOI 10.3389/fcvm.2022.994359

Check for updates

OPEN ACCESS

EDITED BY
Roney Orismar Sampaio,
Heart Institute, University of São Paulo, Brazil

REVIEWED BY
Zeyi Cheng,
Sichuan University, China
An-Tian Chen,
Chinese Academy of Medical Sciences and Peking Union Medical College, China

*CORRESPONDENCE
Shuang Peng
1451868099@qq.com
Xiaozhu Liu
xiaozhuliu2021@163.com;
xiaozhuliu@hospital.cqmu.edu.cn

†These authors have contributed equally to this work

SPECIALTY SECTION
This article was submitted to Heart Valve Disease, a section of the journal Frontiers in Cardiovascular Medicine

RECEIVED 14 July 2022
ACCEPTED 15 September 2022
PUBLISHED 12 October 2022

CITATION
Peng S, Huang J, Deng J, Sun C, Tang J, Chen H, Cao W, Wang W, Duan X, Luo X, Peng S and Liu X (2022) Interpretable machine learning for 28-day all-cause in-hospital mortality prediction in critically ill patients with heart failure combined with hypertension: A retrospective cohort study based on medical information mart for intensive care database-IV and eICU databases. *Front. Cardiovasc. Med.* 9:994359. doi: 10.3389/fcvm.2022.994359

COPYRIGHT
© 2022 Peng, Huang, Deng, Sun, Tang, Chen, Cao, Wang, Duan, Luo, Peng and Liu. This is an open-access article distributed under the terms of the Creative Commons Attribution License (CC BY). The use, distribution or reproduction in other forums is permitted, provided the original author(s) and the copyright owner(s) are credited and that the original publication in this journal is cited, in accordance with accepted academic practice. No use, distribution or reproduction is permitted which does not comply with these terms.

Interpretable machine learning for 28-day all-cause in-hospital mortality prediction in critically ill patients with heart failure combined with hypertension: A retrospective cohort study based on medical information mart for intensive care database-IV and eICU databases

Shengxian Peng[1†], Jian Huang[2†], Jiewen Deng[3†], Chenyu Sun[4], Juan Tang[1], Huaqiao Chen[5], Wenzhai Cao[6], Wei Wang[6,7], Xiangjie Duan[8], Xianglin Luo[7], Shuang Peng[9*] and Xiaozhu Liu[10*]

[1]Scientific Research Department, First People's Hospital of Zigong City, Zigong, China, [2]Graduate School, Guangxi University of Chinese Medicine, Nanning, China, [3]Department of Neurosurgery, The First Affiliated Hospital of Chongqing Medical University, Chongqing, China, [4]AMITA Health Saint Joseph Hospital Chicago, Chicago, IL, United States, [5]Department of Cardiology, The First Affiliated Hospital of Chongqing Medical University, Chongqing, China, [6]Department of Cardiology, First People's Hospital of Zigong City, Zigong, China, [7]Information Department, First People's Hospital of Zigong City, Zigong, China, [8]Department of Infectious Diseases, The First People's Hospital of Changde City, Changde, China, [9]General Affairs Section, The People's Hospital of Tongnan District, Chongqing, China, [10]Department of Cardiology, The Second Affiliated Hospital of Chongqing Medical University, Chongqing, China

Background: Heart failure (HF) combined with hypertension is an extremely important cause of in-hospital mortality, especially for the intensive care unit (ICU) patients. However, under intense working pressure, the medical staff are easily overwhelmed by the large number of clinical signals generated in the ICU, which may lead to treatment delay, sub-optimal care, or even wrong clinical decisions. Individual risk stratification is an essential strategy for managing ICU patients with HF combined with hypertension. Artificial intelligence, especially machine learning (ML), can develop superior models to predict the prognosis of these patients. This study aimed to develop a machine learning method to predict the 28-day mortality for ICU patients with HF combined with hypertension.

Methods: We enrolled all critically ill patients with HF combined with hypertension in the Medical Information Mart for IntensiveCare Database-IV

(MIMIC-IV, v.1.4) and the eICU Collaborative Research Database (eICU-CRD) from 2008 to 2019. Subsequently, MIMIC-IV was divided into training cohort and testing cohort in an 8:2 ratio, and eICU-CRD was designated as the external validation cohort. The least absolute shrinkage and selection operator (LASSO) Cox regression with internal tenfold cross-validation was used for data dimension reduction and identifying the most valuable predictive features for 28-day mortality. Based on its accuracy and area under the curve (AUC), the best model in the validation cohort was selected. In addition, we utilized the Shapley Additive Explanations (SHAP) method to highlight the importance of model features, analyze the impact of individual features on model output, and visualize an individual's Shapley values.

Results: A total of 3,458 and 6582 patients with HF combined with hypertension in MIMIC-IV and eICU-CRD were included. The patients, including 1,756 males, had a median (Q1, Q3) age of 75 (65, 84) years. After selection, 22 out of a total of 58 clinical parameters were extracted to develop the machine-learning models. Among four constructed models, the Neural Networks (NN) model performed the best predictive performance with an AUC of 0.764 and 0.674 in the test cohort and external validation cohort, respectively. In addition, a simplified model including seven variables was built based on NN, which also had good predictive performance (AUC: 0.741). Feature importance analysis showed that age, mechanical ventilation (MECHVENT), chloride, bun, anion gap, paraplegia, rdw (RDW), hyperlipidemia, peripheral capillary oxygen saturation (SpO_2), respiratory rate, cerebrovascular disease, heart rate, white blood cell (WBC), international normalized ratio (INR), mean corpuscular hemoglobin concentration (MCHC), glucose, AIDS, mean corpuscular volume (MCV), N-terminal pro-brain natriuretic peptide (Npro. BNP), calcium, renal replacement therapy (RRT), and partial thromboplastin time (PTT) were the top 22 features of the NN model with the greatest impact. Finally, after hyperparameter optimization, SHAP plots were employed to make the NN-based model interpretable with an analytical description of how the constructed model visualizes the prediction of death.

Conclusion: We developed a predictive model to predict the 28-day mortality for ICU patients with HF combined with hypertension, which proved superior to the traditional logistic regression analysis. The SHAP method enables machine learning models to be more interpretable, thereby helping clinicians to better understand the reasoning behind the outcome and assess in-hospital outcomes for critically ill patients.

KEYWORDS

MIMIC-IV, interpretable machine learning, neural networks, heart failure, hypertension

Introduction

Cardiac diseases are among the leading causes of overall mortality and hospitalization globally. Amongst them, heart failure (HF) is of the highest socio-economic relevance, and it is a global epidemic with high morbidity, mortality, and readmission rates, affecting more than 64 million people worldwide (1–4). In the United States, the estimated prevalence of HF is expected to increase by 24% to approximately 8.5 million in 2030 (5, 6). Hypertension, the most frequent

comorbidity of HF, promotes the development of the disease and contributes to its progression and poor outcome (7). In the United States, around 10–51% of hospitalized patients with HF have been documented with ICU admission, and ICU-admitted patients have significantly higher adjusted in-hospital mortality compared with those admitted to the general medical floor (8–10). In addition, the in-hospital mortality rate for patients treated in the ICU was 10.6%, compared with 4.0% for all HF patients (11). Because ICU physicians receive large amounts of data from many patients stored in electronic patient-data management systems (PDMS) surpassing the amount limits of the human brain to process information, it is often difficult for physicians to extract the most important information in a short period to make the best decisions for patient care. In addition, the limited ability of humans to process this vast amount of data makes them prone to data overload, change blindness, and task fixation (12), which also increases the risk of clinicians failing to identify and interpret relevant information and act accordingly (13, 14). Low nurse-to-patient ratios in the ICU and insufficient numbers of ICU physicians are associated with higher ICU mortality in patients whose conditions deteriorate and who do not receive timely and appropriate treatment (15–18). Despite recent advances in diagnosis and treatment as well as evidence-based management, the results regarding HF remain unsatisfactory (19).

Risk stratification as a common method for risk classification, deciding the duration of intervention, and assessing the mortality in patients with HF combined with hypertension provide not only a fundamental strategy for clinical decision-making but also practical information for health policy and insurance services (20). For this reason, several in-hospital mortality prediction models have been developed and evaluated for risk stratification and mortality prediction of HF patients in the ICU (21–30). However, an interpretable machine learning (ML) model has not been established to predict 28-day in-hospital mortality for ICU patients with HF combined with hypertension.

Artificial intelligence, such as ML techniques, is excellent at analyzing complex signals in data-rich environments (31). The large amount of data collected in ICU and the public availability of datasets such as MIMIC-III (32) and emergency intensive care unit (eICU) (33) are critical to developing ML in this context. ML is the use of computational algorithms that can learn to identify underlying patterns and classes from large amounts of data. It is an alternative method of using previous or existing data to train computer models to make predictions about the outcome. In this study, we aimed to develop and validate an interpretable prediction model to predict 28-day in-hospital mortality in patients admitted to the ICU with HF combined with hypertension using ML algorithms and leveraging data from the Medical Information Mart for Intensive Care (MIMIC-IV) and eICU database.

Materials and methods

Data source and outcome

This study was a retrospective cohort study based on cohort data extracted from the MIMIC-IV (v.1.4) database, which contains over 70,000 ICU admissions across the United States collected from 2008 to 2019. The database is a large, single-center, publicly available, and de-identified patient database containing comprehensive patient information [e.g., demographics, admission records, International Classification of Diseases-9th and Diseases-10th (ICD-9 and ICD-10) revision diagnoses, laboratory tests, medications, procedures, fluid balance, discharge summaries, vital sign measurements undertaken at the bedside, caregivers notes, radiology reports, and survival data] (34, 35). In addition, the eICU-CRD database (version 2.0), a multicenter database of more than 200,000 ICU admissions in the United States, was used as an independent external validation set. We studied these courses in depth and obtained permission to use the database (record ID:42039823). The requirement for individual patient consent and an ethical approval statement was waived as the program does not affect clinical practice and all patient privacy information in the database was de-identified. The selected primary outcome for this study was the all-cause mortality within 28 days of patients with HF combined with hypertension who were admitted to ICU.

Study patients and definitions

All adult patients in the MIMIC-IV database with a diagnosis of HF who were admitted to the ICU were recruited (only the first admission was included for analysis). The diagnosis was identified by a manual review of ICD-9 and ICD-10 codes. The exclusion criteria for participation in the study were as follows: (1) patients without hypertension, (2) patients with ICU length of stay less than 24 h or more than 28 days, (3) patients with severe liver disease, (4) patients with malignant cancer, and (5) patients with more than 30% missing data. In this study, the patient's first hospitalization time was taken as the starting point for statistics on whether he died, and the patient's death or whether the patient did not die within the period recorded in the database was taken as the statistical endpoint. The primary outcome of this study was in-hospital mortality, defined as the survival status at the time of hospital discharge.

Data collection and variable extraction

Following the variable selection method of Deshmukh et al. (35), 58 candidate variables that were associated

with the results were selected. The extracted variables included the general demographic variables of patients and other important variables, as follows: gender, age, ethnicity, body weight, comorbidities, vital signs, laboratory findings, medical treatments, and first care unit. The severity of the disease was assessed using Sequential Organ Failure Assessment (SOAF), Simplified Acute Physiology Score II (SAPS-II), Oxford Acute Severity of Illness Score (OASIS), and Logistic Organ Dysfunction System scoring system.

Charlson comorbidity index was used, and the comorbidities included hyperlipidemia, atrial fibrillation, paraplegia, renal disease, aids, dementia, diabetes without, diabetes with, peripheral vascular disease, cerebrovascular disease, dementia, chronic pulmonary disease, rheumatic disease, peptic ulcer disease, myocardial infarction, and congestive heart failure. For vital signs, the mean values in the ICU for the following variables were selected: respiratory rate, heart rate (HR), body temperature, mean blood pressure, diastolic blood pressure, systolic blood pressure, creatine kinase MB isoenzyme, creatinine phosphokinase, Troponin, and N-terminal prohormone of B-type natriuretic peptide (NT-proBNP). For the results of the first laboratory examination after admission to the ICU, the mean value for the following variables were selected: RBC, hematocrit, hemoglobin, platelets, MCV, WBC, MCHC, MCH, RDW, anion gap, bicarbonate, BUN, creatinine, calcium, chloride, sodium, potassium, PT, PTT, and INR. Medical treatments included MECHVENT and RRT. Finally, the cumulative urine output within the first 24 h. To reduce the impact of missing data on classification, a modified KNN-based (K-nearest neighbor) classification algorithm to fill in the missing values was proposed. Considering a large number of features still presented in the cohort, the least absolute shrinkage and selection operator (LASSO) regression in the variable selection was utilized to effectively prevent overfitting.

Missing data handling

Missing data with $< 30\%$ in each feature was processed by KNN-based classification algorithm using the " DMwR2" package in R. KNN-based classification algorithm is used as a missing value estimation method, which is a non-parametric ML algorithm based on neighbors. The imputed value is the average of the neighbor's measurements or multiple neighbors' measurements. The estimation of missing values is obtained by using the average of the non-missing values of its neighbors, and in addition, the case where all neighbors in a given set are missing can be circumvented by averaging the overall column for that particular feature. Therefore, this technique is advantageous for dealing with data sets that contain a large number of variables with missing values (36).

Machine learning model building

The original raw data included gender, age, vital signs, laboratory tests, and comorbidities. The processed data included 58 characteristics. In our study, five common algorithms, i.e., logistic regression (LR), Neural Networks (NN), Multi-Layer perceptron (MLP), Naive Bayes (NB), and Random Forest (RF), were applied to build models for predicting 28-day in-hospital mortality of ICU patients with HF combined with hypertension. To improve the stability of the prediction models, all continuous variables were rescaled to a distribution with a mean of 0 and a standard deviation of 1 with scale transformation. Threefold cross-validation of the ML models to be tuned (LR, NN, MLP, NB, and RF) was performed to select the best prediction model for each algorithm with different tuning parameters. During the search process, the accuracy or ROC was set as the metric. The test set was not used during model tuning and was used only for model evaluation after the entire model selection and training process.

Model assessment

The final models were evaluated using the confusion matrix metrics such as sensitivity, specificity, positive prediction value (PPV), negative prediction value (NPV), accuracy, and the area under the curve (AUC) of the receiver operating characteristic (ROC). ROC curves were constructed based on the prediction probabilities and the area under the curve (AUC) values of the models in the testing dataset were compared to identify the model with the best predictive performance.

Features important

Feature ranking evaluation is a measure that evaluates the importance of each feature in a feature set through its impact on the final classification result. We analyzed the importance of features using the DALEX package, which explains the predictions of any classifier in an interpretable and faithful manner by learning an interpretable model locally around the prediction. By calculating the relative importance of variables, the impact of features on the prediction model was plotted.

Statistical analysis

Patients were divided into two groups based on whether they died or survived during their 28-day stay in the ICU. Then, categorical variables were presented as a percentage of the total and continuous variables as mean $\pm$ SD or median and IQR, according to the normality of the distribution. For categorical and continuous variables, between-group differences

were compared by using a two-sided Pearson's $\chi 2$ test or Fisher's and two-sided one-way ANOVA or Wilcoxon rank sum test, respectively. Logistic regression with the LASSO penalization method was performed for predictor selection, which helped to reduce the dimensionality of the prediction model. LASSO regression shrinked the coefficient estimates toward zero, with the degree of shrinkage dependent on an additional parameter, lambda. To determine the penalty factor (lambda), we constructed a tenfold cross-validated error plot for the LASSO model. After that, the patients were randomly divided into two groups, of which 80% were used as the training cohort and the remaining 20% as the test cohort. Five common ML methods were applied to develop the models in the test cohort. The quantitative performance of the models was assessed by comparing the AUC and accuracy in the test cohort. The optimized model with the best mortality prediction performance in the test cohort (i.e., the Neural Network-NN) was defined as the final model. Then the top 7 most important clinical features were screened out of the 22 most influential features in the NN model, and they were used to build the best NN model again and finally used for external validation. The sensitivity performance analysis of the NN model was compared with the seven most important clinical features in the LR model. In addition, the Shapley additive explanations (SHAP) method was adopted to improve the interpretability of the final model. The SHAP values of features were evaluated by the lime package. We selected four cases for the feature's SHAP value evaluation.

All statistical analyses were carried out using R software (v. 3.6.3, R Foundation for Statistical Computing), and statistical significance was set at $p < 0.05$.

Results

Baseline characteristics

As shown in **Figure 1**, data of 15,354 critically ill patients were downloaded from the MIMIC-IV database. Among them, 3,458 HF patients with hypertension were included in our study. Among the included patients, 459 patients passed away and 2,999 survived within 28 days, respectively. **Table 1** summarizes the comparison of baseline characteristics, vital signs, and laboratory parameters within 28 days between non-survivors and survivors. In the non-survivor group, gender, age, ethnicity, body weight, SOFA, SAPS II, OASIS, LODS, Charlson comorbidity index, hyperlipidemia, atrial fibrillation, paraplegia, cerebrovascular disease, congestive heart failure, respiratory rate, HR, creatinine phosphokinase, Troponin, NT-proBNP, platelets, MCV, WBC, MCHC, hematocrit, RDW, anion gap, bicarbonate, bun, creatinine, calcium, chloride, sodium, potassium, PT, INR, MECHVENT, RRT, hematocrit, and the cumulative urine output within 24 h differ significantly compared to those who survived. However, dementia, diabetes and non-diabetes, peripheral vascular disease, chronic pulmonary disease, rheumatic disease, peptic ulcer disease, body temperature, mean blood pressure, diastolic blood pressure, systolic blood pressure, creatine kinase MB isoenzyme, RBC, hemoglobin, and MCH showed no significant difference between the two groups. **Figure 1** is the flow chart describing the procedure for subject selection.

Features selected in models

The LASSO regularization process resulted in 22 potential predictors based on 2,766 patients in the training cohort (**Figures 2A,B**). Using MLP, NN, RF, NB, and LR, the 58 selected variables were used to identify patients who died during their hospital stay in the training cohort. We show the proportional importance of the top 22-ranked input variables in the NN model and the LR model, respectively. **Figure 2B** shows the LASSO-selected predictors (shrinkage parameter, $\lambda = 0.01914052$).

Development and comparison of machine learning models

A total of 58 clinical features were collected during the first 24 h after ICU admission. KNN was used to impute missing data. LASSO regression was employed to identify signature variables for hospital mortality in patients with HF combined with hypertension. Ultimately, 22 out of 58 clinical features were associated with prognosis, and these results are presented in **Table 2**. In addition, we have constructed five ML binary classifiers, namely MLP, NN, RF, NB, and LR, to predict the risk of death in HF patients with hypertension (**Figure 1**). Then the obtained hyperparameters were used to train the ML model with the entire training data, and the performance of the model was evaluated using the testing cohort. **Figure 4** and **Table 3** describe the performance of these predictive models, showing that the NN model with all available variables relatively outperformed the other four models or predictive factors in testing cohorts with an AUC of 0.764 and an accuracy of 0.8731 in the testing cohort, compared with the other ML models (AUC: LR, 0.640; RF, 0.748; NB, 0.751; MLP, 0.730). Therefore, we selected the NN as the most promising approach among the five ML algorithms for further prediction in this study.

Significant predictors and development of the simplified model

We identified the 22 most significant predictors by permuting feature importance techniques, transforming the NN model and LR model into a universally applicable prediction

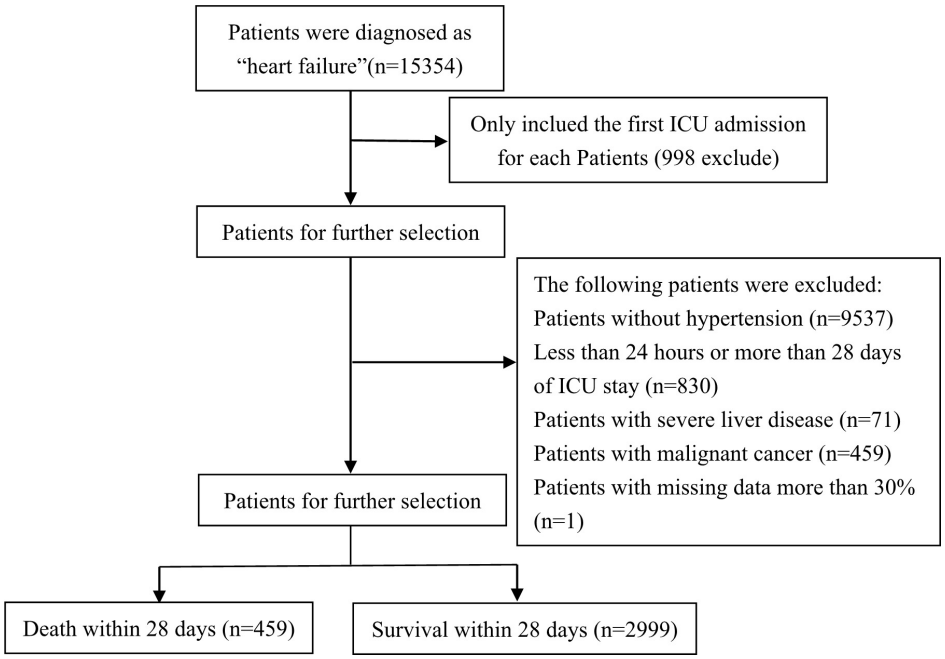


FIGURE 1
A flow chart describing the procedure for subject selection.

model (Figure 3). The features specific to death included age, MECHVENT, chloride, bun, anion gap, paraplegia, RDW, hyperlipidemia, SpO_2, respiratory rate, cerebrovascular disease, HR, WBC, INR, MCHC, glucose, aids, MCV, NT-proBNP, calcium, RRT, and PTT. For the convenience of clinical providers and patients, the order of importance of these features is not the same in the two models. Furthermore, we also assembled a simplified ML model for HF risk stratification by artificial intelligence with the top seven most important high-ranking and readily available variables, namely bun, paraplegia, anion gap, RDW, MECHVENT, chloride, and age. The AUC of SMART-HF reached 0.741 and 0.674 in the test cohort and external validation cohort, respectively (Figure 4C).

Shapley additive explanations values depending on variables

The impact of the top seven factors on the NN model's mortality risk prediction was further explored using the SHAP dependency plot. The probability of death in ICU patients with HF combined with hypertension increases with the following indicators: age, increased anion gap, elevated BUN, elevated RDW, increased serum chloride level, and paraplegia (Figure 5). In contrast, the mortality risk decreases with the increase of the MECHVENT index.

Discussion

Given that HF patients with hypertension have a relatively high chance of ICU admission, prioritization of patients who require higher levels of care or immediate medical attention is critical. Accurately predicting prognosis is the foundation of both patient-centered care and shared decision-making, such as selecting treatment strategies and informing patients. The present study has shown the potential for the NN model to assist physicians with predicting 28-day all-cause in-hospital mortality. Using data derived from the MIMIC-IV database, this study explored and validated five real-time diagnostic and prognostic prediction models based on a ML algorithm for 28-day in-hospital mortality in ICU patients with HF combined with hypertension. These learning models incorporated static and dynamic variables. Ultimately, it was found that an NN model best-stratified patients' risks with good external validation. The algorithm showed that age, MECHVENT, chloride, BUN, anion gap, paraplegia, RDW, hyperlipidemia, SpO_2, respiratory rate, cerebrovascular disease, HR, WBC, INR, MCHC, glucose, AIDS, MCV, NT-proBNP, calcium, RRT, and PTT were associated with an increased risk of death. The NN prediction model may facilitate clinical decision-making for advanced management of ICU-admitted HF patients with hypertension. The proposed model has several advantages over traditional clinical risk models. First, a highly specific cohort of ICU patients with HF combined with hypertension we used, rather than a more generalized cohort such as patients admitted

TABLE 1 Baseline characteristics, vital signs, laboratory parameters and statistic results of mimic-IIV patients with HF combined with hypertension.

Variables	Total (n = 3458)	Survival (n = 2999)	Death (n = 459)	p
Gender, *n* (%)				0.032
0	1756 (51)	1501 (50)	255 (56)	
1	1702 (49)	1498 (50)	204 (44)	
Age, Median (Q1, Q3)	75 (65, 84)	74 (64, 83)	80 (70, 87)	<0.001
Ethnicity, *n* (%)				0.005
0	923 (27)	775 (26)	148 (32)	
1	2535 (73)	2224 (74)	311 (68)	
Weight, Median (Q1, Q3)	79.5 (66.3, 95.9)	80 (67.1, 96.95)	74.2 (60.65, 91.1)	<0.001
Hematocrit, Median (Q1, Q3)	33.6 (28.8, 38.3)	33.4 (28.6, 38.3)	34.5 (29.8, 38.45)	0.011
Hemoglobin, Median (Q1, Q3)	11 (9.4, 12.6)	11 (9.4, 12.6)	11.3 (9.8, 12.5)	0.261
Platelets, Median (Q1, Q3)	202 (152, 266)	202 (151, 264)	210.5 (163.5, 291)	0.003
wbc, Median (Q1, Q3)	10.8 (7.9, 14.8)	10.55 (7.8, 14.6)	12 (8.3, 16.45)	<0.001
mch, Median (Q1, Q3)	30.1 (28.6, 31.5)	30.1 (28.6, 31.5)	30.1 (28.4, 31.4)	0.392
mchc, Median (Q1, Q3)	33 (31.9, 34)	33.1 (32, 34.1)	32.7 (31.5, 33.6)	<0.001
mcv, Median (Q1, Q3)	91 (87, 95)	91 (87, 95)	92 (87, 97)	0.001
rbc, Median (Q1, Q3)	3.69 (3.16, 4.25)	3.69 (3.14, 4.25)	3.73 (3.27, 4.29)	0.178
rdw, Median (Q1, Q3)	14.4 (13.6, 15.6)	14.3 (13.55, 15.45)	14.9 (13.8, 16.4)	<0.001
aniongap, Median (Q1, Q3)	14 (12, 17)	14 (12, 16)	16 (13, 19)	<0.001
Bicarbonate, Median (Q1, Q3)	24 (22, 27)	24 (22, 27)	24 (20, 27)	0.002
Bun, Median (Q1, Q3)	21 (15, 29)	20 (15, 28)	27 (18.5, 39)	<0.001
Calcium, Median (Q1, Q3)	8.5 (8.1, 8.9)	8.5 (8.1, 8.9)	8.5 (7.9, 8.9)	0.014
Chloride, Median (Q1, Q3)	104 (99, 108)	104 (100, 108)	102 (98, 106)	<0.001
Creatinine, Median (Q1, Q3)	1 (0.8, 1.3)	1 (0.8, 1.2)	1.2 (0.8, 1.6)	<0.001
Sodium, Median (Q1, Q3)	139 (136, 141)	139 (136, 141)	138 (135, 141)	0.027
Potassium, Median (Q1, Q3)	4.2 (3.8, 4.6)	4.1 (3.8, 4.6)	4.2 (3.8, 4.8)	0.001
inr, Median (Q1, Q3)	1.3 (1.1, 1.5)	1.3 (1.1, 1.5)	1.3 (1.1, 1.8)	<0.001
pt, Median (Q1, Q3)	14.2 (12.6, 16.9)	14.1 (12.5, 16.7)	14.7 (12.8, 19.5)	<0.001
ptt, Median (Q1, Q3)	31.5 (27.6, 38.2)	31.4 (27.5, 37.75)	32.2 (28.2, 40.65)	0.005
ck.cpk, Median (Q1, Q3)	122 (82, 179)	123 (83.5, 180)	112.5 (71.5, 163)	<0.001
ck.mb, Median (Q1, Q3)	5 (3.5, 6)	5 (3.5, 6)	5 (3, 7)	0.394
Tn.T, Median (Q1, Q3)	0.35 (0.29, 0.51)	0.35 (0.29, 0.5)	0.4 (0.27, 0.63)	0.004
Npro.BNP, Median (Q1, Q3)	2526.5 (1188.5, 4441)	2397 (1156.75, 4348.25)	3339 (1553.5, 4960.25)	<0.001
heart.rate, Median (Q1, Q3)	84 (74, 97)	84 (74, 96)	87 (76, 102)	<0.001
sbp, Median (Q1, Q3)	123 (106, 139)	123 (106, 140)	123 (105, 139)	0.538
dbp, Median (Q1, Q3)	64 (53, 76)	64 (54, 76)	64 (53, 77)	0.75
mbp, Median (Q1, Q3)	80 (70, 93)	80 (70, 93)	78 (67, 92)	0.099
resp.rate, Median (Q1, Q3)	18 (15, 22)	18 (15, 22)	20 (16, 24)	<0.001
Temperature, Median (Q1, Q3)	36.67 (36.33, 37)	36.67 (36.33, 37)	36.61 (36.22, 36.94)	0.211
spo2, Median (Q1, Q3)	98 (95, 100)	98 (96, 100)	98 (95, 100)	<0.001
Glucose, Median (Q1, Q3)	134 (109, 173)	133 (109, 169)	144 (113, 193.5)	<0.001
myocardial.infarct, *n* (%)				0.89
0	2394 (69)	2078 (69)	316 (69)	
1	1064 (31)	921 (31)	143 (31)	
congestive.heart.failure, *n* (%)				0.005
0	897 (26)	803 (27)	94 (20)	
1	2561 (74)	2196 (73)	365 (80)	
peripheral.vascular.disease, *n* (%)			0.09	0.09
0	2900 (84)	2528 (84)	372 (81)	
1	558 (16)	471 (16)	87 (19)	
cerebrovascular.disease, *n* (%)				<0.001
0	2912 (84)	2551 (85)	361 (79)	
1	546 (16)	448 (15)	98 (21)	
Dementia, *n* (%)				0.579
0	3327 (96)	2888 (96)	439 (96)	
1	131 (4)	111 (4)	20 (4)	
chronic.pulmonary.disease, n (%)				0.294
0	2152 (62)	1877 (63)	275 (60)	
1	1306 (38)	1122 (37)	184 (40)	

(Continued)

TABLE 1 (Continued)

Variables	Total (n = 3458)	Survival (n = 2999)	Death (n = 459)	p
rheumatic.disease, *n* (%)				0.654
0	3288 (95)	2854 (95)	434 (95)	
1	170 (5)	145 (5)	25 (5)	
peptic.ulcer.disease, *n* (%)				0.118
0	3383 (98)	2939 (98)	444 (97)	
1	75 (2)	60 (2)	15 (3)	
diabetes.without.cc, n (%)				0.39
0	2332 (67)	2031 (68)	301 (66)	
1	1126 (33)	968 (32)	158 (34)	
diabetes.with.cc, *n* (%)				0.291
0	3216 (93)	2795 (93)	421 (92)	
1	242 (7)	204 (7)	38 (8)	
Paraplegia, *n* (%)				<0.001
0	3343 (97)	2914 (97)	429 (93)	
1	115 (3)	85 (3)	30 (7)	
renal.disease, *n* (%)				0.142
0	3375 (98)	2932 (98)	443 (97)	
1	83 (2)	67 (2)	16 (3)	
Aids, *n* (%)				0.048
0	3455 (100)	2998 (100)	457 (100)	
1	3 (0)	1 (0)	2 (0)	
mechvent, *n* (%)				<0.001
0	1247 (36)	1131 (38)	116 (25)	
1	2211 (64)	1868 (62)	343 (75)	
uo.rt.24 h, Median (Q1, Q3)	1.13 (0.74, 1.55)	1.15 (0.78, 1.57)	0.9 (0.56, 1.4)	<0.001
rrt, *n* (%)				<0.001
0	3424 (99)	2979 (99)	445 (97)	
1	34 (1)	20 (1)	14 (3)	
Hyperlipidemia, *n* (%)				<0.001
0	1633 (47)	1378 (46)	255 (56)	
1	1825 (53)	1621 (54)	204 (44)	
atrialfibrillation, *n* (%)				<0.001
0	1776 (51)	1576 (53)	200 (44)	
1	1682 (49)	1423 (47)	259 (56)	
charlson.comorbidity.index, Median (Q1, Q3)	6 (5, 7)	6 (5, 7)	6 (5, 8)	<0.001
lods, Median (Q1, Q3)	4 (2, 6)	4 (2, 6)	7 (4, 10)	<0.001
sapsii, Median (Q1, Q3)	35 (29, 43)	35 (28, 42)	42 (34, 53)	<0.001
oasis, Median (Q1, Q3)	32 (26, 39)	31 (26, 38)	39 (32, 46)	<0.001
f.sofa, Median (Q1, Q3)	4 (2, 7)	4 (2, 7)	6 (4, 9)	<0.001

to the general medical floor. Second, a simplified ML model for HF risk stratification was also assembled by artificial intelligence with the top seven most important high-ranking variables to avoid the collection of a large number of variables for a prognostic model in real clinical settings. In addition, improving the model predictive performance can directly improve risk assessment even before patients receive a more comprehensive diagnostic evaluation in the ICU.

Hospitalized patients with HF often require admission to the ICU, especially when their condition is complicated by various comorbidities such as hypertension. Data from 341 hospitals in the USA showed a median ICU admission rate of 10% (IQR, 6–16%) for hospitalized HF patients (8). Numerous studies have shown that in-hospital mortality in patients with advanced HF admitted to the ICU is significantly higher than that of HF patients admitted to hospital wards only. All-cause in-hospital mortality was 10.6% for HF patients admitted to the ICU, compared with 4.0% for all HF patients in the ADHERE study (11). Meanwhile, 17.3% mortality among ICU patients versus 6.5% among all hospitalized HF patients was reported in the RO-AHFS study, and 17.8% death rate among ICU patients versus 4.5% among all hospitalized HF patients was observed in the ALARM-HF study (37, 38). It is noteworthy that a decision on whether a patient with HF requires intensive care depends on both clinical judgment and resource availability, which adds unmeasured differences to outcome studies.

Our study population comprised ICU-admitted HF patients with hypertension, and the in-hospital mortality rate was 15.3% (n = 459 patients). This rate was substantially higher than other prediction models for in-hospital mortality based on all

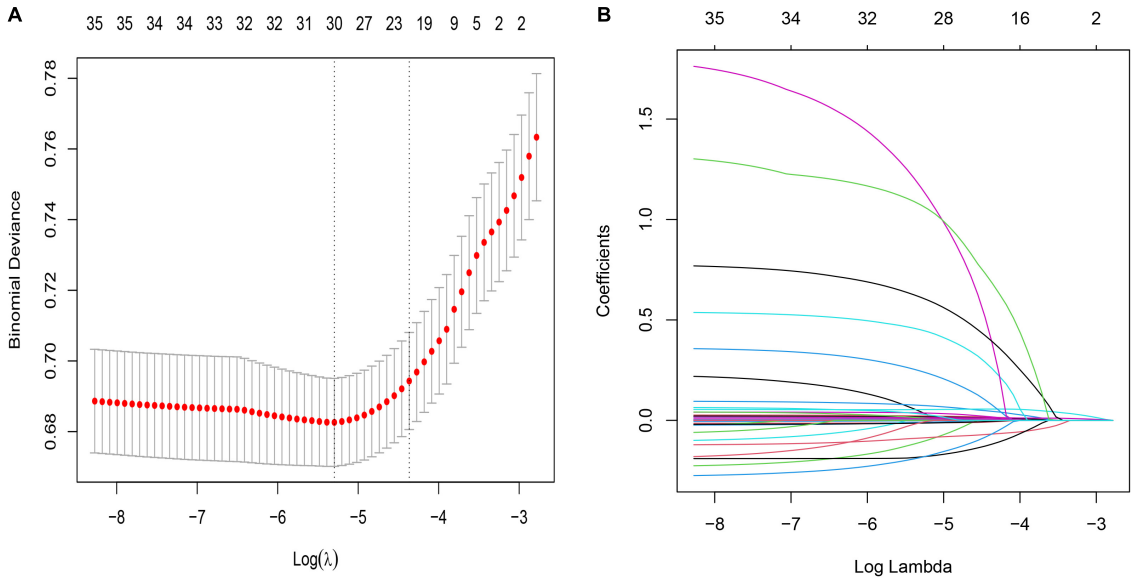


FIGURE 2
Demographic and clinical feature selection using the least absolute shrinkage and selection operator (LASSO) binary logistic regression model. **(A)** Tuning parameter (λ) selection in the LASSO model used 10- fold cross-validation via minimum criteria. The partial likelihood deviance (binomial deviance) curve was plotted versus log(λ). Dotted vertical lines were drawn at the optimal values by using the minimum criteria and the one SE of the minimum criteria (the 1-SE criteria). λ value of 0.01914052, with log(λ), −3.9545 was chosen (1- SE criteria) according to 10-fold cross-validation. **(B)** LASSO coefficient profiles of the 58 features. A coefficient profile plot was produced against the log(λ) sequence. The vertical line was drawn at the value selected using 10-fold cross-validation, where optimal resulted in 20 features with non-zero coefficients.

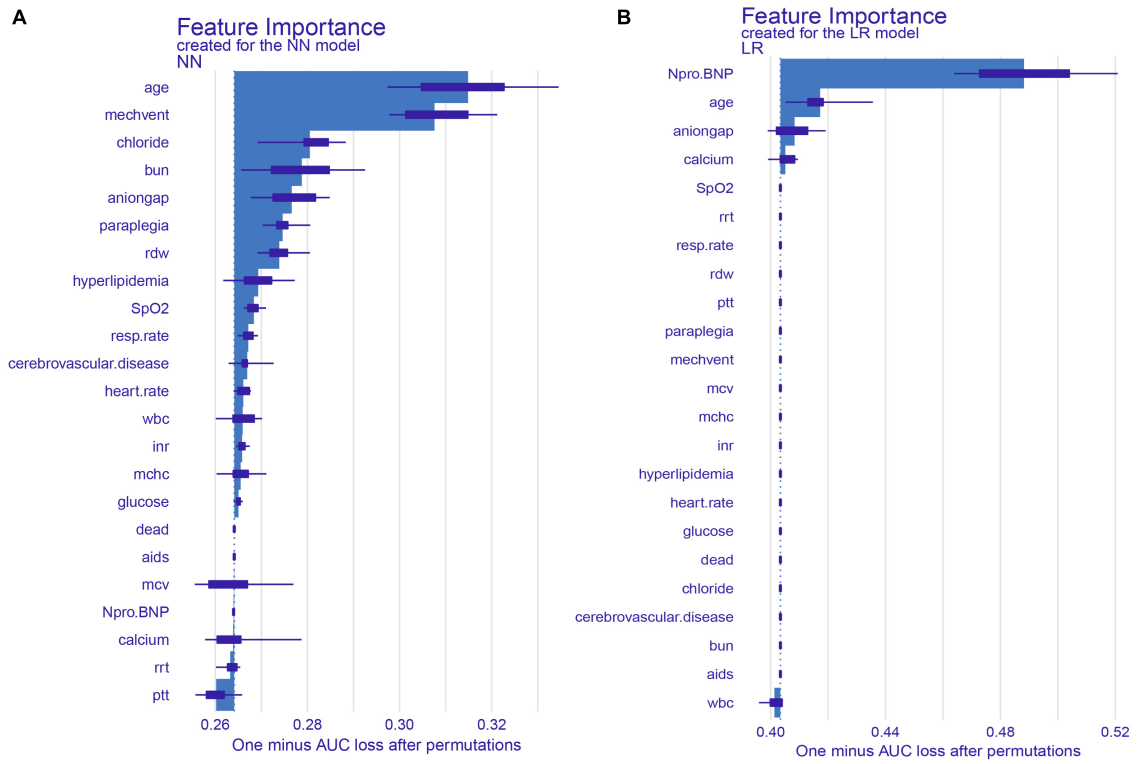


FIGURE 3
SHAP summary plot for the top 22 clinical features contributing to the NN **(A)** and LR **(B)** model. SHAP feature importance is measured as one minus AUC loss after permutations. This matrix plot depicts the importance of each covariate in the development of the final predictive model.

TABLE 2 Comparison of clinical characteristics between the training and testing cohort.

Variables	Total (n = 3458)	Testing (n = 692)	Training (n = 2766)	p
Age, Median (Q1, Q3)	75 (65, 84)	74 (65, 83)	75 (65, 84)	0.742
wbc, Median (Q1, Q3)	10.8 (7.9, 14.8)	10.8 (7.9, 14.83)	10.75 (7.93, 14.78)	0.999
mchc, Median (Q1, Q3)	33 (31.9, 34)	32.9 (31.9, 33.9)	33 (32, 34)	0.074
mcv, Median (Q1, Q3)	91 (87, 95)	91 (86, 95)	91 (87, 95)	0.104
rdw, Median (Q1, Q3)	14.4 (13.6, 15.6)	14.4 (13.7, 15.7)	14.4 (13.6, 15.5)	0.05
Aniongap, Median (Q1, Q3)	14 (12, 17)	14 (12, 17)	14 (12, 17)	0.804
Bun, Median (Q1, Q3)	21 (15, 29)	21 (16, 31)	21 (15, 29)	0.538
Calcium, Median (Q1, Q3)	8.5 (8.1, 8.9)	8.5 (8.1, 8.9)	8.5 (8.1, 8.9)	0.888
Chloride, Median (Q1, Q3)	104 (99, 108)	104 (99, 108)	104 (99, 108)	0.782
inr, Median (Q1, Q3)	1.3 (1.1, 1.5)	1.3 (1.1, 1.6)	1.3 (1.1, 1.5)	0.308
ptt, Median (Q1, Q3)	31.5 (27.6, 38.2)	31 (27.3, 37.1)	31.6 (27.7, 38.4)	0.168
Npro.BNP, Median (Q1, Q3)	2526.5 (1188.5, 4441)	2580.5 (1176.75, 4479.5)	2490 (1193.25, 4440.5)	0.677
heart.rate, Median (Q1, Q3)	84 (74, 97)	85 (74, 98)	84 (74, 97)	0.454
resp.rate, Median (Q1, Q3)	18 (15, 22)	18 (15, 22)	18 (15, 22)	0.66
SpO2, Median (Q1, Q3)	98 (95, 100)	98.5 (96, 100)	98 (95, 100)	0.339
Glucose, Median (Q1, Q3)	134 (109, 173)	137 (109.75, 175)	134 (109, 172)	0.534
cerebrovascular.disease, n (%)				0.978
0	2912 (84)	582 (84)	2330 (84)	
1	546 (16)	110 (16)	436 (16)	
Paraplegia, n (%)				1
0	3343 (97)	669 (97)	2674 (97)	
1	115 (3)	23 (3)	92 (3)	
Aids, n (%)				1
0	3455 (100)	692 (100)	2763 (100)	
1	3 (0)	0 (0)	3 (0)	
mechvent, n (%)				0.214
0	1247 (36)	235 (34)	1012 (37)	
1	2211 (64)	457 (66)	1754 (63)	
rrt, n (%)				0.574
0	3424 (99)	687 (99)	2737 (99)	
1	34 (1)	5 (1)	29 (1)	
Hyperlipidemia, n (%)				0.044
0	1633 (47)	351 (51)	1282 (46)	
1	1825 (53)	341 (49)	1484 (54)	
Dead, n (%)				0.087
0	2999 (87)	586 (85)	2413 (87)	
1	459 (13)	106 (15)	353 (13)	

HF patients, regardless of ICU admission. However, in the ADHERE in-hospital mortality risk stratification model, the in-hospital mortality rate of their study population was only 4.2% (27).In the optimized heart failure prediction model, the GWTG-HF risk scoring model, and a single-center elderly Chinese patient-based model established by Jia et al., the rates were 3.8, 2.86, and 5.58%, respectively (28, 29, 39).

Our model contains only variables that are easily accessible: its simplicity makes risk prediction applicable for different purposes during the hospitalization of HF patients in the ICU. For example, when the calculated risk of death for an individual is high, it indicates the need for more aggressive monitoring or resource allocation, which can help assign patients to different levels of care. This is particularly useful when healthcare resources are limited. The discriminative performance of the model is very high, and its validation was confirmed by testing the model in a cohort of HF patients with hypertension in the eICU database.

Although several published studies provide a wealth of computational tools or predictive models that can be easily used in a variety of settings to assess risk in patients with HF (21, 24, 40–45). Such calculators unfortunately require

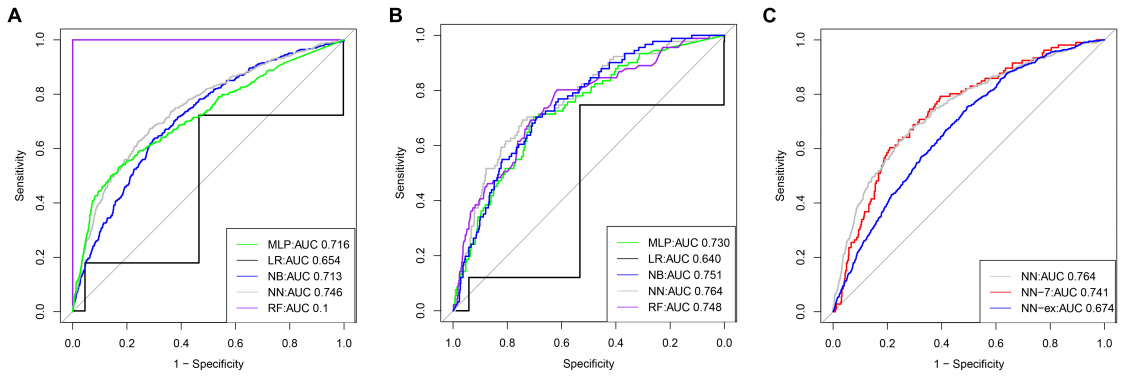


FIGURE 4
The receiver operator characteristic (ROC) curves for the ML models predict in-hospital mortality (The training cohort and testing cohort). ROC curves for five ML models predicting in-hospital mortality in the training **(A)** and testing cohort **(B)**, respectively; **(C)** ROC curves for in-hospital mortality in the test set predicted by the un-simplified NN model and the ROC curves for in-hospital mortality in the test set and external validation set predicted by the simplified NN model, respectively.

TABLE 3 **Predictive performances of the five machine learning models for predicting in-hospital mortality.**

ML	Accuracy	AUC	Sensitivity	Specificity	95% CI
NN					
Training cohort	0.8731	0.746	0.048159	0.993784	0.8727(0.8601,0.8853)
Testing cohort	0.841	0.764	0.028302	0.988055	0.83955(0.8116,0.8675)
LR					
Training cohort	0.8515	0.654	0.17935	0.95458	0.85115(0.8377,0.8646)
Testing cohort	0.8333	0.640	0.12088	0.94157	0.8319(0.8034,0.8604)
NB					
Training cohort	0.8577	0.713	0.11413	0.97167	0.8573(0.8441,0.8705)
Testing cohort	0.858	0.751	0.16484	0.96327	0.85645(0.8297,0.8832)
RF					
Training cohort	1	0.1	1.0000	1.0000	0.999355(0.9987,1)
Testing cohort	0.8681	0.748	0.0000	1.0000	0.86655(0.8406,0.8925)
MLP					
Training cohort	0.8671	0.716	0.0000	1.0000	0.86665(0.8538,0.8795)
Testing cohort	0.8681	0.730	0.0000	1.0000	0.86655(0.8406,0.8925)

tedious data entry. Real-time processing of the predictive model directly from the Electronic Health Record (EHR) provides immediate and seamless calculation, and the score from this calculation is well suited to support clinical decision-making and prioritization when the healthcare system is overloaded. An accurate prognosis is a basis for many clinical decisions regarding patients admitted to the ICU with HF (24). To avoid the shortcomings of using traditional LR analyses such as overfitting and predictor variables with skewed distributions, data on demographic characteristics, vital signs, comorbidities, and laboratory variables were used in the present study for LASSO regression analysis to screen for independent risk factors for in-hospital mortality.

Other predictive models have been published previously, and many variables have been reported to correlate with mortality in HF patients. Variables, such as gender, BUN level, BMI, age, sodium levels, health status, systolic blood pressure, diabetes mellitus, serum creatinine levels, low SBP, chronic obstructive lung disease, NYHA (New York Heart Association) classification, left ventricular ejection fraction (LVEF), smoking, not receiving ACEIs/ARBs (Angiotensin-Converting Enzyme Inhibitors/Angiotensin II Receptor Blockers), and not receiving beta-blockers, have been reported to explain the predictive model (25, 44). Consistent with previous studies, our study identified age as a strong prognostic predictor. When HF worsens, especially in the elderly, it can lead to severe ischemia and hypoxia, respiratory failure, and ultimately death. In our model, BUN levels also substantially contributed to the predicted probabilities, and elevated BUN levels substantially contributed to increased in-hospital mortality, which is

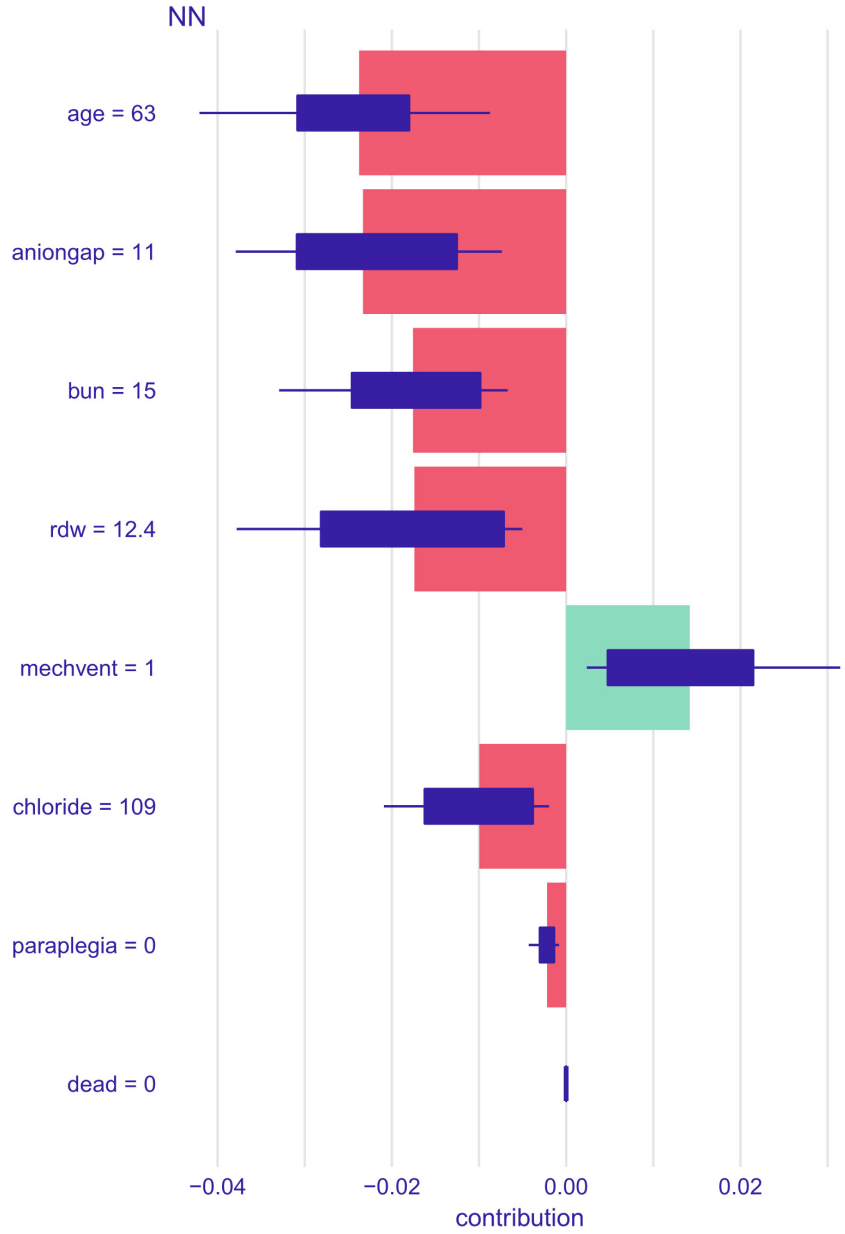


FIGURE 5
SHAP contribution values of different variables for a single sample of the NN model.

consistent with previously published studies (27–29). Elevated BUN levels suggest a high probability of prerenal injury, which may be related to reduced renal blood supply due to insufficient effective blood volume or a decrease in cardiac output after the onset of HF, as well as fluid management (urine output). Some HF mortality prediction models believe that HR affects prognosis strongly (28, 30), while some other models disagree (27, 46, 47). In our study, HR was included in the final model, in contrast to BMI, which was not included in the final model because our study failed to prove that BMI was a predictor of in-hospital mortality of ICU-admitted HF patients with hypertension. This may be related to differences in study populations and our relatively small sample size. Whether the "obesity paradox" biases our results is uncertain, as the "obesity paradox" presented for both critical care-related outcomes (48) and HF (49). Therefore, further studies are still needed to elaborate on the effect of obesity or BMI.

Our study showed that chloride and hyperlipidemia correlated with an unfavorable outcome. Consistent with previous findings, chloride has a more prominent contribution to the pathophysiology and affects the prognosis of HR, which may be related to hyperchloremia, acidosis, inflammation, and

renal injury secondary to hyper chlorination. In clinical practice, it is uncommon to focus on this one marker alone in patients with HF, but it is often integrated with blood gas analysis and evaluation of anion gap (50). Although several studies in acute and chronic HF populations have demonstrated the prognostic value of hypochlorhydria, interventional clinical trials exploring serum chloride as a therapeutic target have been inconclusive to date. Ongoing prospective randomized controlled studies may shed light on the role of serum chloride as a therapeutic target to improve outcomes in patients with HF. These studies should clarify whether serum chloride should be included in current models for predicting prognosis in HF (51). In the general population and patients with atherosclerotic cardiovascular disease, hypercholesterolemia has consistently been shown to be associated with poor outcomes, including mortality, cardiovascular events, and the development of HF (52, 53). Conversely, in patients with established HF, several analyses have now demonstrated an inverse relationship between cholesterol levels and outcomes. That is, low cholesterol levels have been shown to be independently associated with increased mortality, while higher cholesterol levels have been associated with improved survival. It is unclear whether low cholesterol levels play a pathogenic role in adverse outcomes in patients with HF or whether low cholesterol levels simply reflect advanced disease status. Given the observed inverse relationship between cholesterol levels and mortality in patients with HF, the applicability of cholesterol treatment goals recommended for the general population and patients with atherosclerotic CVD to patients with HF is unclear and remains to be determined (54). Consistent with previous studies (39, 55), our study also identified the anion gap as a strong prognostic predictor and found that this factor was independently associated with an increased risk of death.

Our study also showed that the anion gap was also a very important prognostic feature. The anion gap formula ($AnionGap=S_{Na}+S_K-S_{HCO3}^{--}-S_{Cl}^{-}$) itself already shows an interdependent relationship between serum chloride, sodium, potassium, and bicarbonate (50), so it is not surprising why hypochlorhydria often occurs in conjunction with metabolic alkalosis. It is known as "chloride-depleted alkalosis," a state of extracellular fluid volume constriction caused primarily by diuretic-induced diuresis. Although the exact role of pH as a prognostic indicator of HF has not been fully explored, pH is influenced by chloride levels in the form of chloride-depleted alkalosis or hyperchloremic metabolic acidosis (56). Chloride-depleted alkalosis is an independent predictor of in-hospital mortality in patients with decompensated HF (57). In HF, electrolyte depletion is primarily the result of salt restriction and cyclic and thiazide diuretic therapy, whereas metabolic alkalosis often occurs as a result of diuretic usage (58).

Notably, our study found that the use of MECHVENT improved the prognosis of patients with HF (**Figure 5**). The use of MECHVENT often indicates that patients are in serious conditions, such as the occurrence of acute HF and respiratory failure, but the use of MECHVENT as treatment improves the patient's prognosis by rapidly improving respiratory symptoms and ventilatory function compared to conventional drug therapy. The previous study has shown that in-hospital mortality in HF patients receiving non-invasive ventilation (NIV) or non-invasive ventilation (NIV) + invasive mechanical ventilation (IMV) decreases significantly over time, even if the clinical profile is worsening (59).

In our model, paraplegia and high RDW were also high-risk factors for ICU-admitted patients with HR combined with hypertension. When paralysis, prolonged bed rest, and reduced activity occur, the likelihood of thrombosis, crushing pneumonia, and infection increases. Consistent with the previous study (60), RDW is a powerful predictor of poor long-term outcomes in HF patients with acute exacerbation (AHF), and its prognostic value outperforms that of other well-established risk variables or biomarkers.

In addition, we further enhanced the readability of the model by using the SHAP framework, making the individual variables that contribute to the overall prediction easily available and understandable to physicians in real-time, along with the model's risk score.

In comparison with the reported GWTG-HF risk score (29), a well-validated tool for predicting in-hospital mortality in HF patients, both the NN model and the LR model showed superiority in predictive power in our study population. Both models showed good discrimination and calibration power in both the derivation and validation sets. To obtain a more concise and broader range of net benefit threshold probabilities, we chose the NN model to develop our simplified ML model.

Neural networks are constructed from basic units called neurons, which can be easily arranged into layers. The layers are easily connected, and the entire network can be trained end-to-end using a stochastic gradient descent algorithm (61). While single-layer networks can approximate any function to arbitrary accuracy [as implied by the general approximation theorem (62)], the real power of these models lies in providing automatic abstraction by stacking multiple layers into deep neural networks (DNNs). Each layer abstracts its input, providing the next layer with a representation of the data that is more likely to work within the scope of the task being solved. The most advanced models of NNs are DNNs models and have been shown to provide superhuman performance (63, 64) on many tasks involving difficult to abstract data, such as those involving image and audio processing.

In recent literature (65, 66), shallow NNs have been used to predict mortality in heart failure despite training on unbalanced datasets, showing superior performance to other learning methods. DNNs have been used to predict mortality (67, 68) or the risk of heart failure and acute heart failure (69). The authors of these two works compared DNNs with other ML techniques and showed improved performance. Another

interesting recent application of NNs in this field is exploiting their ability to process very complex and related data. This is the case with the Deep Cox Mixture Model (70), where NNs assist the Cox Regression Model to fit the risk ratio of the regression. This work is based on a sound statistical and ML background, is fully disclosed, and provides state-of-the-art performance when working with diverse groups of individuals.

Compared to traditional ML algorithms such as logistic regression, neural networks typically require more data, at least thousands or even millions of labeled samples. This is not an easy problem to solve, but if other algorithms are used, the related ML problem can be solved with less data. At the same time, compared to traditional algorithms, neural networks are computationally more expensive than traditional algorithms. Advanced deep learning algorithms can take weeks to train successfully. Whereas most traditional ML takes less than a few minutes, hours, or days. Of course, the computational power required by NN depends heavily on the size of the data and also on the depth and complexity of the network. The smaller the data set as well as the smaller the depth and complexity of the network, the less computational power is required by the NN.

This study has several limitations: First, as a retrospective study, selection bias was hardly avoidable. However, the inclusion criteria were set strictly so that the cases included in the study reflected the actual conditions as accurately as possible. Second, data were collected from patient medical records and the final performance of our predictive model was strictly dependent on the accuracy of the records. Third, as a single-center study, the scope and number of study populations involved were relatively small. Fourth, the impact of this predictive model on routine patient care in different clinical settings has not been well investigated. Therefore, data with mortality outcomes from other independent healthcare systems will be required to fully assess its generalizability. Finally, our model may only facilitate the rapid identification of critical clinical situations at the bedside but does not provide additional information about the underlying life-threatening pathophysiological mechanisms.

Conclusion

Using ML techniques, we developed a predictive model to predict the 28-day mortality for ICU-admitted patients with HF combined with hypertension based on NN. It was proved with a better predictive value than the traditional logistic regression analysis. With a high AUC of 0.764 and an accuracy of 0.8731 in the testing cohort, this model is promising for routine use in the ICUs to automatically warn the staff at any stage of the disease. The SHAP method enables ML models to be more interpretable, thereby helping clinicians to better understand the reasoning behind the outcome and evaluate in-hospital outcomes for critically ill patients, especially those with uncertain survival outcomes. Also, the model involves a small number of routinely collected variables that can be easily used at the bedside.

Data availability statement

The original contributions presented in this study are included in the article/supplementary material, further inquiries can be directed to the corresponding author.

Ethics statement

The studies involving human participants were reviewed and approved by the Medical Ethics Committee at Zi Gong First People's Hospital. Written informed consent for participation was not required for this study in accordance with the national legislation and the institutional requirements.

Author contributions

SgP, JH, XzL, JD, and SaP contributed to the conception and design. SgP, JH, JD, and HC collected and analyzed the data. JH drew the figures and tables. SgP wrote the draft. CS, JT, WC, WW, and XgL contributed to the manuscript writing and revision. All authors approved the final manuscript.

Funding

This work was supported by the Zigong Science and Technology Project (No. 2015ZC02) and the Medical and Health Own Fund Guiding Project of the Zigong Academy of Medical Sciences (No. 2020YXY03).

Conflict of interest

The authors declare that the research was conducted in the absence of any commercial or financial relationships that could be construed as a potential conflict of interest.

Publisher's note

All claims expressed in this article are solely those of the authors and do not necessarily represent those of their affiliated organizations, or those of the publisher, the editors and the reviewers. Any product that may be evaluated in this article, or claim that may be made by its manufacturer, is not guaranteed or endorsed by the publisher.

References

1. GBD 2017 Disease and Injury Incidence and Prevalence Collaborators. Global, regional, and national incidence, prevalence, and years lived with disability for 354 diseases and injuries for 195 countries and territories, 1990-2017: a systematic analysis for the global burden of disease study 2017. *Lancet.* (2018) 392:1789–858. doi: 10.1016/S0140-6736(18)32279-7

2. Conrad N, Judge A, Canoy D, Tran J, Pinho-Gomes AC, Millett ERC, et al. Temporal trends and patterns in mortality after incident heart failure: a longitudinal analysis of 86 000 individuals. *JAMA Cardiol.* (2019) 4:1102–11. doi: 10.1001/jamacardio.2019.3593

3. Taylor CJ, Ordóñez-Mena JM, Roalfe AK, Lay-Flurrie S, Jones NR, Marshall T, et al. Trends in survival after a diagnosis of heart failure in the United Kingdom 2000-2017: population based cohort study. *BMJ.* (2019) 364:l223. doi: 10.1136/bmj

4. Tromp J, Ferreira JP, Janwanishstaporn S, Shah M, Greenberg B, Zannad F, et al. Heart failure around the world. *Eur J Heart Fail.* (2019) 21:1187–96. doi: 10.1002/ejhf.1585

5. Heidenreich PA, Albert NM, Allen LA, Bluemke DA, Butler J, Fonarow GC, et al. Forecasting the impact of heart failure in the united states: a policy statement from the American heart association. *Circ Heart Fail.* (2013) 6:606–19. doi: 10.1161/HHF.0b013e318291329a

6. Benjamin EJ, Virani SS, Callaway CW, Chamberlain AM, Chang AR, Cheng S, et al. Heart Disease and stroke statistics-2018 update: a report from the American heart association. *Circulation.* (2018) 137:e67–492. doi: 10.1161/CIR.0000000000000558

7. Krum H, Gilbert RE. Demographics and concomitant disorders in heart failure. *Lancet.* (2003) 362:147–58. doi: 10.1016/S0140-6736(03)13869-X

8. Safavi KC, Dharmarajan K, Kim N, Strait KM, Li SX, Chen SI, et al. Variation exists in rates of admission to intensive care units for heart failure patients across hospitals in the United States. *Circulation.* (2013) 127:923–9. doi: 10.1161/CIRCULATIONAHA.112.001088

9. van Diepen S, Bakal JA, Lin M, Kaul P, McAlister FA, Ezekowitz JA. Variation in critical care unit admission rates and outcomes for patients with acute coronary syndromes or heart failure among high- and low-volume cardiac hospitals. *J Am Heart Assoc.* (2015) 4:e001708. doi: 10.1161/JAHA.114.001708

10. Wunsch H, Angus DC, Harrison DA, Collange O, Fowler R, Hoste EA, et al. Variation in critical care services across North America and Western Europe. *Crit Care Med.* (2008) 36:2787–e9. doi: 10.1097/CCM.0b013e318186aec8

11. Adams KF Jr., Fonarow GC, Emerman CL, LeJemtel TH, Costanzo MR, Abraham WT, et al. Characteristics and outcomes of patients hospitalized for heart failure in the United States: rationale, design, and preliminary observations from the first 100,000 cases in the acute decompensated heart failure national registry (ADHERE). *Am Heart J.* (2005) 149:209–16. doi: 10.1016/j.ahj.2004.08.005

12. Goehner NS, Roman PEF. Monitoring technologies in acute care environments: a comprehensive guide to patient monitoring technology. *Can J Anesth.* (2014) 61:891–2. doi: 10.1007/s12630-014-0177-y

13. Fackler JC, Watts C, Grome A, Miller T, Crandall B, Pronovost P. Critical care physician cognitive task analysis: an exploratory study. *Crit Care.* (2009) 13:R33. doi: 10.1186/cc7740

14. Wright MC, Dunbar S, Macpherson BC, Moretti EW, Del Fiol G, Bolte J, et al. Toward designing information display to support critical care. A qualitative contextual evaluation and visioning effort. *Appl Clin Inform.* (2016) 7:912–29. doi: 10.4338/ACI-2016-03-RA-0033

15. Duke G, Green J, Briedis J. Survival of critically ill medical patients is time-critical. *Crit Care Resusc.* (2004) 6:261–7.

16. Numata Y, Schulzer M, van der Wal R, Globerman J, Semeniuk P, Balka E, et al. Nurse staffing levels and hospital mortality in critical care settings: literature review and meta-analysis. *J Adv Nurs.* (2006) 55:435–48. doi: 10.1111/j.1365-2648.2006.03941.x

17. Falk AC, Wallin EM. Quality of patient care in the critical care unit in relation to the nurse-patient ratio: a descriptive study. *Intensive Crit Care Nurs.* (2016) 35:74–9. doi: 10.1016/j.iccn.2016.01.002

18. Wallace DJ, Angus DC, Barnato AE, Kramer AA, Kahn JM. Nighttime intensivist staffing and mortality among critically ill patients. *N Engl J Med.* (2012) 366:2093–101. doi: 10.1056/NEJMsa1201918

19. Ponikowski P, Voors AA, Anker SD, Bueno H, Cleland JG, Coats AJ, et al. 2016 ESC Guidelines for the diagnosis and treatment of acute and chronic heart failure: the task force for the diagnosis and treatment of acute and chronic heart failure of the European society of cardiology (ESC). Developed with the special contribution of the heart failure association (HFA) of the ESC. *Eur J Heart Fail.* (2016) 18:891–975. doi: 10.1002/ejhf.592

20. Yancy CW, Jessup M, Bozkurt B, Butler J, Casey DE Jr., Drazner MH, et al. 2013 ACCF/AHA guideline for the management of heart failure: a report of the American college of cardiology foundation/American heart association task force on practice guidelines. *Circulation.* (2013) 128:e240–327. doi: 10.1161/CIR.0b013e31829e8776

21. Frizzell JD, Liang L, Schulte PJ, Yancy CW, Heidenreich PA, Hernandez AF, et al. Prediction of 30-Day All-cause readmissions in patients hospitalized for heart failure: comparison of machine learning and other statistical approaches. *JAMA Cardiol.* (2017) 2:204–9. doi: 10.1001/jamacardio.2016.3956

22. Wang W, Cai D. Complement components sC5b-9 and CH50 predict prognosis in heart failure patients combined with hypertension. *Am J Hypertens.* (2020) 33:53–60. doi: 10.1093/ajh/hpz140

23. Tohyama T, Ide T, Ikeda M, Kaku H, Enzan N, Matsushima S, et al. Machine learning-based model for predicting 1 year mortality of hospitalized patients with heart failure. *ESC Heart Fail.* (2021) 8:4077–85. doi: 10.1002/ehf2.13556

24. Li F, Xin H, Zhang J, Fu M, Zhou J, Lian Z. Prediction model of in-hospital mortality in intensive care unit patients with heart failure: machine learning-based, retrospective analysis of the MIMIC-III database. *BMJ Open.* (2021) 11:e044779. doi: 10.1136/bmjopen-2020-044779

25. Pocock SJ, Ariti CA, McMurray JJ, Maggioni A, Køber L, Squire IB, et al. Predicting survival in heart failure: a risk score based on 39 372 patients from 30 studies. *Eur Heart J.* (2013) 34:1404–13. doi: 10.1093/eurheartj/ehs337

26. Collier TJ, Pocock SJ, McMurray JJ, Zannad F, Krum H, van Veldhuisen DJ. The impact of eplerenone at different levels of risk in patients with systolic heart failure and mild symptoms: insight from a novel risk score for prognosis derived from the EMPHASIS-HF trial. *Eur Heart J.* (2013) 34:2823–9. doi: 10.1093/eurheartj/eht247

27. Fonarow GC, Adams KF Jr., Abraham WT, Yancy CW, Boscardin WJ, Adhere Scientific Advisory Committee, Study Group, and Investigators. Risk stratification for in-hospital mortality in acutely decompensated heart failure: classification and regression tree analysis. *JAMA.* (2005) 293:572–80. doi: 10.1001/jama.293.5.572

28. Abraham WT, Fonarow GC, Albert NM, Stough WG, Gheorghiade M, Greenberg BH, et al. Predictors of in-hospital mortality in patients hospitalized for heart failure: insights from the organized program to initiate lifesaving treatment in hospitalized patients with heart failure (OPTIMIZE-HF). *J Am Coll Cardiol.* (2008) 52:347–56. doi: 10.1016/j.jacc.2008.04.028

29. Peterson PN, Rumsfeld JS, Liang L, Albert NM, Hernandez AF, Peterson ED, et al. A validated risk score for in-hospital mortality in patients with heart failure from the American heart association get with the guidelines program. *Circ Cardiovasc Qual Outcomes.* (2010) 3:25–32. doi: 10.1161/CIRCOUTCOMES.109.854877

30. Yagyu T, Kumada M, Nakagawa T. Novel risk stratification with time course assessment of in-hospital mortality in patients with acute heart failure. *PLoS One.* (2017) 12:e0187410. doi: 10.1371/journal.pone.0187410

31. Krumholz HM. Big data and new knowledge in medicine: the thinking, training, and tools needed for a learning health system. *Health Aff (Millwood).* (2014) 33:1163–70. doi: 10.1377/hlthaff.2014.0053

32. Johnson AE, Pollard TJ, Shen L, Lehman LW, Feng M, Ghassemi M, et al. MIMIC-III, a freely accessible critical care database. *Sci Data.* (2016) 3:160035. doi: 10.1038/sdata.2016.35

33. Pollard TJ, Johnson AEW, Raffa JD, Celi LA, Mark RG, Badawi O. The eICU Collaborative Research Database, a freely available multi-center database for critical care research. *Sci Data.* (2018) 5:180178. doi: 10.1038/sdata.2018.178

34. Zhou S, Zeng Z, Wei H, Sha T, An S. Early combination of albumin with crystalloids administration might be beneficial for the survival of septic patients: a retrospective analysis from MIMIC-IV database. *Ann Intensive Care.* (2021) 11:42. doi: 10.1186/s13613-021-00830-8

35. Deshmukh F, Merchant SS. Explainable machine learning model for predicting GI bleed mortality in the intensive care unit. *Am J Gastroenterol.* (2020) 115:1657–68. doi: 10.14309/ajg.0000000000000632

36. Gromski PS, Xu Y, Kotze HL, Correa E, Ellis DI, Armitage EG, et al. Influence of missing values substitutes on multivariate analysis of metabolomics data. *Metabolites.* (2014) 4:433–52. doi: 10.3390/metabo4020433

37. Chioncel O, Ambrosy AP, Filipescu D, Bubenek S, Vinereanu D, Petris A, et al. Patterns of intensive care unit admissions in patients hospitalized for heart failure: insights from the RO-AHFS registry. *J Cardiovasc Med (Hagerstown).* (2015) 16:331–40. doi: 10.2459/JCM.0000000000000030

38. Follath F, Yilmaz MB, Delgado JF, Parissis JT, Porcher R, Gayat E, et al. Clinical presentation, management and outcomes in the acute heart failure global

survey of standard treatment (ALARM-HF). *Intensive Care Med.* (2011) 37:619–26. doi: 10.1007/s00134-010-2113-0

39. Jia Q, Wang YR, He P, Huang XL, Yan W, Mu Y, et al. Prediction model of in-hospital mortality in elderly patients with acute heart failure based on retrospective study. *J Geriatr Cardiol.* (2017) 14:669–78. doi: 10.11909/j.issn.1671-5411.2017.11.002

40. Levy WC, Mozaffarian D, Linker DT, Sutradhar SC, Anker SD, Cropp AB, et al. The Seattle heart failure model: prediction of survival in heart failure. *Circulation.* (2006) 113:1424–33. doi: 10.1161/CIRCULATIONAHA.105.584102

41. Rich JD, Burns J, Freed BH, Maurer MS, Burkhoff D, Shah SJ. Meta-analysis global group in chronic (MAGGIC) heart failure risk score: validation of a simple tool for the prediction of morbidity and mortality in heart failure with preserved ejection fraction. *J Am Heart Assoc.* (2018) 7:e009594. doi: 10.1161/JAHA.118.009594

42. Komajda M, Carson PE, Hetzel S, McKelvie R, McMurray J, Ptaszynska A, et al. Factors associated with outcome in heart failure with preserved ejection fraction: findings from the irbesartan in heart failure with preserved ejection fraction study (I-PRESERVE). *Circ Heart Fail.* (2011) 4:27–35. doi: 10.1161/CIRCHEARTFAILURE.109.932996

43. Mortazavi BJ, Downing NS, Bucholz EM, Dharmarajan K, Manhapra A, Li SX, et al. Analysis of machine learning techniques for heart failure readmissions. *Circ Cardiovasc Qual Outcomes.* (2016) 9:629–40. doi: 10.1161/CIRCOUTCOMES.116.003039

44. Angraal S, Mortazavi BJ, Gupta A, Khera R, Ahmad T, Desai NR, et al. Machine learning prediction of mortality and hospitalization in heart failure with preserved ejection fraction. *JACC Heart Fail.* (2020) 8:12–21. doi: 10.1016/j.jchf.2019.06.013

45. Cui X, Zhou J, Pivodic A, Dahlström U, Ge J, Fu M. Temporal trends in cause-specific readmissions and their risk factors in heart failure patients in Sweden. *Int J Cardiol.* (2020) 306:116–22. doi: 10.1016/j.ijcard.2020.02.048

46. Voors AA, Ouwerkerk W, Zannad F, van Veldhuisen DJ, Samani NJ, Ponikowski P, et al. Development and validation of multivariable models to predict mortality and hospitalization in patients with heart failure. *Eur J Heart Fail.* (2017) 19:627–34. doi: 10.1002/ejhf.785

47. Lupón J, de Antonio M, Vila J, Peñafiel J, Galán A, Zamora E, et al. Development of a novel heart failure risk tool: the Barcelona bio-heart failure risk calculator (BCN bio-HF calculator). *PLoS One.* (2014) 9:e85466. doi: 10.1371/journal.pone.0085466

48. Patel JJ, Rosenthal MD, Miller KR, Codner P, Kiraly L, Martindale RG. The critical care obesity paradox and implications for nutrition support. *Curr Gastroenterol Rep.* (2016) 18:45. doi: 10.1007/s11894-016-0519-8

49. Horwich TB, Fonarow GC, Clark AL. Obesity and the obesity paradox in heart failure. *Prog Cardiovasc Dis.* (2018) 61:151–6. doi: 10.1016/j.pcad.2018.05.005

50. Zandijk AJL, van Norel MR, Julius FEC, Sepehrvand N, Pannu N, McAlister FA, et al. Chloride in heart failure: the neglected electrolyte. *JACC Heart Fail.* (2021) 9:904–15. doi: 10.1016/j.jchf.2021.07.006

51. Rivera FB, Alfonso P, Golbin JM, Lo K, Lerma E, Volgman AS, et al. The role of serum chloride in acute and chronic heart failure: a narrative review. *Cardiorenal Med.* (2021) 11:87–98. doi: 10.1159/000515604

52. Pekkanen J, Linn S, Heiss G, Suchindran CM, Leon A, Rifkind BM, et al. Ten-year mortality from cardiovascular disease in relation to cholesterol level among men with and without preexisting cardiovascular disease. *N Engl J Med.* (1990) 322:1700–7. doi: 10.1056/NEJM199006143222403

53. Orso F, Fabbri G, Maggioni AP. Epidemiology of heart failure. *Handb Exp Pharmacol.* (2017) 243:15–33. doi: 10.1007/164_2016_74

54. Bozkurt B, Aguilar D, Deswal A, Dunbar SB, Francis GS, Horwich T, et al. Contributory risk and management of comorbidities of hypertension, obesity, diabetes mellitus, hyperlipidemia, and metabolic syndrome in chronic heart failure: a scientific statement from the American heart association. *Circulation.* (2016) 134:e535–78. doi: 10.1161/CIR.0000000000000450

55. Park JJ, Choi DJ, Yoon CH, Oh IY, Lee JH, Ahn S, et al. The prognostic value of arterial blood gas analysis in high-risk acute heart failure patients: an analysis of the Korean heart failure (KorHF) registry. *Eur J Heart Fail.* (2015) 17:601–11. doi: 10.1002/ejhf.276

56. Kazory A, Ronco C. Emergence of chloride as an overlooked cardiorenal connector in heart failure. *Blood Purif.* (2020) 49:219–21. doi: 10.1159/000503774

57. Khan NN, Nabeel M, Nan B, Ghali JK. Chloride depletion alkalosis as a predictor of in-hospital mortality in patients with decompensated heart failure. *Cardiology.* (2015) 131:151–9. doi: 10.1159/000377669

58. Elfar A, Sambandam KK. The basic metabolic profile in heart failure-marker and modifier. *Curr Heart Fail Rep.* (2017) 14:311–20. doi: 10.1007/s11897-017-0344-x

59. de Miguel-Díez J, Jiménez-García R, Méndez-Bailón M, Muñoz-Rivas N, Hernández-Barrera V, Puente-Maestu L, et al. National trends in mechanical ventilation among patients hospitalized with heart failure: a population-based study in Spain (2001-2017). *Eur J Intern Med.* (2020) 78:76–81. doi: 10.1016/j.ejim.2020.04.016

60. Melchio R, Rinaldi G, Testa E, Giraudo A, Serraino C, Bracco C, et al. Red cell distribution width predicts mid-term prognosis in patients hospitalized with acute heart failure: the RDW in acute heart failure (RE-AHF) study. *Intern Emerg Med.* (2019) 14:239–47. doi: 10.1007/s11739-018-1958-z

61. Robbins H, Monro S. A stochastic approximation method. *Ann Math Stat.* (1951) 22:400–7. doi: 10.1007/978-1-4612-5110-1_9

62. Baker MR, Patil RB. Universal approximation theorem for interval neural networks. *Reliab Comput.* (1998) 4:235–9. doi: 10.1023/A:1009951412412

63. Silver D, Huang A, Maddison CJ, Guez A, Sifre L, van den Driessche G, et al. Mastering the game of go with deep neural networks and tree search. *Nature.* (2016) 529:484–9. doi: 10.1038/nature16961

64. He K, Zhang X, Ren S, Sun J. Delving deep into rectifiers: surpassing human-level performance on imagenet classification. In: *Proceedings of the 2015 IEEE International Conference on Computer Vision (ICCV)*. Santiago: (2015). p. 1026–34. doi: 10.1109/ICCV.2015.123

65. Awan SE, Bennamoun M, Sohel F, Sanfilippo FM, Dwivedi G. Machine learning-based prediction of heart failure readmission or death: implications of choosing the right model and the right metrics. *ESC Heart Fail.* (2019) 6:428–35. doi: 10.1002/ehf2.12419

66. Awan SE, Bennamoun M, Sohel F, Sanfilippo FM, Chow BJ, Dwivedi G. Feature selection and transformation by machine learning reduce variable numbers and improve prediction for heart failure readmission or death. *PLoS One.* (2019) 14:e0218760. doi: 10.1371/journal.pone.0218760

67. Mancia G, Facchetti R, Seravalle G, Cuspidi C, Grassi G. Adding home and/or ambulatory blood pressure to office blood pressure for cardiovascular risk prediction. *Hypertension.* (2021) 77:640–9. doi: 10.1161/HYPERTENSIONAHA.120.16303

68. Jallepalli S, Pathak P, Gupta P, Kar S, Gupta M. *Development and Validation of Artificial Intelligence – Based Cardiovascular Disease (ai-cvd) Risk Score.* Rochester, NY: Social Science Electronic Publishing (2019). doi: 10.2139/ssrn.3444410

69. Kwon JM, Kim KH, Jeon KH, Lee SE, Lee HY, Cho HJ. Artificial intelligence algorithm for predicting mortality of patients with acute heart failure. *PLoS One.* (2019) 14:e0219302. doi: 10.1371/journal.pone.0219302

70. Nagpal C, Yadlowsky S, Rostamzadeh N, Heller K. Deep cox mixtures for survival regression. *ArXiv.* (2021) [Preprint] ArXiv210106536. doi: 10.48550/arXiv.2101.06536

frontiers | Frontiers in Cardiovascular Medicine

TYPE Original Research
PUBLISHED 25 October 2022
DOI 10.3389/fcvm.2022.1042842

Check for updates

OPEN ACCESS

EDITED BY
Miguel Hueso,
Bellvitge University Hospital, Spain

REVIEWED BY
Amirmohammad Khalaji,
Tehran University of Medical Sciences, Iran
Sally Badawi,
United Arab Emirates University, United Arab Emirates

*CORRESPONDENCE
Zhihua Chen
cybweng@sina.com

†These authors have contributed equally to this work and share first authorship

SPECIALTY SECTION
This article was submitted to Cardiovascular Genetics and Systems Medicine, a section of the journal Frontiers in Cardiovascular Medicine

RECEIVED 13 September 2022
ACCEPTED 07 October 2022
PUBLISHED 25 October 2022

CITATION
Zhou K, Cai C, He Y and Chen Z (2022) Using machine learning to find genes associated with sudden death. *Front. Cardiovasc. Med.* 9:1042842. doi: 10.3389/fcvm.2022.1042842

COPYRIGHT
© 2022 Zhou, Cai, He and Chen. This is an open-access article distributed under the terms of the Creative Commons Attribution License (CC BY). The use, distribution or reproduction in other forums is permitted, provided the original author(s) and the copyright owner(s) are credited and that the original publication in this journal is cited, in accordance with accepted academic practice. No use, distribution or reproduction is permitted which does not comply with these terms.

Using machine learning to find genes associated with sudden death

Kena Zhou[1†], Congbo Cai[2†], Yi He[1] and Zhihua Chen[3*]

[1]Department of Gastroenterology, Ningbo No. 9 Hospital, Ningbo, China, [2]Department of Emergency, Yinzhou No. 2 Hospital, Ningbo, China, [3]Department of Emergency, Ningbo First Hospital, Ningbo, China

Objective: To search for significant biomarkers associated with sudden death (SD).

Methods: Differential genes were screened by comparing the whole blood samples from 15 cases of accidental death (AD) and 88 cases of SD. The protein-protein interaction (PPI) network selects core genes that interact most frequently. Machine learning is applied to find characteristic genes related to SD. The CIBERSORT method was used to explore the immune-microenvironment changes.

Results: A total of 10 core genes (MYL1, TNNC2, TNNT3, TCAP, TNNC1, TPM2, MYL2, TNNI1, ACTA1, CKM) were obtained and they were mainly related to myocarditis, hypertrophic myocarditis and dilated cardiomyopathy (DCM). Characteristic genes of MYL2 and TNNT3 associated with SD were established by machine learning. There was no significant change in the immune-microenvironment before and after SD.

Conclusion: Detecting characteristic genes is helpful to identify patients at high risk of SD and speculate the cause of death.

KEYWORDS

sudden death, machine learning, molecular autopsy, characteristic genes, biomarkers

Introduction

Sudden death (SD) is the sudden, non-violent death of a healthy or seemingly healthy person caused by an outbreak of disease or an underlying disease in the body. Those who died within 24 h after the onset of symptoms is called SD. It is common in young or middle-aged adults, which imposes a significant burden on families and society.

The diagnosis of the cause of SD is usually based on autopsy (1). Even with the development of forensic science, there is still a considerable reasons of SD that cannot be inferred (2). With the deepening of research, it is found that genetic factors play a crucial role in SD (3). It is estimated that up 35% of sudden unexplained death cases are associated with genetic variants in cardiac channels (4).

With the development of gene sequencing technology, molecular autopsy is gradually used for forensic identification. This method is especially suitable for SD of unknown causes (5, 6). However, molecular autopsy is still in its infancy, with only preliminary testing in patients with a genetic family history (7). There is still a lack of research on specific genes related to SD.

The Genotype-Tissue Expression (GTEx) database holds data of normal tissue DNA and RNA sequencing (RNA-seq) from donors (8). Now 54 tissues from 948 donors have been preserved, including 17,382 samples. Donor death time in the database were divided into instantaneous death (0 h), short-term death (0–1 h), moderate death (1–24 h) and slow death (> 24 h). This provides a good source of data source for the study of the causes of SD. It can assist forensic medicine to find characteristic genes related to SD.

Machine learning is a collection of data-analytical techniques aimed at building predictive models from multi-dimensional datasets (9). Machine learning outperforms traditional statistical algorithms when faced with complicated problems involving a large number of noisy and heterogeneous predictor (10). It is becoming an integral part of modern data mining and clinical diagnosis (11).

In this study, we searched for the characteristic genes of SD by machine learning based on the GTEx database. These biomarkers can be used to screen patients at high risk of SD. And also characteristic genes provide potential advice for taking early measures in high-risk patients. In addition, theoretical support for molecular autopsy can also be verified.

Materials and methods

Datasets

Donor RNA-seq was downloaded from the GTEx (RRID:SCR_013042) and all sequencing results were normalized by FPKM. The relevant clinical information of the donors can be downloaded from the GTEx official website.[1] The GTEx emphasizes that the database is free and open to the society, but the official website information needs to be marked in the paper. Database use does not require institutional review board approval and informed consent.

Differential gene screening and protein-protein interaction network analysis

The Wilcox test in the "limma" package was used to screen significantly differentially expressed genes between AD and SD in GTEx cohort. We took | LogFC| > 1, false discovery rate (FDR) < 0.05 as the threshold point for differential genes. Simultaneously, volcano plots and heatmaps of differential genes were figured out. There is a close relationship between the biological functions of gene/protein clusters (12). Therefore, proteins usually cooperate to perform biological functions. The protein-protein interaction (PPI) network helps to differentiate the core genes in SD according to the frequency of interaction. PPI analysis was performed on the STRING database[2] with a confidence index of 0.7. The more the interaction relationship, the more important role the gene plays in the process of SD. The connectivity table was drawn in R language, and connectivity ≥ 5 is defined as core genes.

Biological role and disease analysis

Function, pathway enrichment and disease analysis of core genes based on "clusterProfiler," "enrichplot," "org.Hs.eg.db," "ggplot2," "GSEABase" and "DOSE" packages were performed in R language. The biological significance of core genes was analyzed by Gene Ontology (GO) functional enrichment, including Biological Process (BP), Cellular Components (CC), and Molecular Function (MF). Kyoto Encyclopedia of Genes and Genomes (KEGG) enrichment analysis was used to explore the pathways of core genes. Disease Ontology (DO) enrichment analysis was applied to discover major diseases led by core genes. $P < 0.05$ and corrected $P < 0.05$ were considered to be statistically significant in all the analysis process. The visualization of GO, KEGG, and DO could be achieved by the R package "GOplot."

1 www.gtexportal.org/

2 https://www.string-db.org/

TABLE 1 Summary of clinical information for donors.

Characteristic	Accidental death ($N = 15$)	Sudden death ($N = 86$)
Age		
<30	5	3
≥30	10	83
Gender		
Male	11	66
Female	4	20
Death circumstances		
D1	15	0
D2	0	69
D3	0	17
D4	0	0

Death circumstances: D1, Violent and fast death; D2, Fast death of natural causes; D3, Intermediate death; D4, Slow death.

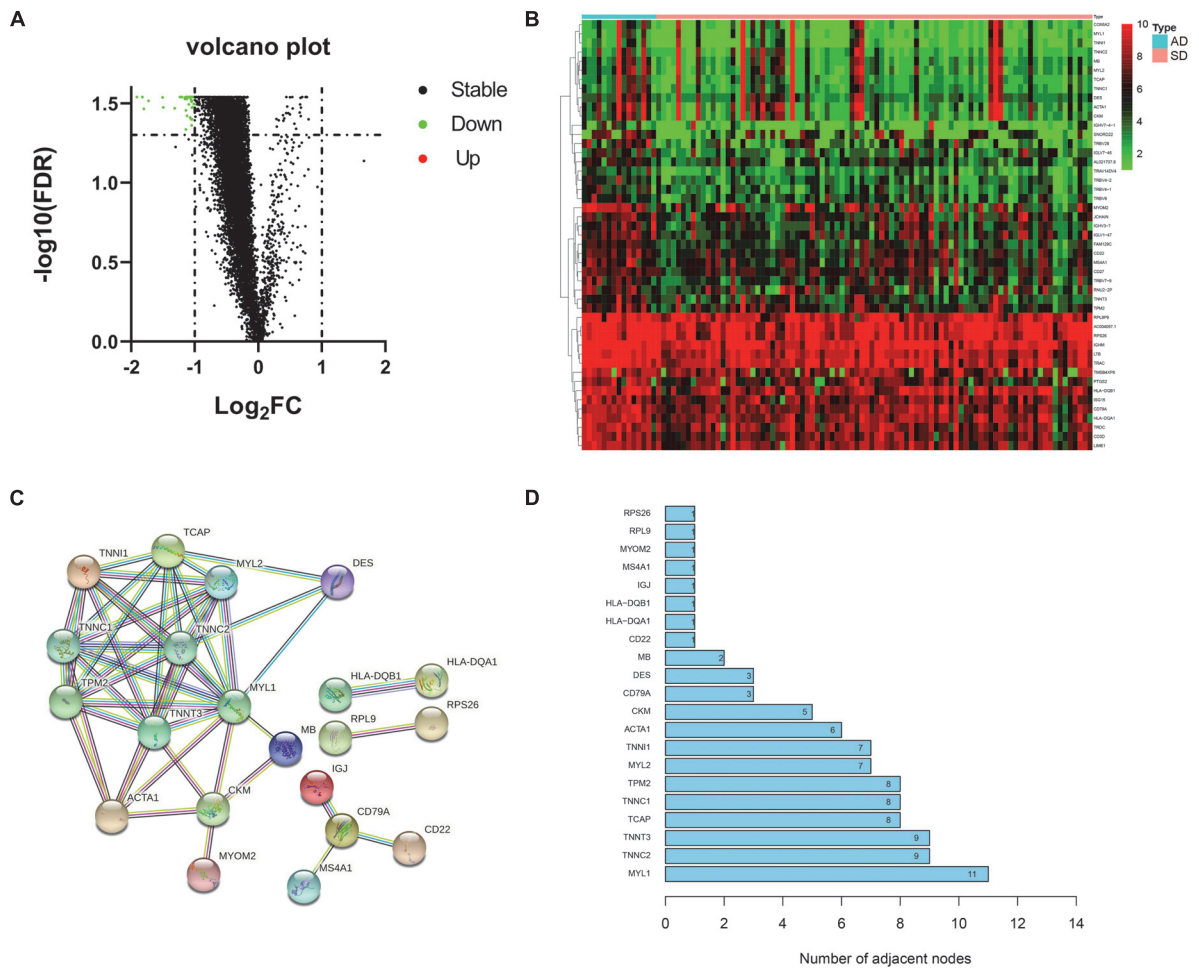


FIGURE 1
Differential expression and core gene screening. **(A)** Volcano plot of all genes. (Red dots represent up-regulated genes and green dots represent down-regulated genes). **(B)** Heatmap of differential genes in AD and SD groups. (Rows represent 47 differential genes and columns represent samples). **(C)** PPI network of differential genes. (Nodes represent hub genes. Lines represent interactions between hub genes). **(D)** Bar graph of all hub genes in the PPI network. (The x-axis represents channel counts. The y-axis represents hub genes). AD, Accidental death; SD, Sudden death.

Machine learning

In order to reduce errors, we used two different machine learning algorithms to seek for potential characteristic genes. The Least Absolute Shrinkage and Selection operator (LASSO) is a machine learning based regression analysis algorithm that uses regularization to remove highly correlated genes, which can avoid overfitting.

Support vector machine recursive feature elimination (SVM-RFE) is a machine learning algorithm based on classification and regression. Gene redundancy can be automatically eliminated and a better, more compact subset of genes can be generated. We use the R packages of "glmnet" and "e1071" to implement machine learning algorithms for LASSO and SVM-RFE. Finally, characteristic genes are obtained by intersection.

Analysis of clinical value of characteristic genes

To test the diagnostic value of the characteristic genes, we compared the expression of characteristic genes in AD and SD groups in R language software. Moreover, receiver operating characteristic (ROC) curves were drawn to analyze the validity of the characteristic genes.

Analysis of the expression of characteristic genes in human tissues

Human anatomy were drawn in R software based on "gganatogram," "dplyr," "viridis," and "gridExtra." The R package of "gganatogram" can draw modular anatomical maps and

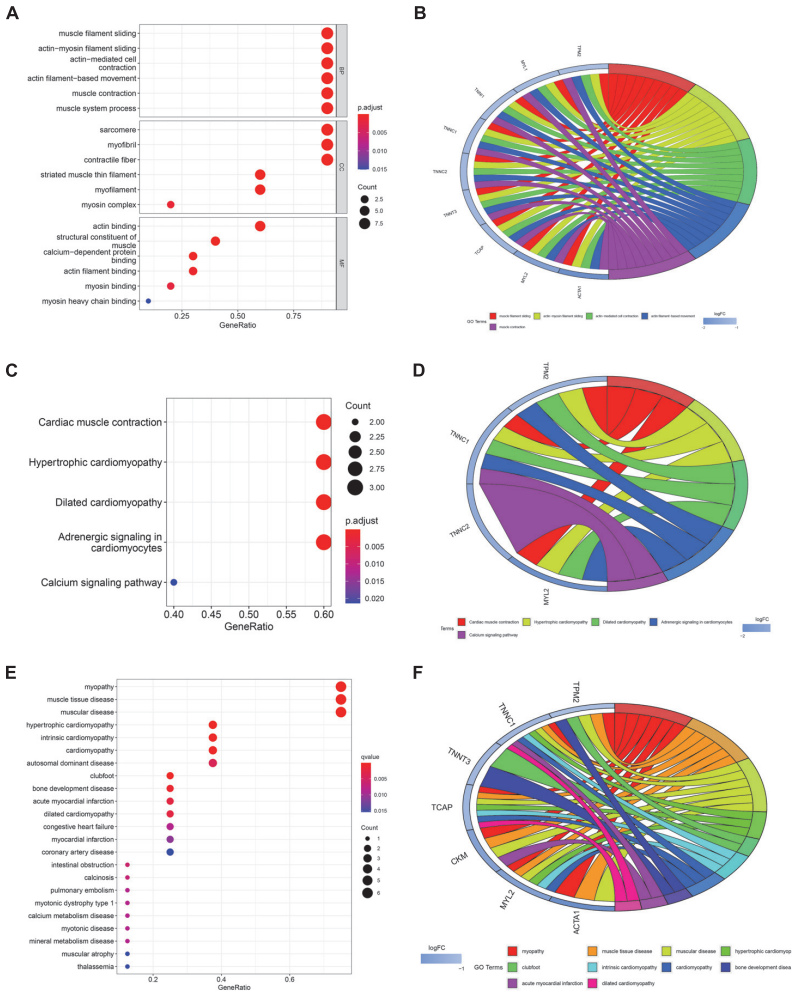


FIGURE 2
Function, pathway, and disease enrichment analysis of core genes. **(A)** Bubble plot of GO function enrichment for core genes. (BP, Biological Process; CC, Cellular Components; MF, Molecular Function). **(B)** Circle plot of GO functional enrichment. **(C)** Bubble map of KEGG pathway enrichment for core genes. **(D)** Circle plot of KEGG enrichment analysis. **(E)** Bubble plot of DO enrichment for core genes. **(F)** Circle plot of DO enrichment analysis. The size of bubbles in the bubble plot represents the number of core genes in the corresponding pathway. The color of the bubbles represents the adjusted *p*-value. The circle plot illustrates certain core genes corresponding to the GO/KEGG terminology or disease. LogFC represents the expression level of gene.

quantify the expression of characteristic genes in various tissues in human body. The Human Protein Atlas (HPA) database[3] was used to validate the protein expression level of the target SD genes.

Analysis of immune-microenvironment

We used the CIBERSORT (RRID:SCR_016955) algorithm to assess the relative proportions of immune cell infiltration in different populations. And the abundance of 22 immune cells can be quantified *via* this method. The R package of "corrplot" visualizes 22 types of immune cells. And the R package of "vioplot" draws violin plots to show differences in immune cell infiltration between different groups.

Results

Clinical information

The clinical information of the patients was obtained on the GTEx official website (see text footnote 1). The AD group consisted of 15 whole blood samples from 15 donors who died unexpectedly (violent and fast death). The SD group included 88 blood samples, including 69 donors with fast death of natural

3 https://www.proteinatlas.org/

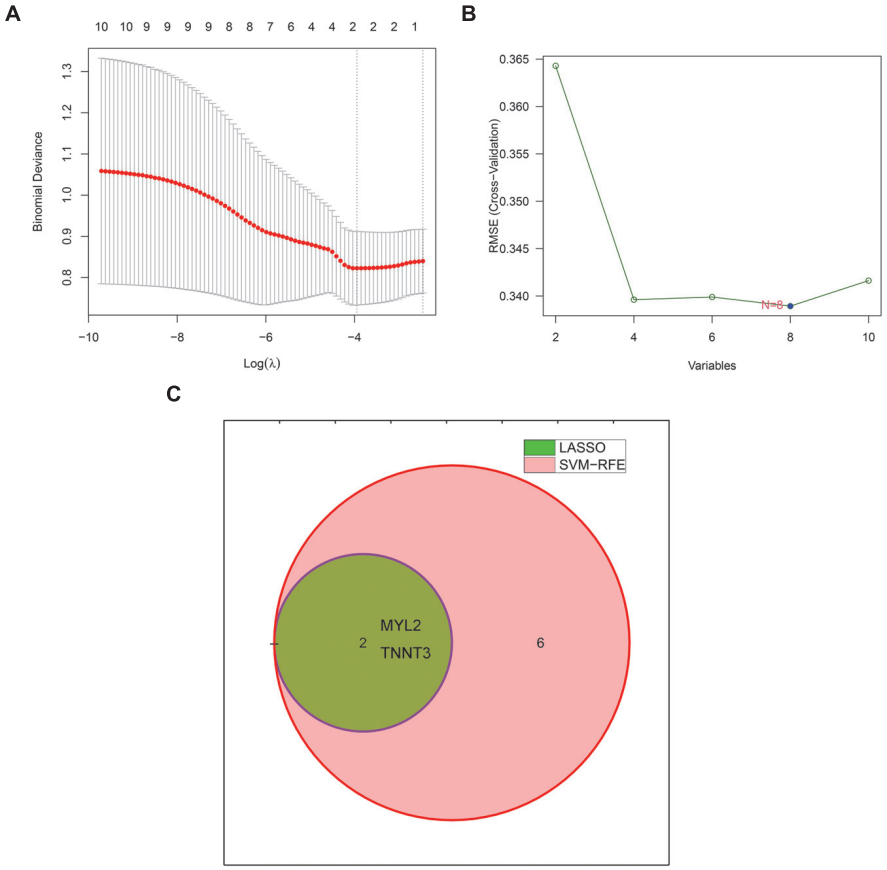


FIGURE 3
Machine learning identifies characteristic genes of sudden death. **(A)** The LASSO regression algorithm was used to select the characteristic genes of sudden death. **(B)** SVM-RFE algorithm to select the characteristic genes of sudden death. (The blue point represents the lowest error rate, correspondingly to the best genome selected by SVM-RFE). **(C)** Venn diagram showing 2 sudden death characteristic genes shared by LASSO (green) and SVM-RFE (pink) algorithms. LASSO, least absolute shrinkage and selector operation. SVM-RFE, support vector machine-recursive feature elimination.

causes (0–1 h) and 17 donors with intermediate death (1–24 h). More details could be referred in **Table 1**.

Analysis of protein-protein interaction network for differential genes

This study retrospectively analyzed whole blood samples from donors of AD and SD. According to the cutoff value, a total of 47 differential genes were obtained and considered to be related to SD (**Supplementary Table 1**). All of these genes were down-regulated in the SD group (**Figure 1A**). The heat map shows the expression levels of all differential genes in different groups (**Figure 1B**). To better understand the interactions between these SD-related genes, we used the STRING online database[4] to construct a PPI network for 47 differential genes (**Figure 1C**). Ten genes with high interaction were identified as core genes (MYL1, TNNC2, TNNT3, TCAP, TNNC1, TPM2, MYL2, TNNI1, ACTA1, CKM). It was suggested that they play an important role in SD process (**Figure 1D**).

Functional correlation analysis of core genes

In order to explore the role of these genes in the process of SD and related diseases. We focused on the function, pathway and disease analysis of 10 core genes related to SD. GO analysis results shows that the annotations of genes come from three ontologies, namely biological process (BP), molecular function (MF), and cellular component (CC). BP terminology mainly contains muscle filament sliding, muscle contraction. MF terminology mainly contains sarcomere, myofibril, contractile fiber. CC terminology mainly contains actin binding, myosin binding (**Figure 2A**). The circle diagram shows that core genes

4 http//:string-db.org

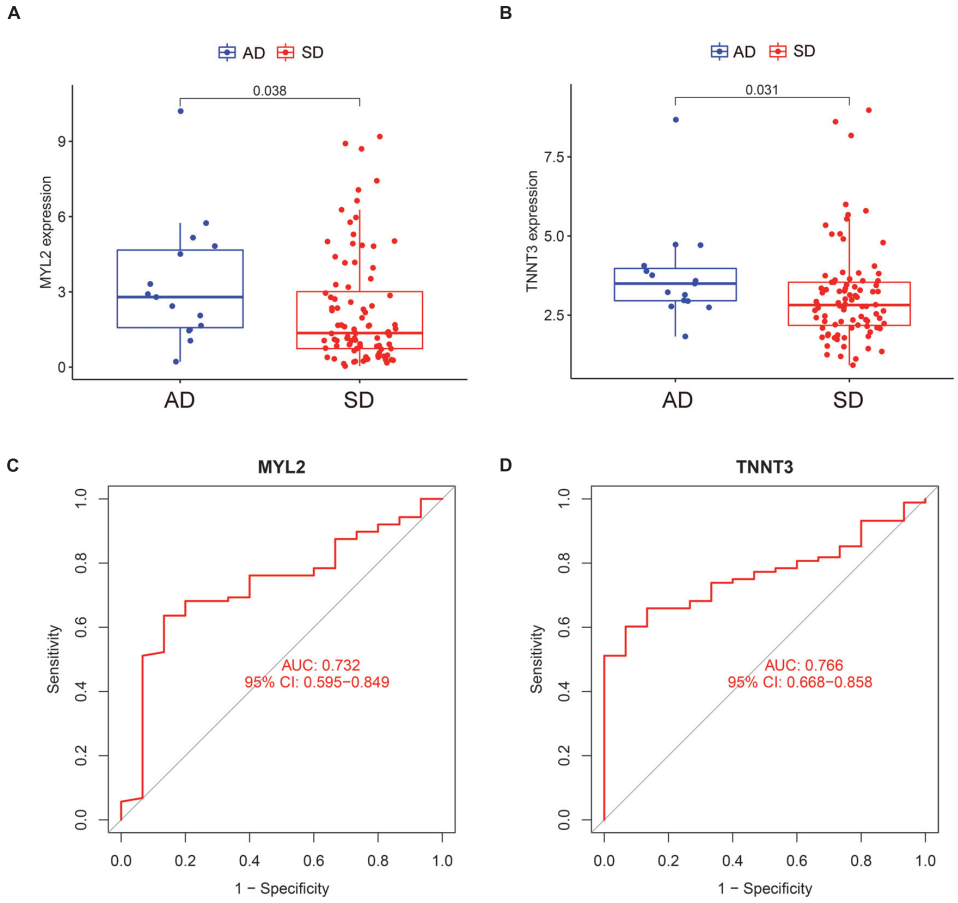


FIGURE 4
Expression and ROC curves of characteristic genes of sudden death. **(A)** The expression level of MYL2 in AD and SD groups. **(B)** The expression level of TNNT3 in AD and SD groups. **(C)** The ROC curve of MYL2. **(D)** The ROC curve of TNNT3. ROC, receiver operating characteristic; AD, Accidental death; SD, Sudden death.

are mainly enriched in muscle contraction, actin filament-based movement, muscle filament sliding, etc. (Figure 2B). The pathways of core genes were mainly enriched in Cardiac muscle contraction, Hypertrophic cardiomyopathy (HCM), Dilated cardiomyopathy (DCM), Adrenergic signaling in cardiomyocytes, and Calcium signaling pathway (Figure 2C). The circle diagram shows certain core genes corresponding to KEGG pathways (Figure 2D). DO analysis shows that the core genes of SD were mainly enriched in myopathy, HCM, cardiomyopathy, autosomal dominant disease, clubfoot, acute myocardial infarction, DCM, pulmonary embolism, and other diseases (Figure 2E). The circle diagram shows top 10 diseases corresponding to SD-associated core genes (Figure 2F).

Machine learning characteristic genes

We used two machine learning methods, LASSO regression and SVM-RFE, to study the core genes of SD. LASSO regression learned from the 10 core genes to obtain 2 characteristic genes of SD (Figure 3A). The SVM-RFE algorithm learned from 10 core genes to obtain 8 characteristic genes of SD (Figure 3B). The two algorithms were intersected by a Venn diagram, and 2 common genes were obtained as the characteristic genes closely related to SD (Figure 3C).

Analysis of clinical value of characteristic genes

We compared the expression of the two characteristic genes in the AD and SD groups. And the ROC curve was exhibited to confirm the clinical value of the characteristic genes. The expression of SD-related characteristic genes (MYL2 and TNNT3) were both decreased in the SD group (Figures 4A,B; all $P < 0.05$). The AUC value of ROC curves for MYL2 was 0.732 (95%CI = 0.595–0.849) (Figure 4C). The AUC value for TNNT3 was 0.766 (95%CI = 0.668–0.858) (Figure 4D). These shows that

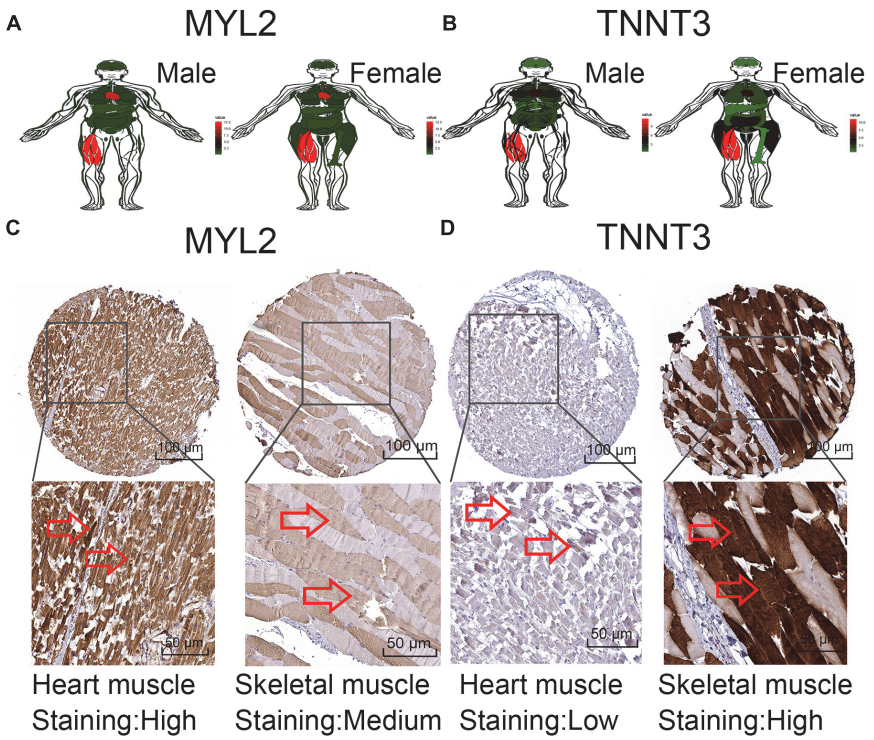


FIGURE 5
Expression of sudden death characteristic genes in human tissues. **(A,B)** MYL2 and TNNT3 expression levels in tissues in males and females. **(C)** Validation of MYL2 in turquoise module by HPA (IHC). **(D)** Validation ofTNNT3 in turquoise module by HPA (IHC). Red represents high expression, green represents low expression, and black represents mediate expression.

the SD-associated characteristic genes have good performance with high diagnostic ability.

Expression analysis of characteristic genes in human body

In order to verify the expression of characteristic genes in the human body, we extracted the expression levels of MYL2 and TNNT3 in various tissues from GTEx database. And an anatomical map was generated (**Figures 5A,B**). Moreover, the protein levels of immunohistochemistry (IHC) staining obtained from the HPA database illustrated that MYL2 was highly expressed in cardiac muscle and moderately expressed in skeletal muscle (**Figure 5C**); while TNNT3 is lowly expressed in cardiac muscle and highly expressed in skeletal muscle (**Figure 5D**).

Immune infiltration analysis

We explored immune cell profiles in patients in AD and SD groups using the CIBERSORT method. The infiltration of 22 immune cells were estimated in SD and AD groups in **Figure 6A**. The ratios of 22 immune cells were further compared in SD and AD groups (**Figure 6B**). The results showed that all immune cell differences were not statistically significant ($P > 0.05$). This suggested that although SD was caused by various diseases, no significant participation of immune cells was witnessed in this short-term process.

Discussion

SD is the most serious clinical adverse phenomenon. Accurate cause of death is difficult to conclude even with the aid of forensic science. Based on the large-scale database of the GTEx platform, we explore the related genes and diseases that cause SD. We screened out 10 core genes (MYL1, TNNC2, TNNT3, TCAP, TNNC1, TPM2, MYL2, TNNI1, ACTA1, CKM) from the database. Two characteristic genes (MYL2, TNNT3) were extruded *via* two machine learning algorithms, with good diagnostic ability. Our study demonstrated that most sudden deaths are acute onsets of chronic diseases without the involvement of the immune microenvironment.

We are the first to put forward 10 core genes related to SD *via* the GTEx database. The biological processes of these core genes mainly focus on myofilament and sarcomere

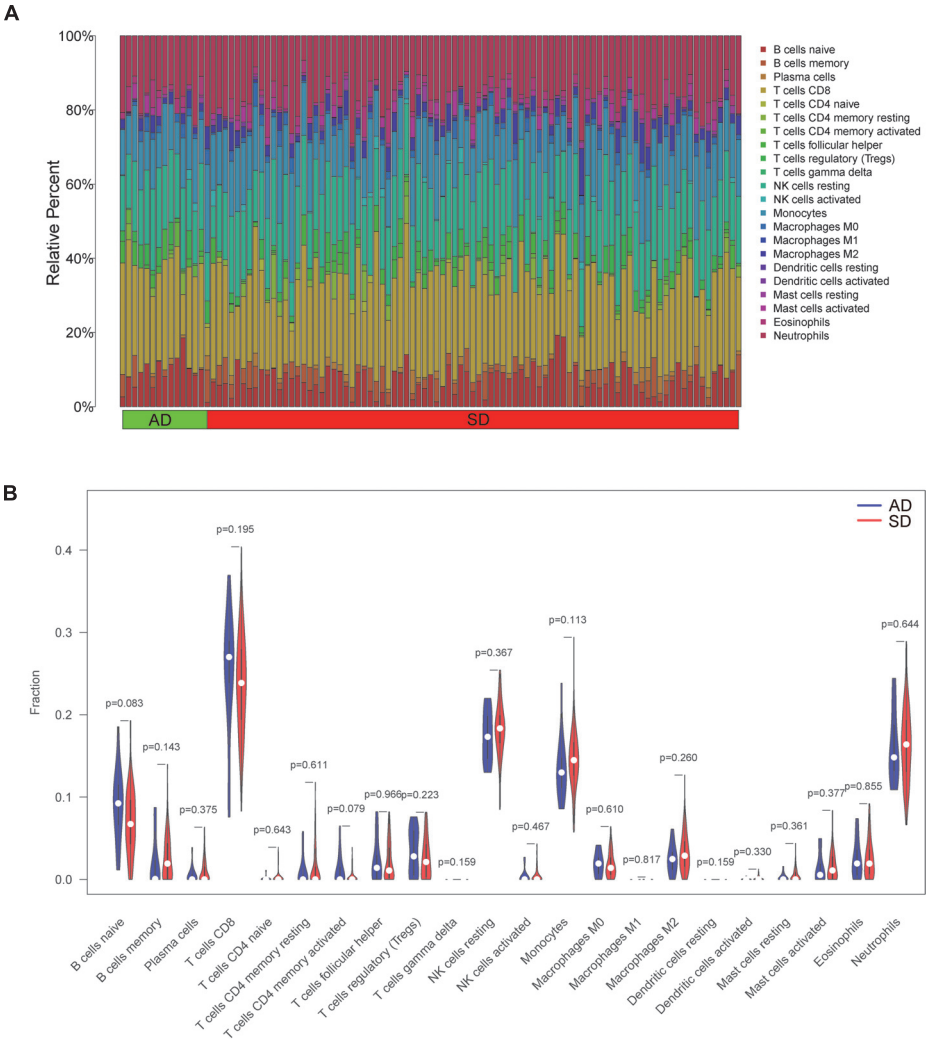


FIGURE 6
Profile and visualization of immune cell infiltration. **(A)** The infiltration of 22 immune cells after quantification by the CIBERSORT algorithm. (The X-axis represents the sample and the Y-axis shows the percentage of 22 immune cells in the sample as stacked bars). **(B)** Violin plot showing comparison based on 22 immune cells. (Blue and red represent AD and SD group samples, respectively). AD, Accidental death; SD, Sudden death.

activities mediated by actin and myosin. Consistent with our study, Klaassen et al. pointed out that sarcomeric protein gene defects can cause various heart diseases (13). Furthermore, the possible causes of SD proposed from the core genes are as follows: myopathy, HCM, cardiomyopathy, autosomal dominant disease, clubfoot, acute myocardial infarction, DCM, pulmonary embolism, etc. These above diseases are clinically common and can lead to death in a short time. The major forms of cardiomyopathy include hypertrophic, dilated, restrictive and arrhythmogenic cardiomyopathy (14). Among them, HCM is usually witnessed with obvious heredity (15). At present, more and more scholars have pointed out the importance of gene detection in HCM risk stratification (16). Our study identified TNNC1, TCAP and MYL2 as the risk genes for SD in HCM. The mutation rate of TNNC1 in HCM patients is approximately 0.4% (17). Multiple studies have shown that mutations in TNNC1 cause HCM and early sudden cardiac death (18, 19). TCAP is a key regulator of muscle growth, and reduced TCAP expression will destroy muscle growth (20). MYL2 is also a risk gene for HCM, and Arg58Gln and R58Q mutations in MYL2 can lead to early sudden cardiac death (21, 22). This is consistent with our research. DCM is a type of cardiomyopathy characterized by left ventricular enlargement and systolic dysfunction. Our study showed that the main SD-related genes in DCM were TCAP and TNNC1. TCAP mutation was detected in DCM patients (23, 24). But whether the mutation of this gene can cause SD in DCM patients has not been reported in the literature. TNNC1 is also a risk gene for

DCM (25). Numerous articles have reported premature sudden cardiac death or heart transplantation would occur in DCM patients with TNNC1-mutated (26, 27). Abnormal expression of core genes in various diseases will lead to the increase of SD rate. Focusing on core genes in hereditary diseases is helpful for the early identification and prevention of deadly outcomes.

Machine learning can discover excellent prognostic genes in the form of self-learning. MYL2 and TNNT3 were extraordinary extruded after machine learning. MYL2 is mainly expressed in the ventricle, and its mutation will cause HCM (28, 29). Statistics found that the probability of MYL2 mutation in HCM patients was 2.1–5% (28, 30–32). Manivannan et al. suggested that mutation in MYL2 in HCM families had resulted in SD of four children before the age of one (29). When MYL2 mutation existed in HCM patients, the clinical lesions appear early, the disease is severe, the prognosis is very poor, and many suffer early SD (21, 33). This is supportive to our study. Thus we advocate that genetic disease guidance can focus on SD associated genes.

Mutations in TNNT3 will cause various muscle disorders, mainly covering distal arthrogryposis (DA) (34). Also there are nemaline myopathy (NEM) (35) and atrial septal defect (36) associated with TNNT3 mutation. DA is a clinically and genetically heterogeneous disease, mainly characterized by congenital spasticity of the joints of the extremities. In 2018, Sandaradura et al. described that TNNT3 mutations had led to non-invasive ventilation in the neonatal period with a result of death at 8 months of age (37). Our study showed that TNNT3 was highly expressed in the heart, as well as in muscle tissues. Therefore, we consider that TNNT3 mutation would cause changes in the myocardium resulting SD. Although these two characteristic genes have less variation in other diseases, the probability of SD is greatly increased with their mutation. Early or aggressive clinical interventions such as heart transplantation or ICD are strongly suggested with characteristic genetic variants.

The AUC values of MYL2 and TNNT3 were 0.732 and 0.766, respectively. We consider that the final result of SD is caused by a large category of SD-related diseases. A single gene can only represent one or several diseases, not all diseases, so the AUC value is not very high. Our study also showed that no changes in the immune-microenvironment before and after death in SD patients. We supposed that SD is the result of a short-term deterioration of the disease without the involvement of immune cells.

This study has some limitations. First, most SD donors died in less than an hour. The main cause of death in these patients is sudden cardiac death, so the characteristic genes are relatively close to the genes related to cardiac death. Second, in order to protect the privacy of donors, GTEx platform only provides the age and gender of the donors, and no other specific clinical data was displayed. Therefore, valid information such as previous diseases, family history and autopsy cannot be obtained in details. Third, there might be bias in our study due to limited sample size, even if we used the PPI network to capture the most active genes as many as possible. Hopefully, we are looking forward to larger cohorts in future validation researches that may require multi-institutional collaboration.

Conclusion

SD is caused by a variety of diseases, most of which are heart disease. Studies have shown that genetics play an important role in SD. Our study found that the cause of SD might be HCM, dilated cardiomyopathy, acute myocardial infarction, pulmonary embolism and so on. MYL2 and TNNT3 were discovered as characteristic genes by machine learning, which could predict the prognosis of SD. For high risk patients with familial SD history, the expression of SD genes can be investigated. For high risk patients, early intervention can be carried out, such as early cardiac surgery or pacemaker placement.

Data availability statement

The datasets presented in this study can be found in online repositories. The names of the repository/repositories and accession number(s) can be found below: www.gtexportal.org.

Ethics statement

Ethical review and approval was not required for the study on human participants in accordance with the local legislation and institutional requirements. Written informed consent for participation was not required for this study in accordance with the national legislation and the institutional requirements.

Author contributions

KZ and ZC contributed to the study conception and design. CC and YH performed the material preparation, data collection, and analysis. KZ and CC wrote the first draft of the manuscript. ZC supervised the whole study. All authors read and approved the final manuscript.

Acknowledgments

We thank the online databases for providing original data in our study.

Conflict of interest

The authors declare that the research was conducted in the absence of any commercial or financial relationships that could be construed as a potential conflict of interest.

Publisher's note

All claims expressed in this article are solely those of the authors and do not necessarily represent those of their affiliated organizations, or those of the publisher, the editors and the reviewers. Any product that may be evaluated in this article, or claim that may be made by its manufacturer, is not guaranteed or endorsed by the publisher.

Supplementary material

The Supplementary Material for this article can be found online at: https://www.frontiersin.org/articles/10.3389/fcvm.2022.1042842/full#supplementary-material

SUPPLEMENTARY FIGURE 1
Graphical abstract.

SUPPLEMENTARY TABLE 1
47 differentiated genes associated with SD.

References

1. Kumar A, Avishay DM, Jones CR, Shaikh JD, Kaur R, Aljadah M, et al. Sudden cardiac death: epidemiology, pathogenesis and management. *Rev Cardiovasc Med.* (2021) 22:147–58. doi: 10.31083/j.rcm.2021.01.207

2. Bayés de Luna A, Elosua R. Sudden death. *Rev Esp Cardiol.* (2012) 65:1039–52. doi: 10.1016/j.rec.2012.03.025

3. Raju H, Behr ER. Unexplained sudden death, focussing on genetics and family phenotyping. *Curr Opin Cardiol.* (2013) 28:19–25. doi: 10.1097/HCO.0b013e32835b0a9e

4. Tester DJ, Medeiros-Domingo A, Will ML, Haglund CM, Ackerman MJ. Cardiac channel molecular autopsy: insights from 173 consecutive cases of autopsy-negative sudden unexplained death referred for postmortem genetic testing. *Mayo Clin Proc.* (2012) 87:524–39. doi: 10.1016/j.mayocp.2012.02.017

5. Miles CJ, Behr ER. The role of genetic testing in unexplained sudden death. *Trans Res.* (2016) 168:59–73. doi: 10.1016/j.trsl.2015.06.007

6. Wijeyeratne YD, Behr ER. Sudden death and cardiac arrest without phenotype: the utility of genetic testing. *Trends Cardiovasc Med.* (2017) 27:207–13. doi: 10.1016/j.tcm.2016.08.010

7. Semsarian C, Hamilton RM. Key role of the molecular autopsy in sudden unexpected death. *Heart Rhythm.* (2012) 9:145–50. doi: 10.1016/j.hrthm.2011.07.034

8. Burgess DJ. Reaching completion for GTEx. *Nat Rev Genet.* (2020) 21:717. doi: 10.1038/s41576-020-00296-7

9. Camacho DM, Collins KM, Powers RK, Costello JC, Collins JJ. Next-generation machine learning for biological networks. *Cell.* (2018) 173:1581–92. doi: 10.1016/j.cell.2018.05.015

10. Van Calster B, Wynants L. Machine learning in medicine. *N Engl J Med.* (2019) 380:2588. doi: 10.1056/NEJMc1906060

11. Saberi-Karimian M, Khorasanchi Z, Ghazizadeh H, Tayefi M, Saffar S, Ferns GA, et al. Potential value and impact of data mining and machine learning in clinical diagnostics. *Crit Rev Clin Lab Sci.* (2021) 58:275–96. doi: 10.1080/10408363.2020.1857681

12. Choi JK, Yu U, Yoo OJ, Kim S. Differential coexpression analysis using microarray data and its application to human cancer. *Bioinformatics.* (2005) 21:4348–55. doi: 10.1093/bioinformatics/bti722

13. Klaassen S, Probst S, Oechslin E, Gerull B, Krings G, Schuler P, et al. Mutations in sarcomere protein genes in left ventricular noncompaction. *Circulation.* (2008) 117:2893–901. doi: 10.1161/CIRCULATIONAHA.107.746164

14. Maron BJ, Towbin JA, Thiene G, Antzelevitch C, Corrado D, Arnett D, et al. Contemporary definitions and classification of the cardiomyopathies: an American heart association scientific statement from the council on clinical cardiology, heart failure and transplantation committee; quality of care and outcomes research and functional genomics and translational biology interdisciplinary working groups; and council on epidemiology and prevention. *Circulation.* (2006) 113:1807–16. doi: 10.1161/CIRCULATIONAHA.106.174287

15. Elliott PM, Anastasakis A, Borger MA, Borggrefe M, Cecchi F, Charron P, et al. 2014 ESC guidelines on diagnosis and management of hypertrophic cardiomyopathy: the task force for the diagnosis and management of hypertrophic cardiomyopathy of the European society of cardiology (ESC). *Eur Heart J.* (2014) 35:2733–79. doi: 10.1093/eurheartj/ehu284

16. Elliott P. Sudden cardiac death in hypertrophic cardiomyopathy: time to change the narrative. *Eur Heart J.* (2021) 42:3945–7. doi: 10.1093/eurheartj/ehab608

17. Landstrom AP, Parvatiyar MS, Pinto JR, Marquardt ML, Bos JM, Tester DJ, et al. Molecular and functional characterization of novel hypertrophic cardiomyopathy susceptibility mutations in TNNC1-encoded troponin C. *J Mol Cell Cardiol.* (2008) 45:281–8. doi: 10.1016/j.yjmcc.2008.05.003

18. Ploski R, Rydzanicz M, Ksiazczyk TM, Franaszczyk M, Pollak A, Kosinska J, et al. Evidence for troponin C (TNNC1) as a gene for autosomal recessive restrictive cardiomyopathy with fatal outcome in infancy. *Am J Med Genet.* (2016) 170:3241–8. doi: 10.1002/ajmg.a.37860

19. Chung WK, Kitner C, Maron BJ. Novel frameshift mutation in troponin C (TNNC1) associated with hypertrophic cardiomyopathy and sudden death. *Cardiol Young.* (2011) 21:345–8. doi: 10.1017/S1047951110001927

20. Markert CD, Ning J, Staley JT, Heinzke L, Childers CK, Ferreira JA, et al. TCAP knockdown by RNA interference inhibits myoblast differentiation in cultured skeletal muscle cells. *Neuromuscul Disord.* (2008) 18:413–22. doi: 10.1016/j.nmd.2008.03.010

21. Kabaeva ZT, Perrot A, Wolter B, Dietz R, Cardim N, Correia JM, et al. Systematic analysis of the regulatory and essential myosin light chain genes: genetic variants and mutations in hypertrophic cardiomyopathy. *Eur J Hum Genet.* (2002) 10:741–8. doi: 10.1038/sj.ejhg.5200872

22. Zhou W, Bos JM, Ye D, Tester DJ, Hrstka S, Maleszewski JJ, et al. Induced pluripotent stem cell-derived cardiomyocytes from a patient with MYL2-R58Q-mediated apical hypertrophic cardiomyopathy show hypertrophy, myofibrillar disarray, and calcium perturbations. *J Cardiovasc Transl Res.* (2019) 12:394–403. doi: 10.1007/s12265-019-09873-6

23. Hayashi T, Arimura T, Itoh-Satoh M, Ueda K, Hohda S, Inagaki N, et al. Tcap gene mutations in hypertrophic cardiomyopathy and dilated cardiomyopathy. *J Am Coll Cardiol.* (2004) 44:2192–201. doi: 10.1016/j.jacc.2004.08.058

24. Hershberger RE, Parks SB, Kushner JD, Li D, Ludwigsen S, Jakobs P, et al. Coding sequence mutations identified in MYH7, TNNT2, SCN5A, CSRP3, LBD3, and TCAP from 313 patients with familial or idiopathic dilated cardiomyopathy. *Clin Transl Sci.* (2008) 1:21–6. doi: 10.1111/j.1752-8062.2008.00017.x

25. Mazzarotto F, Tayal U, Buchan RJ, Midwinter W, Wilk A, Whiffin N, et al. Reevaluating the genetic contribution of monogenic dilated cardiomyopathy. *Circulation.* (2020) 141:387–98. doi: 10.1161/CIRCULATIONAHA.119.037661

26. van Spaendonck-Zwarts KY, van Tintelen JP, van Veldhuisen DJ, van der Werf R, Jongbloed JD, Paulus WJ, et al. Peripartum cardiomyopathy as a part of familial dilated cardiomyopathy. *Circulation.* (2010) 121:2169–75. doi: 10.1161/CIRCULATIONAHA.109.929646

27. Mogensen J, Murphy RT, Shaw T, Bahl A, Redwood C, Watkins H, et al. Severe disease expression of cardiac troponin C and T mutations in patients with

idiopathic dilated cardiomyopathy. *J Am Coll Cardiol.* (2004) 44:2033–40. doi: 10.1016/j.jacc.2004.08.027

28. Claes GR, van Tienen FH, Lindsey P, Krapels IP, Helderman-van den Enden AT, Hoos MB, et al. Hypertrophic remodelling in cardiac regulatory myosin light chain (MYL2) founder mutation carriers. *Eur Heart J.* (2016) 37:1815–22. doi: 10.1093/eurheartj/ehv522

29. Manivannan SN, Darouich S, Masmoudi A, Gordon D, Zender G, Han Z, et al. Novel frameshift variant in MYL2 reveals molecular differences between dominant and recessive forms of hypertrophic cardiomyopathy. *PLoS Genet.* (2020) 16:e1008639. doi: 10.1371/journal.pgen.1008639

30. Lorenzini M, Norrish G, Field E, Ochoa JP, Cicerchia M, Akhtar MM, et al. Penetrance of hypertrophic cardiomyopathy in sarcomere protein mutation carriers. *J Am Coll Cardiol.* (2020) 76:550–9. doi: 10.1016/j.jacc.2020.06.011

31. Rubattu S, Bozzao C, Pennacchini E, Pagannone E, Musumeci BM, Piane M, et al. A next-generation sequencing approach to identify gene mutations in early- and late-onset hypertrophic cardiomyopathy patients of an italian cohort. *Int J Mol Sci.* (2016) 17:8. doi: 10.3390/ijms17081239

32. Richard P, Charron P, Carrier L, Ledeuil C, Cheav T, Pichereau C, et al. Hypertrophic cardiomyopathy: distribution of disease genes, spectrum of mutations, and implications for a molecular diagnosis strategy. *Circulation.* (2003) 107:2227–32. doi: 10.1161/01.CIR.0000066323.15244.54

33. Li L, Bainbridge MN, Tan Y, Willerson JT, Marian AJA. Potential oligogenic etiology of hypertrophic cardiomyopathy: a classic single-gene disorder. *Circ Res.* (2017) 120:1084–90. doi: 10.1161/CIRCRESAHA.116.310559

34. Daly SB, Shah H, O'Sullivan J, Anderson B, Bhaskar S, Williams S, et al. Exome sequencing identifies a dominant TNNT3 mutation in a large family with distal arthrogryposis. *Mol Syndromol.* (2014) 5:218–28. doi: 10.1159/000365057

35. van de Locht M, Borsboom TC, Winter JM, Ottenheijm CAC. Troponin variants in congenital myopathies: how they affect skeletal muscle mechanics. *Int J Mol Sci.* (2021) 22:17. doi: 10.3390/ijms22179187

36. Wang W, Niu Z, Wang Y, Li Y, Zou H, Yang L, et al. Comparative transcriptome analysis of atrial septal defect identifies dysregulated genes during heart septum morphogenesis. *Gene.* (2016) 575:303–12. doi: 10.1016/j.gene.2015.09.016

37. Sandaradura SA, Bournazos A, Mallawaarachchi A, Cummings BB, Waddell LB, Jones KJ, et al. Nemaline myopathy and distal arthrogryposis associated with an autosomal recessive TNNT3 splice variant. *Hum Mutat.* (2018) 39:383–8. doi: 10.1002/humu.23385

frontiers | Frontiers in Cardiovascular Medicine

TYPE Original Research
PUBLISHED 28 October 2022
DOI 10.3389/fcvm.2022.1036340

Check for updates

OPEN ACCESS

EDITED BY
Oswin Grollmuss,
Université Paris-Sud, France

REVIEWED BY
Bowen Zhu,
Fudan University, China
Pittarello Demetrio,
University Hospital of Padua, Italy

*CORRESPONDENCE
Hui Zhang
zhanghui7012@aliyun.com

†These authors have contributed equally to this work and share first authorship

SPECIALTY SECTION
This article was submitted to Pediatric Cardiology, a section of the journal Frontiers in Cardiovascular Medicine

RECEIVED 04 September 2022
ACCEPTED 05 October 2022
PUBLISHED 28 October 2022

CITATION
Li MW, Wang SX, Zhang H, Zhang HT, Wu YJ and Meng B (2022) The predictive value of pressure recording analytical method for the duration of mechanical ventilation in children undergoing cardiac surgery with an XGBoost-based machine learning model.
Front. Cardiovasc. Med. 9:1036340.
doi: 10.3389/fcvm.2022.1036340

COPYRIGHT
© 2022 Li, Wang, Zhang, Zhang, Wu and Meng. This is an open-access article distributed under the terms of the Creative Commons Attribution License (CC BY). The use, distribution or reproduction in other forums is permitted, provided the original author(s) and the copyright owner(s) are credited and that the original publication in this journal is cited, in accordance with accepted academic practice. No use, distribution or reproduction is permitted which does not comply with these terms.

The predictive value of pressure recording analytical method for the duration of mechanical ventilation in children undergoing cardiac surgery with an XGBoost-based machine learning model

Mingwei Li†, Shuangxing Wang†, Hui Zhang*, Hongtao Zhang, Yongjie Wu and Bing Meng

Department of Cardiac Surgery, Children's Hospital of Capital Institute of Pediatrics, Beijing, China

Objective: Prolonged mechanical ventilation in children undergoing cardiac surgery is related to the decrease in cardiac output. The pressure recording analytical method (PRAM) is a minimally invasive system for continuous hemodynamic monitoring. To evaluate the postoperative prognosis, our study explored the predictive value of hemodynamic management for the duration of mechanical ventilation (DMV).

Methods: This retrospective study included 60 infants who underwent cardiac surgery. Cardiac index (CI), the maximal slope of systolic upstroke (dp/dt_{max}), and cardiac cycle efficiency (CCE) derived from PRAM were documented in each patient 0, 4, 8, and 12 h (T0, T1, T2, T3, and T4, respectively) after their admission to the intensive care unit (ICU). A linear mixed model was used to deal with the hemodynamic data. Correlation analysis, receiver operating characteristic (ROC), and a XGBoost machine learning model were used to find the key factors for prediction.

Results: Linear mixed model revealed time and group effect in CI and dp/dt_{max}. Prolonged DMV also have negative correlations with age, weight, CI at and dp/dt_{max} at T2. dp/dt_{max} outweighing CI was the strongest predictor (AUC of ROC: 0.978 vs. 0.811, $p < 0.01$). The machine learning model suggested that dp/dt_{max} at T2 $\leq$ 1.049 or <1.049 in combination with CI at T0 $\leq$ 2.0 or >2.0 can predict whether prolonged DMV (AUC of ROC = 0.856).

Conclusion: Cardiac dysfunction is associated with a prolonged DMV with hemodynamic evidence. CI measured by PRAM immediately after ICU admission and dp/dt_{max} 8h later are two key factors in predicting prolonged DMV.

KEYWORDS

CHD, congenital heart disease, cardiac surgery, pressure recording analytical method, mechanical ventilation, machine learning model

Introduction

Myocardial dysfunction is a critical challenge for hemodynamic management after cardiac surgery. For infants with congenital heart disease, the continuous decline in cardiac performance may remain long after cardiopulmonary bypass (CPB) (1, 2). Cardiac index (CI) decreased around 30% postoperatively in neonates, reaching the lowest point 9–12 h after surgery (1). Adults show decreasing CI over the first 4–8 h in the ICU but recover to the baseline within 24 h (3). Hemodynamic instability and myocardial dysfunction in infants often cause serious complications, which incur higher mortality, prolong the cardiopulmonary support, and even lead to weaning failure (4, 5).

As cardiac surgeons have widely admitted the duration of mechanical ventilation as an index for patients' prognosis after surgery, many studies have tried to reveal the risk factors associated with delayed extubation. However, most of these studies focused on the direct effects of the respiratory system on mechanical ventilation and failed to consider about the radical hemodynamic changes and heart–lung interactions as a whole (6–8). Though a few studies suggested that weaning failure is associated with increased left ventricular end-diastolic pressure (LVEDP) and left ventricular dysfunction (9, 10), clinical explorations based on the theory of the heart–lung interactions in the perioperative period still lack data evidence and methods on evaluating the appropriate timing for weaning remain limited (11, 12). With the benefits of early extubation wellestablished, fast-track anesthesia is now widely used in cardiac 40 surgery in adult, but less well described in children (13–15). Therefore, it is of great necessity for feasible evaluation on the course of mechanical ventilation.

Our research aimed to reveal that hemodynamic parameters representing cardiac function at the early postoperative time can predict the duration of mechanical ventilation, which provides new insights into postoperative management.

Patients and methods

Patients

This retrospective study included 60 infants who underwent heart defect repaired surgeries in our hospital between January 2017 and March 2021. Patients who expired during hospitalization were excluded. All the open heart surgeries were performed through standard procedures of CPB. Mechanical ventilation was initiated immediately when the patient arrived at the ICU after surgery. Extubation was performed when the patients met the standard criteria: (1) hemodynamic stability with reasonable urination and warm peripheral extremities; (2) PaO_2 ≥75 mmHg and $PaCO_2$ ≤50 mmHg with adequate spontaneous respiration under FiO_2 ≤40% and the end of expiratory pressure ≤5 cm H_2O; (3) awake and able to respond to commands without new neurological symptoms; (4) no active bleeding with a reasonable change in hemoglobin and no requirement for volume replacement; and (5) no reasonable fear of reintubation. The duration of mechanical ventilation (DMV) longer than 24 h was considered with delayed extubation, and patients were divided into two groups according to this.

Hemodynamic monitoring

Postoperative management consists of continuous intravenous infusion of sufentanil, dexmedetomidine, or midazolam. Inotropic and vasoactive drugs include dopamine, milrinone, epinephrine, norepinephrine, or levosimendan to maintain arterial blood pressure. Anti-infective treatment is routinely performed with the intravenous antibiotic. Since the Fick (1870) principle was developed (16), many technological methods have been invented to measure the cardiac output and other hemodynamic parameters. MostCare (Vygon Vytech, Padova, Italy) uses the pressure recording analytical method (PRAM) for direct monitoring based on pulse spectrum analysis methods in the same way as $PICCO_2$. It is a minimally invasive real-time method recorded at a high sampling rate (1,000 pressure/time points) without the need of calibration (17, 18). Most care has shown a good level of agreement with the Fick method measurements and is widely studied in animals and adults but rarely in infants after cardiac surgery. Hemodynamic parameters collected in this study included cardiac index (CI), the maximal slope of systolic upstroke (dp/dt_{max}), and cardiac cycle efficiency (CCE). Data were collected and recorded by the device 0, 4, 8, and 12 h after radial artery cannulation was established (T0, T1, T2, and T3, respectively).

Analysis method

The Shapiro–Wilk method was used to test whether the data followed the normal distribution that were normally distributed and median values with interquartile range (IQR, 25th−75th percentile) for variables that were not normally distributed, and as the frequency with percentage (%) for categorical variables. Hemodynamic data recorded by MostCare are presented as mean ± SD. In univariate analysis, differences between groups were evaluated using the Wilcoxon rank-sum test or *t*-test for continuous variables according to distribution. Chi-square test and Fisher's exact test are used for categorical variables. Linear mixed models were used to deal with the repeated measurement of hemodynamic data. For each CI, CCE, and dp/dt_{max}, we tested for interactions between groups (DMV≤24h or >24h) and time (T0, T1, T2, and T3). The model equation is shown

as follows:

$$Y_{i,j} = \beta_0 + \beta_1 (\text{Time}) + \beta_2 (\text{Group}) + \beta_3 (\text{Group} \times \text{Time}) + b_0 (\text{ID}) + b_1$$

where $Y_{i,j}$ is the hemodynamic variables (CI, CCE, or dp/dt_{max}) for patients i at Time j ($i = 1, 2, \ldots 60$. $j = 0, 1, 2, 3$); Time*Group is the interaction between the group term and the time term. ID is the patients i. β_0, β_1, β_2, and β_3 are the fixed effect coefficients. b_0 and b1 are the random effect coefficients. The Pearson correlation coefficient was calculated to assess the relationship between the cardiac functions and DMV. ROC curves are used to assess the diagnostic performance. *p*-value < 0.05 was considered statistically significant. Statistical analysis and data processing were performed with *R* language (version 4.2.0).

Machine learning model

Yan et al. (20) have designed an XGBoost machine learning-based model that can predict the 92 mortality rates of patients with more than 90% accuracy for COVID-19 prognostic prediction. The treeheatr *R* package creates interpretable decision tree visualizations with the data represented as a heat map at the tree's leaf nodes (21). XGBoost algorithms are based on recursive decision tree building from past residuals and can identify those trees that contribute the most to the decision of the predictive model. The leaf nodes are labeled based on their majority votes and colored to correlate with the true outcome in the decision tree. The models were evaluated by assessing the classification accuracy (ratio of true predictions overall predictions), the precision, sensitivity/recall, and defined scores. The importance of individual feature in XGBoost is determined by its accumulated use in each decision step in trees, computing the relative importance of each feature. Hence, it can estimate features that are the most discriminative of model outcomes. Using this machine learning model, we construct a clinically operable decision model.

Results

Patients' characteristics

Demographic characteristics are shown in Table 1. A total of 60 infants were included in the study, among which 35 (58%) children were extubated within 24 h (DMV≤24h group), while 25 (42%) were over 24 h (DMV>24h group). According to the pathophysiology, congenital heart disease (CHD) is divided into left-right shunt CHD and right-left shunt ones. In our study, the former included atrial septal defect (ASD), ventricular septal defect (VSD), patent ductus arteriosus (PDA), and simple valvular disease, while the latter included tetralogy of Fallot (TOF), double outlet right ventricle (DORV), and Complete endocardium pad defect (CEPD). Infants with a prolonged DMV were characterized by significantly younger ages, lower heights and weights, longer CPB time and aortic cross clamp (ACC) time, as well as longer ICU and postoperative hospital stays (*p*-value < 0.05) (Table 1).

TABLE 1 Baseline characteristics.

Characteristics	DMV ≤ 24h ($n = 35$)	DMV > 24h ($n = 25$)	*p*-value
Age (month)	4.77 (3.50, 6.86)	2.00 (1.57, 4.53)	**<0.001**
Sex			0.493
Female	11 (31%)	10 (40%)	
Male	24 (69%)	15 (60%)	**0.002**
Height (cm)	64.51 ± 5.75	58.76 ± 7.45	
Weight (kg)	6.2 (5.50, 7.40)	5.00 (4.20, 6.20)	**0.001**
CHD*			1.000
Left–right	31 (89%)	22 (88%)	
Right–left	4 (11%)	3 (12%)	0.660
NYHA			
≤II	19 (54%)	15 (60%)	
>II	16 (46%)	10 (40%)	0.357
Preoperative respiratory disease**			
Yes	14 (40%)	13 (52%)	
No	21(60%)	12(48%)	**0.004**
CPB time (min)	76 (66, 92)	104 (86, 136)	**0.016**
ACC time (min)	45 (36, 56)	55 (50, 79)	**<0.001**
Ventilation time (h)	12 (8,20)	49 (45,72)	0.199
Adverse events***			
Yes	18 (51%)	17(68%)	
No	17 (49%)	8(32%)	**<0.001**
ICU stay (days)	2 (1,3)	5 (4,7)	**<0.001**
Postoperative hospital stay (days)	10 (9,12)	14 (12,18)	

Data are presented as mean(IQR)/*n* (%)/mean±SD. The bold values represent the *p*-value < 0.05.

DMV, duration of mechanical ventilation; CPB, cardiopulmonary bypass; ACC, aortic cross clamp; NYAH, NYAH class.

*CHD, congenital heart disease includes left-right shunt congenital heart disease and right-left shunt congenital heart disease.

**Preoperative respiratory disease includes respiratory tract infection, pneumonia, and tracheal chondromalacia.

***Adverse events, whether the patient is subjected to one of the following postoperative complications during the hospitalization: Low cardiac output syndrome, pleural effusion, ascites, arrhythmia, infection, or pneumonia.

Hemodynamic data of the two DMV groups

Mean ± SD of hemodynamic monitoring in the ICU at different time points for each DMV group was recorded (Supplementary Table 1), and the changes in cardiac function over time were shown (Figure 1). The results from the linear mixed model revealed significant main effects of time and group

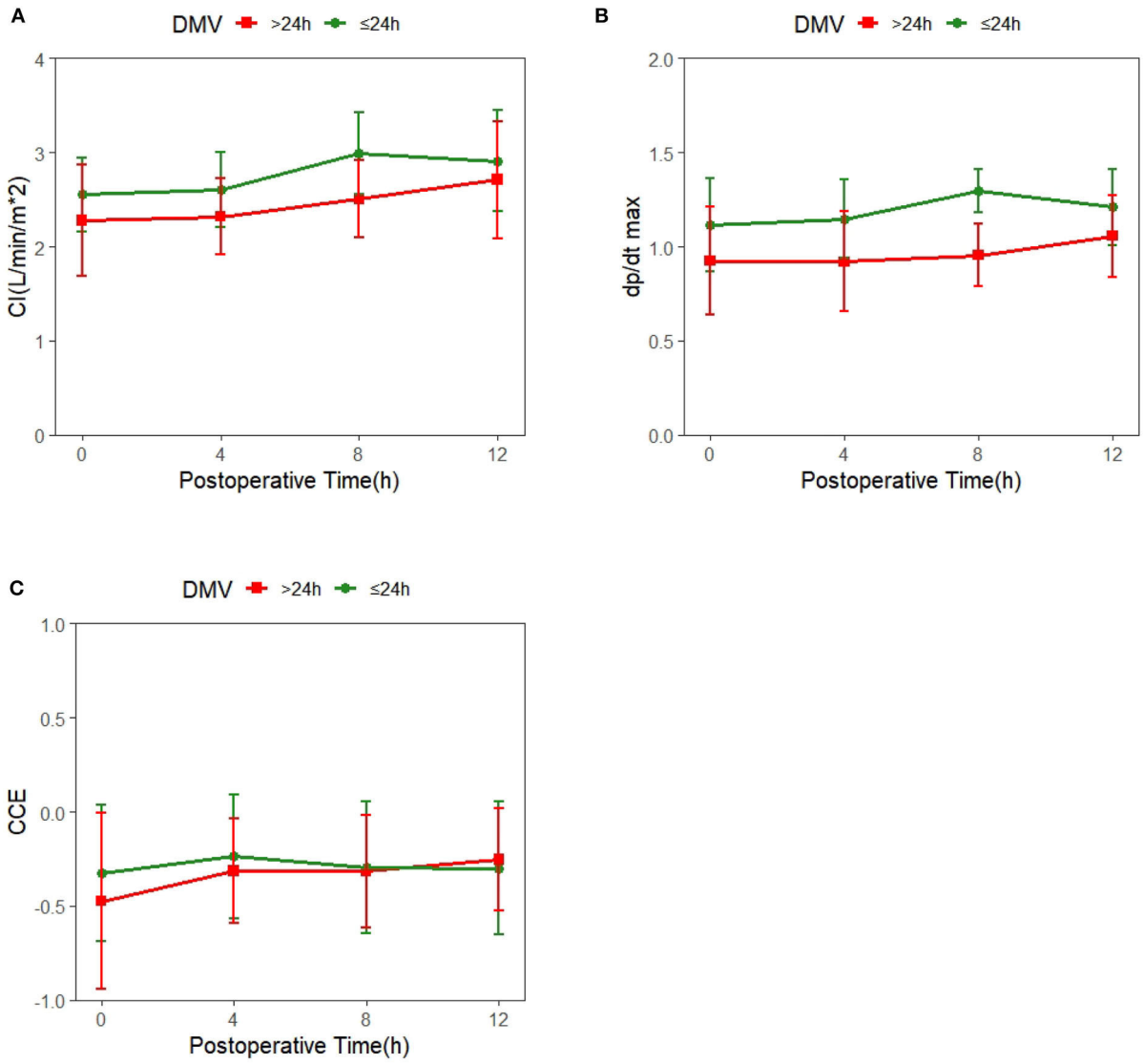


FIGURE 1
Trends of systemic hemodynamic value over time in patients with different duration of mechanical ventilation (DMV); the red line represents DMV >24h, and the green line represents DMV ≤24h. **(A)** Time-dependent changes in cardiac index(CI). **(B)** Time-dependent changes in cardiac cycle efficiency (CCE). **(C)** Time-dependent changes in the maximal slope of the systolic upstroke (dp/dt_{max}).

in CI and dp/dt_{max}, but not CCE (Table 2). DMV ≤24h group showed significant increases in CI and dp/dt_{max} from T0 to T2 (CI, $\beta_1 = 0.44$, SE = 0.09, $p < 0.001$; dp/dt_{max}, $\beta_1 = 0.182$, SE = 0.049, $p<0.001$) and from T0 to T3 (CI, $\beta_1 = 0.35$, SE = 0.09, $p < 0.001$; dp/dt_{max}, $\beta_1 = 0.096$, SE = 0.049, $p < 0.05$). T0 observed a significant difference between the two groups with decreased CI and dp/dt_{max} in patients with a prolonged DMV (CI, $\beta_2 = -0.27$, SE = 0.12, $p < 0.05$; dp/dt_{max}, $\beta_2 = -0.182$, SE = 0.058, $p < 0.01$). Besides, there was a significant group-time interaction in dp/dt_{max} from T0 to T2 ($\beta_3 = -0.152$, SE = 0.075, $p < 0.05$) but not CI or CCE.

Correlation analysis

Age, height, weight, CPB, ACC, which showed a significant difference between the two groups by univariate analysis (Table 1), and CI and dp/dt_{max} at T0, T2, and T3, which showed significant effects of time or group in the linear mixed models (Table 2), were entered for correlation analysis. Figure 3 shows a prolonged DMV has significant and negative correlation with age ($r = -0.48$, $p < 0.01$), weight ($r = -0.42$, $P < 0.05$), CI at T2 ($r = -0.53$, $p < 0.001$), and dp/dt_{max} at T2 ($r = -0.82$, $P < 0.001$). There was no significant correlation in CPB or ACC.

TABLE 2 Linear mixed effects of hemodynamic variables.

	CI	CCE	dp/dt_{max}
Fixed effects			
T0	2.55(0.08)**	−0.327(0.057)	1.113(0.035)**
T0–T1	0.04(0.09)	0.090(0.065)	0.034(0.048)
T0–T2	0.44(0.09)***	0.031(0.065)	0.182(0.049)***
T0–T3	0.35(0.09)***	0.028(0.065)	0.096(0.049)*
Group×T0	−0.27(0.12)	−0.148(0.091)	−0.182(0.058)
Group×T0–T1	−0.004(0.14)	0.070(0.100)	−0.038(0.075)
Group×T0–T2	−0.21(0.14)	0.128(0.100)	−0.152(0.075)*
Group×T0–T3	0.08(0.14)	0.192(0.100)	0.036(0.075)
Random effect			
Individual	0.08(0.28)	0.042(0.20)	0.002(0.046)
Group×Individual	0.29(0.54)	0.064(0.27)	0.022(0.148)
Corr.	−0.96	−0.52	−1.00
Log Likelihood	−154.1	−75.41	15.37
AIC	332.21	174.81	−6.73
BIC	373.98	216.58	35.03

Values indicate estimated effect β and corresponding standard error.
CI, cardiac index; CCE, cardiac cycle efficiency; dp/dt_{max} the maximal slope of the systolic upstroke.
*$p < 0.05$.
**$p < 0.01$.
***$p < 0.001$.

dp/dt_{max} at T2 has a strong correlation, whereas age, weight, and CI at T2 have a moderate correlation.

Predictive values

ROC curves

As shown in Figure 3, dp/dt_{max} outweighing CI at T2 was the strongest predictor of a prolonged DMV ($p < 0.01$). dp/dt_{max} at T2 <1.052 (sensitivity = 1.000, specificity = 0.840), CI at T2 <2.670 (sensitivity = 0.800 specificity = 0.800), and CI at T0 <2.215 (sensitivity = 0.857 specificity = 0.560) could predict prolonged DMV.

XGBoost machine learning-based model

Age, height, weight, CPB, ACC, CI, and dp/dt_{max} at T0, T2, and T3 were also entered into the XGBoost machine learning-based model, which produced a decision tree-heat map. As Figure 4 shows, the model suggested that patients with $dp/dt_{max} \leq 1.049$ at T2 were in DMV>24h group, and those whose $dp/dt_{max} > 1.049$ at T2 was in DMV ≤24h. On the split of CI at T0, although individuals of both branches are all predicted to DMV ≤24h by majority voting, the leaf nodes have different purity, indicating different confidence levels the model has in classifying samples in the two nodes. Therefore, patients with CI≤2 at T0 cannot easily exclude the possibility of being prolonged DMV. The whole model had excellent accuracy and predictive value (accuracy = 0.933, balance accuracy = 0.920, Kappa = 0.860, AUC of ROC = 0.856, AUC of PR = 0.907).

Discussion

Andre' and DelRossi reported that PRAM has been proved to correlate well with "gold-standard" thermodilution (3) in assessing cardiac output. Other methods included Fick, Doppler echocardiography, BNP, and lactate levels (19, 22). Our study initiatively found correlations between the cardiac function characterized by hemodynamic parameters and mechanical ventilation. Prolonged DMV, mainly caused by cardiac dysfunction, is a significant sign of worse prognosis, and successful early extubation is a goal to promote recovery after cardiac surgery with both medical and economic benefits (13, 14). Furthermore, we proved good predictive value of these parameters and provided a visualized decision-making map with the application of machine learning model.

Hemodynamic management with PRAM in the postoperative process

The linear mixed model showed time effects of hemodynamic parameters, indicating that cardiac function presented a significant increase over time in the first 4–8h after the surgery (Figure 1 and Table 2), which contradicted the classic conclusions from Wernovsky et al. (1) and Gil-Anton et al. (4) measured CI of children with CHD 24 h after surgery by femoral arterial thermodilution and found no obvious changes between CI over time. Another exploration of trends of the postoperative hemodynamic based 161 on PRAM found an increase in CCE and dp/dt_{max} in 48 h postoperatively (23). The different trends of postoperative cardiac function between the early study and later ones perhaps resulted from the developed CPB techniques, such as modified ultrafiltration and dexmedetomidine sedative (24–26), which may prevent CPB-related inflammatory responses and lead to better hemodynamic outcomes. Besides, the use of vasoactive agents has proven to be another key factor contributing to improving postoperative cardiac function (27–29).

Cardiac function for predicting DMV

The group effect on hemodynamic parameters revealed by the linear mixed model suggested that patients with a prolonged DMV showed significantly lower CI and dp/dt_{max} after the surgery (Table 2, Figure 1). Cardiac dysfunction is the main risk factor for 80% weaning failure (5). Han et al. and Kadir et al.

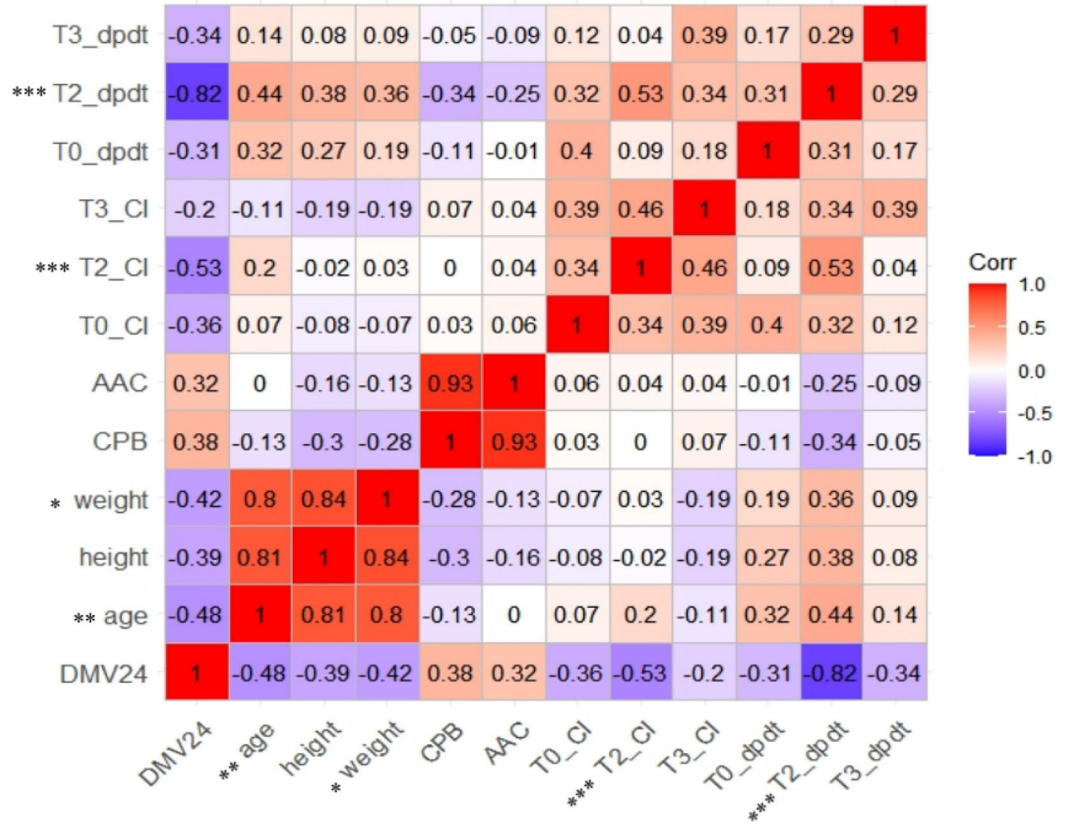


FIGURE 2
Correlation analysis of heat map for relationship between selected the characteristics, hemodynamic parameters, and prolonged DMV. CI, cardiac index. Dp/dt max, the maximal slope of systolic upstroke. DMV24, binary-classified variable, duration of mechanical ventilation leq24h or >24h.

also found that cardiac dysfunction is associated with longer mechanical ventilation duration (30, 31). Both the preload and afterload increase due to the decrease in intrathoracic pressure premature in the process of extubation and increase cardiac work and myocardial oxygen consumption. As a result, premature extubation deteriorates patients' condition by inducing pulmonary edema, pulmonary artery spasm, severe anoxia, heart failure, and reintubation.

dp/dt_{max} measured 8h after the surgery had strongest correlation with a prolonged DMV and was the best hemodynamic predictor (Table 2, Figures 2–4). On the one hand, dp/dt_{max} has generally been used as a sensitive index of cardiac contractility and reserving ability (32). Arterial dp/dt_{max} tracks the left ventricular contractility changes and is mainly determined by myocardial contractility with very limited influence by loading conditions (32–35). Decreased dp/dt_{max} is associated with a myocardial injury even in extracardiac surgery using PRAM (36). Yang et al. also reported that not CI but dp/dt_{max} have a higher correlation with BNP when used PRAM after CHD operation (22). In addition, the exact 8 h after the surgery may be a turning point for restoring cardiac function or prognosis. Yang et al. and Liu et al. observed the nadir of cardiac output, the minimal central venous oxygen saturation, and the peak of BNP and lactate level at 8h after the surgery (22, 37). Su et al. revealed that the increase of troponin-I beyond 8h after CPB was a strong predictor of postoperative hypoperfusion in infants (38).

CI reflects the complex outcomes of the endogenous cardiac, neurohumoral responses, and the exogenous inotropic and vasoactive drugs, dependent more on heart rate, preload, and afterload. Based on the heart–lung interaction theory, an increase in cardiac output is considered a positive response to a volume challenge (39, 40). Although it did not have a linear correlation with delayed extubation, CI measured at T0 is a predictor that could not be neglected (Table 2, Figure 4). Furthermore, the difference of CI and dp/dt_{max} between the two DMV groups at T0 alarmed us that inotropic and vasoactive drugs should be used as early as intraoperatively.

CCE is a unique parameter derived from PRAM, which evaluates the compensating interplay of different cardiovascular

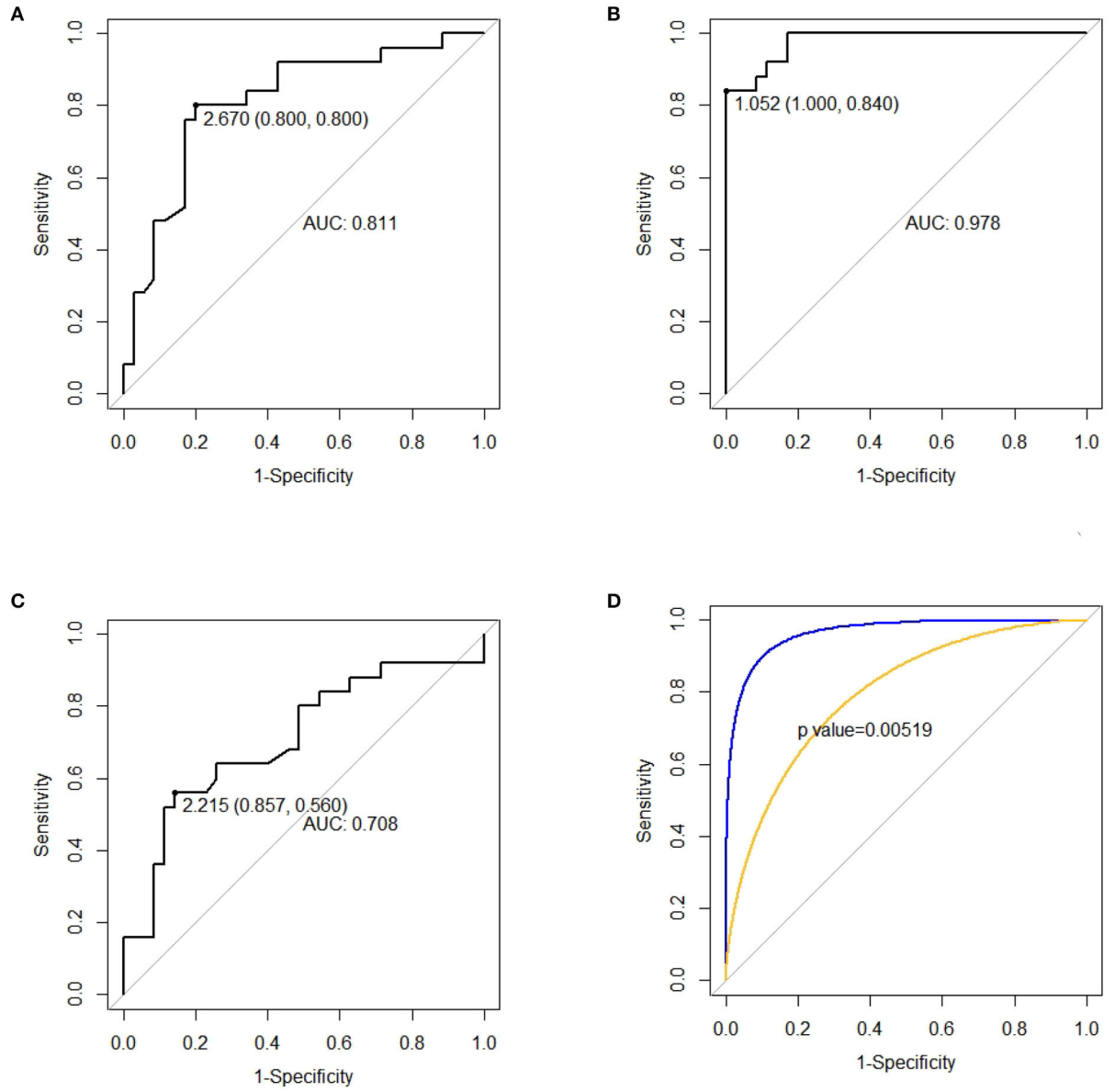


FIGURE 3
ROC curves for predicting prolonged duration of mechanical ventilation (DMV). **(A)** CI, cardiac index, measured at T2 for predicting prolonged DMV. **(B)** dp/dt_{max}, the maximal slope of the systolic upstroke, measured at T2 for predicting prolonged DMV. **(C)** CI, cardiac index, measured at T0 for predicting prolonged DMV. **(D)** Comparison between the AUC of ROC of CI and dp/dt_{max} at T2.

system compartments, including left and right ventricular contractility, preload and afterload, heart rate, reflected waves, as well as elasticity of great arteries and the ventricular-arterial coupling (24, 39). CCE with no significant changes over time in our study (Table 2) indicates the constant condition of cardiac energy expenditure for compensation to maintain cardiovascular homeostasis after the surgery (31, 41). However, influenced by many factors, CCE is too sensitive and variable: McBride et al. (42) reported the inability of negative-pressure ventilation to reduce HR in sedated extubated patients which meant that other hemodynamic benefit increases did not translate into the improved CCE.

XGBoost machine learning-based model

XGBoost machine learning model is a widely used technique for a predictive model for its significant accuracy, which is better than many linear models. It is well designed to prevent overfitting by cross-validation and regularization. Furthermore, the more extended corresponding color column of the outcome

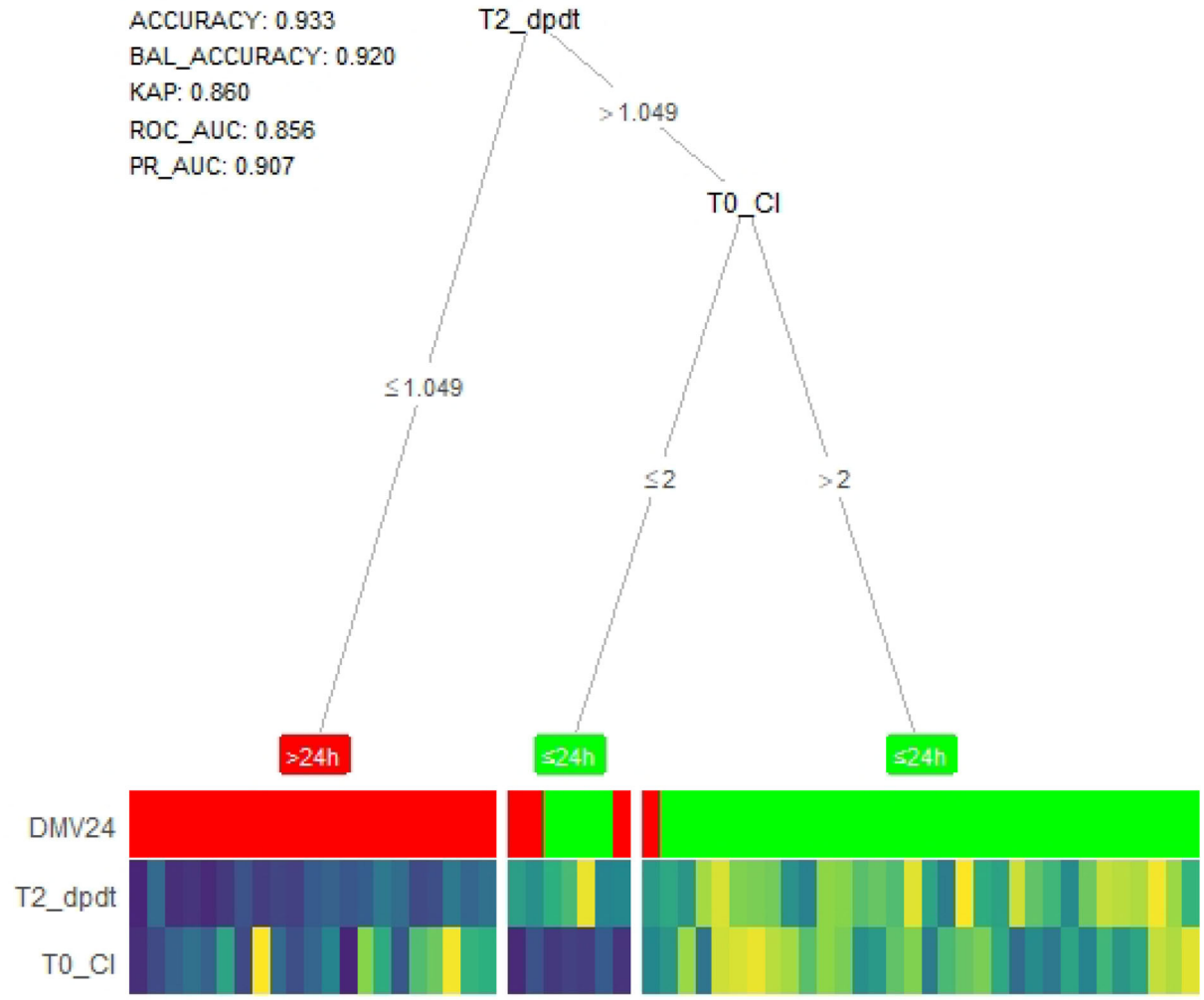


FIGURE 4
Tree-heat map of XGBoost machine learning model for prediction. T2_dpdt, dp/dt_{max} (the maximal slope of systolic upstroke) at T2. T0_CI, CI (cardiac index) at T0. DMV, duration of mechanical ventilation. BAL_ACCURACY, balance accuracy, KAP, kappa. ROC_AUC, Under area curve of ROC.

means more cases of the event and more substantial predictive value of these branches in our XGBoost-based model. Heat map colors present the relative value compared to the rest of the group on each feature (21). Although CI at T2 had good performance in ROC curves, dp/dt_{max} at the same time point probably substitutes for it completely, and CI at T0 improved the predictive value when added into the algorithm. XGBoost machine learning model has been more prevalent in dealing with clinical problems such as treatment evaluation and disease risk management (43).

Other factors affecting DMV in infants

Age and weight are important factors for both early extubation in fast-track management and delayed extubation after congenital heart surgery in children (44). Infants' left ventricle has altered relaxation characteristics that progressively change over the first year of life and reach adult level (45). The less proliferation of cardiomyocytes and sarcoplasmic reticulum in the myocardium contributes to the lower cardiac contractility. Besides, infants with lower body weight had a higher frequency of adverse events and longer DMV, ICU stay and hospital stay (46, 47). Cardiac surgery often necessitates CBP, which causes myocardial ischemia–reperfusion and induces oxidative stress and ventricular dysfunction (48). Children with a prolonged DMV undergo longer CBP and ACC during the surgery (Table 1). However, CBP and ACC did not correlate with a prolonged DMV and could not use for prediction (Figures 2, 4). Tabib et al. and Garci'a-Montes et al. also reported a similar irrelevance to the mechanical ventilation condition (44, 49).

Limitation

There are several limitations to this study. First, the sample size is not big enough, especially for applying the machine learning model. The number of key factors and their priority may change if more patients are included. Extensive multi-center cohort study including complicated cases is needed to confirm our findings. Our general protocol for determining whether patients should be performed extubation may not align with management at other institutions. In addition, MostCare machine records the data at every 30s, but the calculation on postoperative hours is rough and thus the data collected unavoidably have time error.

Conclusion

In summary, postoperative hemodynamic management with PRAM shed light on the interconnection between cardiac function and mechanical ventilation. CI measured by PRAM immediately after ICU admission and dp/dt_{max} 8 h later are two key factors in predicting a prolonged DMV with the application of the machine learning model.

Data availability statement

The original contributions presented in the study are included in the article/Supplementary material, further inquiries can be directed to the corresponding author/s.

Ethics statement

The studies involving human participants were reviewed and approved by Ethical Committee of Capital Institute of Pediatrics. Written informed consent to participate in this study was provided by the participants' legal guardian/next of kin.

Author contributions

ML and SW contributed equally to this work and shared co-first authorship. They were responsible for conceptualization/design, methodology, data curation, investigation, and formal analysis. HuZ was responsible for supervision/oversight and funding resources. HoZ, YW, and BM was responsible for drafting the initial manuscript and reviewing or editing the manuscript. All authors contributed to the article and approved the submitted version.

Funding

This research was supported by the Special Fund of the Pediatric Medical Coordinated Development Center of Beijing Hospitals Authority (XTZD20180301).

Acknowledgments

We thank all the participants in this study including Dan lei Chen and Xinpeng Qu who were not listed in the author list for their assistance in patients' management.

Conflict of interest

The authors declare that the research was conducted in the absence of any commercial or financial relationships that could be construed as a potential conflict of interest.

Publisher's note

All claims expressed in this article are solely those of the authors and do not necessarily represent those of their affiliated organizations, or those of the publisher, the editors and the reviewers. Any product that may be evaluated in this article, or claim that may be made by its manufacturer, is not guaranteed or endorsed by the publisher.

Supplementary material

The Supplementary Material for this article can be found online at: https://www.frontiersin.org/articles/10.3389/fcvm.2022.1036340/full#supplementary-material

References

1. Wernovsky G, Wypij D, Jonas RA, Mayer Jr JE, Hanley FL, Hickey PR, et al. Postoperative course and hemodynamic profile after the arterial switch operation in neonates and infants: a comparison of low-flow cardiopulmonary bypass and circulatory arrest. *Circulation.* (1995) 92:2226–35. doi: 10.1161/01.CIR.92.8.2226

2. Epting LC, McBride EM, Wald LE, Costello MJ. Pathophysiology of post-operative low cardiac output syndrome. *Curr Vasc Pharmacol.* (2016) 14:14–23. doi: 10.2174/1570161113666151014123718

3. Andr ACS, DelRossi A. Hemodynamic management of patients in the first 24 hours after cardiac surgery. *Critical Care Med.* (2005) 33: 2082–93. doi: 10.1097/01.CCM.0000178355.96817.81

4. Gil-Anton J, López-Bayón J, López-Fernández Y, Morteruel E, Pérez-Estevez E, López-Herce J. Cardiac index monitoring by femoral arterial thermodilution after cardiac surgery in children. *J Crit Care.* (2014) 29:1132–e1. doi: 10.1016/j.jcrc.2014.06.004

5. He H, Liu W, Ju M, Liu Y, Gu W, Luo Z. Analysis of factors related to weaning failure of prolonged mechanical ventilation after cardiac surgery. *Chin J Clin Med.* (2019) 26:727–31.

6. Silva MGB, Borges DL, Costa MdAG, Baldez TEP, Silva LNd, Oliveira RL, et al. Application of mechanical ventilation weaning predictors after elective cardiac surgery. *Braz J Cardiovasc Surgery*. (2015) 262:605–609. doi: 10.5935/1678-9741.20150076

7. Sun Y, Shen SE, Deng XM, Cai Y, Du Y. Lung protective ventilation in infants undergoing cardiopulmonary bypass surgery for congenital heart disease: a prospective randomized controlled trial. *Pediatric Anesthesia.* (2020) 30:814–22. doi: 10.1111/pan.13894

8. Murata T, Maeda M, Amitani R, Hiromoto A, Shirakawa M, Kambe M, et al. Postoperative changes in pulmonary function after valve surgery: oxygenation index early after cardiopulmonary is a predictor of postoperative course. *J Clin Med.* (2021) 10:3262. doi: 10.3390/jcm10153262

9. Grübler MR, Wigger O, Berger D, Blöchlinger S. Basic concepts of heart-lung interactions during mechanical ventilation. *Swiss Med Weekly*. (2017) 262:w14491. doi: 10.4414/smw.2017.14491

10. Bennett VA, Aya HD, Cecconi M. Evaluation of cardiac function using heart-lung interactions. *Ann Transl Med* 6:356. (2018). doi: 10.21037/atm.2018.08.10

11. Liu J, Wang Cj, Ran Jh, Lin Sh, Deng D, Ma Y, et al. The predictive value of brain natriuretic peptide or n-terminal pro-brain natriuretic peptide for weaning outcome in mechanical ventilation patients: evidence from sroc. *J Renin-Angiotensin-Aldosterone Syst.*. (2021) 22:1470320321999497. doi: 10.1177/1470320321999497

12. Dessap AM, Roche-Campo F, Kouatchet A, Tomicic V, Beduneau G, Sonneville R, et al. Natriuretic peptide–driven fluid management during ventilator weaning: a randomized controlled trial. *Am J Resp Crit Care Med.* (2012) 186:1256–1263. doi: 10.1164/rccm.201205-0939OC

13. Polito A, Patorno E, Costello JM, Salvin JW, Emani SM, Rajagopal S, et al. Perioperative factors associated with prolonged mechanical ventilation after complex congenital heart surgery. *Pediatr Crit Care Med.* (2011) 12:e122–6. doi: 10.1097/PCC.0b013e3181e912bd

14. Alam S, Shalini A, Hegde RG, Mazahir R, Jain A. Predictors and outcome of early extubation in infants postcardiac surgery: a single-center observational study. *Ann Card Anaesth.* (2018) 21:402. doi: 10.4103/aca.ACA_209_17

15. Tekindur S, Yetim M, Kilickaya O. Timing of extubation after cardiac surgery. *J Cardiothorac Vasc Anesth.* (2018) 32:e35. doi: 10.1053/j.jvca.2016.04.019

16. Fick A. *Uber die messung des Blutquantums in den Hertzvent rikeln.* Sitzber Physik Med Ges Wurzburg (1870).

17. Urbano J, López J, González R, Solana MJ, Fernández SN, Bellón JM, López-Herce J. Measurement of cardiac output in children by pressure-recording analytical method. *Pediatr Cardiol.* (2015) 36:358–64. doi: 10.1007/s00246-014-1014-3

18. Favia I, Rizza A, Garisto C, Haiberger R, Di Chiara L, Romagnoli S, et al. Cardiac index assessment by the pressure recording analytical method in infants after paediatric cardiac surgery: a pilot retrospective study. *Interact Cardiovasc Thorac Surg.* (2016) 23:919–23. doi: 10.1093/icvts/ivw251

19. Alonso-Iñigo JM, Escribá FJ, Carrasco JI, Fas MJ, Argente P, Galvis JM, et al. Measuring cardiac output in children undergoing cardiac catheterization: comparison between the fick method and pram (pressure recording analytical method). *Pediatr Anesthesia.* (2016) 26:1097–1105. doi: 10.1111/pan.12997

20. Yan L, Zhang HT, Goncalves J, Xiao Y, Wang M, Guo Y, et al. An interpretable mortality prediction model for covid-19 patients. *Nat Mach Intel.* (2020) 2:283–8. doi: 10.1038/s42256-020-0180-7

21. Le TT, Moore JH. treeheatr: an r package for interpretable decision tree visualizations. *Bioinformatics.* (2021) 37:282–4. doi: 10.1093/bioinformatics/btaa662

22. Yang F, Iacobelli R, Wang JM, et al. Assessment of cardiac function in infants with transposition of the great arteries after surgery: comparison of two methods. *World J Pediatr.* (2018) 14:373–7. doi: 10.1007/s12519-018-0178-y

23. Lou X, Liu Y, Cui Y, Li J, Li L, Ma L, et al. Contemporary trends and risk factors of hemodynamic and myocardial mechanics derived by the pressure recording analytical method after pediatric cardiopulmonary bypass. *Front Cardiovasc Med.* (2021) 8. doi: 10.3389/fcvm.2021.687150

24. Ricci Z, Polito A, Netto R, De Razza F, Favia I, Carotti A, et al. Assessment of modified ultrafiltration hemodynamic impact by pressure recording analytical method during pediatric cardiac surgery. *Pediatric Crit Care Med.* (2013) 14:390–5. doi: 10.1097/PCC.0b013e31828a7113

25. Cui J, Gao M, Huang H, Huang X, Zeng Q. Dexmedetomidine improves lung function by promoting inflammation resolution in patients undergoing totally thoracoscopic cardiac surgery. *Oxidati Med Cell Longevity*. (2020) 2020:8638301. doi: 10.1155/2020/8638301

26. Xiao Y, Li J, Qiu L, Jiang C, Huang Y, Liu J, et al. Dexmedetomidine protects human cardiomyocytes against ischemia-reperfusion injury through α2-adrenergic receptor/ampk-dependent autophagy. *Front Pharmacol.* (2021) 12:615424. doi: 10.3389/fphar.2021.615424

27. Yunhai S, Zhuoming X, Limin Z, Ling C, Zhaokang S. Reasonable application of positive inotropic agent during the postoperative period in patients with complicated congenital heart disease. *Chin J Cardiovasc Med.* (2010) 15:281–4. doi: 10.3969/j.issn.1007-5410.2010.04.012

28. Wang A, Cui C, Fan Y, Zi J, Zhang J, Wang G, et al. Prophylactic use of levosimendan in pediatric patients undergoing cardiac surgery: a prospective randomized controlled trial. *Crit Care.* (2019) 23:1–11. doi: 10.1186/s13054-019-2704-2

29. Xu J, Jiang W, Li Y, Shen B, Shen Z, Wang Y, et al. Volume-associated hemodynamic variables for prediction of cardiac surgery-associated acute kidney injury. *Clin Exp Nephrol.* (2020) 24:798–805. doi: 10.1007/s10157-020-01908-6

30. Han D, Pan S, Li H, Meng L, Luo Y, Ou-Yang C. Prognostic value of cardiac cycle efficiency in children undergoing cardiac surgery: a prospective observational study. *Br J Anaesth.* (2020) 125:321–9. doi: 10.1016/j.bja.2020.05.042

31. Kadir S, Yetman A, Cramer J, Tsai S. Analyze the clinical characteristics of adult congenital heart disease (achd) patients with intensive care unit admission and its impact on outcome. *Chest.* (2020) 157:A39. doi: 10.1016/j.chest.2020.05.045

32. Sorbara C, Romagnoli S, Rossi A, Romano SM. Circulatory failure: Bedside functional hemodynamic monitoring. In: Perioperative Critical Care Cardiology. *Topics in Anaesthesia and Critical Care*. Milano: Springer (2007). p. 89–108. doi: 10.1007/978-88-470-0558-7_6

33. Monge Garcia MI, Jian Z, Settels JJ, Hunley C, Cecconi M, Hatib F, et al. Performance comparison of ventricular and arterial dp/dt_{max} for assessing left ventricular systolic function during different experimental loading and contractile conditions. *Crit Care*. (2018) 22:1–12. doi: 10.1186/s13054-018-2260-1

34. Scolletta S, Bodson L, Donadello K, Taccone FS, Devigili A, Vincent JL, et al. Assessment of left ventricular function by pulse wave analysis in critically ill patients. *Intensive Care Med.* (2013) 39:1025–33. doi: 10.1007/s00134-013-2861-8

35. Ostadal P, Vondrakova D, Krger A, Janotka M, Naar J. Continual measurement of arterial dp/dt_{max} enables minimally invasive monitoring of left ventricular contractility in patients with acute heart failure. *Crit Care.* (2019) 23:1–8. doi: 10.1186/s13054-019-2654-8

36. Dou X, Liu W, Wang Q, Yu W. Accuracy of pram in predicting myocardial injury during pediatric liver transplantation in infants. *Chin J Anesthesiol.* (2020) 1237–1241. doi: 10.3760/cma.j.cn131073.20200413.01021

37. Liu C, Li L, Hou J, Wei D, Liu Y. Contrast study of cardiac output and oxygen metabolism in infants with congenital heart disease after cardiopulmonary bypass. *Zhonghua yi xue za zhi.* (2012) 92:3113–6.

38. Su JA, Kumar SR, Mahmoud H, Bowdish ME, Toubat O, Wood JC, et al. Postoperative serum troponin trends in infants undergoing cardiac surgery. *Semin Thor Cardiovasc Surg.* (2019) 31:244–51. doi: 10.1053/j.semtcvs.2018.08.010

39. Fan G, Cui Y, Chen X. Application advances of pressure recording analytical method for postoperative monitoring of infants with congenital heart disease. *Chin J Pediatr Surg.* (2020) 41:1138–1142.

40. Song Y, Hou H, Bai J, Gu H. Prediction of fluid responsiveness by stroke volume variation in children undergoing fontan operation. *BioMed Res Int.* (2020) 2020. doi: 10.21203/rs.3.rs-22897/v1

41. Yang F, Wang J, Gu J, Yao J, Zhui X, Zhang X, et al. Comparison of two methods for hemodynamic assessment in children with tetralogy of fallot after radical surgery. *Chin J Clin Thor Cardiovas Surg.* (2019) 26:873–7.

42. McBride WT, Ranaldi G, Dougherty MJ, Siciliano T, Trethowan B, Elliott P, et al. The hemodynamic and respiratory effects of continuous negative and control-mode cuirass ventilation in recently extubated cardiac surgery patients: Part 2. *J Cardiothorac Vasc Anesth.* (2012) 26:873–7. doi: 10.1053/j.jvca.2012.05.021

43. Zhang Z, Ho KM, Hong Y. Machine learning for the prediction of volume responsiveness in patients with oliguric acute kidney injury in critical care. *Crit Care*. (2019) 23:1–10. doi: 10.1186/s13054-019-2411-z

44. Tabib A, Abrishami SE, Mahdavi M, Mortezaeian H, Totonchi Z. Predictors of prolonged mechanical ventilation in pediatric patients after cardiac surgery for congenital heart disease. *Res Cardiovasc Med.* (2016) 5. doi: 10.5812/cardiovascmed.30391

45. Kulkarni A, Morisawa D, Gonzalez D, Kheradvar A. Age-related changes in diastolic function in children: echocardiographic association with vortex formation time. *Echocardiography*. (2019) 36:1869–75. doi: 10.1111/echo.14479

46. Ergün S, Genç SB, Yildiz O, Öztürk E, Kafali HC, Ayyildiz P, et al. Risk factors for major adverse events after surgical closure of ventricular septal defect in patients less than 1 year of age: a single-center retrospective. *Braz J Cardiovasc Surg.* (2019) 34:335–43. doi: 10.21470/1678-9741-2018-0299

47. Siehr SL, Hanley FL, Reddy VM, Miyake CY, Dubin AM. Incidence and risk factors of completeatrioventricular block after operative ventricular septal defect repair. *Congenit Heart Dis.* (2014) 9:211–5. doi: 10.1111/chd.12110

48. Sznycer-Taub N, Mackie S, Peng YW, Donohue J, Yu S, Aiyagari R, et al. Myocardial oxidative stress in infants undergoing cardiac surgery. *Pediatr Cardiol.* (2016) 37:746–750. doi: 10.1007/s00246-016-1345-3

49. Garca-Montes JA, Caldern-Colmenero J, Casanova M, Zarco E, Fernndez de. la Reguera G, Buenda A. Risk factors for prolonged mechanical ventilation after surgical repair of congenital heart disease .*Archivos de cardiologi'a de Me'xico.* (2005) 75:402–7. Available online at: www.scielo.org.mx/pdf/acm/v75n4/v75n4a4.pdf

frontiers | Frontiers in Cardiovascular Medicine

TYPE Original Research
PUBLISHED 05 December 2022
DOI 10.3389/fcvm.2022.1042996

Check for updates

OPEN ACCESS

EDITED BY
Yanwu Xu,
Baidu, China

REVIEWED BY
Hongliang Yi,
Shanghai Jiao Tong University, China
Xiangdong Tang,
Sichuan University, China

*CORRESPONDENCE
Shinan Wu
wshinana99@163.com
Xiaoyong Ren
cor_renxiaoyong@126.com

†These authors have contributed equally to this work and share first authorship

SPECIALTY SECTION
This article was submitted to Hypertension, a section of the journal Frontiers in Cardiovascular Medicine

RECEIVED 13 September 2022
ACCEPTED 21 November 2022
PUBLISHED 05 December 2022

CITATION
Shi Y, Ma L, Chen X, Li W, Feng Y, Zhang Y, Cao Z, Yuan Y, Xie Y, Liu H, Yin L, Zhao C, Wu S and Ren X (2022) Prediction model of obstructive sleep apnea–related hypertension: Machine learning–based development and interpretation study. *Front. Cardiovasc. Med.* 9:1042996. doi: 10.3389/fcvm.2022.1042996

COPYRIGHT
© 2022 Shi, Ma, Chen, Li, Feng, Zhang, Cao, Yuan, Xie, Liu, Yin, Zhao, Wu and Ren. This is an open-access article distributed under the terms of the Creative Commons Attribution License (CC BY). The use, distribution or reproduction in other forums is permitted, provided the original author(s) and the copyright owner(s) are credited and that the original publication in this journal is cited, in accordance with accepted academic practice. No use, distribution or reproduction is permitted which does not comply with these terms.

Prediction model of obstructive sleep apnea–related hypertension: Machine learning–based development and interpretation study

Yewen Shi[1†], Lina Ma[1†], Xi Chen[1†], Wenle Li[2], Yani Feng[1], Yitong Zhang[1], Zine Cao[1], Yuqi Yuan[1], Yushan Xie[1], Haiqin Liu[1], Libo Yin[3], Changying Zhao[1], Shinan Wu[4*] and Xiaoyong Ren[1*]

[1]Department of Otorhinolaryngology Head and Neck Surgery, The Second Affiliated Hospital of Xi'an Jiaotong University, Xi'an, China, [2]Molecular Imaging and Translational Medicine Research Center, State Key Laboratory of Molecular Vaccinology and Molecular Diagnostics, Xiamen University, Xiamen, China, [3]Department of Otorhinolaryngology Head and Neck Surgery, Xi'an Central Hospital, Xi'an, China, [4]Eye Institute of Xiamen University, School of Medicine, Xiamen University, Xiamen, China

Background: Obstructive sleep apnea (OSA) is a globally prevalent disease closely associated with hypertension. To date, no predictive model for OSA-related hypertension has been established. We aimed to use machine learning (ML) to construct a model to analyze risk factors and predict OSA-related hypertension.

Materials and methods: We retrospectively collected the clinical data of OSA patients diagnosed by polysomnography from October 2019 to December 2021 and randomly divided them into training and validation sets. A total of 1,493 OSA patients with 27 variables were included. Independent risk factors for the risk of OSA-related hypertension were screened by the multifactorial logistic regression models. Six ML algorithms, including the logistic regression (LR), the gradient boosting machine (GBM), the extreme gradient boosting (XGBoost), adaptive boosting (AdaBoost), bootstrapped aggregating (Bagging), and the multilayer perceptron (MLP), were used to develop the model on the training set. The validation set was used to tune the model hyperparameters to determine the final prediction model. We compared the accuracy and discrimination of the models to identify the best machine learning algorithm for predicting OSA-related hypertension. In addition, a web-based tool was developed to promote its clinical application. We used permutation importance and Shapley additive explanations (SHAP) to determine the importance of the selected features and interpret the ML models.

Results: A total of 18 variables were selected for the models. The GBM model achieved the most extraordinary discriminatory ability (area under the receiver

operating characteristic curve = 0.873, accuracy = 0.885, sensitivity = 0.713), and on the basis of this model, an online tool was built to help clinicians optimize OSA-related hypertension patient diagnosis. Finally, age, family history of hypertension, minimum arterial oxygen saturation, body mass index, and percentage of time of SaO_2 < 90% were revealed by the SHAP method as the top five critical variables contributing to the diagnosis of OSA-related hypertension.

Conclusion: We established a risk prediction model for OSA-related hypertension patients using the ML method and demonstrated that among the six ML models, the gradient boosting machine model performs best. This prediction model could help to identify high-risk OSA-related hypertension patients, provide early and individualized diagnoses and treatment plans, protect patients from the serious consequences of OSA-related hypertension, and minimize the burden on society.

KEYWORDS

obstructive sleep apnea, hypertension, machine learning, risk factor, Shapley additive explanations, gradient boosting machine (GBM)

Introduction

Obstructive sleep apnea (OSA) is a sleep disorder characterized by intermittent hypoxemia, autonomic fluctuation, and sleep fragmentation. As of 2019, the prevalence of OSA aged 30–69 years (men and women) in China has reached 24.2%, ranking first in the world (1). Aside from the fact that OSA causes difficult symptoms, many studies demonstrated that OSA is closely associated with many complications, such as cardiovascular diseases, metabolic disorders, and cognitive impairment (2–4). Among them, cardiovascular diseases have received extensive attention because of their serious consequences and high morbidity, especially hypertension. Observational studies have illustrated that 45–68% of subjects with OSA have hypertension (5, 6), and the prevalence of OSA is more than 30% among hypertension patients (7).

Hypertension that is primarily caused or exacerbated by OSA is called OSA-related hypertension after excluding other definite secondary etiologies (e.g., renal artery stenosis, renal parenchymal disease, primary aldosteronism, pheochromocytoma, and Cushing's disease) (8). In addition, OSA-related hypertension is characterized by high rates of masked hypertension, elevated nocturnal blood pressure, a non-dipper pattern of nocturnal hypertension, and an increased blood pressure variability (9). Notably, patients with OSA and hypertension seem to be associated with more severe outcomes. Studies based on ambulatory blood pressure monitoring (ABPM) showed that participants with a non-dipper pattern of nocturnal hypertension and those who have elevated blood pressure at night demonstrate a greater degree of end-organ damage, higher risk of stroke, increased risk of incident heart failure, and increased risk of renal disease progression (10). Regrettably, OSA-related hypertension is easily disregarded by patients.

As for the general population, the reference method for blood pressure testing is primarily an in-office measurement. However, this diagnostic method is unreliable in the OSA population because of the specific characteristics of OSA-related hypertension. Previous studies have shown that among OSA patients, masked hypertension was found in 30% of patients, and white-coat hypertension was found in approximately 33% of patients (11–13). It means that there is a high risk that OSA patients may be underdiagnosed or overdiagnosed with hypertension. The application of ABPM to systematically and correctly assess blood pressure is recommended in clinically normotensive OSA patients (14). However, ABPM is not cost-efficient and often burdensome, and in clinical practice, it seems challenging to propose ABPM to all OSA patients with normal clinic blood pressure. Thus, the necessity of a simple and convenient clinical tool to assess OSA-related hypertension in daily clinical practice is emphasized, which can allow the use of ABPM selectively rather than routinely.

Machine learning (ML) has been widely developed and used in the medical field because of its remarkable performance

Abbreviations: OSA, obstructive sleep apnea; ML, machine learning; AUC, area under the curve; SHAP, Shapley additive explanations; SaO_2, arterial oxygen saturation; OAI, obstructive apnea index; BMI, body mass index; GBM, gradient boosting machine; ABPM, ambulatory blood pressure monitoring; AHI, apnea–hypopnea index; CT90/10, percentage of time of SaO_2 < 90%/10.

in recent years. It can extract information from complex and non-linear data, establish models through science, reveal hidden dependencies between factors and diseases in the big data environment, and help clinicians better understand the diseases (15). Especially in cardiovascular diseases, machine learning has a wide range of applications and satisfactory diagnostic performance. For example, Ward et al. demonstrated that the gradient boosting machine (GBM) model has good discrimination for atherosclerotic cardiovascular disease risk (16). Although ML has gained extensive attention because of its powerful predictive capabilities, it is often criticized for being a black box model, making it hard for clinicians to understand and trust these complex models. Hence, this has limited its widespread use in medical decision-making (17).

Timely blood pressure screening and early accurate identification of OSA-related hypertension are crucial in minimizing the associated negative health effects. Regrettably, no ML models are available to predict the risk of OSA-related hypertension. In this study, we aimed to develop ML-based prediction models for OSA-related hypertension based on available clinical data from patients to identify high-risk patients. In addition, we used Shapley additive explanations (SHAP) (18), a method for interpreting results made by machine learning models, to explore the relationship between features and the risk of OSA-related hypertension. In addition, we further provide individual interpretations of the model's decisions through SHAP. Moreover, we established a web-based risk calculator based on the most predictive maximum likelihood algorithm to promote its clinical application, which provided clinicians with valuable tools for risk assessment in OSA-related hypertension.

Materials and methods

Study design and subjects

This is a retrospective observational study. It retrospectively included the OSA patients admitted to the Department of Otorhinolaryngology—Head and Neck Surgery of the Second Affiliated Hospital of Xi'an Jiaotong University between October 2019 and December 2021. All study subjects underwent nighttime polysomnography or home sleep apnea testing and blood pressure monitoring, additionally, cardiologists assessed their blood pressure. OSA was diagnosed on the basis of apnea–hypopnea index (AHI) $\geq$ 5 events per hour through polysomnography (19). Hypertension was defined as a previous diagnosis with current antihypertensive therapy. Additionally, patients with elevated nocturnal blood pressure who had no history of hypertension were further examined and identified as newly diagnosed with hypertension by a cardiologist with more than 10 years of working experience. The definition of hypertension is described in detail in the **Supplementary material**.

The inclusion criteria were as follows: (1) patients with age $\geq$ 18 years, (2) patients with AHI $\geq$ 5 events per hour, and (3) patients who have not received OSA-related treatment in the past. The exclusion criteria were as follows: (1) patients with incomplete baseline data; (2) patients with disease potentially affecting blood pressure regulation, such as multiple organ dysfunction syndrome, uremia, severe cardiac heart failure, renal, or cardiac transplantation; (3) patients with the most common causes of secondary hypertension, namely, renal parenchymal disease, renovascular diseases, coarctation of the aorta, Cushing's syndrome, primary hyperaldosteronism, pheochromocytoma, hyperthyroidism, and hyperparathyroidism; (4) pregnant women; (5) patients with history of snoring shorter than the duration of hypertension; and (6) patients who were diagnosed with central sleep apnea (central AHI $\geq$ 5 events per hour).

This study was approved by the ethics committee of the Second Affiliated Hospital of Xi'an Jiaotong University (approval no. 2021031). In addition, all patients who participated in the research provided informed consent. The inspection items and processes involved in this study are in line with the Declaration of Helsinki.

Data elements

Twenty-seven relevant clinical indicators were collected, and overall, the 27 candidate variables included were as follows: (1) demographic characteristics, namely, gender, heart disease family history of hypertension, diabetes, hypothyroidism, body mass index (BMI), waist circumference, neck circumference, and age/10; (2) lifestyle behaviors, namely, drinking, smoking, high-salt diet, high-fat diet, poor sleep quality, sedentariness, emotionally stable, mental stress, and smoking amount; and (3) OSA-related medical history and indicators, namely, memory decline, inattention, Epworth Sleepiness Scale (20), course of snoring, course of choking, AHI, obstructive apnea index (OAI), minimum arterial oxygen saturation/10 (minimum SaO_2/10), and percentage of time of SaO_2 < 90%/10 (CT90/10).

Development and validation of prediction models

By comparing the clinical characteristics of the hypertension and non-hypertension groups, the risk factors for predicting OSA-related hypertension were analyzed using the univariate analysis, and they were incorporated into machine learning as characteristic variables. Additionally, they were also used in the multivariate logistic regression analysis to obtain independent predictors associated with OSA-related hypertension.

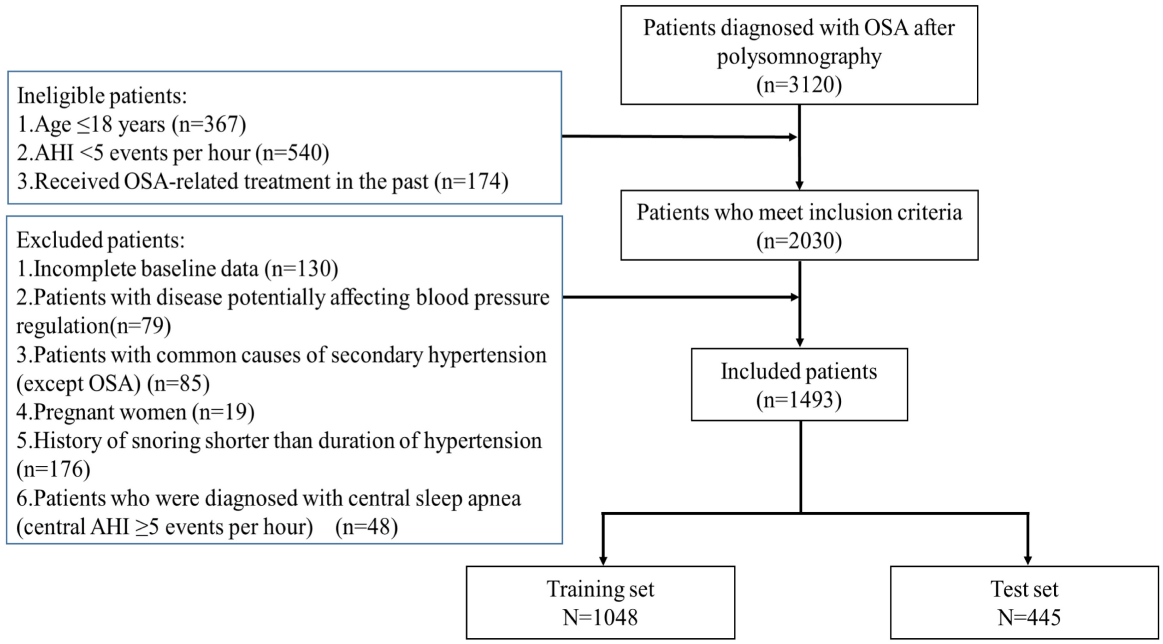


FIGURE 1
Summary of patient inclusion. AHI, apnea–hypopnea index; OSA, obstructive sleep apnea.

All patients were randomly divided into a training set for constructing the predictive model and a test set for the model validation at a ratio of 7:3. The following six representative supervised ML algorithms were used for model construction in the training dataset: adaptive boosting, GBM, multilayer perceptron, bootstrapped aggregating, logistic regression, and extreme gradient boost (21–24). During training, the training cohort internal validation method used 10-fold cross-validation to evaluate the predictive power of each ML classifier in plotting the average area under the receiver operating characteristic curve (AUC). With the use of the validation cohort, the receiver operating characteristics of the six ML models were plotted, and AUC values were calculated to evaluate the predictive ability of the different models in cohorts. By comparing the predictive performance of our ML models, the model with the best predictive performance was selected as the final model. In addition, a confusion matrix was used to evaluate the prediction model performance. Subsequently, on the basis of the best predictive ability model, an online risk calculator that can make predictions using newly entered data of OSA patients was created.

Model interpretation

Shapley additive explanations (SHAP) is a model-agnostic explanation technique based on cooperative game theory that helps interpret the results from a predictive model. The interpretation is based on quantifying the SHAP value for each feature, representing the contribution of a feature to the predicted risk of OSA-related hypertension (25, 26). For each sample, the model produces a prediction value, and the sum or average of the absolute Shapley value of each feature of all individuals is the overall feature importance. Components with large fundamental Shapley values are very important. In addition, the SHAP method also proves each feature value's positive or negative influence on the predicted results, similar to coefficient values in logistic regression. A positive SHAP value indicates that the corresponding feature contributes to a higher risk of the result, whereas a negative SHAP value indicates that the corresponding feature leads to a lower risk of the result. To determine the main predictors of OSA-related hypertension, we identified the importance of ranking features from the final model through the SHAP summary plot and provided individual interpretations of the model's decisions.

Statistical analysis

All analyses and random division of training and validation sets were performed with R software (version 3.6.0). Continuous variables were represented as the median (p25, p75), whereas categorical variables were represented as numbers (n) and proportions (%). The Wilcoxon rank-sum test compared the two groups' differences for continuous variables, and categorical variables were evaluated using the chi-squared test. Logistic regression analysis was used to analyze the relationship between various predictor variables (either categorical or

continuous) and an outcome that is binary (dichotomous). The Python programming language (version 3.8) was also used to develop and evaluate ML models and design network calculators. For model interpretation, the SHAP was implemented using the Python Shap package. $P < 0.05$ was considered statistically significant.

Results

Patient characteristics

After the screening process, a total of 1,493 OSA patients were eligible for the study (**Figure 1**). The baseline characteristics of these patients are summarized in **Table 1**. For the demographic variables, the two groups were significantly different in heart disease, family history of hypertension, diabetes, BMI, waist circumference, neck circumference, and age/10 (all $P < 0.05$). For the lifestyle behavior variables, high-salt diet, poor sleep quality, and smoking amount were significant variables (all $P < 0.05$). For OSA-related medical history and indicators, memory decline, Epworth Sleepiness Scale, course of snoring, course of choking, AHI, OAI, minimum SaO_2/10, and CT90/10 were all significantly different between the two groups (all $P < 0.05$).

Univariate and multivariate logistic regression

Variables with a $P < 0.05$ in the univariate analysis were selected for multivariate logistic regression analysis to identify the independent risk factors of OSA-related hypertension patients (**Table 2**), and all regression coefficients are shown in **Supplementary Table 1**. In addition, the results indicated that family history of hypertension, BMI, age/10, minimum SaO_2/10, and CT90/10 were independent risk factors for OSA-related hypertension (all $P < 0.05$).

Performance of the machine learning algorithm

The average AUC of the six models determined by 10-fold cross-validation is displayed in **Figure 2A**, with the GBM model achieving the best performance (AUC = 0.837). The model validation results based on the validation set are displayed in **Figure 2B**, and the GBM model still exhibited the best performance in predicting OSA-related hypertension (AUC = 0.873). Moreover, we further evaluated the stability and accuracy of GBM through five cross-validations, and the results reveal that the GBM has good stability (average AUC = 0.810 ± 0.048) (**Figure 2C**). The radar plot of the six ML models is shown in **Supplementary Figure 1**. A comparison of model performance on the validation set is shown in **Table 3**. Generally, all models performed satisfactorily in AUC, but not ideally in the sensitivity. Among them, the GBM exhibited the highest sensitivity at 0.713. Because GBM yielded the best results for AUC and sensitivity, we chose the GBM model as the final prediction model and then evaluated it (**Figure 3**). Meanwhile, on the basis of this model, we developed a prediction tool for the web, which can be accessed to further facilitate clinical use through an online risk calculator at https://shimunana-true-ml-vmz425.streamlitapp.com/ (**Figure 4**). The receiver operating characteristic properties of other ML models are shown in **Supplementary Figure 2**.

Model interpretability

To identify the features that influenced the prediction model the most, we illustrated the SHAP summary plot of GBM and the top 15 features of the prediction model in decreasing order (**Figures 5A,B**). The SHAP summary plot shows that age/10, family history of hypertension, minimum SaO_2/10, BMI, and CT90/10 were the five most critical predictive features of the GBM model and had the most significant impact on the prediction results.

Shapley additive explanations (SHAP) values not only could show the contribution of each feature to the final prediction but also could effectively clarify and explain model predictions for individual patients. We provided two living examples to illustrate the role of the SHAP method in describing the machine learning model: a 46-year-old female patient who was diagnosed with OSA but with normal blood pressure and a 54-year-old male patient who was diagnosed with OSA-related hypertension (**Figures 5C,D**). The constructed model predicted the probability of OSA-related hypertension to be 23% and 57%, respectively. The model predicted the outcome as non-OSA-related hypertension for the female patient, which was consistent with the actual outcome (true negative). In addition, the model prediction result was OSA-related hypertension for the male patient, which was consistent with the actual situation (true positive).

Discussion

The present study is the first study to assess the predictive performance of several machine learning algorithms for OSA-related hypertension, obtain a GBM model that can be used to predict OSA-related hypertension clinically, and explain the model. GBM is a commonly used ML algorithm with satisfactory performance in managing large and complex non-linear datasets and avoiding overfitting (27). Subsequently, we designed a network risk calculator based on the GBM model to

TABLE 1 Demographic and clinical characteristics.

Characteristic	Total (n = 1,493)	Non-hypertension (n = 1,134)	Hypertension (n = 359)	P value
Gender, n (%)				0.143
Female	224 (15.0)	161 (14.2)	63 (17.5)	
Male	1,269 (85.0)	973 (85.8)	296 (82.5)	
Heart disease, n (%)				< 0.001
No	1,394 (93.4)	1,085 (95.7)	309 (86.1)	
Yes	99 (6.6)	49 (4.3)	50 (13.9)	
Family history of hypertension, n (%)				< 0.001
No	1,063 (71.2)	905 (79.8)	158 (44.0)	
Yes	430 (28.8)	229 (20.2)	201 (56.0)	
Diabetes, n (%)				< 0.001
No	1,437 (96.2)	1,113 (98.1)	324 (90.3)	
Yes	56 (3.8)	21 (1.9)	35 (9.7)	
Hypothyroidism, n (%)				0.278
No	1,464 (98.1)	1,109 (97.8)	355 (98.9)	
Yes	29 (1.9)	25 (2.2)	4 (1.1)	
Body mass index, median (Q1, Q3)	26.7 (24.6, 29.4)	26.2 (24.4, 28.7)	28.1 (25.9, 30.5)	< 0.001
Waist circumference, median (Q1, Q3)	98.0 (92.0, 105.0)	97.0 (92.0, 103.0)	102.0 (95.0, 108.0)	< 0.001
Neck circumference, median (Q1, Q3)	40.0 (37.5, 42.0)	39.0 (37.0, 41.0)	41.0 (38.0, 43.0)	< 0.001
Age/10, median (Q1, Q3)	4.0 (3.3, 4.9)	3.7 (3.2, 4.6)	4.8 (4.0, 5.6)	< 0.001
Drinking, n (%)				0.965
No	901 (60.3)	684 (60.3)	217 (60.4)	
Yes	592 (39.7)	450 (39.7)	142 (39.6)	
Smoking, n (%)				0.112
No	834 (55.9)	647 (57.1)	187 (52.1)	
Yes	659 (44.1)	487 (42.9)	172 (47.9)	
High-salt diet, n (%)				< 0.05
No	1,124 (75.3)	869 (76.6)	255 (71.0)	
Yes	369 (24.7)	265 (23.4)	104 (29.0)	
High-fat diet, n (%)				0.069
No	1,049 (70.3)	811 (71.5)	238 (66.3)	
Yes	444 (29.7)	323 (28.5)	121 (33.7)	
Poor sleep quality, n (%)				< 0.05
No	808 (54.1)	634 (55.9)	174 (48.5)	
Yes	685 (45.9)	500 (44.1)	185 (51.5)	
Sedentariness, n (%)				0.182
No	573 (38.4)	424 (37.4)	149 (41.5)	
Yes	920 (61.6)	710 (62.6)	210 (58.5)	
Emotionally stable, n (%)				0.157
No	416 (27.9%)	305 (26.9)	111 (30.9)	
Yes	1,077 (72.1%)	829 (73.1)	248 (69.1)	
Mental stress, n (%)				0.099
No	1,092 (73.1)	842 (74.3)	250 (69.6)	
Yes	401 (26.9)	292 (25.7)	109 (30.4)	
Smoking amount, median (Q1, Q3)	0.0 (0.0, 1.0)	0.0 (0.0, 1.0)	0.0 (0.0, 1.0)	< 0.05
Memory decline, n (%)				< 0.01
No	549 (36.8)	439 (38.7)	110 (30.6)	
Yes	944 (63.2)	695 (61.3)	249 (69.4)	
Inattention, n (%)				0.744
No	687 (46.0)	525 (46.3)	162 (45.1)	
Yes	806 (54.0)	609 (53.7)	197 (54.9)	
Epworth sleepiness scale, median (Q1, Q3)	9 (6, 14)	8.5 (5, 13)	11 (7, 16)	< 0.001
Course of snoring, median (Q1, Q3)	9.0 (4.0, 12.0)	8.0 (3.6, 10.0)	10.0 (6.0, 20.0)	< 0.001
Course of choking, median (Q1, Q3)	3.0 (1.0, 6.0)	2.0 (1.0, 5.0)	4.0 (1.0, 8.0)	< 0.001
AHI, median (Q1, Q3)	46.2 (23.0, 67.9)	41.8 (19.8, 66.1)	57.7 (33.1, 70.8)	< 0.001
OAI, median (Q1, Q3)	21.1 (5.2, 46.6)	17.5 (4.2, 43.5)	32.5 (14.7, 53.1)	< 0.001
Minimum SaO_2/10, median (Q1, Q3)	7.6 (6.5, 8.4)	7.9 (6.8, 8.5)	6.9 (5.7, 7.8)	< 0.001
CT90/10, median (Q1, Q3)	0.7 (0.1, 3.0)	0.5 (0.1, 2.6)	1.5 (0.3, 4.0)	< 0.001

AHI, apnea–hypopnea index; OAI, obstructive apnea index; SaO_2, arterial oxygen saturation; CT90/10, percentage of time of SaO_2 < 90%/10.

TABLE 2 Univariate analysis and multivariate logistic regression analysis of variables.

		Univariate analysis		Multivariate analysis	
Characteristics	**Category**	**OR (95% CI)**	***P* value**	**OR (95% CI)**	***P* value**
Gender	Female	Ref	Ref	Ref	Ref
	Male	0.777 (0.565–1.070)	0.122	–	–
Heart disease	No	Ref	Ref	Ref	Ref
	Yes	3.583 (2.369–5.419)	< 0.001	1.437 (0.845–2.446)	0.181
Family history of hypertension	No	Ref	Ref	Ref	Ref
	Yes	5.027 (3.9–6.48)	< 0.001	5.388 (3.975–7.302)	< 0.001
Diabetes	No	Ref	Ref	Ref	Ref
	Yes	5.725 (3.287–9.973)	< 0.001	1.849 (0.934–3.662)	0.078
Hypothyroidism	No	Ref	Ref	Ref	Ref
	Yes	0.500 (0.173–1.446)	0.201	–	–
Body mass index	–	1.148 (1.109–1.188)	< 0.001	1.121 (1.038–1.210)	< 0.01
Waist circumference	–	1.051 (1.039–1.064)	< 0.001	1.014 (0.984–1.045)	0.368
Neck circumference	–	1.099 (1.061–1.138)	< 0.001	1.017 (0.953–1.085)	0.607
Age/10	–	1.901 (1.707–2.118)	< 0.001	2.136 (1.834–2.487)	< 0.001
Drinking	No	Ref	Ref	Ref	Ref
	Yes	0.995 (0.780–1.268)	0.965	–	–
Smoking	No	Ref	Ref	Ref	Ref
	Yes	1.222 (0.963–1.551)	0.099	–	–
High-salt diet	No	Ref	Ref	Ref	Ref
	Yes	1.337 (1.025–1.746)	< 0.05	1.083 (0.776–1.511)	0.639
High-fat diet	No	Ref	Ref	Ref	Ref
	Yes	1.277 (0.99–1.646)	0.060	–	–
Poor sleep quality	No	Ref	Ref	Ref	Ref
	Yes	1.348 (1.063–1.710)	< 0.05	1.058 (0.784–1.428)	0.711
Sedentariness	No	Ref	Ref	Ref	Ref
	Yes	0.842 (0.661–1.072)	0.163	–	–
Emotionally stable	No	1.217 (0.939–1.577)	0.139	–	–
	Yes	Ref	Ref	Ref	Ref
Mental stress	No	Ref	Ref	Ref	Ref
	Yes	1.257 (0.968–1.633)	0.086	–	–
Smoking amount	–	1.383 (1.109–1.723)	< 0.01	1.152 (0.869–1.527)	0.325
Memory decline	No	Ref	Ref	Ref	Ref
	Yes	1.430 (1.109–1.844)	< 0.01	1.070 (0.777–1.474)	0.679
Inattention	No	Ref	Ref	Ref	Ref
	Yes	1.048 (0.826–1.331)	0.698	–	–
Epworth sleepiness scale	–	1.070 (1.048–1.093)	< 0.001	1.021 (0.993–1.049)	0.145
Course of snoring	–	1.068 (1.051–1.085)	< 0.001	1.009 (0.986–1.033)	0.443
Course of choking	–	1.064 (1.041–1.088)	< 0.001	1.004 (0.971–1.037)	0.825
AHI	–	1.014 (1.009–1.018)	< 0.001	0.994 (0.982–1.006)	0.341
OAI	–	1.014 (1.010–1.019)	< 0.001	1.007 (0.995–1.019)	0.282
Minimum SaO_2/10	–	0.638 (0.584–0.697)	< 0.001	0.552 (0.456–0.668)	< 0.001
CT90/10	–	1.160 (1.104–1.219)	< 0.001	0.842 (0.751–0.944)	< 0.01

AHI, apnea–hypopnea index; OAI, obstructive apnea index; SaO_2, arterial oxygen saturation; CT90/10, percentage of time of SaO_2 < 90%/10; OR, odds ratio; 95% CI, 95% credible interval.

estimate the probability of hypertension in individuals with OSA so as to help clinicians make targeted diagnoses and treatment plans, making precision medicine possible.

As hypothesized, our multivariate logistic regression suggested that BMI, age/10, and minimum SaO_2/10 were significant independent risk factors for OSA-related

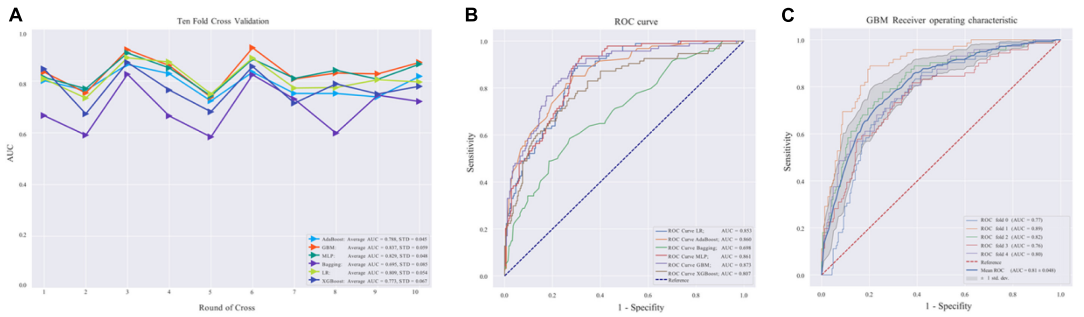


FIGURE 2
(A) Area under the curve (AUC) values of 10-fold cross-validation. **(B)** Validation of machine learning algorithms. **(C)** Receiver operating characteristic curve in the gradient boosting machine (GBM) model. AdaBoost, adaptive boosting; LR, logistic regression; Bagging, bootstrapped aggregating; MLP, multilayer perceptron; GBM, gradient boosting machine; XGBoost, extreme gradient boost; AUC, average area under the curve; ROC, receiver operating characteristic. AUC is used as an indicator of performance, the GBM model achieved the best predictive performance, and the Bagging model had the lowest predictive performance.

hypertension, which converges with previous research. Pan et al. found that among police officers in southern China, the prevalence of OSA-related hypertension was associated with the age of the patients. However, their study population was small and occupation-specific (28). Furthermore, Natsios and colleagues reported that age, BMI, comorbidity, daytime SaO_2, and indices of hypoxia during sleep were estimated to be the most precise predictors of hypertension (29). Additionally, because of the differences in study design and study population, we found some different results from previous studies. Family history of hypertension and CT90/10 were also found to be risk factors for OSA-related hypertension in our study. Interestingly, to further confirm how input factors contribute to the model, we calculated SHAP feature importance and feature effects. The importance of variables also showed that the BMI, age/10, and minimum SaO_2/10, family history of hypertension, and CT90/10 were the most important input parameters that contribute to the predicted risk of OSA-related hypertension. This strongly demonstrates that these five variables were significant contributors to OSA-related hypertension, and proved the accuracy and reliability of the GBM model. Surely, a prospective study and animal experiments are essential to confirm the accuracy and reliability of our proposed model.

Interestingly, in addition to identifying several known risk factors, multivariate logistic regression and SHAP analysis also found that CT90/10, a variable that had been overlooked in previous cardiovascular studies, also plays an important role in OSA-related hypertension. Previous studies have shown a significant association between CT90 and Coronary Artery Calcium, cerebral small vessel disease and diabetic nephropathy (30–32), but the relationship between CT90 and hypertension has not been explored. The underlying causes by OSA and hypertension have not been fully elucidated. A few pathophysiological mechanisms have been suggested to participate in it, such as elevated sympathetic nervous system activity, renin-angiotensin aldosterone system activity, endothelial dysfunction, inflammation, and metabolic dysregulation (33). And López-Cano et al. showed a positive and significant association between the nocturnal concentration of urine metanephrines and the CT90 (34), suggesting that CT90 may influence sympathetic activity. And this also explains the important role of CT90 in OSA-related hypertension, and needs more attention in the future. Surprisingly, in our statistical model, AHI, as a diagnostic indicator of adult OSA, participates weakly. Whether there is a dose–response relationship between the severity of OSA and the cumulative incidence of hypertension has been debated. The Wisconsin Sleep Cohort Study discovered a dose–response association between OSA and the presence of hypertension 4 years later (35). At the same time, the Sleep Heart Health Study and the Victoria Sleep Cohort Study found that the relationship between hypertension and OSA was no longer significant after age and BMI were controlled for O'Connor et al. (36) and Cano-Pumarega et al. (37). Additionally, AHI is a simple measure of the average number of respiratory events (apneas and hypopneas) per hour of sleep, and it does not reflect adequately the various phenotypes and comorbidities of OSA. Our results

TABLE 3 Performance comparison of six machine learning (ML) models.

Model	F1 score	AUC	Accuracy	Sensitivity	Specificity
AdaBoost	0.757	0.860	0.832	0.553	0.925
LR	0.716	0.853	0.810	0.468	0.925
Bagging	0.481	0.698	0.759	0.353	0.916
MLP	0.719	0.861	0.807	0.489	0.914
GBM	0.841	0.873	0.885	0.713	0.943
XGBoost	0.719	0.807	0.807	0.489	0.914

AUC, area under the curve; AdaBoost, adaptive boosting; LR, logistic regression; Bagging, bootstrapped aggregating; MLP, multilayer perceptron; GBM, gradient boosting machine; XGBoost, extreme gradient boost; ML, machine learning.

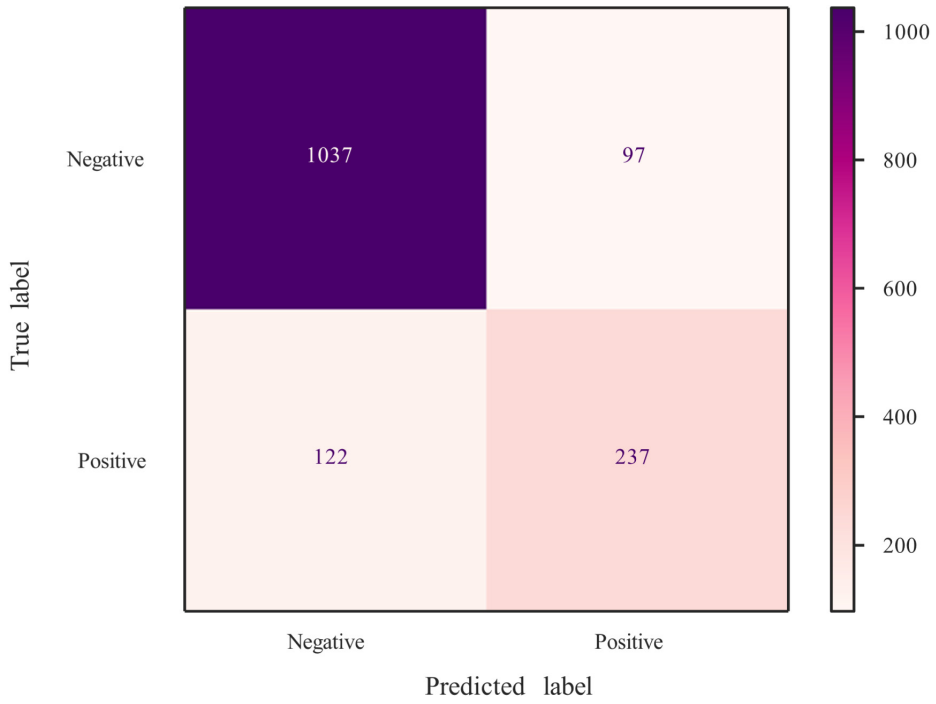


FIGURE 3
Confusion matrix of GBM. GBM, gradient boosting machine.

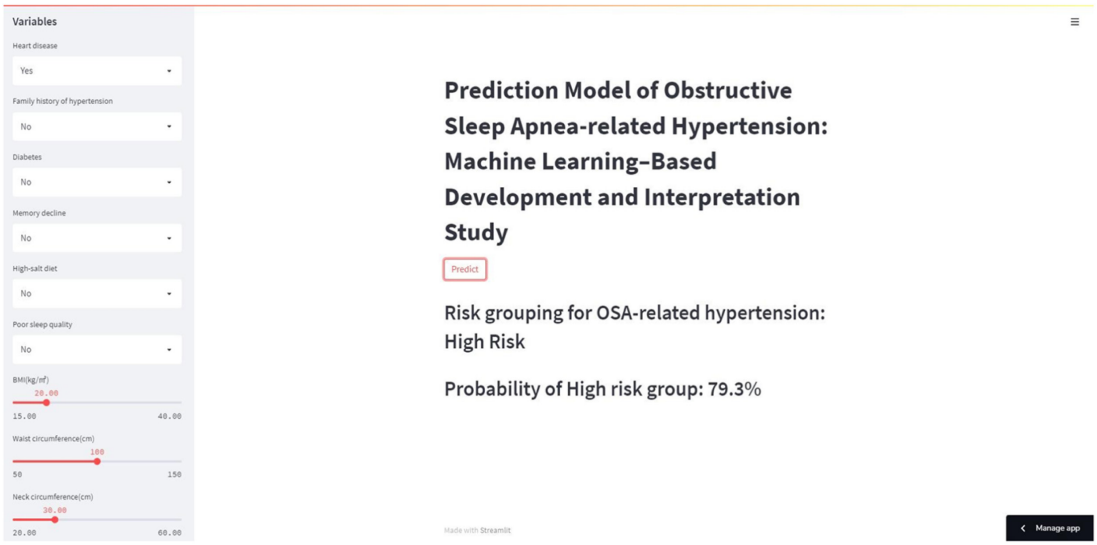


FIGURE 4
Web calculator for predicting OSA-related hypertension. OSA, obstructive sleep apnea.

disclosed that blood oxygen indicators (e.g., minimum SaO_2/10 and CT90/10) might be better predictors of OSA-related hypertension than AHI.

Notably, the risk for OSA-related hypertension is increased most by family history of hypertension in the multivariate logistic regression, followed by age/10. However, the SHAP analysis showed that minimum SaO_2/10 has the highest predictive value for OSA-related hypertension. The discrepancy between multivariate logistic regression and SHAP values can be explained by the prevalence of a variable. Odds ratios were calculated only for patients associated with this variable, but the mean SHAP value for all patients was calculated. In addition, the

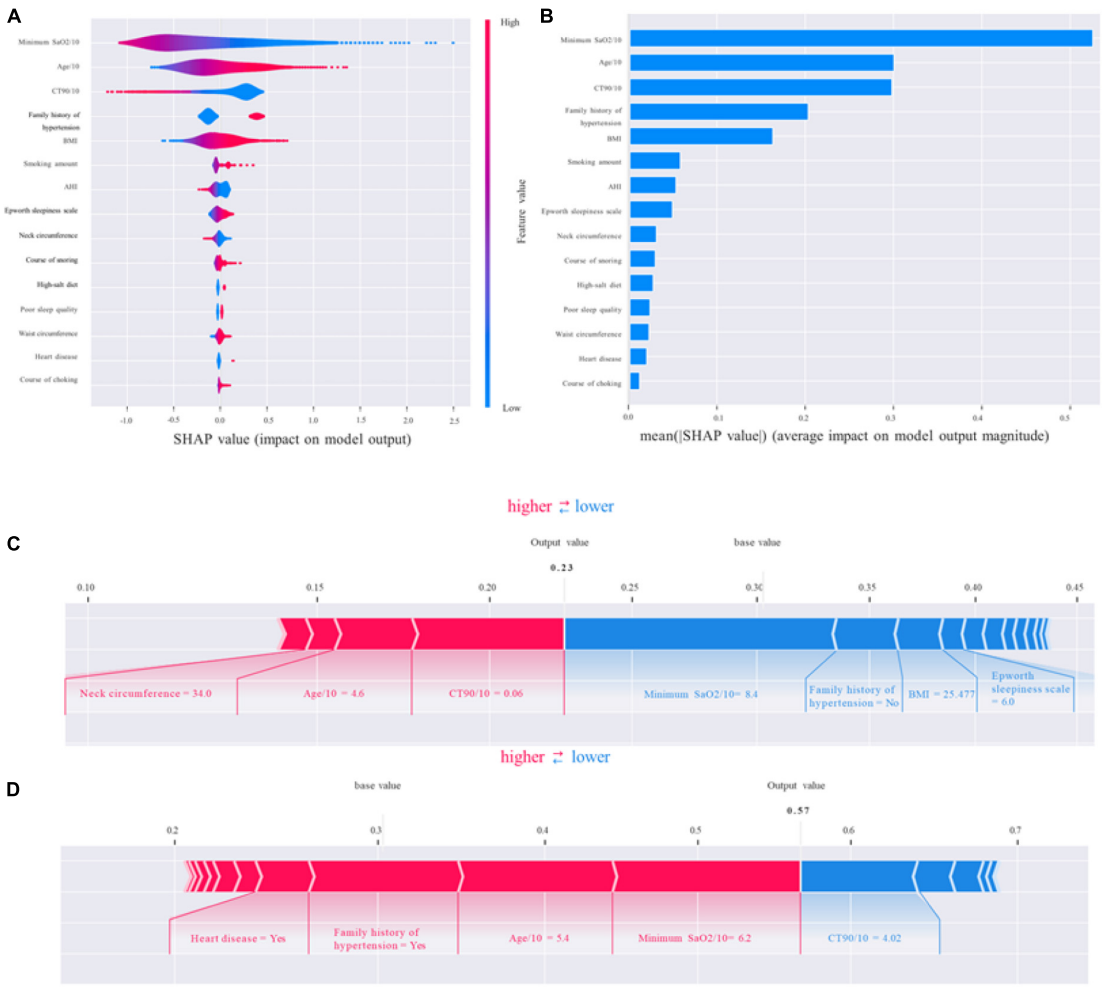


FIGURE 5
Shapley additive explanations (SHAP). **(A,B)** The standard and classified bar charts of the SHAP summary plots showed the influence of each parameter on the gradient boosting machine (GBM) model. **(C,D)** SHAP model explanation of two typical predictions. The features are ranked according to the sum of the SHAP values for all patients, and the SHAP values are used to show the distribution of the effect of each feature on the GBM model outputs. Each dot represents a case in the dataset. The color of a dot indicates the value of the feature, with blue indicating the lowest range and red the highest range. The horizontal axis shows the corresponding SHAP value of the feature. A positive SHAP value contributes to the prediction of rupture and vice versa. SHAP, Shapley additive explanations; GBM, gradient boosting machine; SaO_2, arterial oxygen saturation; BMI, body mass index; AHI, apnea–hypopnea index; CT90/10, percentage of time of SaO_2 < 90%/10.

average SHAP value was further used to evaluate the importance of features and rank them. Hence, variables with low impact and high prevalence will have low odds ratios but high SHAP values.

In our study, full integration of the standard clinical variables with Polysomnography parameters was performed during the construction of the ML model. The model can thus predict OSA-related hypertension risk stratification for the patient, using all relevant covariates rather than individual measures. Our approach was also validated with repeated 10-fold cross-validation to provide a robust estimation of prediction accuracy with minimal bias. The six models performed well, with AUC ranging from 0.698 to 0.873 and sensitivity from 0.353 to 0.713 in the test dataset. And the GBM prediction model with the highest AUC, accuracy, and sensitivity was identified as the final model for this study and clinical use. The GBM model with 0.873 AUC and 0.713 sensitivity proves good discrimination and stability. What's more, we introduce the Shapley value to explain the GBM model. SHAP is a model-independent interpretation technique that interprets black box models globally and locally, and can provide a rational explanation for the prediction, which can significantly enhance the confidence of clinicians in the model.

However, despite our best efforts to improve it, this study still has some limitations. First, this is a single-center retrospective study, and the performance of machine learning algorithms may vary for datasets with different distributions

of patient characteristics and various institutions. Therefore, more patients from multiple sources are required to validate our model's robustness and repeatability in the future. Second, the undesirable sensitivity may be that the ML algorithm learns from input features, and some discreet relationships may have been lost because of unknown or disregarded features not registered by doctors. In the future, we will conduct prospective validation based on this model, continue to explore crucial risk factors for OSA-related hypertension, and modify the model further to improve the accuracy and reliability of the GBM prediction model.

Conclusion

We established a risk prediction model for OSA-related hypertension patients using the ML method and demonstrated that the GBM model performs best among the six ML models. This prediction model could help to identify high-risk OSA-related hypertension patients, provide early and individualized diagnoses and treatment plans, protect patients from the serious consequences of OSA-related hypertension, and reduce the burden on society.

Data availability statement

The raw data supporting the conclusions of this article will be made available by the authors, without undue reservation.

Ethics statement

The studies involving human participants were reviewed and approved by the Ethics Committee of The Second Affiliated Hospital of Xi'an Jiaotong University (approval no. 2021031). Written informed consent for participation was not required for this study in accordance with the national legislation and the institutional requirements.

Author contributions

YS, SW, and XR designed the research. XC and LM wrote the manuscript. YF, YY, HL, and LY collected the data. YX, ZC, and CZ performed data curation. YZ, LM, and WL analyzed and processed the data. XR directed the research and the guarantor of the manuscript and takes full responsibility for the integrity of the work, from its inception to the published manuscript. All authors reviewed the results and approved the final version of the manuscript.

Funding

This work was supported by the National Natural Science Foundation of China (grant no. 62076198) and the Key Research and Development Program in the Social Development Field of Shaanxi, China (grant nos. 2020GXLH-Y005 and 2021SF-286).

Acknowledgments

We wish to thank all who volunteered to participate in this study.

Conflict of interest

The authors declare that the research was conducted in the absence of any commercial or financial relationships that could be construed as a potential conflict of interest.

Publisher's note

All claims expressed in this article are solely those of the authors and do not necessarily represent those of their affiliated organizations, or those of the publisher, the editors and the reviewers. Any product that may be evaluated in this article, or claim that may be made by its manufacturer, is not guaranteed or endorsed by the publisher.

Supplementary material

The Supplementary Material for this article can be found online at: https://www.frontiersin.org/articles/10.3389/fcvm.2022.1042996/full#supplementary-material

References

1. Benjafield AV, Ayas NT, Eastwood PR, Heinzer R, Ip MSM, Morrell MJ, et al. Estimation of the global prevalence and burden of obstructive sleep apnoea: a literature-based analysis. *Lancet Respir Med.* (2019) 7:687–98.

2. Shi Y, Luo H, Liu H, Hou J, Feng Y, Chen J, et al. Related biomarkers of neurocognitive impairment in children with obstructive sleep apnea. *Int J Pediatr Otorhinolaryngol.* (2019) 116:38–42. doi: 10.1016/j.ijporl.2018.10.015

3. Shi Y, Feng Y, Chen X, Ma L, Cao Z, Shang L, et al. Serum neurofilament light reflects cognitive dysfunctions in children with obstructive sleep apnea. *BMC Pediatr.* (2022) 22:449. doi: 10.1186/s12887-022-03514-9

4. Yeghiazarians Y, Jneid H, Tietjens JR, Redline S, Brown DL, El-Sherif N, et al. Obstructive sleep apnea and cardiovascular disease: a scientific statement from the American heart association. *Circulation.* (2021) 144:e56–67. doi: 10.1161/CIR.0000000000000988

5. Kiely JL, McNicholas WT. Cardiovascular risk factors in patients with obstructive sleep apnoea syndrome. *Eur Respir J.* (2000) 16:128–33. doi: 10.1034/j.1399-3003.2000.16a23.x

6. Millman RP, Redline S, Carlisle CC, Assaf AR, Levinson PD. Daytime hypertension in obstructive sleep apnea. Prevalence and contributing risk factors. *Chest.* (1991) 99:861–6. doi: 10.1378/chest.99.4.861

7. Worsnop CJ, Naughton MT, Barter CE, Morgan TO, Anderson AI, Pierce RJ. The prevalence of obstructive sleep apnea in hypertensives. *Am J Respir Crit Care Med.* (1998) 157:111–5. doi: 10.1164/ajrccm.157.1.9609063

8. HPCO Chinese. Medical association expert consensus on clinical diagnosis and treatment of obstructive sleep apnea-related hypertension. *Chin J Pract Intern Med.* (2013).

9. Kario K, Hettrick DA, Prejbisz A, Januszewicz A. Obstructive sleep apnea-induced neurogenic nocturnal hypertension: a potential role of renal denervation? *Hypertension.* (2021) 77:1047–60. doi: 10.1161/HYPERTENSIONAHA.120.16378

10. Ahmad M, Makati D, Akbar S. Review of and updates on hypertension in obstructive sleep apnea. *Int J Hypertens.* (2017) 2017:1848375. doi: 10.1155/2017/1848375

11. Pio-Abreu A, Moreno H Jr, Drager LF. Obstructive sleep apnea and ambulatory blood pressure monitoring: current evidence and research gaps. *J Hum Hypertens.* (2021) 35:315–24. doi: 10.1038/s41371-020-00470-8

12. Baguet JP, Lévy P, Barone-Rochette G, Tamisier R, Pierre H, Peeters M, et al. Masked hypertension in obstructive sleep apnea syndrome. *J Hypertens.* (2008) 26:885–92. doi: 10.1097/HJH.0b013e3282f55049

13. García-Río F, Pino JM, Alonso A, Arias MA, Martínez I, Alvaro D, et al. White coat hypertension in patients with obstructive sleep apnea-hypopnea syndrome. *Chest.* (2004) 125:817–22. doi: 10.1378/chest.125.3.817

14. Parati G, Lombardi C, Hedner J, Bonsignore MR, Grote L, Tkacova R, et al. Recommendations for the management of patients with obstructive sleep apnoea and hypertension. *Eur Respir J.* (2013) 41:523–38. doi: 10.1183/09031936.00226711

15. Schwalbe N, Wahl B. Artificial intelligence and the future of global health. *Lancet.* (2020) 395:1579–86. doi: 10.1016/S0140-6736(20)30226-9

16. Ward A, Sarraju A, Chung S, Li J, Harrington R, Heidenreich P, et al. Machine learning and atherosclerotic cardiovascular disease risk prediction in a multi-ethnic population. *NPJ Digit Med.* (2020) 3:125. doi: 10.1038/s41746-020-00331-1

17. Molnar C. *Interpretable Machine Learning.* Morrisville: Lulu.com (2020).

18. Lundberg SM, Lee S-I. A unified approach to interpreting model predictions. In: Guyon I, Von Luxburg U, Bengio S, Wallach H, Fergus R, Vishwanathan S, et al. editors. *Advances in Neural Information Processing Systems 30.* San Jose, CA: Curran Associates, Inc (2017).

19. Sateia MJ. International classification of sleep disorders-third edition: highlights and modifications. *Chest.* (2014) 146:1387–94. doi: 10.1378/chest.14-0970

20. Johns MW. A new method for measuring daytime sleepiness: the epworth sleepiness scale. *Sleep.* (1991) 14:540–5. doi: 10.1093/sleep/14.6.540

21. Chen T, Guestrin C. X: a scalable tree boosting system. *Proceedings of the 22nd ACM SIGKDD International Conference on Knowledge Discovery and Data Mining-KDD 2016.* San Francisco, CA: (2016). p. 785–94. doi: 10.1145/2939672.2939785

22. Singh A, Thakur N, Sharma A. A review of supervised machine learning algorithms. *2016 3rd International Conference on Computing for Sustainable Global Development (INDIACom).* Piscataway: IEEE (2016). p. 1310–5.

23. Ngiam KY, Khor IW. Big data and machine learning algorithms for health-care delivery. *Lancet Oncol.* (2019) 20:e262–73. doi: 10.1016/S1470-2045(19)30149-4

24. Zhang Z, Zhao Y, Canes A, Steinberg D, Lyashevska O. Predictive analytics with gradient boosting in clinical medicine. *Ann Transl Med.* (2019) 7:152. doi: 10.21037/atm.2019.03.29

25. Rodríguez-Pérez R, Bajorath J. Interpretation of compound activity predictions from complex machine learning models using local approximations and shapley values. *J Med Chem.* (2020) 63:8761–77. doi: 10.1021/acs.jmedchem.9b01101

26. Lundberg SM, Erion G, Chen H, DeGrave A, Prutkin JM, Nair B, et al. From local explanations to global understanding with explainable AI for trees. *Nat Mach Intell.* (2020) 2:56–67. doi: 10.1038/s42256-019-0138-9

27. Sheridan RP, Wang WM, Liaw A, Ma J, Gifford EM. Extreme gradient boosting as a method for quantitative structure-activity relationships. *J Chem Inf Model.* (2016) 56:2353–60. doi: 10.1021/acs.jcim.6b00591

28. Pan M, Ou Q, Chen B, Hong Z, Liu H. Risk factors for obstructive sleep apnea-related hypertension in police officers in Southern China. *J Thorac Dis.* (2019) 11:4169–78. doi: 10.21037/jtd.2019.09.83

29. Natsios G, Pastaka C, Vavougios G, Zarogiannis SG, Tsolaki V, Dimoulis A, et al. Age, body mass index, and daytime and nocturnal hypoxia as predictors of hypertension in patients with obstructive sleep apnea. *J Clin Hypertens.* (2016) 18:146–52. doi: 10.1111/jch.12645

30. Liu X, Lam DC, Mak HK, Ip MS, Lau KK. Associations of sleep apnea risk and oxygen desaturation indices with cerebral small vessel disease burden in patients with stroke. *Front Neurol.* (2022) 13:956208. doi: 10.3389/fneur.2022.956208

31. Seo MY, Lee SH, Hong SD, Chung SK, Kim HY. Hypoxemia during sleep and the progression of coronary artery calcium. *Cardiovasc Toxicol.* (2021) 21:42–8. doi: 10.1007/s12012-020-09593-3

32. Zhang R, Zhang P, Zhao F, Han X, Ji L. Association of diabetic microvascular complications and parameters of obstructive sleep apnea in patients with type 2 diabetes. *Diabetes Technol Ther.* (2016) 18:415–20. doi: 10.1089/dia.2015.0433

33. Salman LA, Shulman R, Cohen JB. Obstructive sleep apnea, hypertension, and cardiovascular risk: epidemiology, pathophysiology, and management. *Curr Cardiol Rep.* (2020) 22:6. doi: 10.1007/s11886-020-1257-y

34. López-Cano C, Gutiérrez-Carrasquilla L, Sánchez E, González J, Yeramian A, Martí R, et al. Sympathetic hyperactivity and sleep disorders in individuals with type 2 diabetes. *Front Endocrinol.* (2019) 10:752. doi: 10.3389/fendo.2019.00752

35. Peppard PE, Young T, Palta M, Skatrud J. Prospective study of the association between sleep-disordered breathing and hypertension. *N Engl J Med.* (2000) 342:1378–84. doi: 10.1056/NEJM200005113421901

36. O'Connor GT, Caffo B, Newman AB, Quan SF, Rapoport DM, Redline S, et al. Prospective study of sleep-disordered breathing and hypertension: the Sleep Heart Health Study. *Am J Respir Crit Care Med.* (2009) 179:1159–64. doi: 10.1164/rccm.200712-1809OC

37. Cano-Pumarega I, Durán-Cantolla J, Aizpuru F, Miranda-Serrano E, Rubio R, Martínez-Null C, et al. Obstructive sleep apnea and systemic hypertension: longitudinal study in the general population: the Vitoria sleep cohort. *Am J Respir Crit Care Med.* (2011) 184:1299–304. doi: 10.1164/rccm.201101-0130OC

frontiers | Frontiers in Cardiovascular Medicine

TYPE Original Research
PUBLISHED 23 December 2022
DOI 10.3389/fcvm.2022.1053697

Check for updates

OPEN ACCESS

EDITED BY
Guangdong Yang,
Laurentian University, Canada

REVIEWED BY
Francesco Ferrara,
Ospedali Riuniti San Giovanni di Dio e Ruggi d'Aragona, Italy
Ruihuan Yu,
Yale University, United States

*CORRESPONDENCE
Yulong Liu
✉ 22646911@qq.com
Xiaobian Dong
✉ dongxiaobian0317@163.com
Qingsong Hu
✉ hqssyshospital@163.com

†These authors have contributed equally to this work and share first authorship

SPECIALTY SECTION
This article was submitted to Cardiovascular Genetics and Systems Medicine, a section of the journal Frontiers in Cardiovascular Medicine

RECEIVED 26 September 2022
ACCEPTED 05 December 2022
PUBLISHED 23 December 2022

CITATION
Guo Y, Jiang H, Wang J, Li P, Zeng X, Zhang T, Feng J, Nie R, Liu Y, Dong X and Hu Q (2022) 5mC modification patterns provide novel direction for early acute myocardial infarction detection and personalized therapy. *Front. Cardiovasc. Med.* 9:1053697. doi: 10.3389/fcvm.2022.1053697

COPYRIGHT
© 2022 Guo, Jiang, Wang, Li, Zeng, Zhang, Feng, Nie, Liu, Dong and Hu. This is an open-access article distributed under the terms of the Creative Commons Attribution License (CC BY). The use, distribution or reproduction in other forums is permitted, provided the original author(s) and the copyright owner(s) are credited and that the original publication in this journal is cited, in accordance with accepted academic practice. No use, distribution or reproduction is permitted which does not comply with these terms.

5mC modification patterns provide novel direction for early acute myocardial infarction detection and personalized therapy

Yiqun Guo[1†], Hua Jiang[1†], Jinlong Wang[2†], Ping Li[2†], Xiaoquan Zeng[3], Tao Zhang[2], Jianyi Feng[2], Ruqiong Nie[4], Yulong Liu[5*], Xiaobian Dong[2*] and Qingsong Hu[2*]

[1]Department of Interventional Radiology and Vascular, Guangzhou Women and Children's Medical Center, The Affiliated Hospital of Guangzhou Medical University, Guangzhou, Guangdong, China, [2]Department of Cardiology, The First Affiliated Hospital of Jinan University, Guangzhou, Guangdong, China, [3]Department of Cardiology, Xinfeng County People's Hospital, Shaoguan, Guangdong, China, [4]Department of Cardiology, Sun Yat-sen Memorial Hospital, Sun Yat-sen University, Guangzhou, Guangdong, China, [5]Department of Intervention and Vascular Surgery, The First Affiliated Hospital of Jinan University, Guangzhou, Guangdong, China

Background: Most deaths from coronary artery disease (CAD) are due to acute myocardial infarction (AMI). There is an urgent need for early AMI detection, particularly in patients with stable CAD. 5-methylcytosine (5mC) regulatory genes have been demonstrated to involve in the progression and prognosis of cardiovascular diseases, while little research examined 5mC regulators in CAD to AMI progression.

Method: Two datasets (GSE59867 and GSE62646) were downloaded from Gene Expression Omnibus (GEO) database, and 21 m5C regulators were extracted from previous literature. Dysregulated 5mC regulators were screened out by "limma." The least absolute shrinkage and selection operator (LASSO) and support vector machine recursive feature elimination (SVM-RFE) algorithm were employed to identify hub 5mC regulators in CAD to AMI progression, and 43 clinical samples (Quantitative real-time PCR) were performed for expression validation. Then a logistic model was built to construct 5mC regulator signatures, and a series of bioinformatics algorithms were performed for model validation. Besides, 5mC-associated molecular clusters were studied *via* unsupervised clustering analysis, and correlation analysis between immunocyte and 5mC regulators in each cluster was conducted.

Results: Nine hub 5mC regulators were identified. A robust model was constructed, and its prominent classification accuracy was verified *via* ROC curve analysis (area under the curve [AUC] = 0.936 in the training cohort and AUC = 0.888 in the external validation cohort). Besides, the clinical effect of the model was validated by decision curve analysis. Then, 5mC modification

clusters in AMI patients were identified, along with the immunocyte infiltration levels of each cluster. The correlation analysis found the strongest correlations were TET3—Mast cell in cluster-1 and TET3-MDSC in cluster-2.

Conclusion: Nine hub 5mC regulators (*DNMT3B*, *MBD3*, *UHRF1*, *UHRF2*, *NTHL1*, *SMUG1*, *ZBTB33*, *TET1*, and *TET3*) formed a diagnostic model, and concomitant results unraveled the critical impact of 5mC regulators, providing interesting epigenetics findings in AMI population vs. stable CAD.

KEYWORDS

acute myocardial infarction, coronary heart disease, epigenetics, bioinformatics, 5mC

1 Introduction

Acute myocardial infarction (AMI) continues to be a common cardiac emergency incidence with significant morbidity and mortality worldwide and is caused by the rupture or erosion of a flawed, lipid-laden, chronic atherosclerotic coronary plaque, which causes an acute interruption of myocardial blood flow and ischemic myocardial necrosis (1, 2). According to prior findings, older individuals with coronary artery disease (CAD) have worse results, such as increased all-cause mortality and recurrent events (3, 4). Early and correct diagnosis may decrease mortality (5). Previous research reported some risk factors linked to the occurrence of AMI, including age, gender, alcohol use, diabetes, hypertension, physical labor, and smoking (6–9). However, there is growing evidence that genetics and epigenetics contribute to the occurrence and development of AMI (10).

Epigenetics is a collective term referring to processes that change the activity of the genome in a heritable way without affecting the DNA sequence (11). And the critical modification of 5-methylcytosine (5mC) is a dynamic and reversible modification process in epigenetics (12). DNA methyl transferase enzymes (writers) are responsible for DNA methylation in mammalian cells (13). They do so by adding a methyl group to the cytosine base's carbon-5 position, which inhibits transcription in the genome (14). Researchers discovered that by altering DNA methylation, 5mC regulators (methyl transferase: writers; signal transducers: readers; and demethylase: erasers) are essential for a variety of cellular biological activities, including the silencing of retroelements, the stabilization of centrioles, and the regulation of gene expression (14–16). While it was reported that DNA methylation plays a major regulatory role in atherosclerosis, myocardial hypertrophy, heart failure as well as AMI (17–19), and diverse therapeutic targets for AMI and other diseases have been identified through the study of genetic factors (20–22). Studies examined 5mC regulators and molecular typing based on 5mC regulator gene expression are still limited. Consequently, research into new, highly sensitive and specific biomarkers for the diagnosis of cardiovascular disease is essential, and DNA methylation seems to be a promising new approach.

In this study, we systematically evaluate the modification pattern of 5mC regulators in AMI and CAD. Then, LASSO and SVM-RFE algorithms were employed to screen out the hub 5mC regulators. We also established a 5mC regulator-based classifier that can discriminate AMI from CAD *via* a machine-learning method. Afterward, we clustered AMI samples according to 21 5mC regulators, and two distinct 5mC modification clusters were identified. The immune cell differences as well as the correlations between hub 5mC regulators and 28 immunocytes were observed between the clusters. Besides, 64 5mC phenotype-related genes were identified and their biological functions were investigated. These findings may provide novel diagnostic biomarkers and a new perspective for individualized therapy in AMI patients.

2 Materials and methods

2.1 Ethics statement

This study gained the approval of the Ethics Committee of Guangdong Provincial People's Hospital (GDREC2016255H). in accordance with the ethical standards of the Declaration of Helsinki. Written informed consent was collected from all participants.

2.2 Patient sample collections

We recruited 43 participants with complete information on biochemical and clinical parameters, and medical history, from Guangdong Provincial People's Hospital between January 2022 and June 2022. The coronary angiography was performed on all patients, and two observers independently verified the angiographic results. Twenty-four patients diagnosed with

AMI (23) were included in the test group, and nineteen patients diagnosed with Stable CAD (24) were included in the control group. The inclusion and exclusion criteria (25) and TIMI scores of the participants used in this research were in **Supplementary Table 1**. Blood samples were collected from each patient within 1 h from the admission, which were centrifuged at 2,000 rpm at 4°C for 30 min. The serum samples were isolated and stored at −80°C until analysis.

2.3 Animals

All animal experiments were conducted in compliance with the Guide for the Care and Use of Laboratory Animals by the US National Institutes of Health (NIH Publication No. 85-23, revised 1996) and approved by the Ethics Committee of Guangdong Provincial People's Hospital. Sixty ApoE$^{-/-}$ mice were housed in a pathogen-free environment at animal laboratory of Sun Yat-sen University. The animals were allowed access to food and water *ad libitum* on a 12-h light/dark cycle. ApoE$^{-/-}$ mice were initially fed a standard rodent chow diet until 8 weeks of age and then switched to a high-fat diet (D12109C Formula) (New Brunswick, NJ). Afterward, the sixty mice were randomly divided into group A (AMI group, n = 30) and group C (CAD group, n = 30), They were anesthetized by intraperitoneal injection of sodium pentobarbital (50 mg/kg). AMI was performed on group A by ligation of the proximal left anterior descending coronary artery. Subsequently, the mice were sacrificed, and the infarcted myocardium in group A and the controls in group C were obtained for further experiments.

2.4 Western blots

The AMI and CAD tissues were lysed using strong RIPA buffer containing Halt Protease Inhibitor Cocktails (Thermo Fisher Scientific, Waltham, USA). Protein concentrations were evaluated with a bicinchoninic acid assay kit (Beyotime, Nantong, China). Primary antibodies targeting to beta actin (ab8226, Abcam), UHRF2 (ABE1028, MilliporeSigma), TET3 (ab153724, Abcam), UHRF2 (ZBTB33, MilliporeSigma), TET1 (ab19198, Abcam), DNMT3B (ab2851, Abcam), NTHL1 (ab191413, Abcam), UHRF1 (ab213223, Abcam), MBD3 (ab157464, Abcam), and SMUG1 (ab192240, Abcam), were incubated with targeted proteins at 4°C overnight, followed by incubating with appropriate horseradish peroxidase-conjugated secondary antibodies. Detection of horseradish peroxidase was performed with the Super Signal West Pico Chemiluminescent Substrate (Pierce).

2.5 RNA isolation and quantitative real-time PCR

Followed by total RNA extraction using TRIzol LS (Invitrogen) and examination of RNA quality and concentration using a NanoDrop ND-1000 analyzer according to the manufacturer's instructions. Total RNA was subjected to reverse transcription using the GoScript^{TM}Reverse Transcription Mix (Promega). GAPDH was selected as an internal control gene, the primers are listed in **Supplementary Table 2**. Quantitative real-time PCR (qRT-PCR) was performed on Applied Biosystems QuantStudio 6 machine with SYBR-Green dye (Takara). The internal control was GAPDH, and data were calculated by the $2^{(-\Delta\Delta Ct)}$ method.

2.6 Public data obtaining

The integration of bioinformatic analyses and experiment data is illustrated by the flowchart in **Figure 1**. Expression microarray data were downloaded from the Gene Expression Omnibus (GEO) database: GSE59867 dataset (26), which contained peripheral blood mononuclear cell (PBMC) samples from 111 patients with STEMI and 46 patients with stable CAD at admission; GSE62646 (27), which contained PBMC samples from 28 patients with STEMI and 14 patients with stable CAD at admission. The two independent datasets were both based on the GPL6244 platform of [HuGene-1_0-st] Affymetrix Human Gene 1.0 ST Array [transcript (gene) version]. Since AMI can hasten atherosclerosis 1 day after AMI, causing recurrent occurrence due to status altering of coronary artery walls or plaques (28), only admission patient data with STEMI and stable CAD were included in this study. We used GSE59867 (included 157 PBMC specimens at admission) in the screening of feature genes and as the training cohort during model construction, whereas GSE62646 was deployed as the external validation cohort (included 42 PBMC specimens at admission). In this article, 21 5mC regulators from previous studies (29–32) were systematically included: three writers (*DNMT1*, *DNMT3B,* and *DNMT3A*), 14 readers (*NEIL1*, *NTHL1*, *SMUG1*, *UHRF1*, *UHRF2*, *MBD1*, *MBD2*, *MBD3*, *MBD4*, *UNG*, and *MECP2*) and four erasers (*TDG*, *TET1*, *TET2,* and *TET3*).

2.7 Alteration analysis of 5mC regulator between AMI and CAD

The protein-protein interaction network of 21 5mC regulators was obtained from the STRING (33) database,[1]

1 https://string-db.org/

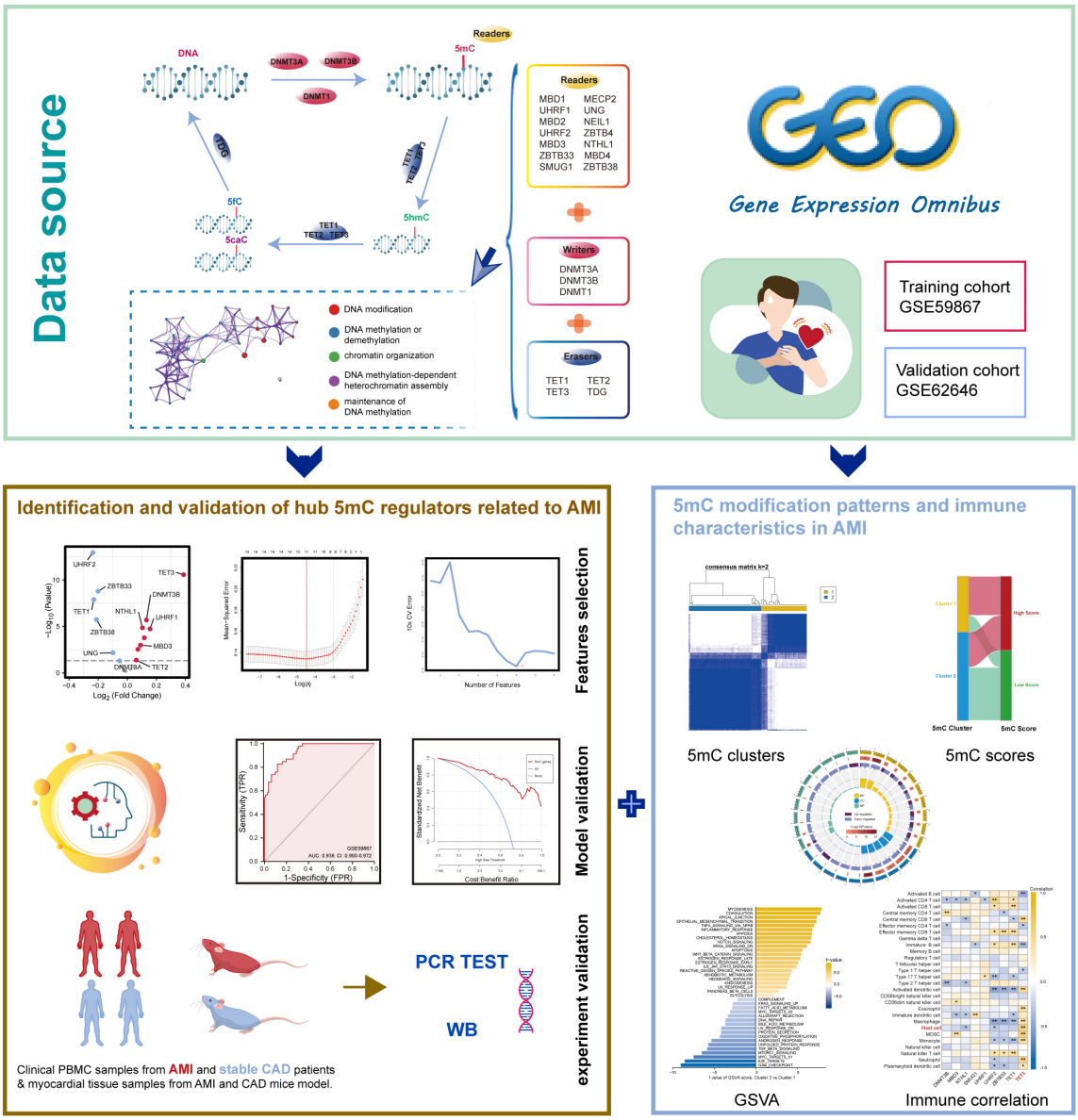


FIGURE 1
The illustrations for this study. The overall protocol utilized in the current study to identify hub 5mC regulators that can be potential biomarkers in unstable plaques and CAD progression and explore the characteristics of 5mC modification patterns in AMI.

and the PPI network was then visualized *via* Cytoscape (34) software, V3.8.3. Besides, the biological processes these 5mC regulators participate were analyzed by Metascape (35). Then, the expression value was pre-processed by the "normalize between arrays" function in the "limma" package (36), and differential gene expression analysis was conducted. A $|\log2FoldChange|$ value > 0, and a p-value < 0.05 were considered statistically significant. The expression relationship among 21 5mC regulators was evaluated by Spearman correlation analysis in AMI and CAD samples, respectively. Afterward, the expression status differences of 21 5mC regulators between AMI and CAD were compared by the Wilcox test.

2.8 Identification of hub AMI-related 5mC regulators and establishment of a classifier

The differentially expressed 5mC regulators were defined as the AMI-related 5mC regulators. Subsequently, these AMI-related 5mC regulators were subjected to least absolute

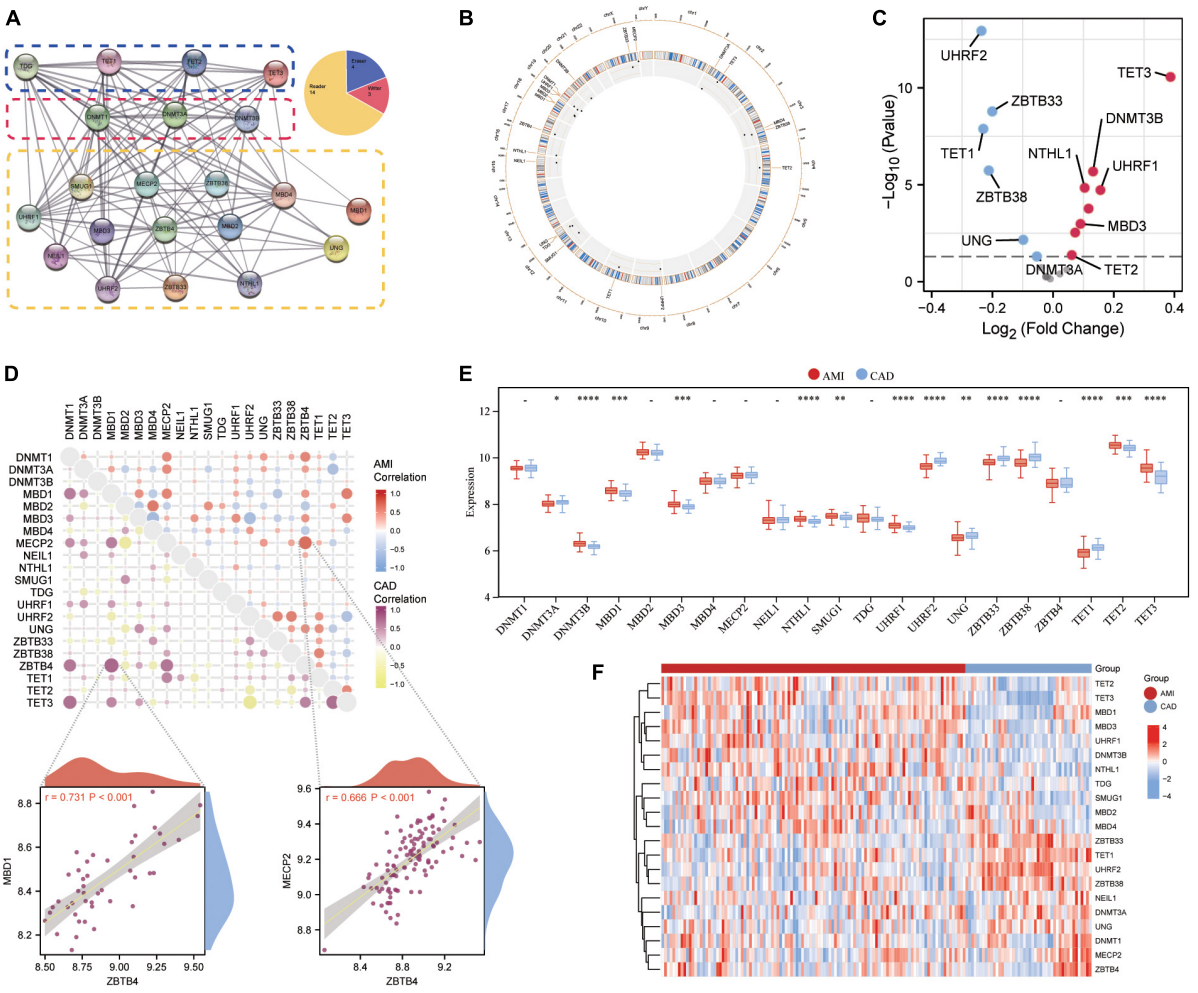


FIGURE 2
Expression landscape of 5mC regulators in AMI and CAD. **(A)** The protein-protein interactions among 21 5mC DNA methylation regulators and the composition summary of them. **(B)** Circle diagram of 5mC-related genes. **(C)** The volcano plot shows the expression changes of 21 5mC-related genes between AMI and CAD samples, and the statistically significant 14 5mC regulators are labeled. **(D)** Correlations among the expression of 21 5mC regulators in AMI and CAD samples, the correlation scatter plot shows the pair of genes with the most positive correlations in AMI and CAD, respectively. The box plot **(E)** and heatmap plot **(F)** demonstrated the transcriptome expression status of 21 5mC regulators between AMI and CAD samples.

shrinkage and selection operator (LASSO) regression (37) and support vector machine recursive feature elimination (38) (SVM-RFE) with 10-fold cross-validation, the R package "glmnet" and "e1071" helped implemented the above process. These two machine learning methods were used for feature selection and dimension reduction, so the hub AMI-related 5mC regulators were identified. Furthermore, by using "rms" package, we developed a 5mC regulator-related AMI-CAD classifier based on the hub 5mC regulator gene expression values, and receiver operating characteristic (ROC) curve analysis was used to evaluate the distinguishing performance of the classifier (39). Besides, a nomogram, a calibration plot, decision curve analysis (DCA) and a clinical impact curve were visualized based on the results, the above analyses can help assess the predictive power of the classifier and evaluated the clinical value of the classifier (40, 41).

2.9 Identification of 5mC-associated molecular clusters

To confirm distinct 5mC methylation modification patterns, unsupervised clustering analysis based on 21 5mC regulators expression profiles was conducted by the R package "ConsensusClusterPlus" (42). To guarantee the stability of the clustering, a thousand repetitions were performed, and each iteration contained 80% of the samples. The cumulative distribution function (CDF) curve of the consensus score

was used to define the optimal cluster number. Then, similar to previous studies (43–47), principal component analysis was further performed on these 5mC regulators to calculate principal component 1, which was used for 5mC score calculation in this study.

$$5mC\ score\ =\ \Sigma PC1i$$

i shows the expression of 5mC regulator genes.

2.10 Exploration of immune characteristics and hallmark pathway activity in the clusters

Gene set variation analysis (GSVA) *via* the R package "GSVA" was performed to explore Hallmark pathways on biological differences between two clusters (48). Besides, the enrichment scores that represented the 28 immunocytes infiltration levels in each sample were evaluated using single-sample GSEA (ssGSEA) algorithm, and immunocyte scores of the samples in CAD group were calculated as well. The marker genes of the 28 immunocytes were acquired from a previous study (49). The Kruskal-Wallis test was used to analyze the infiltration levels of each immunocyte between two clusters. Then the correlation between hub 5mC regulators and immunocytes was determined by Spearman correlation analysis. Subsequently, DEGs between clusters were identified by the R package "limma." Then, Gene ontology (GO) and Kyoto Encyclopedia of Genes and Genomes (KEGG) functional enrichment analyses were conducted on these 5mC phenotype-related DEGs to observe the functions or pathways in which the 5mC regulators may affect.

2.11 Association of identified 5mC regulators and AMI

To further investigate the follow-up relationship between 5mC regulators and AMI. Two datasets (GSE59867 and GSE62646) were employed. The GSE59867 dataset contains relevant gene expression pattern at four time points of AMI patients: admission, discharge, after 1 month, and after 6 months. The GSE62646 dataset contains relevant gene expression pattern at three time points of AMI patients: admission, discharge, and after 6 months. The expression status of the hub 5mC regulators were compared between admission and other time points using Wilcoxon rank sum test.

2.12 Statistical analysis

R software 4.1.1 was conducted in this study for statistical analyses and visualization. The R package "ggplot2" was used to make statistical plots, and a two-tailed P-value < 0.05 was considered statistical significance unless otherwise specified.

3 Results

3.1 An overview of 5mC regulator genes in AMI and CAD

Twenty-one 5mC regulators were investigated in this study, including 3 writers, 14 readers, and 4 erasers. A protein-protein network (**Figure 2A**) depicting the regulation interactions of these 5mC regulators was found to have multiple close connections. Besides, the biological processes these 5mC regulators take part in were exhibited in **Supplementary Figure 1**, and they are mainly involved in the DNA modification process just as anticipated. **Figure 2B** displays the location of the 5mC regulator genes *via* a circle diagram, which was mainly distributed on Chromosomes 2, 3, 12, 18, 19, and X. Besides, we analyzed the transcriptome links and discovered strong correlations between writers, readers, and erasers (**Figure 2C**): most regulators statistically correlated with each other in expression in both group of samples; in the CAD samples, reader MBD1 and reader ZBTB4 are the most correlated 5mC regulators; while in the AMI samples, reader MECP2 and read ZBTB4 showed the closest correlation, indicating these readers may function as a complex. Then, differentially expressed analysis found 14 dysregulated 5mC regulators, where eraser TET3 had the largest fold change, and the well-studied writer DNMT3A did not alter noticeably (**Figure 2D**), indicating that it might not be crucial in unstable plaques and CAD progression. The expression variations of the 21 5mC regulators were depicted in the boxplot (analyzed by the Wilcox test) and heatmap (**Figures 2E, F**), and the immunocytes alteration were shown in **Supplementary Figure 2**.

3.2 Hub 5mC regulator genes were selected *via* integrated machine learning methods

As mentioned earlier, 14 5mC regulators were dysregulated between AMI and CAD. Then, the abovementioned genes in the training cohort were used as inputs for both LASSO (**Figures 3A, B**) and the SVM-RFE algorithm (**Figure 3C**) with 10-fold cross-validation. By taking the intersection of the outputs of LASSO and SVM-RFE algorithms, nine hub 5mC regulator genes were identified (**Figure 3D**), including one writer (DNMT3B), six readers (MBD3, UHRF1, UHRF2, NTHL1, SMUG1, and ZBTB33), and two erasers (TET1 and TET3). Furthermore, a diverse 5mC regulator expression pattern between AMI and CAD was also shown by PCA results (**Figure 3E**), and the contribution of each hub regulator

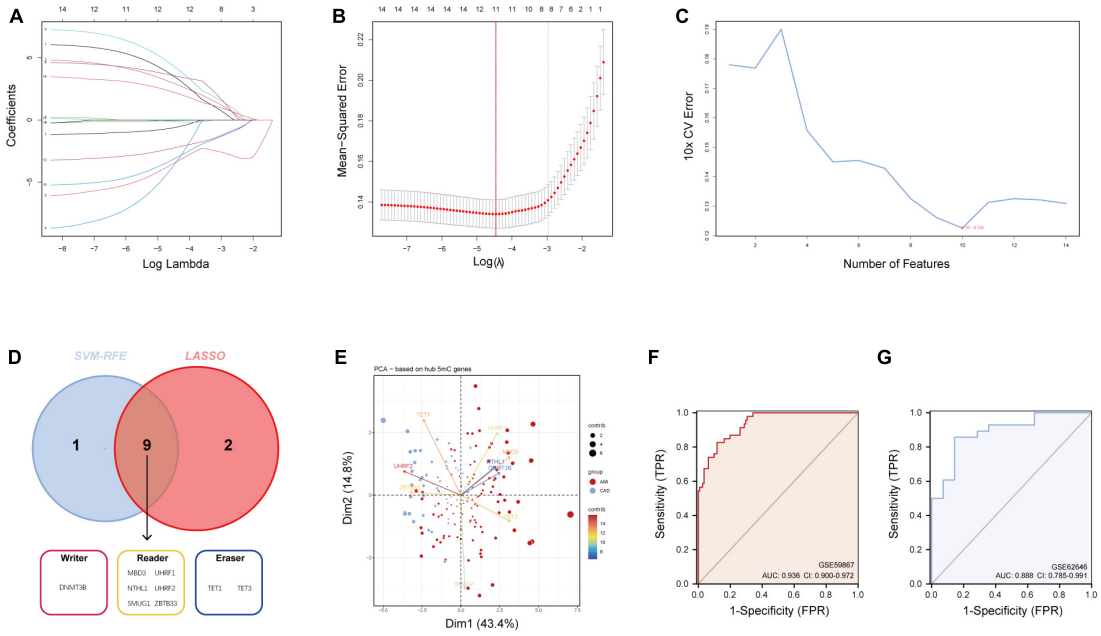


FIGURE 3
Identification of hub 5mC regulators. **(A)** The least absolute shrinkage and selection operator (LASSO) coefficient profiles of the 14 5mC regulators. **(B)** 10-fold cross-validation for optimum tuning parameter (λ) selection using LASSO. **(C)** Estimating 10-fold cross-validation error using the support vector machine recursive feature elimination (SVM-RFE). **(D)** Intersections of diagnostic gene outputs generated by LASSO and SVM-RFE. **(E)** Principal component analysis of nine hub 5mC regulators between AMI and CAD. The ROC curve and evaluated by the AUC value in the training cohort **(F)** and the external validation cohort **(G)** based on the constructed logistic model.

was shown: the erasers contribute more than other regulators, suggesting some potential roles of which in unstable plaques and CAD progression.

3.3 Construction and assessment of a logistic regression model for AMI diagnosis

The R package "Rms" was utilized to constructed a logistic regression model for AMI diagnosis based on the hub 5mC regulators (DNMT3B, MBD3, UHRF1, UHRF2, NTHL1, SMUG1, ZBTB33, TET1, and TET3). The ROC curve was plotted (**Figures 3F, G**), and the classification model showed a satisfactory discrimination capability in both the training cohort (area under the curve [AUC] = 0.936, concordance index [CI] = 0.900–0.972) and the external validation cohort (AUC = 0.888, CI = 0.785–0.991). According to the logistic regression model, a nomogram was generated (**Figure 4A**). Afterward, a calibration curve was plotted to assess the predictive capability of the classifier and very little difference between the actual and predicted AMI risks was shown, demonstrating the robustness of the model (**Figure 4B**). Besides, the DCA of the model was conducted, and patients who use this model would be more beneficial than either the treat-none or the treat-all scheme (**Figure 4C**). Furthermore, the clinical impact curve based on the DCA curve was plotted to test the clinical influence of the logistic regression model (**Figure 4D**). At high risk threshold from 0.4 to 1, the "Number high risk with event" curve was close to the "Number high risk" curve, suggesting that the logistic regression model has the exceptional predictive capability. In certain ways, these findings also suggested that the 10 hub 5mC regulators may be crucial in unstable plaques and CAD progression. To validate our findings, experiments were conducted, and qRT-PCR (**Figures 5A–I**) and Western blot (WB) (**Figure 5J**) results showed significantly differentiated expressions of the genes between AMI and CAD clinical samples, which were consistent with our bioinformatics results.

In addition, information on the association between genes change level and AMI outcome was also analyzed. Based on patients TIMI risk score, 5mC regulators' expression level in patients with high, intermediate, low-risk score was evaluated (**Supplementary Figure 3**).

3.4 The association of identified nine 5mC regulators and AMI

To investigate the relationship between these nine 5mC regulators and AMI, the expression status of these 5mC regulator genes were evaluated. Of interest, we found that the

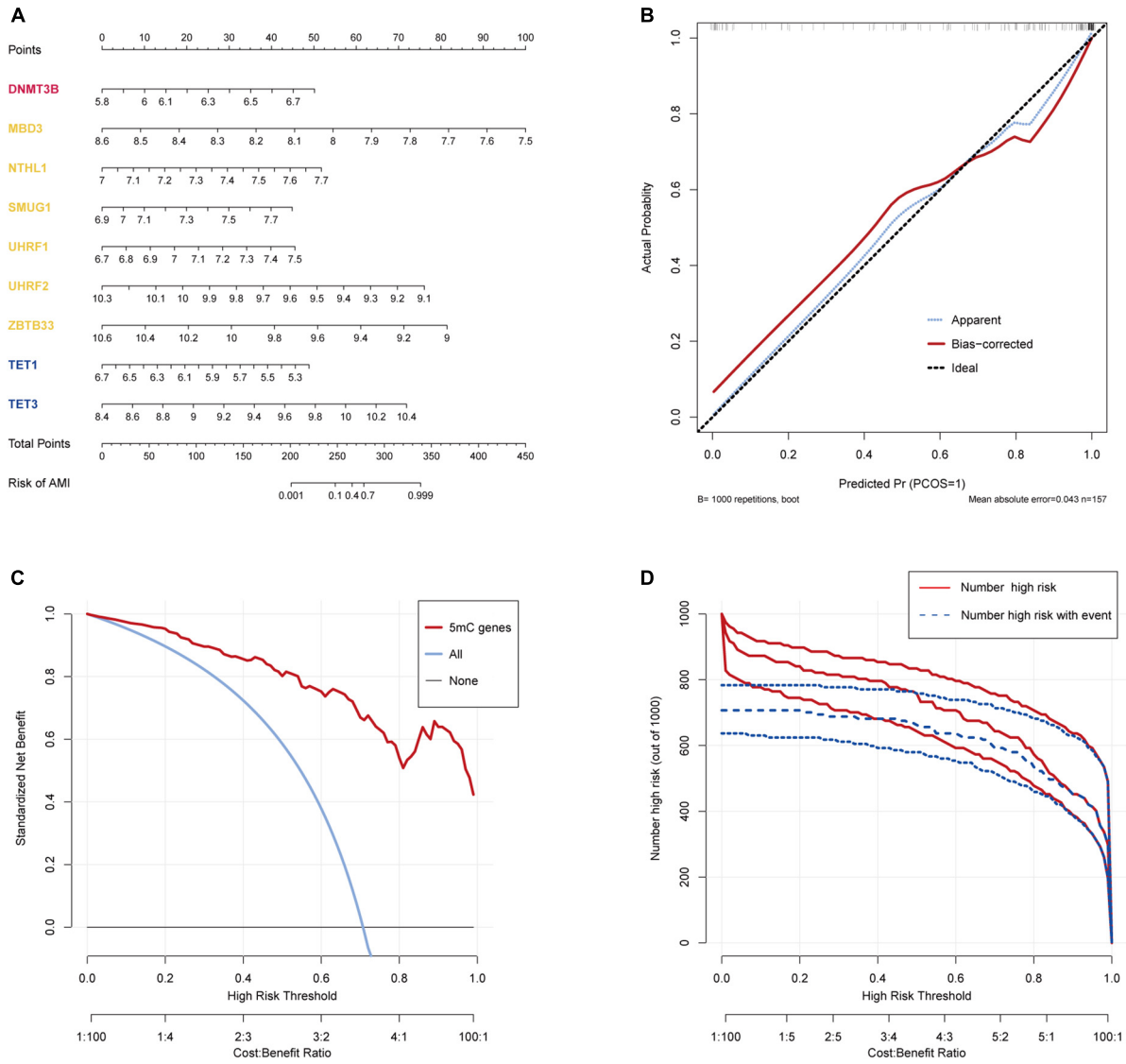


FIGURE 4
Construction and validation of a logistic model for AMI diagnosis based on the training dataset GSE59867. **(A)** Nomogram to predict the occurrence of AMI. **(B)** Calibration curve to assess the predictive power of the logistic model. **(C)** DCA curve to evaluate the clinical value of the logistic model. **(D)** Clinical impact curve based on the DCA curve to assess the logistic model.

expression levels of "eraser" TET3 was the most significantly varied in both training cohort (Figure 6) and external validation cohort (Supplementary Figure 4).

3.5 5mC methylation modification patterns mediated by 21 regulators in AMI

Based on the expression levels of 21 5mC regulators in AMI, the pam clustering algorithm with two clusters (including 43 samples in cluster-1 and 68 samples in cluster-2) was found achieved the clearest population clusters, and k = 2 was determined as the optimal value (Figures 7A–C), and the detail of the clusters and samples were listed in Supplementary Table 2. Besides, the PCA results showed distinct 5mC modification patterns between the two clusters (Figure 7D), and the 5mC score of each sample was calculated based on the abovementioned calculation formula. We found that cluster-1 members have a much higher 5mC score than cluster-2 members (Figure 7E), and the correlations between the 5mC score samples and 5mC cluster samples were shown by a Sankey diagram (Figure 7F). Afterward, the expression

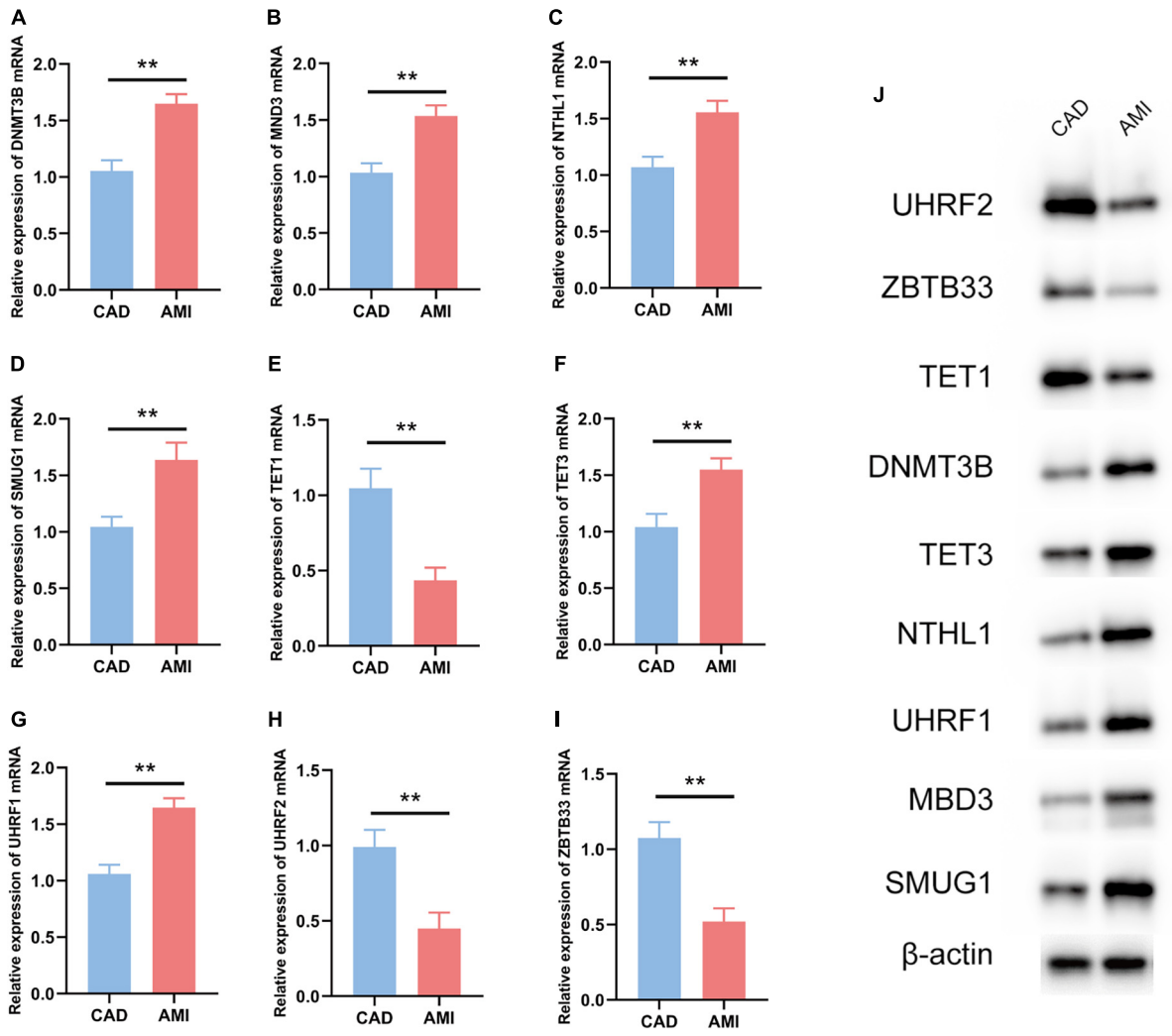


FIGURE 5
Experiment validation of the nine hub 5mC regulators. **(A–I)** DNMT3B, MND3, NTHL1, SMUG1, TET1, TET3, UHRF1, UHRF2, ZBTB33. The results were presented as mean ± standard deviation (*t*-testing). $^{**}p < 0.01$, **(J)** Western blot analysis of hub 5mC regulators.

values of the 21 5mC regulators were compared, and the majority of them notably altered between cluster-1 and cluster-2, demonstrating distinct expression patterns between the two clusters (Figure 7G).

3.6 Function and immunocyte infiltration analysis based on molecular typing

Besides, based on the ssGSEA results, the enriched scores of 28 types of immunocytes were evaluated, and some immunocytes differ between the two subtypes. For example, cluster-1 owned a greater monocyte count, while cluster-2 owned a greater immature and activated B cell count (Figure 8A). The distinct immunological features were explored, we then explored other biological functions between the two clusters. The different HALLMARK pathways activity between the clusters were analyzed *via* GSVA algorithm (Figure 8B), and we found that the MYOGENESIS pathway and the G2M_CHECKPOINT pathway were the most significantly dysregulated ones, indicating their potential linkages. Then, the correlation between immunocytes and hub 5mC regulators were analyzed in separate cluster (Figures 8C, D), the results show that the most positively correlated immunocyte and 5mC regulator pair in cluster-1 was TET3 and Mast cell whereas the most positively correlated immunocyte and 5mC regulator pair in cluster-2 was TET3 and Myeloid-derived suppressor cell (MDSC). Then 64 DEGs between the clusters were identified (Supplementary Figure 5), and these DEGs were subjected to GO and KEGG functional enrichment analyses (Figures 8E, F).

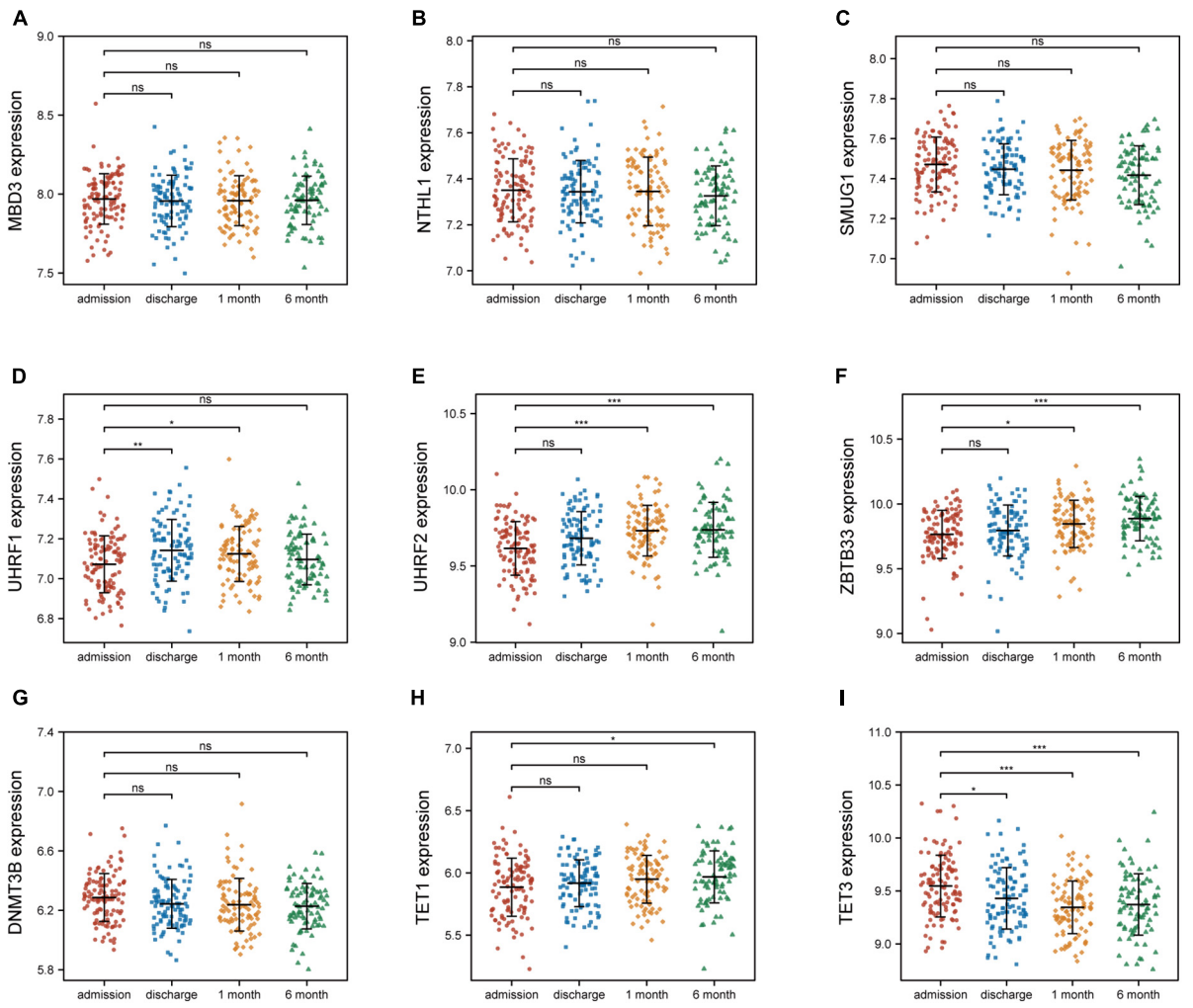


FIGURE 6
Nine 5mC regulators expression level at four time points of AMI patients in GSE59867. **(A–I)** MND3, NTHL1, SMUG1, UHRF1, UHRF2, ZBTB33, DNMT3B, TET1, TET3. *$p < 0.05$; **$p < 0.01$; ***$p < 0.001$; ns, not significant.

The enrichment results showed that they were mainly involved in cytokine-related pathways and immune-related pathways.

4 Discussion

AMI, a leading cause of morbidity and mortality globally, is increasingly being researched by academics in terms of its early diagnosis and treatment (50). Prior studies reported the bidirectional relationship between plaques progression and CAD progression: stable CAD to STEMI can induce plaques progression and plaque progression can worsen CAD progression (28, 51). Nevertheless, the therapeutic targets and predictive biomarkers are currently few, and AMI continues to be a major factor in death and disability. Thus, more research is needed to find novel biomarkers for the early detection of AMI.

To add more theoretical bases to the urgent issue, here, we systematically investigated the 21 5mC regulators under the "stable CAD to AMI" circumstance. A set of bioinformatics algorithms were performed, and 14 differentially expressed 5mC regulators genes were identified which correlated and interacted with each other, resulting in a 5mC regulation network in AMI and CAD. Then, examined by the integrated machine learning methods (LASSO and SVM-RFE), the nine most important 5mC regulators (DNMT3B, MBD3, UHRF1, UHRF2, NTHL1, SMUG1, ZBTB33, TET1, and TET3) were screened out. Afterward, similar to previous studies (52, 53), a logistic model was established for the AMI diagnosis. Satisfactory discrimination ability was shown, for which C-index is 0.936 in the training cohort and 0.888 in the external validation cohort. The calibration, DCA and clinical impact curve plots indicated the pleasant fit of the model, suggesting

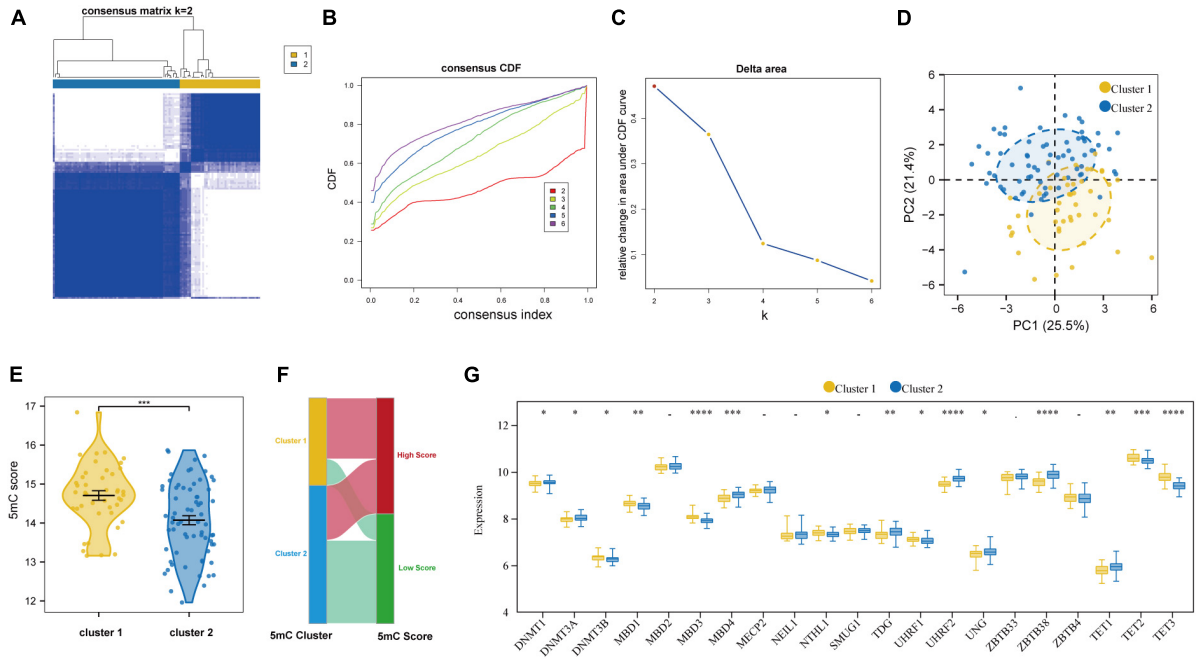


FIGURE 7
Identifying 2 distinct 5mC modification pattern clusters in AMI by unsupervised clustering of 21 5mC regulators. **(A)** Heatmap of the matrix of co-occurrence proportions for AMI specimens. **(B)** Consensus clustering cumulative distribution function (CDF) for $K = 2–6$. **(C)** Relative change in area under CDF curve for $K = 2–6$. **(D)** Principal component analysis for the transcriptome profiles of two 5mC clusters. **(E)** The differences in the 5mC score between the 5mC clusters. **(F)** Sankey plot showing the correlations between the 5mC score groups and 5mC clusters. **(G)** The expression status of 21 5mC regulators between the two 5mC clusters. $^{*}p < 0.05$; $^{**}p < 0.01$; $^{***}p < 0.001$; $^{****}p < 0.0001$.

DNA methylation may be a crucial molecular variable in the development of AMI.

Given the individual heterogeneity of 5mC methylation modification, unsupervised clustering of the AMI specimens based on 5mC regulator expression profiles was performed, and the results led us to two clusters with distinctive 5mC modification patterns, and distinct immunocyte characteristics were observed. Of interest, we found that many significant correlations between hub 5mC regulators and immune cells in the clusters, respectively. The most correlated pair in cluster-2 is TET3-MDSC (correlation coefficient = 0.65, $p < 0.001$), while TET3- Mast cell (correlation coefficient = 0.59, $p < 0.001$) in cluster-1. MDSCs are pathologically activated monocytes and neutrophils with formidable immunosuppressive activity (54), and current studies found that MDSCs mobilization were closely related to AMI (55). By preventing the local inflammatory response and inflammation-mediated apoptosis, MDSCs may have a positive and protective effect on the process of ventricular remodeling after AMI (56). However, Yao et al. reported that myocardial damage in AMI mice can get worse by the growing MDSCs infiltration (57). Besides, DNA methylation can in a way regulate MDSC metabolism. Smith et al. reported that MDSC survival could be affected by DNA methylation *via* an independent mechanism (58). According to our findings, a tight bond of mast cell and 5mC regulator was revealed in AMI subclusters. Mast cells have been seen in AMI and are multifunctional cells that contain a variety of mediators, including histamine, tryptase, and cytokines (59). Kupreishvili et al. reported that excessive mast cell infiltration can give rise to increased risk of AMI, possibly increasing the risk of re-infarction (60). In addition, Leoni et al. found that DNA methylation is crucial in regulating mast cell reactivity (61). Regarding TET3, i.e., tet methylcytosine dioxygenase 3, which is one of the DNA methylation eraser regulators and can oxidize 5mC into 5-hydroxymethylcytosine (5hmC) (62). It has been verified that TET3 was closely associated with the process of stem cell renewal, epigenetic modulation, tumor, and embryonic development (63–66). However, the relationship between TET3 and AMI or between TET3 and MDSC is yet to be found. Furthermore, based on the GSVA results, distinct pathway overview between clusters were drawn. As demonstrated by a previous literature, the pathophysiology of heart failure (HF) is caused by the inappropriate resolution of inflammation following post-myocardial injury, which is linked to failed left ventricular remodeling (67). Apparently, immune-related pathways were more activated in cluster-1, suggesting patients in this cluster may suffer a poor prognosis. Last, we identified the 5mC phenotype-related genes, and the GO and KEGG enrichment analyses results were mainly involved

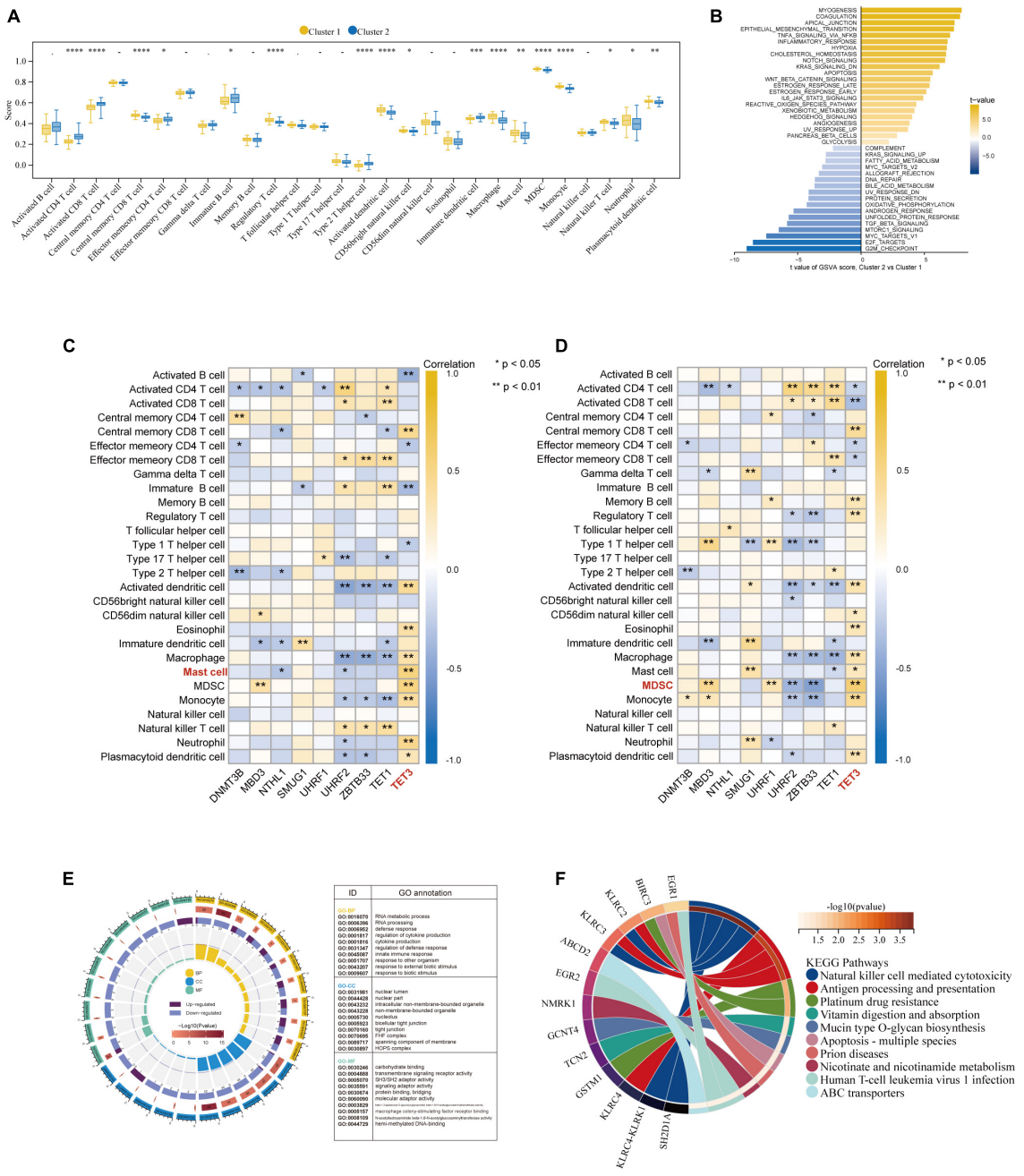


FIGURE 8
Further exploration of the characteristics between the two AMI clusters. **(A)** The abundance differences of each infiltrating immunocyte in 2 5mC modification clusters. **(B)** The differences in HALLMARKS pathway enrichment score between 5mC modification cluster-1 and cluster-2. The correlation between 28 immunocytes and hub 5mC regulators in cluster-1 **(C)**, and cluster-2 **(D)**. **(E)** Gene Ontology enrichment analysis of DEGs between cluster-1 and cluster-2, the outermost ring represented the name of pathways. The second outer ring represented the number of genes in pathways, and the heights of the columns in the inner ring indicate the value of GeneRatio. **(F)** Chord plot depicting the relationship between genes and KEGG signaling pathways. *$p < 0.05$; **$p < 0.01$.

in cytokine-related pathways and immune-related pathways, indicating these processes may mainly contribute to 5mC mediation in AMI. Abundant discoveries were found, and other researchers in the field will get directions to catch the key 5mC regulator and immune features in AMI rapidly.

To our best knowledge, our study is the first one to systematically explored the biomarkers for stable CAD to AMI progression regarded to 5mC regulators. Fruitful findings were generated: hub 5mC regulators were identified and validated by qRT-PCR; an AMI

diagnosis model was built and validated; subclusters of AMI were identified, as well as their unique immune characteristics.

4.1 Limitations of the present study

However, there are still some limitations that we must admit. This research is mainly based upon silico analysis, and most findings are theoretically sound but haven't been tested in actual experiments. Although nine hub 5mC regulators were validated by a robust model, an external validation cohort, and qRT-PCR, the biological function and specific mechanism they may involve in AMI is still a giant gap. Besides, the method for immunocyte infiltration analysis is based on the most widely applied ssGSEA algorithm, although single-cell sequencing is still needed to obtain the most precise number of immunocytes. More importantly, some important information were not reported in the current study, such as biomarkers, echo, EKG and clinical characteristics of the population.

5 Conclusion

In brief, a non-negligible impact of 5mC regulators on the diagnostic effect of stable CAD to AMI was determined. Nine hub 5mC regulators are identified to be latent biomarkers in AMI (DNMT3B, MBD3, UHRF1, UHRF2, NTHL1, SMUG1, ZBTB33, TET1, and TET3). Besides, two 5mC molecular clusters were identified, and the immunocyte infiltration and pathway activity of each cluster was analyzed in this study. The findings may provide a novel direction for the follow-up exploration of the molecular mechanism of 5mC regulators in the progression of stable CAD to AMI and provide a new reference for the personalized treatment of patients.

Data availability statement

Publicly available datasets were analyzed in this study. This data can be found here: https://www.ncbi.nlm.nih.gov/geo/query/acc.cgi.

Ethics statement

This study gained the approval of the Ethics Committee of Guangdong Provincial People's Hospital. The patients/participants provided their written informed consent to participate in this study.

Author contributions

QH, XD, and YL: conceptualization and design. YG, HJ, JW, and PL: formal analysis, visualization, and manuscript writing. PL: sample collection. XZ: data processing and revision. YG and HJ: animal experiments. TZ, RN, and JF: writing – review and editing. All authors critically reviewed and approved the final version of the work.

Funding

This work was supported by the National Natural Science Foundation of China (No. 82100348), the Basic and Applied Basic Research Foundation of Guangdong Province of China (No. 2020A1515110865), the Guangzhou Women and Children's Medical Center Foundation [No. (2018)293], the Science and Technology Projects in Guangzhou City of China (No. 202102021124), and the Medical Science Technology Research Foundation of Guangdong Province of China (No. B2021162).

Acknowledgments

We thank Guangdong Provincial Key Laboratory of South China Structural Heart, Guangdong Provincial People's Hospital, Guangzhou, China for support.

Conflict of interest

The authors declare that the research was conducted in the absence of any commercial or financial relationships that could be construed as a potential conflict of interest.

Publisher's note

All claims expressed in this article are solely those of the authors and do not necessarily represent those of their affiliated organizations, or those of the publisher, the editors and the reviewers. Any product that may be evaluated in this article, or claim that may be made by its manufacturer, is not guaranteed or endorsed by the publisher.

Supplementary material

The Supplementary Material for this article can be found online at: https://www.frontiersin.org/articles/10.3389/fcvm.2022.1053697/full#supplementary-material

References

1. Boateng S, Sanborn T. Acute myocardial infarction. *Dis Mon.* (2013). 59:83–96.

2. Pollard TJ. The acute myocardial infarction. *Prim Care.* (2000) 27:631–49.

3. Rodondi N, Marques-Vidal P, Butler J, Sutton-Tyrrell K, Cornuz J, Satterfield S, et al. Markers of atherosclerosis and inflammation for prediction of coronary heart disease in older adults. *Am J Epidemiol.* (2010) 171:540–9.

4. Roger VL, Go A, Lloyd-Jones D, Benjamin E, Berry J, Borden W, et al. Executive summary: heart disease and stroke statistics–2012 update: a report from the American Heart Association. *Circulation.* (2012) 125:188–97. doi: 10.1161/CIR.0b013e3182456d46

5. Kadire SR, Udelson J, Budoff MJ. Imaging in coronary artery disease risk stratification. *N Engl J Med.* (2021) 385:655–7.

6. Mittleman MA, Maclure M, Tofler G, Sherwood J, Goldberg R, Muller J. Triggering of acute myocardial infarction by heavy physical exertion. protection against triggering by regular exertion. determinants of myocardial infarction onset study investigators. *N Engl J Med.* (1993) 329:1677–83. doi: 10.1056/NEJM199312023292301

7. Mittleman MA, Mintzer D, Maclure M, Tofler G, Sherwood J, Muller J. Triggering of myocardial infarction by cocaine. *Circulation.* (1999) 99:2737–41.

8. Mihas C, Kantzanou M. Body-Weight fluctuations and outcomes in coronary disease. *N Engl J Med.* (2017) 377:94.

9. Mittleman MA, Maclure M, Sherwood J, Mulry R, Tofler G, Jacobs S, et al. Triggering of acute myocardial infarction onset by episodes of anger. determinants of myocardial infarction onset study investigators. *Circulation.* (1995) 92:1720–5. doi: 10.1161/01.cir.92.7.1720

10. Kullo IJ, Fan X, Ding K. Genetic risk, lifestyle, and coronary artery disease. *N Engl J Med.* (2017) 376:1192–3.

11. Waddington CH. The epigenotype. 1942. *Int J Epidemiol.* (2012) 41:10–3.

12. Schübeler D. Function and information content of DNA methylation. *Nature.* (2015) 517:321–6.

13. Ficz G. New insights into mechanisms that regulate DNA methylation patterning. *J Exp Biol.* (2015) 218(Pt. 1):14–20.

14. Skvortsova K, Stirzaker C, Taberlay P. The DNA methylation landscape in cancer. *Essays Biochem.* (2019) 63:797–811.

15. Mohandas T, Sparkes RS, Shapiro LJ. Reactivation of an inactive human X chromosome: evidence for X inactivation by DNA methylation. *Science.* (1981) 211:393–6.

16. Feinberg AP, Koldobskiy MA, Göndör A. Epigenetic modulators, modifiers and mediators in cancer aetiology and progression. *Nat Rev Genet.* (2016) 17:284–99.

17. Li P, Ge J, Li H. Lysine acetyltransferases and lysine deacetylases as targets for cardiovascular disease. *Nat Rev Cardiol.* (2020) 17:96–115.

18. Xie M, Hill JA. HDAC-dependent ventricular remodeling. *Trends Cardiovasc Med.* (2013) 23:229–35.

19. Eom GH, Kook H. Posttranslational modifications of histone deacetylases: implications for cardiovascular diseases. *Pharmacol Ther.* (2014) 143:168–80.

20. Karakas M, Schulte C, Appelbaum S, Ojeda F, Lackner K, Münzel T, et al. Circulating microRNAs strongly predict cardiovascular death in patients with coronary artery disease-results from the large AtheroGene study. *Eur Heart J.* (2017) 38:516–23. doi: 10.1093/eurheartj/ehw250

21. Liang C, Wang S, Zhang M, Li T. Diagnosis, clustering, and immune cell infiltration analysis of m6A-related genes in patients with acute myocardial infarction-a bioinformatics analysis. *J Thorac Dis.* (2022) 14:1607–19. doi: 10.21037/jtd-22-569

22. Chen H, Wang Z, He Y, Peng L, Zhu J, Zhang X. Pyroptosis may play a crucial role in modifications of the immune microenvironment in periodontitis. *J Periodontal Res.* (2022) 57:977–90. doi: 10.1111/jre.13035

23. Thygesen K, Alpert J, Jaffe A, Simoons M, Chaitman B, White H, et al. Third universal definition of myocardial infarction. *J Am Coll Cardiol.* (2012) 60:1581–98.

24. Task Force Members, Montalescot G, Sechtem U, Achenbach S, Andreotti F, Arden C, et al. 2013 ESC guidelines on the management of stable coronary artery disease: the task force on the management of stable coronary artery disease of the European society of cardiology. *Eur Heart J.* (2013) 34:2949–3003. doi: 10.1093/eurheartj/eht296

25. Tan B, Liu Q, Yang L, Yang Y, Liu D, Liu L, et al. Low expression of PRMT5 in peripheral blood may serve as a potential independent risk factor in assessments of the risk of stable CAD and AMI. *BMC Cardiovasc Disord.* (2019) 19:31. doi: 10.1186/s12872-019-1008-4

26. Maciejak A, Kiliszek M, Michalak M, Tulacz D, Opolski G, Matlak K, et al. Gene expression profiling reveals potential prognostic biomarkers associated with the progression of heart failure. *Genome Med.* (2015) 7:26. doi: 10.1186/s13073-015-0149-z

27. Kiliszek M, Burzynska B, Michalak M, Gora M, Winkler A, Maciejak A, et al. Altered gene expression pattern in peripheral blood mononuclear cells in patients with acute myocardial infarction. *PLoS One.* (2012) 7:e50054. doi: 10.1371/journal.pone.0050054

28. Dutta P, Courties G, Wei Y, Leuschner F, Gorbatov R, Robbins C, et al. Myocardial infarction accelerates atherosclerosis. *Nature.* (2012) 487:325–9.

29. Chen YT, Shen J, Chen D, Wu C, Guo R, Zhang P, et al. Identification of cross-talk between m(6)A and 5mC regulators associated with onco-immunogenic features and prognosis across 33 cancer types. *J Hematol Oncol.* (2020) 13:22. doi: 10.1186/s13045-020-00854-w

30. Ginder GD, Williams DC Jr. Readers of DNA methylation, the MBD family as potential therapeutic targets. *Pharmacol Ther.* (2018) 184:98–111.

31. DeNizio JE, Dow B, Serrano J, Ghanty U, Drohat A, Kohli R, et al. TET-TDG active DNA demethylation at CpG and Non-CpG Sites. *J Mol Biol.* (2021) 433:166877. doi: 10.1016/j.jmb.2021.166877

32. Hu J, Othmane B, Yu A, Li H, Cai Z, Chen X, et al. 5mC regulator-mediated molecular subtypes depict the hallmarks of the tumor microenvironment and guide precision medicine in bladder cancer. *BMC Med.* (2021) 19:289. doi: 10.1186/s12916-021-02163-6

33. Szklarczyk D, Franceschini A, Wyder S, Forslund K, Heller D, Huerta-Cepas J, et al. STRING v10: protein-protein interaction networks, integrated over the tree of life. *Nucleic Acids Res.* (2015) 43:D447–52. doi: 10.1093/nar/gku1003

34. Shannon P, Markiel A, Ozier O, Baliga N, Wang J, Ramage D, et al. Cytoscape: a software environment for integrated models of biomolecular interaction networks. *Genome Res.* (2003) 13:2498–504. doi: 10.1101/gr.1239303

35. Zhou Y, Zhou B, Pache L, Chang M, Khodabakhshi A, Tanaseichuk O, et al. Metascape provides a biologist-oriented resource for the analysis of systems-level datasets. *Nat Commun.* (2019) 10:1523. doi: 10.1038/s41467-019-09234-6

36. Ritchie ME, Phipson B, Wu D, Hu Y, Law CW, Shi W, et al. limma powers differential expression analyses for RNA-sequencing and microarray studies. *Nucleic Acids Res.* (2015) 43:e47. doi: 10.1093/nar/gkv007

37. Friedman J, Hastie T, Tibshirani R. Sparse inverse covariance estimation with the graphical lasso. *Biostatistics.* (2008) 9:432–41.

38. Sanz H, Valim C, Vegas E, Oller J, Reverter F. SVM-RFE: selection and visualization of the most relevant features through non-linear kernels. *BMC Bioinform.* (2018) 19:432. doi: 10.1186/s12859-018-2451-4

39. Muschelli J. ROC and AUC with a binary predictor: a potentially misleading metric. *J Classif.* (2020) 37:696–708. doi: 10.1007/s00357-019-09345-1

40. Vickers AJ, Elkin EB. Decision curve analysis: a novel method for evaluating prediction models. *Med Decis Making.* (2006) 26:565–74.

41. Pan X, Jin X, Wang J, Hu Q, Dai B. Placenta inflammation is closely associated with gestational diabetes mellitus. *Am J Transl Res.* (2021) 13:4068–79.

42. Wilkerson MD, Hayes DN. ConsensusClusterPlus: a class discovery tool with confidence assessments and item tracking. *Bioinformatics.* (2010) 26:1572–3. doi: 10.1093/bioinformatics/btq170

43. Zhang B, Wu Q, Li B, Wang D, Wang L, Zhou Y. m(6)A regulator-mediated methylation modification patterns and tumor microenvironment infiltration characterization in gastric cancer. *Mol Cancer.* (2020) 19:53. doi: 10.1186/s12943-020-01170-0

44. Zeng D, Li M, Zhou R, Zhang J, Sun H, Shi M, et al. Tumor microenvironment characterization in gastric cancer identifies prognostic and immunotherapeutically relevant gene signatures. *Cancer Immunol Res.* (2019) 7:737–50.

45. Liu D, Yang X, Wu X. Tumor immune microenvironment characterization identifies prognosis and immunotherapy-related gene signatures in melanoma. *Front Immunol.* (2021) 12:663495. doi: 10.3389/fimmu.2021.663495

46. Zeng D, Wu J, Luo H, Li Y, Xiao J, Peng J, et al. Tumor microenvironment evaluation promotes precise checkpoint immunotherapy of advanced gastric cancer. *J Immunother Cancer.* (2021) 9:e002467. doi: 10.1136/jitc-2021-002467

47. Li H, Hu J, Yu A, Othmane B, Guo T, Liu J, et al. RNA modification of N6-methyladenosine predicts immune phenotypes and therapeutic opportunities in kidney renal clear cell carcinoma. *Front Oncol.* (2021) 11:642159. doi: 10.3389/fonc.2021.642159

48. Hänzelmann S, Castelo R, Guinney J. GSVA: gene set variation analysis for microarray and RNA-seq data. *BMC Bioinformatics.* (2013) 14:7. doi: 10.1186/1471-2105-14-7

49. Charoentong P, Finotello F, Angelova M, Mayer C, Efremova M, Rieder D, et al. Pan-cancer immunogenomic analyses reveal genotype-immunophenotype relationships and predictors of response to checkpoint blockade. *Cell Rep.* (2017) 18:248–62. doi: 10.1016/j.celrep.2016.12.019

50. Cai Y, Yang Y, Chen X, Wu G, Zhang X, Liu Y, et al. Circulating 'lncRNA OTTHUMT00000387022' from monocytes as a novel biomarker for coronary artery disease. *Cardiovasc Res.* (2016) 112:714–24. doi: 10.1093/cvr/cvw022

51. Marino A, Zhang Y, Rubinelli L, Riemma M, Ip J, Di Lorenzo A, et al. Pressure overload leads to coronary plaque formation, progression, and myocardial events in ApoE-/- mice. *JCI Insight.* (2019) 4:e128220. doi: 10.1172/jci.insight.128220

52. Xu M, Guo Y, Li D, Cen X, Qiu H, Ma Y, et al. Screening of lipid metabolism-related gene diagnostic signature for patients with dilated cardiomyopathy. *Front Cardiovasc Med.* (2022) 9:853468. doi: 10.3389/fcvm.2022.853468

53. Chen H, Peng L, Wang Z, He Y, Tang S, Zhang X, et al. Exploration of cross-talk and pyroptosis-related gene signatures and molecular mechanisms between periodontitis and diabetes mellitus via peripheral blood mononuclear cell microarray data analysis. *Cytokine.* (2022) 159:156014. doi: 10.1016/j.cyto.2022.156014

54. Veglia F, Sanseviero E, Gabrilovich DI. Myeloid-derived suppressor cells in the era of increasing myeloid cell diversity. *Nat Rev Immunol.* (2021) 21:485–98. doi: 10.1038/s41577-020-00490-y

55. Yu Z, Ling Y, Xu Q, Cao Y, Tang S, Fu C, et al. Blocking the A(2B) adenosine receptor alleviates myocardial damage by inhibiting spleen-derived MDSC mobilisation after acute myocardial infarction. *Ann Med.* (2022) 54:1616–26. doi: 10.1080/07853890.2022.2084153

56. Reddy K, Khaliq A, Henning RJ. Recent advances in the diagnosis and treatment of acute myocardial infarction. *World J Cardiol.* (2015) 7:243–76.

57. Yao T, Lu W, Zhu J, Jin X, Ma G, Wang Y, et al. Role of CD11b+Gr-1+ myeloid cells in AGEs-induced myocardial injury in a mice model of acute myocardial infarction. *Int J Clin Exp Pathol.* (2015) 8:3238–49.

58. Smith AD, Lu C, Payne D, Paschall A, Klement J, Redd P, et al. Autocrine IL6-Mediated activation of the STAT3-DNMT axis silences the TNFα-RIP1 necroptosis pathway to sustain survival and accumulation of myeloid-derived suppressor cells. *Cancer Res.* (2020) 80:3145–56. doi: 10.1158/0008-5472.CAN-19-3670

59. Kwon JS, Kim Y, Cho A, Cho H, Kim J, Hong M, et al. The novel role of mast cells in the microenvironment of acute myocardial infarction. *J Mol Cell Cardiol.* (2011) 50:814–25. doi: 10.1016/j.yjmcc.2011.01.019

60. Kupreishvili K, Fuijkschot W, Vonk A, Smulders Y, Stooker W, Van Hinsbergh V, et al. Mast cells are increased in the media of coronary lesions in patients with myocardial infarction and may favor atherosclerotic plaque instability. *J Cardiol.* (2017) 69:548–54. doi: 10.1016/j.jjcc.2016.04.018

61. Leoni C, Montagner S, Rinaldi A, Bertoni F, Polletti S, Balestrieri C, et al. Dnmt3a restrains mast cell inflammatory responses. *Proc Natl Acad Sci USA.* (2017) 114:E1490–9. doi: 10.1073/pnas.1616420114

62. Tahiliani M, Koh K, Shen Y, Pastor W, Bandukwala H, Brudno Y, et al. Conversion of 5-methylcytosine to 5-hydroxymethylcytosine in mammalian DNA by MLL partner TET1. *Science.* (2009) 324:930–5. doi: 10.1126/science.1170116

63. Tan L, Shi YG. Tet family proteins and 5-hydroxymethylcytosine in development and disease. *Development.* (2012) 139:1895–902.

64. He YF, Li B, Li Z, Liu P, Wang Y, Tang Q, et al. Tet-mediated formation of 5-carboxylcytosine and its excision by TDG in mammalian DNA. *Science.* (2011) 333:1303–7.

65. Pulikkottil AJ, Bamezai S, Ammer T, Mohr F, Feder K, Vegi N, et al. TET3 promotes AML growth and epigenetically regulates glucose metabolism and leukemic stem cell associated pathways. *Leukemia.* (2022) 36:416–25. doi: 10.1038/s41375-021-01390-3

66. Liu Y, Wang D, Zhou M, Chen H, Wang H, Min J, et al. The KRAS/Lin28B axis maintains stemness of pancreatic cancer cells via the let-7i/TET3 pathway. *Mol Oncol.* (2021) 15:262–78. doi: 10.1002/1878-0261.12836

67. Kologrivova I, Shtatolkina M, Suslova T, Ryabov V. Cells of the immune system in cardiac remodeling: main players in resolution of inflammation and repair after myocardial infarction. *Front Immunol.* (2021) 12:664457. doi: 10.3389/fimmu.2021.664457

frontiers | Frontiers in Cardiovascular Medicine

TYPE Original Research
PUBLISHED 04 January 2023
DOI 10.3389/fcvm.2022.1059543

Check for updates

OPEN ACCESS

EDITED BY
Miguel Hueso,
Bellvitge University Hospital, Spain

REVIEWED BY
Xueping Gao,
Third Military Medical Univeristy, China
Marlin Touma,
University of California, Los Angeles, United States

*CORRESPONDENCE
Meng Li
✉ lim331@163.com
Taohong Hu
✉ hutaohong2010@163.com

†These authors have contributed equally to this work

SPECIALTY SECTION
This article was submitted to Cardiovascular Genetics and Systems Medicine, a section of the journal Frontiers in Cardiovascular Medicine

RECEIVED 01 October 2022
ACCEPTED 08 December 2022
PUBLISHED 04 January 2023

CITATION
Li H, Sun X, Li Z, Zhao R, Li M and Hu T (2023) Machine learning-based integration develops biomarkers initial the crosstalk between inflammation and immune in acute myocardial infarction patients.
Front. Cardiovasc. Med. 9:1059543.
doi: 10.3389/fcvm.2022.1059543

COPYRIGHT
© 2023 Li, Sun, Li, Zhao, Li and Hu. This is an open-access article distributed under the terms of the Creative Commons Attribution License (CC BY). The use, distribution or reproduction in other forums is permitted, provided the original author(s) and the copyright owner(s) are credited and that the original publication in this journal is cited, in accordance with accepted academic practice. No use, distribution or reproduction is permitted which does not comply with these terms.

Machine learning-based integration develops biomarkers initial the crosstalk between inflammation and immune in acute myocardial infarction patients

Hongyu Li[1,2†], Xinti Sun[3†], Zesheng Li[4], Ruiping Zhao[2], Meng Li[2*] and Taohong Hu[1*]

[1]Medical College of Soochow University, The People's Liberation Army of China (PLA) Rocket Force Characteristic Medical Center, Beijing, China, [2]Department of Cardiovascular Medicine, Baotou Central Hospital, Institute of Cardiovascular Diseases, Translational Medicine Center, Baotou, China, [3]Department of Thoracic Surgery, Tianjin Medical University General Hospital, Tianjin, China, [4]Key Laboratory of Post-Neuroinjury Neuro-Repair and Regeneration in Central Nervous System, Tianjin Medical University General Hospital, Tianjin, China

Great strides have been made in past years toward revealing the pathogenesis of acute myocardial infarction (AMI). However, the prognosis did not meet satisfactory expectations. Considering the importance of early diagnosis in AMI, biomarkers with high sensitivity and accuracy are urgently needed. On the other hand, the prevalence of AMI worldwide has rapidly increased over the last few years, especially after the outbreak of COVID-19. Thus, in addition to the classical risk factors for AMI, such as overwork, agitation, overeating, cold irritation, constipation, smoking, and alcohol addiction, viral infections triggers have been considered. Immune cells play pivotal roles in the innate immunosurveillance of viral infections. So, immunotherapies might serve as a potential preventive or therapeutic approach, sparking new hope for patients with AMI. An era of artificial intelligence has led to the development of numerous machine learning algorithms. In this study, we integrated multiple machine learning algorithms for the identification of novel diagnostic biomarkers for AMI. Then, the possible association between critical genes and immune cell infiltration status was characterized for improving the diagnosis and treatment of AMI patients.

KEYWORDS

acute myocardial infarction, prognosis, immune infiltration, machine learning, bioinformatics

Introduction

Acute myocardial infarction (AMI) is a medical emergency caused by acute occlusion of the coronary arteries resulting in hypoperfusion and ischemic necrosis of myocardial cells. The pathophysiology of AMI is complex involving hemodynamic and circulatory dysfunction, organ failure, and even crosstalk between inflammation and immune disorders. The high incidence and mortality of AMI cause a serious social and healthy economic burden and affect the quality of human life (1, 2). It is vital to diagnose and treat AMI as soon as possible to reduce myocardial injury and malignant consequences, reduce mortality to a certain extent, and improve the patient's prognosis (3). As of now, the evaluation of myocardial enzyme (CKMB) and cardiac troponin I (cTnI) remains the gold standard for the diagnosis of acute myocardial infarction. Nevertheless, some researchers have pointed out that patients with chronic kidney disease and heart failure also have elevated cTnI levels, making the diagnosis of AMI based on these biomarkers still unsatisfactory due to their low specificity and sensitivity (4–6). In addition, with an aging global population and an increasing life expectancy, it has become more crucial than ever to diagnose and prevent AMI.

In recent years, new technologies such as next-generation sequencing have allowed us to make great advances in diagnosing cardiovascular disease and identifying therapeutic biomarkers. With the rapid development of bioinformatics, novel methods are being developed for the prediction of AMI. It is worth noting that traditional differential gene expression analysis (DEGs) is mainly used to identify hub genes, but may lead to the loss of intrinsic biological information. Furthermore, although multi-biomarker approaches have been reported to significantly improve the diagnostic accuracy of AMI, they still lack robust capabilities due to complex genetic structures and inadequate methods (7–9). Many predictive models with poor accuracy and low efficiency may not enough for screening and early detection of AMI. Fortunately, the development of machine-learning algorithms, such as random forest (RF) and support vector machine-recursive feature elimination (SVM-REF), have been successfully applied to biomarker discovery and to build accurate prognostic risk models (10, 11).

Hence, in the present study, we integrated weighted gene co-expression network analysis (WGCNA) and DEGs analysis to identify candidate genes related to the pathogenesis of AMI. Then by combining the utilization of multiple machine-learning algorithms including the least absolute shrinkage and selection operator (LASSO), RF, and SVM-REF, we finally obtained seven optimal feature genes. Then we evaluated their predictive performance of them using the receiver operating characteristic (ROC) curve. Thereafter, the mechanism by which they contribute to AMI was investigated by functional enrichment analyses such as GO, KEGG, DO, and GSEA. Besides, immune-related algorithms such as ssGSEA were conducted to assess of the levels of infiltration of different immune cell types and functions. In conclusion, we found that seven powerful diagnostic efficacy genes were present in patients with AMI, indicating that they may provide new potential targets for diagnosis and prognosis of AMI, thus leading to improved outcomes.

Materials and methods

Data collection and processing

The study flowchart is presented in **Figure 1**. AMI-related raw gene expression profiles data were downloaded from the Gene Expression Omnibus database (GEO).[1] Two microarray datasets GSE48060 (GPL570, Control: 21, AMI: 31) and GSE66360 (GPL570, Control: 50, AMI: 49) were included in subsequent bioinformatics analysis. Three microarray datasets GSE19339 (GPL570, Control: 4, AMI: 4), GSE97320 (GPL570, Control: 3, AMI: 3), and GSE61145 (GPL6106, GPL6884, Control: 17, AMI: 31) were used as independent validation sets. Information on the datasets was displayed in **Supplementary Table 1**. It should be noted that if a gene has multiple probe loci during the conversion of probe ID and gene symbol, we use the average value of probe loci as the gene expression level. A further step was taken to convert the probe IDs to the gene symbols based on the annotation files from the respective platforms and to remove the probes which did not correspond to the gene symbols. Next, the microarray data were transformed into log2 values for further analysis. And we integrated them using Combat algorithm implemented in R package "sva" (12) and removed batch effects to form a merged dataset.

Differential expression analysis

Differential expression analyses between AMI and control samples were conducted to identify DEGs using R package "limma" (criteria: $|\log FC| > 0.75$, P-value < 0.05). Significantly upregulated genes and downregulated genes were visualized by volcano plot and heatmap.

Weighted gene co-expression network analysis

Weighted gene co-expression network analysis was performed *via* the R package "WGCNA" to identified potential functional modules that could characterize the biological function of the AMI samples (12). It was checked

1 http://www.ncbi.nlm.nih.gov/geo

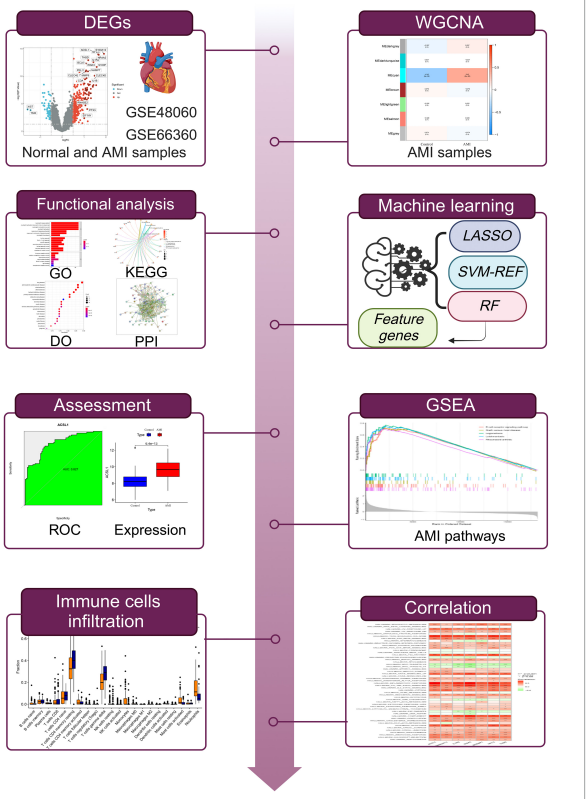


FIGURE 1
The workflow of this study.

to ensure that no anomalous samples had escaped clustering of samples and were excluded from the merged gene matrix. In brief, on the basis of weighted correlation adjacency matrices and cluster analyses, genes with similar expression patterns were assigned to co-expression modules. From the adjacency matrix, a topological overlap matrix (TOM) was derived, based on which genes were divided into modules according to the degree of dissimilarity between them in the TOM. The cut height, minimal module size, and soft-thresholding power were set as 0.25, 50, and 24 (scale-free R^2 = 0.9), respectively. Finally, gene importance (GS) and module membership (MM) were calculated. Then spearman correlation coefficients as well as the corresponding *P*-value between control, AMI groups, and functional modules were calculated by using the Spearman method. Finally, the hub module extracted the corresponding genes were selected for in-depth analysis.

Functional enrichment analysis and protein-protein interaction network

To identify the putative significant functional terms between the AMI and control groups, we applied the gene sets enrichment analysis (GSEA) using GSEA software with reference gene set (c2.cp.kegg.v11.0.symbols) and the significance levels for enriched gene sets were determined at *q*-value [false discovery rate (FDR)] < 0.05 and $P < 0.05$ (13). The upregulated pathways had a normalized enrichment score (NES) greater than zero, whereas the downregulated pathways had a NES less than zero. We further obtained the overlapped candidate genes between DGEs and module genes based on above mentioned analyses. Venn diagrams were created using the Venn Diagrams software[2] to display the overlap genes. Gene ontology (GO), Kyoto Encyclopedia of Genes and Genomes (KEGG), and Disease ontology (DO) enrichment analyses were performed using "clusterProfiler" and "DOSE" R packages to explore the function and pathways of the overlapped candidate genes (14). Besides, we mapped a protein-protein Interaction (PPI) network to explore the interaction of overlapped candidate genes using the online mapping tool "STRING.[3]" The co-expression network was plotted by using R package "igraph" to explore the correlation intensity between score genes.

Screening optimal feature genes

We applied a combination of machine learning algorithms (LASSO, SVM-REF, and RF) to predict disease status and identify significant prognostic variables. The LASSO regression analysis tool selects variables and regularizes them simultaneously to improve the predictive capability of statistical models (14). The SVM, a supervised machine learning method, is used for regression and classification; the FRE algorithm was used to prevent overfitting while producing interpretable results (15, 16). As a result, the SVM-RFE algorithm was used to identify the gene sets with the highest discriminatory powers that would be used to identify the most appropriate feature genes. The classification tree is the basis for the RF method, which is one of the most popular approaches to various prediction problems (17). The optimal tree number was determined by the tree number with the lowest error rate and the best stability among 1–500 trees. Following this, an RF was constructed based on the selected parameter, and the important genes were selected as the key genes for AMI diagnosis based on the decreasing accuracy method (Gini coefficient). Considering the gene importance greater than 2 is a common screening criterion in the RF algorithm, which has been used in similar studies (18), the top 10 important genes (importance > 2) were chosen as the novel gene signatures for predicting prognosis in AMI. Finally, the commonly shared genes from the intersection of a couple of machine learning algorithms were the optimal feature genes.

2 http://bioinformatics.psb.ugent.be/webtools/Venn/
3 https://string-db.org/cgi/input.pl

The expression and diagnosis significance of optimal feature genes

The expression levels of the optimal feature genes in AMI samples and control samples were calculated using Wilcoxon rank-sum test. We further validated the predictive value of the optimal feature genes using receiver operator characteristics (ROC) curves.

Assessment of hallmark gene sets and immune cell infiltration

The CIBERSORT algorithm is a deconvolutional arithmetic on the foundation of genetics expressions, and it can be used to assess variations in a gene group within a specimen in comparison with the variations in the rest of the genes (19). The CIBERSORT algorithm was used to identify the infiltration of 22 immune cells in normal and AMI samples, and box plots were used to illustrate the immune cell composition of patients with varying immune patterns. The Wilcoxon rank-sum test was used to evaluate the differences in immune cell proportions, and $P < 0.05$ was considered statistically significant. Additionally, the relative levels of the 50 hallmark gene sets (h.all.v7.5.1.symbols.gmt) in the merge dataset were quantified using the ssGSEA algorithm (20). Additionally, Spearman's correlations for the 50 hallmark genes sets and the optimal feature genes were calculated.

GSEA and correlation analysis of optimal feature genes

In addition, GSEA was utilized to determine the biological significance of optimal feature genes, utilizing the gene set of "c2.cp.kegg.v11.0.symbols" from the Molecular Signature Database[4] as a reference. A gene set permutation with 1,000 times was conducted for each analysis in order to obtain a normalized enrichment score. An FDR < 0.05 was regarded as significant enrichment. Besides, correlations between optimal feature gene expression levels were calculated using Pearson correlation analysis.

Sample collection

Six AML patients and six healthy subjects of peripheral blood was stored inside 1.5 ml RNase-free tubes at −80°C until use. All blood samples were randomly sampled from the Baotou Central Hospital from August 2021 to September 2022. Diagnosis of AMI was based on the Fourth Universal Definition of Myocardial Infarction. This study was approved by the Ethics Committee of the Baotou Central Hospital and was conducted in accordance with the Declaration of Helsinki.

RNA extraction and quantitative reverse transcription PCR (qRT-PCR)

RNA was extracted from blood samples using Trizol reagent and then cDNA was synthesized by reverse transcription using the PrimeScript^{TM} RT Reagent Kit (RR037, TaKaRa, China) based on the manufacturer's protocol. GAPDH was used as the internal references, then qRT-PCR was conducted using the SYBR Green PCR Kit (RR820, TaKaRa, China) based on the manufacturer's protocol. The expression level was quantized by $2^{-\Delta\Delta CT}$ mode. All reactions were repeated in triplicate. The primers used are shown in **Supplementary Table 2**.

Statistical analysis

All data processing, statistical analysis, and plotting were conducted in R software (version 4.1.1) and GraphPad Prism (version 8.0.2). Wilcoxon rank-sum test or Student's *t*-test was utilized for analyzing the difference between the two groups. The correlation between the variables was determined using Pearson's or Spearman's correlation test. All statistical *P*-values were two-side, and $P < 0.05$ was regarded as statistical significance.

Results

Identification of DEGs between control and AMI samples

In this study, we merged two microarray datasets including GSE48060 and GSE66360 datasets from the GEO database and totally obtained 71 control and 80 AMI samples. Before data analysis, we removed the batch effect from different batches between the datasets (**Figure 2A**). Next, a total of 118 DEGs (**Supplementary Table 3**) including 11 downregulated genes and 107 upregulated genes were identified, which were intuitively presented in the heatmap (**Figure 2B**). Among them, some genes were significantly upregulated, such as ACSL1, S100A12, NFIL3, THBD, NR4A2, IL1R2, BCL6, IRAK3, S100P, PELI1, NAMPT, CLEC4E, MMP9, CLEC4D, CDA, IL1B, RNASE2, PTX3, EIF1AY, etc. While genes like XIST, TSIX were significantly downregulated (**Figure 2C**). To further clarify the differences in functional and biological pathways between AMI and control samples, we performed GSEA analysis of KEGG and screened significant enriched signaling pathways

4 http://software.broadinstitute.org/gsea/msigdb

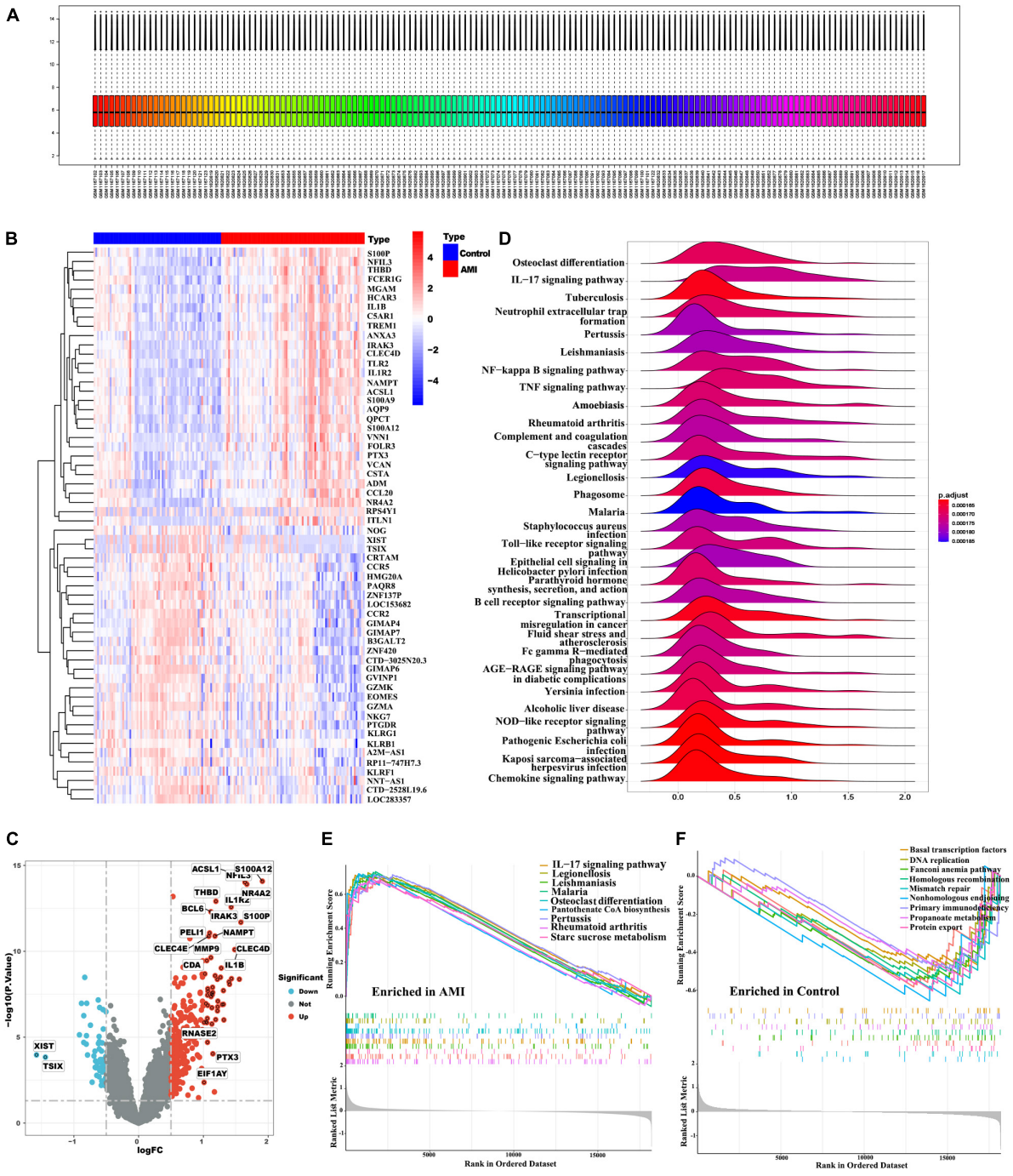


FIGURE 2
Identification of DEGs and functional annotation. **(A)** Gene expression level statistics of the integrated dataset after removed batch effect. **(B)** The heatmap of AMI-related DEGs expression levels: blue-low gene expression; red-high gene expression. **(C)** The volcano plot of AMI-related DEGs expression. **(D)** Ridgeline plot of GSEA results. **(E,F)** The main signaling pathways that are significantly enriched in the AMI group **(E)**, and in the control group **(F)**.

(Supplementary Table 4). Ridgeline plot showed that there were changes in various immune-related biological functions and processes in AMI, such as the activation of IL-17, NF-kB, and TNF signaling pathways, and the formation of centriole extracellular traps (NETs) (Figure 2D). Additionally, IL-17 signaling pathway, starch and sucrose metabolism, and pantothenate and CoA biosynthesis were significantly enriched in the AMI group (Figure 2E). In contrast, basal transcription

factors, DNA replication, mismatch repair, fanconi anemia, etc. were significantly enriched in the control group (Figure 2F).

WGCNA and screening of hub modules

The co-expression network was constructed by WGCNA. A total of 21,654 genes, 71 control and 80 AMI samples were preferred to cluster the samples and exclude the obviously aberrant samples by setting a threshold, as shown in Figure 3A. Then, based on scale-free R^2 = 0.9 and a high average connectivity, we set the soft power threshold to 24 (Figure 3B). In total, seven modules were identified for further study after the strongly associated modules were merged according to a 0.25 clustering height limit. The primed and merged modules were eventually displayed under the clustering tree (Figure 3C). The correlation between modules was assessed, and the results revealed that there was no significant association between them (Figure 3D). The reliability of modules delineation was demonstrated by transcription correlation analysis within modules, which revealed no substantial linkage between modules (Figure 3E). Similarly, an examination of the correlation between ME values and clinical features was conducted using frontal correlations to investigated the relationships between ME values and clinical symptoms. The cyan module showed a strong correlation with AMI (R = 0.42, P < 6.3e-39) (Figures 3F, G). In total 519 candidate genes in the cyan module were included in the subsequent analysis (Supplementary Table 5).

Functional enrichment analysis of overlapping DEGs

In total 96 overlapping genes (Supplementary Table 6) were screened from above mentioned DEGs and cyan module hub genes, which were also named candidate feature genes (Figure 4A). To reveal the possible biological function and enrichment pathways of the candidate feature genes, GO, KEGG, and DO analyses were carried out, subsequently. Among them, GO analysis consisted of three categories: biological process (BP), cellular component (CC), and molecular function (MF). In the BP category, the candidate feature genes were mainly enriched in neutrophil degranulation, neutrophil activation involved in immune response, neutrophil mediated immunity and neutrophil activation, etc. For the CC category, the candidate feature genes were enriched in many aspects, such as tertiary granule, ficolin-1-rich granule, specific granule and secretory granule membrane. For the MF category, the candidate feature genes were significantly enriched in immune receptor activity, pattern recognition receptor activity, chemokine activity and carbohydrate binding (Figure 4B). In addition, these genes were particularly associated with IL-17 signaling pathway, TNF signaling pathway, lipid and atherosclerosis, toll-like receptor signaling pathway, C-type lectin receptor signaling pathway, legionellosis, osteoclast differentiation, rheumatoid arthritis and NF-kappa B signaling pathway in the KEGG enrichment analysis (Figures 4C–E). DO analysis showed that the candidate feature genes mainly enriched in arteriosclerotic cardiovascular disease, bacterial infectious disease, arteriosclerosis and atherosclerosis (Figure 4F). The above functional enrichment analyses show that the immune system of AMI patients has changes in multiple dimensions, and it may have a common pathological process with the occurrence and progression of other autoimmune diseases. Then, to further reveal protein-protein interactions in the pathogenesis of AMI, we analyzed the protein-protein interaction (PPI) network of the candidate feature genes and constructed a PPI network using the String website. The PPI network for these proteins was shown in Figures 4G, H. Taken together, candidate feature genes play an important role in the pathogenesis of AMI.

Identification of optimal feature genes by integrating multiple machine learning algorithms

To identify the putative feature genes, three different machine learning algorithms were employed. Specifically, we identified 30 feature genes as the diagnostic markers for AMI form the aforementioned 96 candidate feature genes obtained from the LASSO analysis (Figure 5A and Supplementary Table 7). Furthermore, using the SVM-REF algorithm, 60 feature genes were selected after 5-fold cross-validation of the 96 candidate feature genes (Figure 5B, Supplementary Table 8). Besides, for the RF algorithm, top 10 feature genes with importance >2 were determined, including MCEMP1, SLC11A1, IRAK3, THBD, MMP9, NFIL3, IL1R2, ACSL1, BCL6, and GABARAPL1 (Figures 5C, D). Finally, the intersection of the feature genes obtained from the above three machine learning algorithms was taken and a total of seven optimal feature genes were identified, including ACSL1, GABARAPL1, IL1R2, IRAK3, MCEMP1, NFIL3, and THBD, that could be used as potential diagnostic markers for AMI and may be critical genes involved in AMI progression (Figure 5E).

Assessment of the expression and diagnosis significance of optimal feature genes

We further validated the expression levels of the 7 optimal feature genes in 80 AMI samples and 71 normal samples. Additionally, the expression levels of the 7 genes were significantly upregulated in the AMI samples, indicating their

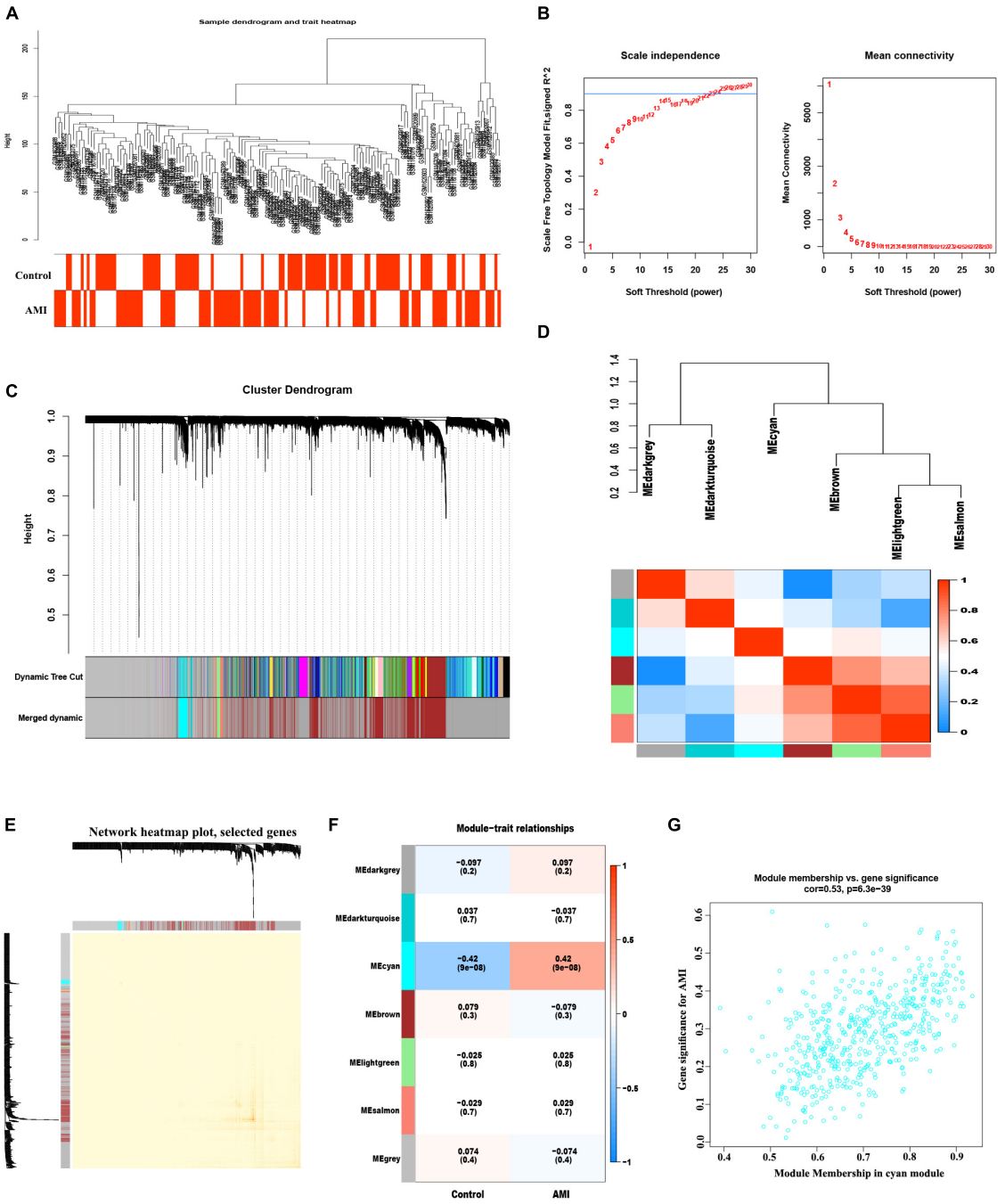


FIGURE 3
Weight correlation network analysis. **(A)** Sample clustering dendrogram with tree leaves corresponding to individual samples. **(B)** Analysis of the scale-free fit index (R^2) and the mean connectivity for various soft-thresholding powers. **(C)** The original and combined modules under the clustering tree with cut-off values height of 0.25. **(D)** Collinear heat map of module feature genes. Red color indicates a high correlation, blue color indicates the opposite results. **(E)** Clustering dendrogram of module feature genes. **(F)** Heat map of module–trait correlations. Red represents positive correlations and blue represents negative correlations. **(G)** MM vs. GG scatter plot of AMI for cyan module.

potential roles during the progression of AMI (Figures 6A–G, $P < 0.01$). Besides, to quantitatively assess the diagnostic and predictive value of the optimal feature genes, we conducted a ROC curve analysis (Figure 6H). The AUC values of ROC curves were ACSL1 of 0.827 (Figure 6I), GABARAPL1 of 0.841 (Figure 6J), IL1R2 of 0.849 (Figure 6K), IRAK3 of 0.845 (Figure 6L), MCEMP1 of 0.844 (Figure 6M), NFIL3 of 0.833 (Figure 6N), THBD of 0.843 (Figure 6O), demonstrating that

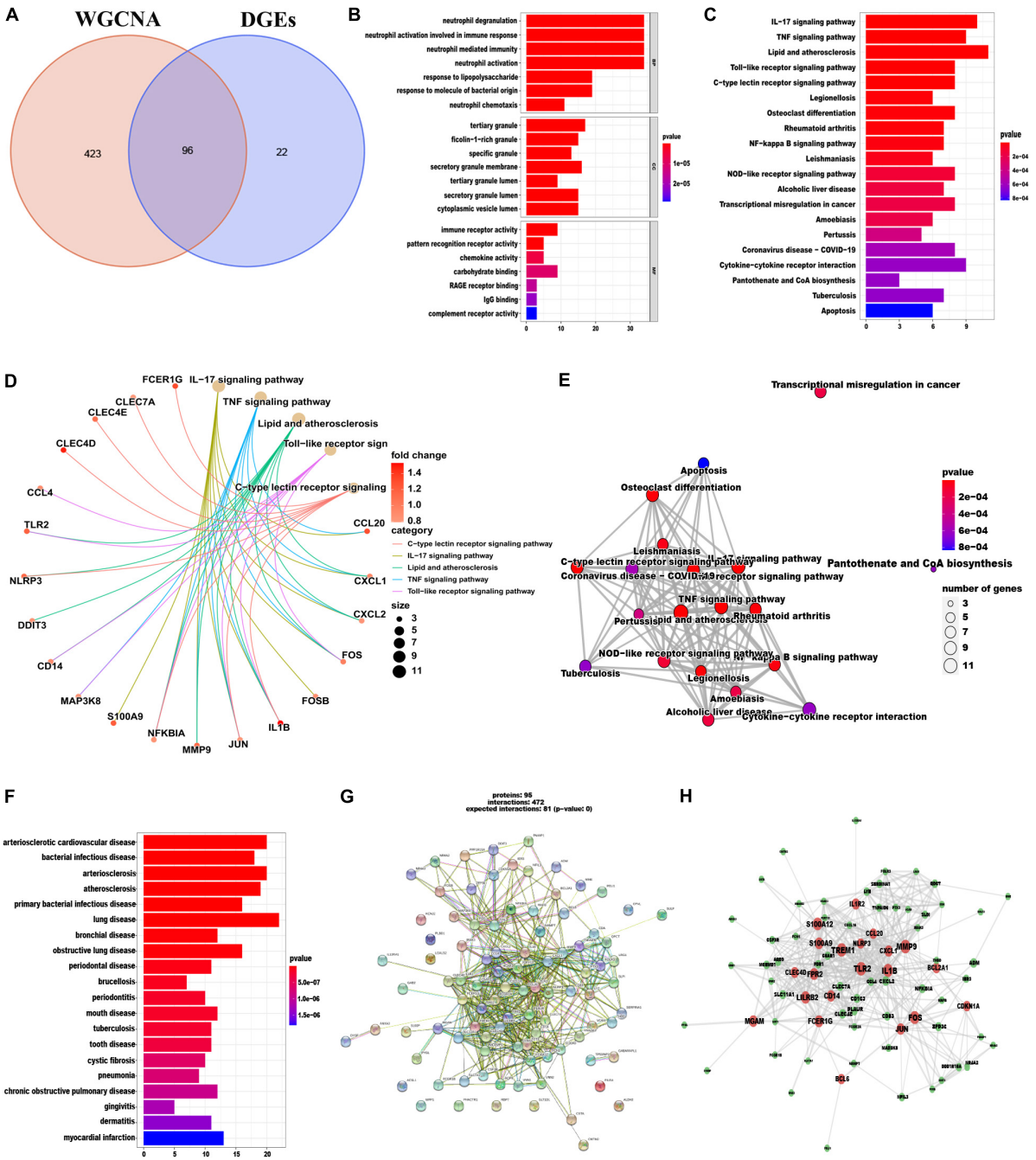


FIGURE 4
Identification and functional enrichment analyses of overlapping candidate genes. **(A)** Venn diagram showed the intersection of DEGs and module genes of WGCNA. **(B–F)** GO **(B)**, KEGG **(C–E)**, and DO **(F)** enrichment analysis of the overlapping candidate genes. **(G)** Protein-Protein Interaction (PPI) network of overlapping candidate genes. **(H)** The co-expression network showing correlation intensity of hub genes from overlapping candidate genes.

these optimal feature genes enable to estimate the progression and had a high diagnostic value for AMI.

In addition, for accurate and reliable results, we further validated the expression levels of the optimal feature genes in external validation dataset including 38 AMI samples and 24 control samples. The GSE19339, GSE97320, and GSE61145 datasets were also normalized before analysis (**Supplementary Figure 1**). As shown in **Figures 7A–G**, the expression of the seven optimal feature genes were significantly upregulated in the AMI samples relative to the control samples (all $P < 0.05$).

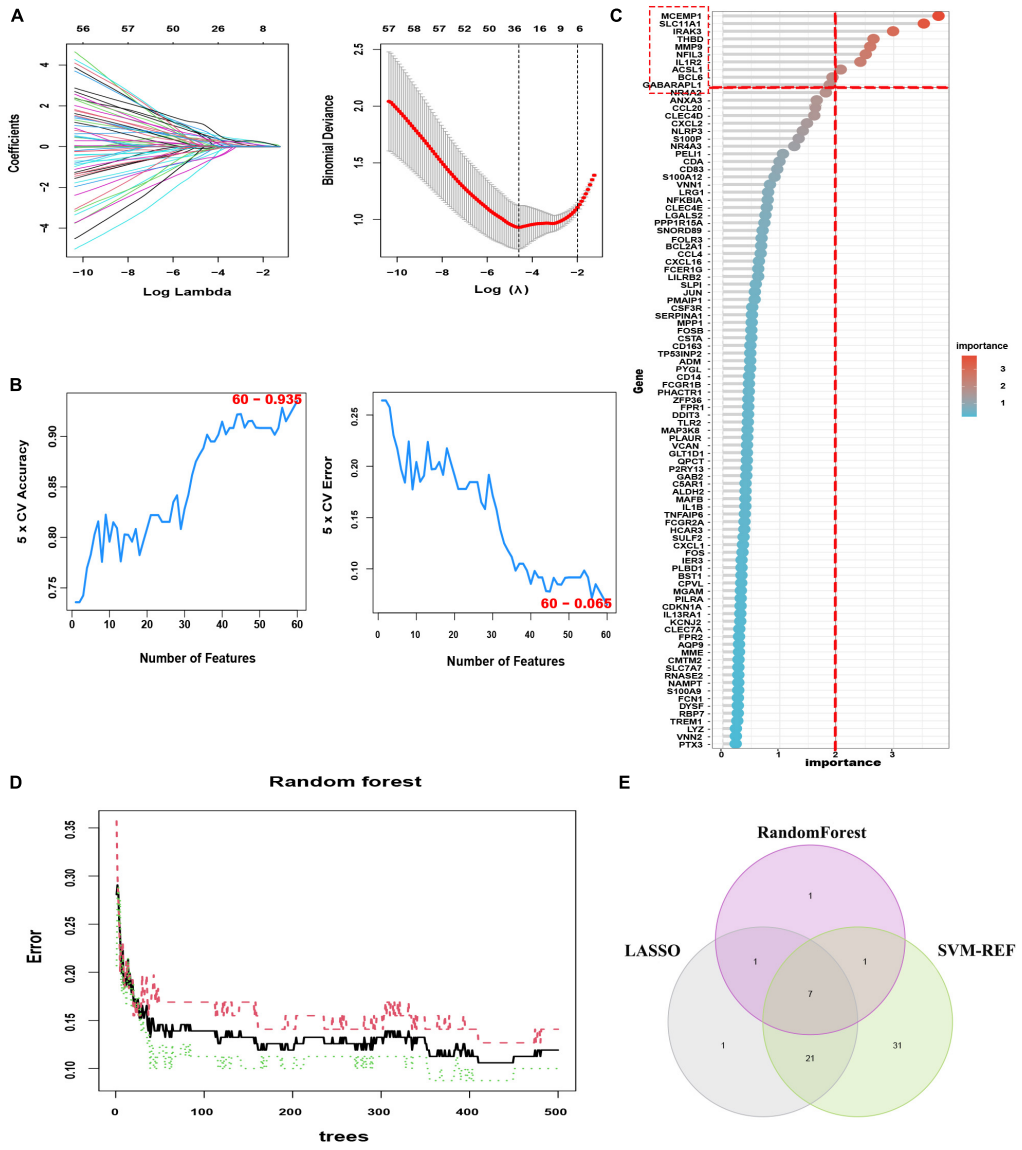


FIGURE 5
Three machine learning algorithms were integrated to identify the optimal feature genes. **(A)** LASSO coefficient profiles of the candidate optimal feature genes and the optimal lambda was determined when the partial likelihood deviance reached the minimum value. Each coefficient curve in the left picture represents a single gene. The solid vertical lines in right picture represent the partial likelihood deviance, and the number of genes (n = 30) corresponding to the lowest point of the cure is the most suitable for LASSO. **(B)** The SVM-RFE algorithm was used to further candidate optimal feature genes with the highest accuracy and lowest error obtained in the curves. The x-axis shows the number of feature selections, and the y-axis shows the prediction accuracy. **(C)** Relative importance of overlapping candidate genes calculated in random forest (Top 10 genes' importance > 2). Importance indexes on the x-axis and genetic variables are plotted on the y-axis. **(D)** Random forest for the relationships between the number of trees and error rate. The x-axis represents the number of decision trees and the y-axis is the error rate. **(E)** Venn diagram showing the seven optimal feature genes shared by LASSO, Random Forest, and SVM-REF algorithms.

Meanwhile, the external validation dataset also presented high AUC values: ACSL1 (AUC: 0.705), GABARAPL1 (AUC: 0.664), IL1R2 (AUC: 0.747), IRAK3 (AUC: 0.737), MCEMP1 (AUC: 0.783), NFIL3 (AUC: 0.671), THBD (AUC: 0.716) (**Figures 7H–O**). The results of external validation strongly proved that all optimal feature genes are involved in AMI and have a high diagnostic value for AMI.

Identification of the function of seven feature genes

Since these seven characteristic genes have a high guiding significance for judging prognosis, we then performed GSEA analysis on them to clarify their potential biological functions. Based on median expression levels of the optimal

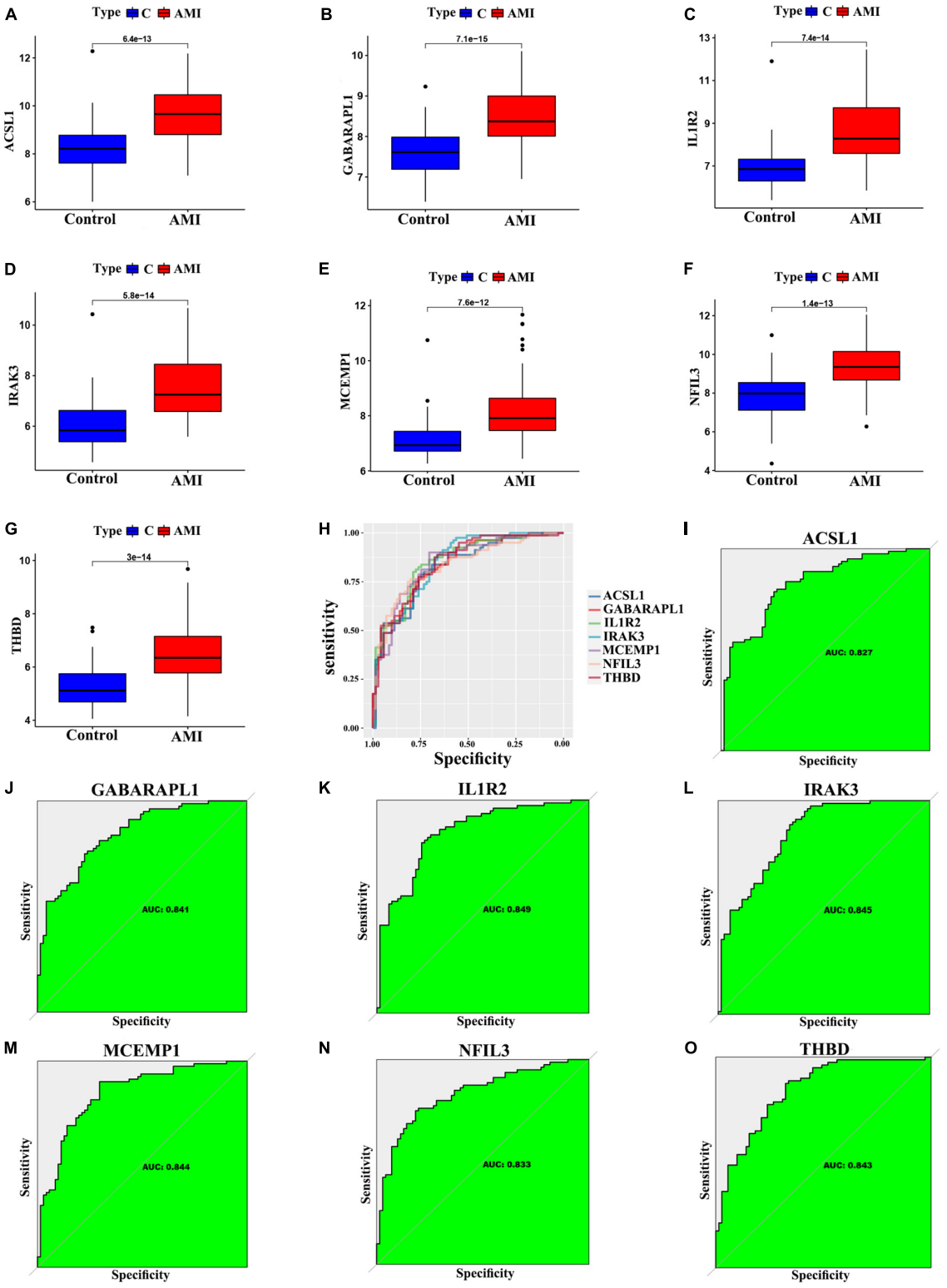


FIGURE 6
Verification of expression and diagnostic efficacy in predicting AMI progression of optimal feature genes. **(A–G)** Box plots showing the expression of ACSL1 **(A)**, GABARAPL1 **(B)**, IL1R2 **(C)**, IRAK3 **(D)**, MCEMP1 **(E)**, NFIL3 **(F)**, and THBD **(G)** in control and AMI samples. Statistic tests: Wilcoxon rank-sum test. **(H–O)** Roc curves **(H)** estimating the diagnostic performance of ACSL1 **(I)**, GABARAPL1 **(J)**, IL1R2 **(K)**, IRAK3 **(L)**, MCEMP1 **(M)**, NFIL3 **(N)**, and THBD **(O)**.

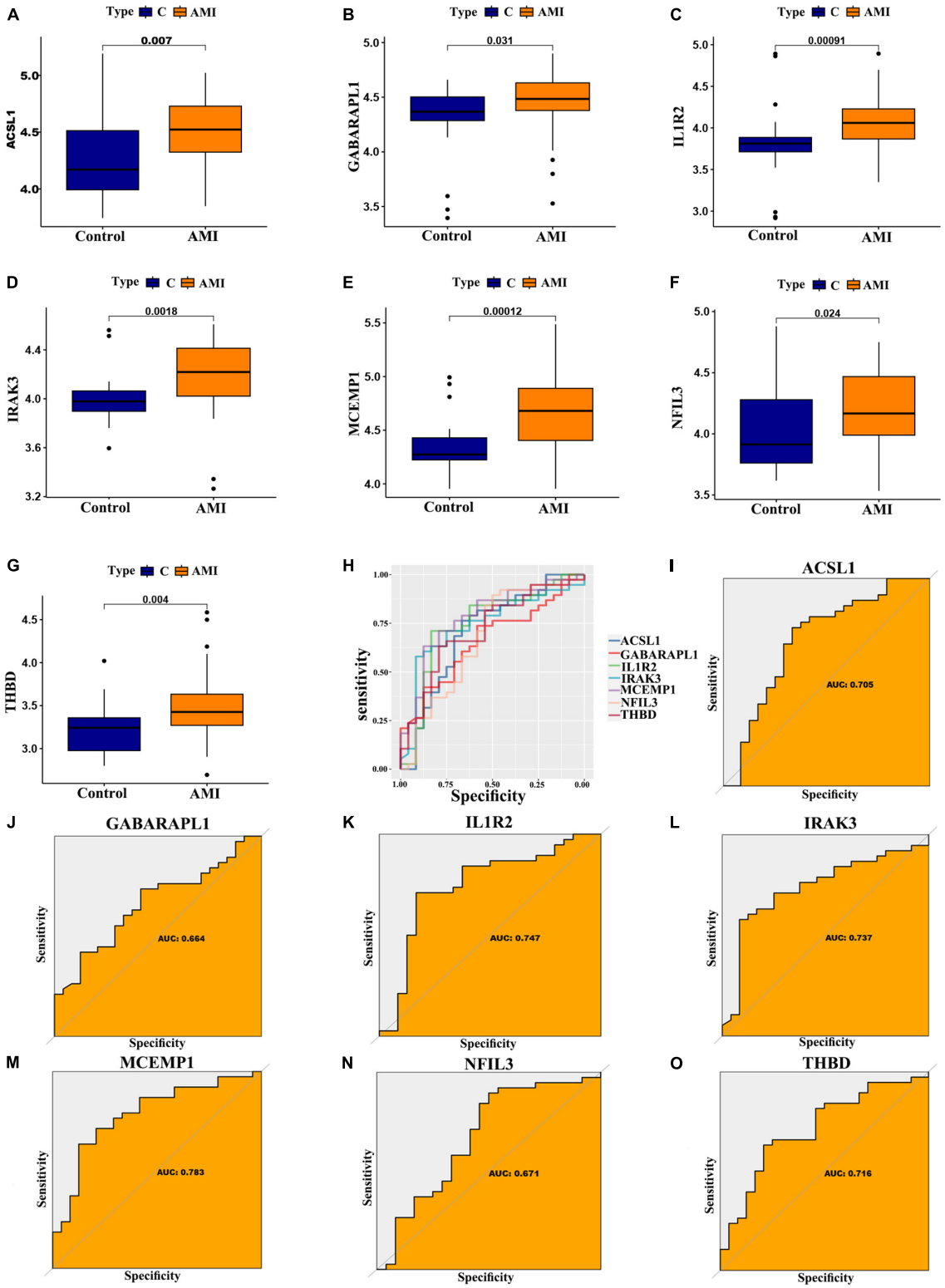


FIGURE 7
Verification of expression and diagnostic efficacy for optimal feature genes using external validation dataset. **(A–G)** Box plots showing the expression of ACSL1 **(A)**, GABARAPL1 **(B)**, IL1R2 **(C)**, IRAK3 **(D)**, MCEMP1 **(E)**, NFIL3 **(F)**, and THBD **(G)** in control and AMI samples. Statistic tests: Wilcoxon rank-sum test. **(H–O)** Roc curves **(H)** estimating the diagnostic performance of ACSL1 **(I)**, GABARAPL1 **(J)**, IL1R2 **(K)**, IRAK3 **(L)**, MCEMP1 **(M)**, NFIL3 **(N)**, and THBD **(O)**.

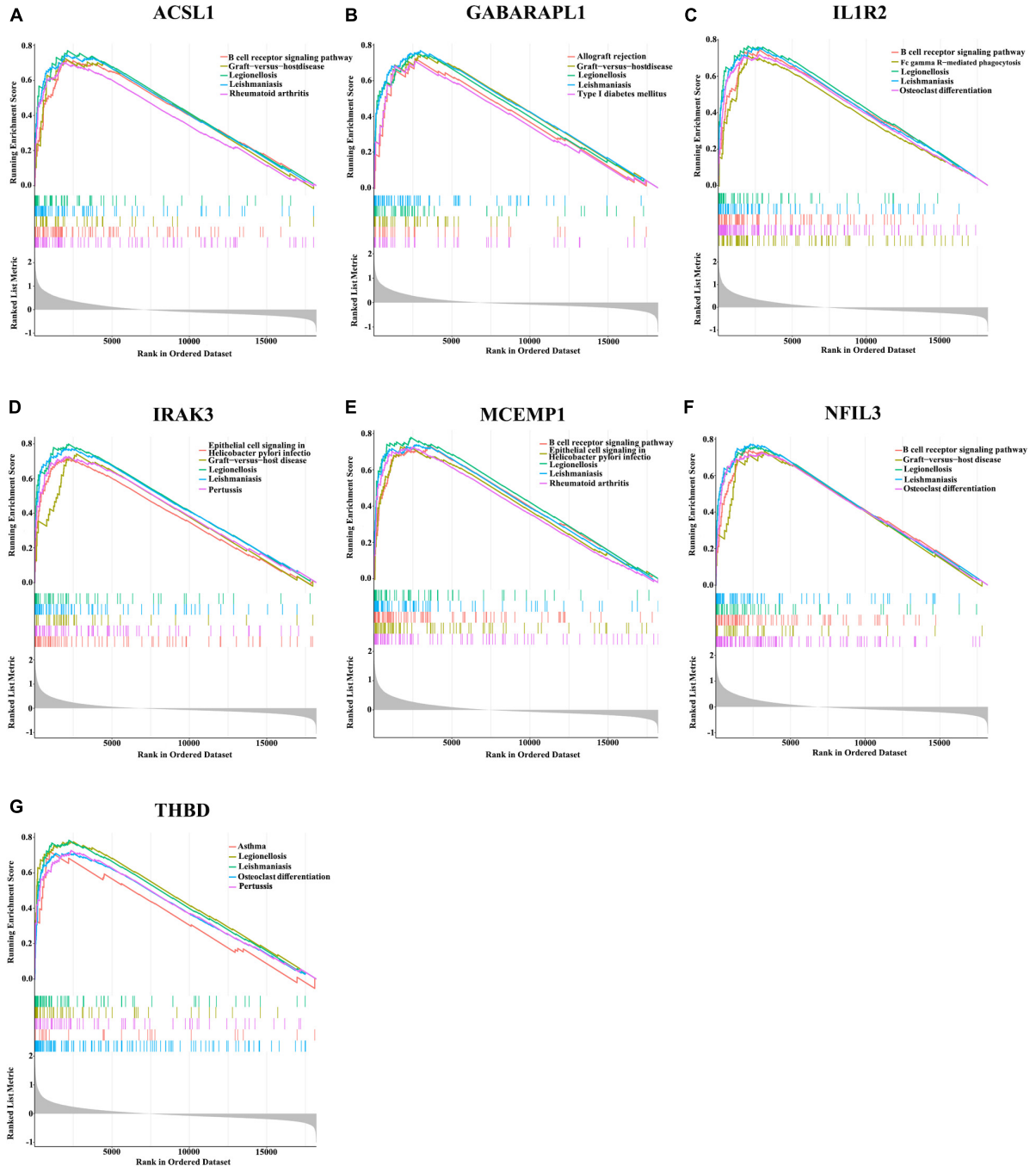


FIGURE 8
Gene sets enrichment analysis (GSEA) identifies signaling pathways in the optimal feature genes. **(A–G)** Top five signaling pathways that are significantly enriched in the high expression of ACSL1 **(A)**, GABARAPL1 **(B)**, IL1R2 **(C)**, IRAK3 **(D)**, MCEMP1 **(E)**, NFIL3 **(F)**, and THBD **(G)**.

feature genes, we divided AMI samples into two groups, respectively. Additionally, immune-related pathways such as B cell receptor signaling pathway, graft-vs.-host disease, legionellosis, leishmaniasis, and rheumatoid arthritis were significantly enriched in the high ACSL1 subgroup (Figure 8A), while metabolism-related pathways such as butanoate metabolism, linoleic acid metabolism, and taurine and hypotaurine metabolism were significantly enriched in the low ACSL1 subgroup (Supplementary Figure 2A). Allograft rejection, graft-vs.-host disease, legionellosis, leishmaniasis and type I diabetes mellitus were significantly enriched in the high GABARAPL1 subgroup (Figure 8B), whereas

metabolism of xenobiotics by cytochrome P450, aminoacyl-tRNA biosynthesis, butanoate metabolism, and valine, leucine and isoleucine degradation were significantly enriched in the low GABARAPL1 subgroup (**Supplementary Figure 2B**). B cell receptor signaling pathway, fc gamma R-mediated phagocytosis, legionellosis, leishmaniasis and osteoclast differentiation were significantly enriched in the high IL1R2 subgroup (**Figure 8C**), whereas linoleic acid metabolism, taurine and hypotaurine metabolism, and maturity onset diabetes of the young were significantly enriched in the low IL1R2 subgroup (**Supplementary Figure 2C**). Epithelial cell signaling in helicobacter pylori infection, graft-vs.-host disease, legionellosis, leishmaniasis and pertussis were significantly enriched in the high IRAK3 subgroup (**Figure 8D**), while aminoacyl-tRNA biosynthesis, primary immunodeficiency, and RNA polymerase were significantly enriched in the low IRAK3 subgroup (**Supplementary Figure 2D**). B cell receptor signaling pathway, epithelial cell signaling in helicobacter pylori infection, legionellosis, leishmaniasis and rheumatoid arthritis were significantly enriched in the high MCEMP1 subgroup (**Figure 8E**), whereas taste transduction and olfactory transduction were significantly enriched in the low MCEMP1 subgroup (**Supplementary Figure 2E**). B cell receptor signaling pathway, graft-vs.-host disease, legionellosis, leishmaniasis and osteoclast differentiation were significantly enriched in the high NFIL3 subgroup (**Figure 8F**), whereas drug metabolism - cytochrome P450, Linoleic acid metabolism, and nicotine addiction were significantly enriched in the low NFIL3 subgroup (**Supplementary Figure 2F**). Asthma, legionellosis, leishmaniasis, osteoclast differentiation and pertussis were significantly enriched in the high THBD subgroup (**Figure 8G**), whereas alanine, aspartate and glutamate metabolism, primary immunodeficiency, and ribosome were significantly enriched the low THBD subgroup (**Supplementary Figure 2G**). Interestingly, we noticed that B cell receptor signaling pathway was enriched multiple times, especially was enriched in the apical position in NFIL3, MCEMP1 and IL1R2 high expression groups.

Hallmark gene sets and immune cell infiltration

To further assess the differences in the immune cell infiltration and hallmark gene sets between AMI and control samples, the CIBERSORT algorithm was employed. The results for differential immune cell infiltration are shown in **Figures 9A, B**. Relative to control samples, the proportions of monocytes, mast cells activated and neutrophils were significantly upregulated in AMI samples, while the proportion of T cells CD4 memory resting and T cells gamma delta was significantly downregulated. Additionally, correlation analysis for the immune cell types with the seven optimal feature genes suggested that all seven optimal feature genes were significantly positively correlated with infiltration of neutrophils, mast cells activated, monocytes, NK cells resting, while correlated negatively with the infiltration of T cells CD4 memory resting and mast cells resting (**Figures 9C–I**). For example, ACSL1 gene is positively correlated with neutrophils ($R = 0.65$, $P < 2.2e\text{-}16$), but highly negatively correlated with T cell CD4 memory resting ($R = -0.48$, $P = 6.4e\text{-}10$) (**Supplementary Figure 3**). Gene correlations were also examined, as shown in **Figures 9J, K**. These seven optimal feature genes showed a significant positive correlation. For example, the correlation coefficient between ACSL1 and IL1R2 was 0.85, indicating that seven optimal feature genes had a significant functional similarity.

To further investigate whether the enrichment of hallmark gene sets differs between the AMI group and the control group, we judged the significance of the difference between the two groups for 50 hallmark gene sets based on the enrichment score by using ssGSEA algorithm. The detailed distribution of the 50 hallmark gene sets between AMI and control samples was illuminated in **Figure 10A**. A number of hallmark gene sets exhibited a significant difference, including KRAS-signaling-up, IL2-STAT5-signaling, angiogenesis, UV-response-up, P53-pathway, glycolysis, xenobiotic-metabolism, inflammatory-response, epithelial-mesenchymal-transition, complement, hedgehog-signaling, apical-surface, apical-junction, myogenesis, estrogen-response-late, estrogen-response-early, apoptosis, IL6-JAK-STAT3-signaling, mitotic-spindle, cholesterol-homeostasis, hypoxia, and TNFα-signaling-*via*-NFKB. So, we can infer that compared with the normal group, these hallmark gene sets were over-activated in the AMI group. Additionally, we can find that the seven optimal feature genes are generally consistent in the majority of hallmark gene sets. For instance, all of the seven optimal feature genes were positively correlated with the inflammatory-response hallmark gene set. However, across a small subset of hallmark gene sets, the seven genes were not consistently correlated. For example, GABARAPL1 was positively correlated with the G2M checkpoint, while the other six genes are negatively correlated with the G2M checkpoint (**Figure 10B**). These data will require us further reinforce the comprehensive interrogation of the various roles of the optimal feature genes in AMI pathogenesis.

qRT-PCR validation of optimal feature genes

We examined the relative expression of seven optimal feature genes in AMI patients and healthy subjects. The detailed baseline information was summarized in **Supplementary Table 9**. Compared to healthy subjects, the expression of ACSL1 (**Figure 11A**), GABARAPL1 (**Figure 11B**), IL1R2 (**Figure 11C**), IRAK3 (**Figure 11D**), MCEMP1 (**Figure 11E**),

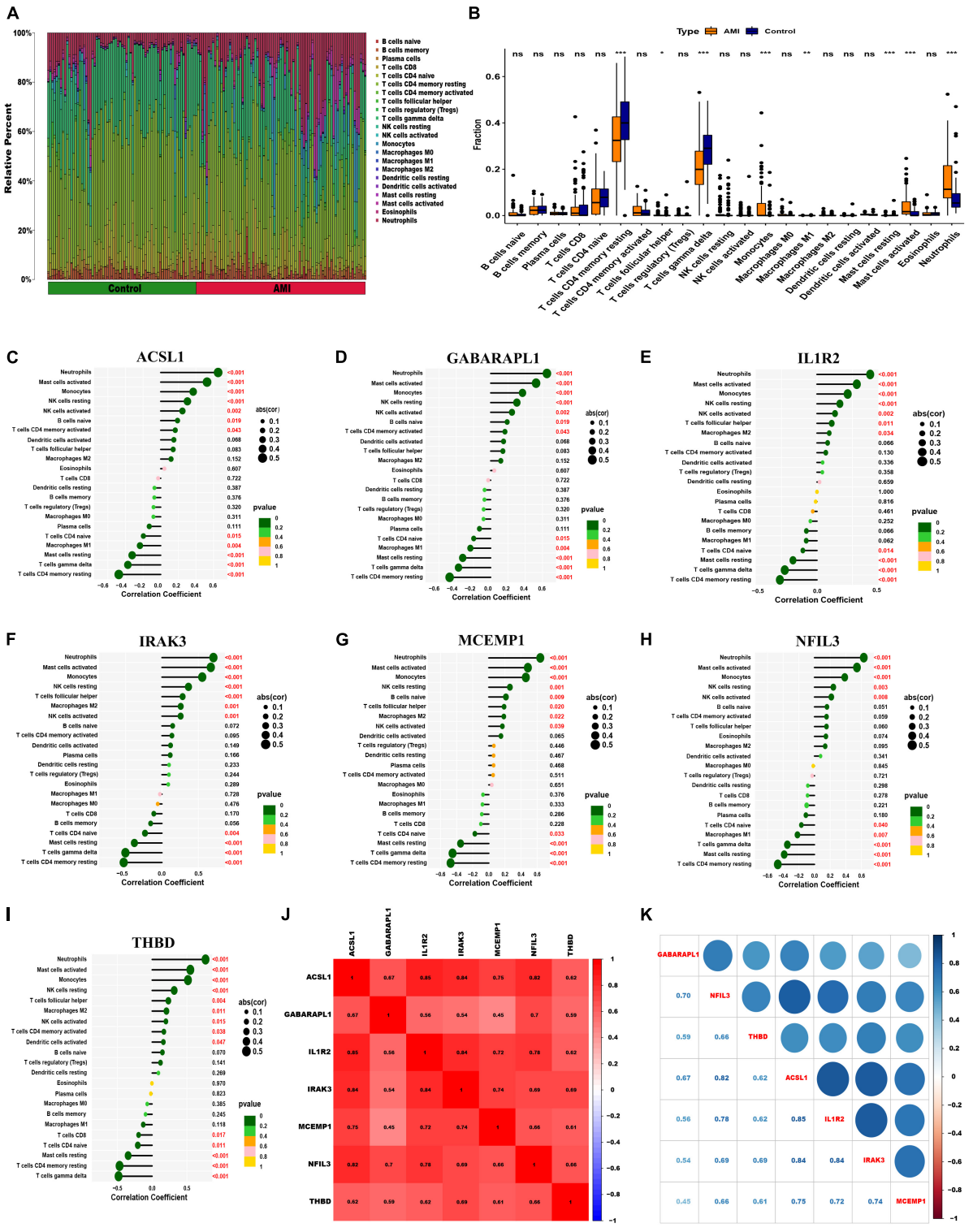


FIGURE 9
Visualization of immune cell infiltration. **(A)** The relative proportions of 22 immune cells types between control samples and AMI samples. Panel **(B)** representative boxplot shows the differences of infiltrated immune cells between control samples and AMI samples. Statistic tests: Wilcoxon rank-sum test. ($P < 0.05$*; $P < 0.01$**; $P < 0.001$***; ns, no significance). **(C–I)** Correlation between immune cells and optimal feature genes ACSL1 **(C)**, GABARAPL1 **(D)**, IL1R2 **(E)**, IRAK3 **(F)**, MCEMP1 **(G)**, NFIL3 **(H)**, and THBD **(I)**; the larger the dots, the stronger the correlation. The color of the dots represents the *P*-value; the greener the color, the lower the *P*-value. **(J,K)** Correlation analysis of seven optimal feature genes in AMI samples.

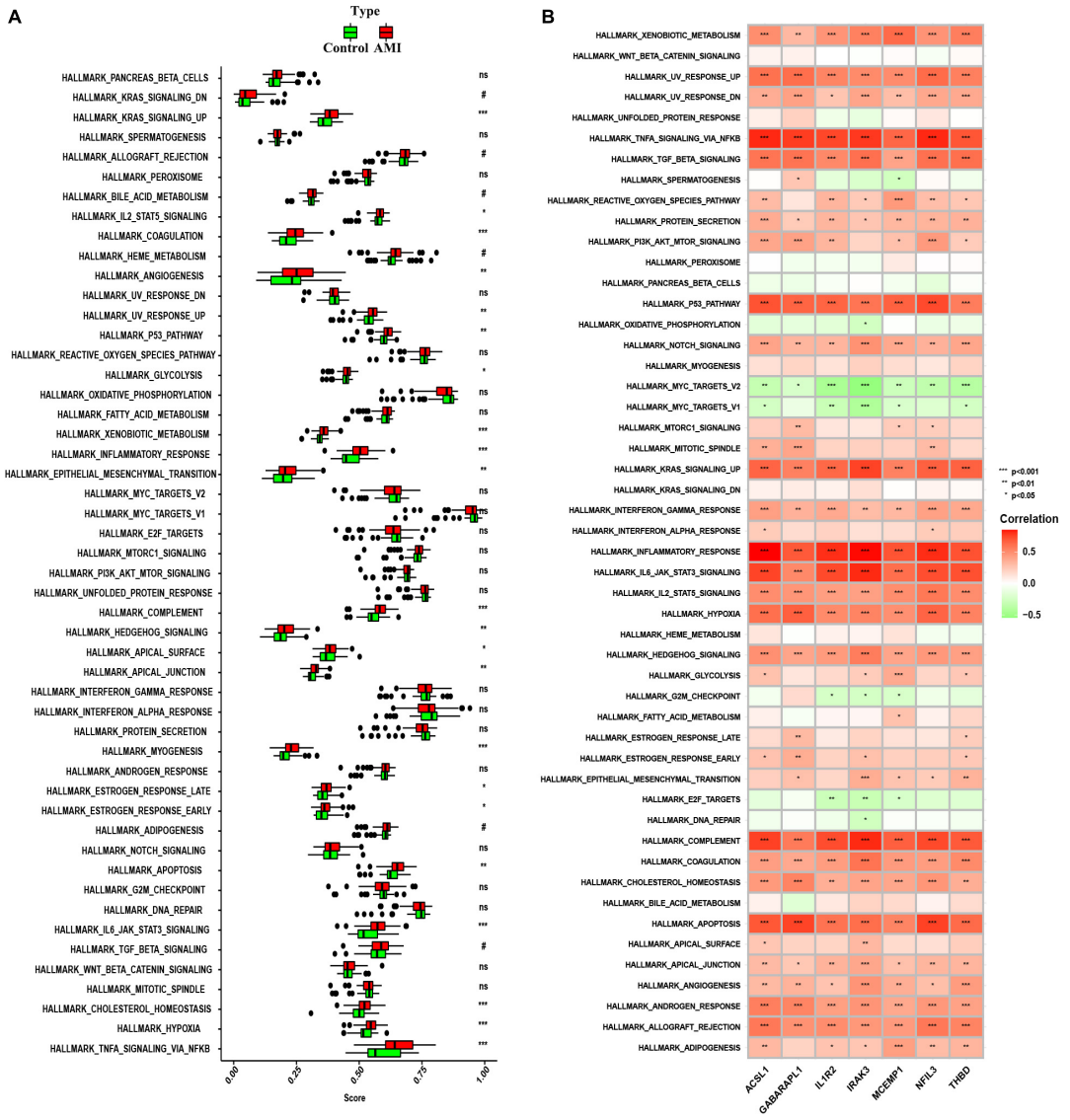


FIGURE 10
Analysis of hallmark gene sets. **(A)** The specific distribution of the 50 hallmark gene sets in AMI and control samples. **(B)** Correlation analysis of the 50 hallmark gene sets with seven optimal feature genes. Statistic tests: Wilcoxon rank-sum test ($P < 0.2^{\#}$; $P < 0.05$*; $P < 0.01$**; $P < 0.001$***; ns, no significance).

NFIL3 (Figure 11F), and THBD (Figure 11G) were significantly up-regulated in AMI patients (all $P < 0.05$), which was in line with the bioinformatics analysis.

Discussion

The core pathological process of AMI is currently considered to be an imbalance between myocardial oxygen demand (oxygen consumption) and actual oxygen supply (21, 22). Although existing studies have pointed out that the sensitivity of the troponin-dependent AMI diagnostic method has been greatly improved, and it has shown that it can be valuable for the prognosis of AMI patients, it is a pity that this detection method is currently used for precise diagnosis and treatment (23). AMI still has some deficiencies, especially in the face of complex subtypes of AMI. Based on previous research experience, biomarkers based on the gene level are often more accurate in distinguishing the disease state of patients and can also more deeply explain the mechanism behind the disease, to guide more reasonable and effective clinical treatment strategies. Therefore, in this study, we downloaded the genetic data of AMI patients from the GEO database, used the WGCNA algorithm to find the differential genes most related to the progression

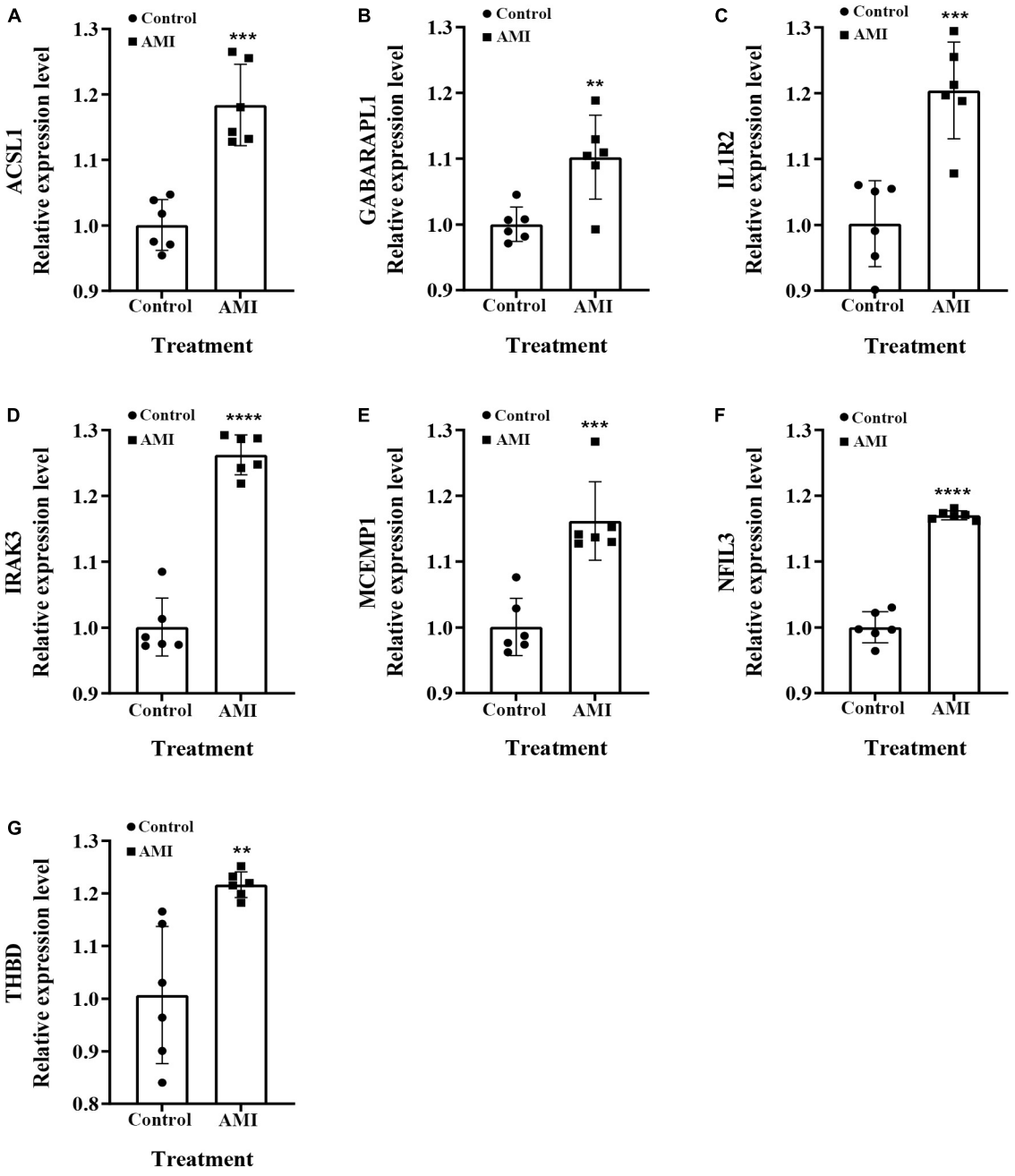


FIGURE 11
The relative expressions of optimal feature genes were validated by qRT-PCR. **(A–G)** The expressions of ACSL1 **(A)**, GABARAPL1 **(B)**, IL1R2 **(C)**, IRAK3 **(D)**, MCEMP1 **(E)**, NFIL3 **(F)**, and THBD **(G)** between AMI patients and healthy subjects. Statistic tests: Student's *t*-test ($P < 0.01$**; $P < 0.001$***; $P < 0.0001$****).

of AMI disease, and comprehensively used machine algorithms such as LASSO regression, SVM-REF, and Random Forest. Finally, seven optimal feature genes (ACSL1, GABARAPL1, IL1R2, IRAK3, MCEMP1, NFIL3, and THBD) that were verified to be closely related to the diagnosis and maybe, progression, of AMI were found, and further functional enrichment analyses of these genes were carried out.

To explore the role of these seven optimal feature genes in AMI, we reviewed previous studies. Among the seven genes closely related to AMI identified in this study, three genes, ACSL1, IL1R2, and THBD, have more preliminary studies in AMI. ACSL1 (chain acyl-CoA synthase 1) encodes an enzyme that plays an important role in the activation of triglyceride synthesis (24). Early studies have shown that high expression

of this gene in mouse cardiomyocytes often leads to the consequence of high myocardial triglyceride deposition, so this gene is also considered a risk factor for AMI (25). In a 2020 study, Tingting Li et al. pointed out that the same triglyceride deposition phenomenon also occurs in leukocytes overexpressing ACSL1 in the peripheral blood of AMI patients, and this process is likely to be achieved through the PPARγ pathway (26). In addition, except for participating in lipid metabolism, Yuanlong Li et al.'s study also found that the high regenerative activity of the myocardium in neonatal mice was also regulated by ACSL1 within 7 days. In the neonatal mouse MI model, mice knocked out of this gene showed more good recovery (27). IL1R2 is considered to mediate the anti-inflammatory response in the traditional inflammatory response (28). Surprisingly, the study of Amit Saxena et al. also pointed out that IL-1 can cause the infiltration of leukocytes at the AMI site and thereby prevent fibroblasts from entering the body (29). The contractile phenotype is transformed to provide a better survival microenvironment for mesenchymal stem cells, thereby improving the recovery of damaged myocardium in AMI. Similar findings were also mentioned in a clinical study by Hilde L Orrem et al. (30). It is worth mentioning that the latest study by Mingzhe Li et al. directly regarded IL1R2 as a suppressor of ischemic myocardial fibrosis and found that the main reason for the inactivation/downregulation of this gene after AMI is that its promoter region is blocked by POU2F1 (31). In addition, some research methods based on gene sequencing also pointed out that IL1R2 is closely related to AMI process (32). Interestingly, we found that the study by Enfa Zhao et al. simultaneously identified IL1R2, IRAK3, and THBD as prognostic diagnostic markers for acute myocardial infarction and found a high enrichment of the IL-17 pathway in the functional analysis, which was consistent with ours (33). The results are consistent with ours. In addition, an earlier study by Wei Chen et al. also demonstrated that another gene in the IRAK family, IRAK-M knockout mice, developed more severe ventricular remodeling and systolic dysfunction after MI (34). THBD (thrombomodulin gene) belongs to the protein C anticoagulation system, which is of great significance in maintaining the balance of hemorrhage and hemostasis in the body. Current research believes that the variation of THBD is one of the important causes of thrombosis, and coronary microthrombi Formation is also an important risk factor in the pathogenesis of AMI (35). In 2011, a clinical study by Ilaria Guella et al. pointed out that SNPs at 12 loci, including THBD, showed a high correlation with an increased risk of death after AMI (36). Unfortunately, there is still a lack of basic experimental research on the gene and the pathogenesis of AMI, but the existing clinical studies have demonstrated the potential value of this gene in AMI. The relationship between the remaining few genes and AMI has not been thoroughly studied, but some indicative studies have emerged. For example, the study of Fan Qiu et al. pointed out that GABARAPL1, by interacting with STBD1, counteracted the energy protection provided by glycoautophagy and mitophagy of OGD-treated cardiomyocytes, and aggravated myocardial injury after ischemia (37). This is consistent with the results we obtained in the ssGSEA single-gene association test. While NFIL3 (38) and MCEMP1 (39) currently with only a few omics studies demonstrated their potential relationship with AMI, our study points to the potential clinical value of both, which may be a viable direction for future research. It is worth noting that the expression levels of these key genes were verified by qRT-PCR, and the results were consistent with the results of bioinformatics.

In the analysis of immune infiltration, we found that B cells and neutrophils were deeply related to AMI. When single-gene GSEA analysis was performed, we found that the B cell receptor signaling pathway was enriched in the apical position in NFIL3, MCEMP1 and IL1R2 high expression groups. As one of the resident immune cells in the heart, during myocardial ischemia, B cells can release a variety of cytokines (including CCL2, CCL7, etc.) that chemoattract monocytes and neutrophils, thereby greatly increasing peripheral blood leukocytes myocardial infiltration (40). As early as 2013, research by Yasmine Zouggari et al. pointed out that this recruitment of B cells after MI aggravates further damage to ischemic myocardium (41). The mechanism behind this phenomenon was recently pointed out by Margarete Heinrichs et al. through the CXCL13-CXCR5 axis (42). And recently, researcher Claudia Monaco believes that B cells may be an important "middleman" in the formation of distal atherosclerosis after MI. He believes that the necrosis of cardiomyocytes can lead to the release of specific antigens that are not recognized and induce humoral immunity through B cells. Immunoglobulin deposition, which in turn leads to atherosclerosis after MI (43). A similar phenomenon was also found in the study of Tin Kyaw et al. (44). However, it is interesting that B cells are not all damaged in the biological process after MI. For example, the study by Lan Wu et al. found that after mice suffered AMI, there will be a special, mainly secreted, in the pericardial fat of mice. B cell subsets of IL-10 are infiltrated, and this group of cells exhibits anti-inflammatory and prognostic effects (45). The above studies all suggest that B cells have a strong potential in the treatment of AMI. The three genes identified in our study, which are closely related to the B cell receptor pathway, may be key to balancing the double-edged sword of B cell injury-protection. In addition, in multiple GSEA analyses, we found that the IL-17 signaling pathway was significantly enriched in AMI patients. As early as 2013, in the clinical study of Tabassome Simon et al., it was pointed out that low serum IL-17 level was the main cardiovascular time risk correlation in AMI patients (46). In the same year, the work of Onno J de Boer et al. also pointed out that IL-17A can promote thrombus formation by enhancing platelet aggregation (47). This process can feed back with the formation and release of Nets, aggravating coronary thrombosis and thus aggravating the progress of AMI (48). This is consistent with Our original

GSEA analysis was consistent. Encouragingly, recent studies by Rafael Blanco-Domínguez et al. have confirmed that Th17 cells are a characteristic of AMI, and the microRNA mmu-miR-721 produced by them has diagnostic significance for AMI (48). The above evidence directly or indirectly illustrates the important role of IL-17 signaling pathway in the progression of AMI.

In addition, in the analysis of immune cell infiltration, we also found that neutrophil infiltration was significantly increased in patients with AMI. Neutrophils, as one of the most important cells in the inflammatory response, have long been considered to be involved in various stages of myocardial ischemia and coronary injury (49, 50), especially in reperfusion injury after myocardial ischemia (51). Some studies in recent years believe that neutrophils are expected to become an important target for the treatment of AMI. For example, Qing Wan et al. found that PDE4B can mediate neutrophil infiltration in mouse myocardium after AMI, and induce neutrophils to release a variety of cytokines, aggravating myocardial injury, which was obtained after administration of PDE4B inhibitors. Improve (52); Ji'e Yang et al. found that the neutrophil glycosylation product Nε- (carboxymethyl) lysine can also aggravate myocardial ischemia-reperfusion injury (53). In addition, the neutrophil extracellular traps (Nets) proposed in recent years have linked various pathological changes such as coronary thrombosis (54), coronary atherosclerosis, and myocardial inflammation in series (55). However, with further research, it has been found that neutrophils may also exhibit anti-inflammatory, pro-angiogenic and pro-reparative protective effects in AMI (56). Based on this, the regulation of neutrophils after AMI must have considerable clinical therapeutic value.

It is true that our research is based on RNA sequencing results from existing databases, and due to the data set, there will be some bias in our research results. In addition, our findings rely on bioinformatics analysis methods and simply verified the expression of these key genes by qRT-PCR, more *in vivo* and *in vitro* experiments are needed to verify the results. Taken together, our research aims to provide new ideas and directions for clinical diagnosis and precise treatment management of AMI.

Conclusion

Overall, we found that seven powerful diagnostic efficacy genes were present in patients with AMI, indicating that they provide new potential targets for diagnosis and maybe progression of AMI, thus leading to improved outcomes. Different from other similar studies, we used more machine learning methods to enhance the accuracy of gene screening, and focused on exploring the specific genes that have the most obvious impact on AMI. It can also provide more accurate direction guidance for future AMI research. Overall, our research aims to provide new ideas and directions for clinical diagnosis and precise treatment management of AMI.

Data availability statement

The original contributions presented in this study are included in the article/**Supplementary material**, further inquiries can be directed to the corresponding authors.

Author contributions

HL, XS, ML, and TH designed the study. HL and ZL analyzed the data, participated in the data collection, and prepared the manuscript. TH and XS helped the analysis with constructive discussions. All authors critically revised the manuscript.

Conflict of interest

The authors declare that the research was conducted in the absence of any commercial or financial relationships that could be construed as a potential conflict of interest.

Publisher's note

All claims expressed in this article are solely those of the authors and do not necessarily represent those of their affiliated organizations, or those of the publisher, the editors and the reviewers. Any product that may be evaluated in this article, or claim that may be made by its manufacturer, is not guaranteed or endorsed by the publisher.

Supplementary material

The Supplementary Material for this article can be found online at: https://www.frontiersin.org/articles/10.3389/fcvm.2022.1059543/full#supplementary-material

References

1. Mir T, Uddin M, Shanah L, Hussain T, Parajuli T, Shafi O, et al. Acute myocardial infarction and acute heart failure among renal transplant recipients: a national readmissions database study. *J Nephrol.* (2022) 35:1851–62. doi: 10.1007/s40620-022-01252-w

2. Reed GW, Rossi JE, Cannon CP. Acute myocardial infarction. *Lancet.* (2017) 389:197–210. doi: 10.1016/S0140-6736(16)30677-8

3. Wang Q, Liu B, Wang Y, Bai B, Yu T, Chu X. The biomarkers of key miRNAs and target genes associated with acute myocardial infarction. *PeerJ.* (2020) 8:e9129. doi: 10.7717/peerj.9129

4. Zhou J, Wen T, Li Q, Chen Z, Peng X, Wei C, et al. Single-cell sequencing revealed pivotal genes related to prognosis of myocardial infarction patients. *Comput Math Methods Med.* (2022) 2022:6534126. doi: 10.1155/2022/6534126

5. Ding H, Chen W, Chen X. Serum miR-96-5p is a novel and non-invasive marker of acute myocardial infarction associated with coronary artery disease. *Bioengineered.* (2022) 13:3930–43. doi: 10.1080/21655979.2022.2031392

6. Wang C, Jing Q. Non-coding RNAs as biomarkers for acute myocardial infarction. *Acta Pharmacol Sin.* (2018) 39:1110–9. doi: 10.1038/aps.2017.205

7. Chen Y, Tao Y, Zhang L, Xu W, Zhou X. Diagnostic and prognostic value of biomarkers in acute myocardial infarction. *Postgrad Med J.* (2019) 95:210–6. doi: 10.1136/postgradmedj-2019-136409

8. Wu Y, Chen H, Li L, Zhang L, Dai K, Wen T, et al. Construction of novel gene signature-based predictive model for the diagnosis of acute myocardial infarction by combining random forest with artificial neural network. *Front Cardiovasc Med.* (2022) 9:876543. doi: 10.3389/fcvm.2022.876543

9. Vernon ST, Hansen T, Kott K, Yang J, O'Sullivan J, Figtree G. Utilizing state-of-the-art "omics" technology and bioinformatics to identify new biological mechanisms and biomarkers for coronary artery disease. *Microcirculation.* (2019) 26:e12488. doi: 10.1111/micc.12488

10. Grobman WA, Stamilio DM. Methods of clinical prediction. *Am J Obstet Gynecol.* (2006) 194:888–94. doi: 10.1016/j.ajog.2005.09.002

11. Meng XW, Cheng Z, Lu Z, Tan Y, Jia X, Zhang M, et al. MX2: identification and systematic mechanistic analysis of a novel immune-related biomarker for systemic lupus erythematosus. *Front Immunol.* (2022) 13:978851. doi: 10.3389/fimmu.2022.978851

12. Langfelder P, Horvath S. WGCNA: an R package for weighted correlation network analysis. *BMC Bioinformatics.* (2008) 9:559. doi: 10.1186/1471-2105-9-559

13. Godec J, Tan Y, Liberzon A, Tamayo P, Bhattacharya S, Butte A, et al. Compendium of immune signatures identifies conserved and species-specific biology in response to inflammation. *Immunity.* (2016) 44:194–206. doi: 10.1016/j.immuni.2015.12.006

14. Sepulveda JL. Using R and bioconductor in clinical genomics and transcriptomics. *J Mol Diagn.* (2020) 22:3–20. doi: 10.1016/j.jmoldx.2019.08.006

15. Kanehisa M, Goto S. KEGG: kyoto encyclopedia of genes and genomes. *Nucleic Acids Res.* (2000) 28:27–30. doi: 10.1093/nar/28.1.27

16. Yu G, Wang L, Yan G, He QY. DOSE: an R/Bioconductor package for disease ontology semantic and enrichment analysis. *Bioinformatics.* (2015) 31:608–9. doi: 10.1093/bioinformatics/btu684

17. Li H, Lai L, Shen J. Development of a susceptibility gene based novel predictive model for the diagnosis of ulcerative colitis using random forest and artificial neural network. *Aging (Albany NY).* (2020) 12:20471–82. doi: 10.18632/aging.103861

18. Tian Y, Yang J, Lan M, Zou T. Construction and analysis of a joint diagnosis model of random forest and artificial neural network for heart failure. *Aging (Albany NY).* (2020) 12:26221–35. doi: 10.18632/aging.202405

19. Newman AM, Steen C, Liu C, Gentles A, Chaudhuri A, Scherer F, et al. Determining cell type abundance and expression from bulk tissues with digital cytometry. *Nat Biotechnol.* (2019) 37:773–82. doi: 10.1038/s41587-019-0114-2

20. Leek JT, Johnson WE, Parker HS, Jaffe AE, Storey JD. The sva package for removing batch effects and other unwanted variation in high-throughput experiments. *Bioinformatics.* (2012) 28:882–3. doi: 10.1093/bioinformatics/bts034

21. Thygesen K, Alpert JS, White HD. Universal definition of myocardial infarction. *J Am Coll Cardiol.* (2007) 50:2173–95. doi: 10.1016/j.jacc.2007.09.011

22. Ambrose JA. Myocardial ischemia and infarction. *J Am Coll Cardiol.* (2006) 47(Suppl. 11):D13–7. doi: 10.1016/j.jacc.2006.04.013

23. Sandoval Y, Jaffe AS. Type 2 myocardial infarction: JACC review topic of the week. *J Am Coll Cardiol.* (2019) 73:1846–60. doi: 10.1016/j.jacc.2019.02.018

24. Li LO, Ellis J, Paich H, Wang S, Gong N, Altshuller G, et al. Liver-specific loss of long chain acyl-CoA synthetase-1 decreases triacylglycerol synthesis and beta-oxidation and alters phospholipid fatty acid composition. *J Biol Chem.* (2009) 284:27816–26. doi: 10.1074/jbc.M109.022467

25. Chiu HC, Kovacs A, Ford D, Hsu F, Garcia R, Herrero P, et al. A novel mouse model of lipotoxic cardiomyopathy. *J Clin Invest.* (2001) 107:813–22. doi: 10.1172/JCI10947

26. Allouch A, Di Primio C, Paoletti A, Lê-Bury G, Subra F, Quercioli V, et al. SUGT1 controls susceptibility to HIV-1 infection by stabilizing microtubule plus-ends. *Cell Death Differ.* (2020) 27:3243–57. doi: 10.1038/s41418-020-0573-5

27. Li Y, Yang M, Tan J, Shen C, Deng S, Fu X, et al. Targeting ACSL1 promotes cardiomyocyte proliferation and cardiac regeneration. *Life Sci.* (2022) 294:120371. doi: 10.1016/j.lfs.2022.120371

28. Garlanda C, Dinarello CA, Mantovani A. The interleukin-1 family: back to the future. *Immunity.* (2013) 39:1003–18. doi: 10.1016/j.immuni.2013.11.010

29. Saxena A, Chen W, Su Y, Rai V, Uche O, Li N, et al. IL-1 induces proinflammatory leukocyte infiltration and regulates fibroblast phenotype in the infarcted myocardium. *J Immunol.* (2013) 191:4838–48. doi: 10.4049/jimmunol.1300725

30. Orrem HL, Shetelig C, Ueland T, Limalanathan S, Nilsson P, Husebye T, et al. Soluble IL-1 receptor 2 is associated with left ventricular remodelling in patients with ST-elevation myocardial infarction. *Int J Cardiol.* (2018) 268:187–92. doi: 10.1016/j.ijcard.2018.05.032

31. Li M, Wu J, Hu G, Song Y, Shen J, Xin J, et al. Pathological matrix stiffness promotes cardiac fibroblast differentiation through the POU2F1 signaling pathway. *Sci China Life Sci.* (2021) 64:242–54. doi: 10.1007/s11427-019-1747-y

32. Yao Y, Zhao J, Zhou X, Hu J, Wang Y. Potential role of a three-gene signature in predicting diagnosis in patients with myocardial infarction. *Bioengineered.* (2021) 12:2734–49. doi: 10.1080/21655979.2021.1938498

33. Zhao E, Xie H, Zhang Y. Predicting diagnostic gene biomarkers associated with immune infiltration in patients with acute myocardial infarction. *Front Cardiovasc Med.* (2020) 7:586871. doi: 10.3389/fcvm.2020.586871

34. Chen W, Saxena A, Li N, Sun J, Gupta A, Lee D, et al. Endogenous IRAK-M attenuates postinfarction remodeling through effects on macrophages and fibroblasts. *Arterioscler Thromb Vasc Biol.* (2012) 32:2598–608. doi: 10.1161/ATVBAHA.112.300310

35. Manderstedt E, Halldén C, Lind-Halldén C, Elf J, Svensson P, Engström G, et al. Thrombomodulin (THBD) gene variants and thrombotic risk in a population-based cohort study. *J Thromb Haemost.* (2022) 20:929–35. doi: 10.1111/jth.15630

36. Guella I, Duga S, Ardissino D, Merlini P, Peyvandi F, Mannucci P, et al. Common variants in the haemostatic gene pathway contribute to risk of early-onset myocardial infarction in the Italian population. *Thromb Haemost.* (2011) 106:655–64. doi: 10.1160/TH11-04-0247

37. Qiu F, Yuan Y, Luo W, Gong Y, Zhang Z, Liu Z, et al. Asiatic acid alleviates ischemic myocardial injury in mice by modulating mitophagy- and glycophagy-based energy metabolism. *Acta Pharmacol Sin.* (2022) 43:1395–407. doi: 10.1038/s41401-021-00763-9

38. Chen J, Yu L, Zhang S, Chen X. Network analysis-based approach for exploring the potential diagnostic biomarkers of acute myocardial infarction. *Front Physiol.* (2016) 7:615. doi: 10.3389/fphys.2016.00615

39. Xu J, Yang Y. Integrated gene expression profiling analysis reveals potential molecular mechanisms and candidate biomarkers for early risk stratification and prediction of STEMI and Post-STEMI heart failure patients. *Front Cardiovasc Med.* (2021) 8:736497. doi: 10.3389/fcvm.2021.736497

40. Swirski FK, Nahrendorf M. Cardioimmunology: the immune system in cardiac homeostasis and disease. *Nat Rev Immunol.* (2018) 18:733–44. doi: 10.1038/s41577-018-0065-8

41. Zouggari Y, Ait-Oufella H, Bonnin P, Simon T, Sage A, Guérin C, et al. B lymphocytes trigger monocyte mobilization and impair heart function after acute myocardial infarction. *Nat Med.* (2013) 19:1273–80. doi: 10.1038/nm.3284

42. Heinrichs M, Ashour D, Siegel J, Büchner L, Wedekind G, Heinze K, et al. The healing myocardium mobilizes a distinct B-cell subset through a CXCL13-CXCR5-dependent mechanism. *Cardiovasc Res.* (2021) 117:2664–76. doi: 10.1093/cvr/cvab181

43. Monaco C, Cole J. Does a myocardial infarction boost your (B cell) memory? *Eur Heart J.* (2021) 42:948–50. doi: 10.1093/eurheartj/ehaa1059

44. Kyaw T, Loveland P, Kanellakis P, Cao A, Kallies A, Huang A, et al. Alarmin-activated B cells accelerate murine atherosclerosis after myocardial infarction via plasma cell-immunoglobulin-dependent mechanisms. *Eur Heart J.* (2021) 42:938–47. doi: 10.1093/eurheartj/ehaa995

45. Wu L, Dalal R, Cao C, Postoak J, Yang G, Zhang Q, et al. IL-10-producing B cells are enriched in murine pericardial adipose tissues and ameliorate the outcome of acute myocardial infarction. *Proc Natl Acad Sci USA*. (2019) 116:21673–84. doi: 10.1073/pnas.1911464116

46. Simon T, Taleb S, Danchin N, Laurans L, Rousseau B, Cattan S, et al. Circulating levels of interleukin-17 and cardiovascular outcomes in patients with acute myocardial infarction. *Eur Heart J*. (2013) 34:570–7. doi: 10.1093/eurheartj/ehs263

47. de Boer OJ, Li X, Teeling P, Mackaay C, Ploegmakers H, van der Loos C, et al. Neutrophils, neutrophil extracellular traps and interleukin-17 associate with the organisation of thrombi in acute myocardial infarction. *Thromb Haemost*. (2013) 109:290–7. doi: 10.1160/TH12-06-0425

48. Jain S. Role of interleukin-17 signaling pathway in the interaction between multiple sclerosis and acute myocardial infarction. *Mult Scler Relat Disord*. (2022) 58:103515. doi: 10.1016/j.msard.2022.103515

49. Weber C, Noels H. Atherosclerosis: current pathogenesis and therapeutic options. *Nat Med*. (2011) 17:1410–22. doi: 10.1038/nm.2538

50. Libby P, Pasterkamp G, Crea F, Jang I. Reassessing the mechanisms of acute coronary syndromes. *Circ Res*. (2019) 124:150–60. doi: 10.1161/CIRCRESAHA.118.311098

51. Jordan JE, Zhao ZQ, Vinten-Johansen J. The role of neutrophils in myocardial ischemia-reperfusion injury. *Cardiovasc Res*. (1999) 43:860–78. doi: 10.1016/S0008-6363(99)00187-X

52. Wan Q, Xu C, Zhu L, Zhang Y, Peng Z, Chen H, et al. Targeting PDE4B (Phosphodiesterase-4 Subtype B) for cardioprotection in acute myocardial infarction via neutrophils and microcirculation. *Circ Res*. (2022) 131:442–55. doi: 10.1161/CIRCRESAHA.122.321365

53. Yang J, Zhang F, Shi H, Gao Y, Dong Z, Ma L, et al. Neutrophil-derived advanced glycation end products-Nε-(carboxymethyl) lysine promotes RIP3-mediated myocardial necroptosis via RAGE and exacerbates myocardial ischemia/reperfusion injury. *FASEB J*. (2019) 33:14410–22. doi: 10.1096/fj.201900115RR

54. Laridan E, Martinod K, De Meyer SF. Neutrophil extracellular traps in arterial and venous thrombosis. *Semin Thromb Hemost*. (2019) 45:86–93. doi: 10.1055/s-0038-1677040

55. Zhou J, Chen R, Liu C, Zhou P, Li J, Wang Y, et al. Associations of NETs with inflammatory risk and atherosclerotic severity in ST-segment elevation myocardial infarction. *Thromb Res*. (2021) 203:5–11. doi: 10.1016/j.thromres.2021.04.015

56. Ma Y. Role of neutrophils in cardiac injury and repair following myocardial infarction. *Cells*. (2021) 10:1676. doi: 10.3390/cells10071676

frontiers | Frontiers in Cardiovascular Medicine

TYPE Original Research
PUBLISHED 10 January 2023
DOI 10.3389/fcvm.2022.1077992

Check for updates

OPEN ACCESS

EDITED BY
Jedrzej Kosiuk,
Helios Clinic Köethen, Germany

REVIEWED BY
Li-Da Wu,
Nanjing Medical University, China
Mario Matta,
AOU Città della Salute e della Scienza, Italy

*CORRESPONDENCE
Yucai Xie
✉ drxieyucai@163.com
Tong Yin
✉ yintong0101@163.com
Liqun Wu
✉ wuliqun89@hotmail.com

†These authors have contributed equally to this work and share first authorship

SPECIALTY SECTION
This article was submitted to Cardiac Rhythmology, a section of the journal Frontiers in Cardiovascular Medicine

RECEIVED 23 October 2022
ACCEPTED 19 December 2022
PUBLISHED 10 January 2023

CITATION
Lin M, Bao Y, Du Z, Zhou Y, Zhang N, Lin C, Xie Y, Zhang R, Li Q, Quan J, Zhu T, Xie Y, Xu C, Xie Y, Wei Y, Luo Q, Pan W, Wang L, Ling T, Jin Q, Wu L, Yin T and Xie Y (2023) Plasma protein profiling analysis in patients with atrial fibrillation before and after three different ablation techniques. *Front. Cardiovasc. Med.* 9:1077992. doi: 10.3389/fcvm.2022.1077992

COPYRIGHT
© 2023 Lin, Bao, Du, Zhou, Zhang, Lin, Xie, Zhang, Li, Quan, Zhu, Xie, Xu, Xie, Wei, Luo, Pan, Wang, Ling, Jin, Wu, Yin and Xie. This is an open-access article distributed under the terms of the Creative Commons Attribution License (CC BY). The use, distribution or reproduction in other forums is permitted, provided the original author(s) and the copyright owner(s) are credited and that the original publication in this journal is cited, in accordance with accepted academic practice. No use, distribution or reproduction is permitted which does not comply with these terms.

Plasma protein profiling analysis in patients with atrial fibrillation before and after three different ablation techniques

Menglu Lin[1†], Yangyang Bao[1†], Zunhui Du[1†], Yanting Zhou[2], Ning Zhang[1], Changjian Lin[1], Yinyin Xie[2], Ruihong Zhang[2], Qiheng Li[1], Jinwei Quan[1], Tingfang Zhu[1], Yuan Xie[3], Cathy Xu[1], Yun Xie[1], Yue Wei[1], Qingzhi Luo[1], Wenqi Pan[1], Lingjie Wang[1], Tianyou Ling[1], Qi Jin[1], Liqun Wu[1*], Tong Yin[2*] and Yucai Xie[1*]

[1]Department of Cardiovascular Medicine, Ruijin Hospital, Shanghai Jiao Tong University School of Medicine, Shanghai, China, [2]State Key Laboratory of Medical Genomics, Shanghai Institute of Hematology, National Research Center for Translational Medicine at Shanghai, Ruijin Hospital, Shanghai Jiao Tong University School of Medicine, Shanghai, China, [3]College of Osteopathic Medicine, Kansas City University, Kansas City, MO, United States

Background: There are controversies on the pathophysiological alteration in patients with atrial fibrillation (AF) undergoing pulmonary vein isolation using different energy sources.

Objectives: We evaluated the changes in plasma proteins in acute phase post-ablation in patients receiving cryoballoon ablation, radiofrequency balloon ablation, or radiofrequency ablation.

Methods: Blood samples from eight healthy controls and 24 patients with AF were taken on the day of admission, day 1, and day 2 post-ablation and analyzed by the Olink proximity extension assay. Proteins were identified and performed with enrichment analysis. Protein–protein interaction network and module analysis were conducted using Cytoscape software.

Results: Of 181 proteins, 42 proteins in the cryoballoon group, 46 proteins in the radiofrequency balloon group, and 43 proteins in the radiofrequency group significantly changed after ablation. Most of the proteins altered significantly on the first day after ablation. Altered proteins were mainly involved in cytokine–cytokine receptor interaction. Both balloon-based ablations showed a similar shift toward enhancing cell communication and regulation of signaling while inhibiting neutrophil chemotaxis. However, radiofrequency ablation presented a different trend. Seed proteins, including osteopontin, interleukin-6, interleukin-10, C-C motif ligand 8, and matrix

metalloproteinase-1, were identified. More significant proteins associated with hemorrhage and coagulation were selected in balloon-based ablations by machine learning.

Conclusion: Plasma protein response after three different ablations in patients with AF mainly occurred on the first day. Radiofrequency balloon ablation shared similar alteration in protein profile as cryoballoon ablation compared with radiofrequency ablation, suggesting that lesion size rather than energy source is the determinant in pathophysiological responses to the ablation.

KEYWORDS

proteomics, bioinformatics, Olink, atrial fibrillation, catheter ablation

Introduction

Atrial fibrillation (AF) is the most common arrhythmia around the world, which can cause a variety of clinical outcomes, such as stroke, heart failure, and cardiovascular mortality. The two main strategies of treatment are anti-arrhythmic drugs and catheter ablation. Although the primary treatment for AF is pharmacology therapy, it has limited effectiveness (1). Previous studies have demonstrated that catheter ablation outperforms drug therapy in terms of recurrence rate and quality of life in long term (2–4). Accordingly, catheter ablation is recommended by the most recent guidelines (5, 6).

Currently, radiofrequency (RF) ablation and cryoballoon (CB) ablation are the most common techniques to treat AF, with no significant difference in terms of safety or efficacy (7, 8). Experimental data suggested that the use of cryoablation is different from radiofrequency ablation due to its preservation of the extracellular matrix and reduction of endothelial and thrombus formation (9–11). In clinical studies, however, there was a comparable increase in markers of cell damage, platelet activation, and inflammatory response between CB and RF ablation (12, 13). Radiofrequency balloon (RB) ablation, also called hot balloon ablation, is an emerging approach for AF ablation with favorable safety and effectiveness (14, 15). However, there are few data about the biomarkers' changes compared to the CB or RF ablation.

In order to resolve the controversy, we utilized a new proteomic assay platform—Olink proximity extension assay, which has been widely applied in the biomarker discovery of the cardiovascular disease field (16, 17), to assess the change in 181 different proteins during the acute post-procedure phase from the cryoballoon ablation group and irrigated-tip RF catheter ablation group. We also introduced the RB ablation group into comparison to avoid alteration resulting from lesion size rather than energy sources (18).

Abbreviations: AF, atrial fibrillation; CB, cryoballoon; RB, radiofrequency balloon; RF, radiofrequency; PPI, protein–protein interaction; LOD, limit of detection; NPX, normalized protein expression; GO, gene ontology; KEGG, Kyoto encyclopedia of genes and genomes; FDR, false discovery rate.

Materials and methods

Patient samples

After the Institutional Review Committee and Ethics Committee approved the study, 24 patients diagnosed with paroxysmal or persistent AF at our institution who gave informed written consent were included, in which pulmonary vein isolation was performed with the CB catheter (Arctic Front Advance Cardiac Cryoablation Catheter, Medtronic), RB catheter (HELIOSTAR^{TM} Balloon Ablation Catheter, Biosense Webster Inc.), or RF catheter (NaviStar^{TM}RMT, ThermoCool^{TM}; Biosense Webster, CA, USA). In our study, all patients met the following inclusion criteria: (1) Non-valvular AF or flutter. The exclusion criteria were as follows: (1) <18 or >80 years old; (2) history of left atrial surgery; (3) transesophageal echocardiography-witnessed left atrial thrombus; (4) uncontrolled hyperthyroidism; (5) pregnancy; (6) history of obstructive sleep apnea syndrome; and (7) history of myocardial infarction, percutaneous coronary intervention, heart surgery, transient ischemic attack, or stroke within 3 months before the procedure. Patients were treated with oral anticoagulation at least 1 month before the ablation procedure. During the procedure, 100-IU/kg heparin was administered to maintain an activated clotting time of ≥300 s. Eight healthy controls were also enrolled as a comparison. A blood sample of 2 ml from the peripheral vein was taken and added to the ethylene diamine tetraacetic acid (EDTA) anticoagulant tube on three-time points, the admission day, day 1 (D1), and day 2 (D2) after ablation. The samples were immediately centrifuged and frozen at −80°C until analysis. All the patients were monitored by the telemetry electrocardiogram during hospitalization, and electrocardiogram data were collected for analysis.

TABLE 1 Clinical characteristics at baseline.

	Controls (n = 8)	Cryoballoon (n = 8)	Radiofrequency (n = 8)	Radiofrequency balloon (n = 8)	P-value
Age (years)	65.13 ± 3.56	65.63 ± 3.25	63.50 ± 1.69	58.63 ± 4.13	0.610
Male (n%)	5 (62.5%)	4 (50%)	3 (37.5%)	4 (50%)	0.801
BMI (kg/m2)	22.13 ± 0.92	22.96 ± 0.87	24.07 ± 0.77	23.73 ± 0.83	0.373
Smoking history (n%)	3 (37.5%)	2 (25%)	0 (0%)	2 (25%)	0.324
Alcohol history (n%)	1 (12.5%)	1 (12.5%)	0 (0%)	2 (25%)	0.515
Past medical history					
Hypertension (n%)	4 (50%)	2 (25%)	4 (50%)	4 (50%)	0.677
Diabetes (n%)	0 (0%)	0 (0%)	2 (25%)	1 (12.5%)	0.257
Coronary heart disease (n%)	1 (12.5%)	0 (0%)	1 (12.5%)	1 (12.5%)	0.776
Cerebral ischemia (n%)	2 (25%)	1 (12.5%)	0 (0%)	1 (12.5%)	0.515
Peripheral vascular disease (n%)	0 (0%)	0 (0%)	0 (0%)	0 (0%)	/
CHA_2DS_2-VASc score					
Score ≤1 (n%)	/	5 (62.5%)	2 (25%)	4 (50%)	/
Score ≥2 (n%)	/	3 (37.5%)	6 (75%)	4 (50%)	/
Atrial fibrillation type					
Paroxysmal (n%)	/	6 (75%)	5 (62.5%)	8 (100%)	/
Persistent (n%)	/	2 (25%)	3 (37.5%)	0 (0%)	/
Atrial fibrillation duration (months)	/	26.63 ± 17.43	15 ± 13.29	13.25 ± 8.54	/
Echocardiography					
Left atrium diameter (mm)	37.63 ± 0.56	40.00 ± 1.18	40.50 ± 1.31	38.13 ± 1.69	0.095
Ejection fraction (%)	64.50 ± 1.54	68.88 ± 1.29	66.00 ± 1.52	66.00 ± 1.52	0.223
Transesophageal echocardiography					
Normal (n%)	8 (100%)	7 (87.5%)	6 (75%)	7 (87.5%)	0.515
Dense echo (n%)	0 (0%)	1 (12.5%)	2 (25%)	1 (12.5%)	0.515
Thrombus (n%)	0 (0%)	0 (0%)	0 (0%)	0 (0%)	/
Thrombus in other places (n%)	0 (0%)	0 (0%)	0 (0%)	0 (0%)	/
Medicine history					
Beta blockers (n%)	2 (25%)	3 (37.5%)	1 (12.5%)	3 (37.5%)	0.637
alpha blockers (n%)	1 (12.5%)	0 (0%)	0 (0%)	0 (0%)	0.377
ACEI/ARB (n%)	2 (25%)	1 (12.5%)	2 (25%)	2 (25%)	0.908
Diuretics (n%)	1 (12.5%)	0 (0%)	1 (12.5%)	1 (12.5%)	0.776
Ca2 + antagonist (n%)	2 (25%)	2 (25%)	1 (12.5%)	1 (12.5%)	0.845
Digitalis (n%)	0 (0%)	0 (0%)	0 (0%)	0 (0%)	/
Antiarrhythmic drugs (n%)	0 (0%)	2 (25%)	3 (37.5%)	4 (50%)	0.144
Antiplatelet drugs (n%)	2 (25%)	0 (0%)	0 (0%)	0 (0%)	0.094
Anticoagulant (n%)	0 (0%)	8 (100%)	8 (100%)	8 (100%)	<0.01
Lab results					
WBC (*10^9/L)	5.05 ± 0.55	5.13 ± 0.33	5.61 ± 0.49	5.89 ± 0.98	0.646
RBC (*10^12/L)	4.30 ± 0.11	4.55 ± 0.14	4.43 ± 0.15	4.34 ± 0.11	0.574
Platelet (*10^9/L)	185.63 ± 14.16	198.13 ± 18.96	207.75 ± 19.45	206.63 ± 20.82	0.924

(Continued)

TABLE 1 (Continued)

	Controls (n = 8)	Cryoballoon (n = 8)	Radiofrequency (n = 8)	Radiofrequency balloon (n = 8)	P-value
Hb (g/L)	134.25 ± 3.82	139.38 ± 4.44	136.13 ± 5.63	133.88 ± 3.20	0.862
ALT (IU/L)	16.13 ± 1.88	31.25 ± 8.38	24.63 ± 3.24	24.88 ± 5.83	0.151
AST (IU/L)	21.38 ± 0.91	30.50 ± 8.64	21.63 ± 1.52	25.13 ± 6.25	0.903
Cr (μml/L)	78.75 ± 4.83	74.75 ± 6.70	68.25 ± 3.07	70.50 ± 5.62	0.504
TC (mmol/L)	4.41 ± 0.28	4.14 ± 0.35	4.58 ± 0.28	4.13 ± 0.20	0.654
LDL (mmol/L)	2.55 ± 0.36	2.36 ± 0.32	2.76 ± 0.16	2.53 ± 0.19	0.804
HbA1c (%)	5.48 ± 0.09	5.83 ± 0.17	6.43 ± 0.59	5.55 ± 0.17	0.401
pro-BNP (pg/ml)	75.56 ± 29.57	359.54 ± 196.27	256.65 ± 84.54	312.08 ± 226.52	0.186
TnI (ng/ml)	0.39 ± 0.37	0.01 ± 0.00	0.66 ± 0.48	0.01 ± 0.00	0.217
D-dimer (mg/L)	0.23 ± 0.04	0.24 ± 0.03	0.50 ± 0.32	0.30 ± 0.02	0.073

Continuous variables were shown as mean ± SD. Categorical variables were shown as counts and percentages. *N*, number; BMI, body mass index; CHA_2DS_2-VASc, risk score for thromboembolism; ACEI, angiotensin-converting enzyme inhibitors; ARB, angiotensin receptor blockers; WBC, white blood cells; RBC, red blood cells; Hb, hemoglobin; ALT, alanine transaminase; AST, aspartate transaminase; Cr, creatine; TC, total cholesterol; LDL, low-density lipoprotein; HbA1c, glycated hemoglobin; BNP, brain natriuretic peptides; TnI, troponin I.

Olink proteomic profiling

The proteomic analyses were performed at the National Research Center for Translational Medicine, Ruijin Hospital, Shanghai Jiao Tong University School of Medicine. The Olink multiplex cardiovascular disease III and inflammation panels comprise 184 proteins. Three protein markers were available on both panels, resulting in 181 unique markers. Samples were run in duplicates. The limit of detection (LOD) was defined as three standard deviations above the background, and values below this limit were reported as <LOD. The results from each assay were rendered as normalized log_2 protein expression (NPX) data, which are relative values, and one-unit higher NPX represents a doubling of the measured protein concentration. NPX values for proteins with >75% of measurements below LOD were removed from the analysis.

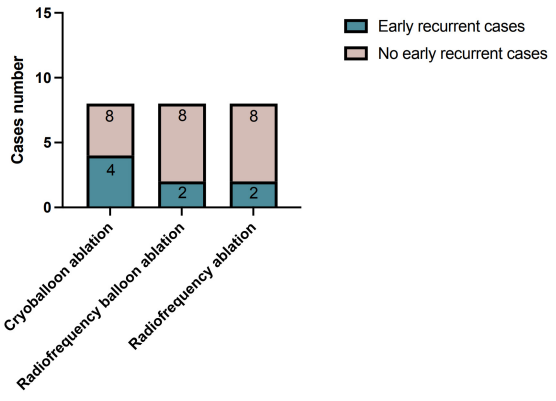


FIGURE 1
Early recurrence of atrial arrhythmia post-different ablations during hospitalization. The early recurrent cases of atrial arrhythmia post-ablations were not significantly different between three ablation groups (p = 0.472).

Statistic analysis

Statistical analysis was performed using GraphPad Prism nine software and SPSS 25. Normally distributed continuous variables were shown as mean ± SD. Categorical variables were shown as counts and percentages. Categorical variables were compared with the chi-square test. Wilcoxon matched-pairs signed-rank test was used to assess differences for each analyte before and after ablation. The Kruskal–Wallis H-test was used to assess differences in the clinical characteristics and the levels of analytes according to the ablation type. A P-value of <0.05 was considered statistically significant.

Proteins bioinformatic analysis

Heatmap was plotted by http://www.bioinformatics.com.cn, a free online platform for data analysis and visualization. The protein interaction, the gene ontology (GO) functional, and Kyoto Encyclopedia of Genes and Genomes (KEGG) pathway enrichment analysis in the network were performed by Search Tool for the Retrieval of Interacting Genes (STRING, version 11.5) database with the threshold of false discovery rate (FDR) <0.05. The required confidence (combined score) >0.4 was used as the cutoff criterion. In addition, the Molecular Complex Detection (MCODE) plugin in Cytoscape (version 3.7.1) was used to screen the significant modules and seed

TABLE 2 Significantly altered proteins before and after ablation were sorted by three different techniques.

Cryoballoon ablation	
Increased proteins	LDL receptor, MMP-9, GDF-15, PRTN3, OPN, CHI3L1, ST2, IGFBP-2, MB (D1), IL-8, TFG-alpha, IL-10, CCL23, CSF-1, MCP-3, IL-17C, CCL20, IL-6, and OSM
Decreased proteins	IGFBP-1, Ep-CAM, CXCL11, CXCL9, MCP-4, CCL11, CCL19, TRANCE, IL-12B, Flt3L, IFN-gamma, CCL8, CD244, CD6, FGF-21, TNFRSF9, uPA, MCP-1, TRAIL, CST5, CXCL10, CCL25, and TNFB, MB (D2)
Radiofrequency balloon ablation	
Increased proteins	MMP-9, MB, CHI3L1, ST2, IGFBP-2, TNFRSF14, LDL receptor, EPHB4, GRN, LTBR, TR, IL-1RT1, CTSD, CTSZ, TNF-R1, OPN, IL-6, OSM, CASP-8, TNFSF14, and CSF-1
Decreased proteins	TFF3, CSTB, MCP-1, uPA, COL1A1, vWF, TRAIL, CXCL9, CD6, CCL11, MMP-1, CCL19, TRANCE, Flt3L, CXCL6, CXCL10, CCL28, IFN-gamma, MCP-2, TNFB, IL-8, TWEAK, CXCL11, CST5, and MCP-4
Radiofrequency ablation	
Increased proteins	GDF-15, RETN, TR-AP, PRTN3, OPN, ST2, IGFBP-2, CHI3L1, IL-10, MCP-3, CSF-1, IL-6, and CCL23
Decreased proteins	CCL15, uPA, CPB1, MMP-3, CSTB, CD163, BLM hydrolase, IGFBP-1, Ep-CAM, Gal-4, KLK6, PLC, CDH5, FABP4, COL1A1, GDNF, TRAIL, CST5, SLAMF1, CCL11, MMP-1, CCL19, TRANCE, MMP-10, Flt3L, IFN-gamma, CCL25, TWEAK, TNFB, and FGF-21

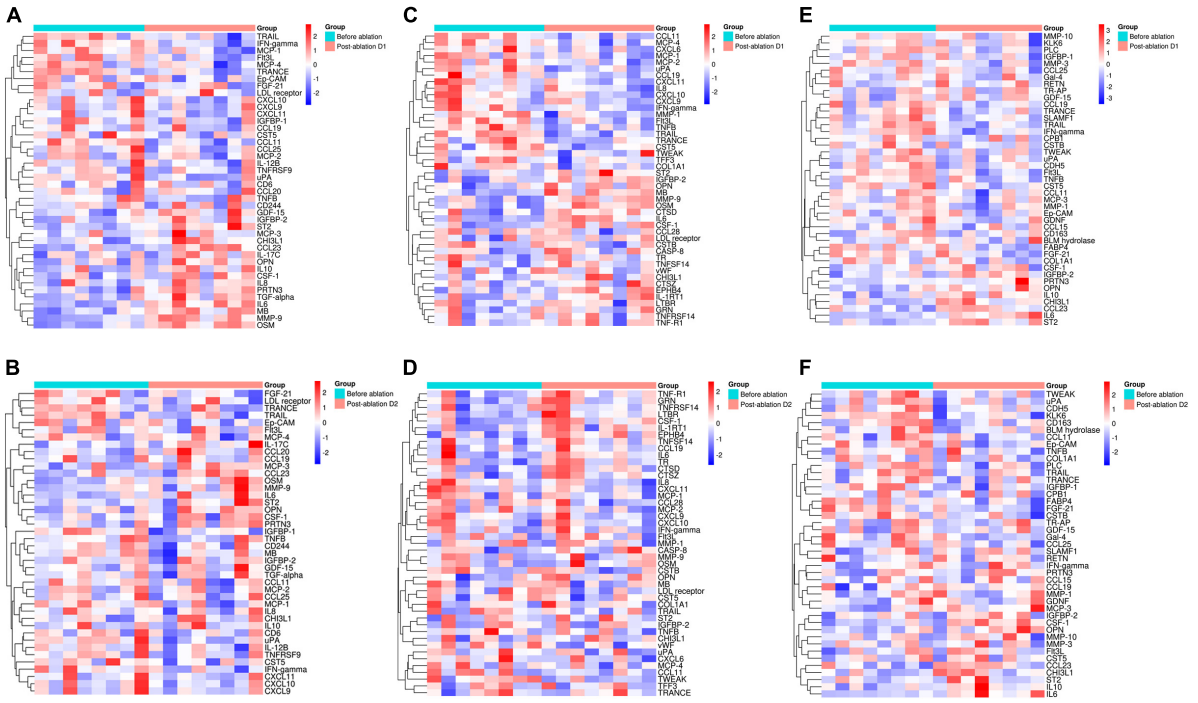


FIGURE 2
Heatmap of altered proteins before and after ablation. Most of the altered proteins changed on the first day after ablation. The heatmap of the altered proteins before and after ablation D1 and D2 in the cryoballoon group **(A,B)**, the radiofrequency balloon group **(C,D)**, and the radiofrequency group **(E,F)** (red: high expression and blue: low expression).

protein in the protein–protein interaction (PPI) network (degree cutoff = 2, node cutoff = 0.2, k-core = 2, and max. depth = 100). Moreover, enrichment analysis for the proteins involved in the most significant module was conducted using the STRING online tool. LASSO logistic regression model was fitted with the glmnet R package. Feature contributions to the models were visualized using the regression coefficients. The random forest model was fitted with random Forest and caret R packages according to Jack Gisby et al. with slight modifications (19). The 4-fold cross-validation that was repeated 100 times was used to estimate the model accuracy. Mtry value was calculated as the square root of the number of features. The random forest feature was extracted using the R randomForestExplainer package. Benjamini–Hochberg

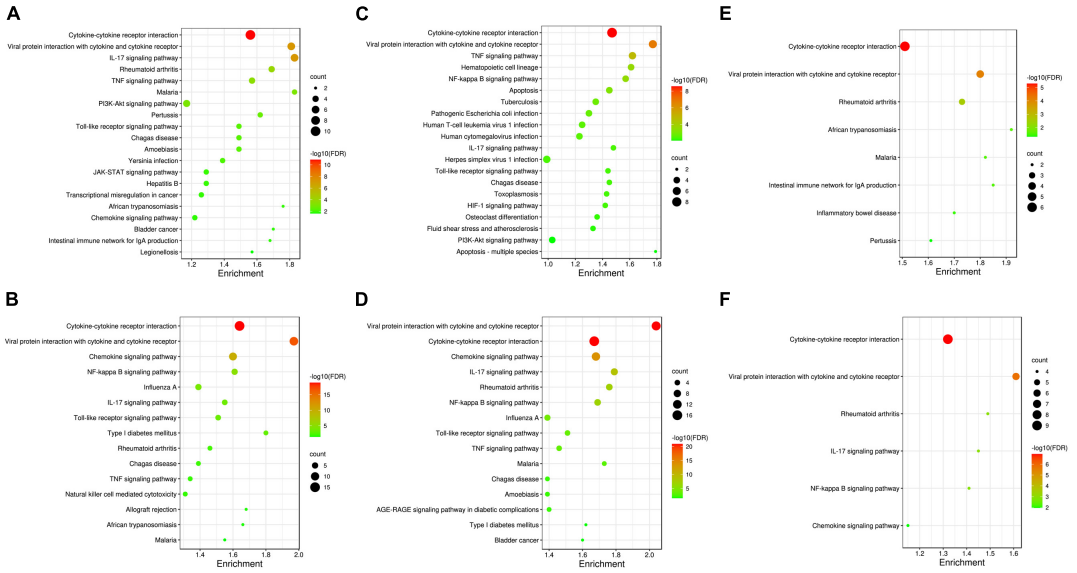


FIGURE 3
Kyoto encyclopedia of genes and genomes pathways analysis of altered proteins in three ablation groups. Altered proteins in three groups are all mainly enriched in cytokine–cytokine receptor interaction and viral protein interaction with cytokine and cytokine receptor. **(A,B)** The top 20 KEGG pathways enriched for the increased proteins and decreased proteins in the cryoballoon ablation group; **(C,D)** the top 20 KEGG pathways enriched for the increased proteins and decreased proteins in the radiofrequency balloon ablation group; **(E,F)** the all KEGG pathways enriched for the increased proteins and decreased proteins in the radiofrequency ablation group. The sizes of the bubbles are illustrated from big to small in descending order of the number of potential targets involved in the pathways.

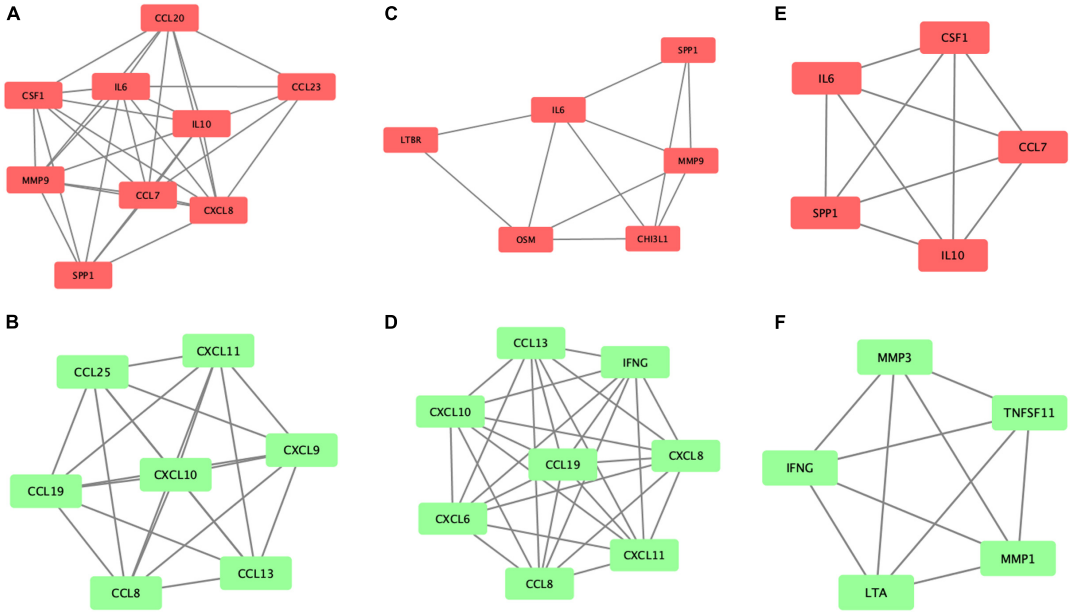


FIGURE 4
Potential functional modules with the best score in the PPI network. The most significant module for the increased proteins **(A)** and decreased proteins **(B)** in the cryoballoon group; **(C,D)** in the radiofrequency balloon group and **(E,F)** in the radiofrequency group, respectively. The significant modules were analyzed by using MCODE plugin, and then module networks were visualized using Cytoscape software.

TABLE 3 GO_BP and KEGG pathways enriched in the most significant module in the CB group (only top five listed).

Category	Term	Count	FDR	Matching proteins in the most significant module
(a)				
GO_BP	GO: 0019221 Cytokine-mediated signaling pathway	8	1.79E-07	CXCL8, CSF-1, CCL20, MMP-9, CCL7, IL-6, IL-10, CCL23
	GO: 0030595 Leukocyte chemotaxis	6	1.79E-07	CXCL8, CCL20, CCL7, IL-6, IL-10, CCL23
	GO: 0006954 Inflammatory response	7	1.02E-06	CXCL8, CSF-1, CCL20, CCL7, SPP1, IL-6, CCL23
	GO: 0097529 Myeloid leukocyte migration	5	2.50E-06	CXCL8, CCL20, CCL7, IL-6, CCL23
	GO: 0002687 Positive regulation of leukocyte migration	5	4.19E-06	CXCL8, CSF-1, CCL20, CCL7, IL-6
PATHWAYS	has04061 Viral protein interaction with cytokine and cytokine receptor	7	2.05E-13	CCL13, CXCL10, CXCL11, CCL19, CXCL9, CCL25, CCL8
	has04657 IL-17 signaling pathway	7	2.05E-13	CCL13, CXCL10, CXCL11, CCL19, CXCL9, CCL25, CCL8
	has04060 Cytokine-cytokine receptor interaction	7	2.05E-13	CCL13, CXCL10, CXCL11, CCL19, CXCL9, CCL25, CCL8
	has05323 Rheumatoid arthritis	7	3.89E-13	CCL13, CXCL10, CXCL11, CCL19, CXCL9, CCL25, CCL8
	has04668 TNF signaling pathway	6	2.87E-12	CCL13, CXCL10, CXCL11, CCL19, CCL25, CCL8
(b)				
GO_BP	GO: 0030593 Neutrophil chemotaxis	7	2.05E-13	CCL13, CXCL10, CXCL11, CCL19, CXCL9, CCL25, CCL8
	GO: 0031640 Killing of cells of other organism	7	2.05E-13	CCL13, CXCL10, CXCL11, CCL19, CXCL9, CCL25, CCL8
	GO: 0070098 Chemokine-mediated signaling pathway	7	2.05E-13	CCL13, CXCL10, CXCL11, CCL19, CXCL9, CCL25, CCL8
	GO: 0061844 Antimicrobial humoral immune response mediated by antimicrobial peptide	7	3.89E-13	CCL13, CXCL10, CXCL11, CCL19, CXCL9, CCL25, CCL8
	GO: 0048247 Lymphocyte chemotaxis	6	2.87E-12	CCL13, CXCL10, CXCL11, CCL19, CCL25, CCL8
PATHWAYS	has04061 Viral protein interaction with cytokine and cytokine receptor	7	3.05E-14	CCL13, CXCL10, CXCL11, CCL19, CXCL9, CCL25, CCL8
	has04062 Chemokine signaling pathway	7	1.37E-12	CCL13, CXCL10, CXCL11, CCL19, CXCL9, CCL25, CCL8
	has04060 Cytokine-cytokine receptor interaction	7	1.59E-11	CCL13, CXCL10, CXCL11, CCL19, CXCL9, CCL25, CCL8
	has04620 Toll-like receptor signaling pathway	3	0.00042	CXCL10, CXCL11, CXCL9
	has04064 NF-kappa B signaling pathway	2	0.038	CCL13, CCL19

(a) The most significant module of increased proteins in cryoballoon ablation; (b) the most significant module of decreased proteins in cryoballoon ablation. CB, cryoballoon; GO, gene ontology; BP, biological process; KEGG, Kyoto encyclopedia of genes and genomes; FDR, false-discovery rate.

adjustment was applied to the *p*-value calculated by the model, and an adjusted value of 0.05 was indicated as the significance threshold. Multiway importance plot was replotted *via* R package ggplot2.

Results

Baseline characteristics and clinical outcomes after ablation

A total of 32 persons were included in this study, of which eight were controls and eight received CB, RB, or RF ablation, respectively. The baseline characteristics of 32 participants are presented in Table 1. There were no significant differences in ages, gender, laboratory values, past medical history, and the history of medication apart from the use of anticoagulants ($p < 0.01$).

All the patients were monitored by the telemetry electrocardiogram during the hospitalization. The recurrent atrial arrhythmia after ablation has no significant differences in the three groups, although four patients presented AF or premature atrial contraction in the CB group, compared with two patients in the RB and RF groups, respectively ($p = 0.472$, Figure 1).

The change in plasma proteins before and after three different ablations

A total of 181 unique proteins in two panels were tested, and 19 (10.5%) analytes were removed with over 75% of samples below LOD. Table 2 shows the biomarkers that

TABLE 4 GO_BP and KEGG pathways enriched in the most significant module in the RB group (only top five listed).

Category	Term	Count	FDR	Matching proteins in the most significant module
(a)				
GO_BP	GO: 0010647 Positive regulation of cell communication	6	0.0085	OSM, LTBR, CHI3L1, MMP-9, SPP1, IL-6
	GO: 0023056 Positive regulation of signaling	6	0.0085	OSM, LTBR, CHI3L1, MMP-9, SPP1, IL-6
	GO: 0001934 Positive regulation of protein phosphorylation	5	0.0093	OSM, LTBR, CHI3L1, MMP-9, IL-6
	GO: 0071310 Cellular response to organic substance	6	0.0093	OSM, LTBR, CHI3L1, MMP-9, SPP1, IL-6
	GO: 0071345 Cellular response to cytokine stimulus	5	0.0093	OSM, LTBR, CHI3L1, MMP-9, IL-6
PATHWAYS	has04060 Cytokine-cytokine receptor interaction	3	0.0199	OSM, LTBR, IL-6
	has04151 PI3K-Akt signaling pathway	3	0.0199	OSM, SPP1, IL-6
	has04672 Intestinal immune network for IgA production	2	0.0199	LTBR, IL-6
	has04061 Viral protein interaction with cytokine and cytokine receptor	2	0.0284	LTBR, IL-6
	has04066 HIF-1 signaling pathway	2	0.0284	LTBR, IL-6
(b)				
GO_BP	GO: 0030593 Neutrophil chemotaxis	7	1.63E-12	CCL13, CXCL6, CXCL10, CXCL8, CXCL11, CCL19, CCL8
	GO: 0070098 Chemokine-mediated signaling pathway	7	1.63E-12	CCL13, CXCL6, CXCL10, CXCL8, CXCL11, CCL19, CCL8
	GO: 0006959 Humoral immune response	8	2.78E-12	CCL13, CXCL6, IFNG, CXCL10, CXCL8, CXCL11, CCL19, CCL8
	GO: 0061844 Antimicrobial humoral immune response mediated by antimicrobial peptide	7	3.10E-12	CCL13, CXCL6, CXCL10, CXCL8, CXCL11, CCL19, CCL8
	GO: 0006954 Inflammatory response	8	2.26E-10	CCL13, CXCL6, IFNG, CXCL10, CXCL8, CXCL11, CCL19, CCL8
PATHWAYS	has04061 Viral protein interaction with cytokine and cytokine receptor	7	2.43E-13	CCL13, CXCL6, CXCL10, CXCL8, CXCL11, CCL19, CCL8
	has04060 Cytokine-cytokine receptor interaction	8	3.54E-13	CCL13, CXCL6, IFNG, CXCL10, CXCL8, CXCL11, CCL19, CCL8
	has04062 Chemokine signaling pathway	7	7.22E-12	CCL13, CXCL6, CXCL10, CXCL8, CXCL11, CCL19, CCL8
	has04657 IL-17 signaling pathway	4	3.15E-06	CXCL6, IFNG, CXCL10, CXCL8
	has05323 Rheumatoid arthritis	3	0.00033	CXCL6, IFNG, CXCL8

(a) The most significant module of increased proteins in radiofrequency balloon ablation; (b) the most significant module of decreased proteins in radiofrequency balloon ablation. RB, radiofrequency balloon; GO, gene ontology; BP, biological process; KEGG, kyoto encyclopedia of genes and genomes; FDR, false-discovery rate.

showed significant differences before and after ablation using three different methods. Forty-two proteins (19 increased and 24 decreased), 46 proteins (21 increased and 25 decreased), and 43 proteins (13 increased and 30 decreased) showed significant changes in the CB, RB, and RF groups, respectively (**Supplementary Figure 4**).

The heatmaps of the altered proteins in three groups before and after ablation are shown in **Figure 2**, which indicates that the change in proteins in the acute phase was mainly on D1 post-ablation, especially in CB and RB groups.

Enrichment analysis and module analysis of PPI network in three ablation groups

Based on the altered proteins and the STRING database, we constructed the PPI network for the increased and decreased proteins separately in three groups (**Supplementary Figures 1–3**). The top KEGG pathways of altered proteins in different groups are shown in **Figure 3**. There was no distinguishment because the altered proteins in three groups were mainly enriched in cytokine–cytokine receptor interaction

TABLE 5 GO_BP and KEGG pathways enriched in the most significant module in the RF group (only top five listed).

Category	Term	Count	FDR	Matching proteins in the most significant module
(a)				
GO_BP	GO: 0032101 Regulation of response to external stimulus	5	0.0048	CSF-1, CCL7, SPP1, IL-6, IL-10
	GO: 0022603 Regulation of anatomical structure morphogenesis	5	0.0048	CSF-1, CCL7, SPP1, IL-6, IL-10
	GO: 0002690 Positive regulation of leukocyte chemotaxis	3	0.0055	CSF-1, CCL7, IL-6
	GO: 0006952 Defense response	5	0.0055	CSF-1, CCL7, SPP1, IL-6, IL-10
	GO: 0006954 Inflammatory response	4	0.0062	CSF-1, CCL7, SPP1, IL-6
PATHWAYS	has04061 Viral protein interaction with cytokine and cytokine receptor	4	1.07E-06	CSF-1, CCL7, IL-6, IL-10
	has04060 Cytokine-cytokine receptor interaction	4	3.71E-05	CSF-1, CCL7, IL-6, IL-10
	has05143 African trypanosomiasis	2	0.0041	IL-6, IL-10
	has04151 PI3K-Akt signaling pathway	3	0.0043	CSF-1, SPP1, IL-6
	has04672 Intestinal immune network for IgA production	2	0.0043	IL-6, IL-10
(b)				
GO_BP	GO: 0019221 Cytokine-mediated signaling pathway	5	0.00066	IFNG, MMP-3, MMP-1, TNFSF11, LTA
	GO: 0050729 Positive regulation of inflammatory response	3	0.0132	IFNG, TNFSF11, LTA
PATHWAYS	has05323 Rheumatoid arthritis	4	6.69E-07	IFNG, MMP-3, MMP-1, TNFSF11
	has04657 IL-17 signaling pathway	3	0.00018	IFNG, MMP-3, MMP-1
	has04060 Cytokine-cytokine receptor interaction	3	0.0033	IFNG, TNFSF11, LTA
	has04940 Type I diabetes mellitus	2	0.0036	IFNG, LTA
	has04064 NF-kappa B signaling pathway	2	0.0182	TNFSF11, LTA

(a) The most significant module of increased proteins in radiofrequency ablation; (b) the most significant module of decreased proteins in radiofrequency ablation. RF, radiofrequency; GO, gene ontology; BP, biological process; KEGG, kyoto encyclopedia of genes and genomes; FDR, false-discovery rate.

and viral protein interaction with cytokine and cytokine receptor.

In order to more accurately elucidate the protein change pattern after different ablations, we used the MCODE plugin in the Cytoscape software to conduct module analysis on the PPI network and obtained a potential protein functional module with the best score, as shown in **Figure 4**. Furthermore, the GO enrichment analysis for six significant modules (**Supplementary Tables 1–5**) showed a similar biological process in CB and RB groups. Proteins involved in the most significant module for the decreased proteins were both enriched in the neutrophil chemotaxis (**Tables 3**, **4**). Proteins in the most significant module for the increased proteins in the CB group mainly enriched in the cytokine-mediated signaling pathway (**Table 3**), which is part of cell communication and regulation of signaling, the two major positively regulated biological processes in the RB group (**Table 4**). However, as seen in **Table 5**, the cytokine-mediated signaling pathway was downregulated in the RF group.

Identification of the seed protein under three different techniques

The MCODE application also provided the highest dense protein complex as the seed protein from the potential functional module, which helps to identify the potential markers for further study in three different techniques. The seed protein of the increased proteins was osteopontin (OPN), also known as secreted phosphoprotein 1, in the CB group and interleukin-6 (IL-6) in the RB group. For patients who received RF ablation, the seed increased protein was IL-10.

Among the proteins decreased after ablation, the seed protein was C-C motif ligand 8 (CCL8), also known as monocyte chemoattractant protein-2, in both CB and RB groups. Differently, the seed protein was matrix metalloproteinase-1 (MMP-1) in the RF group.

The change in OPN, IL-6, IL-10, CCL8, and MMP-1 levels at three-time points in three ablation groups and the control group are shown in **Figure 5**, with a comparable measurement between the groups. No significant difference was observed in these proteins at baseline between the control group and three ablation groups as well, which can exclude the disease-related effect on the change in proteins.

Biomarkers associated with hemorrhage and coagulation activity

As shown in **Table 6**, we identified some altered proteins associated with hemorrhage and coagulation. Proteins changes that increased thrombus formation risk after ablation were noted for OPN and urokinase-type plasminogen activator (uPA) in all groups, along with trefoil factor 3 (TFF3) in the RB group and MMP-1 in the RF group. Proteins changes that caused higher bleeding risk after ablation,

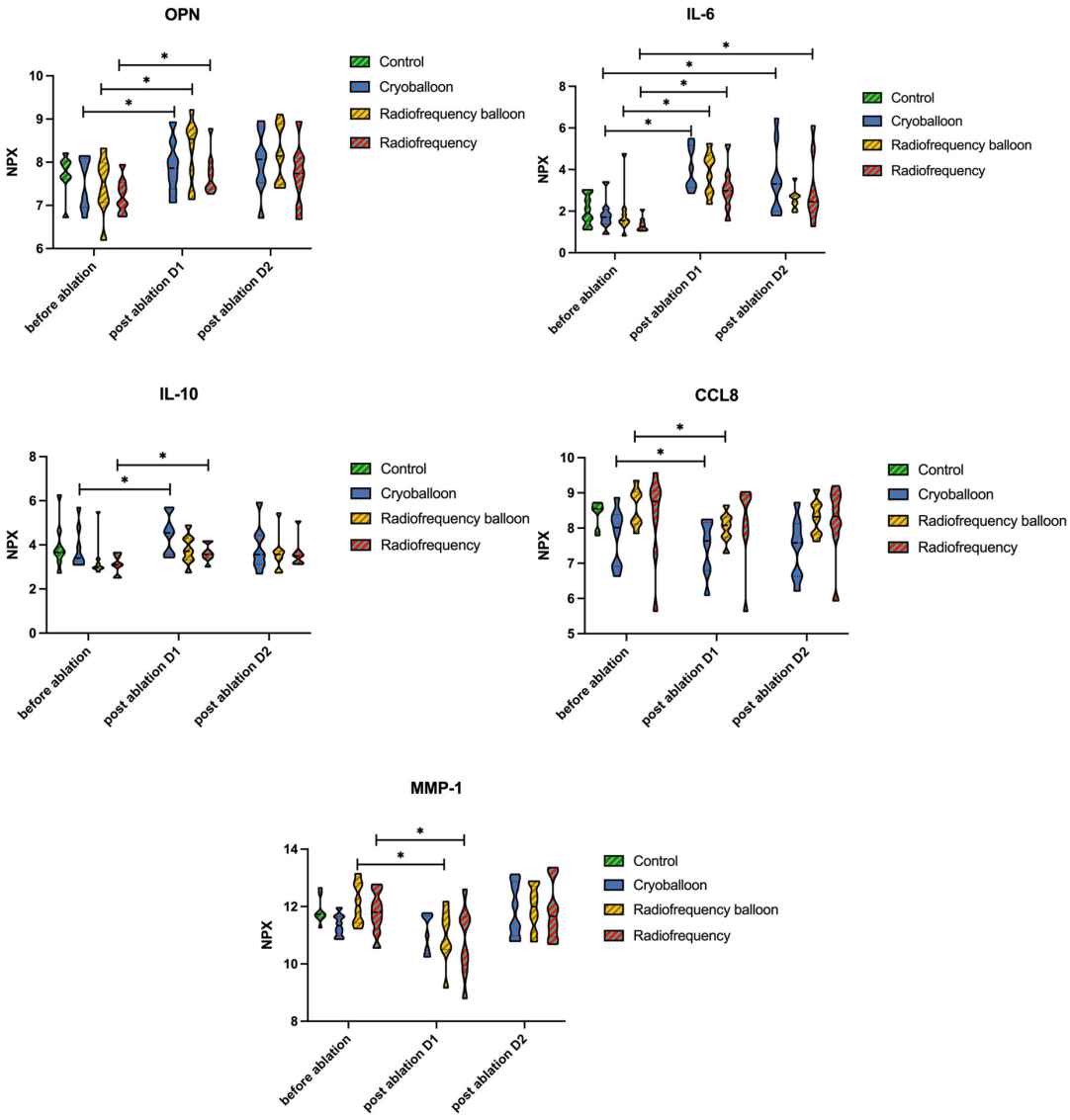


FIGURE 5
Levels of seed proteins before and after ablation. No differences were seen between the groups at any time point. Differences before and after ablation were assessed with the Wilcoxon signed-rank test. *P*-values are given for comparison within the group between different time points. OPN, osteopontin, seed-increased protein in the CB group; IL-6, interleukin-6, seed-increased protein in the RB group; IL-10, interleukin-10, seed-increased protein in the RF group; CCL8, C-C motif ligand 8, seed decreased protein in CB and RB groups; MMP-1, matrix metalloproteinase-1, seed decreased protein in the RF group. NPX, normalized protein expression. $^*P < 0.05$.

include growth/differentiation factor 15, myeloblastin (PRTN3), collagen alpha-1 (I) chain, tumor necrosis factor receptor 1 (TNF-R1), ephrin type-B receptor 4 (EPHB4), and von Willebrand factor (vWF). We also conducted LASSO logistic regression and random forest to select significant proteins (**Figure 6**). Interestingly, two proteins (uPA and PRTN3) in the CB group and three proteins (vWF, uPA, and EPHB4) in the RB group were also the significant proteins selected by LASSO logistic regression and random forest, among which only PRTN3 was related to hemorrhage and coagulation in the RF group. No significant differences in the levels of these proteins were found between three groups (**Figure 7**).

Discussion

Proteins mainly altered on the first day after ablation

In this study, we analyzed a total of 181 different plasma proteins from eight control patients and 24 patients with AF

TABLE 6 Protein changes are associated with hemorrhage and coagulation activity.

Group	Increase thrombus risk	Increase bleeding risk
Cryoballoon ablation	OPN↑, uPA↓	GDF-15↑, PRTN3↓
Radiofrequency balloon ablation	OPN↑, uPA↓, TFF3↓	TNF-R1↑, EPHB4↑, COL1A1↓, vWF↓
Radiofrequency ablation	OPN↑, uPA↓, MMP-1↓	GDF-15↑, PRTN3↑, COL1A1↓

↑, proteins increased after ablation; ↓, proteins decreased after ablation.

before and after interventional ablation using three different techniques. Most of the proteins changed significantly on the first day after ablation. Although clinical studies demonstrated that same-day discharge is safe with a comparable rate of complications in the long term in patients with an overnight stay after ablation (20, 21), the pathophysiological alterations recover until the overnight stay in patients with AF undergoing pulmonary vein isolation. Given that plasma proteins changed mainly limited on the first day after three different ablations, it would be safer for patients to be discharged overnight.

Similar enrichment analysis in both balloon-based ablations

Pathway analysis indicated that the proteins that changed after ablation in the acute phase were mainly in cytokine–cytokine receptor interaction in three groups. Interestingly, the module analysis and enrichment analysis indicated that CB and RB groups showed similar trends in cell communication, the regulation of signaling, and neutrophil chemotaxis. Specifically, the cytokine-mediated signaling pathway in the CB group was upregulated significantly. As part of cell communication and regulation of signaling, this signaling pathway was also positively regulated in the RB group (**Supplementary Table 3**). However, the cytokine-mediated signaling pathway was downregulated in the RF group. Meanwhile, neutrophil chemotaxis was inhibited in both balloon-based ablations (**Tables 3**, **4**) but not in the RF group. To our knowledge, this phenomenon was not noted in previous studies.

Similar response to inflammation in both balloon-based ablations

We also found that both balloon-based ablations shared a similar response to inflammation, while radiofrequency ablation showed different tendencies to inflammatory response as indicated by different seed proteins after ablation. In the CB group, OPN was the most important increased protein after ablation. OPN is a matricellular protein that contributes to acute inflammation by increasing the production of IL-6, IL-12, IL-17, and interferon-gamma (IFN-γ) and inhibiting the expression of IL-10 (22). Since RB ablation is a new technique, there are few comparative studies about markers of inflammation between RB and CB ablation or RF ablation. However, the high risk of inflammation in the RB group was indicated by the seed protein IL-6 in our study. Such a finding was consistent with a previous image study, which describes the regional inflammation pattern occurring after CB ablation and RB ablation in the human left atrium using positron emission tomography (23). The upregulated expression of IL-6 by OPN has been demonstrated in inflammatory disease (24). Thus, IL-6 may trigger IL-6 trans-signaling, contributing to the upregulation of OPN in THP-1 macrophages (25). Of note, higher IL-6 concentrations can also play a role in regulating leukocyte infiltration by suppressing neutrophil recruitment (26). Neutrophil activation, as reflected by the seed protein CCL8 (27, 28), displayed

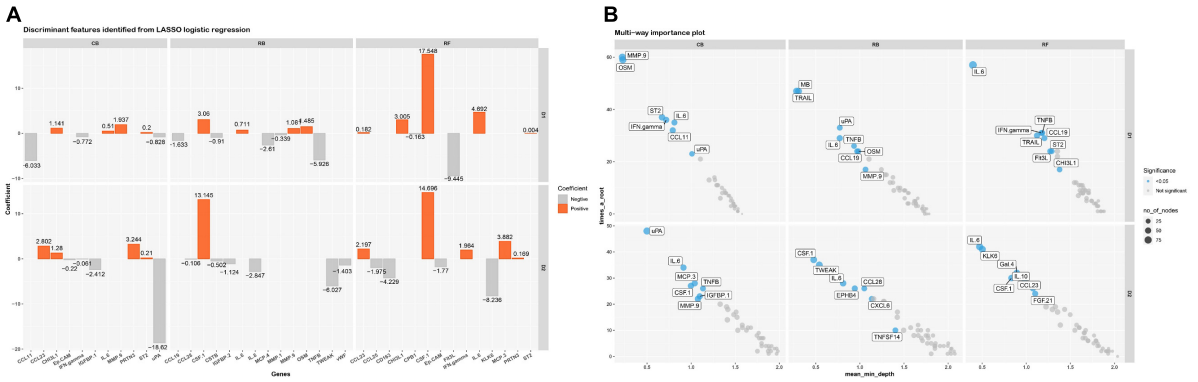


FIGURE 6
LASSO logistic regression and random forest of altered proteins in three ablation groups. **(A)** Significant proteins selected by LASSO logistic regression before and after ablation D1 and D2 in three ablation groups; **(B)** significant proteins selected by random forest before and after ablation D1 and D2 in three ablation groups.

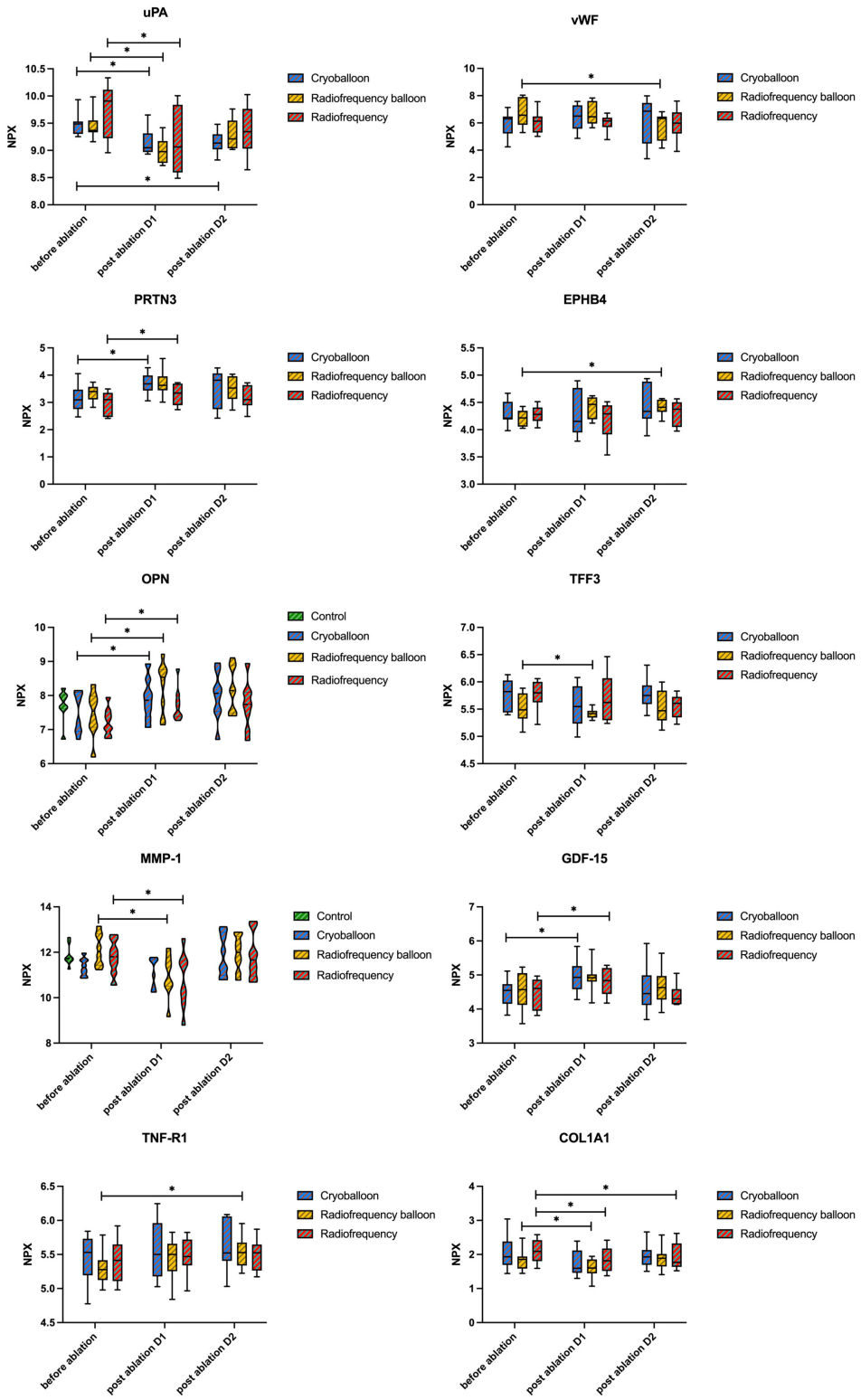


FIGURE 7
Levels of proteins associated with hemorrhage and coagulation activity. No differences were seen between the groups at any time point. Differences before and after ablation were assessed with the Wilcoxon signed-rank test. *P*-values are given for comparison within the group between different time points. uPA, urokinase-type plasminogen activator; TFF3, trefoil factor 3; GDF-15, growth/differentiation factor 15; PRTN3, myeloblastin; COL1A1, collagen alpha-1(I) chain; TNF-R1, tumor necrosis factor receptor 1; EPHB4, ephrin type-B receptor 4; vWF, von Willebrand factor; NPX, normalized protein expression; *$P<0.05$. Note that the levels of OPN and MMP-1 are shown in **Figure 5**.

a similar decreased trend in the CB and RB group in this study. While in the RF group, IL-10 generally recognized as an anti-inflammatory cytokine, was the seed protein of increased proteins in our study. The new report demonstrated that mature neutrophils could potentially dampen local inflammation by IL-10 production (29).

There is no obvious explanation for why these proteins altered significantly, but it could be related to larger lesion size and injury. Previous studies have shown that endothelial injury is related to inflammatory biomarkers, including OPN and IL-6 (30, 31). High levels of IL-6 are also associated with vascularization in sites of inflammation and with wound healing (32, 33). The higher inflammatory tendency in balloon-based ablation might show that the endothelial surface is kept less intact after balloon lesion than what is seen after irrigated RF ablation.

Although this study noted comparable levels of inflammatory markers in the acute phase between the CB and RF ablation, which is supported by other publications (34, 35), the different inflammatory effects of seed proteins indicates greater local inflammatory response in the balloon-based ablation. Along with similar enrichment analysis, these results suggest that pathophysiological response in the acute phase after ablation is more likely to be affected by the lesion size rather than the energy source.

Proteins associated with hemorrhage and coagulation activity in three ablations

Thromboembolism events are uncommon but one of the most feared complications of AF ablation. By using a new proteomic assay, we identified some proteins which are different from the common-used biomarkers in previous studies, such as D-dimer and P-selection.

As shown in **Table 6**, radiofrequency energy affected greater numbers of proteins, indicating a stronger impact on hemorrhage and coagulation activity. This finding is consistent with previous studies showing a higher rate of thrombus formation after RF than after CB ablation (11, 36). However, current data are lacking to define the prevalence of thromboembolism in patients received RB ablation. Compared with the CB group, both radiofrequency energy groups affected one more protein that could increase the risk of thrombus. As the most important decreased protein in the RF group in our study, MMP-1 plays an important role in the occurrence and development of a deep venous thrombus (37, 38), and also in regulating prothrombotic state in patients with AF (39). TFF3 is a protective marker of underlying myocyte damage/ischemia and is moderately correlated with ischemic stroke in patients with AF (40, 41). We also noticed the bleeding tendency with the lower level of vWF after RB ablation, which is commonly increased after CB and RF ablation (13, 42). In an explorative study, TNF-R1 and EPHB4 were independently associated with major bleedings in patients with AF (43), also suggesting higher hemorrhage risk in RB ablation.

Interestingly, results from LASSO logistic regression and random forest presented a different explanation for proteins associated with hemorrhage and coagulation. Among the significant proteins selected in three groups by LASSO logistic regression and random forest, respectively, only one protein in the RF group was associated with hemorrhage and coagulation activity, compared with two related proteins in the CB group and three in the RB group. Although RF ablation affected more proteins associated with thrombus and bleeding events, they are not characteristic enough to distinguish RF from other techniques. The underlying reason for a greater impact on hemorrhage and coagulation activity in balloon-based ablation groups shown in two novel bioinformatic analyses could be attributed to the larger ablation lesion.

In clinical practice, the basis for the selection of ablation technologies for pulmonary vein isolation in patients with AF remains unclear, especially with the emergence of a new technique RB. A recent clinical study showed that all ablation technologies facilitate safe and efficient pulmonary vein isolation, with slight differences in the procedural data and complications (44). To replenish previous clinical studies, the similar alteration of two balloon-based ablations in protein profile in our study provided the pathophysiological evidence from protein levels to support the application of RB in the clinic.

Limitations

This study was limited to the proteins provided by the Olink panel and the evaluation period. Thus, most of the investigated proteins are still not clearly related to the clinical event, although they are useful for the pathophysiological understanding of the ablation lesion mechanism. Finally, the size of this explorative study was small and, as such, did not have enough power to show minor differences between the three ablation techniques.

Conclusion

Multiple plasma proteins were differently expressed after catheter ablation using different techniques, especially on the first day after ablation, suggesting that longer monitoring is not needed in patients with AF undergoing uncomplicated catheter ablation. The pattern of the protein change during the acute phase is mainly affected by the lesion size according to the similar enrichment analysis in the most significant module of CB and RB ablation. We also identified some important plasma proteins that could be of potential interest to future studies.

By comparison, balloon-based ablation (CB and RB) showed a higher tendency of inflammation and had more influence on hemorrhage and coagulation activity. Further studies of these biomarkers and clinical events in patients with AF who received different ablations are warranted.

Data availability statement

The original contributions presented in this study are included in the article/**Supplementary material**, further inquiries can be directed to the corresponding authors.

Ethics statement

The studies involving human participants were reviewed and approved by the Ruijin Hospital Ethics Committee. The patients/participants provided their written informed consent to participate in this study.

Author contributions

ML: data curation-lead, formal analysis-lead, investigation-equal, methodology-equal, validation-equal, visualization-equal, and writing—original draft, review, and editing-equal. YB: conceptualization-lead, investigation-equal, methodology-equal, validation-equal, and writing—original draft, review, and editing-equal. ZD: conceptualization-supporting, data curation-supporting, investigation-equal, methodology-equal, validation-equal, and writing—original draft, review, and editing-equal. NZ, CL, YX, YW, QZL, WP, TL, and QJ: methodology-equal. YYX: conceptualization-supporting and methodology-equal. YZ and RZ: methodology-equal and visualization-equal. QHL: investigation-equal and validation-equal. JQ, TZ, and CX: investigation-equal. YAX, LJW, and LQW: writing—review and editing-equal. TY: conceptualization-supporting, funding acquisition-equal, supervision-equal, and writing—review and editing-equal. YCX: conceptualization-supporting, data curation-supporting, funding acquisition-equal, supervision-equal, and writing—review and editing-equal. All authors contributed to the article and approved the submitted version.

Funding

This study was supported by the National Natural Science Foundation of China (grant number: 81570234) and the National Research Center for Translational Medicine Shanghai Open Project, TMSK-2021-508.

Acknowledgments

We are grateful to the patients who participated in this study.

Conflict of interest

The authors declare that the research was conducted in the absence of any commercial or financial relationships that could be construed as a potential conflict of interest.

Publisher's note

All claims expressed in this article are solely those of the authors and do not necessarily represent those of their affiliated organizations, or those of the publisher, the editors and the reviewers. Any product that may be evaluated in this article, or claim that may be made by its manufacturer, is not guaranteed or endorsed by the publisher.

Supplementary material

The Supplementary Material for this article can be found online at: https://www.frontiersin.org/articles/10.3389/fcvm.2022.1077992/full#supplementary-material

References

1. Goudis C, Vasileiadis I, Liu T. Epicardial adipose tissue and atrial fibrillation: pathophysiological mechanisms, clinical implications, and potential therapies. *Curr Med Res Opin.* (2018) 34:1933–43. doi: 10.1080/03007995.2018.1462786

2. Cosedis Nielsen J, Johannessen A, Raatikainen P, Hindricks G, Walfridsson H, Kongstad O, et al. Radiofrequency ablation as initial therapy in paroxysmal atrial fibrillation. *N Engl J Med.* (2012) 367:1587–95.

3. Packer D, Mark D, Robb R, Monahan K, Bahnson T, Poole J, et al. Effect of catheter ablation vs antiarrhythmic drug therapy on mortality, stroke, bleeding, and cardiac arrest among patients with atrial fibrillation: the CABANA randomized clinical trial. *JAMA.* (2019) 321:1261–74. doi: 10.1001/jama.2019.0693

4. Khan A, Khan S, Sheikh M, Khuder S, Grubb B, Moukarbel G. Catheter ablation and antiarrhythmic drug therapy as first- or second-line therapy in the management of atrial fibrillation: systematic review and meta-analysis. *Circ Arrhythm Electrophysiol.* (2014) 7:853–60.

5. Hindricks G, Potpara T, Dagres N, Arbelo E, Bax J, Blomstrom-Lundqvist C, et al. Corrigendum to: 2020 ESC Guidelines for the diagnosis and management of atrial fibrillation developed in collaboration with the European association for cardio-thoracic surgery (EACTS): the task force for the diagnosis and management of atrial fibrillation of the European Society of Cardiology (ESC) developed with the special contribution of the European heart rhythm association (EHRA) of the ESC. *Eur Heart J.* (2021) 42:4194. doi: 10.1093/eurheartj/ehab648

6. January C, Wann L, Calkins H, Chen L, Cigarroa J, Cleveland J Jr., et al. 2019 AHA/ACC/HRS focused update of the 2014 AHA/ACC/HRS guideline for the management of patients with atrial fibrillation: a report of the american college of cardiology/American heart association task force on clinical practice guidelines and the heart rhythm society in collaboration with the society of thoracic surgeons. *Circulation.* (2019) 140:e125–51. doi: 10.1161/CIR.0000000000000665

7. Andrade J, Champagne J, Dubuc M, Deyell M, Verma A, Macle L, et al. Cryoballoon or radiofrequency ablation for atrial fibrillation assessed by continuous monitoring: a randomized clinical trial. *Circulation.* (2019) 140:1779–88.

8. Wang Y, Wang W, Yao J, Chen L, Yi S. Second-generation cryoballoon vs. contact-force sensing radiofrequency catheter ablation in atrial fibrillation: a meta-analysis of randomized controlled trials. *J Interv Card Electrophysiol.* (2021) 60:9–19. doi: 10.1007/s10840-020-00893-w

9. Ohkawa S, Hackel D, Mikat E, Gallagher J, Cox J, Sealy W. Anatomic effects of cryoablation of the atrioventricular conduction system. *Circulation.* (1982) 65:1155–62.

10. van Oeveren W, Crijns H, Korteling B, Wegereef E, Haan J, Tigchelaar I, et al. Blood damage, platelet and clotting activation during application of radiofrequency or cryoablation catheters: a comparative in vitro study. *J Med Eng Technol.* (1999) 23:20–5.

11. Khairy P, Chauvet P, Lehmann J, Lambert J, Macle L, Tanguay J, et al. Lower incidence of thrombus formation with cryoenergy versus radiofrequency catheter ablation. *Circulation.* (2003) 107:2045–50.

12. Herrera Siklody C, Arentz T, Minners J, Jesel L, Stratz C, Valina C, et al. Cellular damage, platelet activation, and inflammatory response after pulmonary vein isolation: a randomized study comparing radiofrequency ablation with cryoablation. *Heart Rhythm.* (2012) 9:189–96. doi: 10.1016/j.hrthm.2011.09.017

13. Malmborg H, Christersson C, Lonnerholm S, Blomstrom-Lundqvist C. Comparison of effects on coagulation and inflammatory markers using a duty-cycled bipolar and unipolar radiofrequency pulmonary vein ablation catheter vs. a cryoballoon catheter for pulmonary vein isolation. *Europace.* (2013) 15:798–804. doi: 10.1093/europace/eus411

14. Schilling R, Dhillon G, Tondo C, Riva S, Grimaldi M, Quadrini F, et al. Safety, effectiveness, and quality of life following pulmonary vein isolation with a multi-electrode radiofrequency balloon catheter in paroxysmal atrial fibrillation: 1-year outcomes from SHINE. *Europace.* (2021) 23:851–60. doi: 10.1093/europace/euaa382

15. Reddy V, Schilling R, Grimaldi M, Horton R, Natale A, Riva S, et al. Pulmonary vein isolation with a novel multielectrode radiofrequency balloon catheter that allows directionally tailored energy delivery: short-term outcomes from a multicenter first-in-human study (RADIANCE). *Circ Arrhythm Electrophysiol.* (2019) 12:e007541. doi: 10.1161/CIRCEP.119.007541

16. Joshi A, Rienks M, Theofilatos K, Mayr M. Systems biology in cardiovascular disease: a multiomics approach. *Nat Rev Cardiol.* (2021) 18:313–30.

17. Verdonschot J, Ferreira J, Pellicori P, Brunner-La Rocca H, Clark A, Cosmi F, et al. Proteomic mechanistic profile of patients with diabetes at risk of developing heart failure: insights from the HOMAGE trial. *Cardiovasc Diabetol.* (2021) 20:163. doi: 10.1186/s12933-021-01357-9

18. Kurose J, Kiuchi K, Fukuzawa K, Takami M, Mori S, Suehiro H, et al. Lesion characteristics between cryoballoon ablation and radiofrequency ablation with a contact force-sensing catheter: late-gadolinium enhancement magnetic resonance imaging assessment. *J Cardiovasc Electrophysiol.* (2020) 31:2572–81. doi: 10.1111/jce.14664

19. Gisby J, Clarke C, Medjeral-Thomas N, Malik T, Papadaki A, Mortimer P, et al. Longitudinal proteomic profiling of dialysis patients with COVID-19 reveals markers of severity and predictors of death. *eLife.* (2021) 10:e64827. doi: 10.7554/eLife.64827

20. Field M, Goldstein L, Corriveau K, Khanna R, Fan X, Gold M. Same-day discharge after catheter ablation in patients with atrial fibrillation in a large nationwide administrative claims database. *J Cardiovasc Electrophysiol.* (2021) 32:2432–40. doi: 10.1111/jce.15193

21. Prasitlumkum N, Cheungpasitporn W, Chokesuwattanaskul R, Kewcharoen J, Tokavanich N, Navaravong L, et al. Comparison between same-day discharge and overnight stay after atrial fibrillation ablation: systematic review and meta-analysis. *Pacing Clin Electrophysiol.* (2021) 44:2054–66. doi: 10.1111/pace.14380

22. Lund S, Giachelli C, Scatena M. The role of osteopontin in inflammatory processes. *J Cell Commun Signal.* (2009) 3:311–22.

23. Kiuchi K, Fukuzawa K, Mori S, Watanabe Y, Hirata K. Feasibility of imaging inflammation in the left atrium post AF ablation using PET technology. *JACC Clin Electrophysiol.* (2017) 3:1466–7. doi: 10.1016/j.jacep.2017.02.004

24. Yang Y, Gao S, Zhang F, Luo W, Xue J, Lei G. Effects of osteopontin on the expression of IL-6 and IL-8 inflammatory factors in human knee osteoarthritis chondrocytes. *Eur Rev Med Pharmacol Sci.* (2014) 18:3580–6.

25. Uchibori T, Matsuda K, Shimodaira T, Sugano M, Uehara T, Honda T. IL-6 trans-signaling is another pathway to upregulate osteopontin. *Cytokine.* (2017) 90:88–95. doi: 10.1016/j.cyto.2016.11.006

26. Hurst S, Wilkinson T, McLoughlin R, Jones S, Horiuchi S, Yamamoto N, et al. Il-6 and its soluble receptor orchestrate a temporal switch in the pattern of leukocyte recruitment seen during acute inflammation. *Immunity.* (2001) 14:705–14. doi: 10.1016/s1074-7613(01)00151-0

27. Asano K, Takahashi N, Ushiki M, Monya M, Aihara F, Kuboki E, et al. Intestinal CD169(+) macrophages initiate mucosal inflammation by secreting CCL8 that recruits inflammatory monocytes. *Nat Commun.* (2015) 6:7802. doi: 10.1038/ncomms8802

28. Shaath H, Vishnubalaji R, Elkord E, Alajez N. Single-cell transcriptome analysis highlights a role for neutrophils and inflammatory macrophages in the pathogenesis of severe COVID-19. *Cells.* (2020) 9:2374. doi: 10.3390/cells9112374

29. Bergmann C, Salyer C, Beckmann N, Caldwell C. Intraperitoneal Neutrophil IL-10 production is promoted by interferon gamma in a murine model of sepsis model in the acute phase of sepsis. *Biochem Biophys Res Commun.* (2020) 530:278–84. doi: 10.1016/j.bbrc.2020.07.089

30. Batko K, Krzanowski M, Gajda M, Dumnicka P, Fedak D, Woziwodzka K, et al. Endothelial injury is closely related to osteopontin and TNF receptor-mediated inflammation in end-stage renal disease. *Cytokine.* (2019) 121:154729. doi: 10.1016/j.cyto.2019.05.016

31. Montgomery A, Tam F, Gursche C, Cheneval C, Besler K, Enns W, et al. Overlapping and distinct biological effects of IL-6 classic and trans-signaling in vascular endothelial cells. *Am J Physiol Cell Physiol.* (2021) 320:C554–65. doi: 10.1152/ajpcell.00323.2020

32. Catar R, Witowski J, Zhu N, Lucht C, Derrac Soria A, Uceda Fernandez J, et al. IL-6 trans-signaling links inflammation with angiogenesis in the peritoneal membrane. *J Am Soc Nephrol.* (2017) 28:1188–99. doi: 10.1681/ASN.2015101169

33. Mateo R, Reichner J, Albina J. Interleukin-6 activity in wounds. *Am J Physiol.* (1994) 266(6 Pt 2):R1840–4.

34. Antolic B, Pernat A, Cvijic M, Zizek D, Jan M, Sinkovec M. Radiofrequency catheter ablation versus balloon cryoablation of atrial fibrillation: markers of myocardial damage, inflammation, and thrombogenesis. *Wien Klin Wochenschr.* (2016) 128:480–7. doi: 10.1007/s00508-016-1002-0

35. Bin Waleed K, Yin X, Yang X, Dai B, Liu Y, Wang Z, et al. Short and long-term changes in platelet and inflammatory biomarkers after cryoballoon and radiofrequency ablation. *Int J Cardiol.* (2019) 285:128–32. doi: 10.1016/j.ijcard.2019.02.054

36. Herrera Siklody C, Deneke T, Hocini M, Lehrmann H, Shin D, Miyazaki S, et al. Incidence of asymptomatic intracranial embolic events after pulmonary vein isolation: comparison of different atrial fibrillation ablation technologies in a multicenter study. *JACC.* (2011) 58:681–8. doi: 10.1016/j.jacc.2011.04.010

37. Trivedi V, Boire A, Tchernychev B, Kaneider N, Leger A, O'Callaghan K, et al. Platelet matrix metalloprotease-1 mediates thrombogenesis by activating PAR1 at a cryptic ligand site. *Cell.* (2009) 137:332–43. doi: 10.1016/j.cell.2009.02.018

38. Zhang T, Li Q, Wang L, Li G. Expression variations and clinical significance of MMP-1, MMP-2 and inflammatory factors in serum of patients with deep venous thrombosis of lower extremity. *Exp Ther Med.* (2019) 17:181–6. doi: 10.3892/etm.2018.6922

39. Marin F, Roldan V, Climent V, Garcia A, Marco P, Lip G. Is thrombogenesis in atrial fibrillation related to matrix metalloproteinase-1 and its inhibitor, TIMP-1? *Stroke.* (2003) 34:1181–6. doi: 10.1161/01.STR.0000065431.76788.D9

40. Liu S, Tefft B, Roberts D, Zhang L, Ren Y, Li Y, et al. Cardioprotective proteins upregulated in the liver in response to experimental myocardial ischemia. *Am J Physiol Heart Circ Physiol.* (2012) 303:H1446–58.

41. Hijazi Z, Wallentin L, Lindback J, Alexander J, Connolly S, Eikelboom J, et al. Screening of multiple biomarkers associated with ischemic stroke in atrial fibrillation. *J Am Heart Assoc.* (2020) 9:e018984.

42. Hajas O, Bagoly Z, Toth N, Urbancsek R, Kiss A, Kovacs K, et al. Intracardiac fibrinolysis and endothelium activation related to atrial fibrillation ablation with different techniques. *Cardiol Res Pract.* (2020) 2020:1570483. doi: 10.1155/2020/1570483

43. Siegbahn A, Lindback J, Hijazi Z, Aberg M, Alexander J, Eikelboom J, et al. Multiplex protein screening of biomarkers associated with major bleeding in patients with atrial fibrillation treated with oral anticoagulation. *J Thromb Haemost.* (2021) 19:2726–37.

44. Seki R, Nagase T, Asano S, Fukunaga H, Inoue K, Sekiguchi Y, et al. Radiofrequency current versus balloon-based ablation for atrial fibrillation. *Am J Cardiol.* (2022) 178:52–9.

frontiers | Frontiers in Cardiovascular Medicine

TYPE Original Research
PUBLISHED 17 March 2023
DOI 10.3389/fcvm.2023.1058834

Check for updates

OPEN ACCESS

EDITED BY
Miguel Hueso,
Bellvitge University Hospital, Spain

REVIEWED BY
Liam Butler,
Wake Forest University, United States
Quhuan Li,
South China University of Technology, China

*CORRESPONDENCE
XingHua Gu
guxh2005@126.com

†These authors have contributed equally to this work

SPECIALTY SECTION
This article was submitted to Cardiovascular Genetics and Systems Medicine, a section of the journal Frontiers in Cardiovascular Medicine

RECEIVED 04 October 2022
ACCEPTED 28 February 2023
PUBLISHED 17 March 2023

CITATION
Kong X, Sun H, Wei K, Meng L, Lv X, Liu C, Lin F and Gu X (2023) WGCNA combined with machine learning algorithms for analyzing key genes and immune cell infiltration in heart failure due to ischemic cardiomyopathy. Front. Cardiovasc. Med. 10:1058834. doi: 10.3389/fcvm.2023.1058834

COPYRIGHT
© 2023 Kong, Sun, Wei, Meng, Lv, Liu, Lin and Gu. This is an open-access article distributed under the terms of the Creative Commons Attribution License (CC BY). The use, distribution or reproduction in other forums is permitted, provided the original author(s) and the copyright owner(s) are credited and that the original publication in this journal is cited, in accordance with accepted academic practice. No use, distribution or reproduction is permitted which does not comply with these terms.

WGCNA combined with machine learning algorithms for analyzing key genes and immune cell infiltration in heart failure due to ischemic cardiomyopathy

XiangJin Kong[1,2†], HouRong Sun[1,2†], KaiMing Wei[1,2], LingWei Meng[1,2], Xin Lv[1,2], ChuanZhen Liu[1,2], FuShun Lin[1,2] and XingHua Gu[1,2*]

[1]Qilu Hospital, Cheeloo College of Medicine, Shandong University, Jinan, China, [2]Department of Cardiovascular Surgery, Qilu Hospital of Shandong University, Jinan, China

Background: Ischemic cardiomyopathy (ICM) induced heart failure (HF) is one of the most common causes of death worldwide. This study aimed to find candidate genes for ICM-HF and to identify relevant biomarkers by machine learning (ML).
Methods: The expression data of ICM-HF and normal samples were downloaded from Gene Expression Omnibus (GEO) database. Differentially expressed genes (DEGs) between ICM-HF and normal group were identified. Kyoto Encyclopedia of Genes and Genomes (KEGG) pathway enrichment and gene ontology (GO) annotation analysis, protein–protein interaction (PPI) network, gene pathway enrichment analysis (GSEA), and single-sample gene set enrichment analysis (ssGSEA) were performed. Weighted gene co-expression network analysis (WGCNA) was applied to screen for disease-associated modules, and relevant genes were derived using four ML algorithms. The diagnostic values of candidate genes were assessed using receiver operating characteristic (ROC) curves. The immune cell infiltration analysis was performed between the ICM-HF and normal group. Validation was performed using another gene set.
Results: A total of 313 DEGs were identified between ICM-HF and normal group of GSE57345, which were mainly enriched in biological processes and pathways related to cell cycle regulation, lipid metabolism pathways, immune response pathways, and intrinsic organelle damage regulation. GSEA results showed positive correlations with pathways such as cholesterol metabolism in the ICM-HF group compared to normal group and lipid metabolism in adipocytes. GSEA results also showed a positive correlation with pathways such as cholesterol metabolism and a negative correlation with pathways such as lipolytic presentation in adipocytes compared to normal group. Combining multiple ML and cytohubba algorithms yielded 11 relevant genes. After validation using the GSE42955 validation sets, the 7 genes obtained by the machine learning algorithm were well verified. The immune cell infiltration analysis showed significant differences in mast cells, plasma cells, naive B cells, and NK cells.
Conclusion: Combined analysis using WGCNA and ML identified coiled-coil-helix-coiled-coil-helix domain containing 4 (CHCHD4), transmembrane protein 53 (TMEM53), acid phosphatase 3 (ACPP), aminoadipate-semialdehyde dehydrogenase (AASDH), purinergic receptor P2Y1 (P2RY1), caspase 3 (CASP3) and aquaporin 7 (AQP7) as potential biomarkers of ICM-HF. ICM-HF may be closely related to pathways such as mitochondrial damage and disorders of lipid metabolism, while the infiltration of multiple immune cells was identified to play a critical role in the progression of the disease.

KEYWORDS

ischemic cardiomyopathy (ICM), heart failure (HF), machine learning (ML), immune cell infiltration, weighted gene co-expression network analysis (WGCNA)

1. Introduction

Heart failure (HF) is a complex clinical syndrome and the end-stage manifestation of cardiovascular disease (1, 2). Ischemic heart disease refers to myocardial degeneration, necrosis and fibrosis caused by coronary artery disease, which leads to severe left ventricular dysfunction (LVEF ≤ 35%–40%) (3). The alterations in neurohumoral, cellular, and molecular mechanisms are triggered by the structural damage and decompensation of the heart and act as a network to maintain its original normal physiological functions. These coordinated, complex processes lead to excessive volume overload, increased sympathetic activity, and circulatory redistribution and result in the distinct, parallel development of clinical signs and symptoms (4). Depending on the cause, HF is divided into ischemic HF caused by ischemic cardiomyopathy (ICM) and non-ischemic HF (5). ICM refers to the damage to the heart muscle caused by ischemia, where the heart is unable to pump blood properly. According to the WHO, ICM is the leading cause of death worldwide (6). Despite new drugs and surgical advances in the treatment of ICM, the prognosis for ischemic HF caused by coronary artery disease remains poor, with a five-year mortality rate of 40%–50% (7). A recent report from China showed that the prevalence of HF among residents aged ≥35 years was 1.3% (8). Thus, research targeting HF, especially ischemic HF, is of great importance. With the advancements in science and technology, we have developed a new understanding of HF caused by ICM, i.e., genetic alterations and immune environmental factors are jointly involved in the progression of the pathological process.

With the advancements in bioinformatics, the available microarray data can be used to identify hub genes, interaction networks, and pathways in ischemic HF. While traditional assays have certain limitations, weighted gene co-expression network analysis (WGCNA) is a highly systematic bioinformatics method (9). WGCNA may be applied to construct expression profiles of mRNAs in HF triggered by ICM by combining multiple informatics approaches to screen for modules and genes that are highly correlated with the disease to reveal potential molecular mechanisms. It can help provide new ideas for the diagnosis and treatment of the disease. WGCNA constructs scale-free networks by linking gene expression levels to clinical features and is commonly used for the bioanalysis of various systems. We first normalized the samples and then removed outlier samples to ensure reliable results in network construction. Soft threshold power had to be selected according to the standard scale-free network, and all differential genes were calculated using the power function. Machine learning (ML) method has very significant advantages in the processing of big data (10). Algorithms for ML analyze training data to uncover hidden patterns, build models, and then make predictions using the most accurate of these patterns. In fact, existing technology, such as support vector machine recursive feature elimination (SVM-RFE) and random forest (RF), have been applied to problems in genomics, proteomics, systems biology and other fields (11). ML methods are distinguished by their capacity to examine large amounts of data in order to discover correlations, provide explanations. These ML methods can assist in enhancing the dependability, performance, predictability and precision of diagnostic systems (12). Recent research suggests that the application of ML techniques may have the potential to improve heart failure outcomes and management by improving existing diagnostic and therapeutic support systems (13).

In the past decades, high-throughput platforms for analyzing gene expression, such as microarray technology, have been widely used to screen for genetic alterations at the genomic level, which helps us identify differentially expressed genes (DEGs), functions and pathways associated with disease pathogenesis and progression. We identified DEGs by using R (v4.0.1) software with Limma package (14) between ICM-HF myocardial tissue and normal tissue. WGCNA, gene ontology (GO), Kyoto gene and genome encyclopedia (KEGG) pathway enrichment analyses were performed and protein-protein interaction (PPI) networks were constructed and various ML approaches were used for further screening to explore the molecular mechanisms behind ICM-HF. Subsequently, we screened the most important modules of the PPI network built by DEG and the hub genes was screened by ML for further discussion. The aim of this study is to explore the underlying molecular mechanisms in ICM through a combination of several common analytical methods and ML approaches. Future research in the field of cardiovascular disease may benefit from the ideas and methods generated by our work.

2. Materials and methods

2.1. Data acquisition and preprocessing

Figure 1 depicts the study flowchart. A sample of 136 normal samples and 95 samples of ICM-HF from the GSE57345 (15) dataset. The GSE42955 (16) dataset was downloaded from the GEO database (https://www.ncbi.nlm.nih.gov/geo/) for validation of the results. ICM-HF was determined by medical history and pathological examination of the explanted hearts (15). Information on the datasets was displayed in **Supplementary Table S1**. Batch effects were removed using R (v4.0.1). Gene annotation was completed based on GPL9052 Illumina Genome Analyzer (Homo sapiens) and GPL6244 Affymetrix Human Gene 1.0 ST Array (Homo sapiens). It should be noted that if a gene has multiple probe loci, the average value of the probe loci is used as the gene expression level when converting probe ID to gene symbol. On the basis of the annotation files from the respective platforms, probe IDs were converted to gene symbols and probes that did not correspond to gene symbols were removed.

2.2. Identification of differentially expressed genes

We compared ICM-HF subjects with normal using R (v4.0.1). We used the limma package in R to distinguish between differentially expressed genes (DEGs) and then set $|\log2\ (\text{fold change})| \geq 0.5$ and adjusted $p < 0.05$ as the threshold for DEGs,

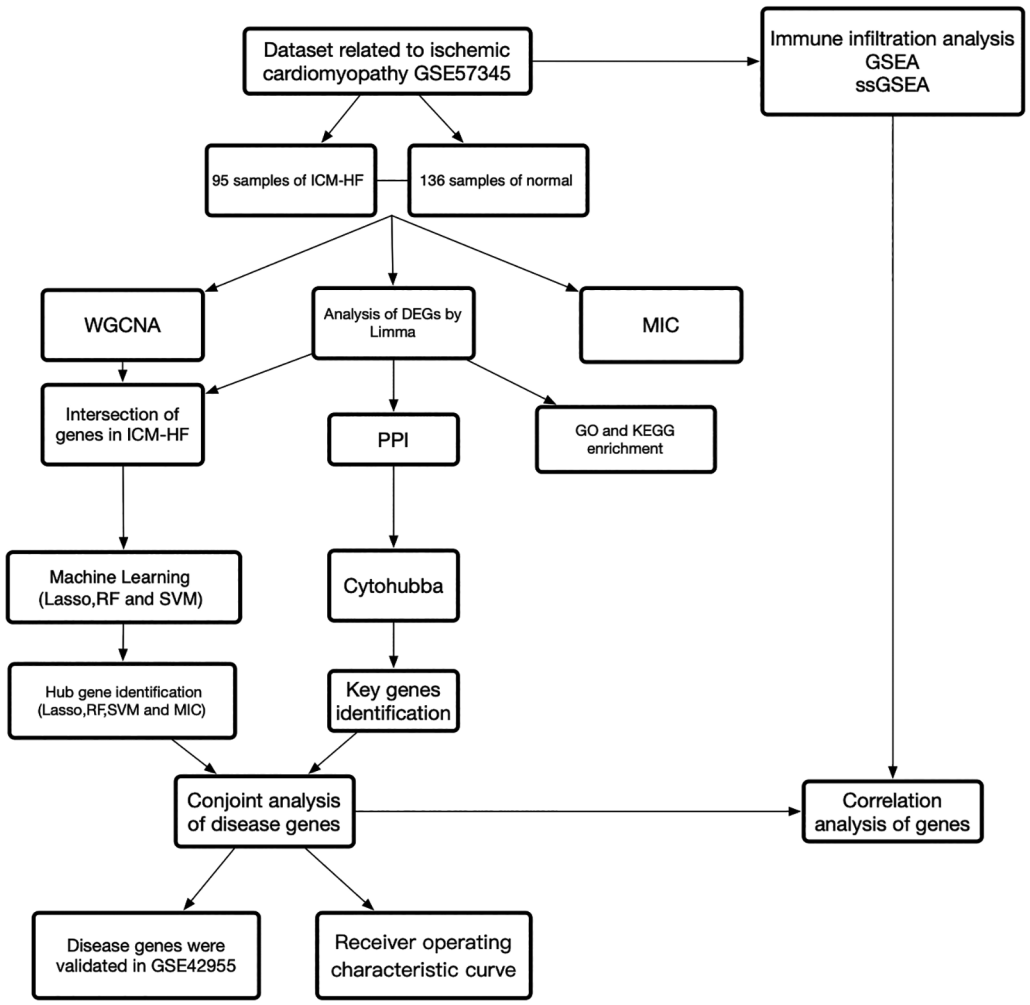


FIGURE 1
Study flowchart, Figure 1 is a summary of our study as a whole.

followed by WGCNA and identification of modules. We also used the MIC algorithm implemented in the minepy class library in Python to screen genes.

2.3. Protein–protein interaction analysis network construction and module analysis

We entered DEGs into the STRING database (http://string-db.org) to collect interactions of target proteins with a medium confidence score >0.4 and constructed a protein–protein interaction (PPI) network (v3.9.0) using Cytoscape software. In addition, we used the Cytoscape plug-in software "cytoHubba" to identify related genes based on mixed character calculations.

2.4. Functional enrichment analysis of DEGs

Gene Ontology (GO) and Kyoto Encyclopedia of Genes and Genomes (KEGG) pathway enrichment analysis are two very important components of bioinformatics analysis. It is difficult to describe the function and relationship among these genes only by gene names. This allows for better insight into the pathways behind the genes. Therefore, we performed a visual analysis in R to analyze all genes in the modules of interest and to identify possible mechanisms by which the module genes play a role in the clinical features of interest. Cutoff criteria were set at a *p*-value <0.05 and a false discovery rate (FDR) <0.1.

2.5. Machine learning analysis of disease genes

Gene fetching intersections using DEGs and WGCNA were used to select gene features using the minimum absolute shrinkage and selection operator (LASSO) algorithms of the glmnet R package (17) and the e1071 package (18), LASSO is a regression method for selecting a variable to improve the predictive accuracy and is also a regression technique for variable selection and regularization to improve the predictive accuracy

and comprehensibility of a statistical model (19), respectively, and the support vector machine recursive feature elimination (SVM-RFE) method (20). Support vector machines (SVM) are a powerful tool to analyze data with a number of predictors approximately equal or larger than the number of observations (20). The "randomForest" R package (21) was used to perform the random forest (RF) analysis. RF is an appropriate approach with the benefits of no limits on variable conditions and better accuracy, sensitivity, and specificity, which can be used to predict continuous variables and provide forecasts without apparent variations (22). The use of Maximal Information Coefficient Maximum mutual information coefficient (MIC) to measure the degree of association between two genes, linear or nonlinear, is more accurate than Mutual Information (MI) mutual information. Next, the intersection-related genes were derived.

2.6. The receiver operating characteristic curve evaluation of candidate genes and tests of relative expression of genes

Receiver operating characteristic (ROC) curves were established to assess the diagnostic value of candidate genes and columnar maps for ICM-HF, and the area under the curve (AUC) and 95% confidence interval (CI) were calculated to quantify their value. AUC > 0.70 was considered the ideal diagnostic value. Differential expression in the experimental and validation groups was then assessed separately using a nonparametric test and visualized through R.

2.7. Immune infiltration analysis

CIBERSORT is a computational method for determining the proportion of immune cells in HF and controls using tissue gene expression profiles to identify different immune cell proportions (23). We performed immune cell infiltration analysis using the "Cibersort" R software package (23). Bar graphs were used to visualize the proportion of each immune cell type in different samples. A comparison of the proportion of different types of immune cells between HF and control groups was visualized by vioplot. Heatmaps depicting the correlation of 22 types of infiltrating immune cells were created using the "corrplot" R package (24).

2.8. GSEA analysis and ssGSEA analysis

For gene set enrichment analysis (GSEA), we obtained the GSEA software (version 3.0) from the GSEA website (DOI: 10.1073/pnas.0506580102, http://software.broadinstitute.org/gsea/index.jsp). We then divided the samples into two groups according to the occurrence of HF and then downloaded the GSEA software from the Molecular Signatures Database (DOI: 10.1093/bioinformatics/btr260, http://www.gsea-msigdb.org/gsea/downloads.jsp) downloaded the c2.cp.kegg.v7.4.symbols.gmt subset to evaluate relevant pathways and molecular mechanisms based on gene expression profiles and phenotypic groupings, setting a minimum gene set of 5 and a maximum gene set of 5,000, with a p-value of <0.05 (as needed) and an FDR of <0.25 (as needed) were considered statistically significant.

3. Results

3.1. Transcriptome profile analysis of the ICM samples and normal samples

A total of 313 DEGs were identified in GSE57345, and 184 upregulated and 129 downregulated genes were identified in the ICM-HF group (**Figure 2A**). The heatmap shows the expression profiles of the top 30 upregulated DEGs and the top 30 downregulated DEGs (**Figure 2B**). We performed GO and KEGG pathway analysis to investigate the biological function of DEGs. Our KEGG analysis revealed that differential genes were mainly enriched in the p53 signaling pathway, cell cycle regulation, and lipid metabolism pathway (**Figure 3A**). BP analysis revealed that differential genes were mainly enriched in numerous immune response pathways, intrinsic organelle damage regulation, and protein transport (**Figure 3B**). CC analysis revealed that differential genes were enriched in numerous organelle peroxidase and organelle membrane regulation (**Figure 3C**). MF enrichment the analysis showed that the differential genes were enriched in the metabolism of nucleotides (**Figure 3D**).

3.2. Weighted gene co-expression network analysis screens for key modules

Before constructing the weighted co-expression network, we selected the soft threshold β parameter as the appropriate weighting parameter for the neighbor-joining function. After calculation, we set the soft threshold β to 6 and chose a correlation coefficient close to 0.86 to construct the gene modules (**Supplementary Figure S1A,B**). In total, about five gene modules were identified using dynamic tree cutting in all samples (**Figure 4A**). The sensitivity was set to 3. In addition, we merged modules with a distance of less than 0.5, resulting in five co-expression modules; notably, the gray module was regarded as the set of genes that could not be assigned to any module and the brown module was considered the most significant gene module (**Figure 4B**). A total of 1,288 genes were identified in the brown gene module. Brown module membership and gene significance were significantly positively correlated ($r^2 = 0.82$, $p =$ 9.9E−324) (**Supplementary Figure S1E**).

3.3. Establishment of PPI protein interactions network to screen out key HUB genes

In order to obtain a protein interaction network map between differential genes, the 313 genes from the limma analysis were

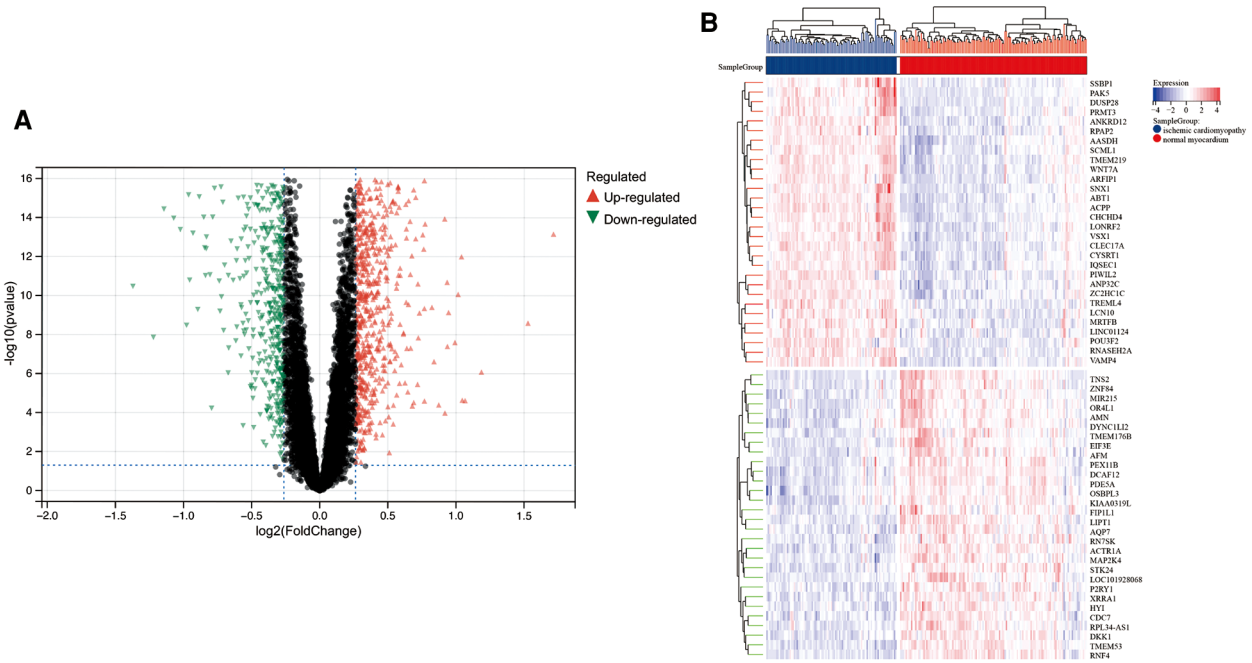


FIGURE 2
Limma analysis of ICM-HF and the normal group. (A) Volcano plot of differentially expressed genes (DEGs) in GSE57345, set |log2(FC)| ≥ 0.5. Red dots are upregulated genes, and green dots are downregulated genes. (B) A heatmap showing the top 30 upregulated and the top 30 downregulated genes in ICM-HF and normal groups.

entered into the STRING database and the PPI (https://cn.string-db.org) network was obtained. The PPI network (v3.9.0) was constructed using Cytoscape software (**Figure 5**), in order to further screen for key hub genes, the *Stress*, *MCC*, *Degree*, *EPC*, *EcCentricity*, *Radiality*, *Closeness* and *Betweenness* algorithms were used to calculate the associated gene scores (**Supplementary Figure S2A–G**). The UpSet graph was used to filter out five common HF-associated genes (**Supplementary Figure S3**). They are G protein subunit alpha O1 (GNAO1), cyclin H (CCNH), caspase 3 (CASP3), mitotic arrest deficient 2 like 1 (MAD2L1) and cyclin E1 (CCNE1).

3.4. Identification of key disease genes by machine learning

A total of 114 disease genes were obtained by taking the common genes of DEGs and WGCNA (**Figure 6A**). For further training of the above mentioned genes, these 114 genes were input into LASSO, RF algorithm and SVM-RFE algorithm were performed on GSE57345. A total of 31 genes were derived from the LASSO algorithm (**Figure 6B**). The top 16 genes from the SVM-RFE calculation were the most significant, with an accuracy of 0.758 (**Figure 6C**) and an error incidence of 0.242 (**Figure 6D**). The RF algorithm yielded 133 genes, and the top 20 in importance were taken as the resultant genes (**Figures 7A, B**). The three algorithms were then intersected with the ML MIC algorithm for a Venn diagram, and the genes with the intersection of the four algorithms were taken as the key disease genes (**Figure 8C**), yielding a total of seven genes. They are coiled-coil-helix-coiled-coil helix domain containing 4 (CHCHD4), transmembrane protein 53 (TMEM53), acid phosphatase 3 (ACPP), aminoadipate-semialdehyde dehydrogenase (AASDH), purinergic receptor P2Y1 (P2RY1), caspase 3 (CASP3), aquaporin 7 (AQP7). Among them, CHCHD4 and CASP3 genes are the causative genes common to all ML algorithms, with CASP3 being the gene shared by multiple cytohubba algorithm-related genes. We evaluated the correlation between the genes derived from cytohubba and ML algorithms (**Figure 8D**). Red dots represent negative correlation between two genes, blue represents positive correlation between two genes. The absolute value corresponding to the dot is the correlation coefficient of the two genes.

3.5. Establishment of ROC to assess the reliability of candidate genes and the relative expression of disease and experimental groups

We further evaluated the diagnostic values of TMEM53, ACPP, AASDH, P2RY1, CASP3, AQP7, GNAO1, CCNH, MAD2L1 and CCNE1 in GSE57345 using ROC curves, in order to improve their diagnostic performance, so we chose AUC > 0.7 as inclusion criteria. Demonstrating that these optimal feature genes have a high diagnostic value for ICM-HF and permit the estimation of

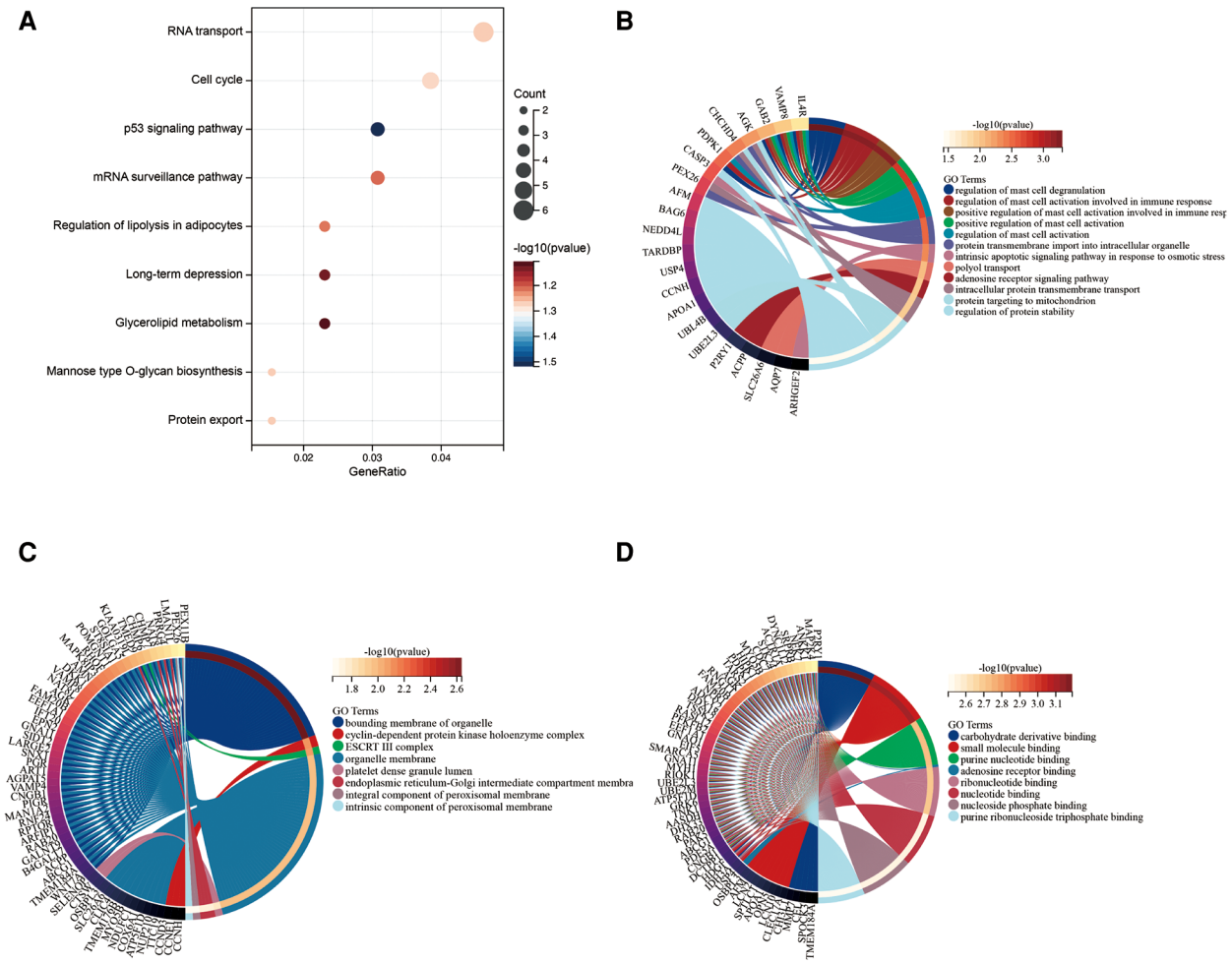


FIGURE 3
Functional enrichment of genes in the object module. The *x*-axis shows the number of ratios of genes, and the *y*-axis shows the pathway terms. The −log10 (*p*-value) of each term is colored according to the legend. (**A**) Kyoto encyclopedia of genes and genomes (KEGG) pathway analysis. (**B**–**D**) Gene ontology (GO) analysis.

progression (**Figures 8A,B**). The relative expression of genes in the experimental cohort was observed using a nonparametric test (**Figure 8C**) and validated using a validation set, the expression of GNAO1 was not statistically significant between the two groups (**Figure 8C**). CHCHD4, CASP3, ACPP, AASDH, CCNH, MAD2L1, and CCNE1 were all significantly upregulated in the ICM-HF group, and TMEM53, P2RY1, and AQP7 were significantly downregulated in the ICM-HF group.

In addition, for accurate and reliable results, we further validated the expression levels of the optimal feature genes in external validation dataset GSE42955 (**Figure 9**). In the dataset GSE42955, the genes CCNH and MAD2L1 were not statistically significant calculated by cytohubba method. Interestingly, the 7 (CHCHD4, CASP3, ACPP, AASDH, AQP7, P2RY1, TMEM53) genes screened by ML methods all share the same trend in the above-mentioned dataset, and at the same time, they are all statistically significant.

3.6. GSEA analysis and ssGSEA analysis

GSEA analysis showed that the enrichment pathway was mainly positively correlated with pathways such as cholesterol metabolism and negatively correlated with pathways such as lipolysis presentation in adipocytes (**Figures 10A,B**). The upregulated pathways in ssGSEA are shown in **Figure 11A** by mountain range plots. The relative significance of each pathway is shown by a box line plot (**Figure 11B**). The most significant differential pathways are mainly focused on lipid metabolism, organelle damage, and oxidative stress-related pathways. We analyzed the correlations of individual genes in the relevant pathways. The correlations of genes screened by ML and genes screened by cytohubba with the pathways are visualized in **Figure 12C**, with red representing positive correlations and green representing negative correlations.

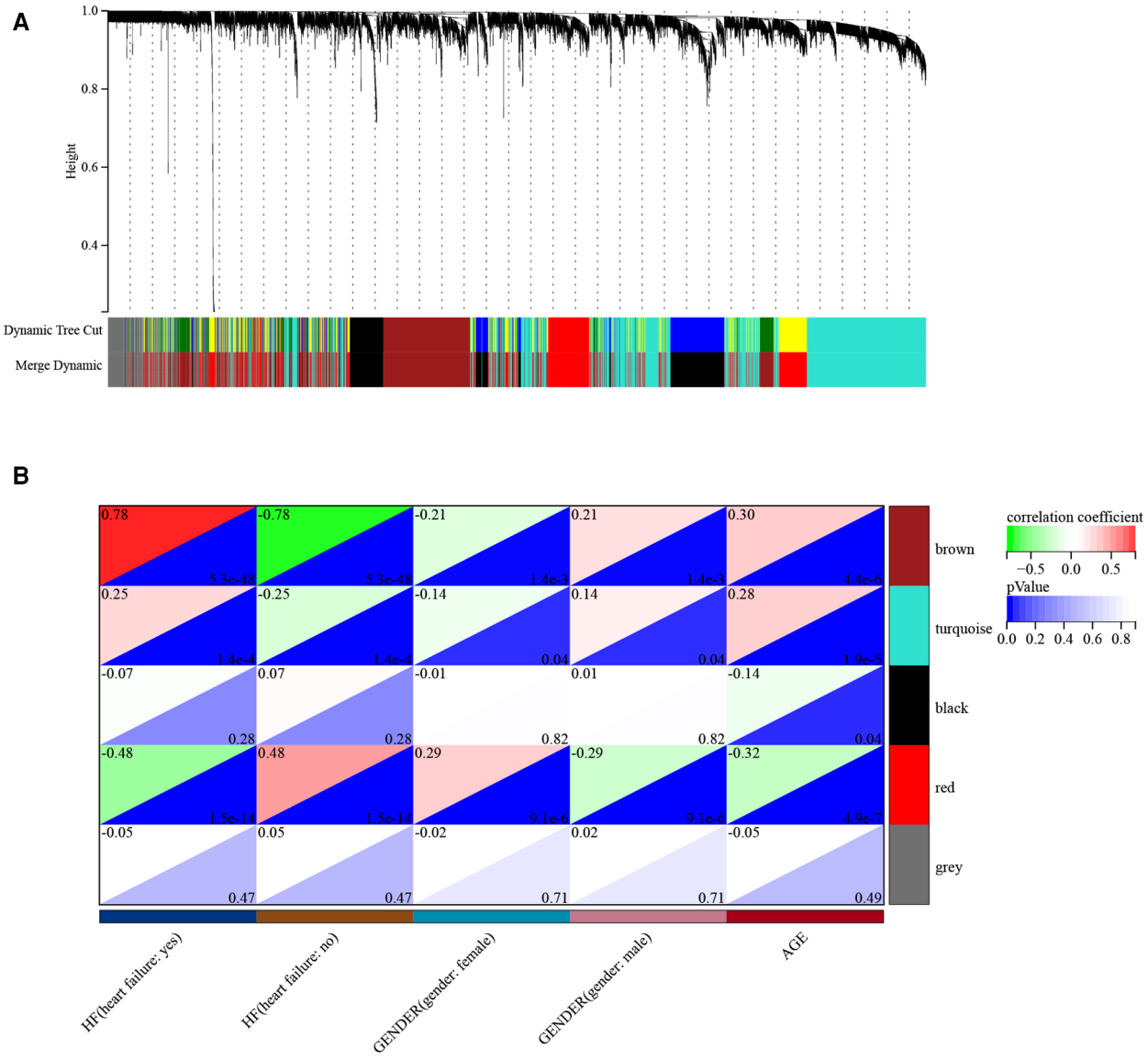


FIGURE 4
Demonstration of the WGCNA process. (A) Gene and trait clustering dendrograms. Gene clustering trees (dendrograms) obtained by hierarchical clustering of neighbor-based differences. (B) Module feature association. Each row corresponds to a module feature, and each column corresponds to a clinical feature. Each cell contains the corresponding correlation in the first row and the corresponding *p*-value in the second row. The table is color-coded by correlation according to the color legend.

3.7. Immune infiltration analysis

Since we observed enrichment of ICM-HF-related genes in immune regulation, immune cell infiltration analysis was performed to better elucidate the immune regulation of ICM-HF.

Regarding the infiltration of 22 immune cells in the ICM-HF and the normal group controls shown in Figure 12A, the violin plot indicates that patients with ICM-HF have higher levels of plasma cells, naive B cells, and resting mast cells and lower levels of activated NK cells and regulatory T cells (Figure 12B). The correlation of individual immune cells is shown in Figure 13A. In general, multiple immune cells are differentially expressed in patients with ICM-HF, which can be used as potential therapeutic targets. Correlation analysis of genes and immune cells (Figure 13B) revealed positive correlations between resting mast cells and several related genes, so we hypothesize that resting mast cells may play an important role in HF due to ICM-HF and CCNH genes correlate with several immune cells, such as negative correlations with memory T cells and resting NK cells and positive correlations with plasma cells and M2 type macrophages. The CCNH gene is associated with several immune cells, such as memory T cells and resting NK cells and with plasma cells and M2 macrophages.

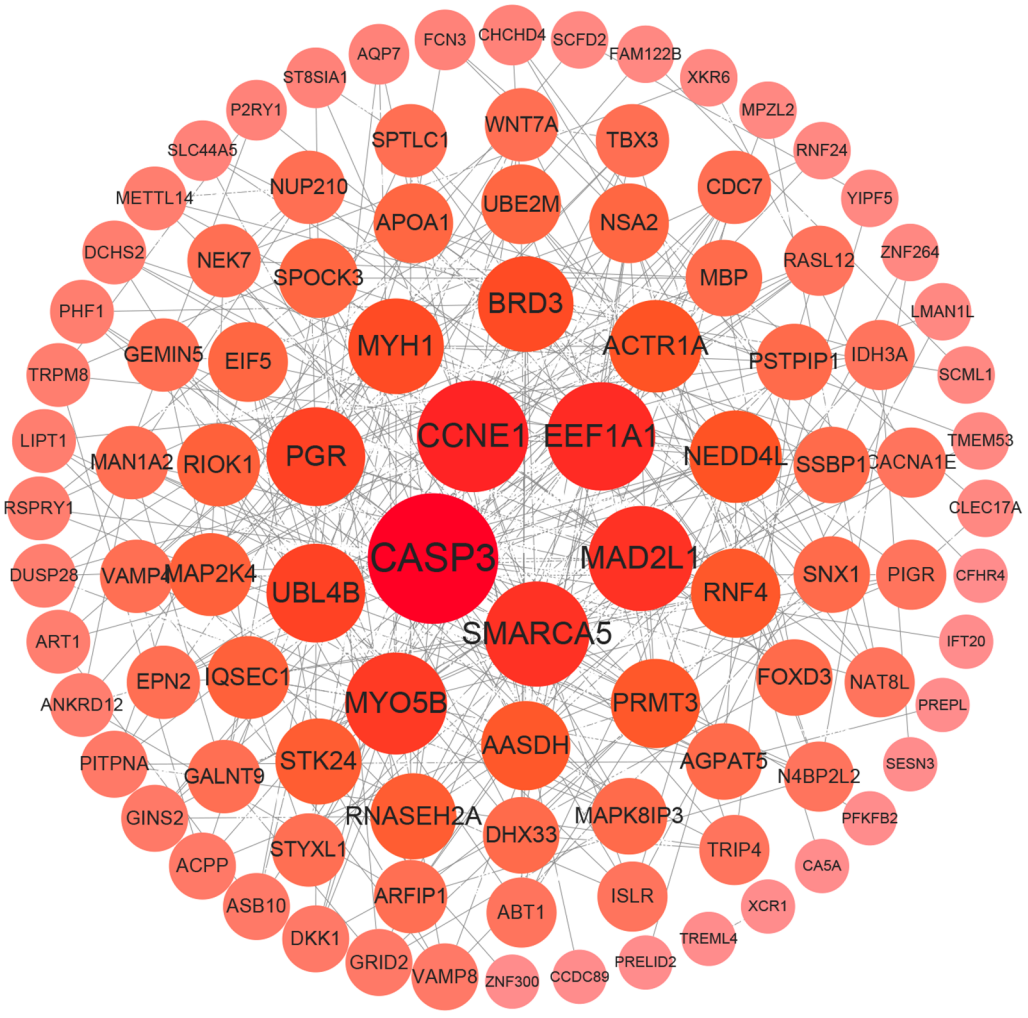


FIGURE 5
Protein–protein interaction (PPI) analysis. PPI network of DEGs. The edges represent the interactions between two genes. Degrees are used to describe the importance of protein nodes in the network; deep red colors indicate high degrees, whereas light red colors indicate low degrees.

4. Discussion

The strong bioinformatics analysis community and technology repositories that have driven advances in modern genetics. Recently, an increasing number of examples of ML-driven analysis are emerging in the field of cardiovascular genetics, including coronary calcium studies (25), pulmonary hypertension (26), and multiple clinically relevant variant assays from next-generation sequencing or proteomic data (27). Modern medical practice is awash with many types of data. In cardiovascular medicine, the range and quality of diagnostic tests, such as non-invasive imaging, such as computed tomography (CT) angiography, physiological tests, and other fractional flow reserves or biomarkers, have increased over the past few decades (28). These tests provide physicians with additional complementary information upon which to base diagnostic and therapeutic decisions, which are widely accessible, less expensive and low-risk. Overall, the high prevalence of cardiovascular disease generates a large amount of patient data related to cardiovascular disease. This provides a large amount of data for training ML models and gives ML the opportunity to assist in more clinical work.

In our research, we used multiple independent algorithms. And then we identified the important genes from dataset. These ML methods are used to find valuable information from complex and large gene expression data. This has enabled researchers to explore potential influences in disease from different perspectives and using different methods. For example, it can identify genes that have not been studied in previous research and provide researchers with new insights and ideas in the study of specific diseases. We screened 7 disease-associated genes using ML (CHCHD4, CASP3, TMEM53, ACPP, AASDH, P2RY1 and AQP7). We used cytohubba to screen for 5 genes (GNAO1, CCNH, MAD2L1, CASP3, CCNE1). Among them, CASP3 was the common gene derived from cytohubba analysis and ML analysis. Based on the results of our study, overall, the diagnostic efficacy of the genes screened by ML may be better than that of cytohubba.

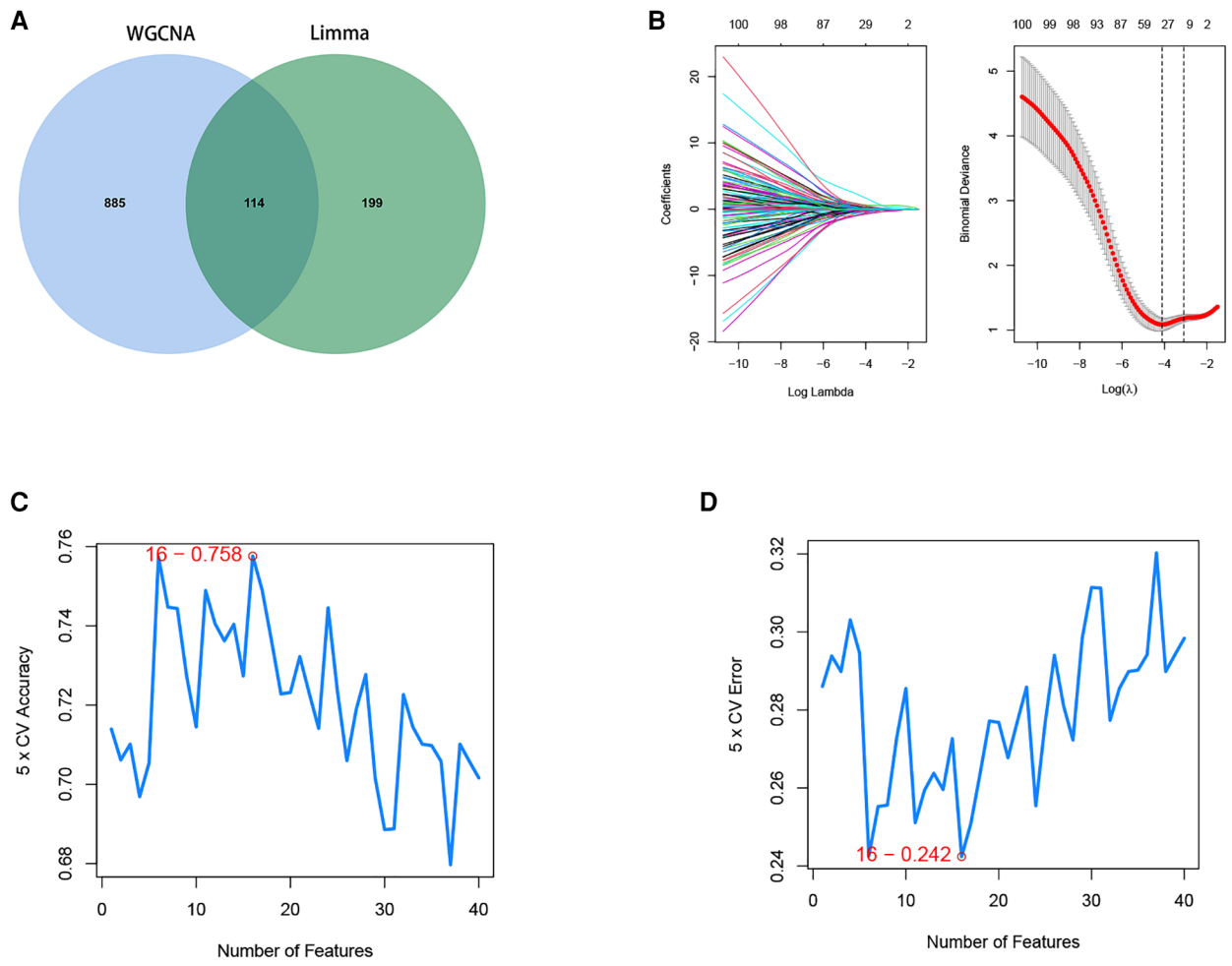


FIGURE 6
Screening of disease intersection genes and machine learning algorithm to identify the optimal feature genes. (A) Strong correlation module of WGCNA and Limma analysis of differential genes to do a Venn diagram screening of intersecting genes. (B) LASSO coefficient profiles of the candidate optimal feature genes and the optimal lambda was determined when the partial likelihood deviance reached the minimum value. Each coefficient curve in the left picture represents a single gene. The solid vertical lines in right picture represent the partial likelihood deviance, and the number of genes ($n = 30$) corresponding to the lowest point of the cure is the most suitable for LASSO. (C,D) The SVM-RFE algorithm was used to further candidate optimal feature genes with the highest accuracy and lowest error obtained in the curves. The x-axis shows the number of feature selections, and the y-axis shows the prediction accuracy. Sixteen gene features were identified through SVM-RFE analysis with an accuracy of 0.758 and an error of 0.242.

CASP3 is a frequently activated death protease that catalyzes the specific cleavage of many key cellular proteins and is involved in apoptotic cell death (29). Studies have demonstrated that CASP3 is involved in the inflammatory activation and immune cell aggregation in cardiovascular disease through the regulation of the Rho-kinase axis by vascular smooth muscle cells (30, 31).

According to our results, CHCHD4 expression was significantly higher in the ICM-HF group compared to normal group, so it is speculated that elevated CHCHD4 may play an important role in the ICM-HF. CHCHD4 plays a key role in oxidative protein folding in the mitochondrial membrane gap, representing a minimal thioredoxin-independent oxidoreductase, which ensures its catalytic function in mitochondrial oxidative folding (32). CHCHD4-based protein import mechanisms are essential for the maintenance of normal mitochondrial functions (33). Damaged mitochondria produce less adenosine triphosphate (ATP) and generate dangerous amounts of ROS. Accumulated ROS may damage mitochondrial DNA, cell membranes, and respiratory complex proteins, leading to catastrophic oxidative damage and cell death (34). We hypothesize that the elevated CHCHD4 protein in the ICM-HF group is a compensatory manifestation of mitochondrial damage due to hypoxia in cardiomyocytes caused by myocardial ischemia. It is expected to be a new target for the diagnosis and treatment of ICM-HF.

Studies have shown that Aquaporins (AQPs) are involved in the regulation of cardiovascular function and the development of related diseases, particularly in cerebral ischemia, congestive HF, hypertension, and angiogenesis (35). AQP7 in AQPs is a hydroglycerol channel protein that is mainly distributed in proximal renal tubules, cardiac muscles, and adipose tissue. Studies have shown that the heart is the second most expressed tissue after adipose tissue for AQP7 mRNA (36). However, the

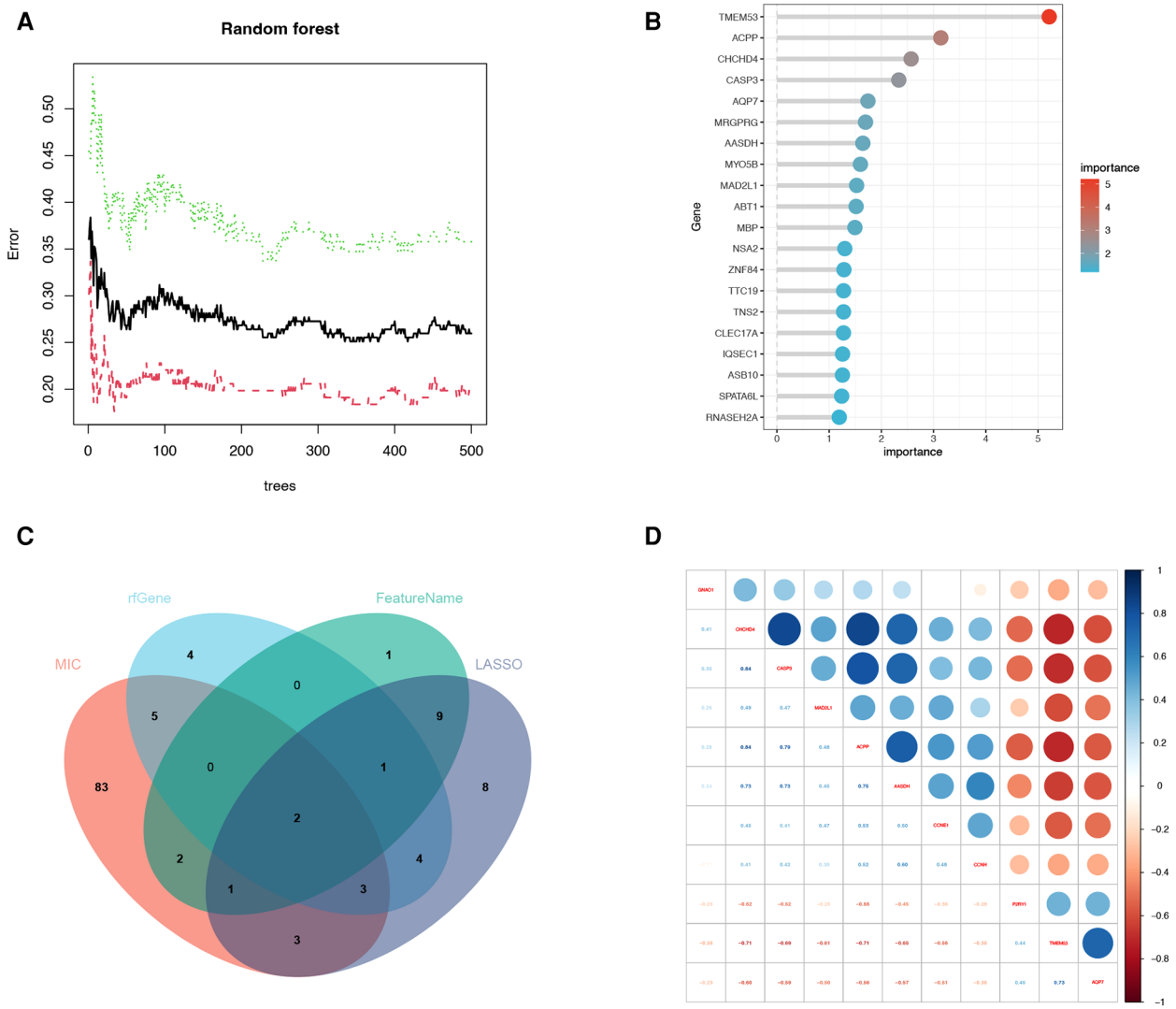


FIGURE 7
Machine learning algorithm and correlation heatmap. (**A**) Relative importance of overlapping candidate genes calculated in random forest (Top 10 genes' importance >2). Importance indexes on the *x*-axis and genetic variables are plotted on the *y*-axis. (**B**) Relative importance of overlapping candidate genes calculated in random forest. Importance indexes on the *x*-axis and genetic variables are plotted on the *y*-axis. (**C**) Four machine learning algorithm genes screened for intersection genes using Venn diagram. (**D**) The correlation heatmap of machine learning algorithm-related genes and cytohubba algorithm-related genes. Red dots represent negative correlation between two genes, blue represents positive correlation between two genes. The absolute value corresponding to the dot is the correlation coefficient of the two genes.

role of AQP7 in the myocardium has been barely investigated. In the above study, AQP7 expression was significantly lower in the disease group than in the control group. During periods of high energy demand and metabolic stress, lipolysis increases and converts triglycerides to free fatty acids and glycerol. AQP7 controls glycerol efflux under these conditions, and the exported glycerol is then taken up by other cells and used as a backbone for energy requirements during high energy demands (37). ICM-HF is often accompanied by the loss of energy metabolic function and disturbances in lipid metabolism. AQP7 is required for carbohydrate metabolism, complex lipid biosynthesis, urea/arginine metabolism, redox homeostasis, amino acid metabolism, and nucleotide metabolism. Thus, AQP7 plays a critical role in regulating lipid metabolism (38).

The analysis with GO, KEGG, and GSEA pathways was enriched in cholesterol metabolism, regulation of lipolysis in adipocytes, and amino acid metabolism. The presence of a significant downregulation of AQP7 in the ICM-HF group relative to the control group was confirmed in our experimental group and validation group. AQP7's deficiency appears to impair metabolic adaptation during cardiac overload by limiting glycerol uptake and reducing intracellular ATP levels (39). This is of fundamental importance because cardiomyocyte metabolism is dependent on fatty acids, but they are converted to glucose and glycerol as energy substrates when the heart is overloaded (40). Overall, AQP7's deficiency may exacerbate the damage to the energy metabolism of the ischemic myocardium, ultimately leading to HF.

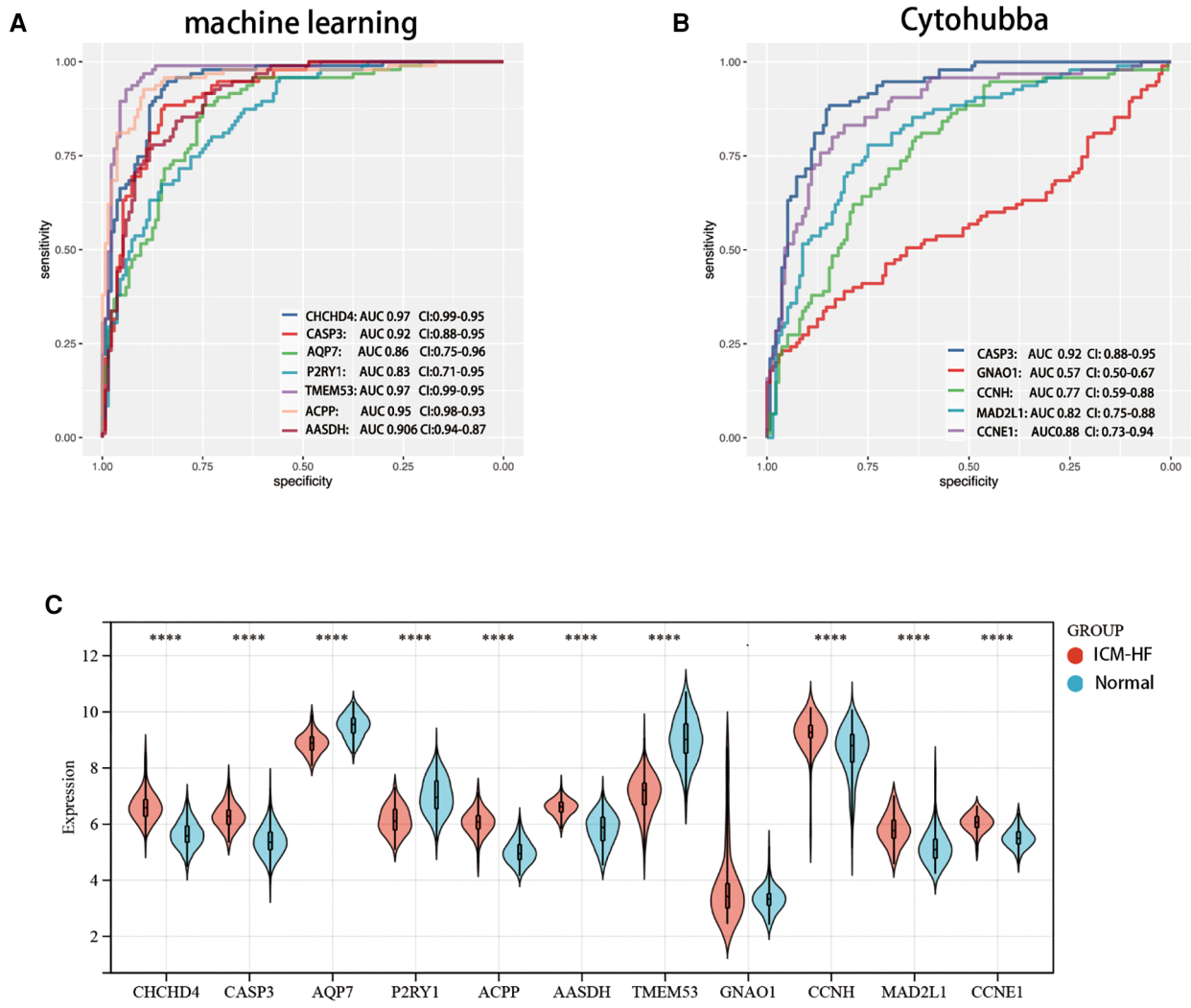


FIGURE 8
Verification of expression and diagnostic efficacy in predicting ICM-HF progression of optimal feature genes. (A) Validation of ROC of genes screened by a machine learning algorithm. (B) ROC validation of genes related to the cytohubba algorithm. (C) Violin plot of the expression of the relevant genes in the experimental set GSE57345. *$p < 0.05$, **$p < 0.01$, ***$p < 0.001$, Wilcoxon rank-sum test.

P2RY1 is a G protein-coupled receptor in which ADP is a physiological agonist that actively couples to phospholipase C *via* Gαq, thereby triggering the release of intracellular stores of Ca^{2+} (41). HF is characterized by the reduced contractile function of cardiac myocytes, resulting in reduced systolic left ventricular contraction. Defective myocardial contractility is associated with impaired excitation–contraction (EC) coupling, a mechanism that converts electrical stimulation from pacemaker cells into contraction through the release of large amounts of Ca^{2+} from the sarcoplasmic reticulum (SR) (42). Interestingly, studies have shown that the dysregulation of intracellular calcium homeostasis in cardiac myocytes is an important factor in exacerbating the cardiovascular disease (43). We found a significant downregulation of P2RY1 in ICM-HF group. Therefore, we consider that P2RY1 may play an important role in ICM-HF.

Growing evidence suggests that immune cell infiltration of the myocardium has a detrimental effect on cardiac function (44–46). Immune cell profiles differ significantly in healthy and diseased hearts (46). In this study, we found that naive B cells and resting mast cells were significantly elevated in the disease genome. Plasma cells, regulatory T cells, and activated NK cells were significantly downregulated within the ICM-HF group. Mast cells exacerbate the progression of ischemic HF by activating matrix metalloproteinases and cardiac fibrosis (47). Myocardial fibrosis and resistance to neo-angiogenesis caused by dysfunction of regulatory T cells are, on the other hand, a very critical step in the pathological progression of cardiovascular disease (48, 49). Through our analysis, we consider that the infiltration of immune cells may provide new ideas and insights in the diagnosis and treatment of ICM-HF.

We identified 11 potentially significant pathogenic genes in ICM-HF through ML and PPI analysis. We focused on the possible roles of the mitochondrial damage and apoptosis genes CHCHD4 and CASP3 and the lipid metabolism regulatory genes AQP7 and P2RY1 in disease development. The differential expression of TMEM53, ACPP and AASDH genes may also play

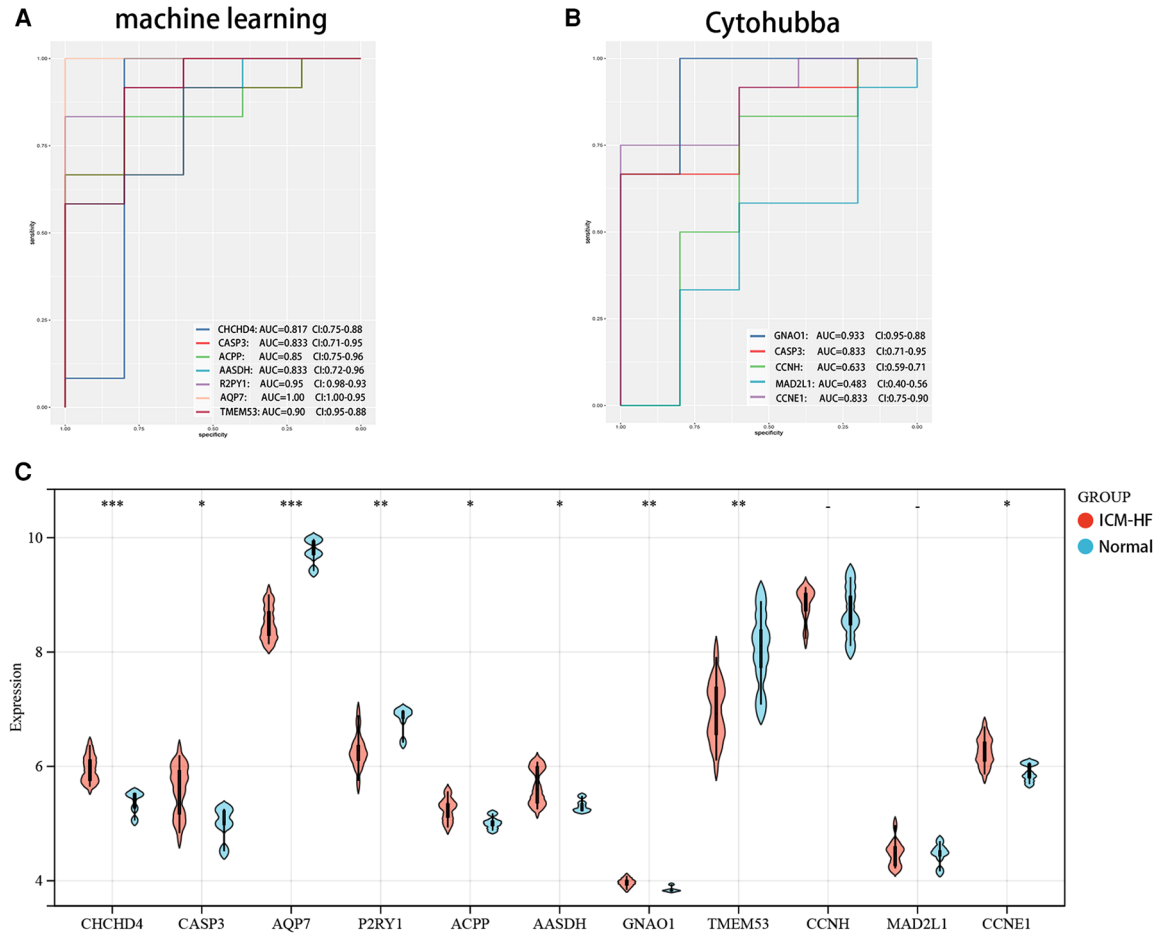


FIGURE 9
Verification of expression and diagnostic efficacy for optimal feature genes using external validation dataset. (A) Validation of ROC of genes screened by a machine learning algorithm. (B) ROC validation of genes related to the cytohubba algorithm. (C) Violin plot of the expression of the relevant genes in the experimental set GSE42955.

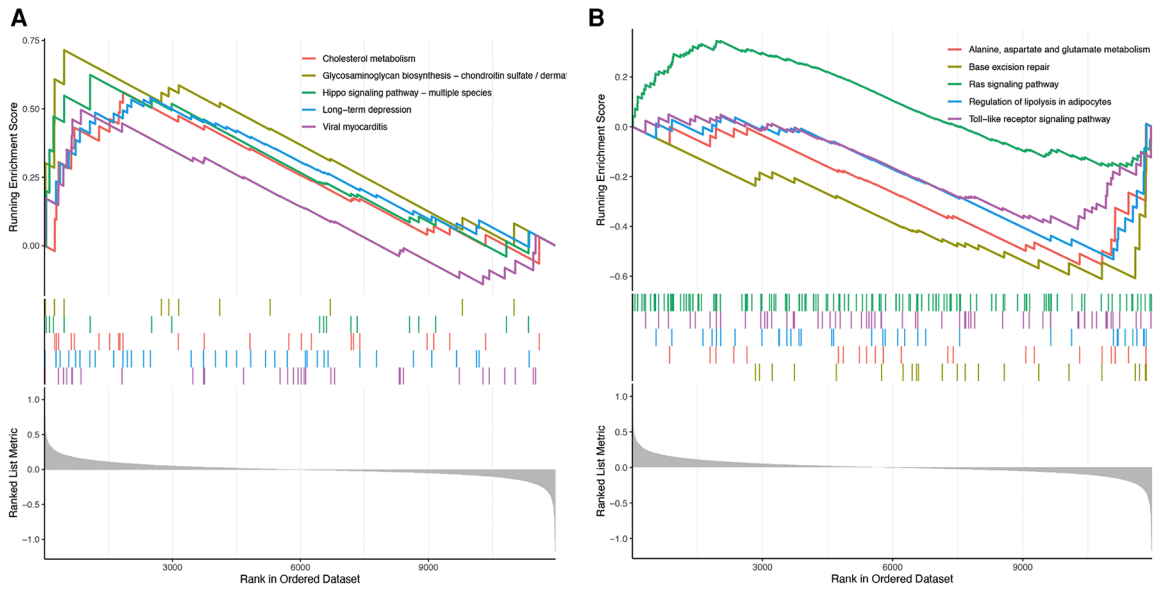


FIGURE 10
Enrichment of GSEA pathway. (A) GSE57345 upregulated gene pathway enriched in GSEA. (B) GSE57345 enriched in GSEA for downregulated gene pathway.

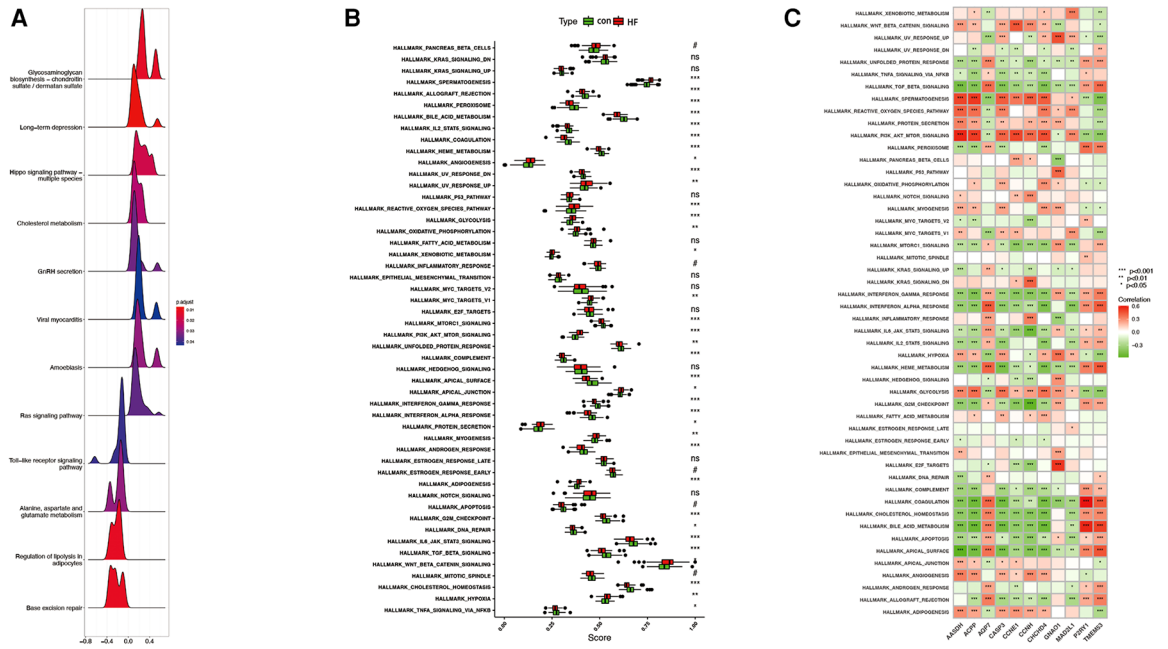


FIGURE 11
Plot of correlated differences in GSEA enrichment. (**A**) Mountain range plot of the correlation pathway of GSE57345 enrichment in GSEA. (**B**) The specific distribution of the hallmark gene sets in ICM-HF and normal samples. (**C**) Correlation analysis of the hallmark gene sets with seven optimal feature genes. Statistic tests: Wilcoxon rank-sum test ($p < 0.2$; *$p < 0.05$; **$p < 0.01$; ***$p < 0.001$; ns, no significance).#.

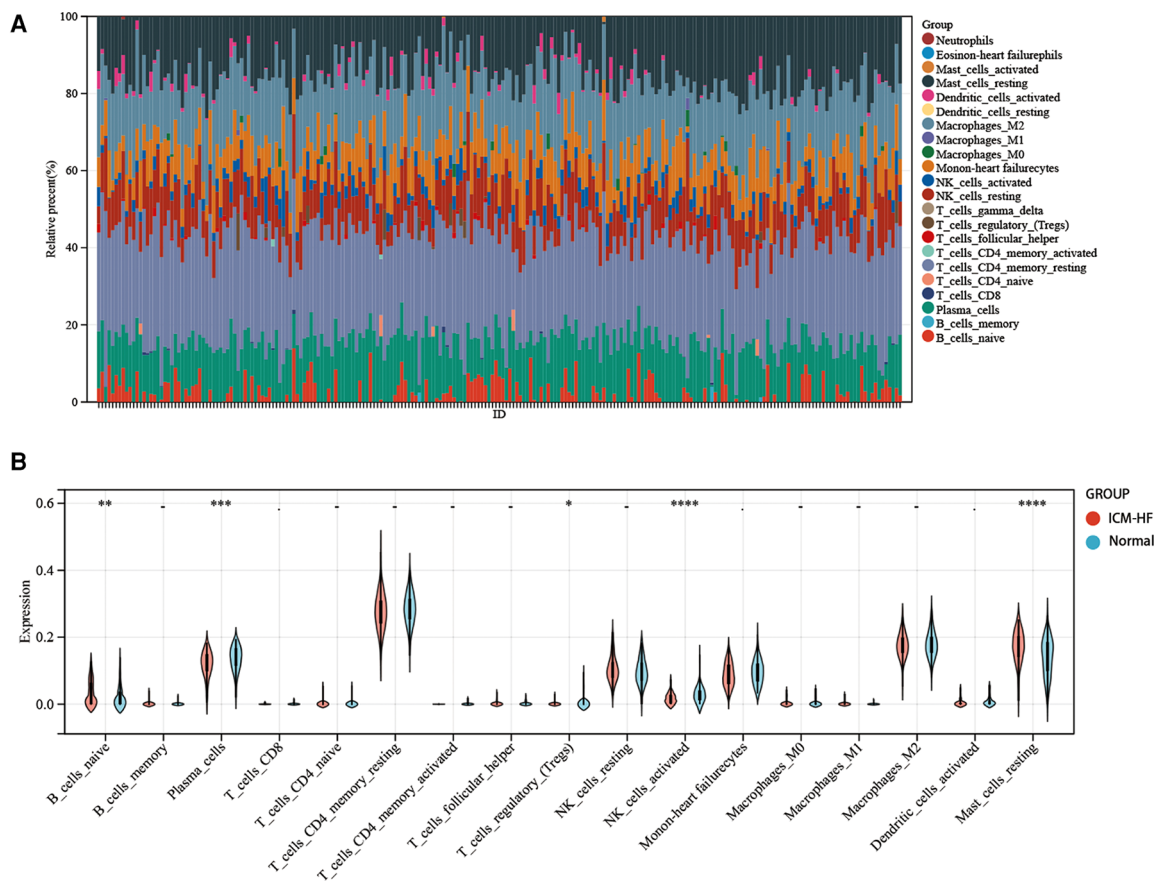


FIGURE 12
Immune infiltration analysis. (**A**) Visualization of stacked plots of various infiltrating immune cells in GSE57345. (**B**) Visualization of violin plots of infiltrating immune cells in the ICM-HF and normal groups. *$p < 0.05$, **$p < 0.01$, ***$p < 0.001$. Wilcoxon rank-sum test.

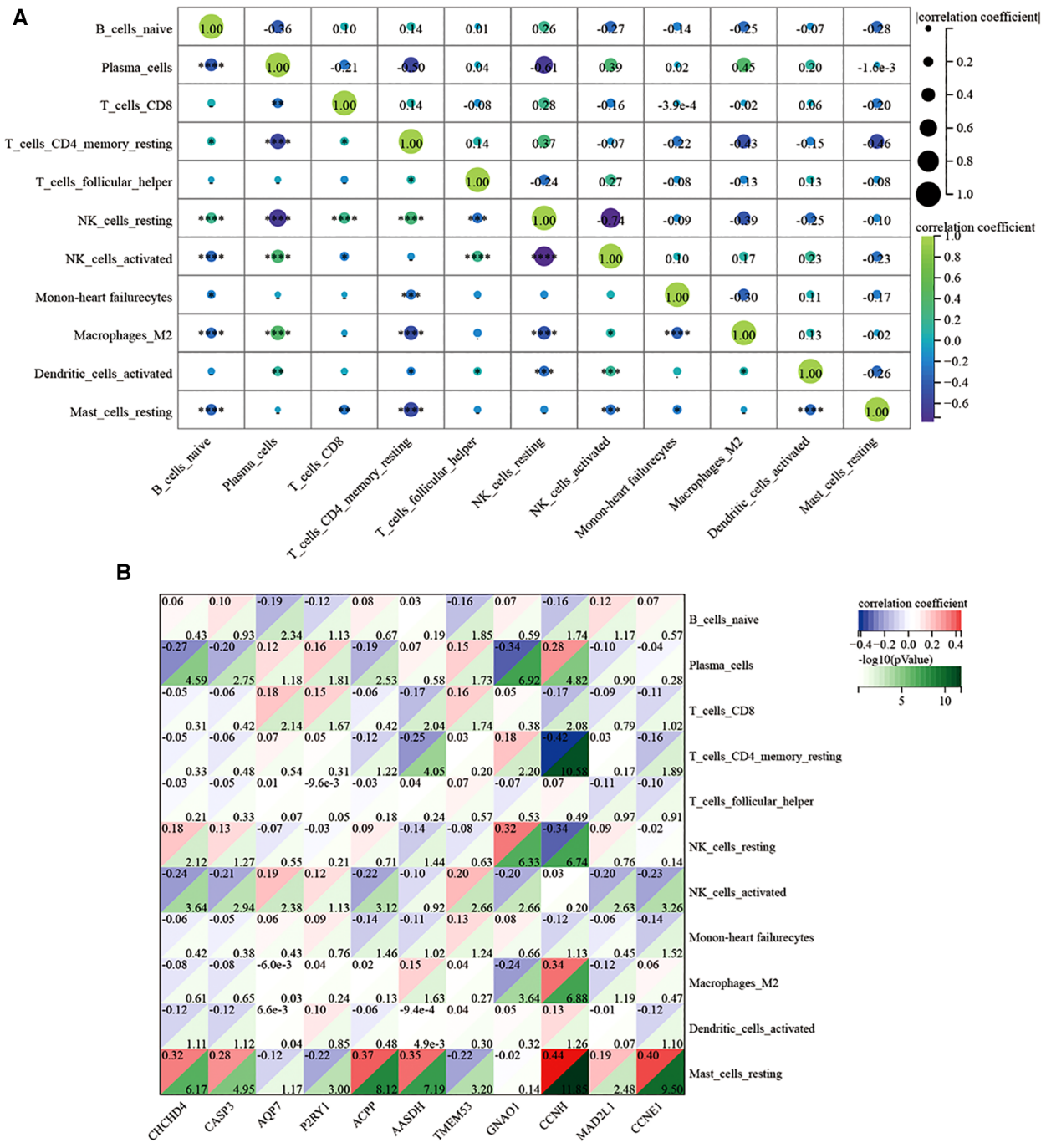


FIGURE 13
Correlation analysis of immune-related infiltration analysis. (A) The relative proportions of 22 immune cells types between normal samples and ICM-HF samples. in GSE57345. (B) Correlation analysis of 11 related disease genes and associated immune cells. *$p < 0.05$, **$p < 0.01$, ***$p < 0.001$.Wilcoxon rank-sum test.

an important role in ICM-HF, but these genes have been barely investigated, so little is known about the function of these genes. These genes may play a critical role in the development and progression of the ICM-HF, and their functions and mechanisms need to be further explored. This is a reflection of the innovation and excellence of ML in the medical field, which has been able to identify many influences that have not been identified by previous studies. At the same time, it can also provide new directions and ideas for the study of ICM-HF. Overall, our study demonstrates for the first time the promising potential of a combined WGCNA and ML approach in transcriptomic data for ICM-HF. Our findings suggest that ML modeling of genome-wide transcriptomic data from cardiac samples collected by clinical heart biopsy can explore potential biomarkers. Finally, our study prioritizes previously unknown genes and genes that have not been studied in ICM-HF as potential candidate

biomarkers. Our work can serve as an important part of future research in the field of ICM-HF. Interestingly, we found that after validation by external gene set GSE42955, all seven genes screened by ML were well validated, while CCNH and MAD2L1 of the five genes screened by PPI were not well validated. This also reflects the superiority of ML compared to common bioinformatics algorithms.

Some limitations of the present study should be noted. First, this is a retrospective study, and further prospective experiments need to be designed. Second, this study can further design animal experiments to explore the mechanism of validating related genes in ICM-HF. Third, the accuracy of our chosen SVM algorithm is only 0.758. However, the use of multiple ML algorithms to analyze the potential causative genes depicting ICM-HF increases the credibility of the study to some extent and explores the correlation between the status of immune infiltrating cells in the tissues of ischemic HF and causative genes, which are biomarkers that may provide guidance for the diagnosis and treatment of patients with ICM-HF.

Data availability statement

The original contributions presented in the study are included in the article/**Supplementary Material**, further inquiries can be directed to the corresponding author.

Author contributions

All authors conceived and designed the study. XK performed the data collection and analysis. HS critically revised the article, XK and HS had equally important contributions to this article. XG supported us in managing the subject in an integrated manner. All authors contributed to the article and approved the submitted version.

Funding

This work was supported by the Natural Science Foundation of Shandong Province (grant no. ZR2021MH347), Funded by Clinical Research Center of Shandong University (grant no. 2020SDUCRCA017).

Conflict of interest

The authors declare that the research was conducted in the absence of any commercial or financial relationships that could be construed as a potential conflict of interest.

Publisher's note

All claims expressed in this article are solely those of the authors and do not necessarily represent those of their affiliated organizations, or those of the publisher, the editors and the reviewers. Any product that may be evaluated in this article, or claim that may be made by its manufacturer, is not guaranteed or endorsed by the publisher.

Supplementary material

The Supplementary Material for this article can be found online at: https://www.frontiersin.org/articles/10.3389/fcvm.2023.1058834/full#supplementary-material.

References

1. Ponikowski P, Voors AA, Anker SD, Bueno H, Cleland JGF, Coats AJS, et al. 2016 ESC guidelines for the diagnosis and treatment of acute and chronic heart failure: the task force for the diagnosis and treatment of acute and chronic heart failure of the European Society of Cardiology (ESC) Developed with the special contribution of the Heart Failure Association (HFA) of the ESC. *Eur Heart J*. (2016) 37 (27):2129–200. doi: 10.1093/eurheartj/ehw128

2. Yancy CW, Jessup M, Bozkurt B, Butler J, Casey DE, Colvin MM, et al. 2017 ACC/AHA/HFSA focused update of the 2013 ACCF/AHA guideline for the management of heart failure: a report of the American college of cardiology/American heart association task force on clinical practice guidelines and the heart failure society of America. *Circulation*. (2017) 136(6):e137–e61. doi: 10.1161/CIR.0000000000000509

3. Jiang M, Xie X, Cao F, Wang Y. Mitochondrial metabolism in myocardial remodeling and mechanical unloading: implications for ischemic heart disease. *Front Cardiovasc Med*. (2021) 8:789267. doi: 10.3389/fcvm.2021.789267

4. Tanai E, Frantz S. Pathophysiology of heart failure. *Compr Physiol*. (2015) 6 (1):187–214. doi: 10.1002/cphy.c140055

5. Barquera S, Pedroza-Tobías A, Medina C, Hernández-Barrera L, Bibbins-Domingo K, Lozano R, et al. Global overview of the epidemiology of atherosclerotic cardiovascular disease. *Arch Med Res*. (2015) 46(5):328–38. doi: 10.1016/j.arcmed.2015.06.006

6. Del Buono MG, Arena R, Borlaug BA, Carbone S, Canada JM, Kirkman DL, et al. Exercise intolerance in patients with heart failure: JACC state-of-the-art review. *J Am Coll Cardiol*. (2019) 73(17):2209–25. doi: 10.1016/j.jacc.2019.01.072

7. Yancy CW, Jessup M, Bozkurt B, Butler J, Casey DE, Drazner MH, et al. 2013 ACCF/AHA guideline for the management of heart failure: a report of the American college of cardiology foundation/American heart association task force on practice guidelines. *J Am Coll Cardiol*. (2013) 62(16):e147–239. doi: 10.1016/j.jacc.2013.05.019

8. Cunningham JW, Claggett BL, O'Meara E, Prescott MF, Pfeffer MA, Shah SJ, et al. Effect of sacubitril/valsartan on biomarkers of extracellular matrix regulation in patients with HFpEF. *J Am Coll Cardiol*. (2020) 76(5):503–14. doi: 10.1016/j.jacc.2020.05.072

9. Langfelder P, Horvath S. WGCNA: an R package for weighted correlation network analysis. *BMC Bioinformatics*. (2008) 9:559. doi: 10.1186/1471-2105-9-559

10. Van Calster B, Wynants L. Machine learning in medicine. *N Engl J Med*. (2019) 380(26):2588. doi: 10.1056/NEJMc1906060

11. Larrañaga P, Calvo B, Santana R, Bielza C, Galdiano J, Inza I, et al. Machine learning in bioinformatics. *Brief Bioinform*. (2006) 7(1):86–112. doi: 10.1093/bib/bbk007

12. Shehab M, Abualigah L, Shambour Q, Abu-Hashem MA, Shambour MKY, Alsalibi AI, et al. Machine learning in medical applications: a review of state-of-the-art methods. *Comput Biol Med*. (2022) 145:105458. doi: 10.1016/j.compbiomed.2022.105458

13. Awan SE, Sohel F, Sanfilippo FM, Bennamoun M, Dwivedi G. Machine learning in heart failure: ready for prime time. *Curr Opin Cardiol*. (2018) 33(2):190–5. doi: 10.1097/HCO.0000000000000491

14. Ritchie ME, Phipson B, Wu D, Hu Y, Law CW, Shi W, et al. limma powers differential expression analyses for RNA-sequencing and microarray studies. *Nucleic Acids Res*. (2015) 43(7):e47. doi: 10.1093/nar/gkv007

15. Liu Y, Morley M, Brandimarto J, Hannenhalli S, Hu Y, Ashley EA, et al. RNA-seq identifies novel myocardial gene expression signatures of heart failure. *Genomics*. (2015) 105(2):83–9. doi: 10.1016/j.ygeno.2014.12.002

16. Molina-Navarro MM, Roselló-Lletí E, Ortega A, Tarazón E, Otero M, Martínez-Dolz L, et al. Differential gene expression of cardiac ion channels in human dilated cardiomyopathy. *PLoS ONE*. (2013) 8(12):e79792. doi: 10.1371/journal.pone.0079792

17. Zhang M, Zhu K, Pu H, Wang Z, Zhao H, Zhang J, et al. An immune-related signature predicts survival in patients with lung adenocarcinoma. *Front Oncol*. (2019) 9:1314. doi: 10.3389/fonc.2019.01314

18. Schroder MS, Culhane AC, Quackenbush J, Haibe-Kains B. Survcomp: an R/bioconductor package for performance assessment and comparison of survival models. *Bioinformatics*. (2011) 27(22):3206–8. doi: 10.1093/bioinformatics/btr511

19. Yang C, Delcher C, Shenkman E, Ranka S. Machine learning approaches for predicting high cost high need patient expenditures in health care. *Biomed Eng Online*. (2018) 17(Suppl 1):131. doi: 10.1186/s12938-018-0568-3

20. Sanz H, Valim C, Vegas E, Oller JM, Reverter F. SVM-RFE: selection and visualization of the most relevant features through non-linear kernels. *BMC Bioinformatics*. (2018) 19(1):432. doi: 10.1186/s12859-018-2451-4

21. Alderden J, Pepper GA, Wilson A, Whitney JD, Richardson S, Butcher R, et al. Predicting pressure injury in critical care patients: a machine-learning model. *Am J Crit Care*. (2018) 27(6):461–8. doi: 10.4037/ajcc2018525

22. Ellis K, Kerr J, Godbole S, Lanckriet G, Wing D, Marshall S. A random forest classifier for the prediction of energy expenditure and type of physical activity from wrist and hip accelerometers. *Physiol Meas*. (2014) 35(11):2191–203. doi: 10.1088/0967-3334/35/11/2191

23. Newman AM, Liu CL, Green MR, Gentles AJ, Feng W, Xu Y, et al. Robust enumeration of cell subsets from tissue expression profiles. *Nat Methods*. (2015) 12 (5):453–7. doi: 10.1038/nmeth.3337

24. Hu K. Become competent within one day in generating boxplots and violin plots for a novice without prior R experience. *Methods Protoc*. (2020) 3(4):64. doi: 10.3390/mps3040064.

25. Oguz C, Sen SK, Davis AR, Fu YP, O'Donnell CJ, Gibbons GH. Genotype-driven identification of a molecular network predictive of advanced coronary calcium in ClinSeq® and framingham heart study cohorts. *BMC Syst Biol*. (2017) 11(1):99. doi: 10.1186/s12918-017-0474-5

26. Bauer Y, de Bernard S, Hickey P, Ballard K, Cruz J, Cornelisse P, et al. Identifying early pulmonary arterial hypertension biomarkers in systemic sclerosis: machine learning on proteomics from the DETECT cohort. *Eur Respir J*. (2021) 57 (6):2002591. doi: 10.1183/13993003.02591-2020

27. Luo R, Sedlazeck FJ, Lam TW, Schatz MC. A multi-task convolutional deep neural network for variant calling in single molecule sequencing. *Nat Commun*. (2019) 10(1):998. doi: 10.1038/s41467-019-09025-z

28. Barrios JP, Tison GH. Advancing cardiovascular medicine with machine learning: progress, potential, and perspective. *Cell Rep Med*. (2022) 3(12):100869. doi: 10.1016/j.xcrm.2022.100869

29. Porter AG, Jänicke RU. Emerging roles of caspase-3 in apoptosis. *Cell Death Differ*. (1999) 6(2):99–104. doi: 10.1038/sj.cdd.4400476

30. Vanhoutte PM. Endothelium-derived free radicals: for worse and for better. *J Clin Invest*. (2001) 107(1):23–5. doi: 10.1172/JCI11832

31. Funakoshi Y, Ichiki T, Shimokawa H, Egashira K, Takeda K, Kaibuchi K, et al. Rho-kinase mediates angiotensin II-induced monocyte chemoattractant protein-1 expression in rat vascular smooth muscle cells. *Hypertension*. (2001) 38(1):100–4. doi: 10.1161/01.HYP.38.1.100

32. Banci L, Bertini I, Cefaro C, Ciofi-Baffoni S, Gallo A, Martinelli M, et al. MIA40 is an oxidoreductase that catalyzes oxidative protein folding in mitochondria. *Nat Struct Mol Biol*. (2009) 16(2):198–206. doi: 10.1038/nsmb.1553

33. Bauer MF, Hofmann S, Neupert W, Brunner M. Protein translocation into mitochondria: the role of TIM complexes. *Trends Cell Biol*. (2000) 10(1):25–31. doi: 10.1016/S0962-8924(99)01684-0

34. Whelan RS, Kaplinskiy V, Kitsis RN. Cell death in the pathogenesis of heart disease: mechanisms and significance. *Annu Rev Physiol*. (2010) 72:19–44. doi: 10.1146/annurev.physiol.010908.163111

35. Tie L, Wang D, Shi Y, Li X. Aquaporins in cardiovascular system. *Adv Exp Med Biol*. (2017) 969:105–13. doi: 10.1007/978-94-024-1057-0_6

36. Sjöholm K, Palming J, Olofsson LE, Gummesson A, Svensson P-A, Lystig TC, et al. A microarray search for genes predominantly expressed in human omental adipocytes: adipose tissue as a major production site of serum amyloid A. *J Clin Endocrinol Metab*. (2005) 90(4):2233–9. doi: 10.1210/jc.2004-1830

37. Hibuse T, Maeda N, Funahashi T, Yamamoto K, Nagasawa A, Mizunoya W, et al. Aquaporin 7 deficiency is associated with development of obesity through activation of adipose glycerol kinase. *Proc Natl Acad Sci U S A*. (2005) 102 (31):10993–8. doi: 10.1073/pnas.0503291102

38. Dai C, Charlestin V, Wang M, Walker ZT, Miranda-Vergara MC, Facchine BA, et al. Aquaporin-7 regulates the response to cellular stress in breast cancer. *Cancer Res*. (2020) 80(19):4071–86. doi: 10.1158/0008-5472.CAN-19-2269

39. Hibuse T, Maeda N, Nakatsuji H, Tochino Y, Fujita K, Kihara S, et al. The heart requires glycerol as an energy substrate through aquaporin 7, a glycerol facilitator. *Cardiovasc Res*. (2009) 83(1):34–41. doi: 10.1093/cvr/cvp095

40. Aggeli IK, Kapogiannatou A, Paraskevopoulou F, Gaitanaki C. Differential response of cardiac aquaporins to hyperosmotic stress; salutary role of AQP1 against the induced apoptosis. *Eur Rev Med Pharmacol Sci*. (2021) 25 (1):313–25. doi: 10.26355/eurrev_202101_24397

41. Smyth SS, Woulfe DS, Weitz JI, Gachet C, Conley PB, Goodman SG, et al. G-protein-coupled receptors as signaling targets for antiplatelet therapy. *Arterioscler Thromb Vasc Biol*. (2009) 29(4):449–57. doi: 10.1161/ATVBAHA.108.176388

42. Braunwald E. The war against heart failure: the lancet lecture. *Lancet*. (2015) 385 (9970):812–24. doi: 10.1016/S0140-6736(14)61889-4

43. Val-Blasco A, Gil-Fernández M, Rueda A, Pereira L, Delgado C, Smani T, et al. Ca mishandling in heart failure: potential targets. *Acta Physiol*. (2021) 232(3):e13691. doi: 10.1111/apha.13691

44. Ren J, Bi Y, Sowers JR, Hetz C, Zhang Y. Endoplasmic reticulum stress and unfolded protein response in cardiovascular diseases. *Nat Rev Cardiol*. (2021) 18 (7):499–521. doi: 10.1038/s41569-021-00511-w

45. Carrillo-Salinas FJ, Ngwenyama N, Anastasiou M, Kaur K, Alcaide P. Heart inflammation: immune cell roles and roads to the heart. *Am J Pathol*. (2019) 189 (8):1482–94. doi: 10.1016/j.ajpath.2019.04.009

46. Farbehi N, Patrick R, Dorison A, Xaymardan M, Janbandhu V, Wystub-Lis K, et al. Single-cell expression profiling reveals dynamic flux of cardiac stromal, vascular and immune cells in health and injury. *Elife*. (2019) 8:e43882. doi: 10.7554/eLife.43882

47. Ngkelo A, Richart A, Kirk JA, Bonnin P, Vilar J, Lemitre M, et al. Mast cells regulate myofilament calcium sensitization and heart function after myocardial infarction. *J Exp Med*. (2016) 213(7):1353–74. doi: 10.1084/jem.20160081

48. Bansal SS, Ismahil MA, Goel M, Patel B, Hamid T, Rokosh G, et al. Activated T lymphocytes are essential drivers of pathological remodeling in ischemic heart failure. *Circ Heart Fail*. (2017) 10(3):e003688. doi: 10.1161/CIRCHEARTFAILURE.116.003688

49. Bansal SS, Ismahil MA, Goel M, Zhou G, Rokosh G, Hamid T, et al. Dysfunctional and proinflammatory regulatory T-lymphocytes are essential for adverse cardiac remodeling in ischemic cardiomyopathy. *Circulation*. (2019) 139 (2):206–21. doi: 10.1161/CIRCULATIONAHA.118.036065

frontiers | Frontiers in Cardiovascular Medicine

TYPE Original Research
PUBLISHED 28 March 2023
DOI 10.3389/fcvm.2023.1121102

Check for updates

OPEN ACCESS

EDITED BY
Miguel Hueso,
Bellvitge University Hospital, Spain

REVIEWED BY
Dmitry A. Sychev,
Ministry of Health, Russia
Serghei Covantsev,
S.P. Botkin Clinical Hospital, Russia
Xue He,
Central South University, China

*CORRESPONDENCE
Kuiwu Yao
✉ yaokuiwu@126.com

These authors have contributed equally to this work and share first authorship

SPECIALTY SECTION
This article was submitted to Cardiovascular Genetics and Systems Medicine, a section of the journal Frontiers in Cardiovascular Medicine

RECEIVED 11 December 2022
ACCEPTED 14 March 2023
PUBLISHED 28 March 2023

CITATION
Sun Z, Lin J, Zhang T, Sun X, Wang T, Duan J and Yao K (2023) Combining bioinformatics and machine learning to identify common mechanisms and biomarkers of chronic obstructive pulmonary disease and atrial fibrillation.
Front. Cardiovasc. Med. 10:1121102.
doi: 10.3389/fcvm.2023.1121102

COPYRIGHT
© 2023 Sun, Lin, Zhang, Sun, Wang, Duan and Yao. This is an open-access article distributed under the terms of the Creative Commons Attribution License (CC BY). The use, distribution or reproduction in other forums is permitted, provided the original author(s) and the copyright owner(s) are credited and that the original publication in this journal is cited, in accordance with accepted academic practice. No use, distribution or reproduction is permitted which does not comply with these terms.

Combining bioinformatics and machine learning to identify common mechanisms and biomarkers of chronic obstructive pulmonary disease and atrial fibrillation

Ziyi Sun[1,2†], Jianguo Lin[1,3†], Tianya Zhang[4†], Xiaoning Sun[1,3], Tianlin Wang[1,2], Jinlong Duan[1] and Kuiwu Yao[1,5*]

[1]Guang'anmen Hospital, China Academy of Chinese Medical Sciences, Beijing, China, [2]Graduate School, Beijing University of Chinese Medicine, Beijing, China, [3]Graduate School, China Academy of Chinese Medical Sciences, Beijing, China, [4]Graduate School, Hebei University of Chinese Medicine, Shijiazhuang, China, [5]Eye Hospital China Academy of Chinese Medical Sciences, China Academy of Chinese Medical Sciences, Beijing, China

Background: Patients with chronic obstructive pulmonary disease (COPD) often present with atrial fibrillation (AF), but the common pathophysiological mechanisms between the two are unclear. This study aimed to investigate the common biological mechanisms of COPD and AF and to search for important biomarkers through bioinformatic analysis of public RNA sequencing databases.
Methods: Four datasets of COPD and AF were downloaded from the Gene Expression Omnibus (GEO) database. The overlapping genes common to both diseases were screened by WGCNA analysis, followed by protein-protein interaction network construction and functional enrichment analysis to elucidate the common mechanisms of COPD and AF. Machine learning algorithms were also used to identify key biomarkers. Co-expression analysis, "transcription factor (TF)-mRNA-microRNA (miRNA)" regulatory networks and drug prediction were performed for key biomarkers. Finally, immune cell infiltration analysis was performed to evaluate further the immune cell changes in the COPD dataset and the correlation between key biomarkers and immune cells.
Results: A total of 133 overlapping genes for COPD and AF were obtained, and the enrichment was mainly focused on pathways associated with the inflammatory immune response. A key biomarker, cyclin dependent kinase 8 (*CDK8*), was identified through screening by machine learning algorithms and validated in the validation dataset. Twenty potential drugs capable of targeting *CDK8* were obtained. Immune cell infiltration analysis revealed the presence of multiple immune cell dysregulation in COPD. Correlation analysis showed that *CDK8* expression was significantly associated with CD8+ T cells, resting dendritic cell, macrophage M2, and monocytes.
Conclusions: This study highlights the role of the inflammatory immune response in COPD combined with AF. The prominent link between *CDK8* and the inflammatory immune response and its characteristic of not affecting the basal expression level of nuclear factor kappa B (*NF-kB*) make it a possible promising therapeutic target for COPD combined with AF.

KEYWORDS

chronic obstructive pulmonary disease, atrial fibrillation, microarray, machine learning, biomarker

Introduction

Chronic obstructive pulmonary disease (COPD) is characterized by progressive airway obstruction. It is estimated that COPD will be the third most deadly disease in the world by 2030 (1). In clinical practice, COPD is often combined with multiple cardiovascular diseases, including heart failure, coronary atherosclerotic heart disease, and atrial fibrillation (AF) (2). AF, the most common type of arrhythmia, has been shown in epidemiological surveys to affect at least 33.5 million people worldwide (3). Heart failure and stroke are severe complications of AF, and the risk of heart failure in AF patients is about twice as high as normal, and the risk of stroke is 4–5 times higher (4, 5).

There is a strong association between COPD and AF, with studies showing a 2.23-fold increased risk of AF in COPD patients compared to non-COPD patients (6). Similarly, the prevalence of COPD in patients with AF reached 25% (7). In addition, combined COPD increases the recurrence rate and the incidence of adverse events after catheter ablation in patients with AF (8, 9). A meta-analysis that included 46 studies involving 4,232,784 AF patients showed that AF patients with comorbid COPD had a significantly increased risk of bleeding, cardiovascular event death, and all-cause mortality compared to AF patients without COPD (10). It is currently thought that enhanced sympathetic activity, altered cardiac structure, immune dysfunction, inflammation, and oxidative stress may be involved in the development of AF in patients with COPD. However, the exact mechanisms have not been fully elucidated (11). Meanwhile, drugs commonly used to treat COPD, such as beta-blockers, theophylline, and glucocorticoids, have been linked to an increased risk of AF development (12, 13). Therefore, it is of practical clinical significance to explore the potential mechanisms of COPD and AF co-morbidity at the genetic level and to find promising therapeutic targets for application.

The field of bioinformatics is developing rapidly, and large amounts of genetic data are publicly available to uncover many unknown pathophysiological mechanisms in the development of diseases and potential connections between diseases. Machine learning, an essential artificial intelligence component, has also been widely applied to bioinformatics research and has become an important tool (14). Based on this, this study integrates COPD and AF mRNA datasets in public databases and attempts to reveal the common biological mechanisms of COPD and AF co-morbidity through weighted gene co-expression network analysis (WGCNA), protein-protein interaction (PPI) network construction, and enrichment analysis. Random forest (RF), support vector machine (SVM), extreme gradient boosting (XGBoost), and generalized linear model (GLM) were used to screen potential biomarkers. A comprehensive analysis of key biomarkers was performed, including co-expression analysis, construction of "transcription factor (TF)-mRNA-microRNA (miRNA)" regulatory networks, and drug prediction. An examination of immune cell infiltration on the COPD dataset was also carried out. **Figure 1** depicts the study flowchart.

Materials and methods

Data source

We applied the Gene Expression Omnibus (GEO) database (15) (http://www.ncbi.nlm.nih.gov/geo/) to filter gene expression datasets for microarrays by qualifying the keywords "COPD" and "AF" with the filter criteria "Homo Sapiens" and "tissues." Four datasets were finally obtained. In the COPD group, GSE76925 (lung tissue samples from 111 COPD patients and 40 control patients) (16) and GSE106986 (lung tissue samples from 14 COPD patients and 5 control patients) were selected. In the AF group, GSE79768 (left and right atrial tissue samples from 7 AF patients and 6 control patients) (17) and GSE115574 (left and right atrial tissue samples from 15 AF patients and 15 control patients) (18) were selected. GSE76925 and GSE79768 were used as training sets, GSE106986 and GSE115574 were used as the external validation set.

Weighted gene co-expression network analysis

WGCNA analysis was performed on GSE76925 and GSE79768, respectively, to obtain modules closely associated with COPD and AF. WGCNA analysis was constructed using the "WGCNA" package in R (19). The genes were ranked based on the standard deviation of gene expression. The top 25% of genes with the largest fluctuations were selected for subsequent analysis, and outlier samples were excluded by hierarchical clustering. The R2 was set greater than 0.9, and a suitable soft threshold (β) was calculated to make the network conform to the scale-free distribution. The co-expression modules are identified by hierarchical clustering to obtain a hierarchical clustering tree. Finally, the module feature values and the correlation between module feature values and clinical features are calculated to obtain the expression spectrum of each module, which is expressed by the correlation coefficient as well as the *p*-value. Finally, we select the genes in the modules closely related to the disease for subsequent analysis.

Identification of overlapping genes and PPI network analyses

The genes in the modules closely related to disease in GSE76925 and GSE79768 obtained by WGCNA analysis were taken to intersect. The Venn diagram was used to visualize the overlapping genes. After that, the overlapping genes were imported into the "Search Tool for Interacting Genes" (STRING) online platform (https://cn.string-db.org/) (20). The species was limited to "Homo sapiens," with the confidence score set to an intermediate value (confidence score > 0.4) to construct the PPI network. The results were exported to Cytoscape 3.7.2 for visualization (21).

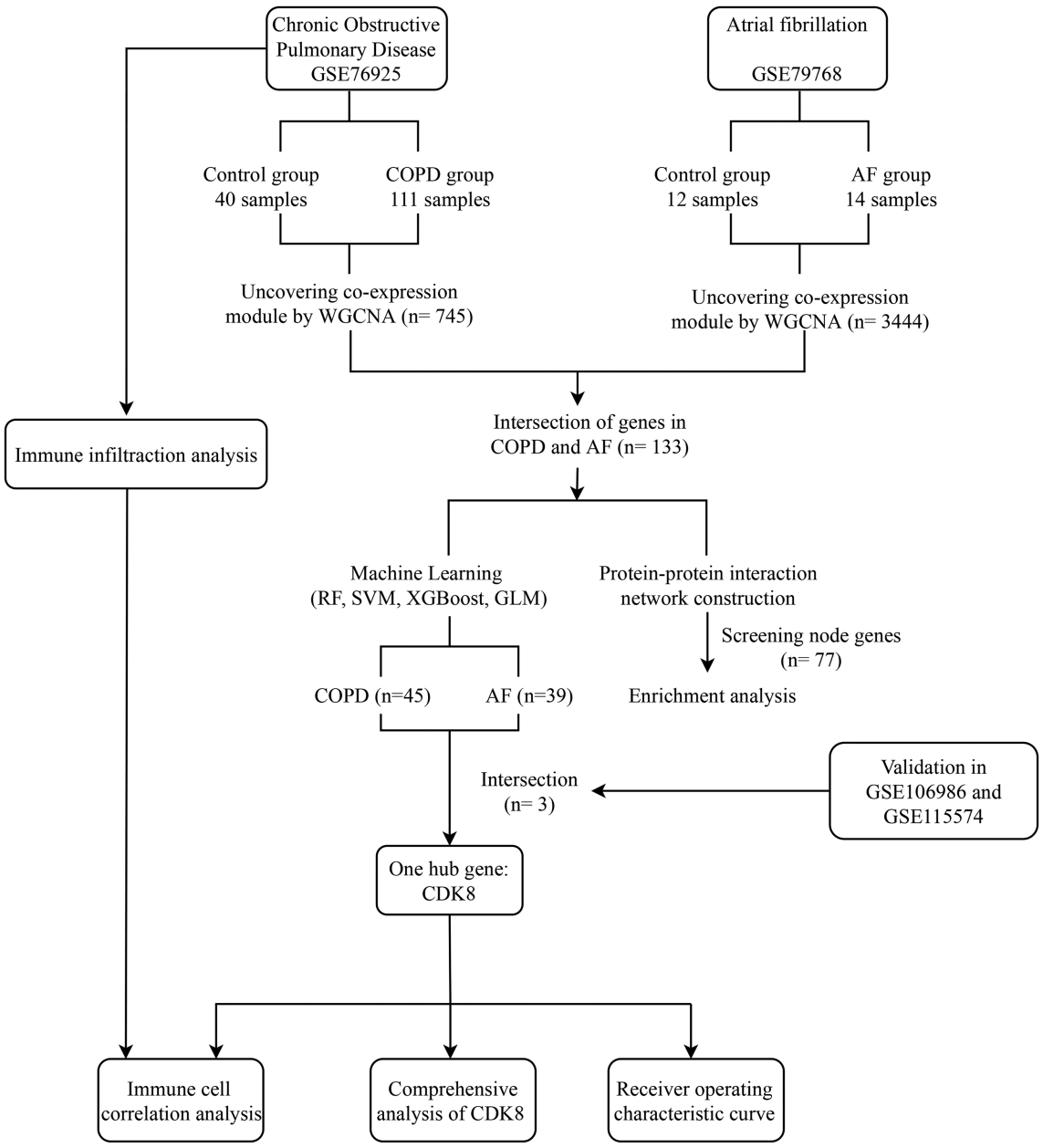


FIGURE 1
Study flowchart. GSE, gene expression omnibus series; WGCNA, weighted gene co-expression network analysis; RF, Random forest support vector machine; SVM, support vector machine; XGBoost, extreme gradient boosting; GLM, generalized linear model.

Functional enrichment analysis

To further understand the common biological mechanisms between the two diseases, the protein information in the PPI network was enriched for Gene Ontology (GO) and Kyoto Encyclopedia of Genes and Genomes (KEGG) pathways using the "clusterProfiler" package in R (22). The GO includes biological process (BP), cellular component (CC), and molecular function (MF) (23). The screening condition was set at adjust -$P < 0.05$, and the visualization was presented using the Sangerbox platform (http://vip.sangerbox.com/). Meanwhile, Gene set enrichment analysis (GSEA) enrichment analysis was performed on the GSE76925 and GSE79768 datasets to comprehensively analyze the key pathways associated with COPD and AF pathogenesis. The reference dataset was "c5.kegg.v7.4.symbols.gmt" from the MSigDB database (24). The significantly enriched pathways were identified with the screening criteria of $P < 0.05$ and FDR < 0.25, and the "enrichplot" package was used for visualization.

Identification of candidate genes based on machine learning algorithms

Machine learning is now widely used to identify characteristic genes. To identify key genes associated with COPD and AF, four

machine learning algorithms, including RF, SVM, XGBoost, and GLM, were used to screen for key genes in COPD and AF, respectively. In both training datasets, the response variable was set to whether the diagnosis was COPD and AF, and the overlapping genes were set as explanatory variables. Use 70% of the data for model construction and 30% for model validation. Models for RF, SVM, XGBoost, and GLM were constructed separately using the "caret" R package (25). It is well known that while building a machine learning model with good results, it is equally important to evaluate the interpretation of the model, as only an interpretable machine learning model is likely to be more widely understood and adopted. The "DALEX" R package is a model interpretation package that has been developed to help understand the links between input variables and model outputs (26). It uses the size of the residuals to assess the quality of the model (smaller residuals mean better model quality) and the root mean square error (RMSE) to assess the importance of the variables (defined as how much the absence of a variable affects the predicted value of the response variable). Once modelling was completed, residual box plots were drawn for the four models using the "DALEX" R package and the RMSE was used to assess the importance of each gene in the model. Also, we use the "predict" function in R to verify the accuracy of the predictions of the model constructed by "caret". Receiver operating characteristic (ROC) curves were then plotted using the "pROC" R package (27) and the area under the curve (AUC) was reported to assess the predictive effectiveness of models. Finally, we selected models with high predictive accuracy based on the quality of the model (assessed by the size of the residuals) and the area of the AUC. According to the gene importance score, select the top 20 genes from the constructed models for COPD and AF respectively, and then perform the intersection for these genes. Afterwards, we compared the differential expression of intersecting genes between the two datasets, with $P < 0.05$ considered to be significantly different, and used the "ggpubr" R package to plot boxplots. Finally, genes that were differentially expressed in the disease and control groups in both sets of data and that showed the same expression trend in both microarrays were identified as candidate hub genes.

Validation of hub genes and evaluation of prediction accuracy

The identified candidate genes were validated in the validation sets for COPD and AF, respectively. The comparison of gene expression between disease group and control group with $P < 0.05$ was considered to be significantly different. The candidate genes with significant differences were finally considered to be hub genes and the boxplot was drawn for visualization. Afterwards, ROC curves of the diagnostic value of hub genes in the training set and validation set were plotted using "pROC" R package, and AUC was calculated to evaluate the accuracy of hub gene prediction.

Comprehensive analysis of hub genes

Hub genes were entered into the GeneMANIA online website (28) (http://genemania.org) for co-expression and functional enrichment analyses. The JASPAR database (29) (http://jaspar.genereg.net/) were used to predict TFs regulating hub genes. Prediction of miRNAs regulated by hub genes using the miRTarBase database (30) (https://mirtarbase.cuhk.edu.cn/), and experimentally validated miRNAs were selected. The results were visualized using Cytoscape to demonstrate the "TF-mRNA-miRNA" regulatory network. In addition, we used the DGIDB 3.0 database (31) (http://www.dgidb.org/) to predict potential drugs that could target the hub gene.

Immune cell infiltration analysis

CIBERSORT can calculate the proportion of different immune cells in the gene expression profile through a deconvolution algorithm (32). We performed an immune cell infiltration analysis of the COPD gene expression matrix (GSE76925) using the CIBERSORT algorithm. The "barplot" and "vioplot" packages were used to show the relative proportions and differences of immune cell types in the expression profile between the control and COPD groups. The "corrplot" package was used to show the correlation heat map of immune cells in the expression profile. The hub gene's expression was then taken from the expression profile. The correlation between the hub gene and immune cells was analyzed by Spearman correlation analysis, with $P < 0.05$ as the screening condition, and visualized by the "ggplot" package.

Results

Construction of co-expressed gene modules

WGCNA analysis was performed on the GSE76925 and GSE79768 datasets to identify co-expression modules associated with COPD and AF, respectively. The β selection analysis of GSE76925 showed that the network was closer to the scale-free network when the $\beta = 4$ (**Figure 2A**). Six modules were also identified, of which the yellow module was positively associated with COPD (correlation coefficient = 0.35, $P = 9e\text{-}06$) and contained 745 genes (**Figures 2B,C**). The β selection analysis of GSE79768 showed that the network was closer to the scale-free network when the $\beta = 10$ (**Figure 2D**). Eleven modules were identified, among which blue (correlation coefficient = 0.55, $P = 0.004$), pink (correlation coefficient = 0.42, $P = 0.03$), turquoise (correlation coefficient = 0.73, $P = 3e\text{-}05$), and yellow (correlation coefficient = 0.61, $P = 0.001$) were positively correlated with AF and contained 3,444 genes (**Figures 2E,F**). Among them, 952 were blue modules, 287 were pink modules, 1,526 were turquoise modules, and 705 were yellow modules. Detailed gene information is listed in **Supplementary Table S1**.

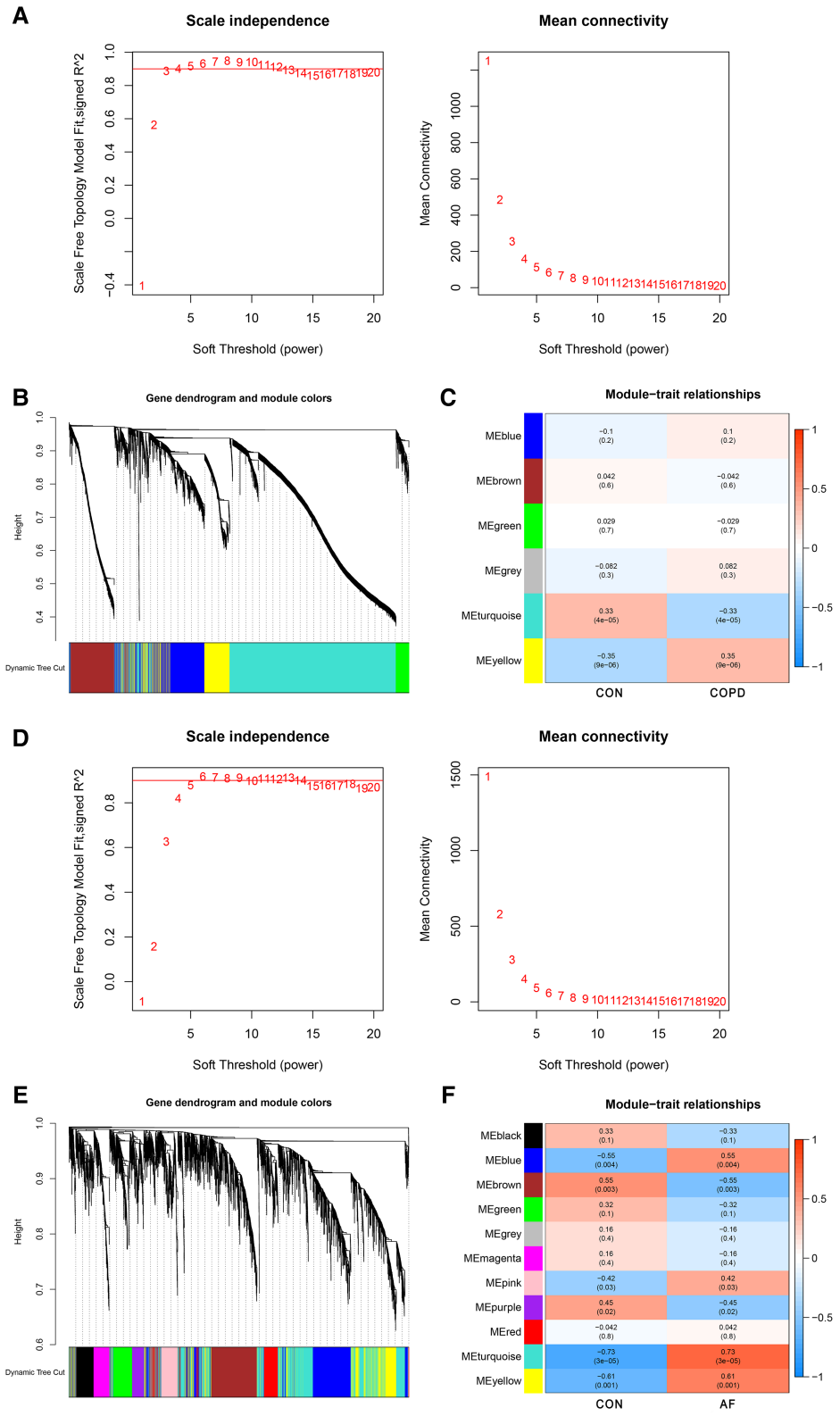


FIGURE 2
Identification of COPD and AF module genes *via* WGCNA. (**A**) The scale-free fit index for soft-thresholding powers and mean connectivity (GSE76925). (**B**) Dendrogram of the genes clustered (GSE76925). (**C**) Module-trait relationships heatmap (GSE76925). The numbers in each cell means the correlation coefficient and *p*-value. (**D**) The scale-free fit index for soft-thresholding powers and mean connectivity (GSE79768). (**E**) Dendrogram of the genes clustered (GSE79768). (**F**) Module-trait relationships heatmap (GSE79768).

Identification of overlapping genes and construction of PPI network

By taking the intersection of the genes of COPD and AF-related modules obtained by WGCNA, 133 genes common to COPD and AF were obtained (**Figure 3A**). After that, we constructed a PPI network of overlapping genes and excluded genes that did not interact. Finally, we obtained 77 interacting genes in the network (**Figure 3B**).

Functional enrichment analysis

77 genes in the PPI network were analyzed for GO and KEGG enrichment to reveal the underlying molecular biological processes shared between COPD and AF. The GO enrichment analysis revealed that 77 genes were primarily enriched in the "Leukocyte migration," "Response to chemokine," "Cellular response to chemokine," "Myeloid leukocyte migration," "Activation of immune response," "Regulation of inflammatory

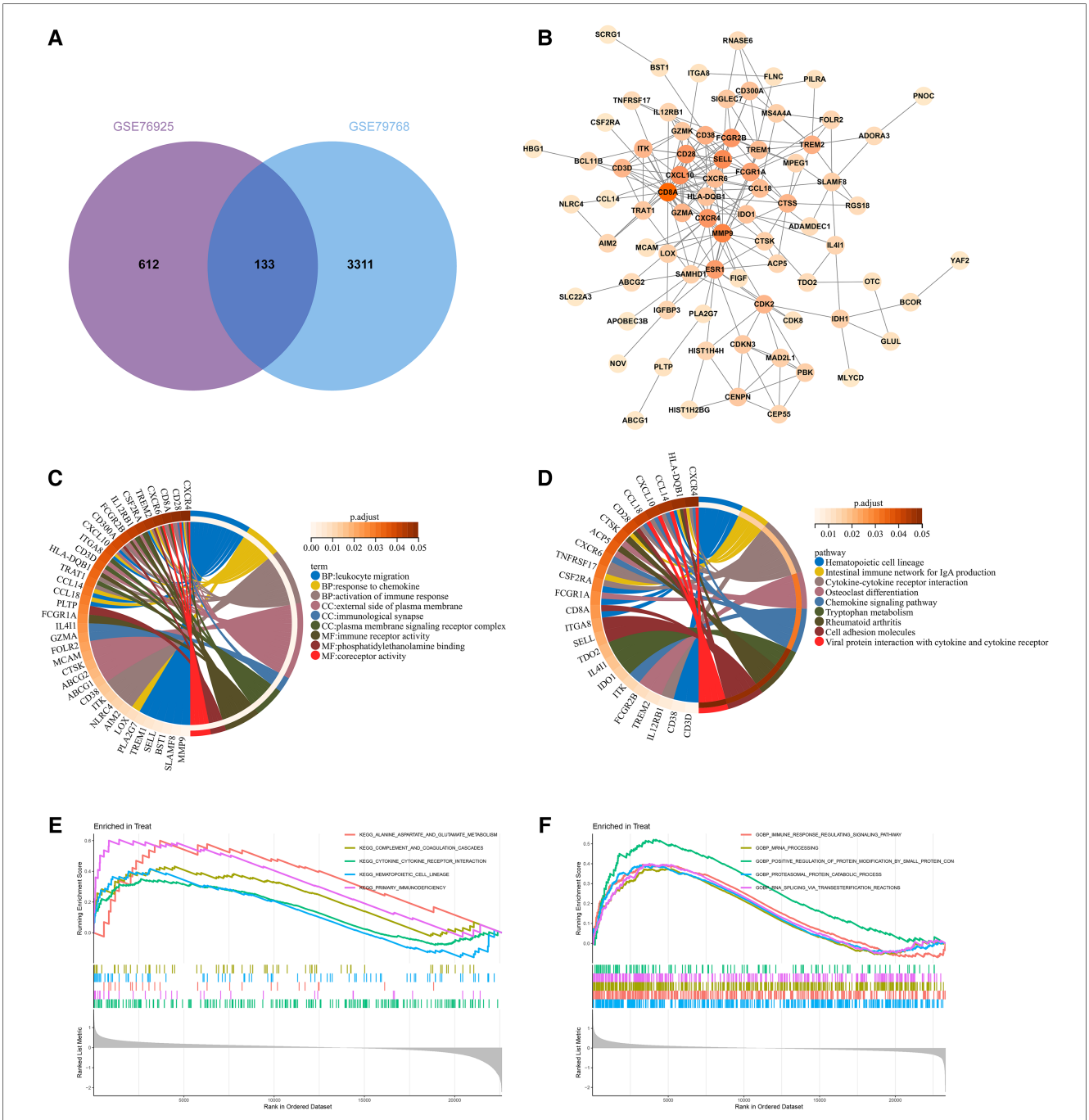


FIGURE 3
Construction of overlapping gene PPI networks and enrichment analysis. (**A**) Venn diagram of COPD and AF module genes. (**B**)PPI network. (**C**) KEGG pathway analysis of genes. Different colors represent various significant pathways and related enriched genes. (**D**) GO analysis of genes. Different colors represent various significant pathways and related enriched genes. (**E**) GSEA enrichment analysis of upregulated genes in the AF dataset. (**F**) GSEA enrichment analysis of upregulated genes in the COPD dataset.

response"(BP); "External side of plasma membrane," "Immunological synapse," "Plasma membrane signaling receptor complex," (CC); "Immune receptor activity," "Phosphatidylethanolamine binding," "Coreceptor activity," (MF) (**Figure 3C**, **Supplementary Table S2**). Also, KEGG analysis showed that genes were enriched in "Hematopoietic cell lineage," "Intestinal immune network for IgA production," "Cytokine-cytokine receptor interaction," "Chemokine signaling pathway," "Cell adhesion molecules," "T cell receptor signaling pathway" (**Figure 3D**, **Supplementary Table S3**). GSEA enrichment analysis revealed that genes upregulated in the GSE76925 dataset were mainly enriched in signaling pathways such as "Cytokine-cytokine receptor interaction," "Primary immunodeficiency," "Alanine aspartate and glutamate metabolism," "Hematopoietic cell lineage," "Complement and coagulation cascade" (**Figure 3E**). The genes upregulated in the GSE79768 dataset were mainly enriched in "RNA degradation," "Ubiquitin-mediated proteolysis," "Spliceosome," "Leukocyte transendothelial migration," and "Natural killer cell-mediated cytotoxicity" (**Figure 3F**).

Identification of hub genes based on machine learning algorithms

To identify key genes associated with COPD and AF, we constructed models using four machine learning methods and evaluated the models based on residuals and ROC. Box line plots of residuals and ROC are shown in **Figures 4A–D**. It can be seen that the SVM, XGB and RF models all exhibit similar excellent performance. Therefore, we selected the top 20 genes predicted by RF, SVM, and XGB in each of these two datasets based on the importance scores of the genes assessed by RMSE. Forty-five genes in total in the GSE76925 dataset and 39 in GSE79768, and 11 intersecting genes were obtained after taking the intersection. (**Figure 4E**, **Supplementary Tables S4, S5**). After verifying the differential expression and expression trends, three candidate genes, cyclin dependent kinase 8 (*CDK8*), solute carrier family 22 member 15 (*SLC22A15*), and TNF receptor superfamily member 17 (*TNFRSF17*), were finally obtained, and the box plots of differential expression are shown in **Figure 5**.

Validation of hub genes and assessment of predictive accuracy

The differential expression of *CDK8*, *SLC22A15*, and *TNFRSF17* was confirmed in the external validation set. Only *CDK8* showed a significant increase in expression in both the training and validation sets ($P < 0.05$) **Figure 5**. Thus, *CDK8* was finally identified as a hub gene that may be related to AF and COPD. the *CDK8*′*s* ROC curves demonstrated that in all four data sets, the AUC was near to or greater than 0.7 (**Figure 6**). It is suggested that *CDK8* may be effective for detecting COPD combined with AF.

Comprehensive analysis of hub genes

Twenty genes associated with hub genes were predicted by GeneMANIA, along with 1,326 interactions. This suggests a complex interaction between the hub gene and the remaining 20 genes. The functional enrichment results were mainly associated with DNA-templated transcription, positive regulation of DNA-templated transcription, and regulation of transcription initiation from the RNA polymerase II promoter (**Figure 7A**). The "TF-mRNA-miRNA" regulatory network contains 11 TFs that regulate *CDK8*, and five miRNAs (**Figure 7B**). DGIDB predicted 20 drugs targeting *CDK8*, including ALVOCIDIB, ACACETIN, and RONICICLIB (**Figure 7C**).

Immune cell infiltration analysis

By observing the enrichment analysis results, we found that immune-related pathways were significantly enriched, suggesting that immune dysfunction may be involved in the development of AF in COPD patients. Therefore, we performed an immune cell infiltration analysis of gene expression profiles in COPD. **Figure 8A** shows the ratio of immune cells in the control group to the COPD group. Compared to the control group, the COPD group had higher levels of plasma cells, CD8+ T cells, T follicular helper cells, Gamma-delta (γδ) T cells, macrophage M0, and resting dendritic cells, and lower levels of monocytes, macrophage M1, and activated dendritic cell (**Figure 8B**). Positive correlations were found between activated mast cells and neutrophils ($r = 0.60$), T cells and plasma cells ($r = 0.42$), and γδ T cells and T follicular helper cells ($r = 0.42$). In contrast, Macrophage M1 and activated dendritic cells were negatively correlated ($r = -0.54$) (**Figure 8C**). This suggests that patients with COPD have a different immune pattern compared to normal patients and that there are interactions between different types of immune cells. Detailed results of the immune cell infiltration analysis are shown in **Supplementary Table S6**.

Correlation analysis of *CDK8* and immune cells showed that *CDK8* expression correlated with four immune cell types, positively with CD8+ T cells, resting dendritic cells, and macrophage M2, and negatively with monocytes (**Figure 8D**).

Discussion

COPD affects more than 300 million people worldwide and causes approximately 3 million deaths yearly (33). COPD increases the incidence of AF and the risk of subsequent cardiovascular death. Similarly, comorbid AF increases the incidence of ischemic stroke, respiratory failure, and heart failure events in patients with COPD (34–37). The vicious circle relationship between COPD and AF, and the contradiction of pharmacological treatment, makes it urgent to explore the mechanisms of COPD and AF co-morbidity and to find potential therapeutic targets. It is generally believed that COPD-induced structural changes in the heart, increased

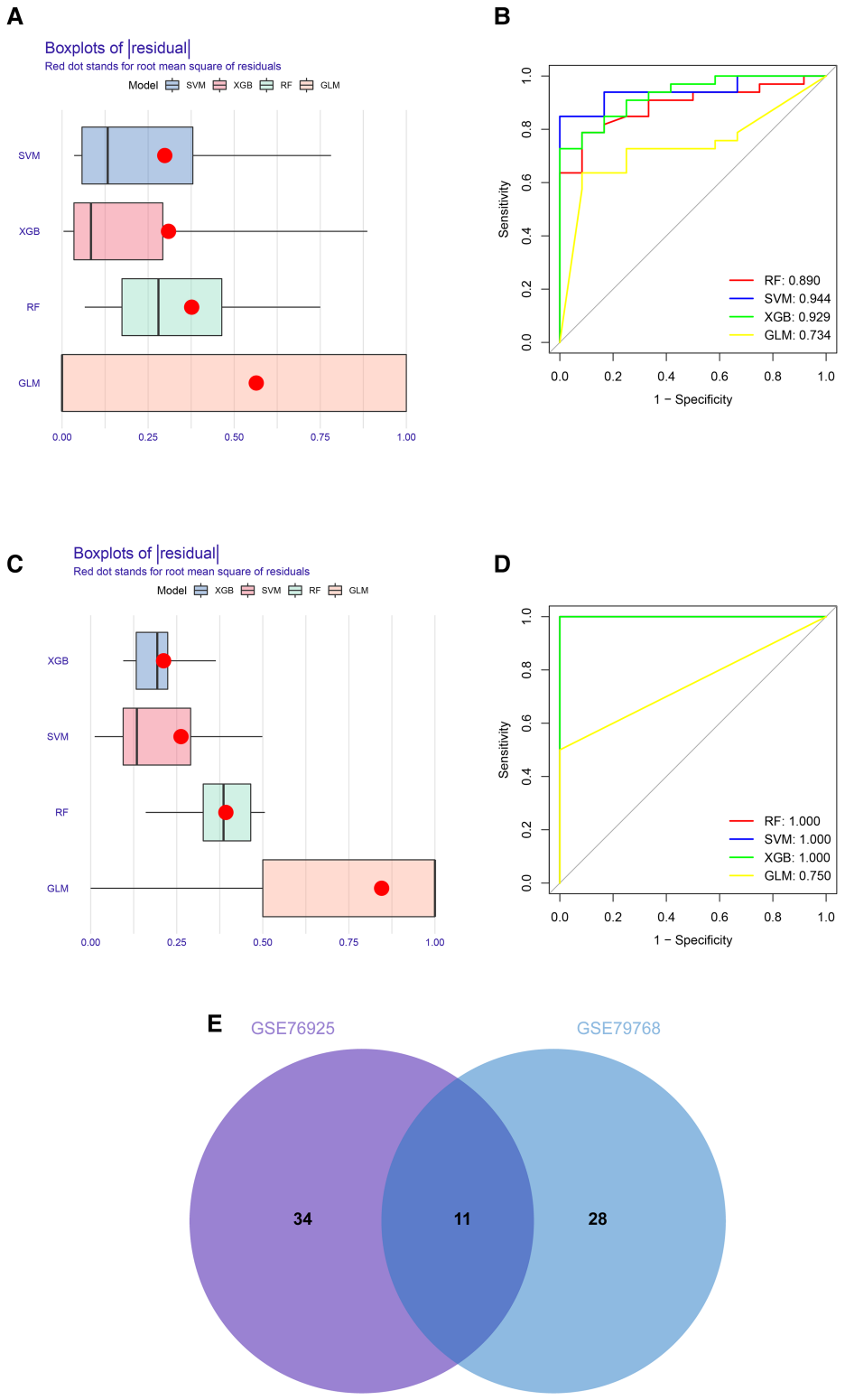


FIGURE 4
Construction and assessment of machine learning models for COPD and AF. (**A**) Boxplots of the residuals of the COPD. Red dot stands for root mean square of residuals. (**B**) ROC curves for model prediction accuracy in COPD dataset. (**C**) Boxplots of the residuals of the AF. (**D**) ROC curves for model prediction accuracy in AF dataset (**E**) Venn diagram of COPD and AF model prediction genes.

sympathetic activity, and hypoxia-induced oxidative stress accelerates the development of AF. But recent studies have highlighted the role of immune dysfunction in the pathogenesis of both diseases, finding that immune dysfunction may play a prominent role in the subsequent inflammatory response, cardiac remodeling, structural remodeling, and neural remodeling (11, 38). However, the exact

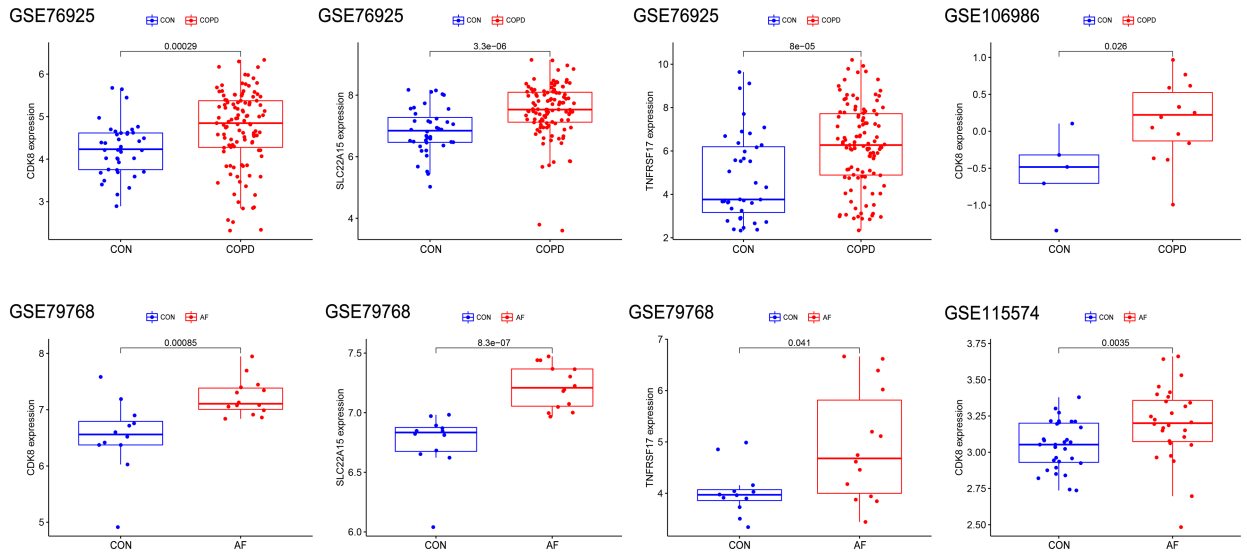


FIGURE 5
Validation of Hub gene expression levels in training and validation sets. The red box represents the disease group, and the blue represents the control group.

mechanisms have not been fully elucidated. In this context, we performed the first joint analysis of genetic datasets from both diseases to reveal common mechanisms and key biomarkers for the development of both diseases and to reveal changes in immune cells in COPD by immune cell infiltration analysis.

After screening of overlapping genes and the construction of PPI networks, 77 genes with interactions were obtained. They are mainly involved in biological processes such as activation of the immune response, regulation of inflammatory response, leukocyte migration, response to chemokines, immune receptor activity, and signaling pathways such as hematopoietic cell lineage, IgA-producing intestinal immune network, cytokine-cell receptor interactions, and T cell receptors. Combined with the results of GSEA enrichment analysis, we suggest that immune and inflammatory responses are the key mechanisms linking these two diseases, as confirmed by the results of previous studies (39–41). COPD is accompanied by a long-term and persistent chronic inflammatory response in the airways and lung parenchyma, leading to subsequent airway remodeling and destruction of the lung parenchyma (42). After inhalation of smoke or other toxic particles, the immune response is activated, after which macrophages release various cytokines and chemokines, including tumor necrosis factor-alpha (*TNF-α*), interleukin 1 beta (*IL-1β*), interleukin 6 (*IL-6*), C-X-C motif chemokine ligand 1 (*CXCL1*), and C-X-C motif chemokine ligand 8 (*CXCL8*), which attract circulating neutrophils, monocytes, and lymphocytes in the lungs leading to an inflammatory response (39, 43). At the same time, the activation of immune and inflammatory responses is not limited to the lungs, as studies have shown that COPD patients are accompanied by elevated circulating c-reactive protein (*CRP*), *IL-6*, *CXCL8*, and *TNF-α* (44). Changes in immune cells, especially macrophages, and increases in cytokines and chemokines such as *TNF-α, IL-6, IL-1β*, C-X-C motif chemokine ligand 1 (*CXCL1*), and C-X-C motif chemokine ligand 2 (*CXCL2*) have also been observed in AF (45, 46).

In response to these results, we performed an immune cell infiltration analysis in GSE76925, which showed a higher proportion of plasma cells, CD8+ T cells, T follicular helper cells, γδ T cells, macrophage M0, and resting dendritic cells, and a lower proportion of monocytes, macrophage M1, and activated dendritic cells in COPD lung tissue compared with controls. Studies have shown that CD8+ T lymphocytes increase in number and activity in COPD and produce many cytokines such as Interferon gamma (*IFN-γ*) and *TNF-α* (47). γδ T cells are nontraditional T cells, and despite their small number, a study by Murdoch (48) et al. found that γδ T cells increase interleukin 17A (*IL-17*) production during acute allergic airway disease and are involved in disease pathogenesis. Plasma cells are widely present in the connective tissue of the lamina propria of the respiratory tract and participate in the adaptive humoral immune response by synthesizing antibodies in response to the invasion of the respiratory tract (49). Studies have shown that the severity of COPD is positively correlated with the development of tertiary lymphoid organs (TLOs), and IL-21 T-follicular-helper (Tfh)-like cells have been observed in TLOs of COPD patients, suggesting that Tfh may be involved in the formation of TLOs (50, 51). Dendritic cells are critical antigen-presenting cells involved in adaptive immune activation in COPD. However, Givi (52) et al. found that chronic exposure to harmful particles impairs dendritic cells maturation and inhibits antigen-presenting capacity. Macrophages are differentiated from monocytes and play a key role in chronic inflammation in COPD patients. Naive macrophage M0 can be induced to differentiate into M1- and M2-type macrophages under different conditions, with M1-type mainly playing a pro-inflammatory role (53). Interestingly, our study found a lower proportion of M1-type macrophages in the

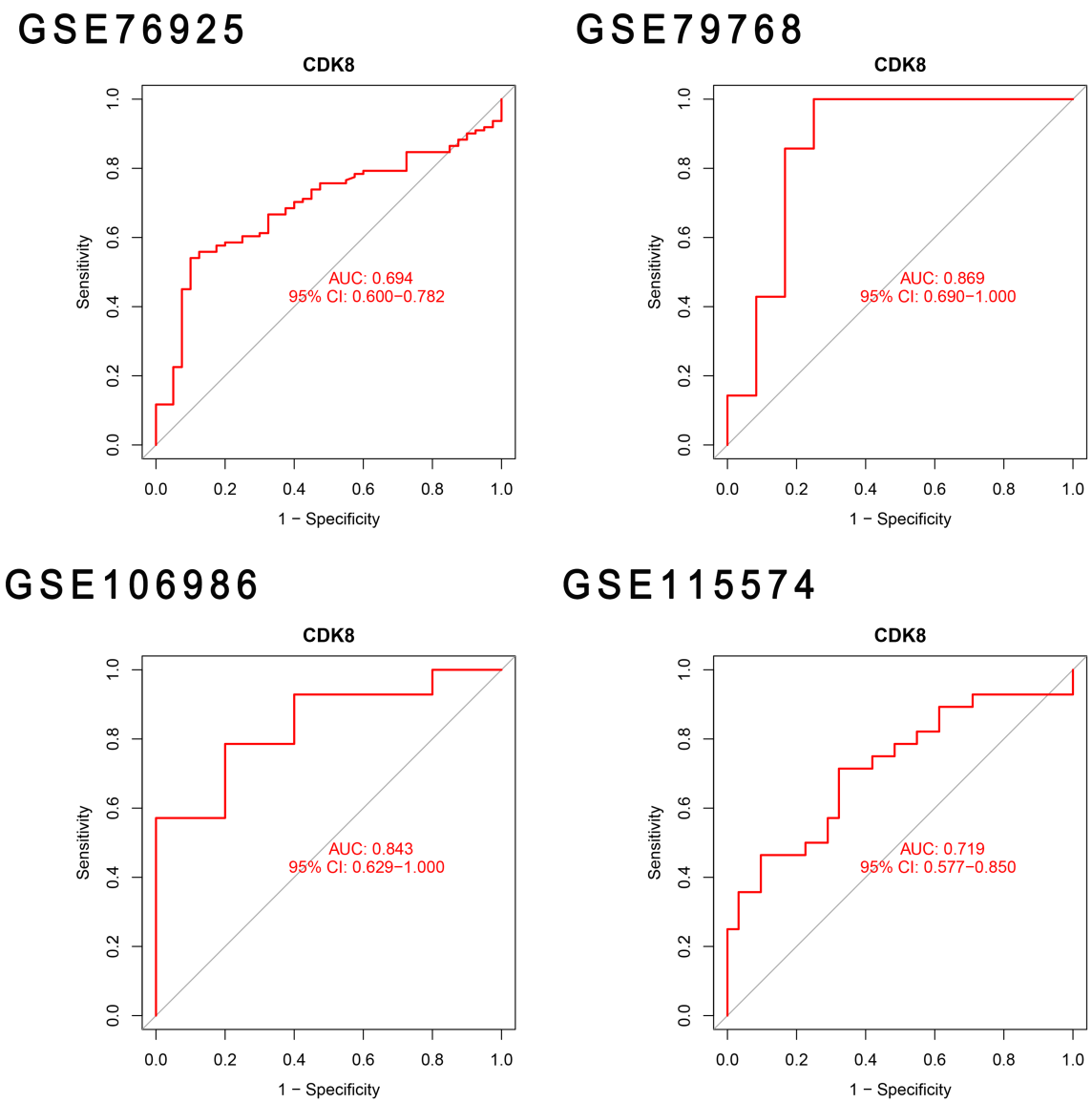


FIGURE 6
Validation hub genes are used as marker genes.

COPD group compared with controls, the reason for which needs to be further investigated. Similarly, immune cells are the primary cell type in the heart, and one study showed that immune cells accounted for 10.4% of all cell types in atrial tissue (54). More dendritic cells were found in the left atrial myocardium of patients with AF compared to those with sinus rhythm. Increased numbers of neutrophils, lymphocytes, and macrophages were also observed in the atrial adipose tissue (55, 56). These findings suggest that immune cell changes in COPD may also be involved in developing AF.

A biomarker, *CDK8*, was identified by a machine learning algorithm and validated in the validation set, and it was significantly upregulated in both COPD and AF groups. *CDK8* is a serine/threonine protein kinase that plays an important role in transcriptional regulation by binding to cell cycle protein C (57). Recent studies have shown that *CDK8* is also involved in the inflammatory response, as Chen et al. (58) found that in response to *TNF-α* stimulation, nuclear factor kappa B (*NF-kB*) and *CDK8* are jointly recruited to the promoters of response genes, driving the expression of *NF-kB* early response genes *CXCL8*, *CXCL2*, and C-X-C motif chemokine ligand 3 (*CXCL3*). In addition, *CDK8* is involved in the activation of hypoxia inducible factor 1 subunit alpha (*HIF1A*) (59). lungs of COPD patients overexpress *HIF1A*, which is associated with hypoxia and inflammatory response (60). Elevated expression of *HIF1A* is also observed during AF, which may be involved in the structural remodeling of the left atrium (61). *CDK8* also highlights potential advantages as a therapeutic target, and *NF-kB* plays an important role in activating immune inflammatory responses in COPD and AF by encoding chemokines and cytokines (62, 63). Transcription of *NF-kB* requires activation of *CDK8*. Studies have shown that reducing *CDK8* activity inhibits *NF-kB*-driven

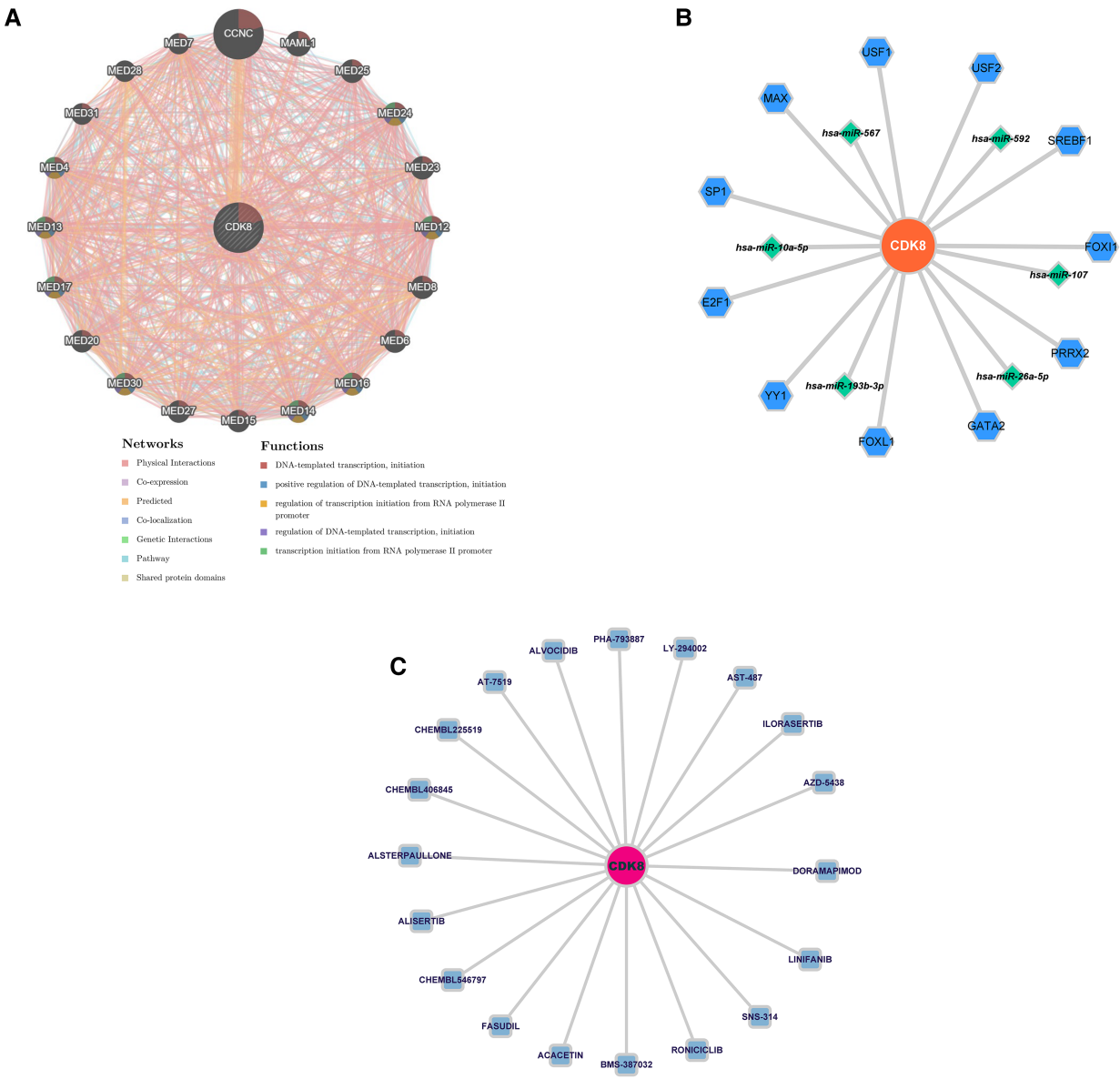


FIGURE 7
(**A**) Co-expression network of CDK8. (**B**) The "TF-mRNA-miRNA" regulatory network of CDK8. Blue hexagons are TFs; green diamonds are miRNAs. (**C**) Drug prediction for CDK8 based on DIGDB database. Blue squares are potential drugs.

transcription but has no effect on the basal expression of *NF-kB*-regulated genes or promoters (58). This avoids the detrimental effects of *NF-kB* blockers due to reduced *NF-kB* expression levels, making *CDK8* a more promising therapeutic target. In addition, we performed a co-expression analysis of CDK8, "TF-mRNA-miRNA" network construction, and drug prediction. These *CDK8*-associated mRNAs, TFs, and miRNAs also contribute to understanding the *CDK8* association network. At the same time, the results predicted by DGIDB may become new drugs for treating COPD combined with AF. Several studies have shown that inhibitors of *CDK8* have an inhibitory effect on inflammatory immune responses (64, 65). Studies by Schmerwitz et al. (66) have found that ALVOCIDIB (also known as Flavopiridol) is able to against inflammation by effectively blocking the activation of endothelial cells through the inhibition of *NF-kB* consensus promoter activity and thereby disrupting the interaction between inflammatory-induced leukocytes and endothelial cells. This suggests that drugs targeting *CDK8* may be promising for treating COPD combined with AF.

Analysis of the correlation between *CDK8* and immune cell infiltration showed a positive correlation between *CDK8* and CD8+ T cells, resting dendritic cells, and macrophage M2 and a negative correlation with monocytes. Patients with COPD have increased infiltration of CD8+ T cells in lung tissue and produce pro-inflammatory factors such as *TNF-α* (47). The involvement of *TNF-α* in AF involves multiple mechanisms, and *TNF-α* has been shown to disrupt intracellular calcium homeostasis in atrial myocytes by decreasing the expression of T-type calcium channel

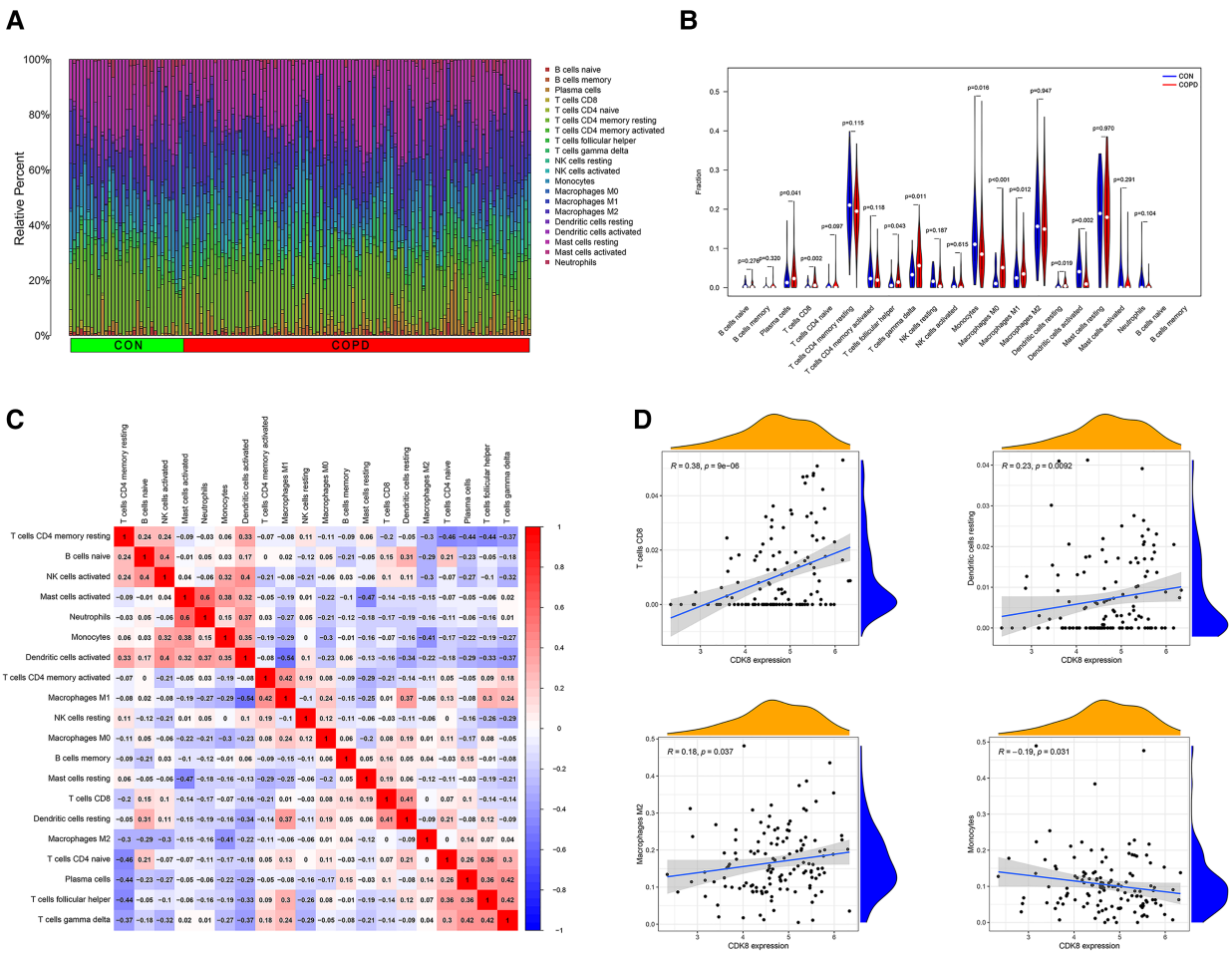


FIGURE 8
Immune cell infiltration analysis of GSE76925 and immune cell correlation analysis of CDK8. (**A**) The proportion of immune cells in different samples. (**B**) Comparison of immune cell ratios in the COPD and control groups. (**C**) Heat map of correlation analysis between immune cells. (**D**) Analysis of the correlation between CDK8 and immune cells.

α1G subunit (TCCA 1G) and sarcoplasmic reticulum Ca-ATPase (SERCA2a) thereby participating in AF (67, 68). In addition, *TNF-α* directly reduces collagen synthesis in cardiomyocytes, enhances matrix metallopeptidase 2 (*MMP-2*) and matrix metallopeptidase 9 (*MMP-9*) activities, promotes collagen breakdown, and exacerbates myocardial fibrosis (69, 70). M2 macrophage infiltration in the lungs of patients with COPD is significantly increased. A study by Kaku (71) et al. showed that M2 macrophages are strongly associated with the severity of COPD and a predicted reduction in expiratory force volume in one second (FEV), suggesting the involvement of M2 macrophages in the development of COPD. Macrophages also secrete elastolytic enzymes, such as *MMP-2* and *MMP-9*, which directly lead to the destruction of lung structures and fibrosis of the atria (72–74). Increased sympathetic nervous system activity triggered by COPD promotes the development of AF (11). Studies have revealed that high catecholamine levels induce sympathetic remodeling by acting on the β1-adrenergic receptors on macrophages to produce inflammatory factors such as *TNF-α*, nerve growth factor (*NGF*), and interleukin 1 alpha (*IL-1*). This process may cause the onset of AF (75). Dendritic cell function in AF and COPD is still being studied. Ravi (76) et al. found that monocyte migration capacity was reduced in COPD patients, which may partially explain the negative correlation between *CDK8* and monocytes. However, the exact mechanism still needs further investigation. In conclusion, our findings provide a new perspective on the pathogenesis of COPD combined with AF from the viewpoint of the inflammatory immune response and suggest a biomarker *CDK8* that could potentially be a therapeutic target.

This study also has several limitations. First, the data in this study were obtained based on the GEO database. Although a dataset containing more samples was selected and validated in an external dataset, the results may be biased due to the different platforms from which they were obtained. Additionally, due to COPD being a heterogeneous disease, there are various phenotypes of COPD, such as small airway-predominant disease, frequent exacerbators, and asthma-COPD overlap, which have different pathophysiological mechanisms that are not completely the same (77). Recent studies have shown that within 90 days of

an acute exacerbation of COPD, patients are at a significantly increased risk of an emergency department visit or hospital admission related to AF (78). Another cohort study also found an increased risk of AF in asthmatic patients (79). However, our study was unable to analyze the association between the different phenotypes of COPD and AF separately, so further research is needed to investigate the relationship between these different COPD phenotypes and AF at the genetic level. Secondly, the AUC area of *CDK8* in the COPD training set was less than 0.7, and although the AUC area was improved in the validation set, its value in practical clinical applications still needs further validation. Finally, the specific mechanisms of immune inflammatory response and *CDK8* in COPD with AF and the association between *CDK8* and immune cells need further proof from subsequent *in vivo* and *in vitro* experiments.

Conclusion

In this study, through bioinformatic analysis, we found that disturbances in immune regulation and subsequent activation of the inflammatory response may have a significant role in COPD combined with AF. Through machine learning algorithms, *CDK8* was finally identified as a key biomarker, and inhibitors targeting *CDK8* may be able to be promising therapeutic agents for COPD combined with AF by inhibiting *NF-kB*-induced immune inflammatory responses.

Data availability statement

The original contributions presented in the study are included in the article/**Supplementary Material**, further inquiries can be directed to the corresponding author/s.'

Ethics statement

Our data comes from the GEO database, GEO belongs to public databases. The patients involved in the database have obtained ethical approval. Users can download relevant data for free for research and publish relevant articles. Our study is based on open source data, so there are no ethical issues or other conflicts of interest. Written informed consent for participation was not required for this study in accordance with the national legislation and the institutional requirements.

Author contributions

KY, ZS and JL conceived of and designed the research plans. ZS, TZ and XS completed data processing and bioinformatics analyses. ZS, JL and TW drafted the manuscript. KY, ZS, and JD checked the manuscript. All authors contributed to the article and approved the submitted version.

Funding

This study was funded by grants from General Program of National Natural Science Foundation of China (81473466, 81873173) and the National Key Research and Development Program of China (2019YFC1708703).

Acknowledgments

We thank the Sangerbox for providing us with the platform as part of the data analysis.

Conflict of interest

The authors declare that the research was conducted in the absence of any commercial or financial relationships that could be construed as a potential conflict of interest.

Publisher's note

All claims expressed in this article are solely those of the authors and do not necessarily represent those of their affiliated organizations, or those of the publisher, the editors and the reviewers. Any product that may be evaluated in this article, or claim that may be made by its manufacturer, is not guaranteed or endorsed by the publisher.

Supplementary material

The Supplementary Material for this article can be found online at: https://www.frontiersin.org/articles/10.3389/fcvm.2023.1121102/full#supplementary-material.

References

1. Decramer M, Janssens W, Miravitlles M. Chronic obstructive pulmonary disease. *Lancet*. (2012) 379:1341–51. doi: 10.1016/S0140-6736(11)60968-9

2. Leong P, Macdonald M, Ko B, Bardin P. Coexisting chronic obstructive pulmonary disease and cardiovascular disease in clinical practice: a diagnostic and therapeutic challenge. *Med J Aust*. (2019) 210:417–23. doi: 10.5694/mja2.50120

3. Chugh S, Havmoeller R, Narayanan K, Singh D, Rienstra M, Benjamin EJ, et al. Worldwide epidemiology of atrial fibrillation: a global burden of disease 2010 study. *Circulation*. (2014) 129:837–47. doi: 10.1161/CIRCULATIONAHA.113.005119

4. Nicoli C, O'Neal W, Levitan E, Singleton M, Judd S, Howard G, et al. Atrial fibrillation and risk of incident heart failure with reduced versus preserved ejection fraction. *Heart*. (2022) 108:353–9. doi: 10.1136/heartjnl-2021-319122

5. Massera D, Wang D, Vorchheimer DA, Negassa A, Garcia M. Increased risk of stroke and mortality following new-onset atrial fibrillation during hospitalization. *Europace*. (2017) 19:929–36. doi: 10.1093/europace/euw110

6. Liao K, Chen C. Incidence and risk factors of atrial fibrillation in Asian COPD patients. *Int J Chron Obstruct Pulmon Dis*. (2017) 12:2523–30. doi: 10.2147/COPD.S143691

7. Konecny T, Park J, Somers K, Konecny D, Orban M, Soucek F, et al. Relation of chronic obstructive pulmonary disease to atrial and ventricular arrhythmias. *Am J Cardiol*. (2014) 114:272–7. doi: 10.1016/j.amjcard.2014.04.030

8. Proietti M, Laroche C, Drozd M, Vijgen J, Cozma D, Drozdz J, et al. Impact of chronic obstructive pulmonary disease on prognosis in atrial fibrillation: a report from the EURObservational research programme pilot survey on atrial fibrillation (EORP-AF) general registry. *Am Heart J*. (2016) 181:83–91. doi: 10.1016/j.ahj.2016.08.011

9. Gu J, Liu X, Tan H, Zhou L, Jiang W, Wang Y, et al. Impact of chronic obstructive pulmonary disease on procedural outcomes and quality of life in patients with atrial fibrillation undergoing catheter ablation. *J Cardiovasc Electrophysiol*. (2013) 24:148–54. doi: 10.1111/j.1540-8167.2012.02448.x

10. Romiti G, Corica B, Pipitone E, Vitolo M, Raparelli V, Basili S, et al. Prevalence, management and impact of chronic obstructive pulmonary disease in atrial fibrillation: a systematic review and meta-analysis of 4,200,000 patients. *Eur Heart J*. (2021) 42:3541–54. doi: 10.1093/eurheartj/ehab453

11. Simons S, Elliott A, Sastry M, Hendriks J, Arzt M, Rienstra M, et al. Chronic obstructive pulmonary disease and atrial fibrillation: an interdisciplinary perspective. *Eur Heart J*. (2021) 42:532–40. doi: 10.1093/eurheartj/ehaa822

12. Wilchesky M, Ernst P, Brophy J, Platt R, Suissa S. Bronchodilator use and the risk of arrhythmia in COPD: part 2: reassessment in the larger Quebec cohort. *Chest*. (2012) 142:305–11. doi: 10.1378/chest.11-1597

13. Huerta C, Lanes S, García Rodríguez L. Respiratory medications and the risk of cardiac arrhythmias. *Epidemiology*. (2005) 16:360–6. doi: 10.1097/01.ede.0000158743.90664.a7

14. Auslander N, Gussow A, Koonin E. Incorporating machine learning into established bioinformatics frameworks. *Int J Mol Sci*. (2021) 22:2903. doi: 10.3390/ijms22062903

15. Barrett T, Wilhite S, Ledoux P, Evangelista C, Kim I, Tomashevsky M, et al. NCBI GEO: archive for functional genomics data sets–update. *Nucleic Acids Res*. (2013) 41:D991–995. doi: 10.1093/nar/gks1193

16. Morrow J, Zhou X, Lao T, Jiang Z, DeMeo D, Cho M, et al. Functional interactors of three genome-wide association study genes are differentially expressed in severe chronic obstructive pulmonary disease lung tissue. *Sci Rep*. (2017) 7:44232. doi: 10.1038/srep44232

17. Tsai F, Lin Y, Chang S, Chang G, Hsu Y, Lin Y, et al. Differential left-to-right atria gene expression ratio in human sinus rhythm and atrial fibrillation: implications for arrhythmogenesis and thrombogenesis. *Int J Cardiol*. (2016) 222:104–12. doi: 10.1016/j.ijcard.2016.07.103

18. Çubukçuoğlu D, Durdu S, Doğan Y, Erdemli E, Özdağ H, Akar A. Molecular signatures of human chronic atrial fibrillation in primary mitral regurgitation. *Cardiovasc Ther*. (2021) 2021. doi: 10.1155/2021/5516185

19. Langfelder P, Horvath S. WGCNA: an R package for weighted correlation network analysis. *BMC Bioinformatics*. (2008) 9:559. doi: 10.1186/1471-2105-9-559

20. Szklarczyk D, Gable A, Nastou K, Lyon D, Kirsch R, Pyysalo S, et al. The STRING database in 2021: customizable protein-protein networks, and functional characterization of user-uploaded gene/measurement sets. *Nucleic Acids Res*. (2021) 49:D605–12. doi: 10.1093/nar/gkaa1074

21. Shannon P, Markiel A, Ozier O, Baliga N, Wang J, Ramage D, et al. Cytoscape: a software environment for integrated models of biomolecular interaction networks. *Genome Res*. (2003) 13:2498–504. doi: 10.1101/gr.1239303

22. Yu G, Wang L, Han Y, He Q. Clusterprofiler: an R package for comparing biological themes among gene clusters. *OMICS*. (2012) 16:284–7. doi: 10.1089/omi.2011.0118

23. Gene Ontology Consortium. The gene ontology resource: enriching a GOld mine. *Nucleic Acids Res*. (2021) 49:D325–34. doi: 10.1093/nar/gkaa1113

24. Subramanian A, Tamayo P, Mootha V, Mukherjee S, Ebert B, Gillette M, et al. Gene set enrichment analysis: a knowledge-based approach for interpreting genome-wide expression profiles. *Proc Natl Acad Sci USA*. (2005) 102:15545–50. doi: 10.1073/pnas.0506580102

25. Jiang H, Zhang X, Wu Y, Zhang B, Wei J, Li J, et al. Bioinformatics identification and validation of biomarkers and infiltrating immune cells in endometriosis. *Front Immunol*. (2022) 13:944683. doi: 10.3389/fimmu.2022.944683

26. Biecek P. DALEX: explainers for complex predictive models in R. *J Mach Learn Res*. (2018) 19:3245–9.

27. Grau J, Grosse I, Keilwagen J. PRROC: computing and visualizing precision-recall and receiver operating characteristic curves in R. *Bioinformatics*. (2015) 31:2595–7. doi: 10.1093/bioinformatics/btv153

28. Franz M, Rodriguez H, Lopes C, Zuberi K, Montojo J, Bader G, et al. GeneMANIA update 2018. *Nucleic Acids Res*. (2018) 46:W60–4. doi: 10.1093/nar/gky311

29. Castro-Mondragon J, Riudavets-Puig R, Rauluseviciute I, Lemma R, Turchi L, Blanc-Mathieu R, et al. JASPAR 2022: the 9th release of the open-access database of transcription factor binding profiles. *Nucleic Acids Res*. (2022) 50. doi: 10.1093/nar/gkab1113

30. Huang H, Lin Y, Cui S, Huang Y, Tang Y, Xu J, et al. miRTarBase update 2022: an informative resource for experimentally validated miRNA-target interactions. *Nucleic Acids Res*. (2022) 50:D222–30. doi: 10.1093/nar/gkab1079

31. Cotto K, Wagner A, Feng Y, Kiwala S, Coffman A, Spies G, et al. DGIdb 3.0: a redesign and expansion of the drug-gene interaction database. *Nucleic Acids Res*. (2018) 46:D1068–73. doi: 10.1093/nar/gkx1143

32. Chen B, Khodadoust M, Liu C, Newman A, Alizadeh A. Profiling tumor infiltrating immune cells with CIBERSORT. *Methods in Mol Biol (Clifton, NJ)*. (2018) 1711. doi: 10.1007/978-1-4939-7493-1_12

33. GBD 2015 Chronic Respiratory Disease Collaborators. Global, regional, and national deaths, prevalence, disability-adjusted life years, and years lived with disability for chronic obstructive pulmonary disease and asthma, 1990-2015: a systematic analysis for the global burden of disease study 2015. *Lancet Respir Med*. (2017) 5:691–706. doi: 10.1016/S2213-2600(17)30293-X

34. Grymonprez M, Vakaet V, Kavousi M, Stricker B, Ikram M, Heeringa J, et al. Chronic obstructive pulmonary disease and the development of atrial fibrillation. *Int J Cardiol*. (2019) 276:118–24. doi: 10.1016/j.ijcard.2018.09.056

35. Huang B, Yang Y, Zhu J, Liang Y, Zhang H, Tian L, et al. Clinical characteristics and prognostic significance of chronic obstructive pulmonary disease in patients with atrial fibrillation: results from a multicenter atrial fibrillation registry study. *J Am Med Dir Assoc*. (2014) 15:576–81. doi: 10.1016/j.jamda.2014.04.009

36. Liu C, Chen Y, Chang Y, Chien W, Lin H, Cheng C, et al. New-Onset atrial fibrillation is a risk factor of ischemic stroke in chronic obstructive pulmonary disease. *Healthcare (Basel)*. (2022) 10:381. doi: 10.3390/healthcare10020381

37. Chen C, Liao K. The impact of atrial fibrillation in patients with COPD during hospitalization. *Int J Chron Obstruct Pulmon Dis*. (2018) 13:2105–12. doi: 10.2147/COPD.S166534

38. Yao Y, Yang M, Liu D, Zhao Q. Immune remodeling and atrial fibrillation. *Front Physiol*. (2022) 13:927221. doi: 10.3389/fphys.2022.927221

39. Barnes P. Inflammatory mechanisms in patients with chronic obstructive pulmonary disease. *J Allergy Clin Immunol*. (2016) 138:16–27. doi: 10.1016/j.jaci.2016.05.011

40. Caramori G, Casolari P, Barczyk A, Durham A, Di S, Adcock I. COPD Immunopathology. *Semin Immunopathol*. (2016) 38:497–515. doi: 10.1007/s00281-016-0561-5

41. Hu Y, Chen Y, Lin Y, Chen S. Inflammation and the pathogenesis of atrial fibrillation. *Nat Rev Cardiol*. (2015) 12:230–43. doi: 10.1038/nrcardio.2015.2

42. Hogg J, Chu F, Utokaparch S, Woods R, Elliott W, Buzatu L, et al. The nature of small-airway obstruction in chronic obstructive pulmonary disease. *N Engl J Med*. (2004) 350:2645–53. doi: 10.1056/NEJMoa032158

43. Saqib U, Sarkar S, Suk K, Mohammad O, Baig M, Savai R. Phytochemicals as modulators of M1-M2 macrophages in inflammation. *Oncotarget*. (2018) 9:17937–50. doi: 10.18632/oncotarget.24788

44. Agustí A, Edwards L, Rennard S, MacNee W, Tal-Singer R, Miller B, et al. Persistent systemic inflammation is associated with poor clinical outcomes in COPD: a novel phenotype. *PLoS One*. (2012) 7:e37483. doi: 10.1371/journal.pone.0037483

45. Sun Z, Zhou D, Xie X, Wang S, Wang Z, Zhao W, et al. Cross-talk between macrophages and atrial myocytes in atrial fibrillation. *Basic Res Cardiol*. (2016) 111:63. doi: 10.1007/s00395-016-0584-z

46. Zhang Y, Cao H, Han X, Teng F, Chen C, Yang J, et al. Chemokine receptor CXCR-2 initiates atrial fibrillation by triggering monocyte mobilization in mice. *Hypertension*. (2020) 76:381–92. doi: 10.1161/HYPERTENSIONAHA.120.14698

47. Williams M, Todd I, Fairclough L. The role of CD8 + T lymphocytes in chronic obstructive pulmonary disease: a systematic review. *Inflamm Res*. (2021) 70:11–8. doi: 10.1007/s00011-020-01408-z

48. Murdoch J, Lloyd C. Resolution of allergic airway inflammation and airway hyperreactivity is mediated by IL-17-producing {gamma}{delta}T cells. *Am J Respir Crit Care Med*. (2010) 182:464–76. doi: 10.1164/rccm.200911-1775OC

49. Kato A, Hulse K, Tan B, Schleimer R. B-lymphocyte lineage cells and the respiratory system. *J Allergy Clin Immunol*. (2013) 131:933–57; quiz 958. doi: 10.1016/j.jaci.2013.02.023

50. Polverino F, Cosio B, Pons J, Laucho-Contreras M, Tejera P, Iglesias A, et al. B cell-activating factor. An orchestrator of lymphoid follicles in severe chronic obstructive pulmonary disease. *Am J Respir Crit Care Med*. (2015) 192:695–705. doi: 10.1164/rccm.201501-0107OC

51. Ladjemi M, Martin C, Lecocq M, Detry B, Nana F, Moulin C, et al. Increased IgA expression in lung lymphoid follicles in severe chronic obstructive pulmonary disease. *Am J Respir Crit Care Med*. (2019) 199:592–602. doi: 10.1164/rccm.201802-0352OC

52. Givi M, Folkerts G, Wagenaar G, Redegeld F, Mortaz E. Cigarette smoke differentially modulates dendritic cell maturation and function in time. *Respir Res*. (2015) 16:131. doi: 10.1186/s12931-015-0291-6

53. Akata K, van Eeden S. Lung macrophage functional properties in chronic obstructive pulmonary disease. *Int J Mol Sci*. (2020) 21:853. doi: 10.3390/ijms21030853

54. Litviňuková M, Talavera-López C, Maatz H, Reichart D, Worth C, Lindberg E, et al. Cells of the adult human heart. *Nature*. (2020) 588:466–72. doi: 10.1038/s41586-020-2797-4

55. Smorodinova N, Bláha M, Melenovský V, Rozsívalová K, Přidal J, Ďurišová M, et al. Analysis of immune cell populations in atrial myocardium of patients with atrial fibrillation or sinus rhythm. *PLoS One*. (2017) 12:e0172691. doi: 10.1371/journal.pone.0172691

56. Begieneman M, Rijvers L, Kubat B, Paulus W, Vonk A, van Rossum A, et al. Atrial fibrillation coincides with the advanced glycation end product N(ε)-(carboxymethyl)lysine in the atrium. *Am J Pathol*. (2015) 185:2096–104. doi: 10.1016/j.ajpath.2015.04.018

57. Wang X, Wang J, Ding Z, Ji J, Sun Q, Cai G. Structural flexibility and functional interaction of mediator Cdk8 module. *Protein Cell*. (2013) 4:911–20. doi: 10.1007/s13238-013-3069-y

58. Chen M, Liang J, Ji H, Yang Z, Altilia S, Hu B, et al. CDK8/19 Mediator kinases potentiate induction of transcription by NFκB. *Proc Natl Acad Sci U S A*. (2017) 114:10208–13. doi: 10.1073/pnas.1710467114

59. Perez-Perri J, Dengler V, Audetat K, Pandey A, Bonner E, Urh M, et al. The TIP60 Complex is a conserved coactivator of HIF1A. *Cell Rep*. (2016) 16:37–47. doi: 10.1016/j.celrep.2016.05.082

60. Shukla S, Walters E, Simpson J, Keely S, Wark P, O'Toole R, et al. Hypoxia-inducible factor and bacterial infections in chronic obstructive pulmonary disease. *Respirology*. (2020) 25:53–63. doi: 10.1111/resp.13722

61. Xu Y, Sharma D, Du F, Liu Y. The role of toll-like receptor 2 and hypoxia-induced transcription factor-1α in the atrial structural remodeling of non-valvular atrial fibrillation. *Int J Cardiol*. (2013) 168:2940–1. doi: 10.1016/j.ijcard.2013.03.174

62. Sun X, Feng X, Zheng D, Li A, Li C, Li S, et al. Ergosterol attenuates cigarette smoke extract-induced COPD by modulating inflammation, oxidative stress and apoptosis in vitro and in vivo. *Clin Sci*. (2019) 133:1523–36. doi: 10.1042/CS20190331

63. Liu M, Li W, Wang H, Yin L, Ye B, Tang Y, et al. CTRP9 Ameliorates atrial inflammation, fibrosis, and vulnerability to atrial fibrillation in post-myocardial infarction rats. *J Am Heart Assoc*. (2019) 8:e013133. doi: 10.1161/JAHA.119.013133

64. Chen X, Yan Y, Cheng X, Zhang Z, He C, Wu D, et al. A novel CDK8 inhibitor with poly-substituted pyridine core: discovery and anti-inflammatory activity evaluation in vivo. *Bioorg Chem*. (2023) 133:106402. doi: 10.1016/j.bioorg.2023.106402

65. Guo Z, Wang G, Lv Y, Wan Y, Zheng J. Inhibition of Cdk8/Cdk19 activity promotes treg cell differentiation and suppresses autoimmune diseases. *Front Immunol*. (2019) 10:1988. doi: 10.3389/fimmu.2019.01988

66. Schmerwitz U, Sass G, Khandoga A, Joore J, Mayer B, Berberich N, et al. Flavopiridol protects against inflammation by attenuating leukocyte-endothelial interaction via inhibition of cyclin-dependent kinase 9. *Arterioscler Thromb Vasc Biol*. (2011) 31:280–8. doi: 10.1161/ATVBAHA.110.213934

67. Rao F, Xue Y, Wei W, Yang H, Liu F, Chen S, et al. Role of tumour necrosis factor-a in the regulation of T-type calcium channel current in HL-1 cells. *Clin Exp Pharmacol Physiol*. (2016) 43:706–11. doi: 10.1111/1440-1681.12585

68. Kao Y, Chen Y, Cheng C, Lee T, Chen Y, Chen S. Tumor necrosis factor-alpha decreases sarcoplasmic reticulum Ca2+-ATPase expressions via the promoter methylation in cardiomyocytes. *Crit Care Med*. (2010) 38:217–22. doi: 10.1097/CCM.0b013e3181b4a854

69. Goudis C, Kallergis E, Vardas P. Extracellular matrix alterations in the atria: insights into the mechanisms and perpetuation of atrial fibrillation. *Europace*. (2012) 14:623–30. doi: 10.1093/europace/eur398

70. Siwik D, Chang D, Colucci W. Interleukin-1beta and tumor necrosis factor-alpha decrease collagen synthesis and increase matrix metalloproteinase activity in cardiac fibroblasts in vitro. *Circ Res*. (2000) 86:1259–65. doi: 10.1161/01.res.86.12.1259

71. Kaku Y, Imaoka H, Morimatsu Y, Komohara Y, Ohnishi K, Oda H, et al. Overexpression of CD163, CD204 and CD206 on alveolar macrophages in the lungs of patients with severe chronic obstructive pulmonary disease. *PLoS One*. (2014) 9:e87400. doi: 10.1371/journal.pone.0087400

72. Vlahos R, Bozinovski S. Role of alveolar macrophages in chronic obstructive pulmonary disease. *Front Immunol*. (2014) 5:435. doi: 10.3389/fimmu.2014.00435

73. Xu J, Cui G, Esmailian F, Plunkett M, Marelli D, Ardehali A, et al. Atrial extracellular matrix remodeling and the maintenance of atrial fibrillation. *Circulation*. (2004) 109:363–8. doi: 10.1161/01.CIR.0000109495.02213.52

74. Abe I, Teshima Y, Kondo H, Kaku H, Kira S, Ikebe Y, et al. Association of fibrotic remodeling and cytokines/chemokines content in epicardial adipose tissue with atrial myocardial fibrosis in patients with atrial fibrillation. *Heart Rhythm*. (2018) 15:1717–27. doi: 10.1016/j.hrthm.2018.06.025

75. Lyu J, Wang M, Kang X, Xu H, Cao Z, Yu T, et al. Macrophage-mediated regulation of catecholamines in sympathetic neural remodeling after myocardial infarction. *Basic Res Cardiol*. (2020) 115:56. doi: 10.1007/s00395-020-0813-3

76. Ravi A, Plumb J, Gaskell R, Mason S, Broome C, Booth G, et al. COPD Monocytes demonstrate impaired migratory ability. *Respir Res*. (2017) 18:90. doi: 10.1186/s12931-017-0569-y

77. Segal L, Martinez F. Chronic obstructive pulmonary disease subpopulations and phenotyping. *J Allergy Clin Immunol*. (2018) 141:1961–71. doi: 10.1016/j.jaci.2018.02.035

78. Hirayama A, Goto T, Shimada Y, Faridi M, Camargo C, Hasegawa K. Acute exacerbation of chronic obstructive pulmonary disease and subsequent risk of emergency department visits and hospitalizations for atrial fibrillation. *Circ Arrhythm Electrophysiol*. (2018) 11:e006322. doi: 10.1161/CIRCEP.118.006322

79. Cepelis A, Brumpton B, Malmo V, Laugsand L, Loennechen J, Ellekjær H, et al. Associations of asthma and asthma control with atrial fibrillation risk: results from the nord-trøndelag health study (HUNT). *JAMA Cardiol*. (2018) 3:721–8. doi: 10.1001/jamacardio.2018.1901

frontiers | Frontiers in Cardiovascular Medicine

TYPE Original Research
PUBLISHED 02 October 2023
DOI 10.3389/fcvm.2023.1189293

Check for updates

OPEN ACCESS

EDITED BY
Alfredo Vellido,
Universitat Politecnica de Catalunya, Spain

REVIEWED BY
Angela Lungu,
Technical University of Cluj-Napoca, Romania
Elena Tolkacheva,
University of Minnesota Twin Cities,
United States

*CORRESPONDENCE
Sanjiv M. Narayan
✉ sanjiv1@stanford.edu

RECEIVED 18 March 2023
ACCEPTED 18 September 2023
PUBLISHED 02 October 2023

CITATION
Feng R, Deb B, Ganesan P, Tjong FVY, Rogers AJ, Ruipérez-Campillo S, Somani S, Clopton P, Baykaner T, Rodrigo M, Zou J, Haddad F, Zahari M and Narayan SM (2023) Segmenting computed tomograms for cardiac ablation using machine learning leveraged by domain knowledge encoding.
Front. Cardiovasc. Med. 10:1189293.
doi: 10.3389/fcvm.2023.1189293

COPYRIGHT
© 2023 Feng, Deb, Ganesan, Tjong, Rogers, Ruipérez-Campillo, Somani, Clopton, Baykaner, Rodrigo, Zou, Haddad, Zahari and Narayan. This is an open-access article distributed under the terms of the Creative Commons Attribution License (CC BY). The use, distribution or reproduction in other forums is permitted, provided the original author(s) and the copyright owner(s) are credited and that the original publication in this journal is cited, in accordance with accepted academic practice. No use, distribution or reproduction is permitted which does not comply with these terms.

Segmenting computed tomograms for cardiac ablation using machine learning leveraged by domain knowledge encoding

Ruibin Feng[1], Brototo Deb[1], Prasanth Ganesan[1], Fleur V. Y. Tjong[1,2], Albert J. Rogers[1], Samuel Ruipérez-Campillo[1,3], Sulaiman Somani[1], Paul Clopton[1], Tina Baykaner[1], Miguel Rodrigo[1,4], James Zou[5], Francois Haddad[1], Matei Zahari[6] and Sanjiv M. Narayan[1]*

[1]Department of Medicine and Cardiovascular Institute, Stanford University, Stanford, CA, United States, [2]Heart Center, Department of Clinical and Experimental Cardiology, Amsterdam UMC, University of Amsterdam, Amsterdam, Netherlands, [3]Bioengineering Department, University of California, Berkeley, Berkeley, CA, United States, [4]CoMMLab, Universitat Politècnica de València, Valencia, Spain, [5]Department of Biomedical Data Science, Stanford University, Stanford, CA, United States, [6]Department of Computer Science, Stanford University, Stanford, CA, United States

Background: Segmentation of computed tomography (CT) is important for many clinical procedures including personalized cardiac ablation for the management of cardiac arrhythmias. While segmentation can be automated by machine learning (ML), it is limited by the need for large, labeled training data that may be difficult to obtain. We set out to combine ML of cardiac CT with domain knowledge, which reduces the need for large training datasets by encoding cardiac geometry, which we then tested in independent datasets and in a prospective study of atrial fibrillation (AF) ablation.

Methods: We mathematically represented atrial anatomy with simple geometric shapes and derived a model to parse cardiac structures in a small set of $N = 6$ digital hearts. The model, termed "virtual dissection," was used to train ML to segment cardiac CT in $N = 20$ patients, then tested in independent datasets and in a prospective study.

Results: In independent test cohorts ($N = 160$) from 2 Institutions with different CT scanners, atrial structures were accurately segmented with Dice scores of 96.7% in internal (IQR: 95.3%–97.7%) and 93.5% in external (IQR: 91.9%–94.7%) test data, with good agreement with experts ($r = 0.99$; $p < 0.0001$). In a prospective study of 42 patients at ablation, this approach reduced segmentation time by 85% (2.3 ± 0.8 vs. 15.0 ± 6.9 min, $p < 0.0001$), yet provided similar Dice scores to experts (93.9% (IQR: 93.0%–94.6%) vs. 94.4% (IQR: 92.8%–95.7%), p = NS).

Conclusions: Encoding cardiac geometry using mathematical models greatly accelerated training of ML to segment CT, reducing the need for large training sets while retaining accuracy in independent test data. Combining ML with domain knowledge may have broad applications.

KEYWORDS

cardiac CT segmentation, machine learning, mathematical modeling, domain knowledge, atrial fibrillation, ablation

1. Introduction

Segmentation of cardiac imaging data is central to several aspects of clinical care, but can be challenging and time consuming. This may hinder the development of large reference databases. In atrial fibrillation (AF), early rhythm control by ablation reduces morbidity and mortality (1), yet segmenting computed tomography (CT) for ablation by annotating the left atrium, pulmonary veins (PVI) and other target sites (2) still requires substantial human intervention even with current cardiac mapping systems (3), which can be time consuming and introduce errors (4).

Machine learning (ML) can automate image segmentation (5). However, one of the biggest challenge in ML applications is the lack of large annotated ground truth data sets identified by LeCun and others (5). This issue is particularly critical in medicine and healthcare applications (6–8) due to technical, privacy, and regulatory concerns. Many publicly available labeled datasets contain ~100 cases (9–11), yet traditional ML studies typically use large cohorts (~70 cases) for training and thus test in only ~30 cases (12–15), which may limit generalizability and hinder wider application (16, 17).

Methods such as transfer learning showed advances in alleviating the need for large training datasets (18, 19). However, many are tailored for medical image classification instead of segmentation (20) or exhibit inconsistent segmentation performance across tasks and datasets (21). Other techniques such as synthetic data generation (22) and data augmentation (23) can artificially enlarge training sets, but risk lacking real-world diversity (24) or introducing bias due to overfitting (25). Indeed, atlases that leverage anatomic knowledge have long been used for image segmentation (26, 27), but their performance will be compromised when faced with anatomic variants unrepresented in the training data (28).

One novel approach is to train ML with conceptual domain (expert) knowledge to potentially reduce the need for massive amounts of data for training (29, 30) (**Figure 1A**), analogous to how humans learn (30). Lake et al. used this approach to generate handwritten characters with human-level performance from 1 exemplar, by parsing characters into simple primitives that were composited to create new characters (31). However, domain knowledge for medical applications is rarely sufficient to reduce training sizes for ML (32, 33).

We hypothesized that ML models could be trained using very small datasets if combined with some mathematical knowledge of the task at hand, or *domain knowledge encoding*. Specifically, we developed mathematical digital models of the cardiac anatomy (the atria) from generic publicly available databases. While we had access to a large dataset of 232 cases, we leveraged domain knowledge to train ML models in a deliberately small cohort,

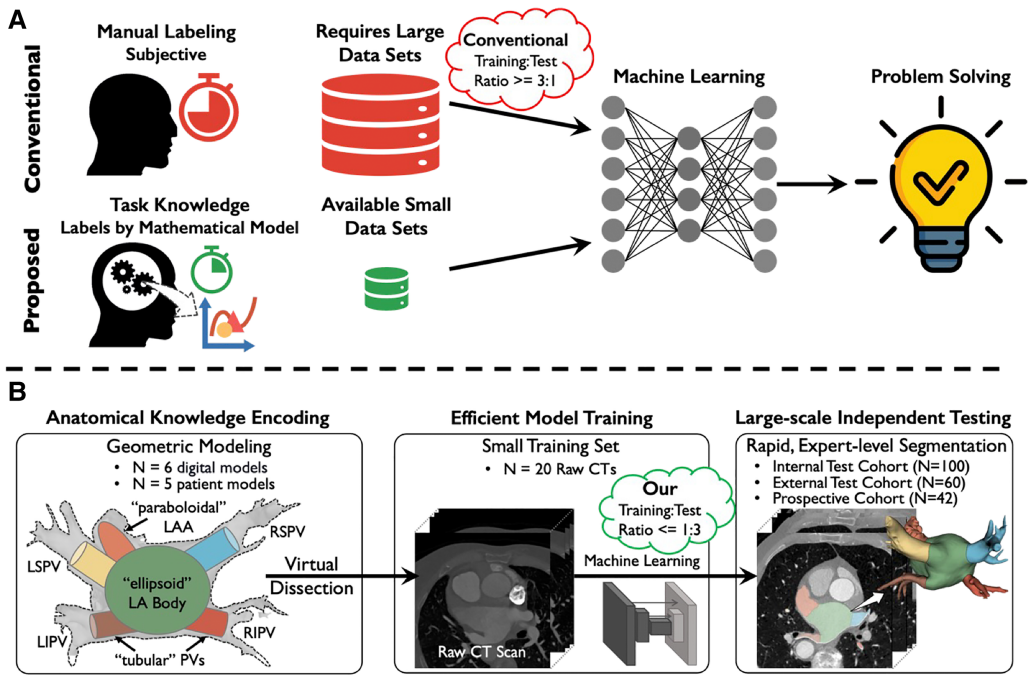


FIGURE 1
Concept and overview. (A) Conventional machine learning (top) can learn patterns in complex data, but requires laborious manual labeling, in large datasets which may be difficult to obtain. Conversely, our proposed approach (bottom) used natural intelligence to replace manual labeling with anatomical concepts encoded mathematically of domain knowledge, to learn rapidly from small datasets. (B) We applied mathematical encoding to segment heart CT scans via ML of small datasets. We represented heart structures as geometric primitives ("virtual dissection"). This was used to train ML on a small dataset ($N = 20$) and was able to accurately segment hearts in 2 larger cohorts from different institutions ($N = 100$, 60). In a prospective study ($N = 42$), the model segmented cardiac CT scans faster, but as accurately as experts. Acronyms: LA, left atrium; LSPV, left superior pulmonary vein; LIPV, left inferior pulmonary vein; RSPV, right superior pulmonary vein; RIPV, right inferior pulmonary vein; LAA, left atrial appendage.

setting aside more cases for testing from 2 large independent datasets. We also tested our model prospectively in a clinical study (**Figure 1B**).

2. Materials and methods

Figure 1B outlines our study design, containing the following steps: (1) We developed algorithms that encode atrial and pulmonary vein anatomies; (2) The algorithm was used to train ML to segment cardiac CT, using a small development cohort; (3) The trained ML was tested in 2 external cohorts from different institutions; (4) The combined domain encoded/ML model was tested prospectively to segment CTs in patients undergoing AF ablation, compared to a panel of 3 experts.

2.1. Development and testing clinical cohort

We identified $N = 130$ consecutive patients who had undergone AF ablation, had CT scans at Stanford Health Care from October 2014 to July 2019, each of whom provided written informed consent. We split this data set randomly into $N = 30$ for algorithm deriving and model training (*Development* cohort), and $N = 100$ patients as a hold-out cohort (*Internal Test* cohort). To further evaluate our approach, we utilized an external publicly available dataset [MM-WHS (10), $N = 60$] from a different institution and different CT scanners (*External Test* cohort).

2.2. Deriving virtual dissection algorithm

We derived our mathematical encoding model from $N = 6$ publicly available 3D heart models (**Figure 2A-1**), built using Gaussian process morphable models (34). We employed these digital models solely as simplified yet accurate templates to facilitate the development, analysis, and tuning of our algorithm.

Inspired by computer graphics (CG) modeling, this "virtual dissection" method identifies critical structures using mathematical encoding (**Figure 2**). CG uses simple geometrical shapes ('primitives') to represent complex objects such as human bodies, that form the basis for techniques such as kinematic modeling that learns 3D human poses from YouTube videos (35) to generate animations. We represented the left atrium (LA) as an ellipsoid; pulmonary veins (PVs) as circular cylinders; and left atrial appendage (LAA) as a paraboloid (**Figure 2A-1**).

We then reasoned that heart structures can be geometrically parsed by separating the ellipsoidal convex LA from the complex concave whole heart. We used mathematical erosion, dilation (36) and subtraction for this purpose (**Figure 2A**). First, we dissected digital shells by a novel application of erosion of concave junctions between tubular PVs and paraboloidal LAA with the ellipsoidal left atrium. We propose an *Erosion Index*, which indicates erosion progression toward a convex shape and can be used to identify the optimal number of erosion iterations (**Figure 2B**). We then applied dilation to ensure the LA retained its original size after erosion and introduced a *Dilation Index* to track the restoration process, which helps determine when to stop dilation before PVs and LAA are re-attached (**Figure 2C**).

To encode the variability of LA geometries across patients, we optimized the virtual dissection algorithm using small clinical seed data from $N = \{0, 5, 10, 20, 30\}$ patients in the *Development* cohort. We trained support vector machines (SVMs) with manually segmented images in patients from the seed sets to predict the optimal number of erosion and dilation iterations.

After the left atrium body is isolated after erosion and dilation, we refined boundaries between the LA body and the PVs and LAA (**Figure 2A-3**) by calculating centerlines from the LA centroid to the centroid of each virtually dissected structure using the Voronoi diagram (37), a method previously used in aorta and great vessels segmentation (9, 38, 39). The original boundaries from the erosion-dilation phase were then refined using a plane aligned perpendicularly to these centerlines. Accuracy of virtual dissection was assessed by centroid-boundary distance and other metrics outlined below in Statistical Analysis.

2.3. Small cohorts of virtually dissected atria can train ML for CT segmentation

We used virtually dissected atria of $N = 20$ patients from the *Development* cohort to train ML to segment chest CT scans. We trained a deep neural network architecture, nnU-Net (**Supplementary Figure 1**), which has been widely used in 23 public datasets (40). For training, we normalized then augmented raw CT scans as input, with the virtual dissected atria as ground truths. We ensured similar voxel spacing for test and training samples. The training protocol is detailed in **Supplementary Methods**. We applied the trained ML to the independent *Internal Test* and the *External Test* cohorts, neither of which was used for training. Accuracy of ML segmentation was assessed by Dice similarity coefficient and other metrics outlined below in Statistical Analysis.

2.4. Prospective study

We prospectively compared our ML approach to experts for segmenting cardiac CT scans in patients prior to AF ablation. The primary endpoints were annotation time and accuracy as assessed by Dice similarity coefficient. The study was approved by the review board of Stanford University Human Subjects Protection Committee, and all subjects gave written informed consent (NCT02997254).

Patient entry criteria were patients undergoing ablation for symptomatic AF refractory to at least one anti-arrhythmic medication between January 1st, 2022, and March 30th, 2022 ($N = 96$). The predefined exclusion criteria were (1) no valid DICOM files (25 cases), (2) CT performed >90 days before ablation (21 cases), and (3) with LAA closure procedures (8 cases). We identified $N = 42$ consecutive patients (Prospective cohort). CT images in our prospective study were scanned using the third-generation dual-source CT system (Somatom Force;

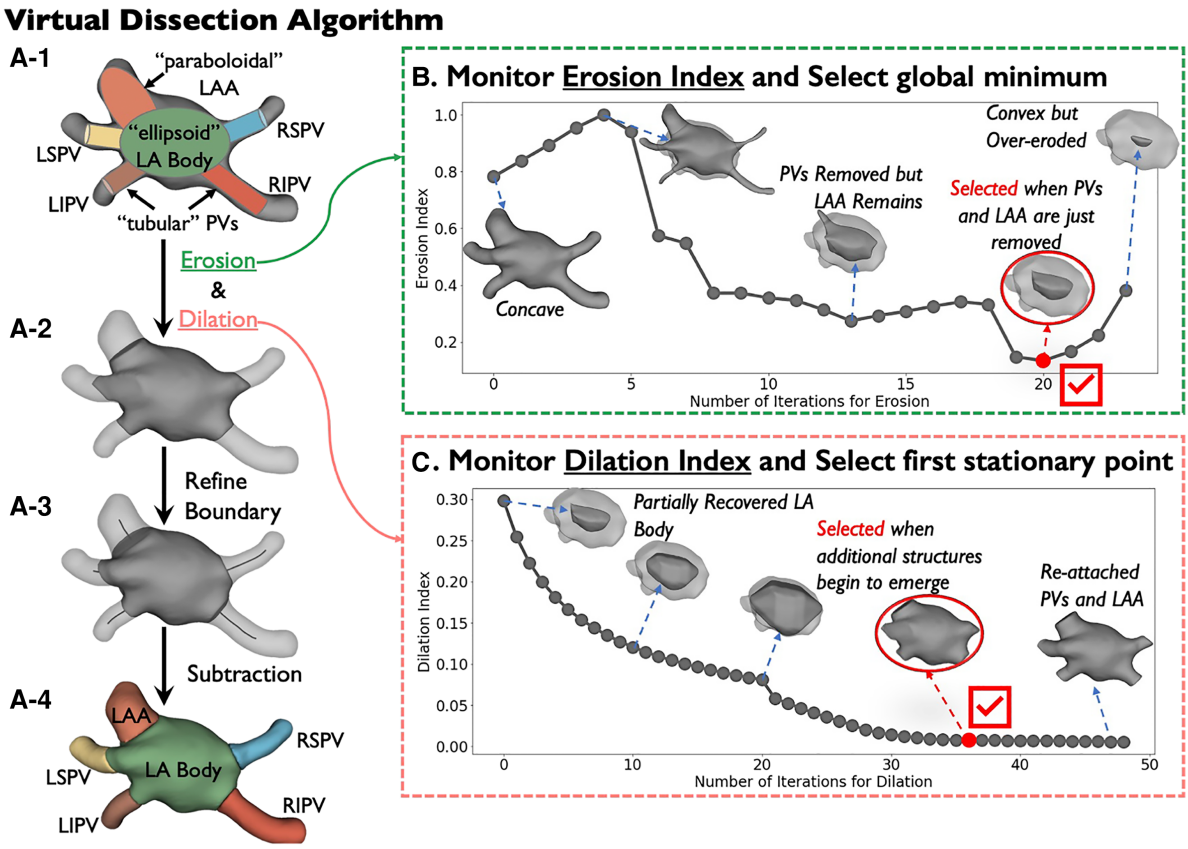


FIGURE 2
Virtual Dissection algorithm. (A) The detailed pipeline. (B) The progress of the iterative erosion. The automatically selected iteration for erosion is highlighted in red. (C) The progress of the iterative dilation. The automatically selected iteration for dilation is highlighted in red. Acronyms: LA, left atrium; LSPV, left superior pulmonary vein; LIPV, left inferior pulmonary vein; RSPV, right superior pulmonary vein; RIPV, right inferior pulmonary vein; LAA, left atrial appendage.

Siemens AG). The CT images had axial sections of 0.7 mm thickness and typical in-plane pixel size of 0.42×0.42 mm.

A panel of 3 experts manually annotated raw CT scans with 3D slicer (41) independently. Each expert had first practiced on several run-in cases, separate from the study cohort, to become familiar with the workflow. During annotation, a bounding box was initially created to identify the LA (including the main branches of PVs and LAA). Several foreground/background seeds were added to these regions, and the region-growing algorithm was applied to get the initial LA geometry. Manual corrections were performed as needed with no further constraints. The final LA segmentation was smoothed using default parameters and exported as a NIFTI file for evaluation. The time taken from loading the CT to exporting the file was recorded for comparison.

2.5. Statistical analysis

We utilized a newly designed metric, the centroid-boundary distance, along with two standard metrics for segmentation tasks (9–15)—Dice similarity coefficient and average surface distance, to evaluate our model's accuracy in capturing 2D LA-PV/LAA boundaries, the global 3D structures, and the local 3D shapes and contours, respectively. Mathematically, the centroid-boundary distance is calculated as the average of all the distances from the centroid of the heart to points on the LA-PV/LAA boundary. The Dice similarity score measures spatial overlap between the model prediction and the ground truth, while 0 indicates no overlap and 1 indicates complete overlap, which can be mathematically expressed as

$$Dice\ Similarity\ Score = \frac{2 \times True\ Positive}{2 \times True\ Positive + False\ Positive + False\ Negative}.$$

The average surface distance is calculated as the average of all the distances from points on the boundary from model prediction to the ground truth boundary. We also measure the success rate of the *virtual dissection* algorithm, where a heart model is successfully parsed if the Intersect over Union (IoU) between the algorithm prediction and expert manual annotation is larger than 0.5. This metric has been widely used for detection tasks (42).

We expressed continuous data by mean ± SD and categorical data by percentages. The distance and Dice scores were summarized as medians and interquartile range (IQR). Pearson correlation's test was used to assess the similarity of LA volumes and LA sphericity Index estimated from model prediction and ground truth. Student's *t*-test, Chi-square test, or McNemar's test was applied as appropriate. $p < 0.05$ was considered as significant.

3. Results

3.1. Study populations

The demographics of the development, internal test and prospective cohorts are shown in **Table 1**. There were no statistical differences in demographics between cohorts except for a higher incidence of diabetes mellitus in the *Development* vs. *Internal Test* cohorts.

3.2. Virtual dissection can automatically parse cardiac geometry

In digital hearts, our developed virtual dissection approach separated the PVs and LAA from left atrial bodies (**Figure 3A**) with a mean difference for the centroid-boundary distances of −0.27 mm (95% CI: −3.87–3.33; $r = 0.99$; $p < 0.0001$; **Figure 3B**). We randomly selected 5 shells of seed data from the *Development* cohort for tuning, with LA sizes from 71 to 140 ml that cover a broad range of patients (43).

In our *Internal Test* cohort ($N = 100$), we compared the optimized-virtual dissection to expert annotation using commercially available software (EnSite Verismo Segmentation Tool; Abbott/St Jude Medical, Inc., St. Paul, Minnesota) refined using 3D Slicer (41). **Figure 3E** shows the success rate of dissection. Accuracy increased from 67% (no tuning) to 94% by tuning with $N = 5$ shells of seed data ($p = 0.034$; McNemar's test), then showed only modest changes when tuning in 10–30 shells (92%–94%). Tuned with $N = 5$ seed data, virtual dissection produced mean difference and limits of agreement for the centroid-boundary distance of 1.46 mm (95% CI: −5.58–8.49; $r = 0.99$; $p < 0.0001$; **Figure 3D**). **Figure 3C** presents two virtually dissected (left) and manually annotated (right) atria.

3.3. ML trained by virtual dissection can accurately segment CT

Figure 4 shows comparisons between ML prediction (left) and manually labeled (right) atria from select samples, representing the 25th, 50th, and 75th percentile accuracy in the hold out *Internal Test* cohort ($N = 100$). Our ML model revealed LA structure, and successfully captured the shape and details of PVs, LAA, and their ostia. The mitral valve plane in the 50th- and 25th-percentile samples showed slight qualitative inconsistencies between ML prediction and ground truth, possibly due to variations in image quality such as density of contrast. Slight differences in LSPV and RSPV measurements were found in the 25th-percentile sample, but the ostia position differences between ML and expert annotations are limited, with LA-LSPV and LA-RSPV boundary errors in a range of 3.54 mm and 0.49 mm, respectively; these differences may not be clinically relevant. Overall, Dice scores were 96.7% (IQR: 95.3% – 97.7%) (**Figure 5A**, left), a median error in surface distance of boundaries of 1.51 mm (IQR: 0.72 – 3.12)) (**Figure 5B**) with a mean boundary distance of 1.16 mm (95% CI: −4.57–6.89) again similar to experts ($r = 0.99$; $p < 0.001$, **Figure 5C-D**).

In our External Test cohort ($N = 60$) of patients from another Institution with different scanners (10), the model segmented structures with a Dice score of 93.5% (IQR: 91.9% to 94.7%) (**Figure 5A**, right) again comparing favorably to experts ($r = 0.99$; $p < 0.0001$).

Thus, this approach enabled a > 10-fold reduction in the relative size of training to test cases for ML, inverting the ratio of training: test cases less than 1:3, from a typical ratio of >3:1.

3.4. Analysis of Anatomical Variants

Despite not pre-screening to eliminate anatomic variants, segmentation accuracy from our virtual dissection technique was maintained for variant anatomy. Overall, 100% cases with 4 PV ostia (the most common configuration, representing 66 cases) were parsed with mean difference and limits of agreement for the centroid-boundary distance of 1.26 mm (95% CI: −5.15–7.68; $r = 0.99$; $p < 0.0001$). We identified 29 cases with one of the 3 main variants: (1) common left PV ostia ($N = 8$; **Supplementary Figure 2A**); (2) LAA occlusion by a closure device ($N = 1$; **Supplementary Figure 2B**); and (3) supplemental PVs or ostial-branch PV ($N = 20$; **Supplementary Figures 2C,D, G,H**). The remaining 5 cases have a combination of these 3 main variants (**Supplementary Figures 2E,F**).

TABLE 1 Clinical demographics of retrospective and prospective study.

	Retrospective cohort ($N = 130$)			Prospective cohort ($N = 42$)	*p*-value	
	Entire cohort ($N = 130$)	Development cohort ($N = 30$)	Internal test cohort ($N = 100$)		Development vs. internal test	Development vs. prospective
Age, year, mean ± SD	64.8 ± 9.8	65.6 ± 10.1	64.6 ± 9.7	65.2 ± 10.6	0.64	0.88
Male gender, *N* (%)	95 (73.1%)	21 (70.0%)	74 (74.0%)	24 (57.1%)	0.39	0.05
Non-paroxysmal AF, *N* (%)	69 (53.1%)	16 (53.3%)	53 (53.0%)	18 (42.9%)	0.97	0.38
BMI, kg/m^2, mean ± SD	29.7 ± 5.7	30.5 ± 5.0	29.43 ± 5.9	29.6 ± 6.9	0.33	0.52
Diabetes, N (%)	16 (12.3%)	7 (23.3%)	9 (9.0%)	5 (11.9%)	0.04	0.20
CHA2DS2-VASc score, mean ± SD	2.2 ± 1.4	2.3 ± 1.2	2.2 ± 1.8	2.1 ± 1.3	0.38	0.37
Smokers, *N* (%)	51 (39.2%)	16 (53.3%)	35 (35.0%)	14 (33.3%)	0.08	0.07
Enlarged LA, *N* (%)	77 (59.2%)	19 (63.3%)	58 (58.0%)	19 (45.2%)	0.60	0.13

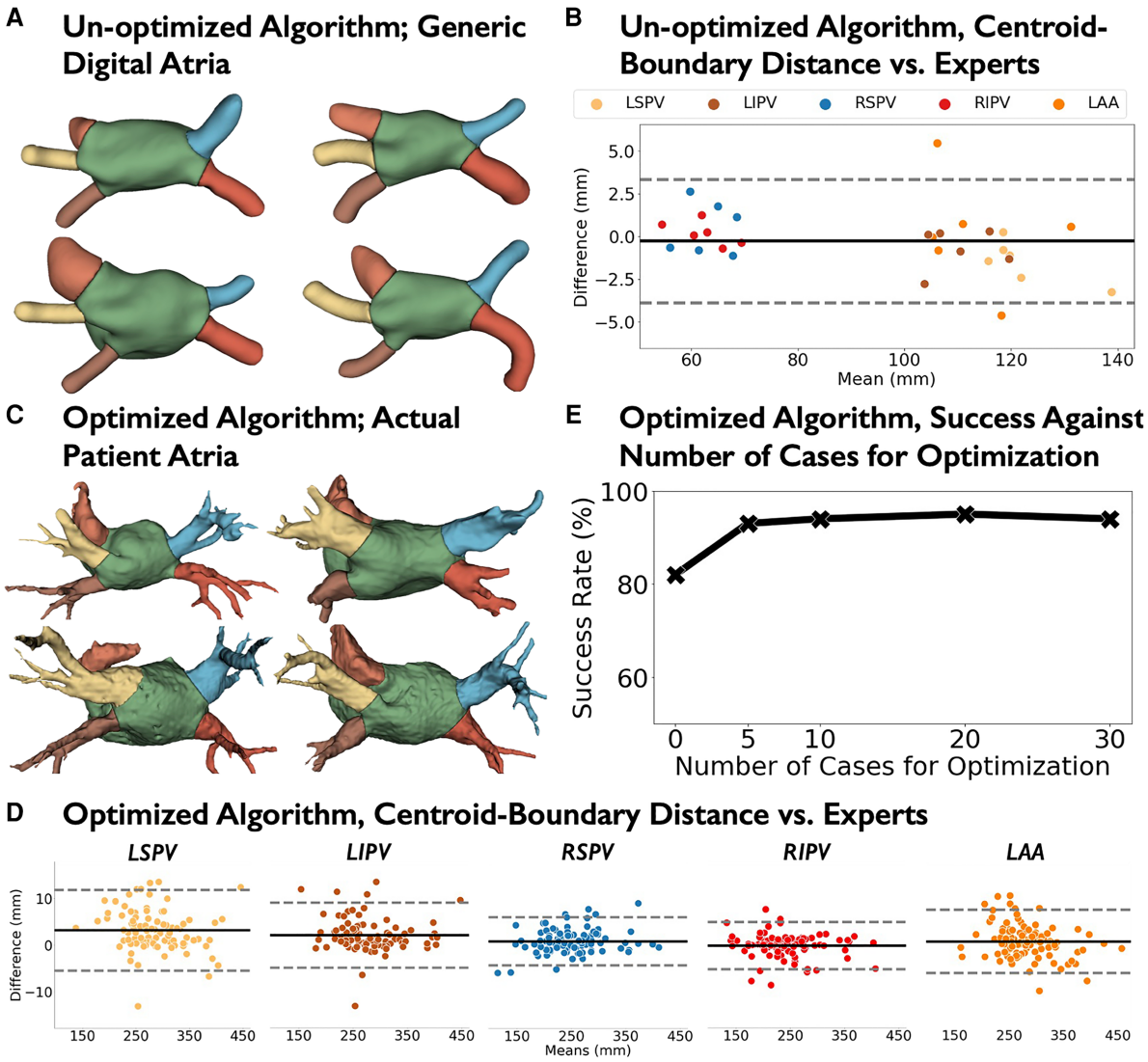


FIGURE 3
Virtual dissection performance. (A) Representative samples of digital atria geometrically parsed by un-optimized algorithm. (B) Bland-Altman plots of the centroid-to-boundary of un-optimized algorithm vs. experts in 6 digital atria. After optimizing Virtual Dissection with $N = 5$ patient cases from the development cohort, (C) Representative patient atria from optimized algorithm in independent Test cohort ($N = 100$). (D) Bland–Altman plots of the centroid-to-boundary distance of optimized algorithm vs. experts in the Test cohort. (E) Success rate of virtual dissection algorithm using N={0, 5, 10, 20, 30} cases. Acronyms: LSPV, left superior pulmonary vein; LIPV, left inferior pulmonary vein; RSPV, right superior pulmonary vein; RIPV, right inferior pulmonary vein; LAA, left atrial appendage.

In summary, 28/34 of identified variants were successfully parsed with anatomic agreement within 1.95 mm (95% CI: −6.34–10.25) which again was in line with experts ($r = 0.99$; $p < 0.0001$), despite lack of specific training in variants. In the remaining 6 cases, errors arose mostly from missing PVs or branches relative to the 4 PV mathematical model (Figure 2A-1), which could be addressed by geometric models that adapt to a range of PVs.

3.5. Prospective validation: using virtual-dissection trained ML to segment left atria

Prospectively, in patients prior to AF ablation, the ML model shortened mean left atrial/PV segmentation time by 85.0% compared to the expert panel (2.3 ± 0.8 vs. 15.0 ± 6.9 min, $p < 0.0001$; Figures 6A,B). Figure 6C shows that our model achieved a Dice score of 93.9% (IQR: 93.0%–94.6%) compared to a panel of 3 experts, statistically indistinguishable from the inter-observer agreement between experts of 94.4% (IQR: 92.8%–95.7%, $p = 0.071$).

To further analyze CT segmentation by our geometrically encoded ML, we compared the left atrial volume and sphericity index between ML and expert readings. These indices are well reported measures of abnormal left atrial size and shape that predict recurrence of AF after drug therapy or ablation (44, 45). Figures 6D,E shows that they were well correlated ($r = 0.99$ and 0.95, respectively; $p < 0.0001$).

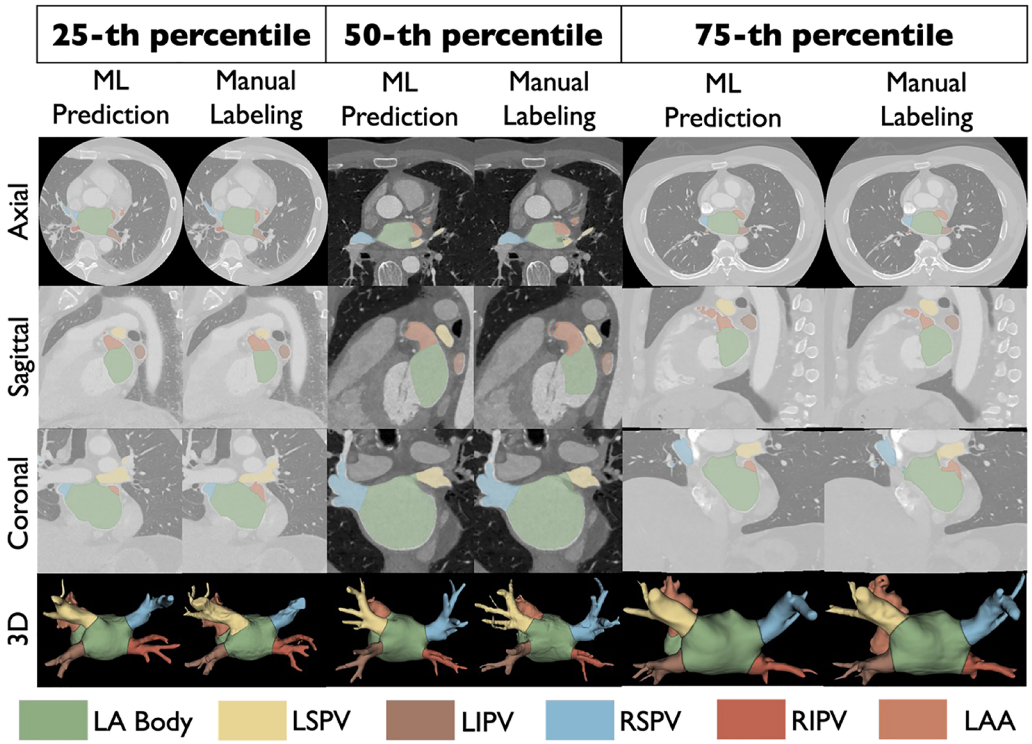


FIGURE 4
Comparison between the ML model predicted CT segmentation (left) and ground truth manual outlining (right) overlaid on the input CT scans in representative samples selected using 25th, 50th and 75th percentiles of segmentation accuracy in an independent test cohort ($N = 100$). Our ML model effectively captured the LA geometry, highlighting key features of PVs, LAA, and their ostia. The mitral valve plane represented in the 50th- and 25th- percentile samples showed slight variation between ML prediction and manual labeling, likely from limited image quality. Slight differences in PV measurements were found in the 25th-percentile sample, which may not be clinically relevant. Acronyms: LA, left atrium; LSPV, left superior pulmonary vein; LIPV, left inferior pulmonary vein; RSPV, right superior pulmonary vein; RIPV, right inferior pulmonary vein; LAA, left atrial appendage.

4. Discussion

Mathematical encoding of geometry was able to accelerate ML for segmentation of CT, and enable its training on very small datasets. In our study, the training: testing ratio was <1 training to 3 test, which indicates a far lower need for training than the conventional published ratios of >3:1 for ML (11–15). This "inversed training-test ratio" paradigm has recently been applied in domains outside medicine such as for Amazon co-purchasing product predictions (46). Our approach was then tested in two independent test datasets and in a prospective study prior to AF ablation, in which the model accelerated segmentation while maintaining similar accuracy to experts. This novel approach could broaden the ease of access and accuracy of AF ablation. More broadly, this approach has analogies to natural intelligence, which has the potential to reduce the need for large annotated datasets to train ML, and could be applied for diverse imaging applications.

4.1. Benefits for clinical applications

Cardiac CT is increasingly used (12, 14, 47) to guide ablation forAF, and to predict clinical endpoints such as the risk of AF recurrence (45, 48). However, segmentation of these large 70–200 MB datasets manually by experts may take up to tens of minutes (9–12) even with the latest commercial software (49, 50). Our prospective validation demonstrated ML models reduced segmentation time by 10–15 min, representing a reduction of 15%–20% from reported PVI case times of 60–100 min (51, 52), and a larger reduction compared to some recently reported segmentation times of 60–120 min (9–12).

Additionally, existing cardiac mapping systems like Carto® 3 (3) require manual input, and their segmentation varies based on the operator's skill and experience. In contrast, our approach offers a fast and fully automatic solution with ensured consistency. It also allows for manual review and editing if desired.

Moreover, our automated segmentation approach provides an efficient way to label and collect large databases—a feature not available in current cardiac mapping systems like Carto® 3 and Rhythmia, which store data in proprietary formats that are not readily accessible to researchers, and require manual input which hinders scalability.

4.2. Comparison to other studies for ML segmentation of cardiac anatomy

We compared our approach with 4 recent ML studies using traditional large training datasets to segment LA from CT scans (12–15). Baskaran et al. and others (12–15) trained in 73–230

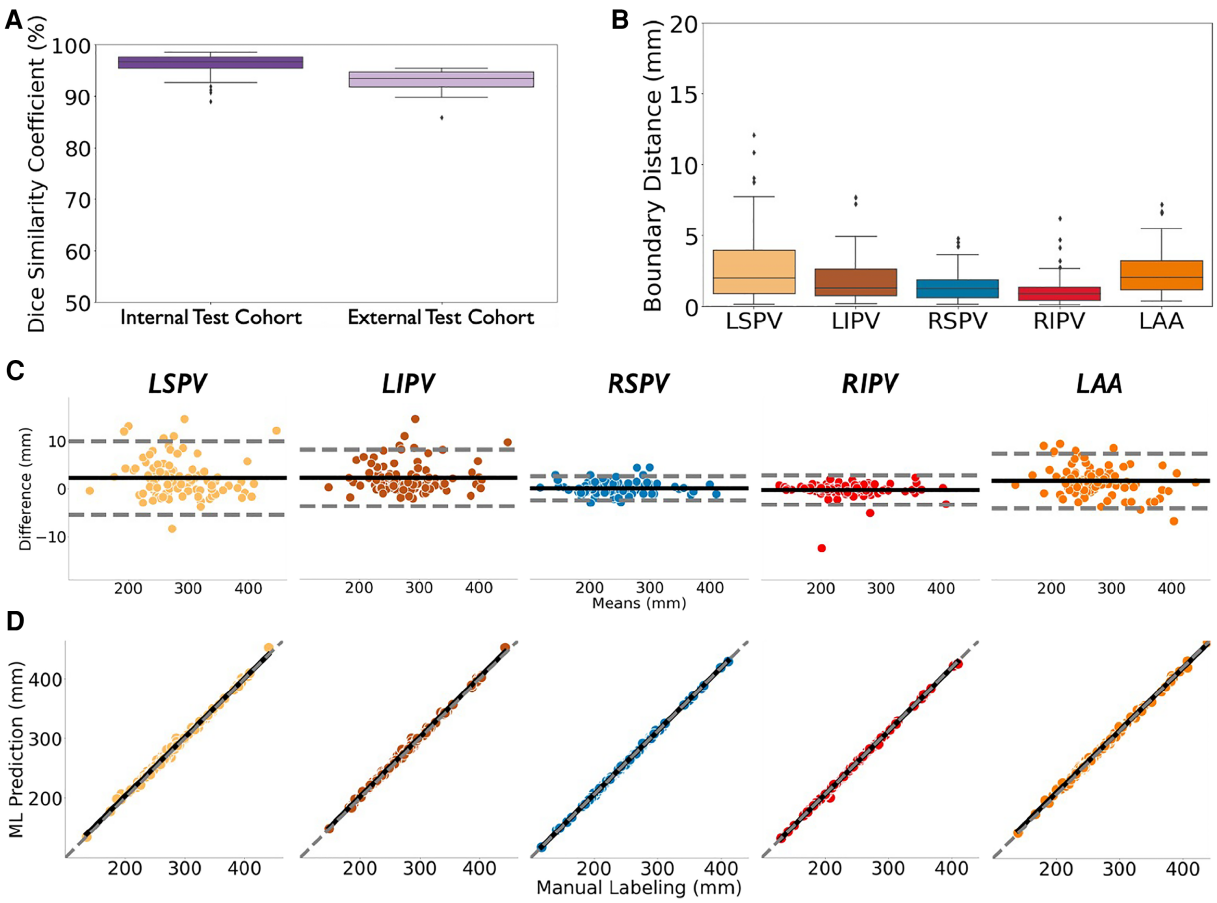


FIGURE 5
Accuracy CT segmentation using ML of optimized virtual dissection in two test cohorts (A) dice score of ML-based CT segmentation in the internal test cohort ($N = 100$; left) and an external test cohort from a different institution with different CT scanners ($N = 60$; right). (B) Boundary surface distances between ML-prediction and expert labelling in the Test Dataset ($N = 100$). (C) and (D) are Bland–Altman plots and linear regression plots of the centroid-to-boundary distance in the Test Dataset ($N = 100$). Acronyms: LSPV, left superior pulmonary vein; LIPV, left inferior pulmonary vein; RSPV, right superior pulmonary vein; RIPV, right inferior pulmonary vein; LAA, left atrial appendage.

cases using manual segmentations, and only tested in 17–37 cases with a maximum Dice of 95.6% (14). Our model used 3–10 times fewer training data yet outperformed on a test set 3–5 times larger. Our model also showed superior generalizability in external and prospective test cohorts, not included in (12–15).

Our approach circumvents the limitation that most CT studies that segmented the LA often did not specifically segment the PVs and LAA (12, 14). Our approach can accurately reveal other anatomical landmarks, evidenced by our ML model's high Dice score (96.7%) compared to experts. **Supplementary Figure 3** illustrates that our ML model successfully identifies the roof and septal walls, which play a significant role in cardiac mapping and AF ablation procedures (53, 54). Our approach can also be applied to other cardiac imaging applications including segmentation of Magnetic Resonance Imaging (MRI) to boost ML by reducing the need for large training data sets.

4.3. Limitations

This study has several limitations. We used only CT and, although this is by far the most widely applied cardiac imaging modality, future studies could extend our approach to MRI through transfer learning. While we tested our approach in cohorts from different institutions, additional studies are needed to define its sensitivity to data from a wide variety of scanners and spatial resolutions. We focused on improving left atrial segmentation, because it is an important and common clinical task, but future studies should extend to other features such as segmenting CT scans to study the aorta for aneurysmal dilation (55), which has a high mortality rate (56), or to plan aortic valve replacement (57), which is commonly performed (58). One limitation and future direction for this work is to adapt our domain knowledge encoding algorithm for different variants, including but not limited to a range of PVs, or congenital variants in the ventricles or aorta (57).

5. Conclusion

Domain knowledge encoding of cardiac geometry was able to train Machine Learning to segment cardiac CT while greatly reducing the need for large training data sets. Our approach

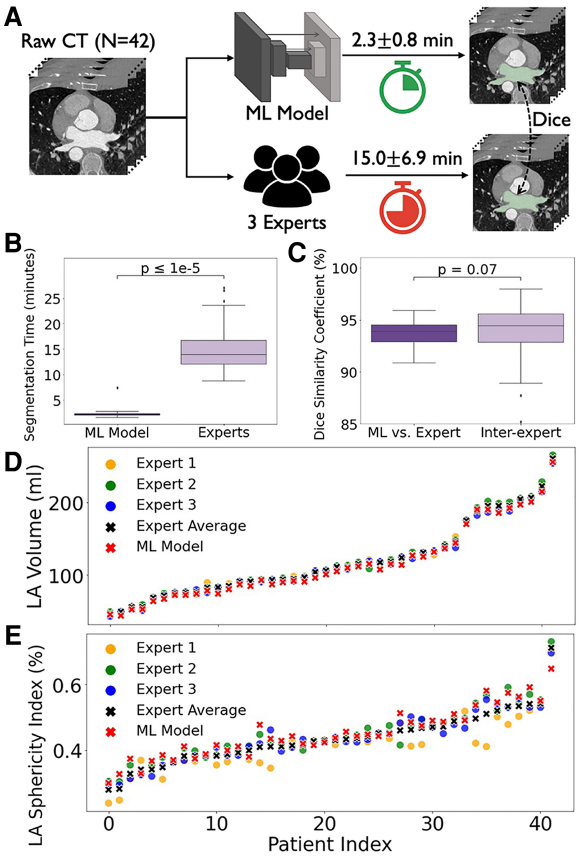


FIGURE 6
Prospective segmentation of cardiac CT scans in 42 consecutive patients undergoing AF ablation by virtual-dissection trained ML vs. experts. (**A**,**B**) Virtual dissection trained ML significantly shortens segmentation time compared to experts. (**C**) Box plots of Dice similarity coefficient between ML and experts were similar. (**D**) and (**E**) LA volume and LA sphericity index marked by Virtual Dissection (red cross) accurately tracks the mean between experts (black cross).

(virtual dissection) derived in very small datasets was able to accurately segment cardiac CT in 2 independent datasets of hundreds of patients and in a prospective study prior to AF ablation. In general, this combined domain knowledge encoding and machine learning approach reduce the dependence of ML on large training datasets and could be applied broadly in imaging and benefit personalized cardiovascular medicine.

Data availability statement

The 3D digital heart models can be found in online repository: https://zenodo.org/record/4309958#%23.YdlOJRPMJqs. The external dataset MM-WHS can be publicly accessed at http://www.sdspeople.fudan.edu.cn/zhuangxiahai/0/mmwhs/. The remaining datasets presented in this article are not readily available because the internal datasets for retrospective and prospective studies are not currently permitted for public release due to the sensitive nature of patient data. Requests to access the datasets should be directed to RF, ruibin@stanford.edu.

Ethics statement

The studies involving humans were approved by Stanford University Human Subjects Protection Committee. The studies were conducted in accordance with the local legislation and institutional requirements. The participants provided their written informed consent to participate in this study.

Author contributions

RF contributed to the conception and design of the study, mathematics and machine learning based modeling, data analysis, and the manuscript writing. BD, PG, and FT contributed to data curation and assisted in the conception and design of the study. AR, SR-C, SS, and MR participated in the design of the study. PC contributed to the design of the study, data analysis, and interpretation of results. JZ and MZ assisted in the conception, design, and supervision of the study. SN participated in the conception and design of the study, contributed to the dataset, analysis and interpretation of results, manuscript writing, supervised and obtained funding for the study. All authors contributed to the article and approved the submitted version.

Funding

Research reported in this publication was supported by grants from the National Institutes of Health under award numbers R01 HL149134 and R01 HL83359.

Acknowledgments

We would like to express our gratitude to Dr. Hui Ju Chang for helping with data collection, and Ms. Kelly Brennan for helping revise the manuscript.

Conflict of interest

SN reports grant support from the National Institutes of Health (R01 HL149134 and R01 HL83359), consulting from Uptodate Inc., and TDK Inc., intellectual property owned by University of California Regents and Stanford University. FT: Consulting honoraria to institution from Abbott, Boston Scientific, Daiichi Sankyo; no personal gain. AR: grants from NIH (F32HL144101), NIH LRP, and Stanford SSPS.

PC: consulting at American College of Cardiology. MR: equity interests in Corify Health Care.

The remaining authors declare that the research was conducted in the absence of any commercial or financial relationships that could be construed as a potential conflict of interest.

Publisher's note

All claims expressed in this article are solely those of the authors and do not necessarily represent those of their affiliated organizations, or those of the publisher, the editors and the reviewers. Any product that may be evaluated in this article, or claim that may be made by its manufacturer, is not guaranteed or endorsed by the publisher.

Supplementary material

The Supplementary Material for this article can be found online at: https://www.frontiersin.org/articles/10.3389/fcvm.2023.1189293/full#supplementary-material

References

1. Kirchhof P, Camm AJ, Goette A, Brandes A, Eckardt L, Elvan A, et al. Early rhythm-control therapy in patients with atrial fibrillation. *N Engl J Med*. (2020) 383 (14):1305–16. doi: 10.1056/NEJMoa2019422

2. Narayan SM, Baykaner T, Clopton P, Schricker A, Lalani GG, Krummen DE, et al. Ablation of rotor and focal sources reduces late recurrence of atrial fibrillation compared with trigger ablation alone: extended follow-up of the confirm trial (conventional ablation for atrial fibrillation with or without focal impulse and rotor modulation). *J Am Coll Cardiol*. (2014) 63(17):1761–8. doi: 10.1016/j.jacc.2014.02.543

3. Biosense Webster I. Carto® 3 System Instructions for Use (V3.2.3) (2015). Available from: https://www.e-ifu.com/search-document-metadata/CARTO%C2%AE%203%20SYSTEM%20INSTRUCTIONS%20FOR%20USE

4. Zhu J, Liu Y, Zhang J, Wang Y, Chen L. Preliminary clinical study of the differences between interobserver evaluation and deep convolutional neural network-based segmentation of multiple organs at risk in Ct images of lung cancer. *Front Oncol*. (2019) 9:627. doi: 10.3389/fonc.2019.00627.

5. LeCun Y, Bengio Y, Hinton G. Deep learning. *Nature*. (2015) 521(7553):436–44. doi: 10.1038/nature14539

6. Topol EJ. High-performance medicine: the convergence of human and artificial intelligence. *Nat Med*. (2019) 25(1):44–56. doi: 10.1038/s41591-018-0300-7

7. Esteva A, Robicquet A, Ramsundar B, Kuleshov V, DePristo M, Chou K, et al. A guide to deep learning in healthcare. *Nat Med*. (2019) 25(1):24–9. doi: 10.1038/s41591-018-0316-z

8. Sapoval N, Aghazadeh A, Nute MG, Antunes DA, Balaji A, Baraniuk R, et al. Current progress and open challenges for applying deep learning across the biosciences. *Nat Commun*. (2022) 13(1):1–12. doi: 10.1038/s41467-022-29268-7

9. Tobon-Gomez C, Geers AJ, Peters J, Weese J, Pinto K, Karim R, et al. Benchmark for algorithms segmenting the left atrium from 3d ct and mri datasets. *IEEE transactions on Medical Imaging*. (2015) 34(7):1460–73. doi: 10.1109/TMI.2015.2398818

10. Zhuang X, Li L, Payer C, Štern D, Urschler M, Heinrich MP, et al. Evaluation of algorithms for multi-modality whole heart segmentation: an open-access grand challenge. *Med Image Anal*. (2019) 58:101537. doi: 10.1016/j.media.2019.101537

11. Xu X, Wang T, Zhuang J, Yuan H, Huang M, Cen J, et al., editors. Imagechd: a 3d computed tomography image dataset for classification of congenital heart disease. *International conference on medical image computing and computer-assisted intervention*. Lima, Peru: Springer (2020). p. 77–87.

12. Baskaran L, Maliakal G, Al'Aref SJ, Singh G, Xu Z, Michalak K, et al. Identification and quantification of cardiovascular structures from ccta: an End-to-End, rapid, pixel-wise, deep-learning method. *Cardiovasc Imaging*. (2020) 13 (5):1163–71.

13. Xu H, Niederer SA, Williams SE, Newby DE, Williams MC, Young AA.editors. Whole heart anatomical refinement from ccta using extrapolation and parcellation. *International conference on functional imaging and modeling of the heart*. Springer (2021). p. 63–70.

14. Chen H-H, Liu C-M, Chang S-L, Chang PY-C, Chen W-S, Pan Y-M, et al. Automated extraction of left atrial volumes from two-dimensional computer tomography images using a deep learning technique. *Int J Cardiol*. (2020) 316:272–8. doi: 10.1016/j.ijcard.2020.03.075

15. Xie W, Yao Z, Ji E, Qiu H, Chen Z, Guo H, et al. Artificial intelligence–based computed tomography processing framework for surgical telementoring of congenital heart disease. *ACM J Emerg Technol Comput Syst*. (2021) 17(4):1–24. doi: 10.1145/3457613

16. Gianfrancesco MA, Tamang S, Yazdany J, Schmajuk G. Potential biases in machine learning algorithms using electronic health record data. *JAMA Intern Med*. (2018) 178(11):1544–7. doi: 10.1001/jamainternmed.2018.3763

17. Futoma J, Simons M, Panch T, Doshi-Velez F, Celi LA. The myth of generalisability in clinical research and machine learning in health care. *Lancet Digit Health*. (2020) 2(9):e489–e92. doi: 10.1016/S2589-7500(20)30186-2

18. Balestriero R, Ibrahim M, Sobal V, Morcos A, Shekhar S, Goldstein T, et al. A cookbook of self-supervised learning. *arXiv preprint arXiv*. (2023). doi: 10.48550/arXiv.2304.12210

19. Brown T, Mann B, Ryder N, Subbiah M, Kaplan JD, Dhariwal P, et al. Language models are few-shot learners. *Adv Neural Inf Process Syst*. (2020) 33:1877–901.

20. Huang S-C, Pareek A, Jensen M, Lungren MP, Yeung S, Chaudhari AS. Self-Supervised learning for medical image classification: a systematic review and implementation guidelines. *NPJ Digital Medicine*. (2023) 6(1):74. doi: 10.1038/s41746-023-00811-0

21. Karimi D, Warfield SK, Gholipour A. Transfer learning in medical image segmentation: new insights from analysis of the dynamics of model parameters and learned representations. *Artif Intell Med*. (2021) 116:102078. doi: 10.1016/j.artmed.2021.102078

22. Chen RJ, Lu MY, Chen TY, Williamson DF, Mahmood F. Synthetic data in machine learning for medicine and healthcare. *Nat Biomed Eng*. (2021) 5(6):493–7. doi: 10.1038/s41551-021-00751-8

23. Shorten C, Khoshgoftaar TM. A survey on image data augmentation for deep learning. *J Big Data*. (2019) 6(1):1–48. doi: 10.1186/s40537-019-0197-0

24. Shen J, Dudley J, Kristensson PO. *The imaginative generative adversarial network: automatic data augmentation for dynamic Skeleton-based hand gesture and human action recognition. 2021 16th IEEE international conference on automatic face and gesture recognition (FG 2021)* (2021).

25. Bhanot K, Qi M, Erickson JS, Guyon I, Bennett KP. The problem of fairness in synthetic healthcare data. *Entropy*. (2021) 23(9):1165. doi: 10.3390/e23091165

26. Vakalopoulou M, Chassagnon G, Bus N, Marini R, Zacharaki EI, Revel M-P, et al., editors. Atlasnet: multi-atlas non-linear deep networks for medical image segmentation. *International conference on medical image computing and computer-assisted intervention*. Granada, Spain: Springer (2018).

27. Qiao M, Wang Y, Berendsen FF, van der Geest RJ, Tao Q. Fully automated segmentation of the left atrium, pulmonary veins, and left atrial appendage from magnetic resonance angiography by joint-atlas-optimization. *Med Phys*. (2019) 46 (5):2074–84. doi: 10.1002/mp.13475

28. Trutti AC, Fontanesi L, Mulder MJ, Bazin P-L, Hommel B, Forstmann BU. A probabilistic atlas of the human ventral tegmental area (vta) based on 7 tesla mri data. *Brain Struct Funct*. (2021) 226(4):1155–67. doi: 10.1007/s00429-021-02231-w

29. Markman EM. *Categorization and naming in children: Problems of induction*. Cambridge, MA, USA: The MIT Press (1989).

30. Van Gerven M. Computational foundations of natural intelligence. *Front Comput Neurosci*. (2017) 11:112. doi: 10.3389/fncom.2017.00112.

31. Lake BM, Salakhutdinov R, Tenenbaum JB. Human-level concept learning through probabilistic program induction. *Science*. (2015) 350(6266):1332–8. doi: 10.1126/science.aab3050

32. Liu L, Wolterink JM, Brune C, Veldhuis RN. Anatomy-aided deep learning for medical image segmentation: a review. *Phys Med Biol*. (2021) 66(11):11TR01. doi: 10.1088/1361-6560/abfbf4

33. Xie X, Niu J, Liu X, Chen Z, Tang S, Yu S. A survey on incorporating domain knowledge into deep learning for medical image analysis. *Med Image Anal*. (2021) 69:101985. doi: 10.1016/j.media.2021.101985

34. Nagel C, Sanchez J, Azzolin L, Zheng T, Schuler S, Dössel O, et al. *A bi-atrial statistical shape model and 100 volumetric anatomical models of the atria*. (2021). doi: 10.5281/zenodo.5571925

35. Peng XB, Kanazawa A, Malik J, Abbeel P, Levine S. Sfv: reinforcement learning of physical skills from videos. *ACM Trans Graph*. (2018) 37(6):1–14. doi: 10.1145/3272127.3275014

36. Soille P. *Erosion and dilation, morphological image analysis*. Berlin: Springer (2004).

37. Piccinelli M, Veneziani A, Steinman DA, Remuzzi A, Antiga L. A framework for geometric analysis of vascular structures: application to cerebral aneurysms. *IEEE Trans Med Imaging*. (2009) 28(8):1141–55. doi: 10.1109/TMI.2009.2021652

38. Krissian K, Carreira JM, Esclarin J, Maynar M. Semi-Automatic segmentation and detection of aorta dissection wall in mdct angiography. *Med Image Anal*. (2014) 18(1):83–102. doi: 10.1016/j.media.2013.09.004

39. Razeghi O, Sim I, Roney CH, Karim R, Chubb H, Whitaker J, et al. Fully automatic atrial fibrosis assessment using a multilabel convolutional neural network. *Circ Cardiovasc Imaging*. (2020) 13(12):e011512. doi: 10.1161/CIRCIMAGING.120.011512

40. Isensee F, Jaeger PF, Kohl SA, Petersen J, Maier-Hein KH. Nnu-net: a self-configuring method for deep learning-based biomedical image segmentation. *Nat Methods*. (2021) 18(2):203–11. doi: 10.1038/s41592-020-01008-z

41. Fedorov A, Beichel R, Kalpathy-Cramer J, Finet J, Fillion-Robin J-C, Pujol S, et al. 3d slicer as an image computing platform for the quantitative imaging network. *Magn Reson Imaging*. (2012) 30(9):1323–41. doi: 10.1016/j.mri.2012.05.001

42. Lin T-Y, Maire M, Belongie S, Hays J, Perona P, Ramanan D, et al., editors. Microsoft Coco: common objects in context. *European Conference on computer vision*. Zurich, Switzerland: Springer (2014). 740–55.

43. Sangsriwong M, Cismaru G, Puiu M, Simu G, Istratoaie S, Muresan L, et al. Formula to estimate left atrial volume using antero-posterior diameter in patients with catheter ablation of atrial fibrillation. *Medicine (Baltimore)*. (2021) 100(29). doi: 10.1097/MD.0000000000026513

44. Shi J, Xu S, Chen L, Wu B, Yang K, Chen S, et al. Impact of left atrial sphericity Index on the outcome of catheter ablation for atrial fibrillation. *J Cardiovasc Transl Res*. (2021) 14(5):912–20. doi: 10.1007/s12265-020-10093-6

45. Nakamori S, Ngo LH, Tugal D, Manning WJ, Nezafat R. Incremental value of left atrial geometric remodeling in predicting late atrial fibrillation recurrence after pulmonary vein isolation: a cardiovascular magnetic resonance study. *J Am Heart Assoc*. (2018) 7(19):e009793. doi: 10.1161/JAHA.118.009793

46. Hu W, Fey M, Zitnik M, Dong Y, Ren H, Liu B, et al. Open graph benchmark: datasets for machine learning on graphs. *Adv Neural Inf Process Syst*. (2020) 33:22118–33.

47. Chen C, Qin C, Qiu H, Tarroni G, Duan J, Bai W, et al. Deep learning for cardiac image segmentation: a review. *Front Cardiovasc Med*. (2020) 7:25. doi: 10.3389/fcvm.2020.00025.

48. Firouznia M, Feeny AK, LaBarbera MA, McHale M, Cantlay C, Kalfas N, et al. Machine learning–derived fractal features of shape and texture of the left atrium and pulmonary veins from cardiac computed tomography scans are associated with risk of recurrence of atrial fibrillation postablation. *Circ Arrhythm Electrophysiol*. (2021) 14(3):e009265. doi: 10.1161/CIRCEP.120.009265

49. Tovia-Brodie O, Belhassen B, Glick A, Shmilovich H, Aviram G, Rosso R, et al. Use of new imaging carto® segmentation module software to facilitate ablation of ventricular arrhythmias. *J Cardiovasc Electrophysiol*. (2017) 28(2):240–8. doi: 10.1111/jce.13112

50. Tops LF, Bax JJ, Zeppenfeld K, Jongbloed MR, Lamb HJ, van der Wall EE, et al. Fusion of multislice computed tomography imaging with three-dimensional electroanatomic mapping to guide radiofrequency catheter ablation procedures. *Heart Rhythm*. (2005) 2(10):1076–81. doi: 10.1016/j.hrthm.2005.07.019

51. Krummen DE, Baykaner T, Schricker AA, Kowalewski CAB, Swarup V, Miller JM, et al. Multicentre safety of adding focal impulse and rotor modulation (firm) to conventional ablation for atrial fibrillation. *Europace*. (2016) 19(5):769–74. doi: 10.1093/europace/euw377

52. Michaud GF, Narayan SM. *Rapid point-by-point pulmonary vein isolation*. Washington, DC: American College of Cardiology Foundation (2019). 787–8.

53. Hocini M, Jaïs P, Sanders P, Takahashi Y, Rotter M, Rostock T, et al. Techniques, evaluation, and consequences of linear block at the left atrial roof in paroxysmal atrial fibrillation: a prospective randomized study. *Circulation*. (2005) 112(24):3688–96. doi: 10.1161/CIRCULATIONAHA.105.541052

54. Wongcharoen W, Tsao HM, Wu MH, Tai CT, Chang SL, Lin YJ, et al. Morphologic characteristics of the left atrial appendage, roof, and septum: implications for the ablation of atrial fibrillation. *J Cardiovasc Electrophysiol*. (2006) 17(9):951–6. doi: 10.1111/j.1540-8167.2006.00549.x

55. Monti CB, van Assen M, Stillman AE, Lee SJ, Hoelzer P, Fung GS, et al. Evaluating the performance of a convolutional neural network algorithm for measuring thoracic aortic diameters in a heterogeneous population. *Radiol Artif Intell*. (2022) 4(2):e210196. doi: 10.1148/ryai.210196

56. Olsson C, Thelin S, Stahle E, Ekbom A, Granath F. Thoracic aortic aneurysm and dissection: increasing prevalence and improved outcomes reported in a nationwide population-based study of more than 14 000 cases from 1987 to 2002. *Circulation*. (2006) 114(24):2611–8. doi: 10.1161/CIRCULATIONAHA.106.630400

57. Zheng Y, John M, Liao R, Boese J, Kirschstein U, Georgescu B, et al., editors. Automatic aorta segmentation and valve landmark detection in C-arm ct: application to aortic valve implantation. *International conference on medical image computing and computer-assisted intervention*. Beijing, China: Springer. (2010). p. 476–83.

58. Hamm CW, Arsalan M, Mack MJ. The future of transcatheter aortic valve implantation. *Eur Heart J*. (2016) 37(10):803–10. doi: 10.1093/eurheartj/ehv574

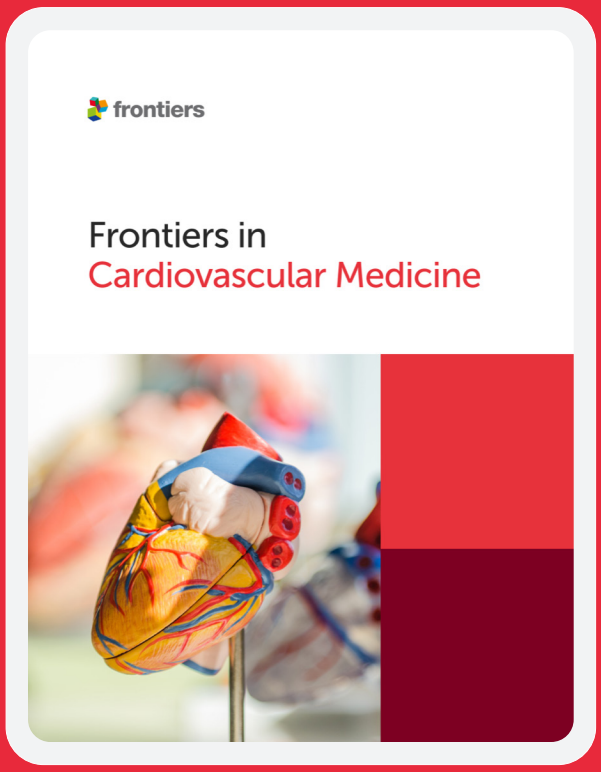
Frontiers in
Cardiovascular Medicine

Innovations and improvements in cardiovascular treatment and practice

Focuses on research that challenges the status quo of cardiovascular care, or facilitates the translation of advances into new therapies and diagnostic tools.

Discover the latest Research Topics

See more →



Frontiers

Avenue du Tribunal-Fédéral 34
1005 Lausanne, Switzerland
frontiersin.org

Contact us

+41 (0)21 510 17 00
frontiersin.org/about/contact